

Visakh P.M.
Oguz Bayraktar
Guillermo Alfredo Picó *Editors*

Polyelectrolytes

Thermodynamics and Rheology

Engineering Materials

More information about this series at <http://www.springer.com/series/4288>

Visakh P.M. · Oguz Bayraktar
Guillermo Alfredo Picó
Editors

Polyelectrolytes

Thermodynamics and Rheology



Springer

Editors

Visakh P.M.
School of Chemical Sciences
Mahatma Gandhi University
Kottayam
Kerala
India

Guillermo Alfredo Picó
Biotechnological Process Laboratory,
Faculty of Biochemical
and Pharmaceutical Sciences
National University of Rosario
Rosario
Argentina

Oguz Bayraktar
Department of Chemical Engineering
İzmir Institute of Technology
Gülbahçe, Urla, Izmir
Turkey

ISSN 1612-1317
ISBN 978-3-319-01679-5
DOI 10.1007/978-3-319-01680-1

ISSN 1868-1212 (electronic)
ISBN 978-3-319-01680-1 (eBook)

Library of Congress Control Number: 2014946747

Springer Cham Heidelberg New York Dordrecht London

© Springer International Publishing Switzerland 2014

This work is subject to copyright. All rights are reserved by the Publisher, whether the whole or part of the material is concerned, specifically the rights of translation, reprinting, reuse of illustrations, recitation, broadcasting, reproduction on microfilms or in any other physical way, and transmission or information storage and retrieval, electronic adaptation, computer software, or by similar or dissimilar methodology now known or hereafter developed. Exempted from this legal reservation are brief excerpts in connection with reviews or scholarly analysis or material supplied specifically for the purpose of being entered and executed on a computer system, for exclusive use by the purchaser of the work. Duplication of this publication or parts thereof is permitted only under the provisions of the Copyright Law of the Publisher's location, in its current version, and permission for use must always be obtained from Springer. Permissions for use may be obtained through RightsLink at the Copyright Clearance Center. Violations are liable to prosecution under the respective Copyright Law. The use of general descriptive names, registered names, trademarks, service marks, etc. in this publication does not imply, even in the absence of a specific statement, that such names are exempt from the relevant protective laws and regulations and therefore free for general use.

While the advice and information in this book are believed to be true and accurate at the date of publication, neither the authors nor the editors nor the publisher can accept any legal responsibility for any errors or omissions that may be made. The publisher makes no warranty, express or implied, with respect to the material contained herein.

Printed on acid-free paper

Springer is part of Springer Science+Business Media (www.springer.com)

Preface

The book on “Polyelectrolytes: Thermodynamics and Rheology” summarizes many of the recent research accomplishments in the area of polyelectrolytes such as state-of-art polyoxymethylene, structure and thermodynamics of polyelectrolyte complexes, polyelectrolytes: science and application, study on biological polyelectrolytes, polyelectrolyte hydrogels: thermodynamics of polyelectrolyte hydrogels rheologys, complexes formation between proteins and polyelectrolytes and its application in the downstream processes of enzyme purification, polyelectrolyte complexes: bridging the ensemble average—single-molecule strategies, stratified interpolyelectrolyte complexes: fabrication, structure, properties, and applications, Monte Carlo studies in polyelectrolyte solutions: structure and thermodynamics. As the title indicates, the book emphasizes on the various aspects of polyelectrolyte and their thermodynamics studies and rheological studies to scientific community. This book is intended to serve as a “one-stop” reference resource for important research accomplishments in this area. This book will be a very valuable reference source for university and college faculties, professionals, postdoctoral research fellows, senior graduate students, researchers from R&D laboratories working in the area of “Polyelectrolyte: Thermodynamics and Rheology.” The various chapters in this book are contributed by prominent researchers from industry, academia, and government/private research laboratories across the globe. It covers an up-to-date record on the major findings and observations in the field of “Polyelectrolyte: Thermodynamics and Rheology.”

The Chapter on “[Polyelectrolyte: Thermodynamics and Rheology](#)” give an overview of the area of state of art, new challenges and opportunities of polyelectrolyte-based studies and research. The following chapter provides an overview of structure and thermodynamics of polyelectrolyte complexes. This chapter explained with many subtopics, such as weak and strong electrostatic coupling, thermodynamics of polyelectrolytes and polyelectrolyte complexes, Flory-Huggins solution theory applied to polyelectrolyte solutions, enthalpy in polyelectrolyte solutions, polyelectrolyte gels, computer simulations and structure, Monte Carlo simulations and other simulation methods, molecular dynamics simulations, experimental characterization, polyelectrolyte complexes and gels, etc.

“Structure and Thermodynamics of Polyelectrolyte Complexes” is mainly concentrated on polyelectrolyte: science and application. The authors of this chapter discussed with recent research on polyelectrolyte, applications of polyelectrolyte, scaling theory, dynamic light scattering, neutron scattering, biopolymers and ionomers. In this section, authors are discussed with very nice subtopics, such as biopolymers, polynucleotides, polypeptides, ionomers, etc. Survey on applications of biological polyelectrolytes done in the “[Biological Polyelectrolytes: Solutions, Gels, Intermolecular Complexes and Nanoparticles](#)”, the authors explained with many subtitles, such as introduction to biological polyelectrolytes, classification of biological polyelectrolytes, biological polyelectrolytes in solutions, intermolecular complexation and coacervation, biological nanoparticles, encapsulation, and drug release, also they explained about other topics, such as carbohydrate, protein, nucleic acids, protein-protein, protein-carbohydrates, protein-DNA, chitosan, gelatin, and pectin. “[Polyelectrolyte Hydrogels: Themodynamics](#)” discussed about the polyelectrolyte hydrogels: Thermodynamics, this chapter discussed about many interesting topics, such as classification of polyelectrolyte hydrogels, synthesis of polyelectrolyte hydrogels, polyelectrolyte hydrogels: thermodynamics, characterization of polyelectrolyte hydrogels, biomedical applications of polyelectrolyte hydrogels.

“[Thermodynamic and Rheological Properties of Polyelectrolyte Systems](#)” deals with the thermodynamic and rheological properties of polyelectrolyte systems. This chapter explained many properties, such as interactions, rheological properties, flow properties, etc. Authors of this chapter explained with different subjects such as interaction of polyelectrolytes with organic molecules, release of drugs from polyelectrolyte-drug dispersions, rheological properties of polyelectrolyte dispersions, flow properties of representative sodium salts of acid polyelectrolytes, flow properties of acid PE-drug dispersions, properties of carbomer-drug hydrogels, effect of the addition of other species on carbomer-drug dispersions, remarks on thermodynamic and rheological properties of polyelectrolytes, finally field of projections based on the properties of PE-drug complexes are also discussed. “[Complexes Formation Between Proteins and Polyelectrolytes and Their Application in the Downstream Processes of Enzyme Purification](#)” discussed about the complexes formation between proteins and polyelectrolytes and their application, from this chapter, we can see many different kinds of applications and use of polyelectrolyte and authors explained with many other topics including uses and applications of polyelectrolytes, aqueous solutions of polyelectrolytes, the formation of complexes between polyelectrolytes and proteins, the downstream processes of proteins and their scaling up process by PE-P formation, application of PE-P in downstream processes. Bridging the ensemble average-single-molecule strategies of polyelectrolyte complexes are discussed in “[Polyelectrolyte Complexes](#)”, this chapter also explained about polyelectrolytes in biology, polyelectrolyte complexes in biology, man-made polyelectrolyte complexes, polyelectrolyte complex formation, nonideal thermodynamics, structure of the polyelectrolyte complexes, experimental observations at the individual complex level, correspondence to observations at the ensemble level and cooperative

effects in DNA condensation. The coming chapter on stratified interpolyelectrolyte complexes explained with fabrication, structure and properties and with several topics, such as fabrication of stratified interpolyelectrolyte complexes, controlling the fabrication of polyelectrolyte multilayers: effect of different physicochemical variables, structure: stratified and nonstratified systems, water content and hydration, rheological properties, permeability and porosity, response to osmotic stress, applications.

“Monte Carlo Studies in Polyelectrolyte Solutions: Structure and Thermodynamics” on Monte Carlo studies in polyelectrolyte solutions: structure and thermodynamics, this chapter discussing about, Monte Carlo studies of polyelectrolytes, theoretical approach of Monte Carlo studies, application level of Monte Carlo in polyelectrolyte, authors of this chapter are also trying to discuss more with many topics, such as coarse-grain model for polyelectrolyte and small ions, ideal gas and excess contribution to the partition function of the system, metropolis Monte Carlo method, Monte Carlo trial moves, conformational and persistence length of a single polyelectrolyte chain, counterions condensation and end-chain effects and morphology of polyelectrolyte complex.

Finally, the editors would like to express their sincere gratitude to all the contributors of this book, who made excellent support to the successful completion of this venture. We are grateful to them for the commitment and the sincerity they have shown toward their contribution in the book. Without their enthusiasm and support, the compilation of a book could have not been possible. We would like to thank all the reviewers who have taken their valuable time to make critical comments on each chapter. We also thank the publisher Springer for recognizing the demand for such a book, and for realizing the increasing importance of the area of “Polyelectrolyte: Thermodynamics and Rheology” and for starting such a new project, in which not many other publishers put their hands on.

Visakh P.M.
Oguz Bayraktar
Guillermo Alfredo Picó

Contents

Polyelectrolyte: Thermodynamics and Rheology	1
Visakh P.M.	
Structure and Thermodynamics of Polyelectrolyte Complexes	19
Johannes Frueh, Meiyu Gai, Simon Halstead and Qiang He	
Polyelectrolyte: Science and Application	87
Emel Akyol, Semra Kirboga and Mualla Öner	
Biological Polyelectrolytes: Solutions, Gels, Intermolecular Complexes and Nanoparticles	113
H.B. Bohidar and Kamla Rawat	
Polyelectrolyte Hydrogels: Thermodynamics	183
Xue-Song Jiang, Mohit Philip Mathew and Jian Du	
Thermodynamic and Rheological Properties of Polyelectrolyte Systems	215
Ruben H. Manzo, Alvaro F. Jimenez-Kairuz, María E. Olivera, Fabiana Alovero and María V. Ramirez-Rigo	
Complexes Formation Between Proteins and Polyelectrolytes and Their Application in the Downstream Processes of Enzyme Purification	245
Ph Guillermo Alfredo Picó and Bc Nadia Woitovich Valetti	
Polyelectrolyte Complexes	275
Rita S. Dias and Bjørn Torgor Stokke	

Stratified Interpolyelectrolyte Complexes: Fabrication, Structure and Properties	299
Eduardo Guzmán, Marta Ruano, Francisco Ortega and Ramón G. Rubio	
Monte Carlo Studies in Polyelectrolyte Solutions: Structure and Thermodynamics	349
Claudio F. Narambuena and Ezequiel P.M. Leiva	

Editor's Short Biodata



Visakh P.M. M.Sc., M.Phil. submitted his Ph.D. thesis to Mahatma Gandhi University, Kottayam, Kerala, India. He edited 9 books from Scrivener (Wiley) and Springer and more than 12 books in press, (from Wiley, Springer, Royal Society of Chemistry and Elsevier). He has been invited as a visiting researcher in Portugal (2013, 2014), Czech Republic (2012, 2013) Italy (2009, 2012), Argentina (2010) Sweden (2010, 2011, 2012), Switzerland (2010), Spain (2011, 2012), Slovenia (2011), France (2011), Belgium (2012) and Austria (2012) for his research work. He visited 15 universities in Europe. He published 5 publications, 3 reviews, and more than 13 book chapters. He has attended and presented more than 28 conferences, he has 68 citations and his h-index is 4. His research interests include polymer nanocomposites, bio-nanocomposites, and rubber-based nanocomposites, fire retardant polymers and liquid crystalline polymers and silicon sensors. Contact: visagam143@gmail.com



Oguz Bayraktar M.Sc., Ph.D. received his M.Sc. and Ph.D. degrees in Chemical Engineering from West Virginia University, USA. He worked as a faculty member in İzmir Institute of Technology between 2001–2014. Now he is working in Ege University, Department of Chemical Engineering, Bornova/İzmir, Turkey. In 2006, he has established a company (Natural Products R & D Ltd. Co.) at İzmir Technology Development Zone. He published more than 30 publications, and 40 conference proceedings. He has 200 citations

and his h-index is 7. His research interests include: biopolymers, bioactivities of natural compounds derived from plants, drug delivery systems, nanotechnology. Contact: oguzbayraktar@iyte.edu.tr



Guillermo Alfredo Picó is a full professor of the National University of Rosario (Argentine) and researcher of the National Council of Scientific and Technical Research of Argentine. Director of the Biotechnological and Chemistry Processes Institute—CONICET. He has worked as researcher in Liege University (post doctoral position), Granada University and Alcala University (Spain). He has been invited as a visiting researcher in Vigo, Spain (2013); Saltillo, Mexico (2012); Bremen, Germany (2011); Ourense (Spain 2008), Pernambuco University, Brazil (2008). His

research interests include aqueous two phase systems, natural polyelectrolytes behavior, downstream processes of enzymes, complex formation between proteins and polyelectrolytes, enzymes stabilization and develop of new matrixes using natural polyelectrolytes. He has published 104 papers in international index journals and he has 391 citations. Contact: gpico@fbioyf.unr.edu.ar

Polyelectrolyte: Thermodynamics and Rheology

State of Art, New Challenges and Opportunities

Visakh P.M.

Abstract The present chapter deals with a brief account on various types topics in polyelectrolyte: thermodynamics and rheology, structure and thermodynamics of polyelectrolyte complexes, polyelectrolyte: science and application, biological polyelectrolytes: relevance to nature and its interactions, polyelectrolyte hydrogels: thermodynamics, thermodynamic and rheological properties of polyelectrolyte systems, complexes formation between proteins and polyelectrolytes and their application in the downstream processes of enzyme purification, polyelectrolyte complexes: bridging the ensemble average—single-molecule strategies, stratified interpolyelectrolyte complexes: fabrication, structure and properties and monte carlo studies in polyelectrolyte solutions: structure and thermodynamics. This chapter also discussed recent technical research accomplishments in the area of polyelectrolyte: thermodynamics and rheology having immense structural possibilities for chemical and mechanical modifications to generate novel properties, functions and applications especially polyelectrolyte.

1 Structure and Thermodynamics of Polyelectrolyte Complexes

Polyelectrolytes (PEs) are polymers with charged monomer groups that can dissociate into a charged macroion and small counterions when the PE is dissolved in a polar solvent [1, 2]. These charged polymers are, in many cases, employed in nature, and not only DNA [3] but also proteins and cellulose can be classified as PEs. Technical applications of PEs include, for example, PE-DNA drug delivery complexes called polyplexes [4, 5]. The interaction and structure of PEs in a solvent (mostly water) are controlled to a large extent by electrostatic interactions.

Visakh P.M. (✉)

School of Chemical Sciences, Mahatma Gandhi University,
Kottayam 686 560, Kerala, India
e-mail: visagam143@gmail.com

In case of a weak coupling, the coupling constant, K , is far below 1 (please note that in some old papers other nomenclature is used). Weak PEs are, in many cases similar to normal polymers. Large parts of the chain are uncharged and the PE structure in solution can be correlated to the solvent quality. In the case of strong PEs, the properties of the PE, and therefore of the enthalpy, are mainly controlled by the strong electrostatic coupling. Strong PEs are, in contrast to weak PEs, insensitive to the surrounding pH. Examples of this type of PE are polystyrenesulphonate (PSS) and polydimethylammonium chloride (PDDA). In contrast to weak electrostatic coupling in weak PEs, strong electrostatic coupling between the ionic groups and their counterions $K \geq 1$ leads to a concentration dependent condensation of counterions [6, 7].

The Flory-Huggins theory (a mean field based approach) and statistical thermodynamic approaches based on the Debye-Hückel theory are the two most frequently used approaches. In the Debye-Hückel approach, the interactions between charges of the same sign cause intramolecular self-repulsion influencing the PE interaction and structure. The thermodynamics of dissolved apolar polymer systems is usually described by the Flory-Huggins theory [8–10]. The Flory-Huggins theory is based on the so called mean field approach which is a theory that assumes, that each part of the monomer-monomer interaction and solvent-solvent interaction has the same energy (PE is not a co-polymer), no overlap of the chains is possible and fluctuations are neglected. Alternatively to the work of the Flory-Huggins theory, other methods like the Hansen solubility parameter can be used to estimate the solvent quality. The behavior of weak PEs is mostly controlled by the pH and ionic strength. If e.g. the pH causes a very low charge density, the interaction between the PEs and also within the same coil is controlled by hydrophobic forces and hydrogen bonds. One of the main interactions in weak PEs that contribute to the enthalpy are hydrogen bonds, which allow the e.g. natural PE to adopt special structures, like helices. The reason for the strong dominance of the entropy is the fact that there is only a little change in the enthalpy of the PE in solid, solution or the complex, in comparison to the entropy of the counter ions. One way to increase the electrostatic interaction energy, and at the same time to decrease the entropy, is to exchange the monovalent counterions with multivalent ions or oppositely charged PEs [11]. A Flory theory based theoretical study of the PE gelation points using di- and trivalent ions was able to show that the free energy of such a system consists of the translational entropy, the combinational free entropy. To understand the rheological and viscous behavior of PE solutions it is vital to understand the behavior of PE molecular structure, entanglement and interactions in solution.

2 Polyelectrolyte: Science and Application

A polymer, large molecules, is made of linked smaller molecules. Firstly, the “rubbery” properties of rubber trees were discovered by the Mayans. A polyelectrolyte is a macromolecule dissolved in water or polar solvent and gets a large

number of elementary charges distributed along the macromolecular chain. Polyelectrolytes carry charged or chargeable groups [12]. The degree of dissociation is controlled by some parameters such as solution pH, temperature, the ionic strength [13]. Weak polyelectrolytes dissociate more or less depending up on pH whereas strong polyelectrolytes dissociate completely independent of pH of the solution. Polyelctrolytes can be used genetic science because of their high charge density and biocompatibility [14]. They are biocompatible materials for medical applications in contact with blood and other biological fluids. Common polyelectrolyte examples are poly_vinyl sulfonic acid, poly_acrylic acid, poly-meric bases poly_vinylamine, poly_vinyl pyridine [15]. The properties of polyelectrolyte have not been well understood in spite of development in theoretical and experimental studies. The first layer can be obtained by dipping the substrate having positive charges into polyanion solution, then into polycation solution. Electrostatic interactions between oppositely charge polyelectrolyte or/and colloidal particles is important for this technique [16].

In the paper industry, polyelectrolytes are used as retention aids, flocculating and coagulating agents to separate solid-liquid phases [17]. Novel applications such as drug and genetic material delivery system utilize polyelectrolytes due to their high charge density and biocompatibility [18]. Biocompatible polyelectrolytes such as chitosan and polystyrene sulfonate (PSS) are also utilized in bio-sensors and biomolecular recognition systems. Polyelectrolytes are solvated in water and surroundend by salt ions in biological system [19]. It is suggested that the driving force for the formation of complex is primarily from the gain in entropy. Furthermore, hydrogen bonding or hydrophobic interactions may have important effects on the complex formation. The PECs and their applications have been studied in recent years. The mechanical, thermal and barrier performance properties increases with the addition of nanoclay instead of clay. Hydrogels are macromelcular polymer networks immersed in a solvent. Their potential application areas are biomedicine, food industry, water purification, building industry and communication technology. Chitosan, pectin, alginate, cellulose derivatives and acrylic polymers have been investigated for the oral controlled release system. Chitosan is derived from natural chitin by alkaline deacetylation and has been used in gastrointestinal drug delivery systems. Polysaccharides, proteins and small molecular weight molecules can be used for biological tissues. Materials used in biological tissues provide the foundation for the biochemical and biomechanical function of tissues. Here we provide a basic introduction into the properties of the neutron scattering. Neutron scattering is an experimental technique which used to investigate materials in modern science. The goal of the neutron scattering technique is to understand material properties on the atomic scale.

3 Biological Polyelectrolytes: Relevance to Nature and Its Interactions

Biological polyelectrolytes are essential component of molecular biophysics. These molecules self-organize to higher order assemblies to yield cells and intelligent organization of cells produce living organism. According to Bohr's Uncertainty Principle "*Physico-chemical properties of the living organisms and the life phenomenon cannot be studied simultaneously*". This implies that cognition of one excludes the other. According to Schrödinger "*An organism is an aperiodic crystal*". Biopolymers such as proteins, nucleic acids and carbohydrates carry a number of charged groups in their monomers. Therefore, they can also be referred to as either *polyampholytes* or *polyelectrolytes*.

All nucleic acids and carbohydrates are high charge density polyelectrolytes whereas proteins are mostly weakly charged polyampholytes. Physics of nucleic acids deals with the study of molecular structure-property relationship in describing the life phenomena, in particular heredity and variability. Proteins comprise the largest percentage of organic molecules in the body. The term protein is derived from the greek word "proteios" meaning the first place. They are nitrogen containing macromolecules. They are twenty in number and can be divided into various classes and these perform a variety of functions. Most cell processes are mediated by proteins.

DNA (a nucleic acid), gelatin (a polyamino acid) and cellulose (a polysaccharide). The solution properties of biopolymers have many dimensions and the least discussed feature is their persistence length. This is a length scale that plays a central role in governing intermolecular interactions. Biopolymer molecules carrying ionizable acid and base groups make the net charge on the molecule strongly dependent on pH. If the pH of protein solution changes, it may affect the molecular structure, along with corresponding change in the surface charge. Thus, monitoring the zeta potential of a protein in solution is one way of observing stability of the dispersion stability at that pH. The term chitosan embraces a series of polymers that vary in molecular weight (from approximately 10,000 to 1 million Da) and degree of deacetylation (in the range of 50–95 %). Chitosan (CS) is the second most abundant naturally occurring polysaccharide which is a cationic polyelectrolyte ($pK_a = 6.3\text{--}7$). This demonstrates that biological agents can be immobilized within the nanoparticle and coacervate matrices and can be used in delivery of the drug, thereby enhancing the circulation time of the drug. Release from these matrices is due to the time dependent swelling in aqueous solutions. The diffusion coefficient of a drug in a matrix is related to its diffusion coefficient in water, its molecular weight, and the percentage of polymer in the matrix.

Zeta potential is a useful indicator of surface charge property and can be employed as an index to the stability of the nano-conjugate. The negative Zeta Potential value of pectin chains imply negative charge on the surface and may be attributed to the presence of ionized carboxyl groups on the pectin surface. Bio-polymer gels remained outside the preview of this chapter because it is a discipline on its own and cannot be dealt in a limited discussion. However, some general observations can be made. Polymer gels constitute a special class of soft matter as far as their supramolecular structure and viscoelastic properties are concerned.

4 Polyelectrolyte Hydrogels: Themodynamics

Polyelectrolyte hydrogels have attracted tremendous research interest over the past few decades owing to their ability in respond to external chemical or physical stimuli. A polyelectrolyte hydrogel is a three dimensional networks forming by charged polymer chains that can swell in water and retain a significant amount of water while maintaining their structure [20]. Many applications require hydrogels that have high sensitivity and a short response times. Because the volume phase transition of hydrogels is a diffusion-limited process, the fast swelling property can be achieved by either reducing the particle size of the hydrogels or creating pore structures in the hydrogels. Alternative types of networks, formed by cleavable bond or physical interactions between polymer chains, have been developed. These biocompatible, nontoxic and biodegradable polymers are now acquiring unique place for biomedical application for various purposes such as scaffolds for tissue engineering [13] and drug delivery system [21–23]. Many methods have been employed for preparation of protein-based hydrogels hydrogels,including thermal gelation, photopolymerization and chemical crosslinking with agents such as glutaraldehyde, genipin, adipic dihydrazide and bis(sulfosuccinimidyl) suberate [24, 25]. Polymers can be converted to hydrogels by crosslinking of polymers containing reactive groups with a bi-functional crosslinking agent like divinyl-sulfone [26] and 1,6-hexanedibromide. Gluteraldehyde has been widely used as a crosslinker to prepare hydrogels of polymers containing primary amine groups (e.g. gelatin, chitosan) [27, 28].

Polyelectrolyte hydrogel swelling and shrinking behavior has an added layer of complexity introduced by the charges that exist within the gel and the charges that can be present as ions in the surrounding liquid. While different models have been developed over the years to describe the thermodynamics of polyelectrolyte hydrogels, this section will focus on the model developed by Maurer and Prausnitz [29]. In addition to this sometimes the kinetics of swelling may be measured wherein the gel is weighed at different times during its incubation in the deionized water bath. The deswelling kinetics may also be determined by transferring the swollen hydrogel after it has reached equilibrium into a deionized water bath at a temperature greater than its Lower Critical Solution. Determination of the interior morphology is generally done using scanning electron microscopy [30, 31]. Here

thin slices of the hydrogel are first allowed to swell in distilled water and then ethanol is gradually added. This treatment makes the gel a little more rigid and opaque. The gel block is then placed in a vacuum to dry and then coated with gold before the sample is examined in a scanning electron microscope. Synthetic hydrogels, with their ability to absorb water, flexibility, and biocompatibility, are ideal carriers for the development for novel pharmaceutical formulations and for the delivery of drugs, proteins, and as targeting agents for drug delivery. Polyelectrolyte hydrogels are attractive as tissue engineering matrices as these hydrophilic networks are capable of absorbing great amounts of water while maintaining structural integrity [32].

5 Thermodynamic and Rheological Properties of Polyelectrolyte Systems

In most of acidic PE the ionizable moiety is the carboxylic group. Such is the case of carbomers (C, also known as carbopol or carboxyvinyl polymers), alginic acid (AA), hyaluronic acid (HA, also known as hyaluronan). Other acidic PE such as dextran sulfate, cellulose sulfate and nucleic acids are based on sulfate, or phosphoric ionizable groups. Among basic PE, the nitrogen atom is the protonable center. The classical description of ion–ion interaction recognizes two relative stable regions: one referred to as a solvent separated ion pair, or as a loose ion pair and the other referred to as a contact ion pair, which is also known as a tight ion pair [33]. The former is the delocalized confinement of the counterions within a condensation volume in the immediate vicinity of the PE, due only to long-range interactions, while the latter is a short range, site-specific interaction [34–36].

Several basic PE has been used for a variety of purposes. In all of them, basic nitrogen is the interacting atom susceptible of protonation in aqueous medium. Among them, chitosan and EE a polymethacrylate with diethylamino pending groups has been extensively studied.

Rheology has been properly defined as the study of the flow and deformation of materials, with special emphasis being usually placed on the former [37]. There exist many fluids whose flow cannot be described by the linear response of the Newtonian flow equations. These materials are called as complex fluids, or non-Newtonian materials, since they display behaviors that range from that of viscous liquids to that of an elastic solid to some combination of the two. PE in aqueous dispersions exhibit behaviors of complex fluids [38].

The rheology of HA-Na is extremely sensitive to protein contamination [39, 40]. Comparable results are obtained using protein free samples obtained from bacterial sources. Some of these studies were conducted in saline aqueous medium to reproduce physiological conditions in which dilute and semidilute HA-Na dispersions exhibit Newtonian behavior in a wide shear rate range. Equilibrium and release properties of aqueous systems PE-drug dispersions can be reasonably

predicted from the physicochemical properties of both partners. However such systems exhibit a wide variability in their rheological properties. In aqueous dispersions of cross-linked PE-drug the osmotic pressure generated by the accumulations of ions inside the microenvironment of the complex is one of the main factors that determine the high level of swelling. Therefore, the addition of inorganic ions decreases the osmotic difference between the macromolecular environment and the bulk medium with the consequent lowering of swelling that affect the rheology of the system [41].

The acid-base reaction renders organic ions that have lower ionic mobility than the small inorganic ions currently used as PE partners. Thus, the electrostatic attraction between the ionized pending groups of the PE and the organic ions yields a high proportion of counterionic condensation with K_{cc} in the range of 10^3 – 10^5 . Available results have shown that the K_{cc} are not affected by the dilution of the dispersions.

There is plenty of experimental evidence to support that rheologic changes are observed when bioadhesive polymers and mucin are mixed. In this context it was shown that when a mucoadhesive polymer and mucin are mixed together there is a synergistic increase in viscosity. It is known that the viscosity of a mucin dispersion is the net result of the resistance to flow exerted by individual chain segments, physical chains entanglements and non-covalent molecular interactions, which are the same as the interactions involved in the process of mucoadhesion.

6 Complexes Formation Between Proteins and Polyelectrolytes and Their Application in the Downstream Processes of Enzyme Purification

The interest is centered in PE obtained from natural polymers which have been chemically modified favoring an increase in their solubility in aqueous media [42]. At present, there are many natural PE, whose use is allowed by the food codex as food additives, for skin products, as drugs carriers and for controlled drug delivery. It is observed that longer chains tend to achieve relatively more compact conformations than shorter ones, and the dimensions of the collapsed structures do not significantly vary with contour length. The influence of contour length and intrinsic stiffness in the process of ion condensation is studied by analysis of the ion-ion nearest-neighbor distribution. The ionic groups can cause repulsion between the chains, which leads to an expansion of the molecule and, consequently, to an increase in solution viscosity. This behavior has been traditionally explained in terms of chain extension of the PE [43]. Weak acid and basic groups present in PE can be titrated with strong basic or acid solutions so; the pK value can be calculated from the titration curve [44]. This experimental pK value is an apparent value because it depends on experimental variables such as ionic strength, dielectric constant of the solvent and the presence of cosolutes which

modifies the structure of the water solvent. When a PE loses protons during acid-base titration, the environment of its acid or basic groups changes because they partially lose contact with the solvent molecules, so the pH_{50} will be a mean of all pK of the acid or basic groups. Then pH_{50} is a macroscopic variable and only represents the overall process of loss of solubility by the effect of pH.

Over the last years, there has been a growing interest in PECs based on natural and synthetic polymers. Chitosan is a natural polyaminosaccharide and a weak base. Its PECs with different natural and synthetic polyacids such as, carboxymethylcellulose, alginic acid [45], poly (acrylic acid) [46] are known. Precipitation with PE requires inexpensive chemicals in small amounts, only the amount of polyelectrolyte required to neutralize the protein charge. Thus, the method is suitable for large-scale processing and for dealing with dilute solutions. The interaction between proteins and synthetic polymers has been extensively studied, in particular for the modulation of living processes, immobilization or stabilization of enzymes, modification of substrate affinity, changing properties of food products, and for the development of many pharmaceutical applications [47]. The forces which contribute to complex formation between PE and proteins are mainly coulombic: ion-ion, ion-dipole and dipole-dipole interaction. According to the pH and ionic strength of the medium, this complex could be soluble; the formation of the soluble complex can be followed by light scattering measurements. In a second step, an interaction is produced between the soluble complex particles, so, a non-soluble complex (of high molecular mass) is produced, and this is evidenced as a precipitate. Production of proteins by genetically engineered microorganisms, yeasts and animal cells became a very important technique for the preparation of pharmaceuticals and other molecules used in Biotechnology. The feedstocks from which proteins are prepared are generally complex, containing solids, soluble and dissolved biomass of various sizes and molecular mass. Precipitation of protein by PE is a novel technique integrating clarification, concentration, and initial purification in a single step [48, 49]. It allows the capture of bio-molecules from feedstock without prior removal of particulates, thus enabling clarification of a cell suspension or cell homogenate and the concentration of the desired product in one operation [50].

7 Polyelectrolyte Complexes

The presence of charge serves as structural motifs underpinning various functionalities. Firstly, it increases the solubility of the molecules in aqueous solution. Even though not much is known about the environment that molecules experience inside a cell, many biological processes are assumed to occur in aqueous environment as thus, the many components should be water soluble and interact in a controllable fashion. Polyelectrolyte complexes adopt structures with extent of order depending on the type of molecules involved and their molecular parameters. The structures of PEC have conceptually been described to span from the formation

of a lattice-like structure where the pairing of the opposite charges are viewed to induce a railway track structure of the polyanion-cation.

The presence of such patches have been shown to induce an inhomogeneous distribution of polyelectrolyte monomers at the protein surface as well as the formation of a stronger complex than a corresponding protein model with a homogeneous surface charge [51]. Experiments [52–54] and computer simulations [55–59] suggest that histone tail bridging may strongly contribute to nucleosomal attraction. Histone tails are flexible chains that extend from the octamer and which carry several positively charged residues. As the stiffness of the polyelectrolyte chains is increased, the polyplexes tend to adopt structures such as toroids or rods [60, 61] but, independently of the morphology of the resulting structures, the forces driving the complexation process are similar as has been reviewed by Bloomfield [62, 63]. It has also long been acknowledged that the presence of a small amount of salt leads to a more uniform distribution of the short chain components among the polyelectrolyte with the longer chains, and thus thermodynamic equilibrium [64].

The successful extraction of thermodynamic parameters relies on the use of nonlinear least squares curve fitting while employing an appropriate model that describes the interaction under study [65]. Recently, the limitations associated with analysis of isothermal titration data of polyelectrolyte complex formation within polypeptide chains applying a lattice-like interaction model has been suggested to be resolved by including a second process [66]. If the compaction of the polyelectrolyte is abrupt above certain charge neutralization, simply the fact that different polyelectrolyte chains experience slightly different environments in solution could lead to the coexistence of extended and compact polyelectrolyte complexes. Monte Carlo simulation results suggest that in polyelectrolyte complexes with some chain length asymmetry of the polyelectrolytes, and below charge neutralization, the shorter polyelectrolyte possesses a significant translational along the longer chain which hinders to some extent the condensation of the longer chain [67].

Semi-flexible chains on the other hand are always broader since the chains fluctuate between stretched and collapsed conformations [68]. On the other hand, and using simple models of stiff chains, no evidence was found that a mixture of fully compact and fully extended polyelectrolytes would have a lower free energy than semi-neutralised chains with homogeneously distributed condensing agents. Returning to the cooperative nature of DNA condensation, the suggestions put forward to explain it in 1972 [69] included (i) the favourable direct interaction between adjacent condensing agents, unlikely for the case of polypeptides but an important mechanism in the case of cationic lipids and surfactants, (ii) the formation of separate phases (complex coacervation), or (iii) a process in which the conformational changes induced in the DNA by the initial binding molecules favour the binding of additional condensing agents. Rod-like polyelectrolyte complexes have been reported for DNA complexes [70–73]. In view of the simulations, such states could represent kinetically trapped states [74, 75]. Other numerical studies suggest that the rod is a ground state, with approximately the same energy as the toroid [76–78].

8 Stratified Interpolyelectrolyte Complexes

In the last 20 years, there has been an increasingly interest on the application of polyelectrolyte based systems in the design and fabrication of new materials [79, 80].

A vast number of applications in different fields of Nanotechnology (interfacial phenomena, colloids, and nanomaterials) have been described for the materials obtained following this approach [81]. The formation and growth of polyelectrolyte multilayers is the result of an intricate balance of interactions [82], among their components: polyelectrolyte–polyelectrolyte, polyelectrolyte–solvent, polyelectrolyte–surface, etc. The different interactions involved are governed by the complex interplay between electrostatic and entropic contributions, as well as solvent quality.

The adsorption of polyelectrolytes onto surfaces can be considered quasi-irreversible and it is possible to assume that once the polyelectrolyte chains are attached to the surface they remain adsorbed [83]. The chemical nature of the polyelectrolytes, and the assembling conditions play a key role in the assembling of polyelectrolyte multilayers, and on their thickness, structure and properties [84, 85]. More specifically, the hydrophobic/hydrophobic balance of the chains is probably the most important factor that affects to the PEMs formation because it determines both the interaction between the polyelectrolytes and the swelling degree of the chains [95]. The effect of the increase of the polymer hydrophobicity on the adsorption of polyelectrolytes is mediated by the existence of a unfavourable contribution to the solvation energy of the chains [86]. Another key variable is the flexibility of the polymer chains. This parameter plays a key role in the interaction between the chains and the adsorbed layers [87].

In general, the increase in the polyelectrolyte concentration provokes the increase in the multilayer thickness [88]. Shen et al. [89] pointed out that the increase in the concentration of hyaluronic acid (HA) induces a strong effect on the growth and intermolecular association in multilayers formed by poly(L-lysine) and HA. The effect of the supporting electrolyte is mainly governed by the well-known Hofmeister serie [90]. In general, the effect of the cations in the growth of polyelectrolyte multilayers is quite limited [91], at least in aqueous systems [92]. The increase of the ions hydrophobicity increases the thickness of the multilayer. The rinsing of the polyelectrolyte multilayers after the deposition of the successive layers allows removing the chains that are not strongly adsorbed to the PEMs. The rinsing step prevents the formation of interpolyelectrolyte complexes in solution when the next layer is formed; such complexes would precipitate onto the multilayer, thus modifying its structure and properties. The first studies on the structural characterization of the multilayers were made in the model system (PAH + PSS)_n by Schmitt et al. [93], and Lösche et al. [94] using different sequences of layers where each certain number of layers the PSS was replaced by deuterated PSS (d-PSS). These authors found certain degree of stratification, even though a total stratification between single layers was not found, and interdigitation of the layers propagating through three bilayers was observed [95]. Furthermore, these authors

found that the degree of stratification was correlated to the multilayer thickness in accordance with the three-zone model for polyelectrolyte multilayers. Singh et al. [96] have revisited recently the existence of different regions in the polyelectrolyte multilayers, using (poly(ethylenimine) + PSS) multilayers. They concluded that the multilayers were formed by an inhomogeneous region near to the substrate due to the influence of the interactions between the surface and the polyelectrolyte, and a second more homogeneous region after a certain number of layers have been deposited.

The control of the mechanical properties of PEMs plays an essential role in the development of materials with potential applications because they control the stability of the PEMs against different external stimuli [97]. In general, the mechanical behavior is reminiscent of both rubber-like and glass-like materials with a wide range of values of the elasticity modulus [98]. The increase in the ionic strength provokes the decrease in the bulk modulus of the films that allows consider this process as a counterion-plastifying phenomena [99]. More recently Blacklock et al. [100] have pointed out that these modifications of the mechanical properties of polyelectrolyte multilayers by the salt content and nature can be used to enhance the cell adhesion onto substrates modified by PEMs. The porosity and permeability of the multilayers play a main role for the development of applications where the exchange of material between the interior of the multilayer and the surrounding environment is needed. In general, it would be expected that rigid films with low water content lead to the formation of non-porous structure, thus hindering the permeability of the molecules along the multilayers.

Big important in the understanding of these systems are the adsorption kinetic and the internal structure of the films which present a strong correlation. The adsorption kinetic includes different steps that determine the distribution of the polyelectrolyte during the adsorption along the multilayers during the deposition. This phenomena allows one different degree of control over the multilayer structure, and more specifically over the stratification of the formed supramolecular architectures.

9 Monte Carlo Studies in Polyelectrolyte Solutions

With the advent of computers with a reasonable calculation capacity could address the application of Monte Carlo method to study of polyelectrolyte systems. The firsts article appears in the 80s [101], and the amount of papers has growing to become a voluminous literature. A comprehensive review of this literature is beyond the reach of this chapter. However, we have been greatly influenced by the work of enormous number of author, in particular a series of articles of Per Linse et al. [102]. This is possible because the species interact via several types of molecular interactions with different length and time scales. Among those involved are hydrogen bonds, electrostatic, hydrophobic, Van der Waals, hydrogen bonds interactions [103]. In order to theoretically understand the Monte Carlo

method, we need use the concepts of statistical mechanics. These concepts are developed in detail in books of fundamental statistical mechanics [104]. This formalism guides us in the task of calculating various quantities and/or properties that describe the behavior of the system. This is accomplished from the partition function that specifies the statistical properties of the system in thermodynamic equilibrium. The exact calculus of the partition function allows us to obtain all thermodynamic and kinetic properties of the system; this is possible for a small number of very simple systems, such as the ideal gas. The stiffness of the polyelectrolyte chain has an important influence on several phenomena, such as the morphology of polyelectrolyte complexes [105–107], and DNA condensation by multivalent cations [108]. This theoretical expression was obtained for a charged chain with a Gaussian statistics in a solution with monovalent salt [109]. The chain was assumed to be of infinite length and the electrostatic interactions were treated at a linear level with a Debye-Hückel screened interaction between charges due to the presence of monovalent salts. The flexible coarse-grained model of a polyelectrolyte chain has the ability to adopt many configurations that are more expanded than that of a neutral polymer but are more compressed than that predicted assuming a rigid rod configuration [110]. The electrostatic potential produced by the flexible model configurations is more attractive than that predicted by the rigid-rod model, being more efficient to condense counterions [111, 112]. Another remarkable physicochemical property of polyelectrolyte is the formation of complexes between oppositely charged polymer in solution [113] or on charged surface [114]. In particular, complex formation on surface by alternate adsorption with oppositely charged polyelectrolyte causes self-assembling into multilayer films [115].

References

1. Barrat, J.L., Joanny, J.F.: Theory of polyelectrolyte solutions. In: Prigogine, I., Rice, S.A. (eds.) *Advances in Chemical Physics, Polymeric Systems*, vol. 94, p. 66. Wiley, Hoboken (1996)
2. Kuhn, W., Künzle, O., Katchalsky, A.: Behavior of polyvalent thread molecule ions in solution. *HCA* **31**, 1994–2037 (1948). doi:[10.1002/hlca.19480310716](https://doi.org/10.1002/hlca.19480310716)
3. Manning, G.S.: The molecular theory of polyelectrolyte solutions with applications to the electrostatic properties of polynucleotides. *Q. Rev. Biophys.* **11**, 179–246 (1978)
4. Jiang, G., Min, S.-H., Hahn, S.K.: DNA/PEI/Alginate polyplex as an efficient in vivo gene delivery system. *Biotechnol. Bioprocess Eng.* **12**, 684–689 (2007)
5. Hamman, J.H.: Chitosan based polyelectrolyte complexes as potential carrier materials in drug delivery systems. *Mar. Drugs* **8**, 1305–1322 (2010). doi:[10.3390/md8041305](https://doi.org/10.3390/md8041305)
6. Osawa, F., Imai, N., Kagawa, I.: Theory of strong polyelectrolyte solutions. *J. Polym. Sci. XIII*, 93–111 (1954)
7. Gennes, P.G., Pincus, P., Velasco, R.M., Brochard, F.: Remarks on polyelectrolyte conformation. *J. Phys. Fr.* **37**, 1461–1473 (1976). doi:[10.1051/jphys:0197600370120146100](https://doi.org/10.1051/jphys:0197600370120146100)
8. Flory, P.J.: Thermodynamics of high polymer solutions. *J. Chem. Phys.* **9**, 660 (1941). doi:[10.1063/1.1750971](https://doi.org/10.1063/1.1750971)

9. Flory, P.J.: Thermodynamics of high polymer solutions. *J. Chem. Phys.* **51**, 51–61 (1942). doi:[10.1063/1.1723621](https://doi.org/10.1063/1.1723621)
10. Huggins, M.L.: Solutions of long chain compounds. *J. Chem. Phys.* **9**, 440 (1941). doi:[10.1063/1.1750930](https://doi.org/10.1063/1.1750930)
11. Michaeli, I., Overbeek, J.T.G., Voorn, M.J.: Phase separation of polyelectrolyte solutions. *J. Polym. Sci.* **23**, 443–450 (1957)
12. Razdan, S.: Novel polyelectrolyte complex based carbon nanotube composite architectures. PhD thesis, Rensselaer Polytechnic Institute (2008)
13. Sui, Z.: Characterization and applications of pH-responsive polyelectrolyte complex and multilayers. PhD thesis, The Florida State University (2004)
14. Amr, I.T.: Control of corrosion in stainless steel using polyelectrolytes multilayer nanofilms. Msc thesis, King Fahd University of Petroleum and Minerals (2006)
15. Nagvekar, M., Tihminlioglu, F., Danner, R.P.: Colligative properties of polyelectrolyte solutions. *Fluid Phase Equilib.* **145**, 15–41 (1998)
16. Fadhillah, F.: Application of polyelectrolyte multilayer reverse osmosis membrane in seawater desalination. PhD thesis, King Fahd University of Petroleum and Minerals (2012)
17. Dou, S.: Synthesis and characterization of ion containing polymers. PhD thesis, The Pennsylvania State University (2007)
18. Jomaa, H.W.: A molecular walk across polyelectrolyte multilayers. PhD thesis, The Florida State University (2005)
19. Jin, Z.: A hybrid density functional theory for solvation and solvent-mediated interactions. PhD thesis, University of California Riverside (2012)
20. Osada, Y., Gong, J.P.: Soft and wet materials: polymer gels. *Adv. Mater.* **10**, 827 (1998)
21. Selktar, D.: Designing cell comparable hydro gels for biomedical applications. *Science* **336**, 1124 (2012)
22. Stuart, M.A.C., Huck, W.T.S., Genzer, J., Muller, M., Ober, C., Stamm, M., Sukhorukov, G.B., Szleifer, I., Tsukruk, V.V., Urban, M., Winnik, F., Zauscher, S., Luzinov, I., Minko, S., et al.: Emerging applications of stimuli-responsive polymer materials. *Nat. Mater.* **9**, 101 (2010)
23. Liu, L., Wang, W., Ju, X.J., Xie, R., Chu, L.Y.: Smart thermo-triggered squirting capsules for nanoparticle delivery. *Soft Matter* **6**, 3759 (2010)
24. Drury, J.L., Mooney, D.J.: Hydrogels for tissue engineering: scaffold design variables and applications. *Biomaterials* **24**, 4337 (2003)
25. Brandl, F., Sommer, F., Goepfertich, A.: Rational design of hydrogels for tissue engineering: impact of physical factors on cell behavior. *Biomaterials* **28**, 134 (2007)
26. Gehrke, S.H., Uhden, L.H., McBride, J.F.: Enhanced loading and activity retention of bioactive proteins in hydrogel delivery systems. *J. Controlled Release* **55**, 21 (1998)
27. Stevens, K.R., Einerson, N.J., Burmania, J.A., Kao, W.Y.J.: In vivo biocompatibility of gelatin-based hydrogels and interpenetrating networks. *J. Biomater. Sci.-Polym. Ed.* **13**, 1353 (2002)
28. Mirzaei, B.E., Ramazani, S.A.A., Shafiee, M., Danaei, M.: Studies on glutaraldehyde crosslinked chitosan hydrogel properties for drug delivery systems. *Int. J. Polym. Mater. Biomater.* **62**, 605 (2013)
29. Maurer, G., Prausnitz, J.M.: Thermodynamics of phase equilibrium for systems containing gels. *Fluid Phase Equilib.* **115**, 113 (1996)
30. Fumio, U., Hiroshi, Y., Kumiko, N., Sachihiko, N., Kenji, S., Yasunori, M.: Swelling and mechanical properties of poly(vinyl alcohol) hydrogels. *Int. J. Pharm.* **58**, 135 (1990)
31. Kim, S., Chu, C.C.: Pore structure analysis of swollen dextran-methacrylate hydrogels by SEM and mercury intrusion porosimetry. *J. Biomed. Mater. Res.* **2000**(53), 258
32. Peppas, N.: Hydrogels in Pharmaceutical Formulations. *Eur. J. Pharm. Biopharm.* **50**, 27 (2000)
33. Grant, D.W., Higuchi, T.: Ion pairs and solubility behavior. Solubility behavior of organic compounds, vol. XXI. In: *Techniques of Chemistry*. Wiley Interscience, New York (1990)

34. Drifford, M., Delsanti, M.: Polyelectrolyte solutions with multivalent added salts: stability, structure, and dynamics. In: Radeva, T. (ed.) *Physical Chemistry of Polyelectrolytes*, vol. 99. *Surfactant Science Series*. Marcel Dekker, NewYork (2001)
35. Porasso, R.D., Benegas, J.C., Van den Hoop, M.A.G.T., Paoletti, S.: Chemical bonding of divalent counterions to linear polyelectrolytes: theoretical treatment within the counterion condensation theory. *Phys. Chem. Chem. Phys.* **3**(6), 1057–1062 (2001)
36. Benegas, J.C., Paoletti, S., Van Den Hoop, M.A.G.T.: Affinity interactions in counterion-polyelectrolyte systems: competition between different counterions. *Macromol. Theor. Simul.* **8**(1), 61–64 (1999)
37. Barnes, H.A.: A handbook of elementary rheology. Cambrian Printers, Wales (2000)
38. Graessley, W.W.: Polymeric liquids and networks: dynamics and rheology. Taylor & Francis Group, New York (2008)
39. Krause, W., Bellomo, E., Colby, R.: Rheology of sodium hyaluronate under physiological conditions. *Biomacromolecules* **2**, 65–69 (2001)
40. Rinaudo, M.: Rheological investigation on hyaluronan-fibrinogen interaction. *Int. J. Biol. Macromol.* **43**, 444–450 (2008)
41. Gutowski, I.: The effect of pH and concentration on the rheology of carbopol gels. Ms Sci thesis. McGill University, Israel (2008)
42. Rinaudo, M.: Chitin and chitosan: properties and applications. *Prog. Polym. Sci.* **31**(7), 603–632 (2006)
43. Klooster, N.T.M., Van der Touw, F., Mandel, M.: Solvent effects in polyelectrolyte solutions. 1. Potentiometric and viscosimetric titration of poly(acrylic acid) in methanol and counterion specificity. *Macromolecules* **17**(10), 2070–2078 (1984)
44. Rinaudo, M.: Polyelectrolyte properties of a plant and animal polysaccharide. *Struct. Chem.* **20**(2), 277–289 (2009)
45. Simsek-Ege, F.A., Bond, G.M., Stringer, J.: Polyelectrolyte complex formation between alginate and chitosan as a function of pH. *J. Appl. Polym. Sci.* **88**(2), 346–351 (2003)
46. Chavasit, V., Torres, J.A.: Chitosan-Poly(acrylic acid): mechanism of complex formation and potential industrial applications. *Biotechnol. Prog.* **6**(1), 2–6 (1990)
47. Cooper, C.L., et al.: Polyelectrolyte–protein complexes. *Curr. Opin. Colloid Interface Sci.* **10**(1–2), 52–78 (2005)
48. Thünemann, A., et al.: Polyelectrolyte Complexes. In: Schmidt, M. (ed.) *Polyelectrolytes with Defined Molecular Architecture II*, p. 113–171. Springer, Berlin (2004)
49. Renault, F., et al.: Chitosan for coagulation/flocculation processes—an eco-friendly approach. *Eur. Polymer J.* **45**(5), 1337–1348 (2009)
50. Cappella, L.V., Boeris, V., Picó, G.: A simple method of chymotrypsin concentration and purification from pancreas homogenate using Eudragit® L100 and Eudragit® S100. *J. Chromatogr. B* **879**(13–14), 1003–1007 (2011)
51. Carlsson, F., Linse, P., Malmsten, M.: Monte carlo simulations of polyelectrolyte–protein complexation. *J. Phys. Chem. B* **2014/01/09** **105**(38), 9040–9049 (2001)
52. Mangenot, S., Leforestier, A., Vachette, P., Durand, D., Livolant, F.: Salt-induced conformation and interaction changes of nucleosome core particles. *Biophys. J.* **82**, 345–356 (2002)
53. Mangenot, S., Raspaud, E., Tribet, C., Belloni, L., Livolant, F.: Interactions between isolated nucleosome core particles. *Eur. Phys. J. E* **7**, 221–231 (2002)
54. Bertin, A., Leforestier, A., Durand, D., Livolant, F.: Role of histone tails in the conformation and interactions of nucleosome core particles. *Biochemistry* **43**, 4773–4780 (2004)
55. Allahyarov, E., Löwen, H., Hansen, J.P., Louis, A.A.: Nonmonotonic variation with salt concentration of the second virial coefficient in protein solutions. *Phys. Rev. E* **67**(051404), 051401–051413 (2003)
56. Boroudjerdi, H., Netz, R.R.: Interactions between polyelectrolyte-macroion complexes. *Europhys. Lett.* **64**, 413–419 (2003)

57. Boroudjerdi, H., Netz, R.R.: Strongly coupled polyelectrolyte-macroion complexes. *J. Phys.: Condens. Matter* **17**, S1137–S1151 (2005)
58. Mühlbacher, F., Schiessel, H., Holm, C.: Tail-induced attraction between nucleosome core particles. *Phys. Rev. E* **74**(3), 031919 (2006)
59. Korolev, N., Lyubartsev, A.P., Nordenskiöld, L.: Computer modeling demonstrates that electrostatic attraction of nucleosomal DNA is mediated by histone tails. *Biophys. J.* **90**, 4305–4316 (2006)
60. Gus'kova, O.A., Pavlov, A.S., Khalatur, P.G.: Complexes based on rigid-chain polyelectrolytes: computer simulation. *Polym. Sci. Ser. A* **48**(7), 763–770 (2006)
61. Narambuena, C.F., Leiva, E.P.M., Chávez-Páez, M., Pérez, E.: Effect of chain stiffness on the morphology of polyelectrolyte complexes. A monte carlo simulation study. *Polymer* **51**, 3293–3302 (2010)
62. Bloomfield, V.: DNA condensation. *Curr. Opin. Struct. Biol.* **6**, 334–341 (1996)
63. Bloomfield, V.: DNA condensation by multivalent cations. *Biopolymers* **44**, 269–282 (1997)
64. Thünemann, A.F., Müller, M., Dautzenberg, H., Joanny, J.F., Löwen, H.: Polyelectrolyte complexes. *Adv. Polym. Sci.* **166**, 113–171 (2004)
65. Brown, A.: Analysis of cooperativity by isothermal titration calorimetry. *Int. J. Mol. Sci.* **10**(8), 3457–3477 (2009)
66. Priftis, D., Laugel, N., Tirrell, M.: Thermodynamic characterization of polypeptide complex coacervation. *Langmuir* **28**(45), 15947–15957 (2012)
67. Dias, R.S., Pais, A.A.C.C., Miguel, M.G., Lindman, B.: Modeling of DNA compaction by polycations. *J. Chem. Phys.* **119**(15), 8150–8157, 15 Oct 2003
68. Dias, R.S., Linse, P., Pais, A.A.C.C.: Stepwise disproportionation in polyelectrolyte complexes. *J. Comput. Chem.* **32**, 2697–2707 (2011)
69. von Hippel, P.H., McGhee, J.D.: DNA-protein interaction. *Annu. Rev. Biochem.* **41**, 231–300 (1972)
70. Danielsen, S., Vårum, K.M., Stokke, B.T.: Structural analysis of chitosan mediated DNA condensation by AFM: influence of chitosan molecular parameters. *Biomacromolecules* **5**, 928–936 (2004)
71. Liu, G., Molas, M., Grossmann, G.A., Pasumarty, M., Perales, J.C., Cooper, M.J., et al.: Biological properties of Poly-L-lysine-DNA complexes generated by cooperative binding of the polycation. *J. Biol. Chem.* **276**(37), 34379–34387 (2001)
72. Rackstraw, B.J., Martin, A.L., Stolnik, S., Roberts, C.J., Garnett, M.C., Davies, M.C., et al.: Microscopic investigations into PEG-cationic polymer-induced DNA condensation. *Langmuir* **17**(11), 3185–3193 (2001)
73. Eickbush, T.H., Moudrianakis, E.N.: The compaction of DNA helices into either continuous supercoils or folded-fiber rods and toroids. *Cell* **13**, 295–306 (1978)
74. Noguchi, H., Saito, S., Kidoaki, S., Yoshikawa, K.: Self-organized nanostructures constructed with a single polymer chain. *Chem. Phys. Lett.* **261**, 527–533 (1996)
75. Noguchi, H., Yoshikawa, K.: First-order phase transition in stiff polymer chain. *Chem. Phys. Lett.* **278**, 184–188 (1997)
76. Noguchi, H., Yoshikawa, K.: Folding path in a semiflexible homopolymer chain: a Brownian dynamics simulation. *J. Chem. Phys.* **113**, 854–862 (2000)
77. Noguchi, H., Yoshikawa, K.: Morphological variation in a collapsed single homopolymer chain. *J. Chem. Phys.* **109**, 5070–5077 (1998)
78. Stevens, M.J.: Simple simulations of DNA condensation. *Biophys. J.* **80**, 130–139 (2001)
79. Ariga, K., Moria, T., Hill, J.P.: Evolution of molecular machines: from solution to soft matter interface. *Soft Matter* **8**, 15–20 (2012)
80. Ariga, K., Hill, J.P., Ji, Q.: Layer-by-layer assembly as a versatile bottom-up nanofabrication technique for exploratory research and realistic application. *Phys. Chem. Chem. Phys.* **9**, 2319–2340 (2007)
81. Decher, G.: Fuzzy nanoassemblies: Toward layered polymeric multicomposites. *Science* **277**, 1232–1237 (1997)

82. von Klitzing, R.: Internal structure of polyelectrolyte multilayer assemblies. *Phys. Chem. Chem. Phys.* **8**, 5012–5033 (2006)
83. Holmberg, K., Jönsson, B., Kronberg, B., Lindman, B.: Surfactants and polymers in aqueous solution. John Wiley & Sons, Chichester (2002)
84. Picart, C., Mutterer, J., Richert, L., Luo, Y., Prestwich, G.D., Schaaf, P., Voegel, J.-C., Lavalle, P.: Molecular basis for the explanation of the exponential growth of polyelectrolyte multilayers. *Proc. Nat. Acad. Sci. USA* **99**, 12531–12535 (2002)
85. Burke, S.E., Barrett, C.J.: Swelling behavior of hyaluronic acid/polyallylamine hydrochloride multilayer films. *Biomacromolecules* **6**, 1419–1428 (2005)
86. Dubas, S.T., Schlenoff, J.B.: Factors controlling the growth of polyelectrolyte multilayers. *Macromolecules* **32**, 8153–8160 (1999)
87. Guzmán, E., Ritacco, H.A., Ortega, F., Rubio, R.G.: Growth of polyelectrolyte layers formed by poly(4-styrenesulfonate sodium salt) and two different polycations: new insights from study of adsorption kinetics. *J. Phys. Chem. C* **116**, 15474–15483 (2012)
88. Guzmán, E., Miguel, V.S., Peinado, C., Ortega, F., Rubio, R.G.: Polyelectrolyte multilayers containing triblock copolymers of different charge ratio. *Langmuir* **26**, 11494–11502 (2010)
89. Shen, L., Chaudouet, P., Ji, J., Picart, C.: pH-Amplified multilayer films based on hyaluronan: influence of HA molecular weight and concentration on film growth and stability. *Biomacromolecules* **12**, 1322–1331 (2011)
90. Record, M.T., Guinn, E., Pegram, L., Capp, M.: Introductory lecture: interpreting and predicting hofmeister salt ion and solute effects on biopolymer and model processes using the solute partitioning model. *Faraday Disc* **160**, 9–44 (2013)
91. Leontidis, E.: Hofmeister anion effects on surfactant self-assembly and the formation of porous solids. *Curr. Opin. Colloid Interface Sci.* **7**, 81–91 (2002)
92. Long, Y., Wang, T., Liu, L., Liu, G., Zhang, G.: Ion specificity at a low salt concentration in water—methanol mixtures exemplified by a growth of polyelectrolyte multilayer. *Langmuir* **29**, 3645–3653 (2013)
93. Schmitt, J., Griinewald, T., Decher, G., Pershan, P.S., Kjaer, K., Losche, M.: Internal structure of layer-by-layer adsorbed polyelectrolyte films: a neutron and x-ray reflectivity study. *Macromolecules* **26**, 7058–7063 (1993)
94. Löschke, M., Schmitt, J., Decher, G., Bouwman, W.G., Kjaer, K.: Detailed structure of molecularly thin polyelectrolyte multilayer films on solid substrates as revealed by neutron reflectometry. *Macromolecules* **31**, 8893–8906 (1998)
95. Korneev, D., Lvov, Y., Decher, G., Schmitt, J., Yaradaikin, S.: Neutron reflectivity analysis of self assembled film superlattices with alternate layers of deuterated and hydrogenated polystyrenesulfonate and polyallylamine. *Phys. B* **213**, 954–956 (1995)
96. Singh, S., Junghans, A., Waltman, M.J., Nagy, A., Iyer, R., Majewski, J.: Neutron reflectometry characterization of PEI–PSS polyelectrolyte multilayers for cell culture. *Soft Matter* **8**, 11484–11491 (2012)
97. Lehaf, A.M., Moussallem, M.D., Schlenoff, J.B.: Correlating the compliance and permeability of photo-cross-linked polyelectrolyte multilayers. *Langmuir* **27**, 4756–4763 (2011)
98. Antipov, A.A., Sukhorukov, G.B., Leporatti, S., Radtchenko, I.L., Donath, E., Mohwald, H.: Polyelectrolyte multilayer capsule permeability control. *Colloids Surf. A* **198–200**, 535–541 (2002)
99. Ladam, G., Schaad, P., Voegel, J.C., Schaaf, P., Decher, G., Cuisinier, F.: In situ determination of the structural properties of initially deposited polyelectrolyte multilayers. *Langmuir* **16**, 1249–1255 (1999)
100. Guzmán, E., Ritacco, H., Rubio, J.E.F., Rubio, R.G., Ortega, F.: Salt-induced changes in the growth of polyelectrolyte layers of poly(diallyldimethylammoniumchloride) and poly(4-styrene sulfonate of sodium). *Soft Matter* **5**, 2130–2142 (2009)
101. Brender, C., Lax, M., Windwer, S.: Monte Carlo study of polyelectrolyte behavior. II. Configurational properties. *J. Chem. Phys.* **74**, 2576 (1981)

102. Wallin, T., Linse, P.: Monte carlo simulations of polyelectrolytes at charged micelles. 1. Effects of chain flexibility. *Langmuir* **12**, 305 (1996)
103. Intermolecular and Surface Forces: Israelchvilli. J. N. Cornell University Press, Ithaca (1985)
104. McQuarrie, D.A.: Statistical mechanics. University Science Books, Sausalito (2000)
105. Maurstad, G., Danielsen, S., Stokke, B.T.: Analysis of compacted semiflexible polyanions visualized by AFM: Influence of chain stiffness on morphologies of polyelectrolyte complexes. *J. Phys. Chem. B* **107**, 8172 (2003)
106. Danielsen, S., Vårum, K.M., Stokke, B.T.: Structural analysis of chitosan mediated DNA condensation by AFM: influence of chitosan molecular parameters. *Biomacromolecules* **5**, 928 (2004)
107. Maurstad, G., Danielsen, S., Stokke, B.T.: The influence of charge density of chitosan in compacting polyanions DNA and xanthan. *Biomacromolecules* **8**, 1124 (2007)
108. Bloomfield, V.A.: DNA condensation. *Curr. Opin. Struct. Biol.* **6**, 334 (1996)
109. Mangui, M., Netz, R.R.: Variational theory for a single polyelectrolyte chain revisited. *Eur. Phys. J. E* **14**, 67 (2004)
110. Narambuena, C.F., Leiva, E.P.M., Chávez-Páez, M., Pérez, E.: Effect of Chain Stiffness on the Morphology of Polyelectrolyte Complexes. A Monte Carlo Simulation Study. *Polymer* **51**, 3293 (2010)
111. Muthukumar, M.: Theory of counter-ion condensation on flexible polyelectrolytes: adsorption mechanism. *J. Chem. Phys.* **120**, 9343 (2004)
112. Muthukumar, M.: Counterion adsorption theory of dilute polyelectrolyte solutions: Apparent molecular weight, second virial coefficient, and intermolecular structure factor. *J. Chem. Phys.* **137**, 034902 (2012)
113. Kabanov, A.V., Bronich, T.K., Kabanov, V.A., Yu, K., Eisenberg, A.: Soluble stoichiometric complexes from poly(N-ethyl-4-vinylpyridinium) cations and poly(ethylene oxide)-block-poly(methacrylate) anion. *Macromolecules* **29**, 6797 (1996)
114. Decher, G.: Fuzzy nanoassemblies: Toward layered polymeric multicomposites. *Science* **277**, 1232 (1997)
115. Decher, G., Schlenoff, J.B. (eds.): *Multilayer thin films: sequential assembly of nanocomposite materials*. Wiley-VCH, Weinheim (2003)

Structure and Thermodynamics of Polyelectrolyte Complexes

Johannes Frueh, Meiyu Gai, Simon Halstead and Qiang He

Abstract Polyelectrolytes (PEs) find applications in many fields of modern life starting from food additives to flocculation and solubility enhancers, down to viscosity adjusting agents in cosmetics and subterranean gelling or drug delivery agents. Most of these properties are related to the PE charge density, structure, counterions, temperature or counter PE. This book chapter gives an overview of the current state of understanding of the thermodynamical properties of PEs in solution. The theoretical predictions and results are compared with current state of the art computer simulations (with a focus on molecular dynamics) as well as experiments on PE structure, complex formation and viscosity properties.

Nomenclature

e	Valence of PE monomer group
$k_B T$	Thermal energy
k_B	Boltzmann constant
ϵ	Dielectric constant
ϵ_L	Local dielectric constant
l_D	Debye length
k	Inverse Debye length
l_0	Persistence length
l_B	Bjerrum length
l_M	Length between two monomers

J. Frueh (✉) · M. Gai · Q. He (✉)

Key Laboratory of Microsystems and Microstructures Manufacturing, Ministry of Education, Micro/Nano Technology Research Centre, Harbin Institute of Technology, Yikuang Street 2, Harbin 150080, China

e-mail: Johannes.frueh@hit.edu.cn

Q. He

e-mail: qianghe@hit.edu.cn

S. Halstead

School of Chemical Engineering and Technology, Harbin Institute of Technology, Xi Da Zhi Street, Harbin 150001, China

l_d	Length of dipole
L	Length of fully elongated PE
L_C	Length of collapsed PE
L_ξ	Correlation length
L_M	Distance between 2 PE chain centers
L_{str}	Length of string between globules
L_ζ	Size of a globule/bead
c_S	Salt concentration
c_P	PE concentration
c^*	Crossover concentration
c_I^{loc}	Local concentration of counterions next to PE
f	Fraction of charged monomers
a	Monomer length/diameter
K	Reduced coupling constant (Based on thermal energy)
K'	Reduced coupling constant (based on excluded volume)
v	Excluded volume per monomer
v_0	Local volume close to monomer
\bar{a}	Elongation per monomer
ζ	Size of electrostatic blob
V_ζ	Volume of electrostatic blob
R	Total length of PE
R_H	Hydrodynamic radius
N	Number of monomers
n^*	Number of charged groups in PE
N_M	Number of monomers in the diameter D of a rodlike molecule
N_{Msr}	Number of monomers in string
N_{Mbead}	Number of monomers in a bead
N_E	Number of monomers in entangled region
N'	Number of P-bonds in strong PE
N_2	Amount of PE molecules
N_1	Amount of solvent molecules
N_{1i}	Amount of solvent molecules inside v_0
N_{1o}	Amount of solvent molecules outside v_0
N_C	Number of counter ions
n_Ψ	Number of Ψ bindings
D	Effective diameter of the rod-like molecule
d	Degree of dissociated charges
M	Mol
L	Liter
b	Charge density
n	Valence of counterions
k	Reaction constant
v_1	Volume fraction of solvent
v_2	Volume fraction of PE

v_3	Volume fraction of counterion
v_l	Molecular volume of solvent
v_c	Molecular volume of counterion
v_{PE}	Molecular volume of PE
V_l	Molar volume of solvent
V_2	Molar volume of PE
x	Number of gratings used in Flory lattice
ΔH	Free enthalpy
H_e	Electrostatic enthalpy
ΔS	Free entropy
S_M	Entropy of mixing
S_K	Kuhn entropy
S_C	Counter ion entropy
F_e	Free energy of electrolyte
F_A	Free energy of ionic atmosphere
F_0	Non electrostatic part of free energy
F	Free energy
χ	Flory Huggins solution parameter
E	Electrostatic based energies
E_D	Debye electrostatic energy of the PE chain
E_a	Energy of the counterion adsorbed on the PE
E_{ela}	Elastic energy of the stretched, charged PE
β	Fraction of free counter ions
β_c	Fraction of condensed counter ions
u	Charge density parameter
k_1	Constant related to k_2
k_2	Concentration parameter $\sim -\log c_P$
λ	Charge density parameter
z_e	Euler number e^x
e_e	Electron charge
Z_1	Effective expansion factor
W	Strength parameter for short ranged effects
A	Å
V_+	Positive ion cloud scaling factor
V_-	Negative ion cloud scaling factor
R_G	Ideal gas constant
F_1	Entropy of condensed counterions
F_2	Translational entropy of ions
F_3	Fluctuations between PE and ions
F_4	Ion pair energy
F_5	Free energy term for partly charged PE
F_6	Correlation term (ion pair PE)
η_s	Viscosity of the solvent
η	Viscosity of the solution

τ_{RZ}, τ_{RR}	Zimm and Rouse relaxation time
τ	Time
D_i	Diffusion coefficient
D_Z, D_R	Zimm and Rouse diffusion coefficient
Z_P	Friction coefficient of the polymer
Z_B	Friction coefficient of the beads
σ_s	Shear stress
$\dot{\gamma}$	Shear rate
β_R	Reduced shear rate
ϕ	Volume fraction
L_a	Tube diameter
T_R	Reduced temperature
θ	Theta temperature of solvent/PE
X	Concentration dependent parameter, which depends on concentration (values used for X are shown below the equations)

1 Introduction

Polyelectrolytes (PEs) are polymers with charged monomer groups that can dissociate into a charged macroion and small counterions when the PE is dissolved in a polar solvent [1, 2]. These charged polymers are, in many cases, employed in nature, and not only DNA [3] but also proteins and cellulose can be classified as PEs [1]. Technical applications of PEs include, for example, PE-DNA drug delivery complexes called polyplexes [4, 5]. PEs are also frequently used in industry. For example, polyethylenimine (PEI) is used in wastewater treatment [6], or biodegradable PEs like dextran sulphate and gelatin PE are used in food science [7]. For the past 20 years, PEs have also been used to fabricate nanofilms [8] and nanostructures [9], called polyelectrolyte multilayers (PEM) which are now being introduced into common products [6]. Due to the existence of excellent review papers on the broad field of cellulose, which is used in the fields of food, medicine, paper, cosmetics, viscosity adjustment and clothing, we omit most of the applications of this type of PE and refer to the other excellent reviews and publications [10–13].

Other fields of application for PEs, which especially rely on the viscosity, are drilling and fracking [14]. In these fields a controlled gelation point and gelation times are also necessary [14]. Due to the growing importance of this field, the basics of this field will also be discussed and references given.

Although PEs and PE solutions have been investigated for a long time [2, 15], a clear understanding of PEs has only emerged within the last decade [16]. The reason that the understanding of this kind of polymer has taken so long is due to the fact that the interaction between charged groups (which can be additionally shielded by counterions), hydrophobic forces and hydrogen bonds occur at the

same time [1]. This interplay between forces leads to several interesting effects of PE solutions which include:

1. Decreasing viscosity upon increasing PE concentration for some strong PEs, whereas the viscosity increases in the case of neutral polymers [2, 17].
2. Formation of electrostatic and Gaussian blobs, necklace-like structures or linear rods, depending on the solvent quality and PE charge [2, 18].
3. Formation of complexes with oppositely charged PEs [19].
4. Due to the release of counterions, the osmotic pressure of PEs is much higher than that of neutral polymers [16].
5. Crossover from dilute to semidilute concentration regions occurs at lower concentrations than in the case of neutral polymers [16].
6. Due to the emerge of regular PE structures in homogeneous solutions, the PE solutions exhibit a peak in the scattering function [2], the intensity of which correlates with $C^{1/2}$ of the PE concentration [16]. In the case of neutral polymers, the lack of regular structure prevents such a peak [16].

This book chapter contains a review of the current state of research in the field of the thermodynamics and viscosity of PEs in solution. In Sect. 2 an overview of the coupling constants in the PE, defining the degree of electrostatic interaction between the PE ionic groups is given. It also contains a review of the interaction and coupling strength between the PE ionic groups and their counterions, and gives definitions of weak and strong PEs. Section 3 reviews the enthalpy of PEs and PE complexes in solution, and Sect. 3.1 contains an overview of the Flory-Huggins solution parameter, which is based on mean field theory and is frequently used to estimate the solution enthalpy and solvent quality. In subsequent parts, this section contains an introduction of enthalpy driven processes that mainly occur in weak PEs. In contrast to weak PEs, entropic processes are the driving force in the case of strong PEs. Section 3 closes with a discussion of the thermodynamic properties of PE complex formation.

Recent results of computer simulations and structure determinations are summarized in Sect. 4. Since Monte Carlo simulations will be reviewed in Sect. 4.1, only a short abstract of the recent state of research of this simulation method relevant to the chapter can be found in Sect. 4.1, along with recent developments in the polymer field theory which has made big advances recently. The recent state of molecular dynamics simulations (Sect. 4.2) is the main focus of Sect. 4.

The experimental results in Sect. 5 are also compared with the simulation methods and thermodynamic calculations. The viscosity and rheology measurements in Sect. 5.1 are the focus of the experimental section, with additional contributions of scattering measurements for PE structure determination in Sect. 5.2 and spectroscopic measurements in Sect. 5.3.

Regarding the layout of each chapter except Sect. 6, it is worth noting that each chapter is structured in such a way that first the PEs are evaluated in solution and then the PE complexes are discussed. Since PE multilayers (and 2D PE complexes) have been reviewed extensively [6, 16, 20], they are only mentioned

briefly in this book chapter and the focus of this chapter is shifted to 0 dimensional gels and dissolved PE complexes. Osmotic pressure and conductivity measurements are omitted in this chapter.

PE complexes and gel properties are mentioned in each section, and their explicit properties and applications are summarized in Sect. 6. For convenience, this book chapter focuses on summarizing the basic properties of PEs. For readers convenience several excellent review papers are cited and recommended for further reading.

2 Weak and Strong Electrostatic Coupling

The interaction and structure of PEs in a solvent (mostly water) are controlled to a large extent by electrostatic interactions [2, 15, 21]. In case of PEs in the strong dilution regime, this interaction leads to an intramolecular charge repulsion and to strongly extended, rod like chains [2]. For this reason the Bjerrum length, l_B , which defines the distance at which the electrostatic interaction reaches the same value as the thermal energy ($k_B T$), is an important parameter [21]:

$$l_B = \frac{e^2}{k_B T \cdot 4\pi\epsilon} \quad (1)$$

In (1) ϵ is the dielectric constant of the solvent (in water ($\epsilon \sim 78$) l_B is ~ 7 Å [21]), and e is the monomer charge. If a PE is dissolved in a salt solution, the charges of the PE are further screened by the ions of the salt, and the interaction strength decays with the Debye length l_D [21]. $l_D = k^{-1}$, with $k = 8\pi c_s l_B$, with c_s being the salt concentration [21]. Compared to uncharged molecules which can be described by simple Gaussian statistics [21], the intramolecular charge repulsion causes an increased persistence length, l_P (a value that defines the stiffness of a polymer). If l_0 is the persistence length of an uncharged chain, the persistence length of a PE in salt solution becomes [21]:

$$l_P = l_0 + \frac{\tau^2 l_B}{4k^2} \quad (2)$$

with $\tau = f/a$, where the fraction of charged monomers are f , and a is the monomer length [2, 21, 22]. The interaction between the polyelectrolyte monomer groups is dependent on the charge density [2]. Some groups, like the R-COOH groups of polyacrylic acid (PAA), show a charge density depending strongly on the pH and are therefore regarded as “weak” polyelectrolytes [21]. In contrast, PEs that carry monomer groups that are almost unaffected by the pH, like the sulphonate group of polystyrenesulphonate (PSS), are considered “strong” polyelectrolytes [15, 21]. One of the first authors who introduced the idea of a coupling constant to describe

the interaction of PEs with each other and the surrounding was nobel laureate De Gennes [22]. In earlier methods like those of Kuhn et al. [2] or Overbeek [23] the average charge density or directly the free energy was used. The scaling method of De Gennes [22], who used the Rouse as well as the Zimm methods for describing the interaction in polyelectrolyte solutions, is the focus of this section [24–28]. The degree of interaction of these electrostatic groups with each other in the same PE [3, 15, 22], with counterions [3, 15, 22], and with oppositely charged PEs is often described by the reduced coupling constant K [22]:

$$K = l/a \quad (3)$$

with a being the monomer unit length and l being the characteristic length, according to Ref. [22]:

$$l = \frac{e^2}{\epsilon k_B T} \quad (4)$$

Another “reduced” coupling constant, is defined by the excluded volume of one monomer length v and the actual volume of the monomer [18, 22, 29]:

$$K' = \frac{v}{a^3} \quad (5)$$

Both reduced coupling constants have in common, that they rely on a volume that excludes same charges. $K \geq 1$ leads to a condensation of counterions on the polyelectrolyte [22]. The coupling constant depends strongly on the type of investigated PE. For this reason PEs can be divided into two main groups.

2.1 Weak PEs with Weak Electrostatic Coupling Constants

In case of a weak coupling, the coupling constant, K , is far below 1 (please note that in some old papers other nomenclature is used) [2, 22]. Due to the weak coupling constant, the elongation (due to electrostatic repulsion) as well as the persistence length of the molecule is quite low [2, 22]. Therefore the average elongation per monomer unit, \bar{a} , due to the electrostatic repulsion force, F , is defined according to de Gennes [22]:

$$\bar{a} = F \frac{a^2}{3T} \quad (6)$$

The weak elongation of the monomers leads to the evolution of so-called electrostatic blobs [2, 18, 22] of blob size ζ [22] in which the PE chain is randomly

oriented. In some cases the chain structure might be rod-like due to an array of blobs with the blob size being the diameter of the chain [18, 22, 29].

$$\zeta \sim a \left(\frac{1}{K} \right)^{1/3} \quad (7)$$

The resulting polymer chain with N monomers and a total chain length R [22, 30] is:

$$R \sim N \zeta \left(\frac{\ln(N)}{3} \right)^{1/3} \quad (8)$$

The blob size correlates with the number of monomers, N_M , in the blob and so, according to de Gennes [18, 26, 29, 30] ζ may be calculated by:

$$\zeta \sim a \sqrt{N_M} \quad (9)$$

At this point it is worth pointing out that other authors use different definitions and models to define a blob, like thermal blobs (that are also called globules or electrostatic blobs), or beads in a necklace model. For a detailed review about these models and structures see references [26, 30]. It is also important to note, that a real PE chain is swollen in solvent and therefore the blob (or effective diameter) size in a real system is larger than in theory [30]:

$$\zeta_{real} \sim a (N_M)^{3/5} \quad (10)$$

Since the electrostatic blobs experience a concentration and solvent dependent repulsion as well as an attraction due to hydrophobic interaction and counterion condensation, the PE concentration dependent correlation length, D , was introduced by de Gennes [22]. This correlation length depends on the length of the PE, the concentration of the PE (c_P) used and the concentration at which the PE blobs start to overlap (c^*), which is known as the crossover concentration. The calculation was developed for cases when $c_P \gg c^*$, where D can be interpreted as a region without chain overlap (intra as well as intermolecular) [22, 26, 30].

$$D = L \left(\frac{c^*}{c_P} \right)^{1/2} = \left(\frac{1}{c_P a} \right)^{1/2} \quad (11)$$

The scaling of D is similar to the Debye length. At low concentrations ($c_P \ll c^*$), the correlation of the screening length due to counterions is the Debye length l_D [22, 29]. The relation of c_P to the polymer-polymer distance d is $c_P = \frac{2N}{d^3}$ [22, 29]. At very low concentrations, the screening length can be larger than the polymer length.

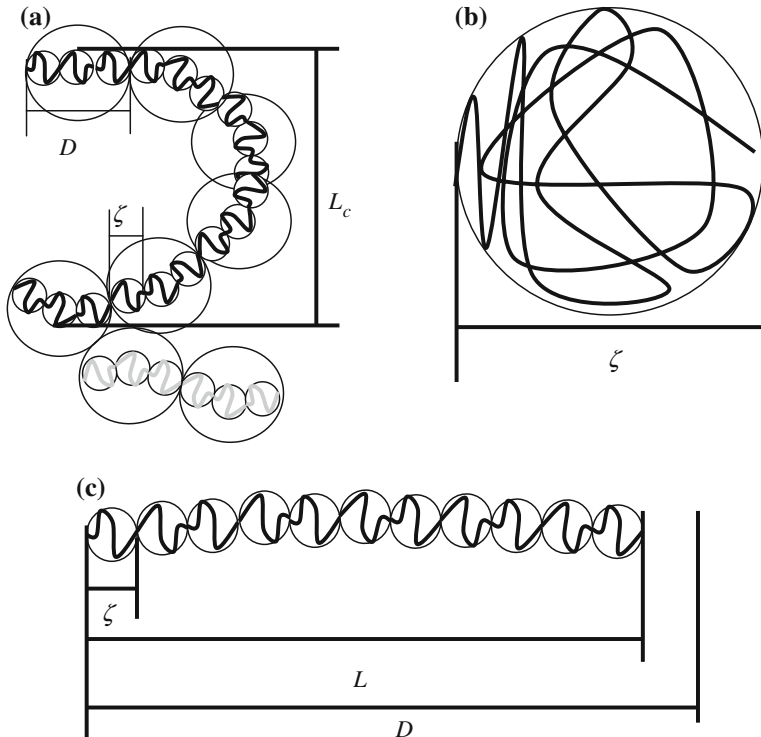


Fig. 1 Illustration of the PE conformation with different coupling and charge repulsion conditions, according to de Gennes. ζ is the blob size, D is the correlation length and L is the length of the polymer, where L_c symbolizes the length of the collapsed polymer chain **a** $\zeta < D < L$ and the polymer chain might exhibit a random walk of correlation of the blobs and the orientation of the chain diameter D , black: chain 1, gray: chain 2 **b** very weak electrostatic interaction ($\zeta > L > D$) the chain is in a Gaussian coil-like formation similar to an uncharged chain. **c** $\zeta < L < D$, strong repulsion of same charges, the chain is strongly elongated. The drawing style of the figure was inspired from Ref. [31]

As a result of the theory of de Gennes [16, 22, 29, 30], the structure of the PE is highly dependent on the coupling constant and the repulsion of the electrostatic blobs. The three parameters D , ζ and R behave strikingly differently depending on the solvent quality, electrostatic charge or the coupling constant. In the case of strong shielding of the charges so that $\zeta < D < L$, the polymer chain exhibits a random walk of correlation of the blobs and the orientation of the chain within the diameter, ζ , is Gaussian (see Fig. 1a). In such a case, the length of the polymer is collapsed and therefore shorter than the length of the elongated polymer, and can be calculated according to following equation [16, 22]:

$$L_c = N_M a \left(\frac{c^*}{c_P} \right)^{1/4} \sim \sqrt{N} K^{1/4} \quad (12)$$

If the solvent is very poor and the electrostatic forces are very weak or strongly shielded ($\zeta > L > D$), the whole chain is in a Gaussian coil-like formation similar to an uncharged chain (see Fig. 1b). In case of a very strong electrostatic repulsion with $\zeta < L < D$, the chain is strongly elongated, as shown in Fig. 1c.

The above formulas and theories were proven experimentally by X-ray and neutron scattering [22], with rheology [2] and spectroscopic measurements in the form of a pyrene labeled PE [32–35]. A summary of these experiments is presented in Sect. 5.

2.1.1 Strong Polyelectrolytes with a Strong Electrostatic Coupling Constants

Recent reviews and simulations mainly focus on weak PEs [16, 26, 30], and this is mainly due to the complexity of counterion condensation and computational limits. For this reason this section summarizes the original work of Osawa and Manning (famous for the Osawa-Manning counterion condensation parameter $\gamma = l_B b$, with b being the charge density) [26], but also mentioning recent studies, of Muthukumar.

Strong PEs are, in contrast to weak PEs, insensitive to the surrounding pH. Examples of this type of PE are polystyrenesulphonate (PSS) and polydimethyl-diammonium chloride (PDDA). In contrast to weak electrostatic coupling in weak PEs, strong electrostatic coupling between the ionic groups and their counterions $K \geq 1$ leads to a concentration dependent condensation of counterions [3, 15, 22]. The interactions of a strong PE along, with the condensation of counterions on the PE, were mainly determined by Osawa and Manning [3, 15]. Counterions that condense on the PE can, according to Osawa and Manning be separated into two major interaction types, namely [3, 15, 36, 37]:

1. π -binding of counterions that are condensed and do therefore not contribute to the coulomb interaction
2. Ψ -binding of counterions that can freely move in solution and that contribute to the coulomb interaction.

According to Osawa (later proven by Manning and others [3, 36]), the counterions within an electrostatic blob are considered inactive, while those outside of the blob are considered active [15, 36, 38]. To estimate the relative amount of the two binding types and therefore the structure of the PE, one can use a simplified relation of the correlation between the blob volume, V_ζ , and the concentration of the added salt. For the precise version of (13), see Ref. [15].

$$V_\zeta \approx \frac{1}{\sqrt{c_S}} \quad (13)$$

Relation (13) is only valid in the case of low amounts of monovalent ions. To distinguish between π and Ψ bonds, the reaction constant of the ionic binding can

be calculated. The Ψ binding reaction constant, k , scales inversely to the blob volume [15].

$$k = \frac{\alpha}{1 - \alpha} \cdot \frac{n_\Psi}{V_\zeta} \quad (14)$$

where the second term in Eq. (14) denotes the average concentration of Ψ bonds with n_Ψ being the number of Ψ bonds. The value of n_Ψ can be measured e.g. via the osmotic pressure of the solution. α defines in (14) the fraction of π bonds, where $\alpha = N'/N_M$. Since N' and (14) depend strongly on the ionic strength, N' is calculated as a function of the ionic strength of the solution [15]. If $N'/N_M < 0.1 M/L$ then α is close to unity [15]. If large amounts of salt are added, then the value of α decreases drastically.

An interesting finding, made in 1954 by Osawa, was that the amount of Ψ bindings decrease with increasing ionic strength [see Eq. (15)]. For the precise version, see Ref. [15]), which correlates with viscosity measurements [15].

$$\Psi \approx \ln \frac{1}{c_S} \quad (15)$$

In case of multivalent (including monovalent) ions, the correlation between the valency of the counterion and the structure of the PE was mainly investigated by Manning [3] and, in recent years, also by Muthukumar [36]. According to Manning [3], the structure parameter, ξ , and the charged fraction of the PE, τ , are:

$$\xi = \frac{q^2}{\epsilon k_b T b} \quad (16)$$

$$\tau = (n\xi)^{-1} \quad (17)$$

where b is the charge density and n is the valency of the counterions. In the case of DNA in a 0.5 M magnesium ion solution, 50 % of the phosphate groups of the DNA are shielded by counterions [3], compared to only 4 % in case of monovalent ions [3]. The local concentration of the counterions, c^{loc} , depends only on the structure parameter and on the local charge but not on the PE concentration [3].

$$c^{loc} = 24.3 \cdot (\xi b^3)^{-1} \quad (18)$$

It was also pointed out by Manning that at $c_S \sim c^{loc}$ the binding of the counterions might become very weak but, due to the low concentrations required for the experiment, measurements were difficult at his time [3]. Such a surprising and counterintuitive finding is in agreement with a recent study, investigating the structure of pyrene labeled PSS at very low concentrations in a salt free solution with fluorescence spectroscopy [33, 39, 40]. In these studies, pronounced coiling of the PEs was found even at very low concentrations and in absence of added salt [39].

Such findings are also in agreement with the theory of Muthukumar [36], which assumes a different dielectric constant close to the PE compared to the bulk. For concentrations higher than c^{loc} , the relations have been proven not only by X-ray and neutron scattering, including corresponding simulations [22, 38], but also with rheology [2] and spectroscopic measurements in form of pyrene labeled PE [32, 39, 41] and EPR spectroscopy [42] (see also Sect. 5).

3 Thermodynamics of Polyelectrolytes and Polyelectrolyte Complexes

In contrast to apolar polymers, the solution behavior of which can be readily explained by the Flory-Huggins theory [43–45], the thermodynamics and solution behavior of PEs is a little more demanding. This is due to the contributions of charged groups, as well as charged group-solvent and additional ion effects [3, 16, 26]. Additionally, the different coupling levels between weak and strong PEs makes the theoretical treatment demanding [29]. For this reason, the following section introduces several approaches used to describe the observed phenomena.

The Flory-Huggins theory (a mean field based approach) and statistical thermodynamic approaches based on the Debye-Hückel theory are the two most frequently used approaches. In the Debye-Hückel approach, the interactions between charges of the same sign cause intramolecular self-repulsion influencing the PE interaction and structure.

The Flory-like approach is based on mean field theory and solvent quality, where a good solvent causes an extended coil and a bad solvent causes phase separation (intra and intermolecular, concentration dependent). The Flory-like approach was used in two ways: in the classical way where charge fraction is neglected and just the solution parameter χ is used; and the modified theory, which contains chain length and charged fraction. The approaches are discussed separately in the following sections, which also contains some new approaches at the end of each section. The enthalpy and entropy of strong and weak PEs are considered separately, since the complex formation and solution behavior depends strongly on the coupling constant.

3.1 Flory-Huggins Solution Theory Applied to Polyelectrolyte Solutions

The thermodynamics of dissolved apolar polymer systems is usually described by the Flory-Huggins theory [43–45]. The Flory-Huggins theory is based on the so called mean field approach which is a theory that assumes, that each part of the monomer-monomer interaction and solvent-solvent interaction has the same

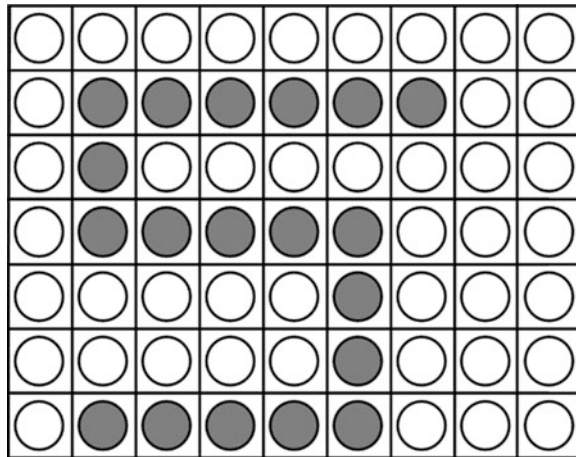


Fig. 2 A graphical visualization of the Flory-Huggins mean field theory. The grating positions with *white circles* illustrate the *solvent* and the *gray circles* illustrate the PE. It's assumed that: Each field has the same size, no overlap of fields or chains, all field positions are occupied, all polymer-polymer interactions are the same (all chain parts are the same)

energy (PE is not a co-polymer), no overlap of the chains is possible and fluctuations are neglected, see Fig. 2 [43–46]. This theory can therefore not directly forecast electrostatic blobs. The approach of averaging over all PE monomer site, allows forecasting solution qualities or general interactions. It is therefore possible to indirectly predict such blobs and the coiling of the molecule via the solvent quality (although Kuhn did not know of the work of Flory, he used a similar approach based on charged fractions and polar solvent) [2, 26]. According to Flory [44] the entropy of mixing for apolar molecules is:

$$\Delta S = k_B[N_1 \ln v_1 + N_2 \ln v_2] \quad (19)$$

where k_B is the Boltzmann constant, N_1 and N_2 are the number of solvent and polymer molecules, and v_1 and v_2 are the volume fractions of the monomers. The enthalpy of mixing, ΔH , for an apolar polymer is, according to Flory [44]:

$$\Delta H = \frac{BN_1N_2V_1V_2}{N_1V_1 + N_2V_2} \quad (20)$$

Here B is a constant, and V_1 and V_2 are the molar volumes where $V_2 = V_1 \cdot x$, with x being the amount of used grating places in the lattice. Despite the Flory-Huggins theory being originally developed for apolar molecules, it was used successfully to describe the swelling of PE complexes in the form of PEM thin films at different humidities [47]. In this study the PEM was considered to be a polymer matrix with the PE charges being compensated. Therefore, only the total interaction of the PE with the solvent was of interest and could therefore be

estimated with the Flory-Huggins solution parameter [47]. Another study (currently in preparation for publication) used the Flory-Huggins solution parameter as well as (19) and (20) to estimate the enthalpy and entropy of elongated PEM thin film complexes. The molecular image of the behavior of such complexes upon macroscopic elongation is that the electrostatic blobs decoil [39]. Such an approach is also successful in explaining the increased hydrophilic behavior of PEM upon mechanical load [48]. The Flory-Huggins solution parameter was also used successfully by other groups to calculate the dilution enthalpy, as well as the excluded volume and elastic energy of the PE chains for chitosan and alkylchitosan [49].

A completely new approach for the simulation of PE solutions was published by Katz and Leibler in 2009, not by using the Flory-Huggins solubility parameter of the polymer backbone, but instead using the one of the counterions [50]. The concept is logical and overdue, since the solubilization of a PE is caused by the release of the counterions and the resulting gain in entropy. Katz and Leibler were able to show all features observed up to now, such as phase separation, meso- and macro-phases and also the calculation of mixing ratio, depended on structure factors [50].

Alternatively to the work of the Flory-Huggins theory, other methods like the Hansen solubility parameter can be used to estimate the solvent quality [51]. In the Hansen approach, the polar, hydration, and dispersion components are considered separately and the contribution of each parameter is considered [46, 51, 52].

An interesting alternative to the Flory-Huggins or other mean field approaches was a study done by Pfeuty using a zero point Langrangian theory and between 1 and 6 dimensions [53]. In this study the authors found a deviation of the asymptotic properties of for high molecular weight PE chains between Flory type calculations and Lagrangian calculations. The authors, however, did not state a comparison with experimental values and the study was not frequently cited in other following reviews [16, 26, 30]. In 1999, Tsonchev et al. published a lattice field approach based on a corrected mean field theory to determine the patrician function, electrical potential, monomer distribution and other thermodynamic parameters such as the free energy [54]. Their approach presented reasonable results for all the variables tested.

3.2 Enthalpy in Polyelectrolyte Solutions

In this section the solution and mixing enthalpy of PEs are reviewed, with weak and strong PEs being reviewed separately due to the mechanics of structure and complex-formation differing greatly between these two types of PE.

3.2.1 Dilution, Mixing and Solution Enthalpy of Weak PEs

Weak PEs are, in many cases similar to normal polymers. Large parts of the chain are uncharged and the PE structure in solution can be correlated to the solvent quality [2, 55]. The only difference between polymers and PEs is the additional contribution of the electrostatic charges. Therefore, it is not surprising that some of the first and, until now, most frequently used thermodynamic approaches were mean field and Flory based [1, 2, 16]. A convenient way to take the charged groups into account is by considering the electrostatic repulsion of the monomers and multiplying it by the fraction of charged groups, f . The free electrostatic energy of a PE is therefore dependent on the dielectric media and fraction of charged monomers [2, 16]:

$$F_{el}(R) \approx k_B T \frac{l_B(fN)^2}{R} \ln\left(\frac{R}{bN^{0.5}}\right) \quad (21)$$

It is worth noting that, depending on the type of PE used, the electrostatic contribution for PEs are the dominating force and therefore it is possible to omit the Flory enthalpy term in this cases [23]. If the PE is very weak, the free enthalpy of dilution, ΔH , is only correctly obtained, when the electrostatic and Flory-Huggins polymer dilution enthalpy terms are added [49].

$$\Delta H_{dil} = \Delta H_{Flory} + \Delta H_{el} \quad (22)$$

$$\Delta F_{Flory} = \chi RT v_2 \quad (23)$$

where χ is the Flory-Huggins solution parameter [44]. ΔH_{el} is calculated from the difference of the total electrostatic energy, H_{tot} , before (b) and after (a) dissolving or diluting the PE [49].

$$\Delta H_{el} = H_{tot(b)} - H_{tot(a)} \quad (24)$$

H_{tot} consists out of 3 parts, namely E_D , which is the Debye electrostatic energy of the PE chain, E_a , the energy of the counterion adsorbed on the PE, and E_{ela} , the elastic energy of the stretched, or charged PE [49]. These parameters are defined according to Safranov [49] with the fraction of free counterions, β , as:

$$E_a = \frac{e^2 N_a}{b \epsilon} (1 - \beta^2) \ln v_2 \quad (25)$$

$$E_D = -\frac{e^2 N_a}{b} \left(\frac{\beta}{\epsilon}\right)^{3/2} \sqrt{A u v_2} \quad (26)$$

$$E_{ela} = \frac{e^2 N_a}{b} \left(\frac{b}{a}\right)^{5/7} \left(\frac{\beta}{\epsilon}\right)^{10/7} u^{-2/7} \quad (27)$$

where the constant $A = \sqrt{8\pi}$, and the charge density parameter, u , is defined as [49]:

$$u = \frac{e^2}{\varepsilon k_B T b} \quad (28)$$

The PE total electrostatic based energy for 1 mol of monomer units is therefore a sum of (25–27) [49]:

$$E_{tot} = \frac{e^2 N_a}{b} \left[(1 - \beta^2) \ln v_2 - \left(\frac{\beta}{\varepsilon} \right)^{3/2} \sqrt{A u v_2} + \left(\frac{b}{a} \right)^{5/7} \left(\frac{\beta}{\varepsilon} \right)^{10/7} u^{-2/7} \right] \quad (29)$$

Equation (29) was investigated with high molecular weight chitosan (MW \sim 20,000 g/mol) [49]. A partial alkylation of the chitosan monomer groups allowed the authors to verify Eq. (29) for different degrees of electrostatic and apolar interactions between PEs and PE with water [49].

Poly(L-glutamic acid) displays a different behavior compared to other weak PEs [56], showing a strong dependence on the degree of polymerization [57]. One of the reasons for such a behavior is the big difference in structure between natural and synthetic polymers e.g. synthetic polymers are coiled, while poly(L-glutamic acid) has a helix like conformation in a low charged state [57]. For such a poly (L-glutamic acid) like system the electrostatic enthalpy dominates [57]. The electrostatic enthalpy of dissolution can be calculated with the semi-empirical formula from Scerjanc [56] who developed his formula originally for a polyacrylic acid system [57]:

$$H_e = \frac{fnRT}{n\lambda} \left[(1 - k_1)k_2 - \ln \left(\frac{(1 - \lambda)^2 - \beta^2}{1 - \beta^2} \right) - \lambda \right] \left(1 + \frac{T}{\varepsilon} - \frac{\Delta\varepsilon}{\Delta T} \right) + \frac{fnRT}{2n\lambda} \left(1 - \beta^2 - \frac{\lambda z_e^{2k_2}}{z_e^{2k_2} - 1} \right) \left(\frac{\Delta \ln V}{\Delta \ln T} + \frac{\Delta \ln R}{\Delta \ln T} \right) \quad (30)$$

In (30), k_1 is a constant related to λ , and the concentration parameter, k_2 , which is proportional to $-\log c_P$. In (30) z_e is the Euler number; n is in this case the valence of the monomer group. V is the volume of the solution and the charge density parameter, λ , is defined as [56]:

$$\lambda = \frac{enfe_0^2}{\varepsilon a k_B T} \quad (31)$$

where a is defined as the monomer length. ΔH of dilution is calculated in the same way as in Eq. (24) [56]. Equation (30) is based on the model of Katchalsky and Kuhn [2], and is not applicable for low degrees of ionization since in such a case non electrostatic interactions become dominant [56, 58]. In this case use of

Eq. (22–29) is suggested. The formulas (22–30) are all normalized for 1 mol of monomer units. Another method is to use the novel method of Muthukumar [59] which allows also the adjustment of the fraction of charged monomers—see formulae in the strong PE section (43–47).

For enthalpy driven PE complex formation and other processes in weak PEs, see Sect. 3.3.

3.2.2 Strong Polyelectrolytes

In the case of strong PEs, the properties of the PE, and therefore of the enthalpy, are mainly controlled by the strong electrostatic coupling (see above). Therefore the Debye-Hückel approach is more frequently used than in case of weak PEs. The enthalpy upon dilution of the PE is mainly influenced by the dissociation of the PE and the counterions [15]. The free electrical energy of the PE upon dilution is, according to Osawa [15]:

$$\frac{E_e}{k_B T} = \frac{1}{2} \frac{e_0^2}{k_B T a} n^{*2} N_M \quad (32)$$

Here n^* is the number of charged groups in the PE. The free energy of the electrolyte part of the PE is, therefore:

$$\frac{F_e}{k_B T} = \frac{E_e - TS_e}{k_B T} \quad (33)$$

where the entropy of the electrolyte part, S_e , is discussed in detail in Sect. 3.4. The total free energy is, according to Osawa, therefore a combination of the free energy of the electrolyte, the mixing entropy, S_M , the Kuhn entropy S_K (which is related to the PE structure) and the contribution of the ion atmosphere, F_A , which is, however, small compared to F_e [15]:

$$F = F_e + F_A - T(S_M + S_K) \quad (34)$$

Since the early approaches which led to the equations presented in references [2, 58] showed a unreliable correlation between the molecular size and the free electrical energy, empirical formulae with free variables were established [60]. These empirical functions are based on an assumption similar to Eq. (34) and can be found in Ref. [15].

A successful theoretical solution to the problem by means of statistical thermodynamics was first achieved by Mandel [61]. This solution was later extended significantly by Manning [3]. The limits of this approach, which is unable to predict the helix to coil transition of DNA and sometimes delivers results one order of magnitude too high, were also pointed out by Manning [3]. The counter ion condensation leading to the famous Manning-Osawa counterion condensation

theory was the focus of Manning's study. Despite the Manning-Osawa theory of counter ion condensation bearing the name of both, the function for the free energy of PE dilution, obtained by Manning, and which incorporates the possibility of multivalent ions [3], is quite different from that of Osawa which is only valid for monovalent ions [compare (35) with (32)].

$$F_{mix} = \theta_n \ln\left(\frac{10^3 \theta_n V_1^{-1}}{c_S}\right) \quad (35)$$

where θ_n is the fraction of associated counterions per monomer and all counter ions have the valence n . θ_n is defined as $\frac{q_{net}}{q} = 1 - N\theta_n$ [3]. The PEs can adopt various structures in solution, such as a coil or helix [3]. To adopt these structures, the free energy of the structural change must be larger than the electrostatic repulsion which is [3]:

$$F_{el} = (1 - N\theta_n)^2 \zeta \ln(1 - e^{kb}) \quad (36)$$

The minimum free energy needed to cause a change in molecular structure for highly diluted solutions ($c_P \rightarrow 0$), where $\theta_n \approx \zeta$ is [3]:

$$\Delta(F_e - F_0) = \Delta(1 - \zeta^{-1}) \ln\left(\frac{c_I^{loc}}{c_I}\right) - \zeta^{-1} \ln(kb) \quad (37)$$

Here, F_0 is the non electrostatic contribution to the free energy. An interesting comparison done by Manning was the comparison of the bending capability of the PE with the persistence length. Although this estimate of the free energy does not contain the entropic contribution, it allows an interesting estimate of the change in electrostatic energy with changes of the persistence length (38) [3].

$$\Delta F = \frac{(RTa)}{2l_P} \theta_n^2 \quad (38)$$

The resulting free energy for a spontaneous structure change from straight to bent is therefore [3]:

$$\Delta F = \Delta F_0 + \left(\frac{\theta^2}{24}\right) \zeta^{-1} \left[2\zeta - 1 \left(\frac{c_I^{loc}}{c_I}\right) \ln(kb) \right] \quad (39)$$

Michaeli and Overbeek used the Debye-Hückel approach to estimate the enthalpy of the PE-PE and PE-solvent interaction [23]. In this model, the Flory entropy is used as the entropic term of the PE chain, and the electrostatic free enthalpy is calculated from the electrostatic energy of a strong PE [23]. By thermodynamic considerations, Michaeli and Overbeek showed that for small univalent counterions no coacervation (complex-formation between PE) occurs

because the entropy of counterions outbalances the enthalpy (see Sect. 3.4), favoring coacervation [23]. This finding was true for two approaches which were compared by Michaeli and Overbeek, one was the Debye-Hückel theory (40) and the second from Lifson and Katchalsky (41) [23]:

$$\frac{G_e}{V} = \frac{k^3 k_B T}{12\pi} = B \left(\sum_j n_j^* v_j \right)^{3/2} \epsilon^{3/2} T^{1/2} \quad (40)$$

with j being the type of molecule carrying the charge, $B = 2/3\pi^{1/2}k_B^{-1/2}e^3$ and e_e the electron charge.

$$G_e = N_M F_e \text{ and } \bar{G}_e = \frac{\nu_1}{\nu_P} F_e \quad (41)$$

Both methods showed that the PE coacervation depends on the PE concentration and on the type and concentration of counterions [23]. Equation (41) is especially tempting to use due to its simplicity. However, since the approach is limited to low concentrations, its applicability for most flexible synthetic polymers at high concentrations is very limited [58]. In contrast, for rod-like, rigid polymers like Tobacco mosaic virus which can not change its shape, it can also be used for higher concentrations [58]. Equation (40) was extended in a subsequent paper by Overbeek for cases where the PE and the counterions are not equal and a second solvent with a low dielectric constant has been added [62].

An interesting novel way to determine the Gibbs free enthalpy of PE-salt complexes within PEM thin films exposed to salt solutions is via the reaction constant [63]:

$$\Delta G_{assoc} = RT \ln K_{assoc} \quad (42)$$

Here K_{assoc} is the association constant. To utilize this method, one must do either an isothermal titration or measure a series of changes in IR-spectra to determine the association constant [63]. It is worth noting that the degree of ion doping and water incorporation correlates with the Hofmeister series [63]. Since PE-PE bonds are broken by incorporation of counter ions, the association constant can also be used indirectly to estimate the PE-PE interaction strength. Calorimetric measurements done by Schlenoff to directly determine the enthalpy of PE complex formation for strong PEs, resulted in values close to 0 [63].

Theoretical determinations of the counterion distribution around a PE were done by Solms by approximating them as tangentially bonded spheres which interact via the coulomb potential [64]. In his work, the Osmotic pressure and thermodynamic properties were determined via analytical integrals [64].

One interesting contribution to the study of PEs was done by Muthukumar [59]. In his extended theory of the counterion condensation of Manning, six contributions to the free energy are considered [59]:

$$F = F_1 + F_2 + F_3 + F_4 + F_5 + F_6 \quad (43)$$

where F_1 is the entropy of the condensed counterions, F_2 is the translational entropy of condensed and free ions (except the PE), F_3 represents fluctuations between the dissociated ions (without PE), F_4 is the gain in energy due to counterion adsorption (ion pair formation), F_5 is the free energy of the PE with its degree of dissociated monomers, and F_6 includes the correlations between ions pairs and the PE. For the entropic contributions (F_{1-3}) of Muthukumar's theory, see Sect. 3.4.2 formulas (56–58). F_4 is defined as the contribution of the ion pair energy to the free energy, with the energy of one ion pair being $-e^2/(\varepsilon_0 \varepsilon_l \pi l_d)$ [59]:

$$\frac{F_4}{N_C k_B T} = -(1-f) \left(\frac{\varepsilon}{\varepsilon_l} \right) \left(\frac{l_M}{l_d} \right) \left(\frac{l_B}{l_M} \right) \quad (44)$$

Here, ε_l is the local dielectric constant, l_M is the length between two monomers, and l_d is the length of the dipole and N_C is the number of counter ions. F_5 depends on the electrostatic repulsion energy and contains the expansion factor $Z_1 = 6R_G/(l_M^2 N_C)$ [59]:

$$\frac{F_5}{k_B T} = \frac{3}{2} (Z_1 - 1 - \log Z_1) + \frac{4}{3} \left(\frac{3}{2\pi} \right)^{3/2} W \sqrt{N_C} \frac{1}{Z_1^{3/2}} + 2 \sqrt{\frac{6}{\pi}} f^2 \tilde{l}_B \frac{N^{3/2}}{Z_1^{1/2}} \Theta_0 \quad (45)$$

R_G is the radius of gyration, W a strength parameter for short ranged effects and Θ_0 and Z_2 are:

$$\begin{aligned} \Theta_0 &= \frac{\sqrt{\pi}}{2} \left(\frac{2}{Z_2^{5/2}} - \frac{1}{Z_2^{3/2}} \right) \exp(Z_2) erfc(\sqrt{Z_2}) + \frac{1}{3Z_2} + \frac{2}{Z_2^2} - \frac{\sqrt{\pi}}{Z_2^{5/2}} - \frac{\sqrt{\pi}}{2Z_2^{3/2}} \\ Z_2 &= \frac{N_C Z_1 \tilde{\kappa}^2}{6} \\ \tilde{\kappa}^2 &= \tilde{l}_B 4\pi (f \rho l_3^3 + 2 c_s l_M^3) \end{aligned} \quad (46)$$

Since several parameters needed to be correlated with the local volume, κ became $\tilde{\kappa} = \kappa l_M$ and the density and salt concentration parameter were multiplied by the monomer volume. The correlation between the ion pairs and the PE are defined as [59]:

$$\frac{F_6}{k_B T} = \frac{4}{3} \left(\frac{3}{2\pi} \right)^{3/2} Z_2 \left(\left(\frac{\varepsilon}{\varepsilon_l} \right) \left(\frac{l_M}{l_d} \right) \right)^2 \tilde{l}_B^2 \left(\frac{l_d}{l_M} \right)^6 (1-f)^2 \sqrt{N_C} \frac{1}{Z_1^{3/2}} \quad (47)$$

This theory allows the PE to bend due to entropy, including at low ionic strength, and allows PE of a finite length, in contrast of Mannings theory. For an alternative definition of F_6 and its derivation, see Ref. [59].

Complex formation of strong PEs is mostly dependent on the entropy. The enthalpy changes of nearly all processes and complexes of strong PEs are 2–15 times smaller than the changes in entropy. For details of the entropy see Sect. 3.4 [63, 65]. The enthalpy of complex formation can be calculated with the formalism of Overbeek (Eq. 40–41) [62], or with the method of Muthukumar (43–47) [19, 59]. Another method is to determine the enthalpy of complex formation by isothermal calorimetric titrations or other calorimetric methods, turbidity titrations or molecular dynamics simulations [19, 63, 65]. Recent molecular dynamics simulations [19] and experimental measurements showed that the enthalpy of PE complex formation decreases with increasing ionic strength, but this value is always below the entropy [23, 62, 63, 65]—see following section for detail.

3.3 Enthalpy-Driven Processes in Weak Polyelectrolytes and Polyelectrolyte Complexes

The behavior of weak PEs is mostly controlled by the pH and ionic strength. If e.g. the pH causes a very low charge density, the interaction between the PEs and also within the same coil is controlled by hydrophobic forces and hydrogen bonds [65]. An interesting finding is that the process of complex formation of two oppositely charged weak PEs is only enthalpy controlled when the PEs are in a region of a low charge [66]. At low or intermediate charge, when the PE is able to form hydrogen bonds, the enthalpy of a weak PE is ~ 3 times the enthalpy of a strong PE [66]. The complex formation can be switched to an endothermic process for conditions where the PE is strongly charged (e.g. change of pH) and then the process is entropy controlled like in the case of strong PEs [66, 67]. The ratio of the PE charge types within the PE–PE complex formed (e.g. positively to negatively charged ratio, with charge neutrality caused by small counter ions) can also be triggered by the pH value [65, 68–71]. The addition of a solvent with a low dielectric constant can decrease the free enthalpy as well [65]. The enthalpy can, if the PE is controlled to a large extent by electrostatic forces, be calculated via the formulas of Overbeek [23]. Equations (40–41) or from Manning [3] (37–39). Despite the formulae being developed for strong PEs, they have been proven to be adequate for weak PEs as well. A special formula for very low charge density or hydrogen bond dominated PE interactions has, to the knowledge of the author, not yet been established. A possible reason for the lack of such a formula might be the large diversity [65] of available weak PEs and the complex interplay between the forces.

One of the main interactions in weak PEs that contribute to the enthalpy are hydrogen bonds, which allow the e.g. natural PE to adopt special structures, like helices [3, 57]. The fact that the initial structure of a weak PE (coil or helix)

influences the stoichiometry of the complex formation further increases the difficulty of establishing a mathematical formalism [72]. In the case of proteins, which are natural PEs, the structure as well as aggregation behavior is often more complex, which has lead to high computational efforts [73]. Due to these high computational efforts [66], measurement based values like direct measurement from the isothermal calorimetric titration [66], crystallography, or from measured reaction constants like in Eq. (42) [63] seem more feasible.

It is to be expected that, in the near future, an extension of novel theories like those of Muthukumar [19, 36, 59] or the 0th order Gaussian equivalent renormalization theory (GER0) from Baeurle [74] will solve some of the afore mentioned problems for the computation of weak PEs. The group of Baeurle solved the problem that long equilibration times, low temperatures and increasing complexity of polymers caused a decreasing efficiency of grand canonical functions by integrating a Monte Carlo Auxiliary field into the grand canonical function at high polymer densities [74, 75]. Especially the GER0 approach solves many problems that emerged in the field theoretical modeling of PEs and has already successfully been used to determine the osmotic pressure of weak PE solution in various concentration regimes [76, 77]. It is, however, already clear that not one function alone will solve all the issues with this type of PE. In particular, since MD functions are too computationally expensive and the observable timescales too short, and the GER0 formalism is not usable for single or polymer nano-structures [78, 79]. For complexes of biological PE, recently a mixture of kinetic Monte-Carlo and Molecular dynamics approaches was used to determine the signaling pathway of proteins [78]. For nanostructures of block copolymers, the same group recently used a self-consistent field method [79]. This will allow a simplified computation of the enthalpy and entropy of complexation and non-coiling structures of synthetic, weak PEs, and some natural ones with simple structure.

3.4 Entropy in Polyelectrolyte Solutions

3.4.1 Weak Polyelectrolytes

In the case of weak PEs, the PE remains stiff and rod like if the PE blob size is small compared to the chain length [22, 29]. Therefore the change in entropy upon dilution or complex formation [21] of such a PE is small. In the case of a weakly charged PE, where the electrostatic repulsion is smaller than $k_B T$, a Gaussian coil like conformation of the PE emerges within afore mentioned blob sizes. The entropic structure of the PE within blobs is the same as in the case of uncharged polymers. Considering both enthalpy and entropy in a Flory-like mean field system to describe the solution behavior of a weak PE, taking the polymerization degree, N , the charged fraction, f , the length of the (coiled or elongated) PE, L , the Bjerrum length, l_B and the thickness of the PE (partially coiled), $b\sqrt{N}$, leads to the approach of Kuhn [2]. The free energy of a PE in solution is therefore [2, 26]:

$$F \approx \frac{L^2}{b^2 N} k_B T + k_B T \frac{l_B(fN)^2}{L} \ln\left(\frac{L}{b\sqrt{N}}\right) \quad (48)$$

The first term of (48) is the contribution of the chain conformation to the free energy and it is inversely related to the entropy. If the entropy decreases (e.g. the chain gets elongated), L increases, and the first term on the right hand side of (48) will increase as well. The second term of (48) represents the electrostatic contribution of the PE to the free energy. Equation (48) is therefore able to determine the overall structure of a PE depending on the fraction of charged monomers. This allowed Kuhn to calculate and evaluate the degree coiling of the PE depending on the charged fraction, as well as to predict the viscosity from the structure of the PE and to compare it with measurements of the viscosity of the corresponding solutions [2].

Since viscosity measurements of uncharged, weak and strong PEs [60] were successfully modeled with the Kuhn entropy [80], it should theoretically be possible to describe weak PE solutions with it as well. This assumption is supported by the fact that the Kuhn entropy is based on the Boltzmann entropy formula, and attempts to use this approach become inaccurate to determine the ion distribution around the charged groups of strong PEs at low salt concentrations, but not the PE structure [81]. Since weak PEs are not strongly affected by counter ion condensation, these effects pose no problem for the Kuhn entropy approach. Another reason for the infrequent use of the Kuhn entropy is the fact that the Flory approach is much simpler and better known than the Kuhn approach [49, 80, 82].

The original theoretical assumption that the low charge density has a negligible influence on the structure is supported by experimental measurements of Safronov et al. [49]. Their results showed no influence from salt concentration, and therefore of the charge density, on the dilution enthalpy or total energy of chitosan, (a weak PE) [49].

3.4.2 Strong Polyelectrolytes

Strong PEs show a fundamentally different dilution and complex formation behavior compared to weak PEs. Dilution is mainly driven by the increase in entropy from the release of counterions and not, like in case of weak PEs, by changes of the enthalpy [15, 62]. The structure of the PE itself, as well as its enthalpy, changes only a little during these processes [63, 65]. The change in the counterion and other ion entropy was calculated by Osawa to be:

$$\begin{aligned} -\frac{S_e}{k_B} = & -\frac{e_e^2}{\varepsilon k_B T a_1} n^{*2} N_C + NN_C \ln \frac{N}{N_{1i}} \frac{1 + \sqrt{1 + \delta^2}}{2} \\ & + c_S \ln \frac{[c_S(N - n_+)N_C][c_S - n_-N_C]}{N_{1O}^2} + NN_C + 2c_S \end{aligned} \quad (49)$$

$$a_1 = n_+^{1/3} 8A \quad (50)$$

$$\delta^2 = \frac{v_0^2}{N^2} \frac{c_S}{V_-} \frac{NN_C + c_S}{V_+} \quad (51)$$

where A represents the unit Å, V_- and V_+ are normalization factors obtained by integrating over the π bonds [15]. The free electric energy of the system is therefore dependent on the entropy of the counter ions and the electrostatic energy of the PE, as shown in Eq. (33) [15]. The function of the total entropy can be found in Eq. (34), where the terms for the entropy of mixing can be approximated by the ideal entropy of mixing at very low PE concentrations. The Kuhn entropy, which adds to the mixing entropy, depends on the size and shape of the PE and emerges due to microbrownian motion. The Kuhn entropy for the PE chain was used by Kagawa et al. [60] in their paper to determine the free energy of strong PEs by means of statistical thermodynamics. The Flory approach combined with a random phase approximation was successfully used in other studies [82, 83] to determine the gelation threshold at high concentrations of strong PEs in presence of multi-valent counterions. Another method also applied to strong PEs is just to use the Flory entropy stated in Eq. (19) [23].

A very simple term for estimating the change in entropy of the counterions upon dilution was used by Manning. Since the association of the counter ions depends on the concentration of added salt, the entropy of the conuterions scales inversely to the salt concentration [3]:

$$S_e \sim nR_G \ln\left(\frac{c_S^{loc}}{c_S}\right) \quad (52)$$

The relation (52) is part of Eqs. (37) and (39).

A volume fraction based term for the determination of the entropic contribution of the (small) counter ions was utilized by Overbeek and Michaeli [23].

$$S_C = \frac{v_1}{v_l} k_B T \ln v_1 + \frac{v_3}{v_C} k_B T \ln v_3 \quad (53)$$

The entropy of the PE chain consists of terms based on volume fractions for the PE and solvent and additionally the ionic species, i , in a Flory-Huggins like expression. For this reason Eq. (49) is more general than Eq. (48) [23].

$$S_{mix} = \frac{k_B T}{v_l} \left(v_1 \ln v_1 + \sum_i \frac{v_i}{r_i} \ln v_i \right) \quad (54)$$

Please note that Eq. (54) is very similar to recent theories and computer simulations based on molecular dynamics [19]. The free enthalpy is therefore [23]:

$$G = G_e + S_{mix} \quad (55)$$

Since the change in molecular entropy of the PE chain itself is often small, compared to the entropy of the counter ions, S_{mix} can often be replaced with the entropy of the counterions S_C . G_e in Eq. (55) can be found in Eqs. (40–41).

The cell model from Katchalsky, Onsager and Manning, which was originally only applicable to linear PEs [26], was extended by Deshkovski in 2001 to a more general two zone model based on the mean field approximation of the nonlinear Poisson Boltzmann equation [84]. In this two zone model, the counter ions around a cylindrical rod (PE) form the area close to the PE, and a spherical volume which extends up to the distances between the PE is the area far away from the PE [84]. This model is able to explain the mean distance of the counterions from the PE chain as a function of the counterion concentration.

The most detailed entropic consideration until now is used by the formalism of Muthukumar. In this formalism, three different entropic contributions to the free energy, which consists of a total of 6 contributions [see Eqs. (43–47)], are considered. The entropies are [59]:

$$\frac{F_1}{N_C k_B T} = f \log f + (1-f) \log(1-f) \quad (56)$$

$$\frac{F_2}{V_l k_B T} = (f c_P) \log(f c_P + c_S) + c_S \log c_S - (f c_P + 2c_S) \quad (57)$$

$$\frac{F_3}{V_l k_B T} = -\frac{1}{3} \sqrt{4\pi l_B^{3/2}} (f c_P + 2c_S)^{3/2} \quad (58)$$

In (56–58) the entropy of the condensed counterions are defined by F_1 ; the translational entropy of the ions is F_2 ; and the fluctuations between PE and ions is given by F_3 . Another way to determine the entropy of the PE solution or complexes is by e.g. isothermal calorimetry measurements with simultaneous determination of the reaction constant [63].

3.5 Entropy-Driven Processes in Strong Polyelectrolytes

In case of strong polyelectrolytes, the complex formation, as well as dilution in a solvent, is driven by counterion release [15, 23, 58, 63]. The reason for the strong dominance of the entropy is the fact that there is only a little change in the

enthalpy of the PE in solid, solution or the complex, in comparison to the entropy of the counter ions [15, 23, 60, 62]. Therefore the entropy outweighs the enthalpy in the described processes by a factor of two to fifteen [63]. As already reported in the 1950s, the PE will not form complexes or phase separations in water with only monovalent counterions at low or moderate concentrations due to the strong contributions of the entropy [23].

One way to increase the electrostatic interaction energy, and at the same time to decrease the entropy, is to exchange the monovalent counterions with multivalent ions or oppositely charged PEs [23]. This way one can achieve concentration dependent complex formation, or coacervation, within the PE solution. At low concentrations, the PE-counterion complex, whereby the counterion is a polymer or multivalent salt, will be strongly charged. The addition of salt to the solution shields the PE charge and decreases the PE-PE or PE-multivalent ion tendency to phase separate due to shielding of the charges [23]. Such a behavior was indeed measured with the dissolution of PE multilayer thin films (two dimensional thin films comprising of complexes of oppositely charged PE) in high ionic strength solutions [85], as long as the PE did not salt out. Figure 2 illustrates this effect, by showing the range of solubility for two PEs of the same size and charge density with opposite charges at different salt and polymer concentrations. It can be clearly seen that high salt concentrations at moderate PE concentrations cause a high solubility (point C in Fig. 3).

3.6 Viscosity of Polyelectrolyte Solutions

To understand the rheological and viscous behavior of PE solutions it is vital to understand the behavior of PE molecular structure, entanglement and interactions in solution. This is because the PE viscosity behavior is dominated by the PE structure, giving PE solutions unique properties compared to uncharged polymers [26, 86]. Another contribution to the solution viscosity is the viscosity of the solvent, η_s , and the interaction of the solvent with the polymer or polyelectrolyte, which is important since the PE will always drag some solvent molecules with it upon movement and shear force [2, 80, 87, 88]. The scaling laws of solution and PE structure in relation to viscosity were mainly developed by de Gennes and Pincus with contributions to the entangled regime by Pfeuty [22, 53, 89]. The friction coefficient of a colloidal particle (here a spherically coiled PE) used in the scaling theory in solution can be determined by the Stokes law [30]:

$$Z_P = 6\pi\eta R \quad (59)$$

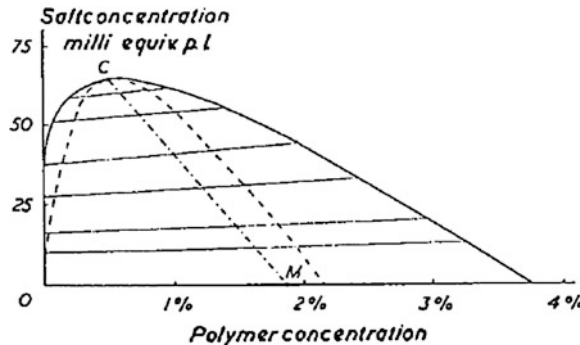


Fig. 3 Addition of a large amount of salt increases solubility of PE and lowers complex formation. The area below the *curve* is the dissolved region, where the *dashed line* shows the spinodal and the line C-M the rectilinear diameter. Image taken from Ref. [23], reprinted with permission of John Wiley and Sons

Here η is the viscosity, which is the proportionality coefficient of the shear, rate $\dot{\gamma}$, and the shear stress, σ_s [30].

$$\eta = \frac{\sigma_s}{\dot{\gamma}} \quad (60)$$

The diffusion coefficient of a spherical particle in a liquid is defined by the Stokes-Einstein relation [30]:

$$D_i = \frac{k_B T}{6\pi\eta R} \quad (61)$$

Equation (61) is especially important because many measurement systems like dynamic light scattering or pulsed field gradient NMR do not measure the absolute diffusion and viscosity, but the relation to the hydrodynamic radius. The hydrodynamic radius, R_H , is defined as [30]:

$$R_H = \frac{k_B T}{6\pi\eta D_i} \quad (62)$$

The volume fraction, ϕ , is calculated from the concentration, the molar mass of the monomer, M_{Mon} , the density ρ and the monomer volume. The Avogadro constant is N_{av} [30].

$$\phi = \frac{c}{\rho} = \frac{c}{M_{Mon}} b^3 N_{av} \quad (63)$$

The time, τ , a polymer or bead needs to travel a distance on the order of its own size is dependent on the friction coefficient, Z_P [30].

$$\tau \approx \frac{R^2}{D_i} \approx \frac{R^2 Z_P}{k_B T} \quad (64)$$

The inverse dependence of τ on the temperature is caused by the fact that the PE travels due to diffusion. The random collisions of the solvent molecules on the PE coil cause an increased diffusion speed with increasing temperature due to introduction of more kinetic energy.

There are two theoretical models to determine the relaxation time, τ_R , and self-diffusion time of the PE in the solution. One is the Rouse model, which is based on the assumption that the PEs are comprised of mass centered points connected with springs these points only interact with these springs. The other is the Zimm model which is an extension of the Rouse model and takes hydrodynamic effects into account [24, 30]. The Rouse model was used to establish the scaling theory of PEs in solution, which allows an estimation of the PE structure from the viscosity in the different solution regimes.

Before the current state of the art of the scaling regimes of viscosity values for PE solutions in different concentration regimes is introduced, it is worth noting, that it can still not explain all observed effects. The calculated values still deviate from measurements, especially at the transition points between concentration regimes. The same is true for osmotic measurements. Novel theories like the GER0 theory can explain all concentration regimes, from dilute to entangled concentrations, while showing a smooth transition. However only the scaling regimes for the osmotic pressure were calculated and tested by the authors [77]. It is expected, that an application of the GER0 theory in the field of rheology in the near future will solve the remaining theoretical gaps.

3.6.1 Unentangled Dilute Regime

The relaxation times determined by the Rouse model, τ_{RR} , and diffusion coefficient, D_R , in the unentangled regime (very low concentration without chain-chain interactions) is [24, 26]:

$$\tau_{RR} = \frac{\eta_s b^3 N^2}{k_B T} \quad (65)$$

The concentration dependent relaxation time of the p modes ($p = 1, 2, \dots N$) [30]:

$$\tau_p \approx \tau_0 \left(\frac{N}{p} \right)^2 \quad (66)$$

The mode $p = 1$ is the longest relaxation mode and is τ_{RR} . For the modulus of the Rouse model, see Ref. [30]. The rouse diffusion constant is defined as [30]:

$$D_R = \frac{k_B T}{N Z_P} \quad (67)$$

The viscosity contribution of the PE to the solution viscosity is defined as [30]:

$$\eta - \eta_S \approx \frac{Z_P}{b} \phi N \quad (68)$$

In contrast to the Rouse model, the Zimm model on the contrary is more precise for low concentrations since the Rouse model is only precise in polymer melts, ignores solvent effects and applies precisely only at high PE concentrations [30]. A comparison of the relaxation times from the Rouse and Zimm models was done in Ref. [30]. For the case when the correlation length is smaller than the screening length (strong dilution), the Zimm time is usually shorter than the Rouse time. This surprising result was explained with the springs in the Rouse model, which hinder free motion of the mass centers. In contrast, a PE in the Zimm model can freely diffuse within the solvent or take part in a mixed motion including additional diffusion of monomers in the chain [30]. The relaxation time and diffusion of the Zimm model, τ_{RZ} and D_Z respectively, in the unentangled regime of an ideal chain are, according to [30].

$$\tau_{RZ} = \frac{1}{2\sqrt{3}\pi k_B T} \frac{\eta_S}{R^3} \quad (69)$$

$$D_Z = \frac{8}{3\sqrt{6\pi^3}} \frac{k_B T}{\eta_S R} \quad (70)$$

The concentration dependent viscosity of the Zimm model is defined as:

$$\eta - \eta_S \approx \eta_S \phi N^{3v-1} \quad (71)$$

where v is ~ 0.5 in θ solvents and ~ 0.666 in good solvents for PEs. This value for good solvents is strikingly different from the ones of uncharged polymers which is ~ 0.588 in good solvents. These differences are caused by charges with the same sign in the PE repelling each other, leading to a final scaling exponent of 1 ($3 \cdot 0.666 - 1 = 1$) [30]. In case of weakly or partially charged PEs, the overlap concentration, c^* , is changed but not the exponent of the PE solution regime [26]. As can be seen in above equations, the contribution of the PE to the solution viscosity is linear at concentrations below c^* . For a comprehensive explanation of the Zimm modes and relaxation time, see Ref. [30].

3.6.2 Unentangle Semidilute Regime

In case of semidilute systems without entanglement ($c > c^*$), in regions above the correlation length, the Rouse motion is faster than the Zimm motion because the Zimm motion is hindered by a coupling between the chains and Rouse dynamics apply [30]. For a detailed derivation of the Rouse and Zimm models, the scaling theory and some older viscosity reviews see references [24, 30, 90].

In the semidiluted unentangled concentration regime the polymer chains begin to overlap but are not entangled. The correlation length decreases with increasing concentration, which agrees with the Fuoss law [17, 24]:

$$\phi \approx \frac{gb^3}{L_\xi^3} \quad (72)$$

With L_ξ being the correlation length which is, in semidilute solutions, equal to the screening length [26, 30]. As can be seen in Eq. (72) the correlation length decreases with increasing concentration, where the size of the chain correlates with the concentration ($L \sim c^{-1/4}$) in a slightly smaller ratio than the distance of the mass centers ($L_M \sim c^{-1/3}$) [26]. This effect allows the unentangled semidilute regime to span over 3–4 decades of the relative entanglement concentration space (c_E/c^*). The correlation of the scaling of the correlation length to the concentration is defined as [30]:

$$L_\xi \approx b\phi^{-v/(3v-1)} \quad (73)$$

v has the values mentioned for Eq. (71): $\frac{1}{2}$ for θ solvents and 0.76 for good solvents. The relaxation time of a chain, τ_{chain} , is therefore [30]:

$$\tau_{chain} \approx \frac{b^3 \eta_S}{k_B T} N^2 \phi^{(2-3v)/(3v-1)} \quad (74)$$

The diffusion constant in the semidiluted unentangled regime as a function of the concentration can be calculated from the relaxation time (74) and the size of the polymer [30]:

$$D \approx \frac{R^2}{\tau_{chain}} \approx \frac{k_B T}{\eta_S b} \frac{\phi^{-(1-v)/(3v-1)}}{N} \quad (75)$$

The concentration dependent viscosity is defined as [30]:

$$\eta - \eta_S \approx \eta_S N \phi^{1/(3v-1)} \quad (76)$$

The result of relation (76) is the concentration dependent viscosity in good solvents increases by an exponent of 1.28, while a value of 0.5 causes an exponent of 2. The values 0.76 and 0.5 are for neutral polymers which show no concentration

depended decrease in chain length like PEs. Therefore the value for ν in Eq. (76) is ~ 1 leading to a total exponent of 0.5. A correlation of the viscosity which also takes the charge density of the PE into account was suggested by Dobrynin and Rubinstein to be [26]:

$$\eta \approx \eta_S (Kf_*^2)^{1/2} (b^3 c)^{1/2} N \quad (77)$$

3.6.3 Entangled Regime and Entanglement Criteria

The entangled regime in the semidilute region starts at the entanglement concentration c_E ($c > c_E$ with c_E being higher than the overlap concentration c^*). The polymer entanglement criteria is assumed to be the same as in the case of uncharged polymers [91–93]. In this criteria only long lived entanglements are considered real entanglements and not temporary overlaps due to fluctuations [91–93]. The effect of tails and dangling bonds are also not considered in this approach due to mean field like assumptions [91–93]. The reason that the overlap concentration, c^* , does not show a significant entanglement effect is due to the fact that PE chain and blob sizes decrease with increasing concentration. Another observation is that a chain needs to overlap with n_e other chains to have significant topological movement for the friction becoming a significant effect, with n_e being a number between 5 and 10 [24]. The dependence of the degree of entanglements and the concentration can be seen below [24]:

$$c_e \approx \frac{n_e}{L^3} \approx c^* \frac{n L^3(c^*)}{L^3(c_e)} \approx n^4 c^* \quad (78)$$

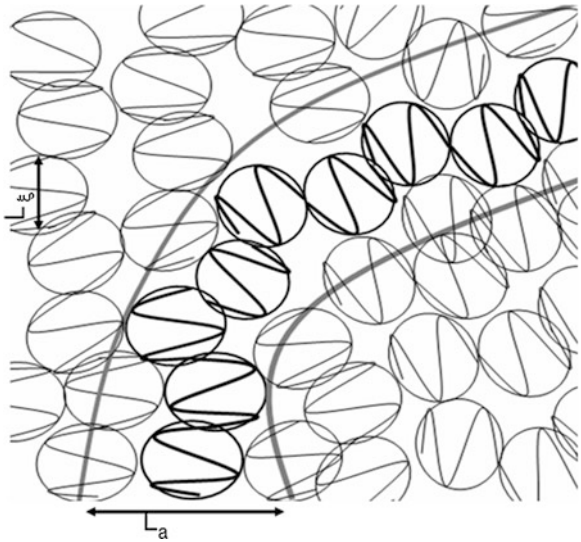
Please note that Eq. (78) was originally published as an equality sign [24]. Since the same author published the same equation as an approximation sign 10 years later in a review paper [26], the equation is shown as an approximation sign [24, 26]. For known crossover, salt and entanglement concentrations, the degree of entanglement points per chain can be calculated [24].

$$n_e \approx (c_e/c^*)^{1/4} ((1 + 2nc_S/c^*)/(1 + 2nc_S/c_e))^{3/8} \quad (79)$$

It is additionally noted that the polymers need a minimum chain length for significant entanglement, which is on the order of 10,000 kDa. For a detailed calculation method of the entanglement chain length, see Ref. [93]. The viscosity at the entanglement concentration is according to Ref. [24]. $\eta \approx n_e^2 \eta_S \approx 50 \eta_S$, which is comparable to the equivalent one for neutral polymers.

The entanglement for the PE is characterized by an imaginary tube diameter, a . The tube itself is considered to surround the PE random walk, and the entanglements are defined by the amounts of other PE laying within the tube volume, a^3 .

Fig. 4 Definition of the tube diameter, a , also called L_a (length a) and the entanglement criterion of n_e . Image adapted with permission from Ref. [26], copyright of the original version, 2005 Elsevier



Therefore, n_e can be determined by Dobrynin et al. [24] and Dobrynin and Rubinstein [26]:

$$\left(\frac{L_a}{\zeta}\right)^3 \approx \frac{n_e N_E}{N_M} \quad (80)$$

$$n_e = \frac{L_a}{\zeta} \quad (81)$$

The definition of a is shown graphically in Fig. 4.

The longest relaxation time, diffusion constant and viscosity of this region for salt free solutions are according to [24, 26]:

$$\tau \approx \tau_\zeta \left(\frac{N_E}{N_M}\right)^2 \left(\frac{N}{N_E}\right)^3 \approx \frac{\eta_S b^3}{k_B T} K f_*^2 n_E^{-2} N^3 \quad (82)$$

$$D_i \approx \frac{L^2}{\tau} \approx \frac{k_B T}{\eta_S b} n_E^2 N^{-2} (K f_*^2)^{-5/6} (c b^3)^{-1/2} \quad (83)$$

$$\eta \approx \eta_S n_E^{-4} N^3 (K f_*^2)^{3/2} (c b^3)^{3/2} \quad (84)$$

By comparing Eq. (82–84) with each other it can be clearly seen that the parameters are affected in different ways by the concentration. While the relaxation time is only affected indirectly via the amounts of entanglement, the diffusion decreases with increasing concentration by the exponent $-1/2$, and the viscosity increases by the exponent $3/2$. An interesting effect was found for the dependence

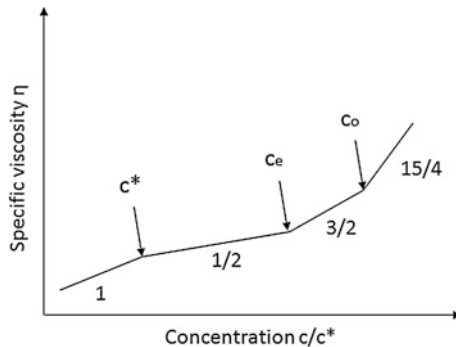


Fig. 5 Illustration of the different concentration regions and their scaling exponent. Image adapted with permission from Ref. [26]. Copyright of the original version 2005, Elsevier

of the viscosity at high salt concentrations. If the concentration of salt is much higher than the PE concentration ($c \ll n c_S$) then the viscosity scales like in the case of neutral polymers in good solvents with $\eta \sim c^{15/4}$ [24]. These regions are illustrated in Fig. 5.

3.6.4 Unentangled and Entangled Hydrophobic Polyelectrolytes in String and Bead Controlled Regions

In case of poor solvents for the PE, like in the case of hydrophobic or partially hydrophobic PEs, formation of necklaces can occur [94]. If the size of the necklace beads reaches the distance between the beads, the PE enters the transition from the diluted to the semidiluted bead controlled regime. The concentration threshold for this regime is defined as [26, 94]:

$$c^* \approx \frac{N}{L_{nec}^3} \approx \frac{N_{Mstr}^{3/2}}{b^3 N^2} \quad (85)$$

An interesting correlation is that the bead size, L_ζ , correlates with the fraction of charged monomers and therefore only weakly and indirectly with the concentration [94].

$$L_\zeta \approx b(Kf^2)^{-1/3} \quad (86)$$

The length of the polymer chain between the beads, called the length of the string, L_{str} , has an inverse correlation with the fraction of charged monomers in the bead [94].

$$L_{str} \approx b(T_R/Kf^2)^{1/2} \quad (87)$$

where T_R is the reduced temperature, $T_R = (\theta - T)/\theta$, with θ being the theta temperature of the PE. In the semidiluted, string controlled, unentangled regime, $c > c^*$, the correlation length can be estimated via following equation [94]:

$$L_\xi \approx R \left(\frac{c^*}{c} \right)^{1/2} \approx b \left(\frac{T_R}{Kf^2} \right)^{1/4} (cb^3)^{1/2} \approx b N_{Mbead}^{1/4} (cb^3)^{-1/2} \quad (88)$$

Here, N_{Mbead} is the amount of molecules in the bead. The concentration at which the bead controlled regime starts can be estimated from either the theta temperature, the charged fraction or from the amount of monomers in the beads [94]:

$$c_b \approx b^{-3} \left(\frac{Kf^2}{T_R} \right)^{1/2} \approx b^{-3} N_{Mbead}^{-1/2} \quad (89)$$

In the bead controlled concentration regime, the correlation length correlates inversely with the concentration, as can be seen in the equation below [94]:

$$L_\xi \approx \left(\frac{T_R}{Kf^2} \right)^{1/3} c^{-1/3} \approx \left(\frac{N_{Mbead}}{c} \right)^{1/3} \quad (90)$$

The overlap concentration of the beads, c_o , is the point at which the concentration of beads reaches values comparable to the PE concentration inside the beads [94]:

$$c_o \approx \frac{N_{Mbead}}{L_\xi^3} \approx \frac{T_R}{b^3} \quad (91)$$

The self-diffusion coefficient in the unentangled string controlled concentration region shows no correlation with the concentration. In the bead controlled region, the diffusion coefficient increases with the concentration. This counterintuitive behavior can be explained with the fact that the friction coefficient is linearly related with the correlation length. Since the correlation length decreases in this concentration regime with increasing concentration, the self-diffusion coefficient increases [94].

$$D_i \approx \frac{k_B T}{\eta_S b} \frac{N_{Mbead}^{1/2}}{N} X \quad (92)$$

Here, X is 1 for the case of $c < c_b$, and $(c/c_b)^{1/3}$ in case of $c_b < c < c_o$.

The relaxation time of the longest mode in the semidilute and bead controlled regime can be determined according to [94]:

$$\tau \approx \frac{\eta_S b^3}{k_B T} \frac{N^2}{N_{Mbead}^{1/2}} X \quad (93)$$

Here, X is $(c_b/c)^{1/2}$ for the case $c < c_b$, and c_b/c in the case of $c_b < c < c_o$. The viscosity also depends on the concentration regimes. In the semidilute regime it scales with the exponent $1/2$, while it is in the bead controlled region independent from the concentration. This phenomena is explained with the inverse correlation of the correlation length to the concentration [94]:

$$\eta \approx \eta_S \frac{N}{N_{Mbead}} X \quad (94)$$

Here, X is $(c/c_b)^{1/2}$ for the case of $c < c_b$, and 1 in case of $c_b < c < c_o$.

Entangled necklaces:

The entanglement criterion for necklaces is similar to that for a normal PE. Also, the number of entanglement sites is the same, and the entanglement concentration can be determined by $c_e = n^4 c^*$ [94]. The only difference is the tube diameter and the correlation length defining it. The relaxation time, self-diffusion coefficient and viscosity of entangled PE necklaces can be determined by [94]:

$$\tau \approx \frac{\eta_S N^3 b^3}{k_B T n_e^2 N_{Mbead}^{3/2}} X \quad (95)$$

Here, X is 1 for the case of $c_e < c < c_b$, and in c_b/c case of $c_b < c < c_o$.

$$D_i \approx \frac{R^2}{T_R} \approx \frac{k_B T n_e^2 N_{Mbead}^{3/2}}{\eta_S b N^2} X \quad (96)$$

Here, X is for the case of $c_e < c < c_b$: $(c_b/c)^{1/2}$ and in case of $c_b < c < c_o$: $(c/c_b)^{1/3}$. The decrease of the self-diffusion coefficient in the entangled regime is surprising, and explained by a strong initial entanglement that decreases due to decreasing correlation length, and an increasing bead diameter along with a decreasing chain length, minimizing interaction sites.

$$\eta \approx \frac{\eta_S N^3}{N_e^4 N_{Mbead}^3} X \quad (97)$$

Here, X is $(c/c_b)^{3/2}$ for the case of $c_e < c < c_b$, and 1 in case of $c_b < c < c_o$. Like in case of Eq. (96), the viscosity shows counter-intuitive behavior. The viscosity increases in the entangled regime, but not in the bead controlled regime. This behavior is explained by the low number of interaction sites in the bead controlled regime. In this regime, however two conditions must be fulfilled: 1. n_e of entanglement is similar to n_e for normal polymers; 2. c_e is be below c_b .

This system behaves more like a dilute solution of beads than like a solution of polymers [94]. This behavior opens interesting new possibilities and applications to this type of polymer solution such as being an additive in polymer melts for extruders, reducing the viscosity and at the same time not disturbing properties, e.g. optical properties, since it is a polymer.

By comparing the string and bead controlled regimes, the following conclusions of the necklace structures can be drawn:

1. As long as the system is controlled by strings (string size larger than bead size) the PE behaves like a linear PE and has similar scaling regimes [94].
2. If the bead size reaches similar distances to the string between the beads, then one enters the bead controlled regime with significantly different scaling factors [94].

Adding salt to necklace solutions:

Adding salt to the PE-bead containing solutions changes the PE structure and rheology. An extensive discussion of the structural properties of the PE necklace structure for different salt concentrations as well as the model of counterion condensation on the string and beads can be found in Ref. [94]. This part of the chapter focuses on the rheological properties for these PE in the semidilute high salt concentration region ($c_s > fc$), for the special conditions of low salt ($c_s \ll fc$) and very high salt concentrations ($c_s \gg fc$), see [94]. The relaxation time (longest mode) and viscosity for the high salt semidiluted unentangled regime of the PE necklace in the string controlled region is [94]:

$$\tau \approx \frac{\eta_S b^3}{k_B T} N_{M\text{bead}}^{-3/4} \left(1 + \frac{2c_s}{fc}\right)^{-3/4} (cb^3)^{-1/2} \quad (98)$$

$$\eta \approx \eta_S N N_{M\text{bead}}^{-3/4} \left(1 + \frac{2c_s}{fc}\right)^{-3/4} (cb^3)^{1/2} \quad (99)$$

In the semidiluted entangled regime, the viscosity and relaxation time change to [94]:

$$\tau \approx \frac{\eta_S N^3 b^3}{k_B T n_e^2} N_{M\text{bead}}^{-3/2} \left(1 + \frac{2c_s}{fc}\right)^{-3/2} \quad (100)$$

$$\eta \approx \eta_S \left(\frac{N^3}{n_e^4}\right) N_{M\text{bead}}^{-9/4} \left(1 + \frac{2c_s}{fc}\right)^{-9/4} (cb^3)^{3/2} \quad (101)$$

In the bead controlled unentangled region, the dependence of the viscosity and relaxation time (longest mode) on the concentration and ionic strength (high ionic strength) is [94]:

$$\tau \approx \frac{\eta_S}{k_B T} N^2 N_{Mbead}^{-1} \left(1 + \frac{2c_S}{fc} \right)^{-5/4} c^{-1} \quad (102)$$

$$\eta \approx \eta_S N N_{Mbead}^{-1} \left(1 + \frac{2c_S}{fc} \right)^{-5/4} \quad (103)$$

In the entangled region Eqs. (102) and (103) become [94]:

$$\tau \approx \frac{\eta_S N^3}{k_B T n_e^2} N_{Mbead}^{-2} \left(1 + \frac{2c_S}{fc} \right)^{-5/2} c^{-1} \quad (104)$$

$$\eta \approx \eta_S \left(\frac{N^3}{n_e^4} \right) N_{Mbead}^{-3} \left(1 + \frac{2c_S}{fc} \right)^{-15/4} \quad (105)$$

The free energy of phase separation (bead formation) in such a necklace solution can be calculated via the free energy according to following relation [26, 95]:

$$\frac{F_{neck}(\phi)}{k_B T} \approx \frac{V}{b^3} \left(\frac{\phi}{N} \ln(\phi) + \phi f \ln T_R \beta_c + f \phi \frac{(1 - \beta_c)^{2/3}}{3} \left(\frac{K}{f} \right)^{2/3} T_R - \phi T_R^2 \right) \quad (106)$$

Here β_c is the fraction of condensed counter ions. Equation (106) was used to calculate the phase diagram of a PE in a poor solvent [95]. The terms on the right hand side are: the entropy of mixing, the entropy of the counterions inside the bead, the free energy of the beads and the monomer-monomer interaction due to short range forces within the beads. The background theory of Eq. (106) is based on Osawa's two zone model of counterion condensation. The increasing concentration of counterions is used to induce a phase separation of the solution, which is dependent on the temperature. The phase separations and, depending on the solution properties, also additional changes of the solution structure, can be measured by changes in the viscosity (see above sections) and/or be followed by SAX or SANS (small angle X-ray and neutron scattering) (see also Sect. 5 for more information about experiments) [95]. Figure 6 shows the solution regimes of PE necklaces in a poor solvent.

3.7 Polyelectrolyte Gels

One interesting feature of PE solutions is the ability of PEs to form cross-linked gel networks [83, 96]. These networks can be formed either by chemical or by ionic thermo-reversible bonds formed by e.g. multivalent ions as cross-linkers [83, 97]. A Flory theory based theoretical study of the PE gelation points using di- and

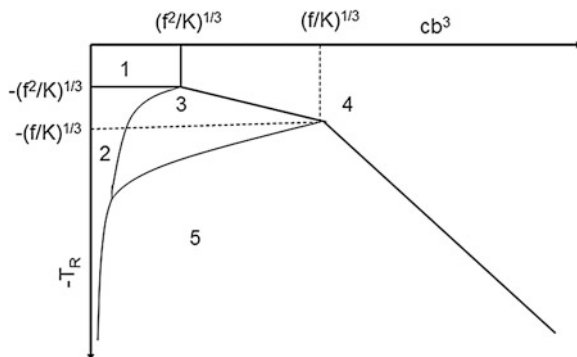


Fig. 6 The different solution regimes of a PE able to form necklaces. Range 1 symbolizes the area of the θ solvent, range 2 the region in which the polymer solvent interaction dominate on small length scales and the PE starts forming the globules of the necklaces. In this region dilute and semidilute regime are possible. In region 3 the PE is in the bead controlled regime while region 4 symbolizes the concentrated solution regime. Region 5 denotes the area of phase separation. Image adapted with permission from Ref. [95]. Copyright 2001, American Chemical Society

tri-valent ions was able to show that the free energy of such a system consists of the translational entropy, the combinational free entropy (entropy of choosing different units) and the free energy of the cross-links [83]. This approach also was additionally able to prove that the weaker the charge of the ionic groups (l_B/a ratio), the more multivalent ions are needed for gelation [83]. If the values of the l_B/a ratio were changed from 5 to 2, the amount of ions needed increased by nearly two orders of magnitude [83]. In a later paper, the same authors were able to show the structural gelation lines of PE gels comprised of different charges and functionalities resulting in different cross-linker energies, and these PE gels were compared with neutral polymer gels [97]. Further, in this study the PE gels in semidilute solutions exhibited a re-entry point of the gelation, which was also described in other models [97].

The same group published another contribution to this topic which describes the complexation of oppositely charged PEs, focusing on the effect of ion pair formation [98]. The free energy was derived from the law of mass action, where the Flory-Huggins parameter was influenced by the polymer fraction [98]. The PE cluster structure, as well as the precipitate properties were described to be salt dependent, which is also in agreement with other theories [16, 98].

4 Computer Simulations and Structure

Experimental methods often require a complicated mathematical treatment to extract the data, e.g. from X-ray and neutron scattering or reflectometry data, which renders the result not univariant but multivariant [99, 100]. Computer simulations, on the contrary, allow a direct observation of the molecular structure

with the option to photograph it by making screen captures [101, 102]. One of the main drawbacks of these methods is that the size of the systems that can be simulated with quantum mechanics is limited to either a few short PEs or one long chain when using a standard PC due to the high computational demand [103, 104]. This limit will be extended in the near future with the emergence of quantum computers [105, 106], like those manufactured by D-wave Systems [107] which have already successfully proven to be capable of the simulation of protein structures [108]. Due to the currently high price, lack of software and computational results of quantum computers, this review focuses on the computational results of current, standard computers.

Using a coarse grain model for PE structures (averaging the mean field similar to the mean field theory over e.g. the monomer groups of the PE) [103, 104, 109] extends the amount of observable PE chain monomers significantly. The great advantage of using a coarse grain model is that the structural change of the whole polymer, which occurs on much longer timescales compared to changes of single atoms, becomes visible [104, 110]. One of the main problems is that the finite system sizes force scientists to use simplifications (e.g. either salt atoms are neglected or the chain-chain interaction) [103, 104, 111, 112].

The best approach is, therefore, to compare the results of simulations made at different length scales with real measurements to determine the validity of the approach since the causes for changes in e.g. viscosity can be caused by changes in local interaction energy or with the PE structure or both [103]. In this section, the results of computer simulations with relation to the PE structure, complex formation and dilution behavior are summarized. The focus lies on molecular dynamics simulations since Monte Carlo simulations [102, 113] are discussed in detail in chapter ‘[Thermodynamic and Rheological Properties of Polyelectrolyte Systems](#)’.

4.1 Brief Summary Monte Carlo Simulations and Other Simulation Methods

Since the results of Monte Carlo (MC) simulations on PE structure are discussed in detail in chapter [‘Thermodynamic and Rheological Properties of Polyelectrolyte Systems’](#), only a brief summary of this simulation method and some results related to this chapter are discussed. In addition, a short overview of recent developments in field theoretical approaches is given.

Monte Carlo simulations [102] are generally less precise in regard to the real reaction time and dynamics of a system compared to MD simulations since MC simulations base on statistics and not real speed of the particles [103]. MC simulations are often lattice based, are easier to program and are also well suited for discontinuous or not differentiable energy functions as well as to define structural equilibration and static properties [103]. With such properties, MC simulations are

well suited for the simulation of the PE conformational structures and also their complex formation [104, 109, 114, 115]. For this reason, simulations of PE-complexes done with MD are very scarce and most PE complexes have been simulated with the MC method or derivations of it, see reviews [16, 104, 109, 116], as well as chapter ‘[Thermodynamic and Rheological Properties of Polyelectrolyte Systems](#)’ for details and corresponding MC based papers. Along with PE complexes, PE gels have also been studied with MC simulation. The focus was on the interaction of the PE gel molecules with strongly charged macro-ions e.g. from surfactants [117]. Other studies focused on the effect of different PE chain lengths as well as polydispersed PE chains in a PE gel, finding that the effect of polydispersity is larger for PE gels than for uncharged gels [118].

Field theoretical approaches have been successful in the area of polymer physics and physical chemistry [74, 77–79]. In particular, for mean field simulations great advances have been made in recent years, as can be seen in the extensive review of Ref. [74]. These advances led also to new developments in the field of PE solutions, e.g. in the simulation of the osmotic pressure of NaPSS solutions [74, 119].

An novel approach is the combination between self-consistent field theoretical approaches and Monte Carlo simulations called theoretically informed coarse grain simulations [120]. It was developed in the field of block copolymers and could easily be extended to PE based copolymers and also thermodynamic calculations [120].

4.2 Molecular Dynamics Simulations

One of the main methods used in computer simulation of explicit atoms, molecular groups and particles is molecular dynamics (MD) [101, 103, 104, 109]. This method allows the simulation of the dynamic movement of particles (atoms or molecular groups), which are usually assumed to be spheres [101, 103, 104]. The special feature of this method is that the movement of these particles is in real time and that each particle has a potential well, which can alter the speed of the particles [101]. This not only allows detailed measurement of self-folding structures, but also the determination of self-folding times, dynamics and temperatures [103]. In contrast to MC simulations which use statistical probabilities and a priori knowledge to determine changes to the system, MD can even be used to simulate the real quantum mechanical probabilities of a atom [103]. Due to the high computational demand and the low observable timescales of these processes, usually molecular groups are merged into a coarse grain model [103, 104].

This part of the book chapter is focused on MD coarse grained simulation results of thermodynamic and rheological properties of PEs. For a detailed introduction into MD simulations and coarse graining see references [103, 104, 109, 121]. MD simulations have been used very successfully in the determination of DNA structures, for excellent reviews of MD coarse graining simulations of these DNA structures and their properties see references [109, 121].

4.2.1 Coupling Constants

The effect of the coupling constant on the PE structure and counterion condensation discussed in Sect. 2 was proven by MD simulations, which showed that an increased coupling constant influences counterion condensation as well as the structure of the PE [122–124].

Monovalent counterions: The effect of counterion condensation at various solvent qualities with different salt concentrations and charge densities have been simulated using PE-MD simulations [125]. By 1995, the structure factor, the coulomb forces, the end to end distances, the polymer and counterion based chain concentration, the osmotic pressure and the persistence length had been simulated by the group of Kremer, and the values were compared with analytical equations and experiments [125]. Later studies of this group extended this approach to poor solvents for strongly charged PEs [126]. The dependence of the degree of polymerization and the monomer width on the crossover point from electrostatic to hydrophobic controlled regime and its effect on the structure factor was determined in this study [126]. The effects of chain ends on PE chains was simulated by Limbach et al. [127] with the result that the chain ends are much more charged than the center of the PE in both strong and weak PEs, as well as in different solvent qualities and ionic strengths. The results of another MD study showed that PEs are not homogeneously stretched supports this finding [128]. Investigations of the effect of counterion concentrations and solvent qualities were able to show the formation of bundles and blobs within PE brushes in MD simulations [129, 130]. Although hard to synthesize for bulk applications, such PE structures in solution could enable new and interesting viscoelastic and/or optical properties.

PSS in water at different degrees of sulphonation, which causes a varying degree of the fraction of charged monomers, showed in atomistic simulations structures depending on the degree of charge (sulphonation) [119]. The transition from elongated to collapsed chains was in agreement with the scaling theory as well as with calculations performed by Kuhn in the 1950s [2, 24, 119]. A coarse grained simulation of strongly charged PEs (a group which includes PSS) was done by Chang and Yethiraj for bad solvents without added salt [122]. In this simulation the solvent parameter was varied from good to bad across a variety of solution phases ranging from dissolved (good to bad solvent) and necklace-bead structures, to phase separation in the case of bad solvents, with various structures depending on the polymer concentration [122]. During these simulations, the structure factor was also determined, and this showed a polymer concentration dependent peak [122].

4.2.2 Necklaces, Poor Solvents and Counterions

The formation of necklace like structures due to poor solvents and counterion condensation was first simulated by the Kremer group and the structure factor was calculated as a function of the wave vector [131]. In a paper about end effects of

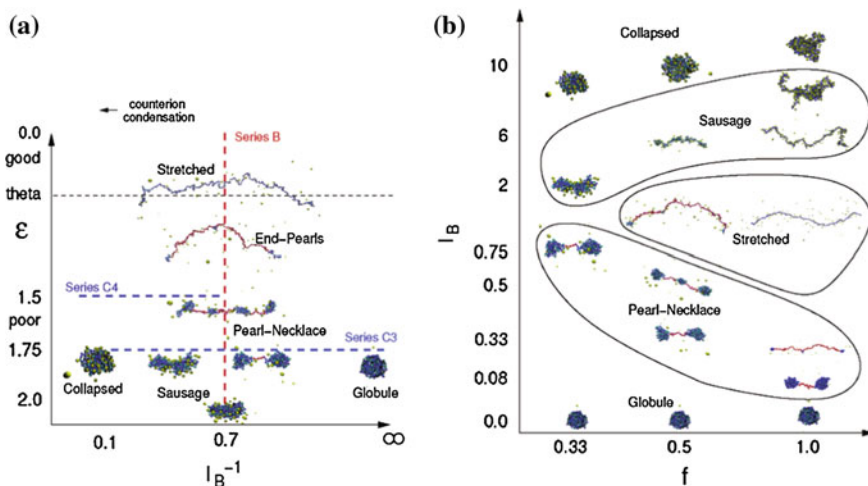
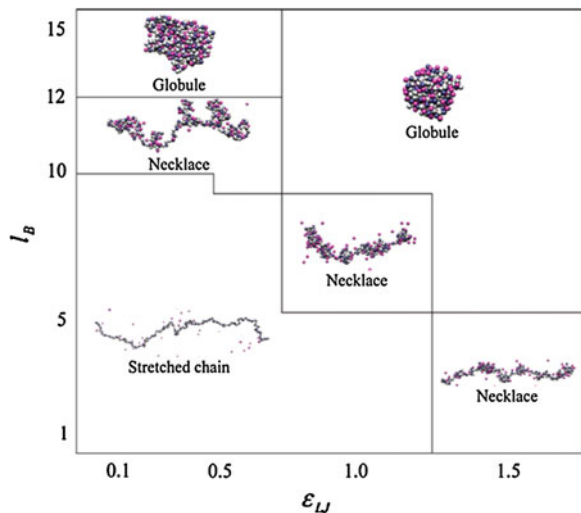


Fig. 7 Chain conformations of a strong PE for varying conditions. **a** Simulated for $f = 1/3$, showing the influence of the Bjerrum length and solvent quality on the PE structure. **b** Bjerrum length versus charge fraction in a poor solvent. Image reprinted with permission from Ref. [135]. Copyright Americal chemical society 2003

strong PEs, the development of necklaces in poor solvents was reported [127]. The necklaces showed in the middle of the PE a nearly balanced charge, while necklaces at the end of the PE exhibited an overcompensated charge [127]. No instability of the necklaces due to counterion condensation in the dilute regime were reported by other papers, and only minor changes in the form factors have been found [132–134]. These small changes in the form factor are a major hindrance to experimental observations, since the change of the form factor is related to changes in the monomer density of $F_S \propto \phi_M^{0.35}$ in case of poor solvents, which differs from the structure factor of good solvents of $F_S \propto \phi_M^{1/2}$ for the dilute and $F_S \propto \phi_M^{1/3}$ for semidilute phase [133]. In a systematic study of the structural conditions of strong PEs in a poor solvent, the necklace regime was reported to be rather small [135]. In this study only small changes in observable parameters like the form factor could be observed despite large changes in the chain conformation simulated for a large variety of possible influences parameters which included Bjerrum length, Manning parameter, string length, number and size of necklaces, chain length, solvent quality, counterions and their distribution, and polymer density [135]. The results of these systematic simulations are shown in Fig. 7.

The simulation of the dissolution or breakup of a big PE globule (called necklace formation) was done in theory and MD simulation by the Dobrynin and Rubinstein groups [124]. The globule is treated in such a simulation like a Rayleigh drop with a certain degree of outer and inner charge, and the globule breaks down into two evenly sized sub PE globules with the PE chain connecting both globules if the charge surpasses a certain degree [26]. The PE chain bridges

Fig. 8 Counterion mediated necklace formation in a good solvent. The chain conformations were simulated with $N = 304$ and a charge fraction of $1/3$. Image reprinted with permission from Ref. [136]. Copyright American Chemical Society 2007



these two globules, which can be split into even smaller globules if the charge is raised further. A convenient summary of the research on PE necklaces in theory and simulation can be found in Ref. [26].

A simple way to form necklaces in good solvents with the introduction of counterions was presented by Jeon and Dobrynin [136]. Such a counterion induced necklace formation was found to be possible by Jeon if the fraction of charged monomers in the simulation was reduced to 0.3 in good, theta and poor solvents [136]. The results of this method are summarized in Fig. 8, which is significantly different from Fig. 7a due to a different necklace forming mechanism and use of different PE.

The theory of the necklace formation for a hydrophobic PE in a poor solvent was done by Liao et al. [124] accompanied by MD simulations which covered different charged fractions, degree of polymerization and different solvent qualities. The MD results support the theory which is discussed in detail in the thermodynamics section of this chapter. The transition regimes of diblock Polyampholytes were investigated with MD and scaling theory by Wang and Rubinstein [137]. They detected three regimes of the electrostatically driven coil to globule transitions, which are known to depend on the electrostatic interaction energy [137].

4.2.3 Monovalent Salt Solutions

The effect of salt solutions on the properties of a flexible PE was investigated by Carillo [138]. It is interesting to note that the results obtained for the persistence length in the dilute regime [138].

$$l_p \propto \frac{1}{\sqrt{\parallel} c_s} \quad (107)$$

deviated from the ones obtained by analytical considerations, which is shown in Eq. (2), but were in agreement with a definition of the Debye length in Ref. [24]. This contradiction can be explained by different theoretical approaches between the two references. It is worth noting that there are 2 regimes in the semidilute region, one which lasts approximately from 0 ionic strength to $c_s/c_{s0} = 1$ (where c_{s0} is defined as the counterion concentration in a salt free solution) and shows a linear decrease of the Debye length [138]. This regime deviates from Eqs. (2) and (107) because it is still a counterion controlled regime and the amount of added salt is still not significant. The second regime shows a decrease of the persistence length according to Eq. (107) [138]. The chain size in the dilute regime correlates with the ionic strength by $R \propto c_s^{-1/5}$ [138] which is in good agreement with the correlation stated in Ref. [24].

$$R \approx bN^{3/5}(c_p b^3)^{-1/5}(Nb/L)^{-2/5}(1 + 2c_s(N(1-f))/c_p)^{-1/5} \quad (108)$$

The scaling of the decrease of the chain size with increasing polymer concentration correlates with $R \propto c_s^{-1/4}$, which is in agreement with current scaling laws, which predicted a similar exponent [24, 138]:

$$R \approx L \left(\frac{c_p}{c^*} \right)^{-1/4} \quad (109)$$

A weaker correlation of $R \propto c_s^{-1/8}$ was found for high salt concentrations, which might be caused the fact that the chains were already quite contracted due to the high ionic strength [138]. The correlation length to salt concentration determined was $\zeta \propto c_s^{-1/2}$, which is in line with Eq. (11) and Ref. [24].

4.2.4 Divalent Counterions

The effects of divalent counterions investigated by Brownian dynamics studies showed that the same concentration of divalent counterions caused a stronger chain contraction, a stronger self-diffusion and a stronger scattering peak compared to monovalent counterions [38].

4.2.5 Multivalent Counterions

The bending rigidity and counterion condensation was investigated with a langevin simulation method with the possibility to insert an arbitrary counterion valency [123]. A detailed investigation of this study showed that, if the Bjerrum length

comes in the range of the bond length, the counterions enrich in an imaginary tube around the polymer and not only coils and rods, but also thyroids can emerge [123].

4.2.6 Weak Polyelectrolytes

One of the few MD studies of weak PEs was done by Konieczny et al. [139]. In this study, the effect of the PE solution without added salt and a charge degree below 20 %, which is below the Manning counterion condensation limit, was assumed [139]. The PE structure was compared with analytical calculations, and good quantitative agreement was found [139]. In the case of a charge >20 %, the PE structure changed from coil to rod and the analytical considerations did not apply anymore [139].

4.2.7 Enthalpy and Entropy of Polyelectrolyte Complex Formation

The thermodynamic properties of two PE molecules of same charge density in the dilute regime of a good solvent with added salt were calculated theoretically and simulated by Langevin [19]. In this study the enthalpy was determined by changes of the coulomb energy before and after the complex formation, while the entropy was determined by the counterion release [19]. The system showed, in case of strong PEs, an entropy controlled complex formation due to a positive enthalpy, while it showed for weak PEs or strong dielectric solvent an enthalpy controlled complex formation due to a negative enthalpy [19]. The authors pointed out that the addition of salt significantly affects the enthalpy of strong PEs and weakly affects the entropy of the released counterions [19]. The functions used by the authors are shown in the above thermodynamic section.

Another study in the field of PE complex formation covered PE-polyampholyte complexes. The resulting structures of this type of complexes were dependent on the structure of the polyampholyte (dibloc, or polyblock) as well as the ionic strength and polymer concentration [140]. The simulation was additionally treated theoretically by a calculation of the free energy based on the Flory theory [140]. In a subsequent study, the same authors discussed the effect of a poor solvent and different ionic strengths on different types of polyampholytes (di- or polyblock) [141]. It was shown that the PE can either form a globule with the polyampholyte or the PE can wrap the polyampholyte, depending on the polyampholyte composition and the ionic strength, resulting in different structure factors [141].

4.2.8 Adsorption of Polyelectrolyte Chains and Formation of Thin Films

The adsorption mechanisms of PEs have been more extensively studied than pure PE complex formation. This, on first glance, contradictory way of studying PE complex formation is result of the large success of layer-by-layer thin films and their large potential in science and applications [6]. Since this topic is only partly related to this book chapter, it is only briefly summarized here.

The adsorption of PE chains on negatively charged surfaces using the example of cellulose surfaces was simulated and compared with AFM images in the PhD thesis of Biermann [13]. The group of Dobrynin investigated the wrapping of dispersed nanoparticles by PEs [142]. The buildup of PEM thin films was investigated by the same group by taking electrostatic, short range interaction, polymerization degree, charged fraction and diffusion into account [143, 144]. In this way it was possible to show that there is a transition from linear to exponential growth of these thin films [143, 144]. The PE adsorption process was investigated in more detail in subsequent publications by the same group by taking the solvent quality, surface charge and surface overcharging into account [145]. In later publications, the adsorption of PE films on nanoporous substrates as well as different salt solutions were also taken into account [138, 146]. The swelling effect of crosslinked PE thin films was investigated by other groups by calculating the osmotic pressure within the PE crosslink complex, which is partly influenced by trapped counterions [147–149].

4.3 Viscosity of Polyelectrolyte Solutions

It has not yet been possible to directly determine the viscosity values of PE solutions by MD simulations. This is because of the difference in time and length scales between the molecular properties and the macroscopically observed regime [74]. It is, however, possible to determine and simulate microscopic effects that have a large influence on the viscosity or to simulate an environment that is constrained so that a viscosity can be determined or extended to the solution regime, although only within a very narrow concentration regime. Such work was done by Carrillo et al. [112] by simulating the shear viscosity of charged bottle brushes for different pressures and grafting densities. The PE brushes exhibited a lower shear viscosity as well as different behavior compared to neutral polymers, which is in agreement with experimental findings and current theory [112] (see also Fig. 9).

The degree of shear thinning was found to depend on the degree of backbone deformation, which is much higher in case of neutral polymers [112]. Another way to deal with this problem, and to avoid the introduction of additional surfaces, is to determine molecular effects that have a strong influence on the PE viscosity like the Rouse dynamic relaxation times [150]. This specific parameter was studied by

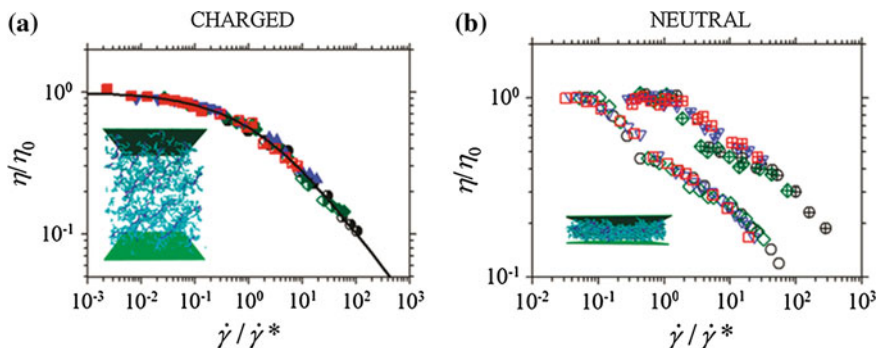


Fig. 9 Molecular dynamics simulation of charged bottle brushes versus neutral polymers, shear viscosity versus shear rate of **a** PE brush and **b** neutral brush, image reprinted with permission from Ref. [112]. Copyright American Chemical Society 2011

the Dobrynin group with a MD bead spring model, which follows the Rouse model by taking counterions as well as different charge degrees into account [150]. In the dilute solution regime, the relaxation time increased exponentially with the chain length $\tau_{RR} \approx N^3$, which was found to be higher than the value obtained from the scaling regime (Eqs. 65, 66), but it was in line with values from entangled regimes (Eq. 82) [150]. The result for the semidilute region, $\tau_{RR} \approx N^2$, was in agreement with Eq. 66 [150]. The relaxation time decreased with increasing polymer concentration due to chain contraction, which depended in the dilute region non monotonically, and in the semidilute region with the exponent $\tau_{RR} \approx c_p^{-1/2}$, on the PE concentration [150]. Such a concentration dependence is in agreement with the scaling theory as can be seen in Eq. (77) [150]. At high polymer concentrations the authors reported an increasing relaxation time, which was explained with an increase of the monomer friction coefficient [150]. It is interesting to note that the authors also determined the self-diffusion coefficient, which also affects the viscosity and depended on the concentration but not on the chain length [150]. The self-diffusion coefficient was also determined by other groups with Brownian MD for short chain PEs in dilute salt free solution, taking long-range hydrodynamic and coulomb interactions into account [151]. The whole chain diffusion was found to be related differently to the coulomb interaction than the short time Kirkwood diffusion which is related inversely to the chain size [151]. This relation to the coulomb interaction proved the importance of taking the hydrodynamic interaction into account [151].

The effect of shear thinning and molecular orientation of uncharged short chain polymers was simulated by Pierleoni et al. [111] in 1995. This simulation showed that the shear thinning is able to destroy blobs (although, due to the short chain length, only 1 blob was present) [111]. According to this report, the amount of blobs per chain, N_B , the blob size and the relaxation time in a polymer solution under shear are inversely dependent on the shear rate [111]:

$$N_B = N\beta_R^{-1/3\nu'} \quad (110)$$

$$\tau_n \sim n^{3\nu'} \sim \dot{\gamma}^{-1} \quad (111)$$

Here $\nu' < \nu$ with ν being the Flory exponent. β_R being a large reduced shear rate ($\beta_R \gg 1$), and $\dot{\gamma}$ being the shear rate. Also the birefringences and structure factor were estimated. These results are also able to explain the shear thinning effects in PE solutions [27, 152], which can (up to now) not be explained by the scaling theory or by Rouse dynamics [27, 152].

An interesting Monte Carlo simulation with embedded dissipative particle dynamics showed that the PE radius of gyration can shrink and swell depending on the concentration of salt added and the solvent quality [114].

PE gels were also investigated by MD dynamics studies. One extensive study of this interesting subject was performed by Pablo [153]. In this study, a crosslinked PE network was assumed and its interaction with mono-, di- and tri-valent counterions were investigated [153]. The osmotic pressure, structure factor, the elastic entropy (which was found to behave nearly classically) and Bjerrum length were calculated [153]. The discontinuous phase transition of PE gels was explained by the authors with the interplay of the elastic energy of the PE chains and the entropy of the counterions [153]. The structure of the PE gel was found to consist of nearly fully extended chains in the swollen state, and chains in a Gauss like state in the collapsed state [153]. In this collapsed state, the internal osmotic pressure of the PE gel was found to be higher than in the extended state [153].

5 Experimental Characterization

The structure of the PE, as mentioned in the computer simulation or theoretical section, has seldom been directly observed. Such a direct observation is, in principle, possible by high resolution TEM, or in case of dried solutions, by AFM as some recent AFM studies demonstrated for non charged polymer brushes in different solutions with different Flory-Huggins solubility parameters [154]. To ensure a measurement in non disturbed conditions, in most cases some indirect measurements, like small angle neutron scattering, X-ray scattering, light scattering, simulations, viscosimetry, or, if one employs proper dyes, also spectroscopic methods, can be employed for observing the features discussed above. This section discusses the different methods for each type of investigation and their relation to the parameters determined. The PE experimental methods of this section are divided into: viscosimetry, scattering techniques and spectroscopic approaches. Electrical measurements are omitted from this section.

5.1 Viscosimetry and Rheology

The effects of a different viscosity behavior of PE solutions compared to apolar polymer solutions was first reported in a book edited by Staudinger, as well as in a publication of Heidelberger in the 1930s [155, 156]. In the following decade, the scaling of the viscosity as a function of the concentration was determined for PE solutions by Fuoss, where the scaling for apolar polymer solutions was determined by Staudinger [17, 157, 158]. The methods and calculations for high precision viscosity measurements as well as for the relaxation times are described in detail in the publications of Adam and Delsanti [87, 88]. Another high precision viscosimeter designed for measuring highly diluted PE solutions was developed by Cohen [159].

At this point it is worth mentioning that the absolute viscosity of PE solutions up to the entanglement concentration is much higher than the one of uncharged polymer solutions [27]. Only the increase of the viscosity upon increasing concentration is lower compared to apolar polymers. This effect is not mentioned in most publications since most publications just compare PE with each other or even use different units [27]. The first contribution known to the authors actually comparing PEs with apolar polymers using the same units was Colby in 2009 [27]. Another problem when dealing with data interpretation is the mixing of the entanglement and the overlap concentration which was, in some old papers, referred to as being the same [27].

Polyvinylpyridonium (PVP) and polyvinylbutyl-pyridonium in water, ethanol and mixtures of these two solvents at different pH and degrees of ionization were used by Fuoss to validate the consistency of his approach [158]. PmAA (poly-methacrylic acid) at different ionization degrees was investigated by Kuhn, and it was found that the viscosity increased with increasing ionization [2]. The effect of adding salt to strong PEs causes a similar effect to decreasing the degree of ionization of weak PEs [159, 160]. The viscosity of cellulose sulphate (strong PE) can be switched from exponentially decreasing, to linear, to exponentially increasing viscosity upon increasing PE concentration, depending on the ionic strength of the solution [160]. This effect can be explained with different degrees of interaction and charge shielding effects of the PE with its surrounding ions and other PEs [160].

PE solutions without addition of salt can also form regular structures that can be detected by viscosity measurements [159]. By plotting the reduced viscosity versus the logarithmic concentration, Cohen was able to detect the strong dependence of the PE viscosity on the concentration, with a maximum of the specific viscosity at $\sim 10\text{--}5 \text{ mol/L}$ [159]. The height and position of the peak maximum depended on the molecular weight, where an increasing molecular weight shifted the maximum of the peak to higher concentrations, and the peak became more pronounced (see scattering and theory sections for more information about PE structures) [159].

The counterion association with the PE also influences the degree of charge, meaning that a stronger association causes a lower ionic PE–PE interaction and therefore lower viscosity [161]. The minimum in the reduced viscosity for a salt free solution of 0.45 N PSS solutions can be explained by the dissociation and mobility of the counterions [161]. Another study of PSS was done by Zebrowski and Fuller, who investigated the relaxation times of this PE. In their paper, a decreasing relaxation time for an increasing PE or salt concentration was reported [162]. In addition, an increasing deviation of the Zimm like behavior at a decreasing PE concentration and PE charge (which can be decreased by increasing the ionic strength) was found [162]. Such a deviation of the Zimm like behavior can be explained by the effect of ionic charges on the PE, which is not included in the original Zimm model [163]. This work was extended by Boris and Colby who increased the concentration range of the PE solutions investigated, and detected that the onset of shear thinning and viscosity is inversely proportional with the relaxation time [164, 165]. In addition, they also found that the fact that the Fuoss law only applies at higher shear rates [164]. A maximum in the relaxation time was found to be at 2×10^{-4} mol/L, and the relaxation time increased again after reaching the entanglement concentration [164]. Such a behavior was not forecast by scaling theory, but was also detected for different PEs and has, to the authors knowledge, so far only been explained in a narrow concentration range [27, 164]. The same effect is true for the modulus [27, 164]. PSS solutions were investigated in salt free solutions by Chen and Archer and unexpected relaxation times, which were caused by PSS aggregates and coupled polyion diffusions, were detected [166]. The inverse dependence of the relaxation time on PE molecular weight for low concentrations could not be explained by their data or by aggregation [166].

Charge density effects on PE solution rheology and solvent properties were investigated by Dou and Colby by measuring the rheological properties of PVP solutions in a good solvent at different PE concentrations [167]. They found the dependence of the chain overlap concentration on the charge density of the PE, which was also in agreement with the theoretical model of Dobrynin [26, 167]. Other measured parameters like the modulus or the relaxation time dependence on the concentration and charge density were in line with the scaling and the observed trends were reproduced theoretically [167].

The onset point of the shear thinning effect of PE solution depends on the inverse of the relaxation time of the PE chain [152]. It is interesting to note that the shear thinning effects in the study of Krause were found only for high molecular weight samples, and therefore no exact relaxation time could be determined [152]. Generally, the trend of shear thinning can be explained by an extension of the PE chain by shear force, and the viscosity is proportional to the size of the chain cross section that is exposed to the flow, as defined by the Pincus blob size, $\xi \sim \dot{\gamma}^{-1/2}$, and therefore $\eta \sim \dot{\gamma}^{-1/2}$ [165]. This behavior was explained with a modified Rouse model and Cox-Merz empiricism [165]. In steady state shear and oscillatory shear the relaxation time modes that are longer than $\dot{\gamma}^{-1}$ do not contribute to the steady

state or dynamic viscosity, and therefore lead to a decrease in the detected viscosity [165].

Amphiphilic and hydrophobically modified PEs were investigated by Di-Cola with various techniques [168]. The increase in viscosity upon increasing concentration was determined to be $\eta \sim c^a$, where a was 0.5 in case of semidilute unentangled and 1.5 in the entangled regime [168]. When the concentration reached the values at which the intramolecular globules overlapped, the specific viscosity increased by the factor $a = 4$ [168].

Studies of non organic PEs are quite scarce. Some of these studies of inorganic PEs were done by Strauss in the 1950s on polyphosphates with a molecular weight ranging from 7,000 to 19,000 [169, 170]. The short branch points of freshly prepared polyphosphates are not stable and needed some time to decay, and therefore the experiments were performed after a conditioning time [169]. The PE viscosity was found to increase nearly linearly with increasing molecular weight [169]. In a subsequent publication it was shown that inorganic PEs also follow the Fuoss equation [170].

At the end of this section on viscosity, a general problem for the measurement of PE solutions without added ionic strength is mentioned. As pointed out by Colby [27], the overlap concentration of PEs is quite small and there are salt residues at the air- water-interface due to the evaporation of water [159, 164]. Therefore deriving values or the interpretation of data can produce errors if the experiment and equipment is not designed carefully. The viscosity properties of PE complexes are discussed in the PE complexation and gel section of this chapter.

5.2 Scattering Approaches (Light, X-ray, Neutron)

It is interesting to note that reports about birefringences caused by PE solutions under shear flow were published in 1948 [2]. In these reports the influence of the molecular confinement of the PE in solution, and the degree of ionization of the PE on birefringence properties had already been taken into account [2]. The absolute value of the birefringences depends not only on the geometry but also on the polarizability and anisotropy of the polymer [2]. This theory was proved in 1988 by experiments with PSS in 95 % glycerol at different NaCl concentrations by Fuller and Zebrowski [162]. An increasing ionic strength led to decreasing birefringences in the equilibrium state of the PE solution, and is known to decrease the PE linear structure due to a shielding of the charges [162]. The birefringences were found to increase upon increasing shear modulus [162]. Such behaviour was explained by the authors by a decoiling of the PE chains due to shear force, which is in agreement with MD simulations [111, 162]. An overshoot in the birefringences, observed for low ionic strength, was explained as an effect that emerges when the relaxation time is larger than the reciprocal shear time [162]. Therefore the chains are unable to change their orientation fast enough to the proper position and overshoot in their alignment [162]. This effect was observed to reach its

maximum at 0.002 M NaCl [162]. Light scattering experiments were utilized for a determination of whether PE agglomerates were present or not [162]. Such agglomerates were found in salt free solutions of PSS at concentrations <10 mg/mL [162].

It is interesting to note that not only differences in refractive indexes, but also relaxation times, can be determined by the birefringence method [166]. The laser birefringence detection method is presented in Ref. [166]. Details of the necessary calculations and a comparison of the results obtained compared with rheological methods are also shown are shown in Ref. [166].

Numerous SANS (small angle neutron scattering) experiments with various parameters were used by De Gennes to establish his scaling theory [171, 172]. In these experiments, a peak was found which becomes broader and moves to higher q values (smaller structural sizes) with increasing PE concentration and, in case of increasing salt concentration, a loss of structure [171, 172]. In some cases a completely deuterated PE was used to gain a better contrast of the PE in aqueous solvents [172]. For example, the results of De Gennes and his group's X-ray and neutron scattering were also used by Pfeuty to verify theoretical approaches [53, 89]. The finding that that the scattering peak decreases upon increasing ionic strength was also confirmed by the SANS and SAXS experiments of Essafi et al. [173] and Bordi et al. [174]. The decrease of structure was attributed to an increase of polymer density fluctuations [173]. In scattering experiments with poly(acrylamide-co-sodium-2 acrylamido-2-methylpropanoate sulphate) at different ionic strengths, the scattering peak at $q \sim 0.1$ was determined to be correlated with the charged fraction [173]. The interdiffusion between PEs in PE complex based layers (PEM) was investigated by Loesche et al., using neutron reflectometry and deuterated layers of PSS [175]. A PE interdiffusion of up to 3 bilayers (~ 1.5 to several nanometers depending on the preparation conditions and type of PE) was reported [175].

Hydrophobic modified PE showed, in the scattering experiments of DiCola, a better resolution for the q range and a wider angular range in X-ray than in neutron scattering [168]. The correlation length scaled with c^{-a} where a was 0.5 in the unentangled, and 1.5 in the entangled regime [168]. In the case when hydrophobic micelles overlap, a was determined to be <0.3 [168].

Light scattering experiments were done by Strauss and Smith on inorganic PEs [169]. A linear increase of scattering intensity upon increasing PE concentration was determined, and the total intensity decreased with increasing ionic strength [169]. The most surprising findings were that the scattering factor, B , and the viscosity were in a linear relationship, and that the charge degree of the polyphosphate was so low that the Donnan term was irrelevant [169]. Light scattering experiments to investigate the effect of the PE structure on the diffusion coefficient were done by Drifford [176]. In this publication, an increasing concentration of PSS was reported to cause a decreasing PE structure, which is in agreement with SANS measurements [168, 176]. For the maximum PE concentration investigated, Drifford determined a minimum diffusion coefficient, though it has to be pointed out that the maximum concentration was overall quite low [176].

Ellipsometric measurements of PE multilayers (PEM) comprising PSS and PDDA formed in the presence of salt, showed that PEM exposed to mechanical stress can undergo humidity dependent swelling instead of compression [48]. Such effects were strongly dependent on the preparation of the PE complex, since the composition of the PE complex (polycation to polyanion and counterion ratios) depends on the preparation conditions [69]. In the case of no added salt, the PE film did not show a swelling, but in the case of added salt, it increased in thickness since the polyanion to polycation ratio is not 1:1 and the glass transition point could be surpassed due to the introduction of mechanical energy [39, 69, 71].

5.3 Spectroscopic Approaches

Another way to determine the PE structure is via the excimer (excited dimer) formation of pyrene labeled PE. This way it is possible to determine the coiling of a PE, pH dependent structural change, PE complex formation, interaction with surfactants (these also disrupt excimers), changes in the chemical structure of pyrene labeled PE, and labeling degree of the PE [35]. The details of these methods are listed in review [35]. Changing the pH of pyrene labeled polyethylenimine (PEI) in an aqueous solution from pH 10 to 1.5 causes a general increase in fluorescence, and this is 50 times lower in the excimer than in the monomer [34]. This pyrene fluorescence based PE system not only utilizes the pyrene excimer formation as a label for the PE coiling but also the total fluorescence intensity, since the PEI aminogroups quench the pyrenes fluorescence and therefore serve as PE density indicators [34]. The pyrene coiling index, which describes the degree of intramolecular coiling of a polymer chain was investigated by labeling PAH with pyrene [177]. It is defined as the fluorescence intensity ratio between the excimer to monomer fluorescence intensities [177]. The coiling index was tested by varying the charge density of the weak PE, PAH, by varying the solution pH [177]. The main motivation of using pyrene as a label was to enhance the hydrophobic properties as well as serving as a label for the PE structure [177]. The PE adsorption was found to be in a stretched condition, and in the form of a dense layer on the substrate, in which the PE recoils during the PEM assembly, leading to a coagulated PE complex [177]. More uniform, flatter and smooth films were achieved by increasing the ionic strength of the solution [177]. The typical “odd-even” effect which defines contraction and extension of a PE complex film every second bilayer, due to an intrinsic charge compensation and overcharging processes was also observed in this study [69, 177].

Upon mechanical elongation of PEM comprised of pyrene labeled PSS and non labeled PDDA, the PEs were found to decoil due to the shear forces, which is in line with other investigations and simulations [39, 111, 165]. During this decoiling process an increase in local polarity was detected by the same group, which was, in the case of PEM, assembled without the presence of salt, even higher than the polarity of water [39]. This finding was explained by the water within the PEM

having an ice like structure [39]. Such an explanation is in agreement with other studies that detected an effect of PE on water rotational motions [174]. Upon drying, the PEM shrinks, and the drying stress itself was found to lead to decoiling of the PE chains [39]. Absorption spectra of the same type of film proved the local polarity of PEM produced in presence of salt to be inhomogeneously distributed, while that of PE complexes produced without added salt is homogeneous [41]. The inhomogeneously distributed local polarity of the PEM is probably induced by a larger degree of interdiffusion, stronger hydrophobic surface effects due to shielding of the charges, or due to the preparation mechanism since the PEM film with added salt is softer [41].

Another spectroscopic method which was applied to PE solutions was dielectric spectroscopy. The theory, as well as a short review of the work of Ito [178], was published by Bordi [174]. Frequency ranges from MHz to GHz were used for the investigations of PE solutions [174]. In this frequency range, waters' rotational motion easily keeps up with the dielectric field and the PE is frozen in space, therefore the counterions can be investigated [174]. In addition to the main results for this intermediate range, a change in the maximum absorption frequency of the water (~ 17 MHz) was found when PEs were added to the water, hinting that the PE affects the rotational motion of the water molecules [174]. Below 1 MHz, the PE is relaxed, making it possible to investigate the mode structure of the PE chain [174]. A simple determination of the PE charge fraction and solvent quality, and with additional knowledge (e.g. diffusion coefficient), also the correlation length and polarizability can be determined by this method [174]. The relaxation time of the counterions decreased by factor 200 when the PE concentration was increased by factor 10 in a study of Bordi [174]. The fraction of charged monomers was found to be dependent on the PE type and concentration [174]. Some PEs were found to increase their fraction of charges upon increasing PE concentration like PSS and PAMS, while others like PAMS-80r-PA20 do not [174]. The solvent quality was also found to be affected by the degree of the charged fraction [174].

Dielectric spectra of divinylpyridine (PMVP) from 1 kHz to 2 GHz in water, ethyleneglycole and mixtures of water and ethyleneglycole were investigated by the same authors [179]. The influence of the dielectric increment, relaxation time of the ions as well as the solvent quality were compared with scaling theory, verifying the predicted exponent [179]. Also, the crossover concentration of the PE was in agreement with the predicted values when taking the degree of charged fraction into account [179]. The same authors used this type of measurement to determine the charged fraction of the same PE in ethyleneglycole [179].

6 Polyelectrolyte Complexes and Gels

This section is not intended to be a complete review of this type of materials as there are already other excellent reviews in this field. This section is intended to inform the interested reader of why and how PE complexes are related to

influences in the viscosity. Further, this section shows the reader interesting applications of PE complexes and gels, and where to find further information about this topic.

6.1 Polyelectrolyte Complexes

Aqueous solutions of PE complexes are applied in many fields of science and technology, ranging from drug delivery to coatings for foods [4, 180]. Since a large number of PE complex properties have already been mentioned in previous chapters, this section summarizes work which is closer to applications. In later parts, this section introduces PE complexes based on their applications to show examples of applications and uses of the previously mentioned properties of PEs.

A detailed description of the preparation methods of PEI and PAA complexes was published by Mueller et al. [181] they investigated the influence of the pH, the molecular weight and the mixing with a model drug [181]. When one of the complexes is formed, a small primary complex is formed first, then the small primary complex rapidly agglomerates into a so called secondary PE complex which consists of hundreds of primary complexes [181]. If such small primary complexes are weakly charged, then the resulting secondary particles are usually more strongly charged than the primary complexes [181]. The size of the complex also scales with the molecular weight of the PE, and so the utilization of higher molecular weight PEs results in larger complexes [181].

Three dimensional aggregates of PSS-PDDA complexes were found to exhibit a porous structure with pore sizes on the order of tens of micrometers [182]. Such pores can be closed upon extraction of water in e.g. PEG, where trapped ions stay within the PE complex and cause a re-swelling and restoration of the pores upon reintroduction of water [182]. The PE complex becomes much harder upon drying, with a kinetic component in the first minutes upon applying mechanical force, which then decays [182]. Such a kinetic component, which is caused by chains sliding and decoiling, is in agreement with other studies of PE decoiling in PEM upon elongation and kinetics in PEM-carbon nanotube networks [39, 182, 183].

PE complexes made out of chitosan and xanthan were found to exhibit pH dependent complex formation. At pH 1.5, only 21 % of the PE form complexes, while this increases to 98 % at pH 6.3 [184]. The fibril structures of the complex exhibited sizes from 50 to 100 nm, with pore sizes ranging from 100 nm to 1 μm , making the formed gel like structure suitable for drug and enzyme encapsulation [184]. The enzymes showed a very different behavior—some exhibited an increase in activity, while others a decreased activity in the encapsulated state [184]. This behavior is probably caused by a reaction to steric hindrance as well as a change in the water structure, and dielectric and ionic fields in such a complex network compared to solution.

An interesting review of chitosan PE complexes was written by Hamman, therefore this chapter only briefly summarizes the properties of chitosan and

recommends the review of Hamman for details [5]. Chitosan is a natural, positively charged PE, which is non toxic, cheap and biodegradable; it even can be dissolved in the stomach [5]. Chitosan PE complexes are usually made out of common industrial PE, as well as a large variety of natural PEs, like DNA, xanthan gum, cellulose and its derivates, dextran sulphate, and polyphosphate [5]. A variety of enzymes (e.g. lysocyme), as well as small molecules like insulin were investigated for drug delivery [5, 185]. Other enzymes were investigated for determining structural changes or enzymatic activities in the complex states [5]. Chitin complexes with xanthan gum were even used to form gels, which exhibited the rheological storage modulus of solids [5].

The stability of PE complexes in solution was investigated surprisingly late [186], given that coacervation was first reported in the 1920s [55] and then again in the 1950s [62], and PE structures have been investigated in detail since the 1930s [155, 156]. In recent publications, PEI-Plasmid DNA complexes were freeze-dried at different freezing speeds, freezing with temperature hold steps and at different sucrose concentrations [186]. The temperature hold step was shown to negatively affect the PE complex stability (determined by an increased swelling size after thawing) by mechanically damaging the PE complex due to the formation of ice crystals [186]. Repeating the freezing progress was found to damage the PE complex further [186]. It was further reported by the same authors that agglomeration and complex formation depends on the system's viscosity, and the reaction rate has a critical temperature at -18°C (freezing of ice was decreased due to the introduction of sucrose as well as controlled ice nucleation) [186]. The reaction rate was found to correlate inversely with the system's viscosity, whereby the reaction rate first increases with time, but decreases rapidly, as soon as the viscosity increases [186].

An interesting study about the influence of various PE effects in particles of poly-L-lysine and chitosane on competing polyanions like DNA and xanthan showed no relative preference of polyanions due to the strong influence of electrostatic forces [187]. The release of ethidium bromide as a marker for ion exchange processes was observed to be quite fast $\sim 1\text{ min}$ [187]. Further experiments showed that PE can be destabilized depending on the type of employed PE, showing that the complex stability can be PE specific [187]. A study about the speed of PE complex formation of chitosan/DNA complexes showed 3 effective times [188]. First, the diffusion limited part, which is around 5 ms; then the exponential growth part, which is from 5 to 1,000 ms; and then, after 1 s, the gaussian chain parts reorganize [188]. This study was investigated by employing spectroscopic techniques of fluorescence energy transfer to quantum dots [188].

The coating of food like apples and peaches was investigated by using pectin based complexes, where the PE coating was optimized for permeability of gases like oxygen, carbon dioxide, water vapor (which was minimized), antimicrobial properties, controlled release and their digestive properties [180]. The favored PEM complex was a pectin, alginate calcium matrix [180].

Other possibilities to use PE complexes are to utilize them as viscosity enhancement agents [11]. Carboxymethyl-cellulosis and polyaryl-amide-co-dimethylammonium

chloride in various mass ratios, at different temperatures and shear rates were investigated by Zhang et al. [11] to determine the viscosity enhancement rates of the PE complexes. The viscosity enhancement factors obtained (a factor calculated from differences between theoretical and real viscosity) of up to 20 enable a variety of applications for this type of PE complex like agents in the mineral or oil industry, food processing, pharmaceuticals as well as in the cosmetics or textile industry [11].

Other applications of PE complexes are gene delivery systems, by using PE complexes of positively charged PE and negatively charged DNA [4]. One such system comprises of DNA and PEI (polyethyleneimine) complexes, which were additionally coated with alginate to prevent agglomeration of red blood cells to the complex [4]. Such a system with a complex size of 280–360 nm was shown to exhibit low toxicity (up to 50 volume% of such complexes showed no damage to cells *in vivo* and *in vitro*). The viscosity of the complex solution could be decreased by decreasing the molecular weight of the PE complexes, as the gene delivery of low viscosity complexes was found to be the highest [4]. The swelling and rheological properties of chitosan and xanthan gum were investigated by Magnin et al. [189]. The coacervation time, molecular weight, pH and acetylation degree were investigated [189]. An increase in coacervation time resulted in a higher density of the network and therefore a decreased swelling of the PE complex, as an increasing pH led to increased swelling (except for pH 1, which might be strong enough to cleave the chains) [189]. It is interesting to note that the storage modulus of PE complexes that gelate increased up to 10^4 s, and gels immediately harden out [189]. A mechanical mixing of the complexes or gels induced a structural change of the complex [189]. The swelling degree of the complex gel obtained was found to be between 600 and 20,000 % while exhibiting a porous structure, which is favorable for drug delivery [189].

6.2 Polyelectrolyte Gels

PE gels are used in many applications starting from basic food products (gelatin, agar, pudding) and water treatment to oil production agents for fracking [14]. Like Sect. 6.1, this section is not intended to give a full review since other recent reviews summarize this field already [96]. This section is merely intended to introduce effects between PE complexes, as well as PE with multivalent ions and show applications.

The PE behavior in the presence of multivalent counterions was studied by Ermoshkin [83, 190]. Multivalent ions can act as bridging agents between PEs, where strong short-range attractions can facilitate gelation [83]. Such a gelation can be hindered by long range electrostatic correlations from e.g. non crosslinked monomers or ions [83]. Strong diluted PE solutions preferably segregate, while semidilute PE solutions are able to gelate when the distance between charged monomers is higher than the ion size [83].

For non geochemists, a very surprising application is the use of PE complex gels for subterrain gel formations to facilitate hydrocarbon extraction [14]. For such applications, PE complex nanoparticles made out of chitosan and dextran sulphate with zinc as the crosslinking agent were used [14]. Such complexes showed depending on their concentration and size, an increase in viscosity due to gel formation after 9–12 days [14]. The gel formation could be facilitated up to 60 °C, which allows a large variety of drilling holes, since the temperature in the boreholes spans from 10 to 180 degrees [14]. The same material with additional alginate and PEG (polyethyleneglycole) was used for oral delivery of Insulin in form of acid proof nanogel capsules, where a replacement of the alginate by albumin showed a preferable decrease of the viscosity [185].

A interesting review paper about the fundamental aspects of PE gels, summarizing most of the important achievements in this section was published by Kwon et al. [96]. A short summary is presented here, and the review paper is cited for the readers' convenience. PE gels can achieve a water uptake of up to 2000× their own weight [96]. Due to the high rate of water uptake, they are not only useful as water absorbers, but also as soft and wet cell scaffolds [96]. They also exhibit unique electrical properties, like shape and movement changes upon application of electrical current. This is similar to muscle cells, and they are therefore also called artificial muscles [96]. PE gels can additionally bind their counterions in a so-called potential valley which traps them as the binding energy is larger than the thermal energy [96]. In this context it is not surprising that the water molecules in such potential valleys are hindered in their movement as well [96]. The total number of counterions also increases with the crosslink density, affecting the PE gel's conductivity [96]. The PE units in the gel show a decreasing relaxation time upon increasing concentration, which is comparable to those in solution [96]. Surfactants can not only stick with their apolar group, but also with their ionic group to PE, and even induce a collapse of the gel. Such a collapse can be hindered by adding salt and shielding the electrostatically driven process [96].

7 Conclusion and Outlook

PEs, which were in the past also considered colloids [191], have been investigated for a long time [191], partially under a different name, and sometimes patented rather than published for the general science community. Nanoencapsulations of PE gels were first patented in 1957 in the US, but for different purposes, and have caught attention again just recently as drug delivery agents [96, 191]. The application of PE complexes in medical applications, which is currently considered a hot topic, has been investigated since the 1920s in basic science.

Currently PEs play a very important role in many fields of application, where their thermodynamic and rheological properties are most important. Applications which need fine tuned thermodynamic properties include: drug delivery agents,

cosmetics, lubricants, subterrain gelation agent or food itself. The measurement of these thermodynamic properties imposes no problems with current methods.

Recent scaling theories based on the Rouse and Zimm model are able to explain most effects in PEs like the correlation length, viscous effects, counterion condensation and changes in chain length. However, there are still many unexplained effects, like the inability of the scaling theory to correctly explain the modulus and in some cases the relaxation time. Despite interesting MD and MC simulations in this field there is a fundamental mismatch between the length and time scales between macroscopic and microscopic effects of PEs, rendering these methods incapable of explaining macroscopic effects like viscosity (with a few exceptions for very constrained areas and surfaces). To solve such questions, sufficient field based theories are currently being developed.

Although omitted in this chapter, the PE conductivity and osmotic pressure play an important role for daily applications of PE, like the design of ion exchangers where the degree of crosslinking in PE gels is important to resist the high osmotic pressure [191]. Another promising application in regard to PE conductivity is PE gels and PE complex gels which react to electrical stimuli and might serve as artificial muscles.

Acknowledgments Acknowledgments: This work was supported by the National Nature Science Foundation of China (91027045), 100-talent Program of HIT, China Postdoctoral Science Foundation (2013M531019) and New Century Excellent Talent Program (NCET-11-0800) and Harbin Institute of Technology.

References

1. Barrat, J.L., Joanny, J.F.: Theory of polyelectrolyte solutions. In: Prigogine, I., Rice, S.A. (eds.) *Advances in Chemical Physics, Polymeric Systems*, vol. 94, p. 66. Wiley, Hoboken (1996)
2. Kuhn, W., Künzle, O., Katchalsky, A.: Verhalten polyvalenter Fadenmolekelionen in Lösung. *HCA* **31**, 1994–2037 (1948). doi:[10.1002/hlca.19480310716](https://doi.org/10.1002/hlca.19480310716)
3. Manning, G.S.: The molecular theory of polyelectrolyte solutions with applications to the electrostatic properties of polynucleotides. *Q. Rev. Biophys.* **11**, 179–246 (1978)
4. Jiang, G., Min, S.-H., Hahn, S.K.: DNA/PEI/Alginate polyplex as an efficient *in vivo* gene delivery system. *Biotechnol. Bioprocess Eng.* **12**, 684–689 (2007)
5. Hamman, J.H.: Chitosan based polyelectrolyte complexes as potential carrier materials in drug delivery systems. *Mar Drugs* **8**, 1305–1322 (2010). doi:[10.3390/md8041305](https://doi.org/10.3390/md8041305)
6. Decher, G., Schlenoff, J.: *Multilayer Thin Films: Sequential Assembly of Nanocomposite Materials*, 2nd edn, p. 1112. Wiley, Weinheim (2012)
7. Antonov, Y.A., Moldenaers, P.: Strong polyelectrolyte-induced mixing in concentrated biopolymer aqueous emulsions. *Food Hydrocolloids* **28**, 213–223 (2012). doi:[10.1016/j.foodhyd.2011.12.009](https://doi.org/10.1016/j.foodhyd.2011.12.009)
8. Decher, G., Hong, J.D., Schmitt, J.: Build up of ultrathin multilayer films by a self-assembly process: III. Consecutively alternating adsorption of anionic and cationic polyelectrolytes on charged surfaces. *Thin Solid Films* **210–211**, 831–835 (1992)

9. Caruso, F., Caruso, R.A., Moehwald, H.: Nanoengineering of inorganic and hybrid hollow spheres by colloidal templating. *Science* **282**(80), 1111–1114 (1998). doi:[10.1126/science.282.5391.1111](https://doi.org/10.1126/science.282.5391.1111)
10. Clasen, C., Kulicke, W.-M.: Determination of viscoelastic and rheo-optical material functions of water-soluble cellulose derivatives. *Prog. Polym. Sci.* **26**, 1839–1919 (2001). doi:[10.1016/S0079-6700\(01\)00024-7](https://doi.org/10.1016/S0079-6700(01)00024-7)
11. Zhang, L., Huang, S.: Viscosity properties of homogeneous polyelectrolyte complex solutions from sodium carboxymethyl cellulose and poly (acrylamide- co - dimethyldiallylammonium chloride). *Polym. Int.* **532**, 528–532 (2000)
12. Rehfeldt, F., Tanaka, M.: Hydration forces in ultrathin films of cellulose. *Langmuir* **19**(5), 1467–1473 (2003)
13. Biermann, O.: Molecular Dynamics Simulation Study of Polyelectrolyte Adsorption on Cellulose Surfaces, p. 163. Universität Dortmund, Dortmund (2001)
14. Berkland, C., Cordova, M., Liang, J.-T., Willhite, G.P.: Polyelectrolyte complexes as delayed gelling agents for oil and gas applications, p. 12 (2008)
15. Osawa, F., Imai, N., Kagawa, I.: Theory of strong polyelectrolyte solutions. *J. Polym. Sci. XIII*, 93–111 (1954)
16. Dobrynin, A.V.: Theory and simulations of charged polymers: from solution properties to polymeric nanomaterials. *Curr. Opin. Colloid Interface Sci.* **13**, 376–388 (2008)
17. Fuoss, R.M.: Viscosity function for polyelectrolytes. *J. Polym. Sci.* **3**, 603–604 (1948). doi:[10.1002/pol.1948.120030414](https://doi.org/10.1002/pol.1948.120030414)
18. Borue, V.Y., Erukhimovich, I.Y.: A statistical theory of weakly charged polyelectrolytes: fluctuations, equation of state, and microphase separation. *Macromolecules* **21**, 3240–3249 (1988)
19. Ou, Z., Muthukumar, M.: Entropy and enthalpy of polyelectrolyte complexation: Langevin dynamics simulations. *J. Chem. Phys.* **124**, 154902 (2006). doi:[10.1063/1.2178803](https://doi.org/10.1063/1.2178803)
20. Ariga, K., Ji, Q., Hill, J.P., et al.: Forming nanomaterials as layered functional structures toward materials nanoarchitectonics. *NPG Asia Mater.* **4**, e17 (2012). doi:[10.1038/am.2012.30](https://doi.org/10.1038/am.2012.30)
21. Schönhoff, M.: Layered polyelectrolyte complexes: physics of formation and molecular properties. *Condens. Matter.* **15**, 1781–1808 (2003)
22. Gennes, P.G., Pincus, P., Velasco, R.M., Brochard, F.: Remarks on polyelectrolyte conformation. *J. Phys. Fr.* **37**, 1461–1473 (1976). doi:[10.1051/jphys:0197600370120146100](https://doi.org/10.1051/jphys:0197600370120146100)
23. Michaeli, I., Overbeek, J.T.G., Voorn, M.J.: Phase separation of polyelectrolyte solutions. *J. Polym. Sci.* **23**, 443–450 (1957)
24. Dobrynin, A.V., Colby, R.H., Rubinstein, M.: Scaling theory of polyelectrolyte solutions. *Macromolecules* **28**, 1859–1871 (1995)
25. De Gennes, P.G.: Dynamics of entangled polymer solutions. I. The Rouse model. *Macromolecules* **9**, 587–593 (1975). doi:[10.1021/ma60052a011](https://doi.org/10.1021/ma60052a011)
26. Dobrynin, A., Rubinstein, M.: Theory of polyelectrolytes in solutions and at surfaces. *Prog. Polym. Sci.* **30**, 1049–1118 (2005). doi:[10.1016/j.progpolymsci.2005.07.006](https://doi.org/10.1016/j.progpolymsci.2005.07.006)
27. Colby, R.H.: Structure and linear viscoelasticity of flexible polymer solutions: comparison of polyelectrolyte and neutral polymer solutions. *Rheol. Acta* **49**, 425–442 (2009). doi:[10.1007/s00397-009-0413-5](https://doi.org/10.1007/s00397-009-0413-5)
28. De Gennes, P.G.: Dynamics of entangled polymer solutions. II. Inclusion of hydrodynamic interactions. *Macromolecules* **9**, 594–598 (1976). doi:[10.1021/ma60052a012](https://doi.org/10.1021/ma60052a012)
29. Gennes, P.G.: Scaling Concepts in Polymer Physics. Cornell University Press, Ithaca (1979)
30. Rubinstein, M., Colby, R.H.: Polymer Physics, p. 454. Oxford University, Oxford (2003)
31. Colby, R.H.: Contributions of Nobel Laureate P. G. de Gennes to Polyelectrolyte Solutions, 2008-08-27 (2008)
32. Stramel, R.D., Nguyen, C., Webber, S.E., Rodgers, M.A.J.: Photophysical properties of pyrene covalently bound to photoelectrolytes. *J. Chem. Phys.* **92**, 2934–2938 (1988)
33. Dong, D.C., Winnik, M.A.: The Py scale of solvent polarities. *Can. J. Chem.* **62**, 2560–2565 (1984)

34. Winnik, M.A., Bystryak, S.M., Liu, Z., Siddiqui, J.: Synthesis and characterization of pyrene-labeled poly (ethylenimine). *Macromolecules* **31**, 6855–6864 (1998)
35. Winnik, F.M.: Photophysics of preassociated pyrenes in aqueous polymer solutions and in other organized media. *Chem. Rev.* **93**, 587–614 (1993)
36. Kundagrami, A., Muthukumar, M.: Theory of competitive counterion adsorption on flexible polyelectrolytes: divalent salts. *J. Chem. Phys.* **128**, 244901 (2008). doi:[10.1063/1.2940199](https://doi.org/10.1063/1.2940199)
37. Deshkovski, A., Obukhov, S., Rubinstein, M.: Counterion phase transitions in dilute polyelectrolyte solutions. *Phys. Rev. Lett.* **86**, 2341–2344 (2001). doi:[10.1103/PhysRevLett.86.2341](https://doi.org/10.1103/PhysRevLett.86.2341)
38. Chang, R., Yethiraj, A.: Brownian dynamics simulations of polyelectrolyte solutions with divalent counterions. *J. Chem. Phys.* **118**, 11315–11324 (2003). doi:[10.1063/1.1575731](https://doi.org/10.1063/1.1575731)
39. Frueh, J., Koehler, R., Moehwald, H., Krastev, R.: Changes of the molecular structure in polyelectrolyte multilayers under stress. *Langmuir* **26**, 15516–15522 (2010). doi:[10.1021/la1015324](https://doi.org/10.1021/la1015324)
40. Winnik, M.A., Bystryak, S.M., Liu, Z.: Synthesis and characterization of pyrene-labeled poly (ethylenimine). *Macromolecules* **9297**, 6855–6864 (1998)
41. Frueh, J., Reiter, G., Möhwald, H., et al.: Orientation change of Polyelectrolytes in linearly elongated polyelectrolyte multilayer measured by polarized UV spectroscopy. *Colloid. Surf. A* **415**, 366–373 (2012). doi:<http://dx.doi.org/10.1016/j.colsurfa.2012.08.070>
42. Hinderberger, D., Spiess, H.W., Jeschke, G.: Radial counterion distributions in polyelectrolyte solutions determined by EPR spectroscopy. *Europhys. Lett.* **70**, 102–108 (2005). doi:[10.1209/epl/i2004-10459-y](https://doi.org/10.1209/epl/i2004-10459-y)
43. Flory, P.J.: Thermodynamics of high polymer solutions. *J. Chem. Phys.* **9**, 660 (1941). doi:[10.1063/1.1750971](https://doi.org/10.1063/1.1750971)
44. Flory, P.J.: Thermodynamics of high polymer solutions. *J. Chem. Phys.* **51**, 51–61 (1942). doi:[10.1063/1.1723621](https://doi.org/10.1063/1.1723621)
45. Huggins, M.L.: Solutions of long chain compounds. *J. Chem. Phys.* **9**, 440 (1941). doi:[10.1063/1.1750930](https://doi.org/10.1063/1.1750930)
46. Lindvig, T., Michelsen, M.L., Kontogeorgis, G.M.: A Flory-Huggins model based on the Hansen solubility parameters. *Fluid Phase Equilib.* **203**, 247–260 (2002). doi:[10.1016/S0378-3812\(02\)00184-X](https://doi.org/10.1016/S0378-3812(02)00184-X)
47. Köhler, R., Dönch, I., Ott, P., et al.: Neutron reflectometry study of swelling of polyelectrolyte multilayers in water vapors: influence of charge density of the polycation. *Langmuir* **25**, 11576–11585 (2009). doi:[10.1021/la901508w](https://doi.org/10.1021/la901508w)
48. Frueh, J., Reiter, G., Moehwald, H., et al.: Novel controllable auxetic effect of linearly elongated supported polyelectrolyte multilayer with amorphous structure. *Phys. Chem. Chem. Phys.* **15**, 483–488 (2013). doi:[10.1039/C2CP43302H](https://doi.org/10.1039/C2CP43302H)
49. Safronov, A.P., Zubarev, A.Y.: Flory Huggins parameter of interaction in polyelectrolyte solutions of chitosan and its alkylated derivative. *Polymer (Guildf)* **43**, 743–748 (2002)
50. Alexander-Katz, A., Leibler, L.: Controlling polyelectrolyte equilibria and structure via counterion–solvent interactions. *Soft Matter* **5**, 2198 (2009). doi:[10.1039/b814653e](https://doi.org/10.1039/b814653e)
51. Hansen, C.M.: Hansen Solubility Parameters a User's Handbook, 2nd edn, p. 546. CRC Press, Boca Raton (2007)
52. Hansen, C.M.: The Three Dimensional Solubility Parameter and Solvent Diffusion Coefficient, p. 102 (1967)
53. Pfeuty, P., Velasco, R.M., DE Gennes, P.G.: Conformation properties of one isolated polyelectrolyte chain in D dimensions. *LE J. Phys.* **38**, 5–7 (1977)
54. Tsonev, S., Coalson, R.D., Duncan, A.: Statistical mechanics of charged polymers in electrolyte solutions: a lattice field theory approach. *Phys. Rev. E* **60**, 4257–4267 (1999)
55. Bungenberg, D.E., Jong, H.G., Kruyt, H.R.: Coacervation (Partial Miscibility in Colloid Systems). Chemistry (Easton), p. 9. DWC, Utrecht (1929)
56. Skerjanc, J.: Heats of dilution of polyacrylic acid at various degrees of ionization. *Biophys. Chem.* **1**, 376–380 (1974). doi:[10.1016/0301-4622\(74\)85007-6](https://doi.org/10.1016/0301-4622(74)85007-6)

57. Godec, A., Skerjanc, J.: Enthalpy changes upon dilution and ionization of poly(L-glutamic acid) in aqueous solutions. *J. Phys. Chem. B* **109**, 13363–13367 (2005). doi:[10.1021/jp050234a](https://doi.org/10.1021/jp050234a)
58. Alfrey, T., Berg, P.W., Morawetz, H.: The counterion distribution in solutions of rod-shaped polyelectrolytes. *J. Polym. Sci.* **VII**, 543–547 (1951)
59. Muthukumar, M.: Theory of counter-ion condensation on flexible polyelectrolytes: adsorption mechanism. *J. Chem. Phys.* **120**, 9343–9350 (2004). doi:[10.1063/1.1701839](https://doi.org/10.1063/1.1701839)
60. Kagawa, I., Nagasawa, M.: Statistical thermodynamics. *J. Polym. Sci.* **XVI**, 299–310 (1955)
61. Mandel, M.: Statistical thermodynamics of polyelectrolyte solutions. In: Selegny, E. (ed.) *Polyelectrolytes*, pp. 39–55. D. Reidel Publishing Company, Dordrecht (1974)
62. Overbeek, J.T., Voorn, M.J.: Phase separation in polyelectrolyte solutions; theory of complex coacervation. *J. Cell Physiol. Suppl.* **49**, 7–22 (1957). (discussion, 22–6)
63. Schlenoff, J.B., Rmaile, A.H., Bucur, C.B.: Hydration contributions to association in polyelectrolyte multilayers and complexes: visualizing hydrophobicity. *J. Am. Chem. Soc.* **130**, 13589–13597 (2008). doi:[10.1021/ja802054k](https://doi.org/10.1021/ja802054k)
64. Von Solms, N., Chiew, Y.C.: Analytical integral equation theory for a restricted primitive model of polyelectrolytes and counterions within the mean spherical approximation. II. Radial distribution functions. *J. Chem. Phys.* **118**, 4321 (2003). doi:[10.1063/1.1539842](https://doi.org/10.1063/1.1539842)
65. Bekturov, E.A., Bimend, L.A.: Interpolymer complexes. In: Dusek, K. (ed.) *Advances in Polymer Science*, vol. 41, pp. 99–147. Springer, Berlin (1980)
66. Feng, X., Leduc, M., Pelton, R.: Polyelectrolyte complex characterization with isothermal titration calorimetry and colloid titration. *Colloids Surf. A Physicochem. Eng. Asp.* **317**, 535–542 (2008). doi:[10.1016/j.colsurfa.2007.11.053](https://doi.org/10.1016/j.colsurfa.2007.11.053)
67. Nyström, R., Hedström, G., Gustafsson, J., Rosenholm, J.B.: Mixtures of cationic starch and anionic polyacrylate used for flocculation of calcium carbonate—fluence of electrolytes. *Colloids Surf. A Physicochem. Eng. Asp.* **234**, 85–93 (2004). doi:[10.1016/j.colsurfa.2003.12.012](https://doi.org/10.1016/j.colsurfa.2003.12.012)
68. Steitz, R., Jaeger, W., Klitzing, Rv: Influence of charge density and ionic strength on the multilayer formation of strong polyelectrolytes. *Langmuir* **17**, 4471–4474 (2001)
69. Klitzing, Rv: Internal structure of polyelectrolyte multilayer assemblies. *Phys. Chem. Chem. Phys.* **8**, 5012–5033 (2006)
70. Köhler, K., Shchukin, D.G., Möhwald, H., Sukhorukov, G.B.: Thermal behavior of polyelectrolyte multilayer microcapsules. 1. The effect of odd and even layer number. *J. Phys. Chem. B* **109**, 18250–18259 (2005). doi:[10.1021/jp052208i](https://doi.org/10.1021/jp052208i)
71. Köhler, K., Biesheuvel, P., Weinkamer, R., et al.: Salt-induced swelling-to-shrinking transition in polyelectrolyte multilayer capsules. *Phys. Rev. Lett.* **97**, 3–6 (2006). doi:[10.1103/PhysRevLett.97.188301](https://doi.org/10.1103/PhysRevLett.97.188301)
72. Hugert, A., Caram-Lelham, N., Sundeloef, L.-O.: The effect of charge density and conformation on the polyelectrolyte complex formation between carrageenan and chitosan. *Carbohydr. Polymers* **34**, 149–156 (1997)
73. Kazuo, H., Akashi, S., Furuya, M., Fukuhara, K.: Rapid confirmation and revision of the primary structure of bovine serum albumin by ESIMS and frit-FAB LC/MS. *Biochem. Biophys. Res. Commun.* **173**, 639–646 (1990)
74. Baeurle, Sa: Multiscale modeling of polymer materials using field-theoretic methodologies: a survey about recent developments. *J. Math. Chem.* **46**, 363–426 (2009). doi:[10.1007/s10910-008-9467-3](https://doi.org/10.1007/s10910-008-9467-3)
75. Baeurle, Sa: Grand canonical auxiliary field Monte Carlo: a new technique for simulating open systems at high density. *Comput. Phys. Commun.* **157**, 201–206 (2004). doi:[10.1016/j.comphy.2003.11.001](https://doi.org/10.1016/j.comphy.2003.11.001)
76. Baeurle, S., Charlot, M., Nogovitsin, E.: Grand canonical investigations of prototypical polyelectrolyte models beyond the mean field level of approximation. *Phys. Rev. E* **75**, 011804 (2007). doi:[10.1103/PhysRevE.75.011804](https://doi.org/10.1103/PhysRevE.75.011804)

77. Baeurle, Sa, Nogovitsin, Ea: Challenging scaling laws of flexible polyelectrolyte solutions with effective renormalization concepts. *Polymer (Guildf)* **48**, 4883–4899 (2007). doi:[10.1016/j.polymer.2007.05.080](https://doi.org/10.1016/j.polymer.2007.05.080)
78. Peter, E., Dick, B., Baeurle, Sa: A novel computer simulation method for simulating the multiscale transduction dynamics of signal proteins. *J. Chem. Phys.* **136**, 124112 (2012). doi:[10.1063/1.3697370](https://doi.org/10.1063/1.3697370)
79. Donets, S., Pershin, A., Christlmaier, M.J., Baeurle, Sa: A multiscale modeling study of loss processes in block-copolymer-based solar cell nanodevices. *J. Chem. Phys.* **138**, 094901 (2013). doi:[10.1063/1.4792366](https://doi.org/10.1063/1.4792366)
80. Kuhn, W.: Über die Gestalt fadenförmiger Moleküle in Lösungen. *Kolloid-Z* **68**, 2–15 (1934)
81. Patra, C.N., Yethiraj, A.: Density functional theory for the distribution of small ions around polyions. *J. Phys. Chem. B* **103**, 6080–6087 (1999). doi:[10.1021/jp991062i](https://doi.org/10.1021/jp991062i)
82. Ermoshkin, A.V., Cruz, M.: Gelation in strongly charged polyelectrolytes. *J Polym Sci* **42**, 766–776 (2004). doi:[10.1002/polb.10752](https://doi.org/10.1002/polb.10752)
83. Ermoshkin, a, Olvera de la Cruz, M.: Polyelectrolytes in the presence of multivalent ions: gelation versus segregation. *Phys. Rev. Lett.* **90**, 125504 (2003). doi:[10.1103/PhysRevLett.90.125504](https://doi.org/10.1103/PhysRevLett.90.125504)
84. Deshkovski, A., Obukhov, S., Rubinstein, M.: Counterion phase transitions in dilute polyelectrolyte solutions. *Phys. Rev. Lett.* **86**, 2341–2344 (2001). doi:[10.1103/PhysRevLett.86.2341](https://doi.org/10.1103/PhysRevLett.86.2341)
85. Mjahed, H., Voegel, J.-C., Senger, B., et al.: Hole formation induced by ionic strength increase in exponentially growing multilayer films. *Soft Matter* **5**, 2269 (2009). doi:[10.1039/b819066f](https://doi.org/10.1039/b819066f)
86. Netz, R.R., Andelman, D.: Polyelectrolytes in solution and at surfaces. In: Bard, A., Stratmann, M. (eds.) *Encyclopedia of Electrochemistry*, vol. 1, pp. 282–322. Wiley-VCH Verlag GmbH & Co, KGaA, Weinheim (2002)
87. Adam, M., Delsanti, M.: Viscosity and longest relaxation time of semi-dilute polymer solutions. I. Good Solvent. *J Phys* **44**, 1185–1193 (1983)
88. Adam, M., Delsanti, M.: Viscosity and longest relaxation time of semi-dilute polymer solutions: II. Theta Solvent. *J. Phys.* **45**, 1513–1521 (1984)
89. Pfeuty, P.: Conformation des polyelectrolytes ordre dans les solutions de polyelectrolytes. *J. Phys.* **39**, C2–149–C2–160 (1978). doi:[10.1051/jphyscol:1978227](https://doi.org/10.1051/jphyscol:1978227)
90. Rubinstein, M., Colby, R., Dobrynin, A.: Dynamics of semidilute polyelectrolyte solutions. *Phys. Rev. Lett.* **73**, 2776–2779 (1994)
91. Kavassalis, T., Noolandi, J.: New view of entanglements in dense polymer systems. *Phys. Rev. Lett.* **59**, 2674–2677 (1987)
92. Kavassalis, T.A., Noolandi, J.: A new theory of entanglements and dynamics in dense polymer systems. *Macromolecules* **21**, 2869–2879 (1988)
93. Kavassalis, T.A., Noolandi, J.: Entanglement scaling in polymer melts and solutions. *Macromolecules* **2720**, 2709–2720 (1989)
94. Dobrynin, A.V., Rubinstein, M.: Hydrophobic polyelectrolytes. *Macromolecules* **32**, 915–922 (1999). doi:[10.1021/ma981412j](https://doi.org/10.1021/ma981412j)
95. Dobrynin, A.V., Rubinstein, M.: Counterion condensation and phase separation in solutions of hydrophobic polyelectrolytes. *Macromolecules* **34**, 1964–1972 (2001)
96. Kwon, H.J., Osada, Y., Gong, J.P.: Polyelectrolyte gels—fundamentals and applications. *Polym. J.* **38**, 1211–1219 (2006). doi:[10.1295/polymj.PJ2006125](https://doi.org/10.1295/polymj.PJ2006125)
97. Ermoshkin, aV, Kudlay, aN, Olvera de la Cruz, M.: Thermoreversible crosslinking of polyelectrolyte chains. *J. Chem. Phys.* **120**, 11930–11940 (2004). doi:[10.1063/1.1753573](https://doi.org/10.1063/1.1753573)
98. Kudlay, A., Ermoshkin, A.V., Olvera de la Cruz, M.: Complexation of oppositely charged polyelectrolytes: effect of ion pair formation. *Macromolecules* **37**, 9231–9241 (2004). doi:[10.1021/ma048519t](https://doi.org/10.1021/ma048519t)
99. Gibaud, A., Hazra, S.: X-ray reflectivity and diffuse scattering. *Curr. Sci.* **78**, 11 (2000)

100. Dietrich, S., Haase, A.: Scattering of X-rays and neutrons at interfaces. *Phys. Rep.* **260**, 1–138 (1995)
101. Alder, B.J., Wainwright, T.E.: Studies in molecular dynamics. I. General Method. *J Chem Phys* **31**, 459 (1959). doi:[10.1063/1.1730376](https://doi.org/10.1063/1.1730376)
102. Metropolis, N., Rosenbluth, A.W., Rosenbluth, M.N., et al.: Equation of state calculations by fast computing machines. *J. Chem. Phys.* **21**, 1087 (1953). doi:[10.1063/1.1699114](https://doi.org/10.1063/1.1699114)
103. Müller-Plathe, F.: Coarse-graining in polymer simulation: from the atomistic to the mesoscopic scale and back. *Chem. Phys. Chem.* **3**, 755–769 (2002)
104. Peter, C., Kremer, K.: Multiscale simulation of soft matter systems—from the atomistic to the coarse-grained level and back. *Soft Matter* **5**, 4357 (2009). doi:[10.1039/b912027k](https://doi.org/10.1039/b912027k)
105. Feynman, R.P.: Simulating physics with computers. *Int. J. Theor. Phys.* **21**, 467–488 (1982). doi:[10.1007/BF02650179](https://doi.org/10.1007/BF02650179)
106. Simon, D.R.: On the power of quantum computation. In: *Proceedings 35th Annual Symposium on Foundations of Computer Science*, pp. 116–123. Santa Fe, NM (1994)
107. D-wave.: D-wave company homepage. Homepage http://www.dwavesys.com/en/dw_homepage.html (2013). Accessed 30 Jul 2013
108. Perdomo-Ortiz, A., Dickson, N., Drew-Brook, M., et al.: Finding low-energy conformations of lattice protein models by quantum annealing. *Sci. Rep.* **2**, 571 (2012). doi:[10.1038/srep00571](https://doi.org/10.1038/srep00571)
109. De Pablo, J.J.: Coarse-grained simulations of macromolecules: from DNA to nanocomposites. *Annu. Rev. Phys. Chem.* **62**, 555–574 (2011). doi:[10.1146/annurev-physchem-032210-103458](https://doi.org/10.1146/annurev-physchem-032210-103458)
110. Bouvard, J.L., Ward, D.K., Hossain, D., et al.: Review of hierarchical multiscale modeling to describe the mechanical behavior of amorphous polymers. *J. Eng. Mater. Technol.* **131**, 041206 (2009). doi:[10.1115/1.3183779](https://doi.org/10.1115/1.3183779)
111. Pierleoni, C., Ryckaert, J.-P.: Deformation and orientation of flexible polymers in solution under shear flow: a new picture for intermediate reduced shear rates. *Macromolecules* **28**, 5097–5108 (1995). doi:[10.1021/ma00118a044](https://doi.org/10.1021/ma00118a044)
112. Carrillo, J.-M.Y., Russano, D., Dobrynin, A.V.: Friction between brush layers of charged and neutral bottle-brush macromolecules. Molecular dynamics simulations. *Langmuir* **27**, 14599–14608 (2011). doi:[10.1021/la203525r](https://doi.org/10.1021/la203525r)
113. Radeva, T.: *Physical Chemistry of Polyelectrolytes*, p. 936. CRC Press, Boca Raton (2001)
114. Alarcón, F., Pérez-Hernández, G., Pérez, E., Gama Goicochea, a: Coarse-grained simulations of the salt dependence of the radius of gyration of polyelectrolytes as models for biomolecules in aqueous solution. *Eur. Biophys. J.* **42**, 661–672 (2013). doi:[10.1007/s00249-013-0915-z](https://doi.org/10.1007/s00249-013-0915-z)
115. Dobrynin, a: Theory and simulations of charged polymers: From solution properties to polymeric nanomaterials. *Curr. Opin. Colloid Interface Sci.* **13**, 376–388 (2008). doi:[10.1016/j.cocis.2008.03.006](https://doi.org/10.1016/j.cocis.2008.03.006)
116. Da Silva, F.L.B., Lund, M., Jönsson, B., Akesson, T.: On the complexation of proteins and polyelectrolytes. *J. Phys. Chem. B* **110**, 4459–4464 (2006). doi:[10.1021/jp054880l](https://doi.org/10.1021/jp054880l)
117. Edgecombe, S., Linse, P.: Monte Carlo simulations of cross-linked polyelectrolyte gels with oppositely charged macroions. *Langmuir* **22**, 3836–3843 (2006). doi:[10.1021/la053193i](https://doi.org/10.1021/la053193i)
118. Edgecombe, S., Linse, P.: Monte Carlo simulation of polyelectrolyte gels: effects of polydispersity and topological defects. *Macromolecules* **40**, 3868–3875 (2007). doi:[10.1021/ma0700633](https://doi.org/10.1021/ma0700633)
119. Carrillo, J.-M.Y., Dobrynin, A.V.: Detailed molecular dynamics simulations of a model NaPSS in water. *J. Phys. Chem. B* **114**, 9391–9399 (2010). doi:[10.1021/jp101978k](https://doi.org/10.1021/jp101978k)
120. Detcheverry, Fa., Pike, D.Q., Nagpal, U., et al.: Theoretically informed coarse grain simulations of block copolymer melts: method and applications. *Soft Matter* **5**, 4858 (2009). doi:[10.1039/b911646j](https://doi.org/10.1039/b911646j)
121. Becker, N., Everaers, R.: From rigid base pairs to semiflexible polymers: Coarse-graining DNA. *Phys. Rev. E* **76**, 021923 (2007). doi:[10.1103/PhysRevE.76.021923](https://doi.org/10.1103/PhysRevE.76.021923)

122. Chang, R., Yethiraj, A.: Strongly charged flexible polyelectrolytes in poor solvents: molecular dynamics simulations with explicit solvent. *J. Chem. Phys.* **118**, 6634 (2003). doi:[10.1063/1.1558312](https://doi.org/10.1063/1.1558312)
123. Ou, Z., Muthukumar, M.: Langevin dynamics of semiflexible polyelectrolytes: rod-toroid-globule-coil structures and counterion distribution. *J. Chem. Phys.* **123**, 074905 (2005). doi:[10.1063/1.1940054](https://doi.org/10.1063/1.1940054)
124. Liao, Q., Dobrynin, A.V., Rubinstein, M.: Counterion-correlation-induced attraction and necklace formation in polyelectrolyte solutions: theory and simulations. *Macromolecules* **39**, 1920–1938 (2006)
125. Stevens, M.J., Kremer, K.: The nature of flexible linear polyelectrolytes in salt free solution: a molecular dynamics study. *J. Chem. Phys.* **103**, 1669 (1995). doi:[10.1063/1.470698](https://doi.org/10.1063/1.470698)
126. Micka, U., Holm, C., Kremer, K.: Strongly charged solvents: flexible polyelectrolytes in poor solvents: molecular dynamics simulations. *Langmuir* **15**, 4033–4044 (1999)
127. Limbach, H.J., Holm, C.: End effects of strongly charged polyelectrolytes: a molecular dynamics study. *J. Chem. Phys.* **114**, 9674 (2001). doi:[10.1063/1.1370077](https://doi.org/10.1063/1.1370077)
128. Liao, Q., Dobrynin, A.V., Rubinstein, M.: Molecular dynamics simulations of polyelectrolyte solutions: nonuniform stretching of chains and scaling behavior. *Macromol.* **36**, 3386–3398 (2003). doi:[10.1021/ma025995f](https://doi.org/10.1021/ma025995f)
129. Sandberg, D.J., Carrillo, J.-M.Y., Dobrynin, A.V.: Molecular dynamics simulations of polyelectrolyte brushes: from single chains to bundles of chains. *Langmuir* **23**, 12716–12728 (2007). doi:[10.1021/la702203c](https://doi.org/10.1021/la702203c)
130. Russano, D., Carrillo, J.-M.Y., Dobrynin, A.V.: Interaction between brush layers of bottle-brush polyelectrolytes: molecular dynamics simulations. *Langmuir* **27**, 11044–11051 (2011). doi:[10.1021/la2018067](https://doi.org/10.1021/la2018067)
131. Micka, U., Kremer, K.: Strongly charged flexible polyelectrolytes in poor solvents—from stable spheres to necklace chains. *Eur. Lett.* **49**, 189–195 (2000)
132. Limbach, H.J., Holm, C.: Conformational properties of poor solvent polyelectrolytes. *Comput. Phys. Commun.* **147**, 321–324 (2002). doi:[10.1016/S0010-4655\(02\)00295-3](https://doi.org/10.1016/S0010-4655(02)00295-3)
133. Limbach, H.J., Holm, C., Kremer, K.: Structure of polyelectrolytes in poor solvent. *Eur. Lett.* **60**, 566–572 (2002)
134. Limbach, H.J., Holm, C., Kremer, K.: Conformations and solution structure of polyelectrolytes in poor solvent. *Macromol. Symp.* **211**, 43–54 (2004). doi:[10.1002/masy.200450703](https://doi.org/10.1002/masy.200450703)
135. Limbach, H.J., Holm, C.: Single-chain properties of polyelectrolytes in poor solvent. *J. Phys. Chem. B* **107**, 8041–8055 (2003)
136. Jeon, J., Dobrynin, A.V.: Necklace globule and counterion condensation. *Macromolecules* **40**, 7695–7706 (2007). doi:[10.1021/ma071005k](https://doi.org/10.1021/ma071005k)
137. Wang, Z., Rubinstein, M.: Regimes of conformational transitions of a diblock polyampholyte. *Macromolecules* **39**, 5897–5912 (2006). doi:[10.1021/ma0607517](https://doi.org/10.1021/ma0607517)
138. Carrillo, J.-M.Y., Dobrynin, A.V.: Polyelectrolytes in salt solutions: molecular dynamics simulations. *Macromolecules* **44**, 5798–5816 (2011). doi:[10.1021/ma2007943](https://doi.org/10.1021/ma2007943)
139. Konieczny, M., Likos, C.N., Löwen, H.: Soft effective interactions between weakly charged polyelectrolyte chains. *J. Chem. Phys.* **121**, 4913–4924 (2004). doi:[10.1063/1.1781111](https://doi.org/10.1063/1.1781111)
140. Jeon, J., Dobrynin, A.V.: Molecular dynamics simulations of polyampholyte-polyelectrolyte complexes in solutions. *Macromolecules* **38**, 5300–5312 (2005)
141. Jeon, J., Dobrynin, A.V.: Molecular dynamics simulations of polyelectrolyte-polyampholyte complexes. Effect of solvent quality and salt concentration. *J. Phys. Chem. B* **110**, 24652–24665 (2006). doi:[10.1021/jp064288b](https://doi.org/10.1021/jp064288b)
142. Jeon, J., Panchagnula, V., Pan, J., Dobrynin, A.V.: Molecular dynamics simulations of multilayer films of polyelectrolytes and nanoparticles. *Langmuir* **22**, 4629–4637 (2006). doi:[10.1021/la053444n](https://doi.org/10.1021/la053444n)
143. Patel, Pa, Jeon, J., Mather, P.T., Dobrynin, A.V.: Molecular dynamics simulations of layer-by-layer assembly of polyelectrolytes at charged surfaces: effects of chain degree of

- polymerization and fraction of charged monomers. *Langmuir* **21**, 6113–6122 (2005). doi:[10.1021/la050432t](https://doi.org/10.1021/la050432t)
144. Patel, Pa, Jeon, J., Mather, P.T., Dobrynin, A.V.: Molecular dynamics simulations of multilayer polyelectrolyte films: effect of electrostatic and short-range interactions. *Langmuir* **22**, 9994–10002 (2006). doi:[10.1021/la061658e](https://doi.org/10.1021/la061658e)
145. Carrillo, J.-M.Y., Dobrynin, A.V.: Molecular dynamics simulations of polyelectrolyte adsorption. *Langmuir* **23**, 2472–2482 (2007). doi:[10.1021/la063079f](https://doi.org/10.1021/la063079f)
146. Carrillo, J.-M.Y., Dobrynin, A.V.: Layer-by-layer assembly of polyelectrolyte chains and nanoparticles on nanoporous substrates: molecular dynamics simulations. *Langmuir* **28**, 1531–1538 (2012). doi:[10.1021/la203940w](https://doi.org/10.1021/la203940w)
147. Mann, Ba, Holm, C., Kremer, K.: Swelling of polyelectrolyte networks. *J. Chem. Phys.* **122**, 154903 (2005). doi:[10.1063/1.1882275](https://doi.org/10.1063/1.1882275)
148. Mann, Ba, Everaers, R., Holm, C., Kremer, K.: Scaling in polyelectrolyte networks. *Europhys. Lett.* **67**, 786–792 (2004). doi:[10.1209/epl/i2004-10121-x](https://doi.org/10.1209/epl/i2004-10121-x)
149. Lu, Z.-Y., Hentschke, R.: Computer simulation study on the swelling of a polyelectrolyte gel by a Stockmayer solvent. *Phys. Rev. E* **67**, 061807 (2003). doi:[10.1103/PhysRevE.67.061807](https://doi.org/10.1103/PhysRevE.67.061807)
150. Liao, Q., Carrillo, J.Y., Dobrynin, A.V., Rubinstein, M.: Rouse dynamics of polyelectrolyte solutions: molecular dynamics study. *Macromolecules* **40**, 7671–7679 (2007)
151. Zhou, T., Chen, S.B.: Computer simulations of diffusion and dynamics of short-chain polyelectrolytes. *J. Chem. Phys.* **124**, 034904 (2006). doi:[10.1063/1.2161205](https://doi.org/10.1063/1.2161205)
152. Krause, W.E., Tan, J.S., Colby, R.H.: Semidilute solution rheology of polyelectrolytes with no added salt. *J. Polym. Sci. B* **37**, 3429–3437 (1999). doi:[10.1002/\(SICI\)1099-0488\(19991215\)37:24<3429:AID-POLB5>3.0.CO;2-E](https://doi.org/10.1002/(SICI)1099-0488(19991215)37:24<3429:AID-POLB5>3.0.CO;2-E)
153. Yin, D.-W., Yan, Q., de Pablo, J.J.: Molecular dynamics simulation of discontinuous volume phase transitions in highly-charged crosslinked polyelectrolyte networks with explicit counterions in good solvent. *J. Chem. Phys.* **123**, 174909 (2005). doi:[10.1063/1.2102827](https://doi.org/10.1063/1.2102827)
154. Sun, F., Dobrynin, A., Shirvanyants, D., et al.: Flory theorem for structurally asymmetric mixtures. *Phys. Rev. Lett.* **99**, 137801 (2007). doi:[10.1103/PhysRevLett.99.137801](https://doi.org/10.1103/PhysRevLett.99.137801)
155. Heidelberger, M., Kendall, F.E.: Some physicochemical properties of specific polysaccharides. *J. Biol. Chem.* **95**, 127–142 (1932)
156. Staudinger, H.: Die hochmolekularen organischen Verbindungen. **540** (1932). doi:[10.1002/bbpc.19320381231](https://doi.org/10.1002/bbpc.19320381231)
157. Staudinger, H.: Der Aufbau der hochmolekularen organischen Verbindungen. *Naturwissenschaften* **22**, 65–71 (1934)
158. Fuoss, R.M., Strauss, U.P.: Polyelectrolytes. II. Poly-4-vinylpyridonium chloride and poly-4-vinyl-N-n-butylpyridonium bromide. *J. Polym. Sci.* **3**, 246–263 (1948). doi:[10.1002/pol.1948.120030211](https://doi.org/10.1002/pol.1948.120030211)
159. Cohen, J., Priel, Z., Rabin, Y.: Viscosity of dilute polyelectrolyte solutions. *J. Chem. Phys.* **88**, 7111 (1988). doi:[10.1063/1.454361](https://doi.org/10.1063/1.454361)
160. Terayama, H., Wall, F.T.: Reduced viscosities of polyelectrolytes in the presence of added salts. *J. Polym. Sci. XVI*, 357–365 (1955). doi:[10.1002/pol.1955.120168224](https://doi.org/10.1002/pol.1955.120168224)
161. Prini, R.F., Lagos, A.E.: Tracer diffusion, electrical conductivity, and viscosity of aqueous solutions of poly styrenesulfonates. *J. Polym. Sci. A* **2**, 2917–2928 (1964). doi:[10.1002/pol.1964.100020640](https://doi.org/10.1002/pol.1964.100020640)
162. Zebrowski, B.E.: Rheo-optical studies of polyelectrolyte solutions in simple shear flow. *J. Rheol. (N Y N Y)* **29**, 943 (1985). doi:[10.1122/1.549823](https://doi.org/10.1122/1.549823)
163. Zimm, B.H.: Dynamics of polymer molecules in dilute solution: viscoelasticity, flow birefringence and dielectric loss. *J. Chem. Phys.* **24**, 269 (1956). doi:[10.1063/1.1742462](https://doi.org/10.1063/1.1742462)
164. Boris, D.C., Colby, R.H.: Rheology of sulfonated polystyrene solutions. *Macromolecules* **31**, 5746–5755 (1998)
165. Colby, R.H., Boris, D.C., Krause, W.E., Dou, S.: Shear thinning of unentangled flexible polymer liquids. *Rheol. Acta* **46**, 569–575 (2007). doi:[10.1007/s00397-006-0142-y](https://doi.org/10.1007/s00397-006-0142-y)

166. Chen, S., Archer, L.A.: Relaxation dynamics of salt-free polyelectrolyte solutions using flow birefringence and rheometry. *J. Polym. Sci. B* **37**, 825–835 (1998). doi:[10.1002/\(SICI\)1099-0488\(19990415\)37:8<825::AID-POLB8>3.0.CO;2-H/pdf](https://doi.org/10.1002/(SICI)1099-0488(19990415)37:8<825::AID-POLB8>3.0.CO;2-H)
167. Dou, S., Colby, R.H.: Charge density effects in salt-free polyelectrolyte solution rheology. *J. Polym. Sci. Part B* **44**, 2001–2013 (2006). doi:[10.1002/polb](https://doi.org/10.1002/polb)
168. Di Cola, E., Plucktaveesak, N., Waigh, T., et al.: Structure and dynamics in aqueous solutions of amphiphilic sodium maleate-containing alternating copolymers. *Macromolecules* **37**, 8457–8465 (2004). doi:[10.1021/ma049260h](https://doi.org/10.1021/ma049260h)
169. Strauss, U.P., Smith, E.H., Winema, P.L.: Polyphosphates as polyelectrolytes. I. Light scattering and viscosity of sodium. *J. Am. Chem. Soc.* **75**, 3935–3940 (1953). doi:[10.1021/ja01112a017](https://doi.org/10.1021/ja01112a017)
170. Strauss, U.P., Smith, E.H.: Polyphosphates as polyelectrolytes. II. Viscosity of aqueous solutions of Graham's salts. *JACS* **75**, 6186–6188 (1953). doi:[10.1021/ja01120a023](https://doi.org/10.1021/ja01120a023)
171. Nierlich, M., Williams, C.E., Boué, F., et al.: Small angle neutron scattering by semi-dilute solutions of polyelectrolyte. *J. Phys.* **40**, 701–704 (1979). doi:[10.1051/jphys:01979004007070100](https://doi.org/10.1051/jphys:01979004007070100)
172. Williams, C.E., Nierlich, M., Cotton, J.P., et al.: Polyelectrolyte solutions: intrachain and interchain correlations observed by SANS. *J. Polym. Sci. Polym. Lett. Ed.* **17**, 379–384 (1979). doi:[10.1002/pol.1979.130170608](https://doi.org/10.1002/pol.1979.130170608)
173. Essafi, W., Lafuma, F., Williams, C.E.: Structural evidence of charge renormalization in semi-dilute solutions of highly charged polyelectrolytes. *Eur. Phys. J. B* **9**, 261–266 (1999). doi:[10.1007/s100510050765](https://doi.org/10.1007/s100510050765)
174. Bordi, F., Cametti, C., Tan, J.S., et al.: Determination of polyelectrolyte charge and interaction with water using dielectric spectroscopy. *Macromolecules* **35**, 7031–7038 (2002). doi:[10.1021/ma020116a](https://doi.org/10.1021/ma020116a)
175. Lösche, M., Schmitt, J., Decher, G., et al.: Detailed structure of molecularly thin polyelectrolyte multilayer films on solid substrates as revealed by neutron reflectometry. *Macromolecules* **31**, 8893–8906 (1998). doi:[10.1021/ma980910p](https://doi.org/10.1021/ma980910p)
176. Drifford, M., Dalbiez, J.-P.: Light scattering by dilute solutions of salt-free polyelectrolytes. *J. Phys. Chem.* **88**, 5368–5375 (1984)
177. Park, J., Hammond, P.T.: Polyelectrolyte multilayer formation on neutral hydrophobic surfaces. *Macromolecules* **38**, 10542–10550 (2005)
178. Ito, K., Yagi, A., Ookubo, N., Hayakawa, R.: Crossover behavior in high-frequency dielectric relaxation of linear polyions in dilute and semidilute solutions. *Macromolecules* **23**, 857–862 (1990). doi:[10.1021/ma00205a027](https://doi.org/10.1021/ma00205a027)
179. Bordi, F., Cametti, C., Sennato, S., et al.: Dielectric scaling in polyelectrolyte solutions with different solvent quality in the dilute concentration regime. *Phys. Chem. Chem. Phys.* **8**, 3653–3658 (2006). doi:[10.1039/b605624e](https://doi.org/10.1039/b605624e)
180. Marudova, M., Rashkov, I.: Pectin and its polyelectrolyte complexes in food coating and encapsulation of food-stuffs. *Internet* **15**
181. Müller, M., Keßler, B., Fröhlich, J., et al.: Polyelectrolyte complex nanoparticles of poly(ethyleneimine) and poly(acrylic acid): preparation and applications. *Polymers (Basel)* **3**, 762–778 (2011). doi:[10.3390/polym3020762](https://doi.org/10.3390/polym3020762)
182. Hariri, H.H., Lehaf, A.M., Schlenoff, J.B.: Mechanical properties of osmotically stressed polyelectrolyte complexes and multilayers: water as a plasticizer. *Macromolecules* **45**, 9364–9372 (2012). doi:[10.1021/ma302055m](https://doi.org/10.1021/ma302055m)
183. Frueh, J., Nakashima, N., He, Q., Moehwald, H.: Effect of linear elongation on carbon nanotube and polyelectrolyte structures in PDMS-supported nanocomposite LbL films. *J. Phys. Chem. B* **116**, 12257–12262 (2012). doi:[10.1021/jp3071458](https://doi.org/10.1021/jp3071458)
184. Dumitriu, S., Magny, P., Montane, D., et al.: Polyionic hydrogels obtained by complexation between Xanthan and Chitosan: their properties as supports for enzyme immobilization. *J. Bioact. Compat. Polym.* **9**, 184–209 (1994). doi:[10.1177/088391159400900205](https://doi.org/10.1177/088391159400900205)
185. Soares, A.F., Oliveira, L.M., Reis, C., Veiga, F.: Characterization of polyelectrolyte interactions of alginate core nanospheres coated with polyelectrolytes and acid-protective

- biomaterials for oral insulin delivery. In: XVth International Workshop on Bioencapsulation, Vienna, Au. 6–8 Sept 2007, pp 10–13. Impascience.eu, Vienna (2007)
186. Kasper, J.C., Pikal, M.J., Friess, W.: Investigations on polyplex stability during the freezing step of lyophilization using controlled ice nucleation—the importance of residence time in the low-viscosity fluid state. *J. Pharm. Sci.* **102**, 9–11 (2012). doi:[10.1002/jps](https://doi.org/10.1002/jps)
187. Danielsen, S., Maurstad, G., Stokke, B.T.: DNA-polycation complexation and polyplex stability in the presence of competing polyanions. *Biopolymers* **77**, 86–97 (2004). doi:[10.1002/bip.20170](https://doi.org/10.1002/bip.20170)
188. Ho, Y.-P., Chen, H.H., Leong, K.W., Wang, T.-H.: The convergence of quantum-dot-mediated fluorescence resonance energy transfer and microfluidics for monitoring DNA polyplex self-assembly in real time. *Nanotechnology* **20**, 095103 (2009). doi:[10.1088/0957-4484/20/9/095103](https://doi.org/10.1088/0957-4484/20/9/095103)
189. Magnin, D.: Physicochemical and structural characterization of a polyionic matrix of interest in biotechnology, in the pharmaceutical and biomedical fields. *Carbohydr. Polym.* **55**, 437–453 (2004). doi:[10.1016/j.carbpol.2003.11.013](https://doi.org/10.1016/j.carbpol.2003.11.013)
190. Ermoshkin, A.V., Cruz, M.: Gelation in strongly charged polyelectrolytes*. *J. Polym. Sci. Part B* **42**, 766–776 (2004)
191. Overbeek, J.T.G.: Polyelectrolytes, past, present and future. *Pure Appl. Chem.* **46**, 91–101 (1976). doi:[10.1351/pac197646020091](https://doi.org/10.1351/pac197646020091)

Polyelectrolyte: Science and Application

Emel Akyol, Semra Kirboga and Mualla Öner

Abstract Polyelectrolytes, which are a macromolecule dissolved in water or polar solvent, have gained a wide attention among scientists and engineers for their wide application areas. Their different properties have allowed them to be used in many areas such as soap, body lotions, electrochromic devices, solid-state reference electrode systems, fuel cell exchange membranes, water treatment, waste treatment, paper production, corrosion protection, fuel cells, electrodialysis, contact lenses, membrane-based separations, drug delivery, and genetic science. Biocompatible polyelectrolytes are also utilized in biosensors and biomolecular recognition systems. Layer-by-layer (LbL) technique can be used to produce polyelectrolyte multilayer. Severe substrate such as gold, quartz, silicon, glass, plastic, stainless steel can be used in LbL technique. LbL technique is reproducible, cost-effective, and environmentally-friendly method. The characteristic properties of polyelectrolyte depend on the interaction between electrostatic forces. The degree of polymer charge can modify the electrostatic interactions. We examine the scaling theory according to Gennes et al. and Beurle and Nogovitsin in this chapter. After having discussed the scaling theory, we provide a basic introduction to properties of the neutron scattering and dynamic light scattering. In the end, we analyzed biopolymers and ionomers briefly.

Polyelectrolytes (PEs) are generally defined as macromolecules, which when dissolved in water, dissociate to give highly charged polymeric molecules [1–3]. As another definition, polyelectrolytes are polymers carrying either positively or negatively charged ionizable groups. These groups dissociate under appropriate conditions, and leaving ions on the chain and counter ions in the solution. Examples of polyelectrolytes include polystyrene sulfonate, polyacrylic and polymethacrylic acids and their salts. DNA, proteins, nucleic acids, polysaccharides and other polyacids are given example to the natural polyelectrolytes [4–8].

E. Akyol · S. Kirboga · M. Öner (✉)
Chemical Engineering Department, Yildiz Technical University,
Davutpasa Campus, 34210 Istanbul, Turkey
e-mail: oner@yildiz.edu.tr

Polyelectrolytes are well known to play a vital role in nature and technology. PEs finds widespread use as solubilizing agents, phase separation agents, and rheological property modifiers in daily life and technological applications. However, despite of their fundamental and practice importance, PEs systems still remain only poorly understood. This relates to the fact that their chemistry and physics are influenced by many controlling parameters, such as molecular weight, salt concentration, pH of the solution, etc. [9, 10].

1 Recent Research on Polyelectrolyte

A polymer, large molecules, is made of linked smaller molecules. Firstly, the “rubbery” properties of rubber trees were discovered by the Mayans. Then, polymers have been used in many application areas such as plastic, fiber, electronic, rubber, etc. [11].

A polyelectrolyte is a macromolecule dissolved in water or polar solvent and gets a large number of elementary charges distributed along the macromolecular chain [1–14]. In fact, macromolecules have been used in nature for a long time. Natural polymers consisting of polypeptides, proteins, DNA and RNA are found in human body to arrange function of body [1, 3, 5]. DNA carrying millions of charged groups is the best known bio-polyelectrolyte [15]. Polyelectrolytes are distinguished from neutral polymer with the presence of covalently attached ionic groups [3, 5]. Polyelectrolytes carry charged or chargeable groups [16]. The degree of dissociation is controlled by some parameters such as solution pH, temperature, the ionic strength [16, 17]. Weak polyelectrolytes dissociate more or less depending up on pH whereas strong polyelectrolytes dissociate completely independent of pH of the solution [2]. An anionic polymer has changes in ionization from pH below the pKa to above the pKa [18]. High dielectric constant media causes to dissolution of polyelectrolyte and it dissociates into polyions each with small ions [19]. Electrostatic forces affect the solution behavior of polyelectrolyte [16]. The properties of polyelectrolyte are related to their macromolecular and electrolyte properties. Polyelectrolytes have been a big attention among scientists and engineering for their wide application areas [20]. They can be utilized in a large number of applications such as soap, body lotions, electrochromic devices, solid-state reference electrode systems, fuel cell exchange membranes, water treatment, waste treatment, paper production, corrosion protection, fuel cells, electrodialysis because of their different properties [11, 14, 15, 16]. Polyelectrolytes can be used genetic science because of their high charge density and biocompatibility [15]. They are biocompatible materials for medical applications in contact with blood and other biological fluids [17]. Common polyelectrolyte examples are poly(vinyl sulfonic acid), poly(acrylic acid), poly-meric bases poly(vinylamine), poly(vinyl pyridine) [13]. The properties of polyelectrolyte have not been well understood in spite of development in theoretical and experimental studies.

In 1966, a new technique related with colloidal oppositely charged particles was explained. In this technique, charged particles could be assembled into layer by layer film. Similar technique was applied for polyelectrolytes multilayer assembly [12, 14]. The systematic way of the technique was reported in 1997 and has attracted a big interest in nature or in field of chemistry. Alternately dipping the substrate into two oppositely charged polyelectrolyte is the classical method to form polyelectrolyte multilayer. The first layer can be obtained by dipping the substrate having positive charges into polyanion solution, then into polycation solution. Electrostatic interactions between oppositely charge polyelectrolyte or/ and colloidal particles is important for this technique [12]. Polyelectrolyte multilayers have been used in contact lenses as hydrophilic coating. In addition, they could be used in food-wrapper to prevent bacterial on fruits and vegetables [17].

Layer by layer (LbL) technique could be used for several materials such as polymers, clay, proteins, colloids, carbon nanotubes and nanoparticles. Severe substrate such as gold, quartz, silicon, glass, plastic, stainless steel can be used in LbL technique. Polyelectrolyte multilayers (PEMs) can be arranged from proteins, DNA, inorganic platelets, dendrimers. The electrostatic interaction between the surface and polyelectrolyte is the driving force to form PEMs. The degree of polymer charge can modify the electrostatic interactions. Polymer charge can be altered by changing pH or using ionic groups. At high salt concentration, the electrostatic repulsion between different polyelectrolyte segments is reduced whereas the electrostatic attraction between polyelectrolyte and oppositely charged surface is reduced. Small molecules transport to the surface and the confirmation of polymer can be changed with associated arrangement of chain at the surface. Many layers can be built by assembling into surface. LbL technique is reproducible, cost effective and environmentally friendly method carried out at room temperature. Multilayer formation is affected by polymer charge density. A multilayer of polystyrene sulfonate (PSS) and copolymer poly(diallyl-dimethyl-ammoniumchloride-*stat*-N-methyl-N-vinylacetamide) P(DADMAC-*stat*-NMVA) can be composed of polyanion (PSS) and copolymer of cationic DADMAC and N-methyl-N-vinylacetamide (NMVA). The film thickness decreased with increasing the charge density because of differences in chain confirmation. The addition of salt to solution can increase the thickness of multilayer. Salt causes to alter the confirmation of polymer chains, thus changing the thickness of multilayer [21].

The adsorption of DNA films assembled from oligonucleotides composed of two homopolymeric diblocks (polyA_nG_n and polyT_nC_n) were studied in the presence of salt. The growth of film increased with salt concentration [22]. The studies on polyelectrolyte complexation have offered wide applications such as water treatment, surface modification, drug delivery system, tissue engineering. To understand the formation of protein-polyelectrolyte complex is important due to the interaction between polyanions or polycations with protein macromolecules or polyelectrolytes. Soluble complexes can be formed and amorphous can be precipitated with the interaction of molecules. Complex formation is generally performed in the bulk solutions. Potentiometry, conductometry, viscosimetry, turbidimetry, or electrophoretic and quasi-elastic light scattering are used to follow

the formation of complex. A new method, assembling onto substrate of polyelectrolyte, was improved for the experiments in bulk solution. Materials having high structure can be obtained with this method and can be utilized in macroscopic devices for non-linear optics, catalysis, microelectronics. In addition, the assembling of polyelectrolytes may give some information about the formation of polyelectrolyte complexes and protein–polyelectrolyte interactions [23].

Ultrathin multilayers of polyelectrolytes onto a substrate are a developing research area. A substrate is dipped into a positively charged polyelectrolyte solution, and then a negatively charged polyelectrolyte solution is followed. The electrostatic interaction between two oppositely charged polyelectrolytes leads to form a thin film. The electrical properties of films are influenced by residual small ions, their mobility, water content, ionic strength and solution pH. The impedance and dielectric characteristics properties of the sequential adsorption of layers of poly(allylamine hydrochloride) (PAH) with poly(acrylic acid) (PAA) and sulfonated polystyrene (SPS) were investigated. Changes in temperature, moisture content and deposition conditions affected the dielectric properties significantly. It is found there was a linear relationship between temperature or moisture content and the conductivity and dielectric constant [24].

Polyelectrolyte with oppositely charged surfactant is a new working area. Many researches are interested in the interaction between polyelectrolyte and ionic surfactant in bulk solution. A complex can be formed with the interaction of polyelectrolyte chain-surfactant. Association of polyelectrolyte and surfactant starts at a well-defined surfactant concentration whereas it finishes at the critical aggregation concentration (CAC). CAC system is affected by polyelectrolyte concentration, charge density of polyelectrolyte, flexibility. CAC is inversely proportional to charge density and flexibility [25].

2 Applications of Polyelectrolyte

In the paper industry, polyelectrolytes are used as retention aids, flocculating and coagulating agents to separate solid-liquid phases [19]. Novel applications such as drug and genetic material delivery system utilize polyelectrolytes due to their high charge density and biocompatibility [11]. Biocompatible polyelectrolytes such as chitosan and polystyrene sulfonate (PSS) are also utilized in biosensors and biomolecular recognition systems [16]. Polyelectrolytes are solvated in water and surrounded by salt ions in biological system [21]. Polyelectrolyte complexes (PECs), which are a special class of polymeric compounds, consist of oppositely charged polyions. A phase separation and formation of liquid coacervates occurred with mixing of oppositely charged natural polyelectrolytes in the early 1930s. The interaction between strongly acidic polyanion and basic polycation was explained for the first by Fuoss and Sadek in 1949 [17].

The first humidity sensor was known a polymer sensor and used to detect the mechanical properties of protein of hair [26]. Sensors have been deeply

investigated for the detection of humidity in air. At high humidity, a high stability could be provided with interpenetrating polymer networks (IPN). IPNs were used in organic medium to test water traces. The Langmuir equation and the dielectric constant of solvents are important to describe the performance of sensors. Detection limit of a sensor is proportional with dielectric constant of the solvent. IPN polyelectrolyte has dynamic variation impedance causing to water sorption mechanism in three steps. These are diffusion of moisture into polymer matrix, concurrent interaction between water ions and solvent, water molecules solvate the ions. Solvated ions causes to electrolytic solution. Poly(4-vinylpyridine) (P4VP) cross-linked with 1,4-dibromobutane (DBB) and poly(glycidyl methacrylate) (PGMA) cross-linked with diethylenetriamine (DETA) are polymer network to produce IPN electrolyte. IPN polyelectrolytes are sensitive materials for the detection water traces in organic solvent. The water concentration causes changes in the resistance and the capacitance of the polyelectrolyte. The strongest conductance changes and high dielectric constant occurred in a narrow range of water concentration. The film resistance and capacitance at the electrodes are inversely proportional to water concentration [26].

In 1961, Michaels and Miekka investigated the interaction between sodium poly(styrene sulfonate) and poly(vinyl benzyl trimethyl ammonium) chloride. Spontaneous aggregation can be provided by mixing of a polyanion and a polycation. It is suggested that the driving force for the formation of complex is primarily from the gain in entropy. Furthermore, hydrogen bonding or hydrophobic interactions may have important effects on the complex formation. The PECs and their applications have been studied in recent years. PECs can be seen in large-scale industrial areas as flocculants, coatings, and binders. Polycation complexes with polynucleotides or oligonucleotides are used in gene therapy. Insoluble PECs are effective to prevent wind and water erosion. Insoluble PECs have been found more effective than industrial polyelectrolytes used in coagulating colloid dispersions [17].

Nowadays, there is a big attention on fuel cells due to their high efficiency, high power density and pollution free fuel utilization. The lack of proper material is the main problem to improve fuel cells as commercial industrial product. The operating temperature of the fuel cells is related to the nature of the electrolyte. Polymer electrolyte fuel cells (PEMFCs) were applied for the first time in Gemini space program in the early 1960s. The oxidative degradation of their sulfonated polystyrene-divinylbenzene copolymer membranes became a big problem for real applications. The PEM platform, trade name Nafion, has been used to improve active catalyst layers, gas diffusion layer optimization and component design. The advantages of usage of PEM materials are cost, operational flexibility and system performance. Therefore, PEMFCs has started commercialization. PEMFCs's high efficiency, high power density and relatively low operating temperatures are the major characteristic properties to develop novel materials in fuel cells. Novel polymer membranes have been researched to improve durability and reliability of PEMFCs [27].

In recent years, the need of new polymeric materials to remove the waste products of industrial applications has increased. The removal and recovery of heavy metal ions has an important range of application areas. The major study has been effective removal of toxic heavy metals. Polymer/clay hydrogel composite with low production cost and high adsorption capacity is a developing research area for removal of heavy metals. Water-absorbing properties of superabsorbent can be increased by grafting monomer onto clay and fabricating a composite. Superabsorbent composites based on sepiolite, montmorillonite, and bentonite have high water absorbency, salt-resistance and low production costs. On the other hand, pure organic superabsorbent polymers have opposite properties for removal of heavy metals [28]. The mechanical, thermal and barrier performance properties increases with the addition of nanoclay instead of clay. Hydrogels are macromolecular polymer networks immersed in a solvent. Their potential application areas are biomedicine, food industry, water purification, building industry and communication technology. The swelling capacity of hydrogels can be increased with ionic groups in the hydrogels. Polyacrylamide hydrogels are used as a specific sorbent. Some multifunctional crosslinkers such as ethylene glycol dimethacrylate (EGDMA) and 1,4 butanediol dimethacrylate (BDMA) were used with Polyacrylamide hydrogels. The adsorption capacity of the hydrogels composed of ionic/anionic comonomer of acrylamide, 2-acrylamido-2-methyl-1-propanesulfonic acid (AMPS), increased with AMPS concentration. The acrylamide (AAm)/(AMPS) hydrogels and AAm/AMPS/Bent (bentonite) can be used as a sorbent in an aquatic field for pharmaceutical, agricultural, environmental, and biomedical applications [28].

Another recent research area on polyelectrolyte is controlled release systems. Target cell or organ is important in the controlled release systems. The stomach-specific delivery, the intestinal delivery and the colon-specific delivery are the sections of oral controlled release systems. Chitosan, pectin, alginate, cellulose derivatives and acrylic polymers have been investigated for the oral controlled release system. Chitosan is derived from natural chitin by alkaline deacetylation and has been used in gastrointestinal drug delivery systems. The main advantages of chitosan are its nontoxic, biocompatible, and biodegradable properties. The application of chitosan is restricted with the dissolving at low pH. Therefore, some modifications are needed for the application areas. Alginate, pectin, dextran sulfate and oxypullulan can be used to modify chitosan. Sodium cellulose sulfate (NaCS) could be used both to prepare the bio-microcapsules in biomedical applications and improve the properties of chitosan. In 2009, a novel colon-specific drug delivery capsule based on chitosan and NaCS was prepared for the oral controlled system and good responses were obtained by using it. The degradation of biomaterials may affect both the release process and the host response in controlled systems. So, the degradation behavior of materials could be investigated before applications [29].

Modelling of the biologic materials, well-organized multifunctional structures and systems found in nature has attracted the interest of scientists working in many scientific disciplines. The constant-composition method has been used to study the

influence of polyelectrolytes on the kinetics of crystal growth of hydroxyapatite (HAP) on HAP seed crystals [30]. A series of acidic acrylate block copolymers have been made, by radical polymerization, with defined molecular weight and structure. Radical polymerization of acrylic acid (AA) was carried out in the presence of a-thio polyethylene glycol monomethylether as a chain transfer agent to produce poly (ethylene glycol block acrylic acid) copolymers. The results indicate that polyelectrolyte concentration and the larger number of negatively charged functional groups markedly affect the growth rate. The fit of the Langmuir adsorption model to the experimental data supports a mechanism of inhibition through molecular adsorption of polymers on the surface of growing crystals [30]. These polyelectrolytes also were tested in spontaneous calcium oxalate crystallization [31, 32]. The inhibition of calcium oxalate crystallization by acrylic polyelectrolytes increased with increasing polymer acid functional group content. Homo and block copolymers of polyacrylates are more effective in inhibiting calcium oxalate growth than polymethylacrylates although they are similar in calcium ion binding. Introduction of a hydrophobic methyl group into a polymer molecule has a negative influence on its inhibiting performance [31, 32]. In addition, copolymers of vinylphosphonic acid and 4-vinylimidazole (poly(4-VIm-co-VPA)) were found to be substrates favoring the precipitation of nanohydroxyapatite (HAP) crystals from stable supersaturated solutions [33]. The rates of HAP crystal growth on the polymeric substrate were found to depend on the amount of seed material and on the phosphate content of the copolymer [33]. The highly reproducible constant composition technique was used to study the influence of biopolymers of crystal growth of calcium carbonate (CaCO_3), on CaCO_3 seed crystals. The crystal growth of calcium carbonate (CaCO_3) was inhibited in the presence of carboxymethyl inulin (CMI) at low concentration [34]. Calcium oxalate (CaOx) crystals exhibiting different shapes and phase structures were produced in the presence of water soluble homopolymer of vinylsulfonic acid [35]. Polyelectrolyte effects were interpreted in terms of the adsorption of inhibitors onto the active growth sites on the crystal surface [35]. The series of water-soluble polyethyleneglycol methacrylate-vinylsulfonic acid graft copolymers [(PEG-MA)-co-VS] and homopolymer of vinylsulfonic acid have been made to investigate the influence of graft polymers on spontaneous batch crystallization of calcium oxalate [36]. The presence of polymers inhibited the crystal growth of calcium oxalate possibly through adsorption onto the active growth sites for crystal growth due to the charge and hydrophilic effects. The higher inhibition efficiency of vinylsulfonic acid homopolymer is related to the maximum surface charge density due to adsorbed polymer [36]. The effect of poly(ethylene oxide)-block-poly(methacrylic acid) (EO-b-MAA) and poly(butylmethacrylate)-block-poly(methacrylic acid) (BuMA-b-MAA) copolymers with different architectures on the spontaneous precipitation of calcium sulfate dihydrate (gypsum) were was investigated [37]. Changing the butyl ester to a hydrophilic ethylene oxide resulted in higher inhibition efficiency. The inhibition efficiency is believed to arise from the closer chain packing on the crystal surface [37]. Ethylenediamine-tetrakis(methylenephosphonic acid) (EDTMP), hexamethylenediamine-tetrakis(methylenephosphonic acid) (HDTMP),

octamethylenediamine-tetrakis-(methylenephosphonic acid) (ODTMP), and dodecamethylenediamine-tetrakis(methylenephosphonic acid) (DDTMP) have been used as polyelectrolytes for the crystallization of calcium sulfate dihydrate ($\text{CaSO}_4 \cdot 2\text{H}_2\text{O}$, gypsum) [38]. The inhibition efficiency is directly proportional to the number of methylene groups in the organic chain that connects the aminobis(methylenephosphonate) moieties [38].

The cells of tissues interact with molecules forming the extracellular matrix (ECM). Existing molecules have ligands interacting with cell membrane receptor proteins. The internal information is obtained with receptors. In addition, renewal of tissue is provided by the ECM molecules. The studies related with development of implant materials have an important role to simplify the regeneration of damaged tissue. The synthetic ECM can be modified with attachment of polymers/proteins and synthetic peptides. They can interact directly with cell surface receptor or indirectly binding serum proteins. The design of implant material is related with two-dimensional model surfaces and three-dimensional ECM of natural biological tissues. Hydrogels having similar mechanical and structural properties to tissues can be used as synthetic three-dimensional ECMs. Alginate, a linear polysaccharide, can be injected at the site of implantation [39].

Polysaccharides, proteins and small molecular weight molecules can be used for biological tissues. Materials used in biological tissues provide the foundation for the biochemical and biomechanical function of tissues. Proteoglycans consisting of negatively charged glycosaminoglycans (GAG) participate in organizing other materials in extracellular matrices. The physical and chemical properties of nanoscale biologically-derived polymer are important for biomedical applications. Nanometer scale may provide new searching areas for the functional biomaterials. Polysaccharides having biochemical and biomechanical functions generally can be obtained at the nanometer scale. Among all polysaccharides, GAGs have a big role for biological systems due to their rich biochemistry properties. Polysaccharides-based polyelectrolytes can be used in drug delivery and tissue engineering. Chitosan, heparin and hyaluronan having amino, sulfate and carboxylate groups respectively, are common polyelectrolytes used biological systems. Electrostatic interactions between charged ions control the biological function of polyelectrolytes. Chitosan is composed of N-deacetylation of chitin and the degree of acetylation (DA) is an important parameter for chitosan. Its antimicrobial activity, biodegradability and biocompatibility properties are useful for tissue applications, drug delivery and cell adhesion systems. Enzymes, growth factors and extra cellular matrix can be bound with heparin. Fibroblast growth factors (FGF) and transforming growth factor beta superfamily (TGF β) can be activated by heparin. Hyaluronan is a weak polyanion composed of D-glucuronic acid and N acetyl-D-glucosamine. It is effective at increasing cell migration and proliferation [40].

Poly(L-lysine) (PLL) and PAA multilayers were investigated for protein adsorption. The adsorption mechanism was studied with multilayers consisting of sodium alginate (SA), cellulose sulfate (CS) and poly(methylene-co-guanidine) (PMCG) [23].

Corrosion is an electrochemical process leading to a decrease in thickness and strength of materials. Steel is the most widely used metal in industry and has weak resistance to corrosion. Corrosion resistance can be increased with addition of chrome and nickel. Adding of metals causes an increase in the production cost of steel. To develop the corrosion resistance, polyelectrolyte multilayers can be used to coat stainless steel with low cost [14]. The main aim to coat a metal is to protect it from corrosion. The layer-by-layer self-assembly method is used to prepare polyelectrolyte multilayers. Corrosion of metals can be reduced with inhibitors. Severe corrosion protective coatings are used in many application areas such as automotive, steel, pipe, petroleum and lining industry. Polyelectrolyte multilayers (PEMs) are an alternative method to protect the materials from corrosion. PEMs can be produced with anionic and cationic polyelectrolytes. In addition, PEMs has wide application areas such as membrane separation, microfluidics, biocatalytic and analytical separations. Cationic polyallylamine hydrochloride (PAH), anionic polystyrene sulfonate (PSS), polystyrene sulfonate-co-maleic acid (PSS-co-MA) and polyacrylic acid (PAA) were used to investigate the corrosion protection efficiency of polyelectrolyte. Corrosion rate, corrosion potential and linear polarization resistance were examined as corrosion process parameters. In addition, polydiallyldimethylammonium chloride (PDADMAC) was used with sulfonated polyetherether ketone (SPEEK) for steel corrosion applications [14].

The most important parameters for facial tissue, bath tissue, paper towels and napkins are softness, water absorbency and strength [41]. One of their characteristic properties is low basis weight. It ranges from 20 to 22.8 g/m² for bath tissue, whereas it ranges from 47 to 52 g/m² for paper towel. The wet strength is especially important. Water absorbency indicates absorption capacity per unit mass of tissue. Softness is important for customer's skin. The priority of desired properties changes according to the application area. The market of tissue has a stable growth in the developed countries. There is a big effort to improve the quality of tissue product in the market due to large consumption. The quality of tissue produced with modern tissue machines is not measured objectively; especially there is no exact method to measure the softness with high accuracy. Creping and through-air-drying consisting of forming, draining, pressing, and drying are commonly used for the production of tissue products. They are capable to develop tissue products with well quality, yet the machinery used in the process is expensive. The cost of process can be reduced with the addition of additives. Recent studies are related with getting more information about tissue property improvement by using chemical additives. Wet strength resins and debonding agents are most widely used chemical additives to improve the tissue properties. Wet strength resins can provide enough strength to tissue products under wet conditions. Debonding agents are used to provide softness. Although the adsorption kinetics of the two kinds of additives is important, there is a little information about the adsorption mechanism of additives. In addition, the effects of molecular structure of the debonder on sheet properties have not fully been studied. A new kind of biodegradable softener has been recently developed [41]. Additives with cationic charges can be used in the paper industry. Fiber system has negative charges so

additives are effective at lower concentration than anionic polymer. Additives both alter the amount of bonding between adjacent fibers and adjust the strength of bond. The synthetic polymers, ureaformaldehyde and melamine-formaldehyde resins, are used in wet strength paper application. Urea-formaldehyde or melamine-formaldehyde form a network protecting the existing fiber-to-fiber bonds, so products can gain resistant to water. There is some usage problem of formaldehyde due to environmental damages. There is a big tendency to alkaline papermaking operations. Therefore natural and alkaline conditions are used for the wet strength resins. Generally, poly (amido-amine)-epichlorohydrin (PAE) resin is used under neutral and alkaline conditions. PAE resins are derived from secondary amino polyamides. Quaternary ammonium compounds are utilized as cationic debonders. Debonder consists of long fatty alkyl with 16–18 carbon atoms. Dimethyl ammonium chloride, di (hydrogenated tallow) dimethyl ammonium chloride, ditallow dimethyl ammonium methyl sulfate, and di (hydrogenated tallow) dimethyl methyl sulfate are known as debonders. Various fatty aliphatic groups such as monoalkyl trimethyl ammonium quaternaries, dialkyl dimethyl ammonium quaternaries and the trialkyl monomethyl ammonium quaternaries have been studied as debonders. Among above debonders, dialkyl dimethyl quaternaries have been found the best debonder. Strong germicidal effect is the most important parameter for debonders. The biodegradation of cationic quaternary compounds is not high, so environmental effects can be negligible. However, there is a trend to usage of more biodegradable debonding agents. Monododecyl imidazolinium compounds are more biodegradable than traditional quaternaries. Monoester ditallow dimethyl ammonium chloride, diester di (hydrogenated) tallow dimethyl quaternary ammonium chloride, diester ditallow dimethyl quaternary ammonium chloride, and diester hydrogenated) tallow dimethyl quaternary ammonium methyl sulfate are esterfunctional quaternary ammonium compounds used to improve the properties of tissue products. A polyamide-epichlorohydrin resin, Kymene® 1,500, was used as wet strength resin while methyl-1 tallow-amidoethyl-2-tallow imidazolinium methyl sulfate was investigated as debonder in Liu's study [41]. The chemical adsorption of additives on the cellulose was examined. The adsorption of Softrite on the fiber was found fast whereas the adsorption of Kymene was slow. The application of dual chemical additives caused to produce sheet with high wet strength, low dry strength, low stiffness and high softness [42].

Polyelectrolyte multilayers (PEMs) are very important materials due to having a wide range of application fields such as encapsulation of drugs and enzymes, membrane-based separations, antibacterial coatings, membrane reactors and fuel cells. Polyelectrolyte multilayer (PEM) has a wide range of transport properties, simple deposition and small thickness, so it can be used in separation membranes. Polyelectrolyte concentration, duration and temperature of adsorption, deposition and solution pH are key parameters for specific separations. In addition the number of polyelectrolyte layers can alter the properties of polyelectrolyte. Poly(styrene sulfonate) (PSS)/poly(diallyldimethylammonium chloride) (PDADMAC) films are utilized in separation membranes. The adsorption of Cu(II) or Fe(III) ions can be carried out with PSS/poly(allylamine hydrochloride) (PAH) membranes.

Poly(acrylic acid) (PAA), poly(styrenesulfonate) (PSS), poly(vinylsulfonic acid), alginic acid, hyaluronic acid (HA), and pectic acid are general polyanions used in PEMs formed by LbL method. LbL method is used in various charged species such as proteins, viruses, nanoparticles, and exfoliated inorganic materials [22]. There is a linear relation between the thickness of a layer pair of PSS/PAH and the ionic strength in deposition solution. The thickness of PSS/PAH multilayer increases linearly with the number of layer. On the other hand, poly(L-glutamic acid) (PGA)/poly(L-lysine) (PLL), PGA/PAH, PDADMAC/PSS and HA/chitosan (CHI) have an exponential growth mechanism. In addition, the molecular weight of PSS has no effect on the thicknesses of PSS/PAH films. The growth of HA/CHI multilayer is proportional to the molecular weight of CHI whereas the growth of PAH/PAA is inversely proportional to molecular weight of PAA. The thickness of PAH and poly(1-[p-(3'-carboxy-4'-hydroxyphenylazo) benzenesulfonamido]-1,2-ethandiyil) (PCBS) multilayer are independent of polyelectrolyte concentration. The thickness with permeability and morphology can be affected by the pH value of weak polyelectrolyte solution [22].

Nanofiltration (NF) is similar to reverse osmosis (RO) and used water softening, removal of organic substance. The cost of energy is lower than RO and NF contains a selective layer on a highly permeable support. While monovalent ions can pass at NF, multivalent ions and organic compounds cannot pass at NF. Generally, NF is consisted of the high surface charge of many PEM films. NF membranes are used for removal of ions, sugars, dyes. (PAH/PSS)₅ film is a selective NF for Cl⁻/SO₄²⁻ and Cl⁻/[Fe(CN)₆]³⁻ in diffusion dialysis. A 60-bilayer film of PAH/PSS membrane which is not practical for large-scale membrane fabrication can be used for NaCl over Na₂SO₄. In order to improve of selectivity of Cl⁻/SO₄²⁻, PSS/PAH/PAA films, (PSS/PDADMAC)₃ PSS film and cross-linking of PAA/PAH can be used. 60-bilayer poly(vinyl amine) (PVA)/poly(vinyl sulfate) (PVS) films on poly(acrylonitrile) (PAN)/poly(ethylene terephthalate) (PET) can be used rejections of chloride and sulfate salts [22].

Microgel is polymeric colloidal dispersion and used in many applications such as drug delivery, paint, ink-jet printing, ceramics, biotechnology. Environmental conditions and temperature causes changes in swelling properties of microgels [18]. The properties of poly(N-isopropylacrylamide/4-vinylpyridine) [poly(NIPAM/4-VP)] having different ratio of 4-VP and NIPAM was investigated by using dynamic light scattering (DLS). Swelling properties make microgels useful in applications. Poly(NIPAM), temperature responsive, is most widely used in microgel systems. It is composed of amide and isopropyl groups. The addition of co-monomer causes essential effects on the properties of microgel. The ratio of NIPAM/4-VP concentrations may alter the temperature/pH sensitivity of microgel which can be used in applications where changes in particle size with small change in pH or temperature. Poly(acrylamide) (PAAm), poly(acrylic acid) (PAA), poly(methacryl acid) (PMAA), poly(diethylaminoethyl methacrylate) (PDEAEMA) and poly(dimethylaminoethyl methacrylate) (PDMAEMA) are most widely known pH-responsive materials. Ionic strength, pH and fixed charges on the polymer matrix

are important for the pH-dependent swelling of the microgel. The transition temperature of poly(NIPAM) has increased with adding of acrylic acid (AAC) [18].

The polyelectrolyte solution has not been understood yet. The characteristic properties of polyelectrolyte depend on not only the interaction between the polyvalent macroion and the counterions but also between the shape or conformation and the ionic state. Macroions usually have flexible chains and the shape of chains alters from random coil to a fully extended. There is a strong relationship between viscosity and the ionic strength and/or polyelectrolyte concentration. A decrease in the viscosity and the size of polymer can be resulted from the addition of salt [13]. In addition, there is a small distance between charged repeat units of polymer in the presence of salt. The thickness of a layer pair of PSS/poly(allylamine hydrochloride) (PAH) is proportional to the ionic strength in deposition solutions [22]. Polyelectrolyte solutions have low counterion activity coefficients, low osmotic coefficients and high extent of counterion binding. The main parameter for the current models is Gibbs free energy expressing the sum of two contributions from long-range and short-range interactions. Spherical and cylindrical chain models are two general models suggested for the polyelectrolyte thermodynamics. The coiled polyions are accepted spherical with the charge density in the first model. While electrostatic potentials are small, polyions size are large in this model. Second model was developed by Alfrey et al. and Fuoss et al. [13]. These two suggested models allow us to calculate osmotic coefficient and counterion activity coefficient of polyelectrolyte solution [13].

3 Scaling Theory

In this section, we discuss the scaling approach. The pioneering studies about scaling theory of polyelectrolytes was started by de Gennes et al. In 1976, de Gennes et al. [43] proposed a simple scaling model for the conformation of polyelectrolytes. Odijk, Skolnick and Fixman contributed significantly to these works [44, 45]. They indicated that the electrostatic persistence length is proportional to the square of the Debye screening length. Then Barrat and Joanny showed that intrinsically flexible chains stay flexible on small length scales in their works [46].

The properties of polyelectrolyte solutions can be summarized as follows:

1. One of the important parameter of polyelectrolyte solution is the concentration dependence of the solution viscosity called the Fuoss law. According to Fuoss law, the viscosity, η , of polyelectrolyte solutions at low concentrations is proportional to the square root of polymer concentration. ($\eta \sim c^{1/2}$). In a dilute solution regime, the viscosity of uncharged polymers in a good solvent scales linearly with polymer concentration or as $c^{1.3}$ in a semidilute solution regime.
2. There is a strong peak in the scattering function of homogeneous polyelectrolyte solutions. The wave vector corresponding to this peak increases with concentration as $c^{1/2}$. There is no such peak in solutions of uncharged polymers.

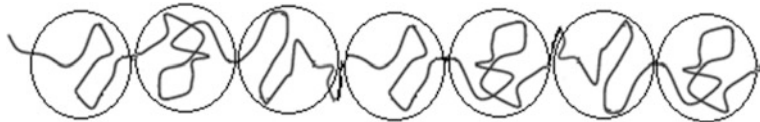


Fig. 1 The Blob model

3. The particular contribution to the osmotic pressure of polyelectrolyte solutions comes from counterions at low salt concentration [47–49].

Firstly we review the scaling theory which was presented by de Gennes et al. [43]. His idea was to break the chain up into blobs as shown in Fig. 1. Inside the blob the chain is self-avoiding but the blobs themselves can imbricate and are fundamentally ideal. If we have g monomers per blob and the blob size is D , then $D \sim g^{v/2} \sim g^{3/5}$. If the blobs can overlap then $R \sim D^{0.5}$ and hence:

$$R \sim n^{0.5} g^{0.1} \quad (1)$$

Here, R is proportional to the square root of the number of bonds, n . The exponent v is given by $v = 6/(D + 2)$, where D is the spatial dimension. So in 3D, $v = 6/5$ and the chain expands beyond its ideal dimensions ($v = 1$).

For an ideal chain $g = 1$ and for a chain with full excluded volume $n = g$ which recaptures the two extreme situations of an ideal and swollen chain above [43].

Mostly, the solvent is water and the uncharged polymer would not dissolve in water (poor solvent). In such a case, the polyelectrolyte is locally collapsed, shielding as many monomers as possible from the prejudicial interaction with water.

The size D_e of these collapsed electrostatic blobs and g_e monomers is given in Eq. (2). This equation shows the balance between the electrostatic energy inside the blob and the interfacial free energy of the electrostatic blob surface [49, 50].

$$\frac{(efg_e)^2}{(D_e \epsilon)} \approx \left(\frac{\tau D_e}{b}\right)^2 kT \quad (2)$$

Here, e is the elementary charge, f is the fraction of monomers bearing an effective charge, ϵ is the dielectric constant, and b is the monomer size. The chain is collapsed inside the electrostatic blob, with $D_e \approx b(g_e/\tau)^{1/3}$. τ is the reduced temperature and it can be calculated by Eq. (3).

$$\tau \equiv (\theta - T)\theta \quad (3)$$

Here, θ is the temperature at which the net interaction between uncharged polymer and water is zero. The electrostatic blob size in poor solvent can be determined by combining Eq. (3) with Eq. (4).

$$D_e \approx \frac{b^{4/3}}{f^{2/3} I_B^{1/3}}, \quad g_e \approx \frac{\tau b}{f^2 I_B} \quad (4)$$

Here, l_B is the Bjerrum length.

$$I_B = \frac{e^2}{\epsilon kT} \quad (5)$$

Here, ϵ is dielectric constant, kT is thermal energy.

If a polyelectrolyte is in a good solvent, it would swell the uncharged chain and then swell the electrostatic blob. In this situation, the electrostatic blob size is determined by a balance between the electrostatic energy inside the blob and the thermal energy kT [43, 49].

$$\frac{(efg_e)^2}{(D_e \epsilon)} \approx kT \quad (6)$$

The chain is swollen inside the electrostatic blob in good solvent, with $D_e \approx bg_e^{3/5}$. Combining with Eq. (6) determines the electrostatic blob size in good solvent [43, 51].

$$D_e \approx \frac{b^{10/7}}{f^{6/7} I_B^{3/7}}, \quad g_e \approx \left(\frac{b}{f^2 I_B}\right)^{5/7} \quad (7)$$

In this section we review the scaling theory which was presented by Baeurle and Nogovitsin [52]. According to Baeurle and Nogovitsin, scaling theory has mainly been effective in cleaning up the static and dynamic behaviors of neutral polymer and PE solutions with added salt. In order to derive scaling laws for PE solutions with no salt, they firstly assayed the condition of neutral polymer solutions. In the dilute regime of neutral polymer solutions $C_m \ll C_m^*$ here C_m^* is the so-called overlap concentration specifying the concentration at which the polymer coils m, where Cm is the so-called overlap concentration defining the concentration at which the polymer coils pack to fill space with unit volume fraction [53] of a virial expansion. If truncated at quadratic order with regard to concentration, the equation was found below:

$$\frac{\pi}{RT} \approx \frac{C_m}{N} + A_2 C_m^2 \quad (8)$$

Where $A_2 = 4\pi^{\frac{3}{2}}\rho(z)N_A R_F^3/N^2$ is the second virial coefficient with $\rho(z)$ as the penetration function, which is a constant in good solvents. The parameter R_F is

showing the Flory radius of the polymers representing the radius of a single chain in the good solvent limit, which varies as $R_F \sim N^{3/5}$. According to the scaling approach of des Cloizeaux [54, 55], the osmotic pressure of neutral polymer solutions in the semidilute regime of concentrations, $C_m \gg C_m^*$, should correspond to the following relation

$$\frac{\pi}{RT} \sim C_m^{9/4} \quad (9)$$

and should not depend on the polymerization index N . According to Odijk [44, 56], the same relations should be valid for semidilute PE solutions in the presence of added salt, provided the influence of the electrostatic interactions between fixed charges on the macromolecular chains is considered. He suggested a Debye Huckel (DH) type of interaction potential between the fixed charges with a screening parameter

$$K^2 = 8\pi\lambda_B I \quad (10)$$

where I is the ionic strength. Odijk gave the osmotic pressure of semidilute PE solutions in the presence of added salt as

$$\frac{\pi}{RT} \sim \left(\frac{L_t}{K}\right)(AC_m)^{9/4} \quad (11)$$

where L_T is the total persistence length of the charged macromolecules [43– 44, 56–58]. The latter quantity may be estimated by a sum of two terms, i.e. $L_t = L_p + L_e + \frac{1}{4K^2 A^2 f^2}$, where L_p is the intrinsic persistence length and L_e the electrostatic persistence length, while A shows the linear charge spacing along the chains and f accounts for the effective charge on the PE chains. If we consider counterion condensation theory [59], one has $f = 1$ if $A > \lambda_B$ and $f = \lambda_B / A$ if $A < \lambda_B$. The scaling approach to PE solutions without added salt, developed by de Gennes et al. [43, 44], specified three concentration regimes. They considered that the PEs are on average widely separated at very low concentrations in the dilute regime and, if strongly charged, they should be fully stretched due to the ineffective screening between the polyions. Above a certain critical concentration in the semidilute regime of PE solutions, there is a considerable overlap between chains and a transient network is formed, whose characteristic mean distance (correlation length) between adjacent chains decreases with increasing concentration as $C_m^{-1/2}$.

In this case the electrostatic energy per monomer is of order kT . According to de Gennes et al., the osmotic pressure contributed from the polyions scales like the free energy per unit volume and is, thus, of order

$$\frac{\pi}{RT} \sim C_m \quad (12)$$

Odijk considered DH screening as being caused by uncondensed counterions only, which implicates that the screening parameter depends on C_m

$$k^2 = 4\pi A C_m \quad (13)$$

To derive the osmotic pressure, the Eqs. (13) and (11) are combined to yield the scaling relation [58]

$$\frac{\pi}{RT} \sim A^{3/8} C_m^{9/8} \quad (14)$$

Baeurle and Nogovitsin showed that the scaling exponent in the latter relation is similar to the exponent in expression (12), obtained by de Gennes et al. [43].

4 Dynamic Light Scattering

In order to measure the size of particles in the sub micron region, Dynamic Light Scattering (DLS) method can be used [60]. The other definition of DLS is a method for measuring scattered light having temporal fluctuations. Fluctuations in the scattered intensity results from the movement of the particles along the scattering vector [61]. The cooperative diffusion coefficient and the angular dependence of the decay rate is measured by DLS [62]. DLS is related to the characterization of particles, emulsions or molecules in a liquid [60]. The advantages of DLS are short experiment duration, automatized and low development cost. The samples having broad distributions can be analyzed with DLS. Besides, DLS can be used to detect very small amounts of higher mass species. Molecular weight, radius of gyration, Translational diffusion constant can be obtained with this technique. The disadvantage of DLS, to analyze non-rigid macromolecules is not easy and molecules fluctuate above the zero degree Kelvin [63].

There are two assumptions for the theory of DLS. The particles which are in Brownian motion is the first assumption [63]. First, it was observed by Robert Brown in 1827. The intensity of the scattered light is concerned with the motion of the scatterers [61]. Brownian motion is measured by DLS giving the information about the size of the particles [60]. The Brownian motion of particles leads to laser light to be scattered at different intensities. Brownian motion is the random movement of particles. The cumulative effect of bombardment by the suspending medium's molecules creates the motion of particles in the solution. The larger particles have the slower Brownian motion [60]. In Brownian motion, the probability density function can be calculated by the formula [63]:

$$P(r, t | 0, 0) = (4\pi D_{Diff})^{-3/2} \exp(-r^2 / 4D_{Diff}) \quad (15)$$

where D_{Diff} is the diffusion constant.

The second assumption is the spherical beads particles are used in the experiment. These particles have a small diameter compared to the molecular dimensions. Hence, the translational diffusion coefficient (D_{T-Diff}) of colloidal particles in dispersions and hydrodynamic radius (R_h) can be measured with DLS technique if Stokes-Einstein relation is applied to particle [62–64]. The translational diffusion coefficient is used to calculate the particle size. [60]. Stokes-Einstein is given in Eq. (16) [11, 60, 63, 65];

$$R_h = \frac{kT}{6\pi\eta D_{T-Diff}} \quad (16)$$

where R_h is hydrodynamic radius; k is Boltzmann's constant, D_{T-Diff} is translational diffusion coefficient, T is absolute temperature and η is viscosity.

Ionic strength of medium, surface structure and non-spherical particles can affect diffusion speed of particles. The thickness of the electric double layer (Debye length) changes with the ions in the medium and the total ionic concentration. An extended double layer of ions around the particle results from a low conductivity medium. So, the diffusion speed reduces and hydrodynamic diameter increases. The diffusion speed can be affected with a change in surface area. The diffusion speed will reduce with an adsorbed polymer layer. Polymer conformation can alter the apparent size.

DLS is depend on the time-dependent interference among electric fields emanating from scattering centers [66]. The time-averaged time correlation function of the intensity $I(q,t)$ of light scattered by the sample in the direction described by the scattering vector can be measured by DLS.

The autocorrelation function of the intensity $I(q,t)$ due to concentration fluctuations in the system is given in Eq. (17) [62].

$$g_2(\tau) = \frac{I(q,t).I(q,t + \tau)}{I^2} \quad (17)$$

q is the scattering wave vector and defined as $4\pi(n/\lambda)\sin(\theta/2)$. Where λ is the wavelength of the scattering radiation in vacuum, n is the refractive index of the medium, and θ is the scattering angle. For the current system, λ is the wavelength of the Argon laser (=514.5 nm) and n is the refractive index of water (=1.33) [62].

5 Neutron Scattering

Here we provide a basic introduction into the properties of the neutron scattering. Neutron scattering is an experimental technique which used to investigate materials in modern science. The goal of the neutron scattering technique is to understand material properties on the atomic scale. The method has led to advances in many areas of science and it has applications in fundamental physics,

Table 1 Basic properties of neutron

Neutron	
Mass	1.675×10^{-27} kg
Charge	0
Spin	$\frac{1}{2}$
Mean life time	≈ 15 min
Magnetic dipole moment	$\mu = \frac{-e\hbar}{2m}$ gs ($g = 3.826$)
Energy	$E[\text{meV}] = \frac{81.81}{\lambda^2 [\text{\AA}]}$
Coulomb interaction	No
Strong-force interaction	Yes
Magnetic dipole-dipole interaction	Yes

solid state physics, chemistry, material science, biology, etc. [67–70]. As known neutrons have zero charge and their electric dipole moment is either zero or too small to be measured by the most sensitive of modern techniques. For these reasons neutrons can interact with matter far better than charged particles. Furthermore, neutrons interact with atoms via nuclear rather than electrical forces. Nuclear forces are very short range (a few fermis, where 1 fermi = 10^{-15} m) and the sizes of nuclei are typically 100,000 smaller than the distances between them. Neutrons can therefore travel long distances in material without being scattered or absorbed. They can be scattered elastically or inelastically. While elastic scattering changes direction but not the magnitude of the wave vector, inelastic scattering changes both direction and magnitude of the neutron wave vector. It is the elastic, coherent scattering of neutrons that gives rise to small-angle scattering. Coherent scattering is “in phase” and thus can contribute to small-angle scattering. Incoherent scattering is isotropic and in a small-angle scattering experiment and thus contributes to the background signal and degrades signal to noise. Basic properties of neutron are summarized in Table 1. These properties provide us determine the relative positions and motions of atoms in a bulk sample of solid or liquid. To investigate atomic-scale structure and dynamics, scientists use a variety of tools and techniques, often based on the scattering of beams of particles. In these studies, it would have zero charge, to avoid strong scattering by charges on the electrons or the nucleus and allow deep penetration into materials. Neutrons interact directly with the atomic nucleus. Therefore the strength of the scattering depends not only on the element, but also on the specific isotope. Moreover, the details of the nuclear and nuclear spin interactions responsible for neutron scattering lead to scattering cross sections that vary in a seemingly random manner from isotope to isotope. These cross sections depend only weakly on the atomic number [71–74].

Basic idea of neutron scattering experiment is showed in Fig. 2.

Neutron scattering is used in many different scientific fields. Neutrons can be used to study the dynamics of chemical reactions at interfaces for chemical and biochemical engineering, in food science, drug synthesis and healthcare. Neutrons have been used to investigate polymers and to reveal the molecular structure of

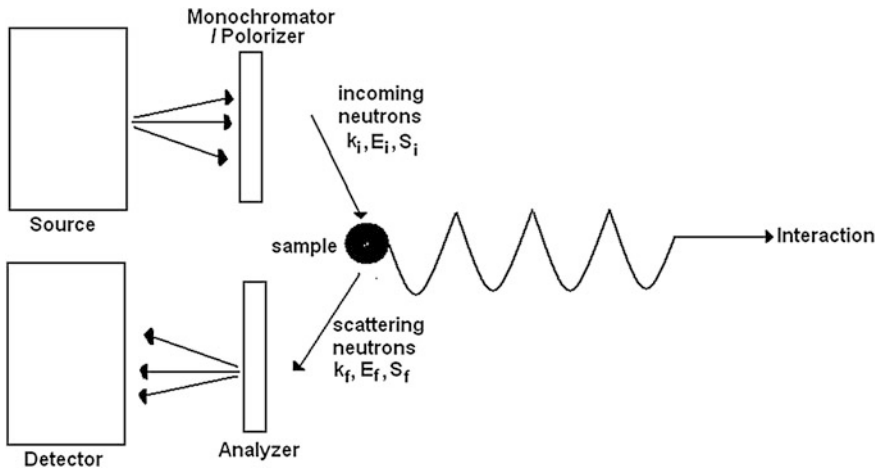


Fig. 2 A neutron scattering experiment

both crystalline and disordered materials. Also Neutron science continues to break new ground in investigating how drug-delivering polymers can move through membranes, how antibodies are structured and how active parts of medicines interact with lipids and proteins. Neutron studies will facilitate the understanding and development of materials that can store hydrogen safely and efficiently. Another application area of neutron scattering is analysis of ancient objects. The delicate, sensitive and deeply penetrating nature of neutron beams enables heritage scientists to determine unique information from historic objects, museum artefacts or geological fossils with no risk to their value or integrity. Additionally, the simplicity of the neutron interaction, and the fact that it can be measured on an absolute scale with high accuracy, gives an easy and direct link to theory and computer modelling. In future it will be the norm for neutron experiments to be coupled with advanced computation [75–83].

The advantages of neutron scattering can be summarized as follows:

- Penetrating: measure bulk properties, can benefit from large samples
- Penetrating: extreme sample environment (high/low temperature, magnetic field, pressure)
- Low-energy, non-ionizing, non-destructive
- Scattered by nuclei and by magnetism
- High contrast for light elements
- Isotope sensitive

Although, neutron scattering has numerous advantages, it includes some handicaps. The disadvantages of neutron scattering can be summarized as follows:

- Low brilliance of sources: low intensity or resolution, large samples, statistical noise.
- Penetrating: background hard to control, need large samples

- Some elements (B, Cd, Gd) strongly absorb
- Neutral: hard to manipulate, accelerate, detect, etc. [83–86].

In conclusion, neutron scattering is a powerful bulk probe to measure fundamental electronic and structural correlations in condensed matter and provides a direct route to the microscopic origin of the physical properties of materials. Neutron experiments have provided definitive data to the chemical industry, which has enabled process optimisation and the saving of millions of pounds in energy costs and improved the environment by reducing waste effluent. Materials testing data have given aerospace companies confidence in new alloy compositions and manufacturing techniques. Health-based research has obtained key datasets required in preparation for clinical trials or to understand why certain drug treatments can be more successful than others.

6 Biopolymers and Ionomers

6.1 Biopolymers

The term biopolymer refers to naturally occurring long-chain molecules which have been derived from bio-based monomers. Most of biopolymers are biodegradable, but this isn't necessarily the case. Although, there is no clear definition for the word biopolymer, we can simply define as a polymer produced by living organisms. Biopolymers have a more complex chemical structure than that of synthetic polymers. Because of the renewable feedstock used to produce them and their biodegradability, they are generally regarded as an eco-friendly alternative to petrochemical polymers [87–91].

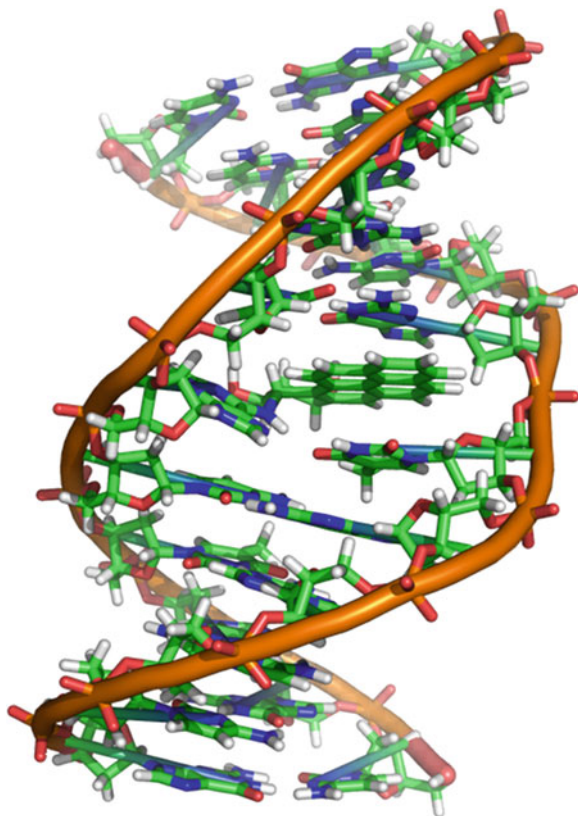
Biopolymers include natural polymers, bio-based polymers, also known as bioplastics, which are extracted from biomass (i.e., natural polymers) or polymerized from bio-based monomers and those polymers produced in microorganisms and extracted [92].

There are three main classes of biopolymers: polynucleotides (RNA and DNA), which are long polymers composed of 13 or more nucleotide monomers; polypeptides, which are short polymers of amino acids; and polysaccharides, which are often linear bonded polymeric carbohydrate structures. Terms such as biopolymers, bioplastics, and biodegradable plastics are used synonymously in certain contexts; however, each has a unique meaning [91, 93] (Fig. 3).

6.1.1 Polynucleotides

A polynucleotide molecule is a biopolymer composed of nucleotide monomers covalently bonded in a chain. DNA (deoxyribonucleic acid) and RNA (ribonucleic acid) are examples of polynucleotides with distinct biological function. DNA

Fig. 3 Microstructure of DNA which is an example of biopolymers
(Credit:Wikipedia)



consists of two chains of polynucleotides, with each chain in the form of a helical spiral. Polynucleotides occur naturally in all living organisms. Polynucleotides have a variety of other roles in organisms. Polynucleotides occur naturally in all living organisms. The genome of an organism consists of complementary pairs of enormously long polynucleotides wound around each other in the form of a double helix. Polynucleotides have a variety of other roles in organisms [94, 95].

6.1.2 Polypeptides

Peptides are short chains of amino acid monomers linked by peptide (amide) bonds, the covalent chemical bonds formed when the carboxyl group of one amino acid reacts with the amino group of another. Peptides are distinguished from proteins on the basis of size, and as a benchmark can be understood to contain approximately 50 amino acids or less. They have vital importance in biotechnology and biomedicine as a new class of biomaterials due to their unique chemical, physical, and biological properties [96, 97].

Polysaccharides

Polysaccharides, otherwise known as carbohydrates, are polymeric structures in biological systems. Polysaccharides are made of many monosaccharides, which are composed primarily of carbon, oxygen, and hydrogen. The most common types of monosaccharide units contain either five or six carbon atoms. Due to the presence of several hydroxyl groups within the monosaccharide structure, hydrogen bonds are formed between polymer chains. Glucose is the most abundant six carbon sugar and is the monomeric unit of both cellulose and starch. Polysaccharide is used widely in food, cosmetic and pharmaceutical industries [92, 98].

There has been heightened interest in using biopolymers in recent years due to having a wide range of applications. The number of possible applications of biopolymers is almost infinite. These materials especially are used in biomedical applications such as pharmaceutical, medical device coatings, and resorbable implants that require biocompatibility and nontoxicity. Bio-based and biodegradable polymers play an important role in the development of controlled delivery devices for a range of applications related to drugs, food-related bioactive ingredients and genes. The most common of the biodegradable materials are blends of thermoplastic starch (TPS) and aliphatic/aromatic polyesters, such as poly(lactic acid) or polylactides (PLA), polycaprolactone (PCL), poly(butylene adipate terephthalate) (PBAT) and polyhydroxybutyrate (PHB) [99, 100].

6.2 Ionomers

Ionomers are thermoplastic polymers that are ionically crosslinked, containing both hydrogen and ionic bonds. An ionomer is a polymer that comprises repeat units of both electrically neutral repeating units and a fraction of ionized units (usually no more than 15 mol%) covalently bonded to the polymer backbone as pendant moieties. This means that most ionomers are copolymers of the neutral segments and the ionized units, which usually consist of carboxylic acid groups. But an ionomer is a special kind of polyelectrolyte. First of all, they are copolymer. They contain both nonionic repeat units, and a small amount of ion containing repeat units. One example of an ionomer is poly(ethylene-co-methacrylic acid) (Fig. 4). This polymer is a sodium or zinc salt (which provides the ions) of copolymers derived from ethylene and methacrylic acid.

The ionic attractions that result strongly influence the polymer properties. In an ionomer, the nonpolar chains are grouped together and the polar ionic groups are attracted to each other. The ionic groups would like to go off into a little corner by themselves, but since they are attached to the polymer chain, they cannot. This allows thermoplastic ionomers to act in ways similar to that of cross-linked polymers or block copolymers [101, 102].

Ionomers have largely evolved over the years. The most important applications for ionomers are in the manufacture of films and extrusion coatings used primarily

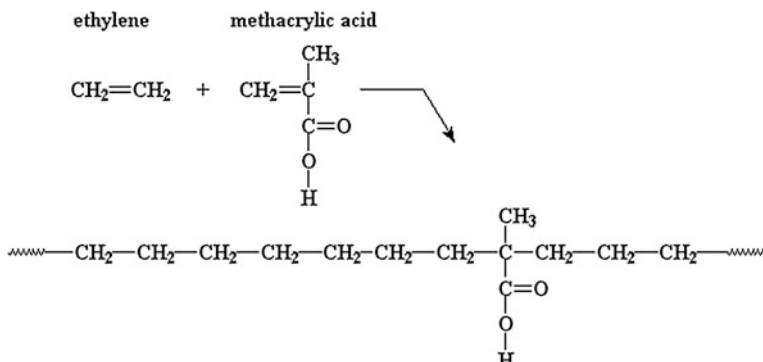


Fig. 4 The scheme of poly(ethylene-co-methacrylic acid)

for various kinds of food packaging. Ionomers have multiple applications within the injection molded, film, and extrusion markets. The major markets for ionomers include meat packaging, skin packaging, medical packaging, automotive injection molding, golf ball covers, condiment packaging, squeeze tube packaging, aseptic brick packaging, nuts and dried fruit packaging, bowling pin covers, bullet proof glass, hair care products packaging, and snack food packaging [102].

References

1. Hara, M.: Polyelectrolytes: Science and Technology. Marcel Dekker, New York (1993)
2. Dautzenberg, H., Jaeger, W., Kotz, J., Philipp, B., Seidel, Ch., Stscherbina, D.: Polyelectrolytes: Formation, Characterization, and Application. Hanser Gardner, Munich (1994)
3. Konieczky, M., Likos, C.N., Löwen, H.: *J. Chem. Phys.* **121**, 4913–4924 (2004)
4. Liao, Q., Carrillo, J.M.Y., Dobrynin, A.V., Rubinstein, M.: *Macromolecules* **40**, 7671–7679 (2007)
5. Csajka, F.S., Netz, R.R., Seidel, C., Joanny, J.F.: *Eur. Phys. J. E.* **4**, 505–513 (2001)
6. Förster, S., Schmidt, M.: *Adv. Polym. Sci.* **120**, 51 (1995)
7. Barrat, J.L., Joanny, J.F.: *Adv. Chem. Phys.* **94**, 1 (1996)
8. Dobrynin, A.V., Rubinstein, M.: *Prog. Polym. Sci.* **30**, 1049 (2005)
9. Allen, M.P., Tildesley, D.J.: Computer Simulation of Liquids. Clarendon Press, Oxford (1996)
10. Von Solms, N., Chiew, Y.C.: *J. Chem. Phys.* **118**, 4321–4330 (2003)
11. Jomaa, H.W.: A molecular walk across polyelectrolyte multilayers. Ph.D. thesis, The Florida State University (2005)
12. Fadhillah, F.: Application of polyelectrolyte multilayer reverse osmosis membrane in seawater desalination. Ph.D. thesis, King Fahd University of Petroleum & Minerals (2012)
13. Nagvekar, M., Tihminlioglu, F., Danner, R.P.: *Fluid Phase Equilib.* **145**, 15–41 (1998)
14. Amr, I.T.: Control of corrosion in stainless steel using polyelectrolytes multilayer nanofilms. M.Sc. thesis, King Fahd University of Petroleum & Minerals (2006)
15. Popov, A.: Assessing polyelectrolyte effective charge. Ph.D. thesis, University of Massachusetts Amherst (2007)

16. Razdan, S.: Novel polyelectrolyte complex based carbon nanotube composite architectures, PhD Thesis, Rensselaer Polytechnic Institute (2008)
17. Sui, Z.: Characterization and applications of pH-responsive polyelectrolyte complex and multilayers. Ph.D. thesis, The Florida State University (2004)
18. Nur, H., Pinkrah, V.T., Mitchell, J.C., Benée, L.S., Snowden, M.J.: *Adv. Colloid Interface Sci.* **158**, 15–20 (2010)
19. Dou, S.: Synthesis and characterization of ion containing polymers. Ph.D. thesis, The Pennsylvania State University (2007)
20. Jin, Z.: A hybrid density functional theory for solvation and solvent-mediated interactions. Ph.D. thesis, University of California Riverside (2012)
21. Neff, P.A., Wunderlich, B.K., Klitzing, R.V., Bausch, A.R.: *Langmuir* **23**, 4048–4052 (2007)
22. Adusumilli, M.: Polyelectrolyte multilayer films for ion separation and water purification. Ph.D. thesis, Michigan State University (2010)
23. Müller, M., Brisssová, M., Rieser, T., Powers, A.C., Lunkwitz, K.: *Mater. Sci. Eng. C* **8–9**, 163–169 (1999)
24. Durstock, M.F., Rubner, M.F.: *Langmuir* **17**, 7865–7872 (2001)
25. Naderi, A., Claesson, P.M.: *Langmuir* **22**, 7639–7645 (2006)
26. Casalbore-Miceli, G., Zanelli, A., Rinaldi, A.W., Camaioni, N., Yang, M.J., Li, Y., Giroto, E.M.: *Sens. Actuators B* **125**, 120–125 (2007)
27. Kang, J.: A new class of polyelectrolyte: Poly(p-phenylene disulfonic acids). Ph.D. thesis, Case Western Reserve University (2008)
28. Kundakci, S., Uzum, O.B., Karadag, E.: *Polym. Compos.* **32**, 994–1001 (2011)
29. Zhu, L.Y., Lin, D.Q., Yao, S.J.: *Carbohydr. Polym.* **82**, 323–328 (2010)
30. Oner, M., Dogan, O.: *Prog. Cryst. Growth Charact. Mater.* **50**, 39–51 (2005)
31. Akyol, E., Bozkurt, A., Oner, M.: *Polym. Adv. Technol.* **17**, 58–65 (2006)
32. Akyol, E., Oner, M.: *J. Cryst. Growth* **307**, 137–144 (2007)
33. Dogan, O., Oner, M.: *Langmuir* **22**, 9671–9675 (2006)
34. Kirboga, S., Oner, M.: *Colloids Surf., B* **91**, 18–25 (2012)
35. Kirboga, S., Oner, M.: *Colloids Surf., B* **78**, 357–362 (2010)
36. Kirboga, S., Oner, M.: *Cryst. Growth Des.* **9**, 2159–2167 (2009)
37. Dogan, O., Akyol, E., Oner, M.: *Cryst. Res. Technol.* **39**, 1108–1114 (2004)
38. Akyol, E., Oner, M., Barouda, E., Demadis, K.D.: *Cryst. Growth Des.* **9**, 5145–5154 (2009)
39. Znidarsic, W.J.: Biomolecular localization: applications in tissue engineering. Ph.D. thesis, Faculties of University of Pennsylvania (2006)
40. Boddohi, S.: Engineering nanostructured polysaccharide-based polyelectrolyte complexes. Ph.D. thesis, Colorado State University (2009)
41. Liu, J.: Effects of chemical additives on the light weight paper. Ph.D. thesis, Georgia Institute of Technology (2004)
42. Cohen Stuart, M.A., Huck, W.T.S., Genzer, J., Müller, M., Ober, C., Stamm, M., et al.: *Nat. Mater.* **9**, 101–113 (2010)
43. de Gennes, P.G., Pincus, P., Velasco, R.M., Brochard, F.: *J. Phys.* **37**, 1461–1473 (1976)
44. Odijk, T.: *J. Polym. Sci., Polym. Phys. Ed.* **15**, 477–483 (1977)
45. Skolnick, J., Fixman, M.: *Macromolecules* **10**, 944 (1977)
46. Barrat, J.L., Joanny, J.F.: *Europhys. Lett.* **24**, 333 (1993)
47. Katchalsky, A.: *Pure Appl. Chem.* **26**, 327 (1971)
48. Oosawa, F.: *Polyelectrolytes*. Marcel Dekker, New York (1971)
49. Dobrynin, A.V., Colby, R.H., Rubinstein, M.: *Macromolecules* **28**, 1859–1871 (1995)
50. Khokhlov, A.R.: *J. Phys. A: Math. Gen.* **13**, 979–987 (1980)
51. Bordi, F., Cametti, C., Colby, R.H.: *J. Phys.: Condens. Matter* **16**, 1423–1463 (2004)
52. Baeurle, S.A., Nogovitsin, E.A.: *Polymer* **48**, 4883–4899 (2007)
53. Fredrickson, G.H.: *The Equilibrium Theory of Inhomogeneous Polymers*. Clarendon Press, Oxford (2006)
54. Des Cloizeaux, J.: *J. Phys.* **36**, 281–291 (1975)

55. Des Cloizeaux, J.: *J. Phys.* **36**, 1199–1203 (1975)
56. Odijk, T.: *J. Polym. Sci. Polym. Phys. Ed.* **16**, 627–639 (1978)
57. Wang, L., Bloomfield, V.A.: *Macromolecules* **23**, 804–809 (1990)
58. Odijk, T.: *Macromolecules* **12**, 688–693 (1979)
59. Manning, G.S.: *J. Chem. Phys.* **51**, 924–933 (1969)
60. Malvern Instruments, DLS Technical notes, MRK656 (<http://chemikalie.upol.cz/skripta/msk/MRK656.pdf>)
61. Aschinger, A., Winter, J.: *New J. Phys.* **14**, 093035 (2012)
62. Kanai, S.: Phase separation kinetics of polyelectrolyte solutions, Ph.D. thesis, University of Massachusetts Amherst (2006)
63. Sartor, M.: Dynamic light scattering. University of California, San Diego
64. Deguchi, S., Ghosh, S.K., Alargova, R.G., Tsujii, K.: *J. Phys. Chem. B* **110**, 18358–18362 (2006)
65. Murphy, R.J.: Translocation of synthetic polyelectrolytes through protein and synthetic nanopores. Ph.D. thesis, University of Massachusetts Amherst (2007)
66. Dzakpasu, R., Axelrod, D.: *Biophys. J.* **87**, 1279–1287 (2004)
67. Pynn, R.: Neutron Scattering -a Non-Destructive Microscope for Seeing Inside Matter Neutron Applications in Earth, Energy and Environmental Sciences, pp. 15–36. Springer, New York (2009)
68. Fitzsimmons, M.R., Schuller, I.K.: *J. Magn. Magn. Mater.* **350**, 199–208 (2014)
69. Dittrich, H., Bieniok, A.L.: Measurement Methods - Structural Properties: X-Ray and Neutron Diffraction. Elsevier, pp. 718–737 (2009)
70. Loong, C.K.: *J. Phys. Chem. Solids* **60**, 1397–1401 (1999)
71. Hall, P.L.: Neutron Scattering Techniques for the Study of Clay Minerals Developments in Sedimentology, pp. 51–75. Elsevier, Amsterdam—Oxford—New York (1982)
72. Band, Y.B., Avishai, Y.: Electronic Properties of Solids Quantum Mechanics with Applications to Nanotechnology and Information Science, pp. 381–544. Elsevier, Amsterdam—Oxford—New York (2013)
73. Lewis, E.E.: Neutron Interactions Fundamentals of Nuclear Reactor Physics, pp. 29–56. Elsevier, Amsterdam—Oxford—New York (2008)
74. Greene, G.L.: *Physica B + C*, 136, pp. 121–125, (1986)
75. Byron, O., Gilbert, R.J.: *Curr. Opin. Biotechnol.* **11**, 72–80 (2000)
76. Loong, C.K.: *J. Phys. Chem. Solids* **60**, 1397–1401 (1999)
77. Fitzsimmons, M.R., Schuller, I.K.: *J. Magn. Magn. Mater.* **350**, 199–208 (2014)
78. Lopez-Rubioa, A., Gilbert, E.P.: *Trends Food Sci. Technol.* **20**, 576–586 (2009)
79. Luk, A., Murthy, N.S., Wang, W., Rojas, R., Kohn, J.: *Acta Biomater.* **8**, 1459–1468 (2012)
80. Colmenero, J., Moreno, A.J., Alegre, A.: *Prog. Polym. Sci.* **30**, 1147–1184 (2005)
81. Ramirez-Cuesta, A.J., Jones, M.O., David, W.I.F.: *Mater. Today* **12**, 54–61 (2009)
82. Ryzewska, K., Herringerb, S., Bilheuxc, H., Walkerb, L., Sheldonb, B., Voisinc, S., Bilheuxc, J.-C., Finocchiaro, V.: *Phys. Procedia* **43**, 343–35 (2013)
83. Siourisa, I.M., Walter, J.: *Phys. B* **385–386**, 225–227 (2006)
84. Sinha, S.K.: *J. Phys. Chem. Solids* **68**, 2048–2051 (2007)
85. Kearley, G.J., Johnson, M.R.: *Vib. Spectrosc.* **53**, 54–59 (2010)
86. Strobl, M.: *Nuc. Instrum. Methods Phys. Res. A* **604**, 646–652 (2009)
87. Song, J.H., Murphy, R.J., Narayan, R., Davies, G.B.H.: *Philos. Trans. Roy. Soc. B* **364**, 2127–2139 (2009)
88. Davis, G., Song, J.: *Ind. Crops Prod.* **23**, 147–161 (2006)
89. Pal, K., Paulson, A.T., Rousseau, D.: Biopolymers in Controlled-Release Delivery Systems, Modern Biopolymer Science, pp. 519–557, (2009)
90. Enderle, J., Blanchard, S., Bronzino, J.: Biomaterials: Properties, Types and Applications Introduction to Biomedical Engineering, pp. 519–557. Academic Press, San Diego, California (2005)
91. Yates, M.R., Barlow, C.Y.: *Resources. Conserv. Recycl.* **78**, 54–66 (2013)

92. Rudin, A., Choi, P.: Biopolymers, the Elements of Polymer Science and Engineering, 3rd edn, pp. 521–535. Academic Press, USA (2013)
93. Tirrell, J.G., Tirrell, D.A.: *Curr. Opin. Solid State Mater. Sci.* **1**, 407–411 (1996)
94. Nanda, R.K., Tewari, R Govil, G.: Govil Structure of Polynucleotide and Nucleic acids. *Bull. Nat. Acad. Sci. In: Proceedings of Kanekar Memorial Symposium*, 40, 226 (1974)
95. Loewen, P.C., Khorana, H.G.: *J. Biol. Chem.* **248**, 3489–3499 (1973)
96. Berg, J.M., Tymoczko, J.L., Stryer, L.: Biochemistry. W.H. Freeman, New York (2002)
97. Chow, D., Nunalee, M.L., Lim, D.W., Simnick, A.J., Chilkoti, A.: *Mater. Sci. Eng. R* **62**, 125–155 (2008)
98. Nitta, Y., Nishinari, K.: *J. Biol. Macromol.* **5**, 47–52 (2005)
99. Soroudi, A., Jakubowicz, I.: *Eur. Polymer J.* **49**, 2839–2858 (2013)
100. Bastioli, C.: Handbook of biodegradable polymers. Rapra Technology Limited (2005)
101. Copek, I.: *Adv. Colloid Interface Sci.* **112**, 1–29 (2004)
102. Iojoiu, C., Genova-Dimitrova, P., Mafechal, M., Sanchez, J.Y.: *Electrochim. Acta* **51**, 4789–4801 (2006)

Biological Polyelectrolytes: Solutions, Gels, Intermolecular Complexes and Nanoparticles

H.B. Bohidar and Kamla Rawat

Abstract In this chapter, a detailed discussion on the salient features of structures of biomolecules like proteins, carbohydrates and nucleic acids is presented. Intermolecular interactions leading to phase separation, coacervation and nanoparticle formation is discussed herein. Biomolecular solutions exist as gels, coacervates, dispersions and melts with each of these phases having its signature physico-chemical properties, which is discussed in this chapter. The discussions are supported by robust experimental data obtained from an array of methods like turbidimetry, elecrophoresis, viscosity, light scattering etc. The inevitability of the phenomenon of self-organization in biopolymers results in the generation of a variety of soft matter phases which do not, however, make it predictable. For instance, the associative aggregation is a process which remains obscure, as every protein aggregates in a different manner under different conditions. One known feature to the aggregation of proteins is the strong dependence upon pH, salt concentration and temperature. Beyond the influence of these factors and their effects on aggregation, the process is not well understood. An increase in protein usage in biomedical and pharmaceutical studies implicates protein aggregation in Alzheimer's, Parkinson's and other diseases, and have placed a growing importance upon understanding this behaviour in general. Comparison of the system to other protein-polyelectrolyte systems suggests that the preferential binding of the two could be a result of complexation of the two molecules which often lead to coacervation. Such association can even occur at pH greater than the isoelectric points (pI), when the net charge of protein is of the same sign as that of

H.B. Bohidar (✉) · K. Rawat

Special Center for Nanosciences, School of Physical Sciences, Jawaharlal Nehru University,
New Delhi 110067, India
e-mail: bohi0700@mail.jnu.ac.in; bohidar@hotmail.com

K. Rawat

e-mail: kamla@aol.in; kamla.jnu@gmail.com

H.B. Bohidar

School of Physical Sciences, Jawaharlal Nehru University, New Delhi 110067, India

polyelectrolyte. Such binding though prevalent in nature is not well understood. In summary, a comprehensive account of biomolecular phase states and their inherent attributes are presented in this review.

1 Introduction to Biological Polyelectrolytes

Biological polyelectrolytes are essential component of molecular biophysics. These molecules self-organize to higher order assemblies to yield cells and intelligent organization of cells produce living organism. These aerobic and anaerobic organisms constitute the biosphere. The living organism and the biosphere are not isolated; they exchange matter and energy continuously. From the thermodynamic perspective “*A living organism feeds on negative entropy*”. More specifically, biophysics is the study of life phenomenon. Several alternative definitions exist. For example, the postulate of life states as “*Life itself should be looked upon as a basic postulate of biology that does not lend itself to further analysis*”. According to Bohr’s Uncertainty Principle “*Physico-chemical properties of the living organisms and the life phenomenon cannot be studied simultaneously*”. This implies that cognition of one excludes the other. According to “*An organism is an aperiodic crystal*”. This is a very well defined in conceptualization of any organism. An organism is a complex many-body system of numerous biomolecules interacting through enumerable physico-chemical reactions in an orderly, coordinated and regulated manner. In physical science, a crystal exhibits spatial order which allows a comprehensive description of this material through statistical means. However, no such order is observed in living organisms. Nonetheless, millions of biochemical reactions are carried out with excellent accuracy and reproducibility inside the numerous cells which constitute the organism.

Biological macromolecules in solutions can be distinctly characterized from their transport behaviour in solution phase. The study of transport processes yields physical parameters like the diffusion coefficient, sedimentation coefficient, intrinsic viscosity, friction constant etc. of the dissolved solute molecule. These coefficients are dependent on two parameters. First, is the size and shape of the solute particle? Second, is the type of the solvent medium and its environment (pH, temperature, pressure, ionic strength etc.). The solvent medium can force the diffusing particles to assume a special shape and/or to get distributed in a special fashion in space through solvent–solute interactions. At the same time a pair of solute molecules will also influence each other’s behaviour and/or their physical shape and size. This process may or may not be mediated by the solvent. To account for all these mechanisms, we need to discuss the solute–solvent, solvent–solvent and solute-solute interactions. Interestingly enough, much of this information is contained in the transport coefficients of a solute and physical parameters describing a solvent.

Biopolymers such as proteins, nucleic acids and carbohydrates carry a number of charged groups in their monomers. Therefore, they can also be referred to as either *polyampholytes* or *polyelectrolytes*. Polyelectrolyte molecules carry only one type of charge regardless of the solution pH. Thus, these can be *polyanionic* or *polycationic*. In contrast, polyampholyte molecules can bear positive or negative charge depending on solution pH. For example, proteins contain both acidic and basic residues that selectively dissociate as per solution pH.

Macromolecules can exist as macro ions or flexible polyelectrolyte chains. The interactions between the charge groups present on them determine their properties. Their charge, in turn, are dictated by the degree of dissociation of ionogenic groups and the surrounding ion atmosphere. The conformation of the polyelectrolyte chains is controlled by the minimum sum of conformational and electrical free energies. Like charges lead to mutual repulsion and uncoiling of the chain and increase in the size of the biopolymer. It is assumed that the coil and solution it immobilises are electrically neutral. It has been proved that the electrostatic interactions in polyelectrolyte chains only expand the coil. This is in concurrence with the experimental data which is clearly seen from the dependence of intrinsic viscosity on molecular weight. Further, because of shielding by counter ions, the charge on those macromolecules which are secluded from each other interact only during fluctuation due to inadvertent approach. This leads us to deduce that the conformational charge on polyelectrolytes is in between that of ideal random coils and rigid rods.

The maximum capacity of a macromolecule to uncoil is revealed at low ionic strength. The expansion of the coil is directly proportional with the dilution of the solution, since at constant degree of dissociation, decrease in concentration results in decreased ionic strength.

The charged group of polyelectrolytes can bind to counter ions specifically. This binding is essentially the formation of salt linkages at precise points on the macromolecule and determines the ion exchange property of the biopolymer of interest. This linked counter ion is located at a much shorter distance from charged group of macroion than the distance between it and the mobile counter ions. Due to this binding, a number of practical applications can be considered. Cross linked insoluble polyelectrolytes which swell in liquid media are made use of as ion exchange resins or *Ionites*. Ionites have the ability of adsorbing particular ions from solutions and can thus be used to purify and separate a number of electrolytes and to purify non-electrolytes from ion impurities.

In polyampholytes salt linkages can form in between anionic and cationic groups in single or multiple chains. The conformation of indigenous molecules of proteins and nucleic acids is influenced greatly by ionic and electrostatic interactions, including the ones with small ions of the medium. The charge state of a biopolymer is determined from the measurement of its electrophoretic mobility. Electrophoresis is the streaming of charged colloids in the presence of an external electric potential. This procedure can be employed for the study of proteins. The electrophoretic mobility of a polyelectrolyte or polyampholyte depends on the geometrical shape and size of the molecule, and ionic strength and pH of solution at constant temperature and pressure.

All nucleic acids and carbohydrates are high charge density polyelectrolytes whereas proteins are mostly weakly charged polyampholytes. Physics of nucleic acids deals with the study of molecular structure-property relationship in describing the life phenomena, in particular heredity and variability. The origin and development of molecular biophysics is associated with the genetic role of nucleic acids and with their interpretation. Physics has played a vital role in providing a foundation to molecular biology. For instance, the discovery of DNA duplex structure was facilitated by data obtained from X-ray diffraction studies by Watson and Crick [118]. They proposed a structure which has two helical chains each coiled around the same axis. The bases are located inside the helix whereas the phosphates on the outside. In case of biomolecules, the relation between the molecular structure and its biological function is not trivially correlated. Due to high linear charge density, DNA molecule acts as a strong polyelectrolyte.

Proteins comprise the largest percentage of organic molecules in the body. The term protein is derived from the Greek word “proteios” meaning the first place. They are nitrogen containing macromolecules. They are twenty in number and can be divided into various classes and these perform a variety of functions. Most cell processes are mediated by proteins. Proteins have both structural and dynamic functions. Structural functions include the formation of collagen and elastin which constitute the bone matrix; keratin present in the epidermis and the vascular system. Dynamic functions include protein containing blood clotting factors, enzymes, hormones, antibodies, membrane receptors etc. Other than their role in genetic control of muscle function.

Soft matter systems consist of charged molecular chains which play a fundamental role in determining structure, stability and the interactions of various molecular assemblies. Their unique properties are being exploited in a wide range of technological and industrial fields. It plays major role in biology and biochemistry. Many biological molecules are polyelectrolytes by nature and we shall be discussing some contemporary issue related to these molecules in this chapter.

2 Classification of Biological Polyelectrolytes

As has already been stated earlier, biological polyelectrolytes comprise of the important constituents: carbohydrates, proteins and nucleic acids. Section 2.1 through 2.3 are adapted from the forthcoming book of the author title.

2.1 Sugars (*Carbohydrates*)

Carbohydrates are the most abundantly occurring organic molecules. They are major dietary sources of energy and are made up of mainly carbon, hydrogen and oxygen. These are made up of monosaccharide repeat units which have a general

molecular formula given by $C_6H_{12}O_6$. The family of monosaccharides, of which glucose happens to be an important member, play most important role in the metabolism of plants and animals.

Carbohydrates are polyhydroxylaldehydes or ketones or compounds which produce them on hydrolysis. The name carbohydrate means ‘hydrates of carbon’. The term ‘sugar’ is used for those carbohydrates which are water soluble and sweet to taste. **Functions:**

- They are the most important source of energy for all organisms.
- Play a part in the structure of cell membrane and regulate functions such as cell growth, fertilization and adhesion.
- Stores forms of energy to meet the needs of the body.
- Serve as precursors for many organic compounds.

Classification: The saccharides can be classified into mainly three groups on the basis of the number of sugar units they possess i.e. into Monosaccharides, Oligosaccharides and Polysaccharides. The first two are crystalline in structure, water soluble and sweet to taste.

2.1.1 Monosaccharides

They are the simplest group of carbohydrates with formula $C_n(H_2O)_n$. They are further of two types:

Aldoses: The functional group in this is an aldehyde e.g. Glyceraldehyde, Glucose.

Ketoses: The functional group in this is a ketone e.g. Dihydroxyacetone, Fructose.

On the basis of number of carbon atoms the monosaccharides are referred to as trioses (3C), tetroses (4C), pentoses (5C), hexoses (6C) and heptoses (7C), e.g. glucose is an aldohexose while fructose is a ketohexose. The aldose and ketose sugar molecules are shown in Fig. 1.

Glyceraldehyde: It is the simplest monosaccharide with a single carbon atom. Its D- and L-isomers are mirror images of each other. The orientation of the –OH and –H group around a carbon atom (C_5 for glucose) adjacent to the terminal primary alcohol carbon atom determines the isomer. In naturally present mammalian tissues, monosaccharides are usually present in D-configuration.

The structures of various monomers of sugar molecules are shown in Fig. 2.

2.1.2 Structure of Glucose

The hydroxyl groups of monosaccharides can react with its own aldehyde or ketone functional group to form Hemiacetals or Hemiketals respectively. Therefore, when the aldehyde group of glucose at C_1 reacts with the alcohol group at C_5 ,

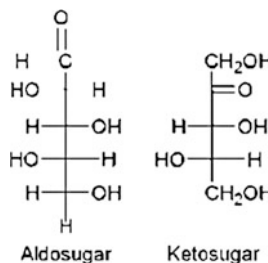


Fig. 1 The aldose and ketose sugar molecules

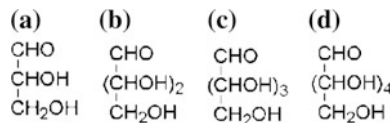
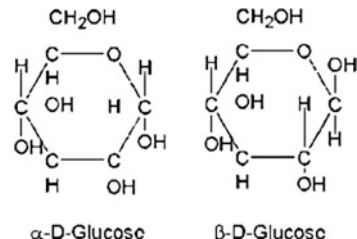


Fig. 2 Sugar monomers **a** triose: glyceraldehydes, **b** tetrose: threose, erythrose, **c** pentose: ribose, arabinose, xylose, lyxose, and **d** hexose: allose, gulose, altose, idose, galactose, mannose, glucose, talose

Fig. 3 The alpha and beta forms of D-glucose



two forms of cyclic hemiacetals are formed. They are known as α and β cyclic hemiacetals and have different optical rotations, structures shown in Fig. 3. Their inter-conversion is called as Mutarotation.

The structure of glucose molecule can be represented either as the Fischer formulae or the Howarth projection formulae. Howarth projection formulae have a six-membered ring pyranose or a five-membered ring furanose. The cyclic forms of glucose are known as α -D-glucopyranose and α -D-glucofuranose. These chemical structures of these molecules are depicted in Fig. 4.

The linear and cyclic conformations of D-glucose is shown in Fig. 5.

Glycosides: Glycosides are formed when the hemiacetal and hemiketal hydroxyl group of a saccharide reacts with that of another saccharide or a non-saccharide. The bond formed between them is called as a Glycosidic Bond. This is depicted in Fig. 6 in case of starch and cellulose molecules.

Some important glycosides are: Cardiac glycosides digoxin and digitoxin which stimulate heart muscle contraction; Streptomycin a commonly used antibiotic.

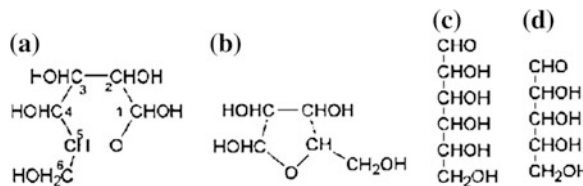


Fig. 4 **a** α -D-glucose in the pyranose form, **b** α -D-ribose in the furanose ring form, **c** aldose structure of D-glucose, and **d** aldose structure of D-ribose

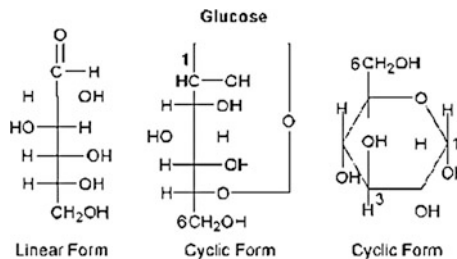


Fig. 5 The linear and cyclic forms of D-glucose

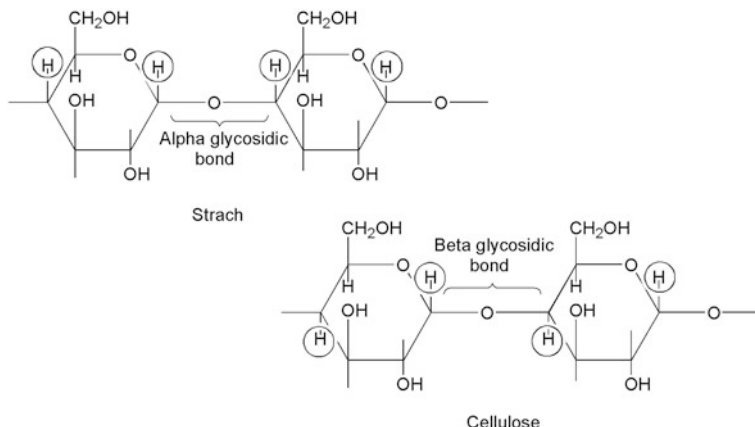


Fig. 6 Glycosidic bond and chemical structure of starch and cellulose

2.1.3 Oligosaccharides

Oligosaccharides contain 2–10 molecules of monosaccharides. Hence, they are further divided into disaccharides, trisaccharides etc.

Table 1 List of common disaccharides and their characteristic glycosidic bond assignments

Disaccharide	Units	Glycosidic bond
Maltose	Two α -D-glucose units	$\alpha(1 \rightarrow 4)$
Isomaltose	-Do-	$\alpha(1 \rightarrow 6)$
Cellobiose	-Do-	$\beta(1 \rightarrow 4)$
Sucrose	One α -D-glucose unit and one β -D-fructose unit	$(\alpha_1 \rightarrow \beta_2)$
Lactose	One β -D-galactose unit and one β -D-glucose unit	$\beta(1 \rightarrow 4)$

2.1.4 Disaccharides

These are the most common oligosaccharides. They consist of 2 monosaccharides held together by a glycosidic bond. They are crystalline, sweet to taste and water soluble (see Table 1 for a list).

They can be divided into two groups.

1. Reducing type with a free aldehyde or ketone group
2. Non-Reducing type with no free groups

2.1.5 Polysaccharides

These are polymers of monosaccharides and have high molecular weight. They can be linear as well as branched and are held together by glycosidic bonds. They are tasteless and insoluble in water. They are divided into two types:

1. Homopolysaccharides

They give only a single type of monosaccharide on hydrolysis and are named accordingly. Thus, glucans are polymers of glucose while fructosans are polymers of fructose. Their main function is storage of energy.

- (a) Starch: It is also known as Glucosan or Glucan. It is the main carbohydrate reserve of plants and the principal dietary source for higher organisms. It composes of D-glucose units held together by α -D-glycosidic bonds. Starch comprises of two polysaccharide components, namely Amylose (long unbranched chain, water soluble) and Amylopectin (branched chain, water insoluble). Amylose chain is linked together by $\alpha(1 \rightarrow 4)$ glycosidic linkages while amylopectin chain is joined together by $\alpha(1 \rightarrow 4)$ bonds and $\alpha(1 \rightarrow 6)$ linkages at branching spots.
- (b) Dextrin: These are the breakdown products of starch by the action of enzyme amylase. Starch undergoes sequential hydrolysis through various dextrins to finally form maltose and glucose.
- (c) Inulin: It is a polymer of fructose. It occurs in dahlia bulbs, onions, garlic etc. It is water soluble and is not utilised by the body.

- (d) Glycogen: It is the main carbohydrate reserve of animals, hence also called as Animal Starch. It is also found in those plants which lack in chlorophyll i.e. fungi, yeast etc. It is a repeating structure of glucose units held together by α (1 → 4) glycosidic bonds and α (1 → 6) glycosidic bonds at branching spots. Glycogen
- (e) Cellulose: It is found only in plants and is the most widely present organic substance in plants. It is a principal constituent of the plant cell wall. It is composed of β -D-glucose units held together by β (1 → 4) glycosidic bonds.
- (f) Agar: Agar comprises mainly of alternating β -(1-4)-D and α -(1-4)-L linked galactose residues in a way that most of α -(1-4) residues are modified by the presence of a 3,6-anhydro bridge. Other modifications commonly observed are mainly substitutes of sulphate, pyruvate, urinate or methoxyl groups. The gelation temperature of agar is primarily decided by the methoxy content of the sample.
- (g) Chitin: It is composed of N-acetyl D-glucosamine units held together by β (1 → 4) glycosidic bonds. It is a structural polysaccharide found in the exoskeleton of some invertebrates.

2. Heteropolysaccharides

They give a mixture of monosaccharides on hydrolysis and their main function is structural. When the polysaccharides are composed of various sugars as well as their derivatives they are called Heteropolysaccharides or Heteroglycans.

Mucopolysaccharides are heteroglycans made up of repeating units of sugars and their derivatives such as amino sugars and uronic acids. These are commonly called as Glycosaminoglycans (GAG). They contain mainly sulphate and carboxylic groups as well as acetylated amino groups. The extracellular tissue spaces consist of a ground substance in which the collagen and elastin fibres are embedded. This ground substance is primarily composed of GAGs. Some mucopolysaccharides combine with proteins to form Proteoglycans or Mucoproteins or Mucoids. Some important mucopolysaccharides are listed in Table 2 along with their functions. Some important mucopolysaccharides

A representative set of monomers of naturally occurring polysaccharides are illustrated in Figs. 7 and 8.

The structural formula of sucrose and amylose are shown in Figs. 9 and 10.

2.2 Amino Acids (Proteins)

Proteins are broken down into by hydrolysis into 20 different monomer units known as amino acids. Proteins comprise the largest percentage of organic molecules in the body. The term protein is derived from the greek word “proteios” meaning the first place. They are nitrogen containing macromolecules. They are 20 in number and can be divided into various classes and these perform a variety of

Table 2 Some important mucopolysaccharides

Glycosaminoglycan	Composition	Found in	Functions
Hyaluronic acid	D-glucuronic acid, N-acetyl glucosamine	Connective tissue, synovial fluid, vitreous humour	Lubricant, shock absorber, enhances wound healing
Chondroitin sulphate	D-glucuronic acid, N-acetyl glucosamine 4-sulphate	Cartilage, bone, skin, blood vessel walls	Maintains structure of tissues
Heparin	D-glucuronate 2-sulphate, N-sulpho glucosamine 6-sulphate	Blood, lung, liver, kidney, spleen	Anticoagulant
Dermatan sulphate	L-iduronic acid, N-acetyl galactosamine 4-sulphate	Blood vessel valves, heart valves	Maintains shape of tissues
Keratan sulphate	D-galactose, N-acetyl glucosamine 6-sulphate	Cartilage, cornea, connective tissue	Keeps cornea transparent

functions. Most cell processes are mediated by proteins. Proteins have both structural and dynamic functions. Structural functions include the formation of collagen and elastin which constitute the bone matrix; keratin present in the epidermis and the vascular system. Dynamic functions include protein containing blood clotting factors, enzymes, hormones, antibodies, membrane receptors etc. Other than their role in genetic control muscle function. Proteins are basically polypeptide chains formed by polymers of amino acids, specifically the L- α -amino acids. Proteins comprise of 5-elements of the periodic table: carbon (maximum), hydrogen, oxygen, nitrogen and sulphur (least).

The general structure of an amino acid is depicted in Fig. 11. There is central C_α carbon atom that is attached to a carboxyl group $-COOH$, an amino group $-NH_2$, H atom and a functional group R that defines the specific amino acid. These are attached at tetrahedral angle to the central C_α carbon atom through covalent bonds. Most amino acids are chiral molecules. The functional groups associated with various amino acids are listed in Table 2.

When dispersed in a solvent, the polar groups $-COOH$ and $-NH_2$ get ionized and attribute dipolar characteristics to the amino acid as shown in Fig. 12.

Amino acids contain two functional groups: amino $-NH_2$ and carboxyl $-COOH$. Amino groups are basic while the carboxylic groups are acidic. Physiologically they exist as dipolar ions commonly called as *Zwitter Ions* (Fig. 12). The $NH_2^+-CHR-COO^-$ amino acid dipole is associated with a large dipole moment. Thus, all protein molecules are dipolar in nature; a property that is used extensively to separate proteins.

- (a) Amino Acids: There exist almost 300 amino acids in nature. Of these, only 20 amino acids have been isolated consistently in all forms of life such as plants, animals and bacteria. This is because the universal nature of the genetic code produces only these 20 amino acids during protein biosynthesis. Hence, these are called as *Standard Amino Acids*.

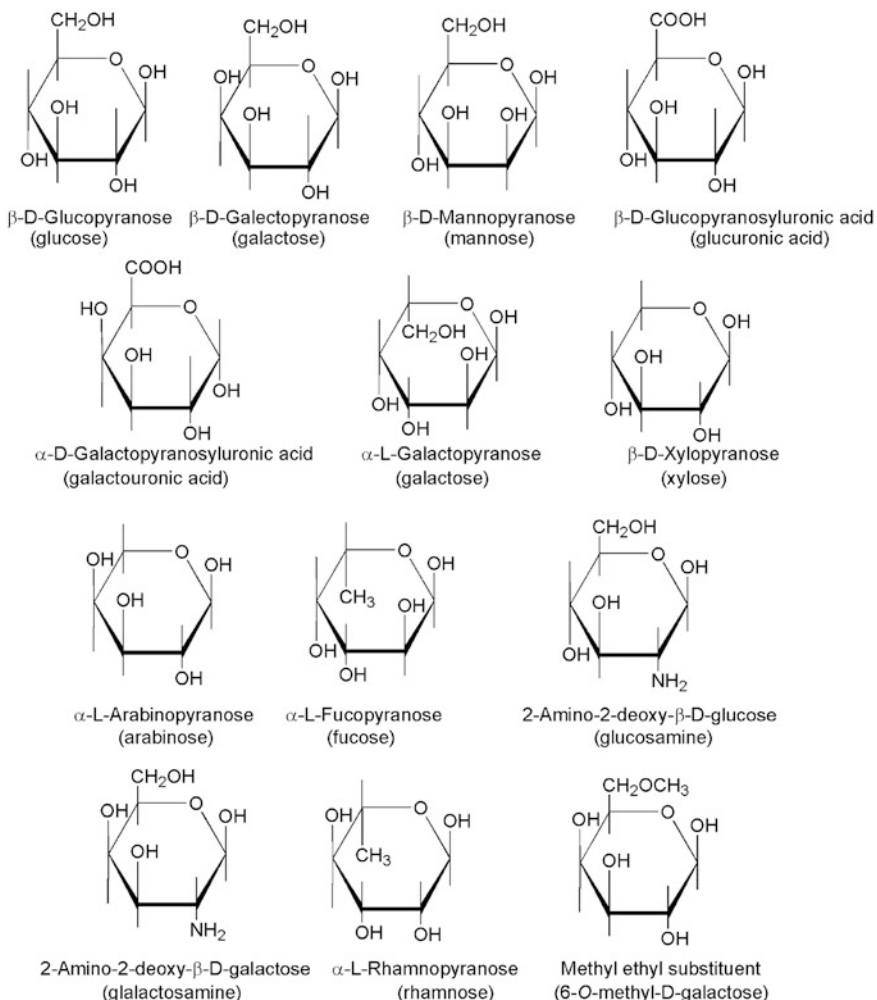
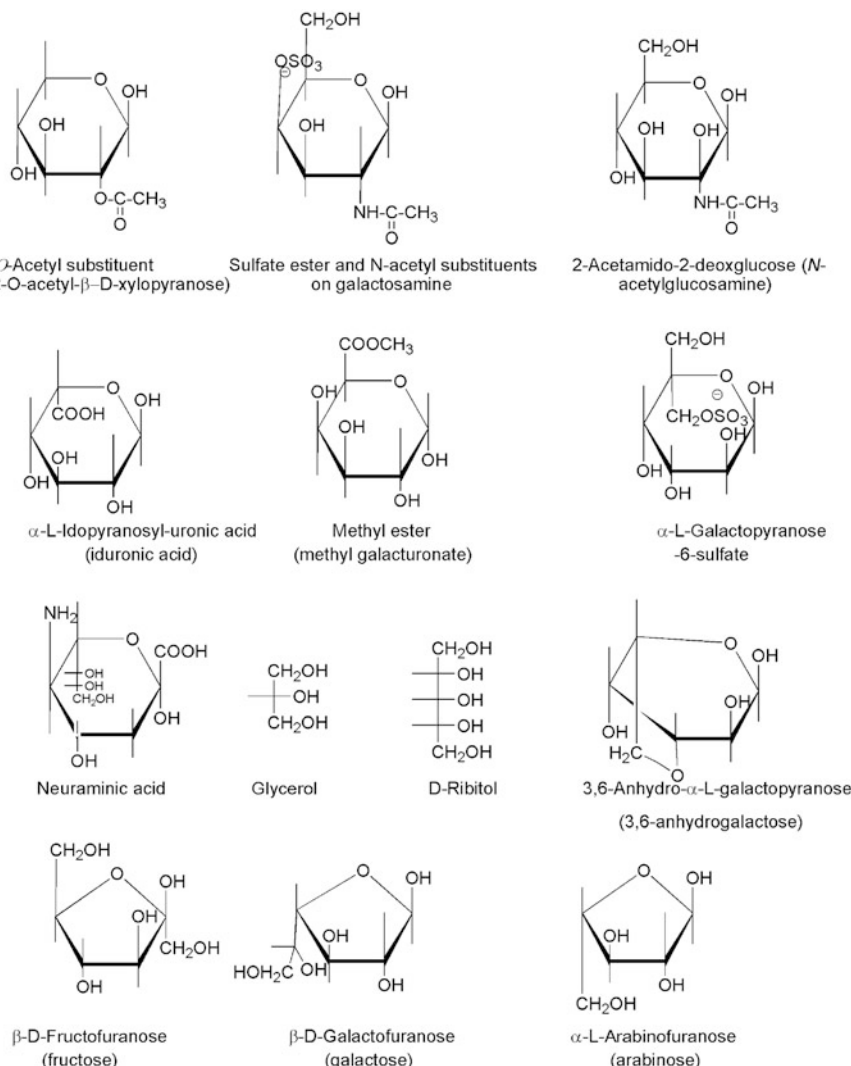
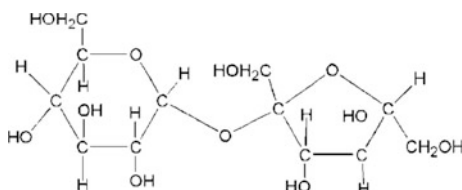
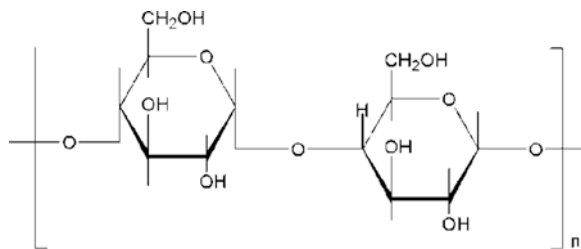
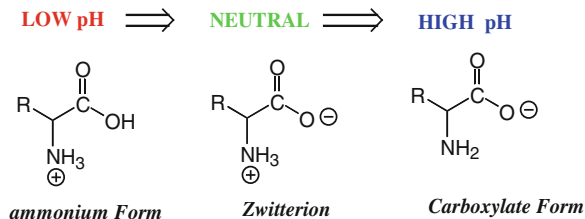


Fig. 7 Common monomers of natural polysaccharides

Other than the 20 amino acids present in proteins, there are numerous *Non-Standard Amino Acids*. Some of these are:

- Collagen which contains 4-hydroxyproline and 5-hydroxylysine.
- Histones contain many methylated, phosphorylated or acetylated amino acids.
- Cystine is a combination of two Cysteines.
- D-amino acids are found in antibiotics. D-serine and D-aspartame is found in brain tissue. D-alanine is found in bacterial cell walls.
- D-penicillamine is a metabolite of penicillin, used to chelate copper.

**Fig. 8** Common monomers of natural polysaccharides**Fig. 9** Chemical formula of sucrose (cane or beet sugar)

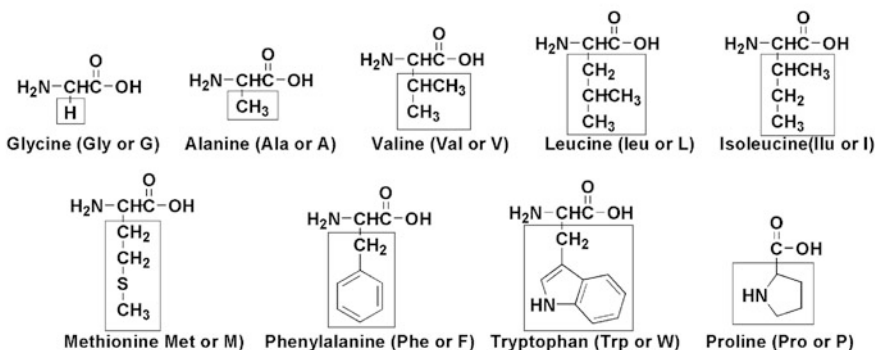
**Fig. 10** Chemical formula of amylose**Fig. 11** Basic structure of an amino acid and charged state shown as function of pH**Fig. 12** Dipolar character of an amino acid

The amino acids are termed as α -amino acids if both the amino and carboxylic groups are attached to same carbon atom. The α -carbon atom is linked to side chain which is different for all the 20 amino acids found in proteins. Table 3 provides a list of all the 20 amino acids. Amino acids are also referred to as residues in molecular biophysics. Of the amino acids, Arginine, Valine, Histidine, Isoleucine, Leucine, Lysine, Methionine, Phenylalanine, Tryptophan and Threonine are *Essential Amino Acids* as they can't be synthesised by the human body. However, Histidine and Arginine can be synthesised in the adult body even if not in growing children, and can therefore also be known as *Semi-Essential Amino Acids*. The rest all are *Non-Essential* or *Dispensable Amino Acids* as they can be formed by the body. Molecular structure of the amino acids is shown in Figs. 13, 14, 15, and 16.

Table 3 List of common amino acids

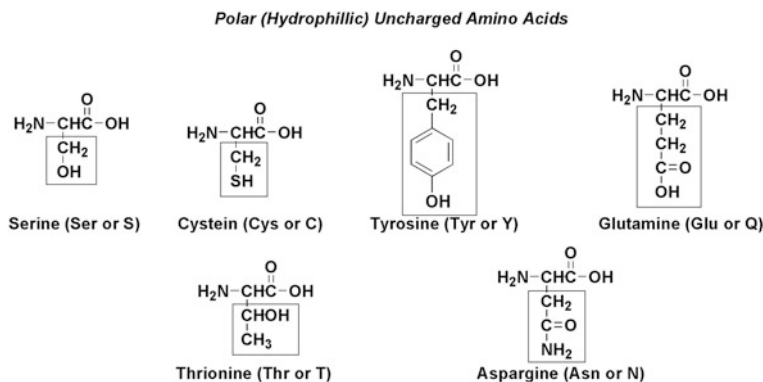
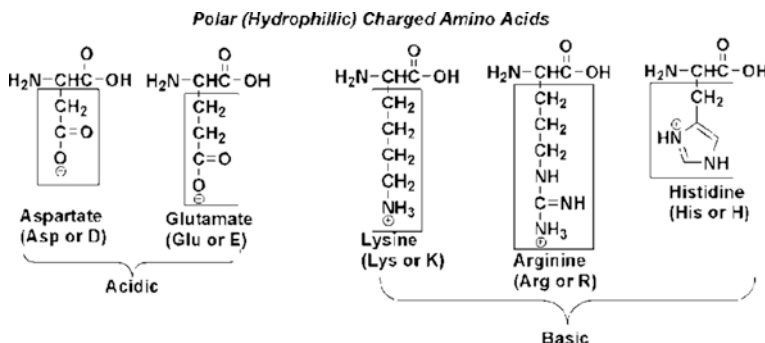
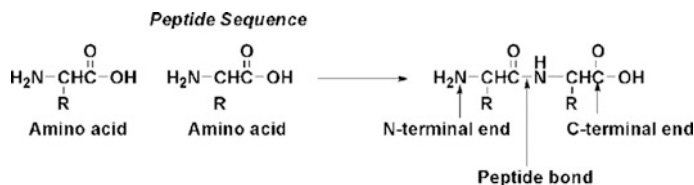
Name	3 Letter symbol	1 Letter symbol
Glycine	GLY	G
Alanine	ALA	A
Leucine	LEU	L
Isoleucine	ILE	I
Valine	VAL	V
Serine	SER	S
Threonine	THR	T
Methionine	MET	M
Cysteine	CYS	C
Glutamic acid	GLU	E
Glutamine	GLN	Q
Aspartic acid	ASP	D
Asparagine	ASN	N
Histidine	HIS	H
Arginine	ARG	R
Lysine	LYS	K
Tyrosine	TYR	Y
Tryptophan	TRP	W
Phenylalanine	PHE	F
Proline	PRO	P

Nonpolar (Hydrophobic) Amino Acids

**Fig. 13** Molecular structure of hydrophobic amino acids

2.2.1 Peptide Bond

The amino acids are held together by specific covalent linkages known as *peptide bonds*. When the amino group of an amino acid combines with the carboxyl group of another amino acid a peptide bond is formed through polycondensation

**Fig. 14** Molecular structure of hydrophilic amino acids**Fig. 15** Molecular structure of polar amino acids**Fig. 16** Formation of peptide bond through condensation reaction

reaction. Molecules containing less than 100 amino acids are known as polypeptides. The peptide bond is rigid and planar. It generally exists in trans-form as shown in Fig. 17. X-Ray structure analysis reveals that the peptide bond --CO--NH-- which joins two adjacent residues in a protein molecule has a specific planar structure. All the four atoms, in the peptide bond, lie on one plane (Fig. 17) which makes the covalent bonds conjugate.



Fig. 17 Planar Structure of peptide bond and its dipolar representation

For instance, the N–C bond in peptide bond is 0.132 nm long whereas in aliphatic amines –C–NH₂– similar bond has a length 0.147 nm. This shortened bond and planar nature of peptide bond allows conjugation of C=O and N–C bonds. Hence, there is considerable overlap of their electron shells and there is a shift of electron density from N to C to O. This makes the N–C bond partially double C=O bond partially single. In addition, the peptide bond attains a dipolar character as shown in Fig. 17.

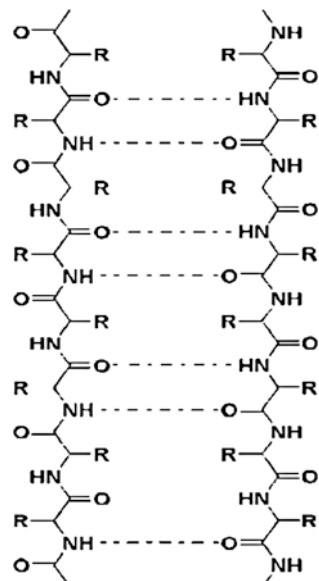
2.2.2 Structure of Proteins

Proteins are polymers of amino acids. The term protein is only used for those assemblies having more than 50 amino acids. Protein biological activity is not manifested in assemblies containing less than this number of residues. Hence, the term polypeptide is normally used to refer to such molecular assemblies. The bio-functionality of the protein molecules owes its origin to many factors of which the conformation is an important component. The conformational state of proteins can be divided into 4 hierarchical levels:

- (a) The *primary structure* largely dictates its function through its amino acid composition. Here the sequence of residues present in the protein molecule is written in a three letter alphabet code. As we shall learn later, this sequence is determined by genes present in DNA. The mRNA, tRNA and rRNA play the roles of transcribing, transferring and linking the amino acid sequence. The primary structure is not biologically active.
- (b) *Secondary Structure* is dictated by the folding strategy based on amino acid interactions. This is the biologically active form of a protein molecule. Two types of structures α -helix and β -sheet have been isolated commonly. The α -helix is a tightly packed coil around a central axis with amino acid chains extending outwards. The structure is maintained by the formation of large number of hydrogen bonds. The right handed helix is more stable. Typically, each turn consists of 3.6 amino acids and the space between each amino acid is 0.15 nm.

The β -sheet consists of two more fragments of fully extended peptide chains which can be arranged in either parallel or anti-parallel direction. The hydrogen bonds are formed by adjacent segments of polypeptides. This structure can be formed by either multiple chains or by a single chain folding onto itself. A typical β -sheet is shown in Fig. 18.

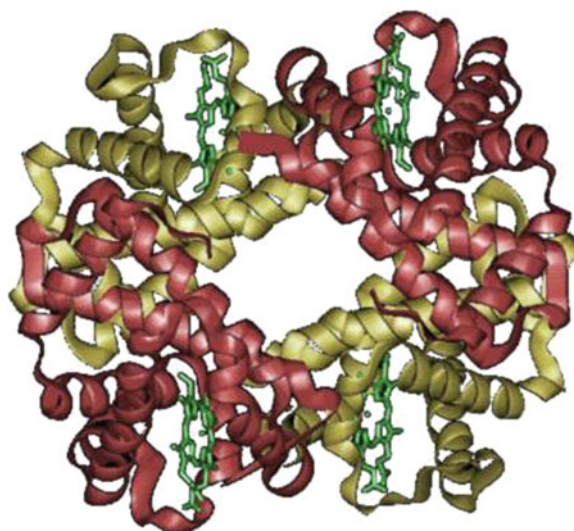
Fig. 18 Typical β -sheet structure representation of a protein molecule



- (c) *Tertiary Structure* of proteins is a three dimensional compact arrangement. The hydrophobic side chains are facing towards the core while the hydrophilic groups are directed towards the periphery. Other than the hydrogen bonds, disulfide bonds, hydrophobic interactions and electrostatic interactions also contribute to stability of the structure. The term ‘domain’ denotes the basic unit of structure and function of protein. A domain of 50–350 amino acids is required to fulfill a specific function.
- (d) *Quaternary Structure* of many proteins consists of two or more polypeptide chains into a single protein with multiple subunits. They are held together by hydrogen and ionic bonds and hydrophobic interactions. These can be dissociated in laboratory experiments but these are quite stable *in vivo*. A common way to describe a quaternary structure is through the quantitative designation of each protein present. For example, a molecule designated as $\alpha\beta\gamma$ indicates existence one unit each of the three distinct protein chains (α , β and γ). On the other hand, $\alpha_1\beta_3\gamma_2$ indicates an assembly of one unit of α , three units of β and two units of γ chains. Common examples of this structure are haemoglobin, DNA polymerase and ion channels. Their function is to regulate cellular function and metabolism. A quaternary structure of haemoglobin is shown in Fig. 19.

Hemoglobin has a tetramer consisting of two dimers that bind to oxygen. It is the oxygen binding protein of red blood cells and is a globular protein with quaternary structure. The structure consists of four polypeptide subunits: 2 alpha chains and 2 beta chains. There are two states of hemoglobin, the T state (the tense state) and the R state (the relaxed state). The T state has a less of an affinity for oxygen than the R state.

Fig. 19 Quaternary structure of Hemoglobin molecule. It contains four polypeptide chains: two alpha chains, each with 141 amino acids and two beta chains, each with 146 amino acids. Thus has quaternary representation $\alpha_2 \beta_2$



Some functionally important proteins are listed in Table 4.

2.3 Nucleic Acids

The genetic information required for the function and replication of biological organism is provided by nucleic acids.

There are mainly two types of nucleic acids, namely *deoxyribonucleic acid* (DNA) and *ribonucleic acid* (RNA). Primarily nucleic acids serve as repositories and transmitters of genetic information. The DNA is organised into genes which are the fundamental units of genetic information. These genes control protein synthesis. Components of nucleic acids are sugar, base and phosphate diester molecules; nucleic acids are polymers of nucleotides held by 3' and 5' phosphate bridges.

- Sugars: RNA contains *D-Ribose* while DNA contains *D-Deoxyribose*. They differ in structure at C₂ where deoxyribose has one oxygen less than ribose. This is shown in Fig. 20.
- Bases: The nitrogenous bases of *purine* and *pyrimidine* derivatives are found in nucleotides. These are aromatic heterocyclic compounds. Purines are numbered in anti-clockwise direction and Pyrimidines in clockwise direction. DNA and RNA contain the same purines i.e. Adenine (A) and Guanine (G). The pyrimidine Cytosine (C) is found in both. However, with respect to the second pyrimidine base DNA contains Thymine (T) while RNA contains Uracil (U). The molecular structure of these nitrogenous bases is illustrated in Fig. 21.

Table 4 List of functionally important proteins

Name	Function
Keratin	Hair and nail growth
Collagen/Gelatin	Bone and muscle function
Hexokinase	Enzymatic/Catalytic
Pepsin	Enzymatic/Catalytic
Haemoglobin	Transport protein
Serum albumin	Transport protein
Insulin	Hormonal protein
Growth hormone	Hormonal protein
Actin	Motor Control
Myosin	Motor Control
Ovalbumin	Storage protein
Glutelin	Storage protein
Nucleoprotein	Genetic protein
Immunoglobulin	Defense protein

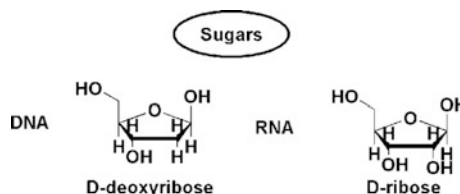
**Fig. 20** Representation of sugar molecule found in DNA and RNA

Fig. 21 Top figure shows various nitrogenous bases, the phosphate diester and the deoxyribose molecules. These three components join to produce a nucleotide shown in the bottom figure

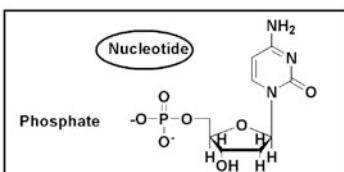
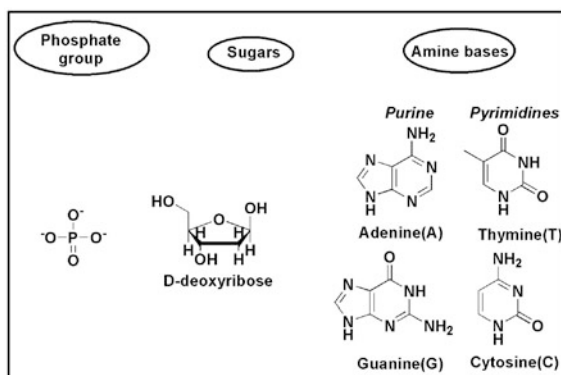


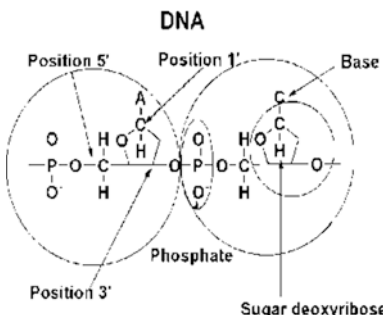
Table 5 Representation of various nucleosides, nucleotides of DNA and abbreviations used to designate these are shown in this table

Base	Deoxyribonucleoside	Deoxyribonucleotide	Abbreviation
Adenine	Deoxyadenosine	Deoxyadenosine 5'-monophosphate	dAMP
Guanine	Deoxyguanosine	Deoxyguanosine 5'-monophosphate	dGMP
Cytosine	Deoxycytidine	Deoxycytidine 5'-monophosphate	dCMP
Thymine	Deoxythymidine	Deoxythymidine 5'-monophosphate	dTMP

Table 6 Representation of various nucleosides, nucleotides of RNA and abbreviations used to designate these are shown in this table

Base	Ribonucleoside	Ribonucleotide	Abbreviation
Adenine	Adenosine	Adenosine 5'-monophosphate	AMP
Guanine	Guanosine	Guanosine 5'-monophosphate	GMP
Cytosine	Cytidine	Cytidine 5'-monophosphate	CMP
Uracil	Uridine	Uridine 5'-monophosphate	UMP

Fig. 22 Sugar, phosphate and base linkage in DNA molecule



- (c) *Nucleotides:* Nucleotides are composed of a nitrogenous base, a pentose sugar and a phosphate. The term nucleoside refers to base + sugar. Therefore nucleotides are nucleoside + phosphate. Nucleotides also perform a variety of cellular functions such as metabolic regulators, energy carriers, secondary messengers etc. A representative nucleotide structure is shown in Fig. 21. Tables 5 and 6 give a comprehensive list of various nucleosides and nucleotides for DNA and RNA molecules. Their abbreviated designations used in molecular biophysics are listed in these tables.
- (4) Structure of DNA: DNA is the chemical basis of heredity which is assembled as genes, the basic unit of genetic information. DNA is a polymer of deoxyribonucleotides, composed of the following units—dAMP, dGMP, dCMP and dTMP. The monomeric units in DNA are held together by 3'-5'-phosphodiester bridges. The horizontal line indicate the carbon chain of sugar with base attached to C_{1'}. At the other end of the line is C_{5'} phosphate linkage. This is clearly shown in Fig. 22.

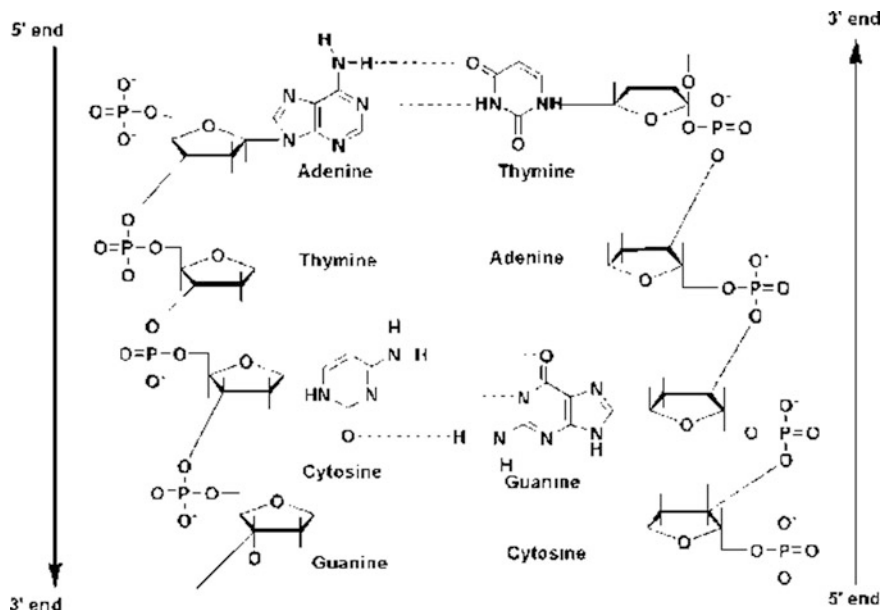


Fig. 23 Stacking of amine bases through hydrogen bonding yields DNA double helix structure. Realize that A-T and G-C are connected through two and three hydrogen bonds respectively. This makes the G-C binding much stronger

- (e) *Chargaff's Rule:* It states that DNA has equal number of adenine and thymine residues ($A=T$) and equal number of guanine and cytosine residues ($G=C$). This is known as Chargaff's Rule of molar equivalence between purines and pyrimidines. The double helical structure of DNA is based entirely upon this rule. RNA (usually single stranded) and single stranded DNA do not follow this rule. A and T, and G and C are called base pairs in DNA. The same in RNA is A and U, and G and C. DNA double helix structure owes its origin to the extensive hydrogen bonding between base pairs, which is shown in Fig. 23.
- (f) **DNA Double Helix:** The double helical structure of DNA was discovered by Watson and Crick in 1953 (Nobel Prize 1962). The structure of DNA double helix is comparable to that of a twisted ladder. Some salient features of the most common form of DNA, called *B-DNA*, are discussed below.

Salient Features:

- The DNA is a right handed double helix. It consists of two polydeoxyribonucleotide chains twisted around each other along a common axis.
- The two polynucleotide chains are complimentary to each other as a result of base pairing.
- The two strands are anti-parallel i.e. one runs in the 3' to 5' direction while the other runs in the opposite direction.
- The width of double helix is 2 nm.

- Each turn i.e. the helix pitch is 3.4 nm with 10 base pairs of nucleotides, each placed at a distance of 0.34 nm (B-DNA).
- Each strand has a hydrophilic deoxyribose phosphate backbone (3'-5'-phosphodiester bonds) on the periphery of the molecule while the hydrophobic bases are packed inside the core.
- The two strands are held together by hydrogen bonds formed by complimentary base pairs. The A-T pair has two hydrogen bonds while the G-C pair has three hydrogen bonds. Therefore the G-C bond is stronger by 50 %.
- The hydrogen bonds are formed between a purine and pyrimidine only. If two purine rings faced each other they would not fit into the available space while the two pyrimidines would be too far away to form a bond.
- The complimentary base pairing proves Chargaff's Rule.
- The genetic information is stored on one of the two strands called as the Template Strand. The other strand is the Antisense Strand. The double helix has major and minor grooves along the phosphodiester backbone where the proteins interact with the DNA without disrupting its structure.

Other than the double helix structure, DNA also exists in other less common forms such as Bent DNA, Triple stranded and four stranded DNA.

- (g) Conformations of the DNA Double Helix: The double helical structure of DNA exists in 6 forms A-E and Z of which the forms B, A and Z are the most important.

B-form of DNA is the most predominant physiologically and is explained above.

The A-form is also right handed helix. It contains 11 base pairs per turn and there is tilting of base pairs by 20° away from the axis.

The Z-form is a left handed helix and contains 12 base pairs per turn. The strands of DNA move in a somewhat zigzag pattern.

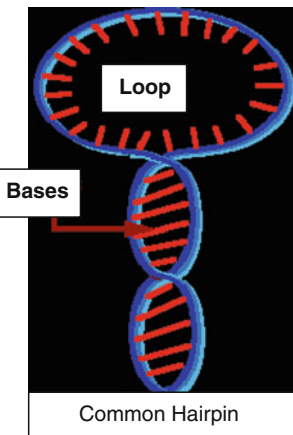
Unit of length of the DNA double strand is expressed as base pairs (bp). A kilobase pair (kbp) is 1,000 bp while a megabase pair (mbp) is 1,000,000 bp. The gigabase pair (gbp) is equal to 1,000 mbp. It may be noted that the genomic length of DNA is much larger as compared to the size of cell or nucleus containing it. For instance a 2 m long DNA is packed compactly in cell nucleus of 10 µm diameter. Prokaryotic DNA is present as a single chromosome in the form of a double stranded circle and is packed as Nucleoids. Eukaryotic DNA is associated with a variety of proteins to form Chromatin. These are further arranged as compact structures called as Chromosomes.

- (h) Structure of RNA

RNA is a polymer of ribonucleotides held together by 3'-5'-phosphodiester bridges. Although it is similar to DNA, it also varies in many aspects of its structure. The sugar in RNA is ribose in contrast to deoxyribose of DNA. It contains Uracil instead of Thymine. It is usually a single stranded structure.

Table 7 Various forms of RNA, their abbreviated representations and biological functions are listed in this table

Type	Abbreviation	Function
Messenger RNA	mRNA	Provides genetic information to ribosomes for protein biosynthesis
Heterogeneous nuclear RNA	hnRNA	Precursor for all types of RNA
Transfer RNA	tRNA	Transfers amino acid to mRNA during protein biosynthesis
Ribosomal RNA	rRNA	Governs structural framework of ribosomes
Small nuclear RNA	snRNA	Processing of mRNA
Small nucleolar RNA	snoRNA	Processing of rRNA
Small cytoplasmic RNA	scRNA	Selects proteins for export
Transfer-messenger RNA	tmRNA	Mostly found in bacteria

Fig. 24 Common hairpin structure of RNA molecule

However, it may fold in many places to give a double stranded structure if complimentary base pairs are in close proximity. Chargaff's rule not obeyed due to single stranded structure. Various known types of RNA, their designations and biological functions are listed in Table 7.

Specific types of RNAs can also function as enzymes named as Ribozymes. These function either as catalysts or assist in self-processing reactions of RNA. RNA assumes many conformations; a commonly occurring hairpin structure is shown in Fig. 24.

3 Biological Polyelectrolytes in Solutions

3.1 Biological Polyelectrolytes in Aqueous Solutions

As has been discussed earlier biological polyelectrolytes are commonly available as nucleic acids, polyamino acids and polysaccharides. In this section, we shall discuss the aqueous state behavior of three representative biopolymers: DNA (a nucleic acid), gelatin (a polyamino acid) and cellulose (a polysaccharide). The solution properties of biopolymers have many dimensions and the least discussed feature is their persistence length. This is a length scale that plays a central role in governing intermolecular interactions. Hence, herein the focus has been centered around the evaluation of persistence length of the aforesaid biopolymers from experimental data.

3.1.1 Cellulose

This section has been adopted from our previous work [3, 4]. Cellulose is world's one of the most abundant biopolymers. It forms skeletal material of plant cell walls. The polymorphic forms and derivatives of cellulose are the subject of a large body of work. Hydroxyethyl cellulose (HEC) is a low charge density hydrophilic biopolymer. Cationic polymers, particularly biopolymers, have found applications as stabilizers and thickeners in paint formulations and as, hair and, eye-care solutions. The remarkable physical properties associated with cellulose polymers accrue from their water and organic solvent solubility, their thermal plasticity, their thickening and colloid stabilizing abilities, which is described in excellent details by Eastman and Rose [31], Archer [2] and Saito et al. [92]. Native cellulose is known to comprise long microfibrils with different cross-sectional dimensions, depending on the source of the specimen [51, 56, 93, 91]. However, most of the cellulose samples show presence of regular fibrils having 3.5 nm diameter. These elementary fibrils have a tendency to coagulate and produce larger crystallite widths in the range 5–10 nm, identified as microfibrils [55].

Polymer theory of dilute solutions predicts universal behaviour for key static properties of the polymer chains in the limit of very high degree of polymerization. The main thing of interest here is that these properties depend only on the overall extension of the chain and not on its chemical character or individual segment size. Thus, it was felt imperative to analyze the molecular properties of HEC in this well established framework. Aqueous solutions of HEC, having molecular weights $M_1 = 9 \times 10^4$ Da, $M_2 = 7.2 \times 10^5$ Da and $M_3 = 1.3 \times 10^6$ Da, were subjected to viscosity studies and the intrinsic viscosity, (η), of each sample was determined (Fig. 25). The calculated value of intrinsic viscosity were 1.16, 7.28, 9.77 dL g⁻¹ for samples with molecular weights M_1 , M_2 and M_3 respectively.

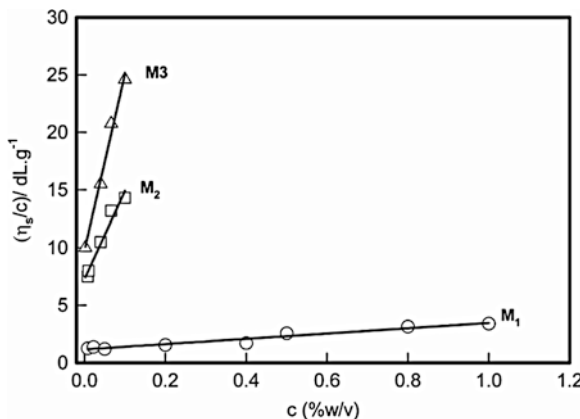
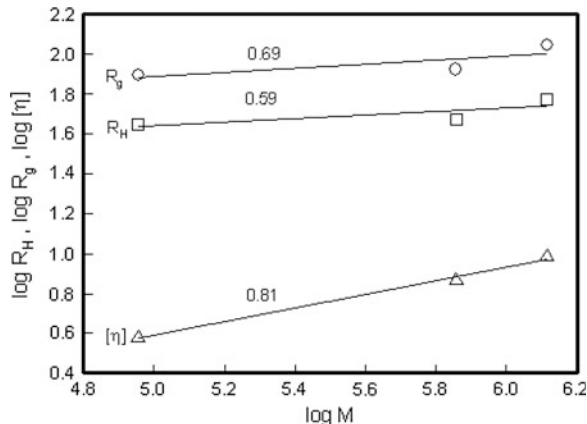


Fig. 25 Plot η_s/c as function of polymer concentration for samples with molecular weights, $M_1 = 9 \times 10^4$, $M_2 = 7.2 \times 10^5$ and $M_3 = 1.3 \times 10^6$ Da. The $c \rightarrow 0$ interpolation yields the intrinsic viscosity value (Reproduced with permission from Elsevier [3, 4])

Fig. 26 Depiction of various scaling relations given by Eqs. (1)–(3). The figures on the solid lines, which show linear fitting of data, indicate the corresponding scaling exponents (Reproduced with permission from Elsevier [3, 4])



The intrinsic viscosity values (η), deduced from data in Fig. 26, were plotted as function of M in Fig. 26. This data was fitted to Mark–Houwink expression [97, 105]

$$[\eta] \sim M^\alpha \quad (1)$$

The fitting yielded $\alpha = 0.81 \pm 0.04$ not too different from the value reported in the literature ($\alpha = 0.80$ was reported by Saito and Nalepa [93, 92] and Erkselius and Karlsson [34] measured $\alpha = 0.76$), polymer theory predicts $\alpha = 0.80$ applicable to random coils. This exponent universally relates to the radius of gyration, R_g and molecular weight (M) exponent, v defined through $R_g \sim M^v$ as $\alpha = 3v - 1$.

This immediately gives $v = 0.60$ implying water was a good solvent for HEC. The measured hydrodynamic and radii gyration scaled with molecular weight as (Fig. 26)

$$R_g \sim M^v; \quad \text{with } v = 0.69 \pm 0.05 \quad (2)$$

and

$$R_H \sim M^{v'}; \quad \text{with } v' = 0.59 \pm 0.04 \quad (3)$$

All the scaling features are explicitly shown in Fig. 2 in chapter “[Polyelectrolyte: Science and Application](#)”. The ratio R_g/R_H is indicative of three dimensional conformation of the polymer molecule and this ratio is exactly 1.8 for a random coil [105]. For the HEC samples used in this study ($M_3 = 1.3 \times 10^6$ Da), $R_g/R_H = 1.78 \pm 0.06$ that attributed random coil conformation to this biopolymer molecule in water at room temperature.

Similarly, the R_g and M exponent measured from light scattering, Eq. (2) was $v = 0.69 \pm 0.05$ and the same estimated through the viscosity data was $v = 0.60$ which are in agreement within acceptable limits. The measured value of $R_g = 120$ nm. For a rod of length, L_{LS} and cross-sectional diameter d , $R_g^2 \approx (L_{LS}^2/12)$, if $L_{LS} \gg d$. This estimates $L_{LS} \approx 0.5$ μm . One can also estimate average end-to-end length R_e of this random coil biopolymer, $R_e = \sqrt{6}R_g$ that gives $R_e \approx 0.3$ μm . Thus, R_e , L_{LS} and L_{SEM} define the typical overall lengths of this biopolymer.

The persistence length (l_p) of HEC molecule was deduced from the knowledge of molecular contour length (L_c), and R_g following Porod-Kratky formalism. Benoit and Doty [8] have shown that in the limit of degree of polymerization going to infinity, the following holds

$$\frac{R_g^2}{l_p^2} + 1 = \frac{x}{3} + \frac{2}{x} - \frac{2}{x^2}(1 - e^{-x}) \quad (4)$$

where $x = L_c/l_p$. The contour length of the chain could be determined from the geometry of the monomer constituting the molecular structure. We have used Gaussian 03 W software to determine the molecular size of such a monomer which yielded 0.465 nm.

The approximate formula weight of this monomer is ≈ 162 Da which attributes $\approx 8,000$ and $4,400$ to the two higher molecular weight samples (M_3 and M_2) of HEC molecules, respectively, as degree of polymerization which yields the value for L_c . Thus, the persistence length was estimated from Eq. (4) in chapter “[Polyelectrolyte: Science and Application](#)” as, $l_p \approx 10$ nm (assuming $R_g = 120$ nm) which attributed considerable chain stiffness to HEC fibers.

We have provided a systematic and comprehensive report on the various aqueous phase states of an important biopolymer, HEC [3, 4]. It has been clearly

shown that there are three distinct concentration phases: dilute [$c < 0.2\% \text{ (w/v)}$] regime, semidilute [$0.2 < c < 1\% \text{ (w/v)}$] regime and melt [$1 < c < 5\% \text{ (w/v)}$] state. The dilute regime attributed $\approx L_{LS} = 0.5 \mu\text{m}$ to the length of HEC fibres dispersed in water and these had a persistence length $\approx 10 \text{ nm}$. Such a persistence length is intermediate between that of a stiff chain like DNA (persistence length $\approx 90 \text{ nm}$) and a flexible polypeptide like gelatin (persistence length $\approx 2 \text{ nm}$). In the semidilute region, these fibres get preferentially hydrated and the solution exhibited viscoelastic behaviour at low frequency. Flow to viscoelastic transition was noticed in the rheology studies on a typical time scale $\approx 450 \text{ ms}$. Presence of networks or crosslinks were not seen.

3.1.2 Gelatin B

This section has been adopted from our previous work [45]. The hydrodynamic radii (R_h) of the gelatin chains were measured at 20°C and close to the Flory temperature by dynamic light scattering. Persistence length (l_p) is the average projection of the end-to-end vector on the tangent to the chain contour at a chain end in the limit of infinite chain length or the integral of the average projections of chain elements of the infinitely long chain on its initial direction [70]. It is a measure of stiffness of the polymer. It is an intrinsic property of a polymer molecule. For polyelectrolytes $l_p = (l_o + l_e)$ where l_o and l_e are bare and electrostatic persistence lengths. The later is a function of solution ionic strength and polyelectrolyte charge density. Benoit and Doty [8] have derived the expression relating the unperturbed radius of gyration (R_g) to l_p and the contour length (L_c) which is given by Eq. (4) which can be approximated to Eq. (5) if $L_c \gg l_p$

$$l_p = 3(R_g^2)/L_m \quad (5)$$

For spherical particles, $R_g^2 = (3/5) R_h^2$ which gives $l_p = (9/5) R_h^2/L_c$ yielding $l_p \approx 2.0 \pm 0.2 \text{ nm}$. This estimation required a priori knowledge about L_c which was estimated as follows. Consider the Gelatin primary structure to be a linear single strand polypeptide chain of monomeric representation (-Gly-X-Pro-)_n. Molecular weights of residues Glycine, Proline and X (average of Glu, 4-Hydroxy Proline etc.) are 57, 97, 115 respectively. So, average molecular weight per monomer is ≈ 270 . There are four peptide bonds of bond length = 1.32 \AA each, three N-C bonds (bond length $\approx 1.47 \text{ \AA}$ each) bond and three C-C bonds (bond length $\approx 1.54 \text{ \AA}$). Thus the monomer length of Gelatin molecule is $\approx 14.31 \text{ \AA}$. Since the average molecular weight established by SDS/PAGE was $\approx 100 \text{ kD}$, the degree of polymerization comes out to be ≈ 370 giving a contour length, $L_c \approx 520 \text{ nm}$. The persistence length determined in this approximate method compares rather well with the value reported in the literature (2 nm) [84].

3.1.3 Persistence Length of DNA

Determination of the persistence length of DNA is discussed in details by [3, 4]. Persistence length (l_p) is the average projection of the end-to-end vector on the tangent to the chain contour at a chain end in the limit of infinite chain length or the integral of the average projections of chain elements of the infinitely long chain on its initial direction [70]. It is a measure of stiffness of the polymer. It is an intrinsic property of a polymer molecule. For polyelectrolytes $l_p = (l_o + l_e)$ where l_o and l_e are bare and electrostatic persistence lengths. The later is a function of solution ionic strength and polyelectrolyte charge density. For spherical particles, $R_g^2 = (3/5) R_h^2$ which gives $l_p = (9/5) R_h^2/L_m$ yielding $l_p \approx 10.3$ nm for GA and $l_p \sim 50$ nm for DNA, taken from Refs. [33, 73].

3.2 Biological Polyelectrolytes in Ionic Liquids

3.2.1 Proteins Dispersions in Ionic Liquid Solutions

This section has been adopted from our previous work [86, 87]. Stability of protein dispersions in ionic liquid solutions has been reported [86, 87]. Room temperature ionic liquids (RTIL) have received considerable attention in the recent past due to their unique physico-chemical attributes in the field of chemical and process engineering [15, 108]. These liquids, comprising of inorganic anions and organic cations, are associated with negligible vapour pressure, high thermal, chemical and electrochemical stability that enable these to be treated as green solvents [30, 48]. The variety of possible combinations of anions and cations can, in principle, generate a wide spectrum of designer solvents. This necessitated a clear understanding of intermolecular hydrogen bonding, Coulombic, hydrophobic and van der Waal interactions occurring in these systems. Due to their characteristic hydrophobic-hydrophilic balance, RTILs are widely used as surface active agents to study micellization behaviour in water [1, 37, 125].

Imidazolium based ILs are quite hygroscopic in nature and are miscible with water so it is important to understand the modified properties of ILs due to their interaction with water before using them for any specified purpose. In order to utilize ILs for specific processes, a complete understanding of their physical properties, phase behavior, safety/environmental hazards was required. Despite the extensive experimental and theoretical studies made on water-IL solutions, to date, our knowledge of interaction between these two liquids is poorly understood, and remains mostly empirical. A molecular level understanding of phase states of ILs and their hydrated structures have been reported in the past [86, 87]. It is important to understand the thermodynamic, viscoelastic and surface active properties of ILs and their interactions with various liquids. Rate of chemical reactions and efficiency of various processes in ILs are reported to be dependent on the absorbed

Table 8 Physical properties of proteins (Reproduced with permission from American chemical society [86, 87])

S. No.	Protein	pI	R _h (nm)	ζ_{\max} (mV) (pH = 3)	ζ_{\min} (mV) (pH = 8)
1	BLG	5.2	3.6	22.83	-46.86
2	HSA	5.3	4.0	35.76	-48.49
3	BSA	4.6	3.5	37.18	-47.49
4	IgG	5.3	5.0	24.29	-23.26
5	Gelatin-A	9.0	58	12.03	-9.43
6	Gelatin-B	4.2	23	30.63	-23.88

water [119]. The interaction of water with ILs has been observed to be strongly dependent on water concentration [35, 43].

A set of 6 common proteins, bovine serum albumin (BSA), human serum albumin (HSA), immunoglobulin (IgG), β -lactoglobulin(β -Lg), gelatin-A and gelatin-B, were examined in two homologous RTIL solutions at room temperature in a systematic manner. This set was chosen using the following criteria: (i) the isoelectric pH (pI) should be $\approx 5.0 \pm 0.2$ and (ii) protein hydrophobicity index should span a broad range. All the proteins used in this study were well characterized biomolecules with known protein data base (PDB) attributes. Except that gelatin A has a pI ≈ 9.0 and gelatin A and B do not have PDB id, their native state being collagen. The summary of the measured physical properties of these proteins is provided in Table 8.

3.2.2 Interaction Between IL and Proteins

Biopolymer molecules carrying ionizable acid and base groups make the net charge on the molecule strongly dependent on pH. If the pH of protein solution changes, it may affect the molecular structure, along with corresponding change in the surface charge. Thus, monitoring the zeta potential of a protein in solution is one way of observing stability of the dispersion stability at that pH. Zeta potential is the electrostatic potential of a macroion at the hydrodynamic slipping plane. Thus, it provides a reasonable estimate of protein charge if the geometrical shape of the molecule is known.

The pH dependence of zeta potential for six selected proteins is shown in Figs. 27, 28 and 29 as function of IL concentration. The observed strong quenching of zeta potential with increase in IL concentration can be attributed to the fact that IL molecules present in the hydration shell located close to the protein molecular surface selectively interact with imidazolium cation and chloride anion through electrostatic forces. A typical zeta potential-pH profile of a protein has three distinctive features: (i) at pH < pI, the protein molecule is highly protonated and has the highest zeta potential (ζ_{\max} at a specific pH), (ii) every protein has a

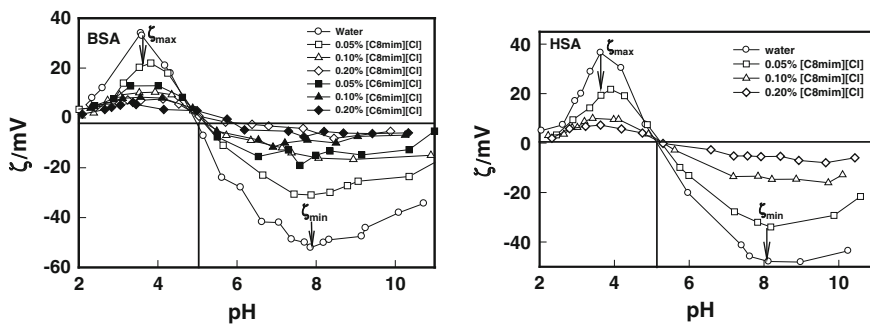


Fig. 27 Plot of mean zeta potential of BSA and HSA molecules as function of pH of the solution (BSA and HSA concentration = 0.25 % w/v) measured at 20 °C. Note the gradual variation of the potential (surface charge neutralization) with increasing ILs concentration. Solid line is guide to the eye (Reproduced with permission from American chemical society [86, 87])

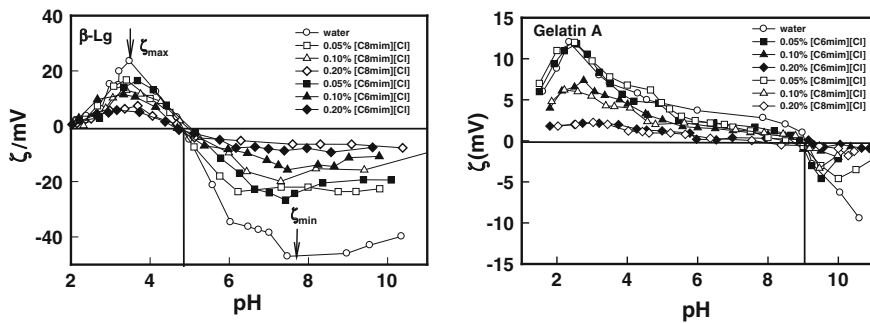


Fig. 28 Plot of mean zeta potential of β -Lg and Gelatin A molecules as function of pH of the solution (β -Lg and Gelatin A concentration = 0.25 and 0.1 % w/v) measured at 20 °C (Reproduced with permission from American chemical society [86, 87])

well defined pI where $\zeta_{\text{pI}} = 0$ and (iii) at $\text{pH} > \text{pI}$, these molecules reside in a deprotonated state yielding minimum zeta potential (ζ_{min} at a specific pH). The data shown in Figs. 27, 28 and 29 clearly retain these attributes.

At low pH (<pI) the protein is cationic in nature (protonated state), therefore is bound to anionic part of ILs (here Cl^-). The maximum zeta potential (ζ_{max}) was observed at $\text{pH} \approx 3$. It is clearly seen from Figs. 27, 28 and 29 that at higher concentration of ionic liquid ζ_{max} reduced considerably and when $[\text{IL}] = 0.2\% (\text{w/v})$, ζ_{max} assumed very low values. This generic behaviour was universally seen in all the protein dispersions.

Another universal observation was the invariance of pI with IL concentration (see Fig. 30) except for IgG samples. At $\text{pH} > \text{pI}$, the protein molecules begin to deprotonate and close to $\text{pH} \approx 8$, minimum zeta potential (ζ_{min}) was noticed in all cases. Here the protein surface is negatively charged, hence, the positively charged

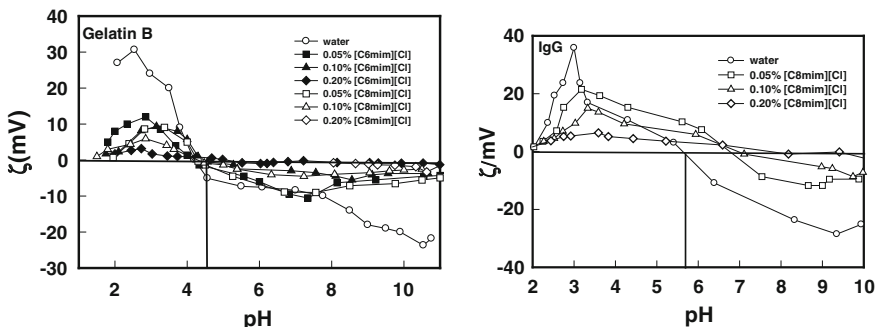
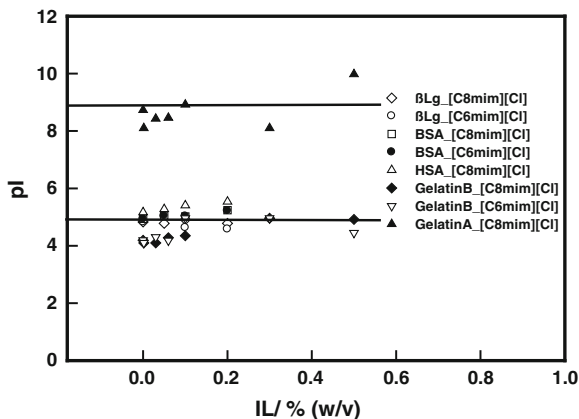


Fig. 29 Plot of mean zeta potential of Gelatin B and IgG molecules as function of pH of the solution (Gelatin B and IgG concentration = 0.1 and 0.025 % w/v) measured at 20 °C (Reproduced with permission from American chemical society [86, 87])

Fig. 30 Plot of isoelectric point, pI as function of concentration of IL measured at 20 °C. Note the invariance of the pI with concentration of ILs (Reproduced with permission from American chemical society [86, 87])



imidazolium ions selectively bind to the protein surface. With increase in IL concentration, ζ_{\min} reduced significantly and close to $[\text{IL}] = 0.2 \%$ (w/v), the ζ_{\min} value vanished completely. The pI, ζ_{\min} and ζ_{\max} data for all six proteins dispersed in water is reported in Table 8. In addition to electrostatic forces, other major forces influencing the interaction between proteins with ILs are hydrophobic interaction, H-bonding and van der Waals forces. ILs can bind to a given protein by H-bonding which is formed between positively charged imidazolium head group and negatively charged amino acid residues lying on the surface of a protein molecule. Hydrophobic interaction between alkyl chains of ILs and the hydrophobic amino acid residues located in the interior of the protein structure do prevail with finite probability.

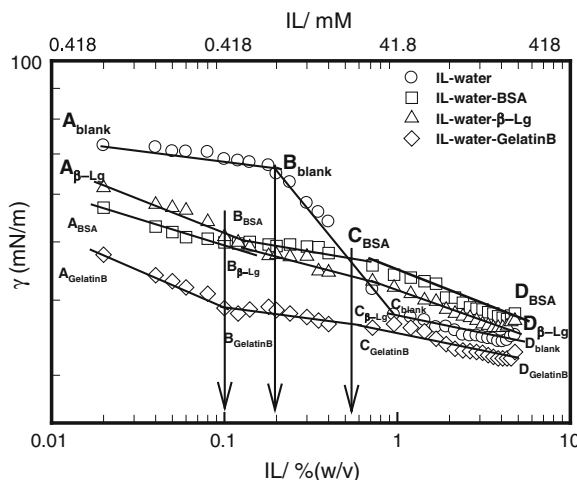


Fig. 31 Surface tension (γ) as a function of IL concentration [$\text{C8mim}][\text{Cl}]$. Various transitions are marked with vertical arrows as a guide to eye. Note that the presence of two transitions (cac and cmc) and significant shift in the cmc of IL with protein (Reproduced with permission from American chemical society [86, 87])

3.2.3 Surface Active Behaviour

The effect of IL on surface active behaviour of proteins was examined systematically and the results are presented in the plots shown in Fig. 31. Let us peruse the surface tension profile as function of IL concentration. The characteristic transition points are marked as A–D. Because of the amphiphilic nature of IL molecules, IL reduces the surface tension of water by adsorbing at the liquid–air interface ($A_{\text{blank}}\text{--}B_{\text{blank}}$ branch in Fig. 31). Initially, IL shows a less pronounced decrease in surface tension from the water value giving a plateau region with a distinct break point (B_{blank} in Fig. 31) indicating the onset of micellization. This IL concentration refers to the well known critical micellar concentration (cmc), which was determined to be 0.2 % (w/v). In the bulk aqueous phase for IL concentrations larger than cmc, IL molecules form aggregates, where the hydrophobic alkyl tails form the core and the hydrophilic imidazolium head groups are in contact with the surrounding liquid giving rise to sharp decline in γ value ($B_{\text{blank}}\text{--}C_{\text{blank}}$ branch). With further addition of IL, γ decreases slowly in a narrow range ($C_{\text{blank}}\text{--}D_{\text{blank}}$ branch).

The surface active behaviour of proteins is known for a long time [25, 42, 101]. Surface active nature of proteins result in the decrease in the surface tension of solutions compared to protein free systems. This is evident from the data shown in Fig. 31 (all A_{protein} points). For BSA and β -Lg solutions, the decrease in γ value with respect to water was between 10 and 14 % whereas for gelatin B solution the same was close to 30 %. Recall that latter is an extended random coil molecule, while the other two have near spherical conformation. Thus, gelatin B is associated

with distinct hydrophobic and hydrophilic chain segments that allow the chain to behave like a surfactant molecule per se. On the other hand, BSA and β -Lg molecules, due to their compactness, cannot have similar attribute. In the present case, the IL consists of $[\text{Cl}]^-$ and $[\text{C8mim}]^+$ ions. These constituent ions (of which $[\text{C8mim}]^+$ possesses amphiphilic character) are capable of interacting with positive and negatively charged moieties on the protein surface electrostatically. In addition, hydrophobic interaction, H-bonding and van der Waals forces also play important role in proteins-IL interaction. Hence, in the presence of proteins, the tendency of IL molecules to populate the interface decreases as these bind preferentially to protein molecules.

In the presence of proteins, the tendency of IL molecules to populate the interface decreased as these bind preferentially to protein molecules. At low concentrations of ILs, at critical aggregation concentration, IL molecules bind to the protein surface. After complete neutralization of surface charge IL molecules tend to undergo self aggregation and free IL-aggregates begin to form. The biological activity and integrity of the proteins studied was found to be mostly unaffected in the presence of IL in the concentration range used.

3.2.4 Nucleic Acid Dispersions in Imidazolium Chloride Ionic Liquid Solutions

The long-term preservation of DNA under ambient conditions is a major challenge. Although DNA is considered to be reasonably stable in aqueous solution, it is susceptible to slow hydrolytic reactions, such as depurination and deamination, which can cause serious damage to the DNA structure [68]. Various other factors, such as temperature, pH, ionic strength, and solvent properties, can also disrupt the DNA helix and cause denaturation. The solubility and stability of DNA has been studied in a variety of non-aqueous [11] and mixed solvent [47] and it was shown that DNA losses its double-helical structure when dissolved in dimethyl sulfoxide, formaldehyde or methanol whereas the structure is retained in ethylene glycol and to some extent in glycerol. Conventionally, in cryogenic storage, the DNA structure is found to be influenced by the storage temperature [66, 89]. However DNA molecules are not stable in solution at ambient temperature for long periods (≥ 1 month). One of the most recent developments in the field is the use of ILs as ideal solvent media for long-term DNA storage. Spectroscopically, it has been demonstrated that the structural and chemical stability of DNA remain preserved up to one year in a series of choline-based ILs [115]. Chandran et al. [21] showed IL cations can enter the DNA grooves and contribute to DNA stability via hydrophobic and polar interactions. The interaction of ILs with the minor groove is via hydrogen bonding, van der Waals contacts, and electrostatic effects of the IL cation, carrying a +1 charge. The high density of IL cations in the DNA solvation shell screens the interstrand phosphate repulsions and helps stabilize the B-conformation of DNA. Moreover, the partial dehydration of DNA by ILs prevents the hydrolytic reactions that slowly depolymerize or degrade DNA. The strong IL

cation–DNA interactions not only lock the DNA in the B-conformation but also prevent intermolecular interactions between the neighboring DNA strands, a phenomenon known to be inevitable for the B to A conformational transition.

3.2.5 Carbohydrate Dispersions in Imidazolium Chloride Ionic Liquid Solutions

Biomaterials have limited solubility in water or conventional organic solvents ILs due to their high solvating ability are the ideal alternative media which can dissolve biomaterials effectively without degrading the material property and from which the material can be regenerated with adequate yield. Further, ILs allow for the chemical, physical, or enzymatic modification of the properties of biomaterials dissolved. ILs can be used in various chemical reactions including, biomaterial processing. The solvation ability of ILs is an important feature which is prerequisite for the processing of biomaterials. Researchers around the globe are actively engaged in studies involving the interaction of biomaterials with ILs. Cellulose is the most widely studied biopolymer for its solubility and functionalization in $[C_2Py][Cl]$ in the presence of nitrogen containing base [44]. Later, [106] demonstrated up to 25 wt% solubility (highly-viscous solution) of cellulosic and lignocellulosic materials by imidazolium based ILs. The high chloride concentration and activity of ionic liquid was found responsible for breaking the extensive hydrogen-bonding network in the polysaccharide and promoting the dissolution. Solubility of cellulose decreases with increase of the alkyl chain length of imidazolium cation. The microwave irradiation (or sonication) enhances the efficiency of dissolution compared to thermal heating [32, 71]. NMR studies were used to propose the mechanism of cellulose solubilization [50, 88]. Zhang et al. [128] demonstrated short alkyl chain in the cation (i.e., 1-Allyl-3-methylimidazolium chloride, [Amim]) enhances the solubility of cellulose when compared to $[C_4mim]$ cation. Various effects were observed for cations containing oxygenated side chains. It was found that the oxygen atom present in the IL serves as a hydrogen-bond acceptor and interacts with cellulose to enhance its solubility in ILs [62, 67]. ILs containing carboxylate anions showed low viscosity and basicity of hydrogen bonding than chloride anion and were found to dissolve same amount of cellulose at lower temperature than chloride ILs [41]. Out of three imidazolium based IL anions ($[CH_3SO_3]^-$, $[CH_3OSO_3]^-$ and $[(CH_3O)_2PO_2]^-$) examined for the solubility of cellulose, it was found that only $[(CH_3O)_2PO_2]^-$ based IL could dissolve cellulose [40]. The extended solubility of cellulose was also found in phosphate containing imidazolium ILs [116]. Recently in a review, Ohno et al. [78] described the design of ILs for dissolution, depolymerization, and energy conversion of cellulose and their derivatives. Existing studies reveal that not only the nature of anion but the alky chain length of the cation is also responsible for controlling the cellulose solubility.

Chitin is another industrially important biopolymer which has been investigated for dissolution using ILs. It is structurally similar to cellulose, though it forms

Table 9 The solubility investigation of different biopolymers in ILs

Biopolymer	IL used	Solubility	References
Amylopectin	[C4mim][Cl]	5 wt%	[39]
Starch	Different IL	Soluble	[9, 122]
Agarose	various ILs	Soluble	[62]
Agarose	[C4mim][Cl], [C4mim][PF ₆] and [C4mim][BF ₄]	Soluble	[5]
β-cyclodextrin	[C4mim][(CN) ₂ N]	High solubility	[67]
β-cyclodextrin	[C4mim][Br]	25 wt%	[10]
Maltodextrin	[C4mim][(CN) ₂ N]	Soluble	[9]
Glucose	Ether containing ILs	Well soluble	[62]
Glucose	[C4mim][(CN) ₂ N]	Soluble	[38, 39, 65, 67, 80]
Fructose, arabinose, mannose, xylose	Different ILs	Soluble	[39, 65]

more complex inter and intra-molecular hydrogen bonded network. Yamazaki et al. [124] dissolved chitin in [Amim][Br], in the amount of 10 wt%. Xie et al. [121] reported dissolution of chitin and its N-deacetylated analogue, chitosan, in concentration up to 10 wt%. Wu et al. [120] obtained only a limited dissolution of chitin with [C4mim][Cl] and no dissolution with [Amim][Cl]. The [C4mim][CH₃COO] dissolved raw chitin of different molecular weights at temperature above 85 °C. The solvability of [C4mim][CH₃COO] is not affected by the crystalline nature of the chitin but strongly depends on the molecular weight. Chloride containing ILs are more capable of dissolving chitosan but limited solubility of chitin was observed. The solubility of other carbohydrates such as amylase, dextrin, pectin and xylan, in [Amim][HCOO] IL was also reported [41]. Amylose, except being soluble in formate based IL [41], is also shown to dissolve in ether-containing ILs, [MeO MC2mim][Br] and [MeOC2mim] [Br] [62]. The solubility of other biopolymer are listed in Table 9.

3.3 Biological Polyelectrolytes in Non-aqueous Solution

This section has been adopted from our previous work [96]. Hydrogen bonding liquids and their mixtures occupy a special place among complex systems due to the existence of directed H-bonds. In contrast to covalent bonds, the H-bonds can be rearranged relatively easily. Although an enormous amount of literature exists which relates to the investigation of H-bonding systems, particularly on glycerol-water mixture systems [7, 22, 26, 49, 99, 104, 109], there is still a lack of clear understanding even of the level of dynamics in “simple” water or alcohols.

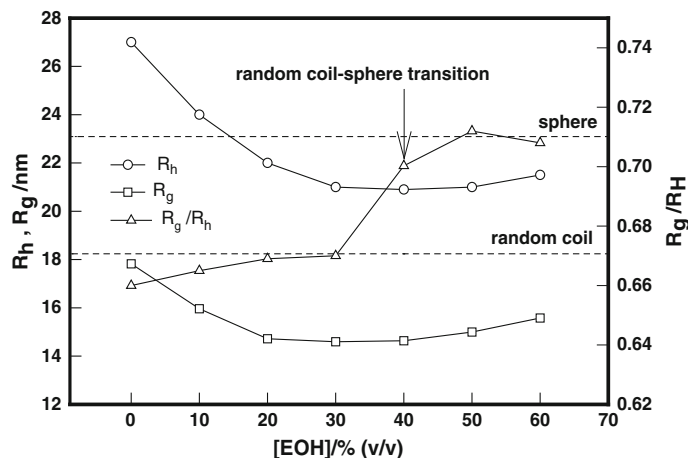


Fig. 32 Variation of the hydrodynamic radius R_h and radius of gyration R_g of the chain as function of ethanol concentration. Note the chain collapse for ethanol concentration exceeding 40 % (v/v)

Among them, alcohols and their mixtures with water are widely used as excellent models to study cooperative dynamics. A variety of physical phenomena owe their origin to the specificity of the first hydration sheath found around a biopolymer which includes protein folding denaturation, DNA condensation and coil-globule transition etc. [6, 27, 85, 127]. In all these processes, the hydrophobicity of the solvent environment and the hydrogen bonding capacity of the solvent with its co-solvent partner plays a decisive role. A systematic way to study the same can be attempted through appropriate tuning of solvent hydrophobicity and its hydrogen bonding capability by choosing alcohol solutions as solvent and a known biopolymer as probe molecule. Herein, we have chosen ethanol, ethylene glycol and glycerol solutions to observe how they affect the hydration of gelatin B (GB) biopolymer.

Gelatin is one of the most versatile and used gelling agents in food industry. It has found many applications in the pharmaceutical and photographic field [60, 83] as it is an abundant raw material, produced all over the world at low cost and with excellent film forming properties [36]. Gelatin is obtained by thermal denaturation of collagen, which is the most common protein in the animal kingdom and consists of three polypeptide chains, each one twisted in a left-handed helix and super-coiled together to form a right-handed triple helix [113].

Gelatin is soluble in water, but not in any of the alcohols. Thus, the aqueous alcohol solution is a marginal solvent for this polypeptide. The measured normalized hydrodynamic radius (R_h) and radius of gyration (R_g) is plotted as a function of ethanol concentration in Fig. 32 which indicates that the chain size is sensitive to propensity of hydrogen bonds that can be formed between the organic solvents and water. The number of hydroxyl groups is least in ethanol, it increases

to two in ethylene glycol and its maximum in glycerol. Thus it was observed that as the number of hydroxyl groups increased in the solvent, the physical size of the polymer decreased considerably. This chain collapse is attributed to the changed hydration environment of the molecule.

The radii values were found to reduce by about 50 % for glycerol, 35 % for ethylene glycol and 30 % for ethanol solutions. Interestingly, the chain collapse was distinctively seen where hydrogen bonding was maximum between the two liquids (freezing point depression point). More specifically, this occurred when glycerol, ethylene glycol and ethanol concentrations were close to 60, 35 and 40 % (v/v) respectively. CT-DNA has been reported to exhibit condensation at ethanol concentration \approx 42 % (v/v) [74].

The three dimensional conformation of the chain can be ascertained from the R_g/R_h ratio. For a random coil polymer this ratio is \approx 0.67 whereas for a globular shape it is \approx 0.77. This data is plotted in Fig. 32 which is very revealing. It is interesting to observe that this ratio remained invariant (0.65 ± 0.04) of alcohol type and their concentration in the concentration range 0–30 % (v/v) and sudden chain collapse was seen for concentration >30 % (v/v). Thus, though the spatial stretch of the chain was reduced in water solutions of alcohols, their conformations did not alter for lower alcohol concentrations. It should be noted here that hydrophobicity of the nonsolvent though was found responsible for causing reduction in solubility of the biopolymer, did not affect chain conformation. This ruled out any possible gelatin-alcohol hydrophobic interaction.

Polymer solution viscosity is an important physical property in polymer research, development, and engineering. When high molecular weight nonionic polymer molecules dissolve in a fluid, they typically expand to form spherical coils. In dilute solutions, the volume associated with each polymer coil contains one polymer molecule surrounded by a much larger mass of solvent. A polymer coil's hydrodynamic volume depends upon the polymer molecular weight and its thermodynamic interaction with the solvent. Polymer–solvent interactions depend upon the polymer molecular structure, chemical composition, solution concentration, solvent molecular structure, and the solution temperature.

Intrinsic viscosity (η) is the viscosity of an infinitely diluted polymer solution. It is a measure of the hydrodynamic volume occupied by a macromolecule, which is closely related to the size and conformation of the chain, but is independent of concentration of macromolecule. In dilute solutions, by definition, the polymer chains are separated and there is negligible interaction between them. Therefore, the (η) of polymer in solution depends only on the dimension and the molecular weight of polymer chain. Experimentally determined values of the relative and specific polymer viscosities were used to calculate it, according to Huggins [53] and Kraemer [64] equations given by

$$\text{Huggins: } \frac{\eta_{sp}}{c} = [\eta] + K_H[\eta]^2 c \quad (6)$$

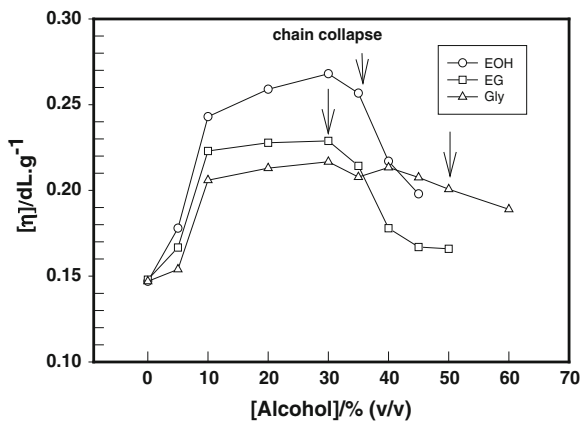


Fig. 33 Variation of intrinsic viscosity with alcohol concentrations at room temperature. Note the sharp drop in $[\eta]$ value at characteristic alcohol concentration (arrows)

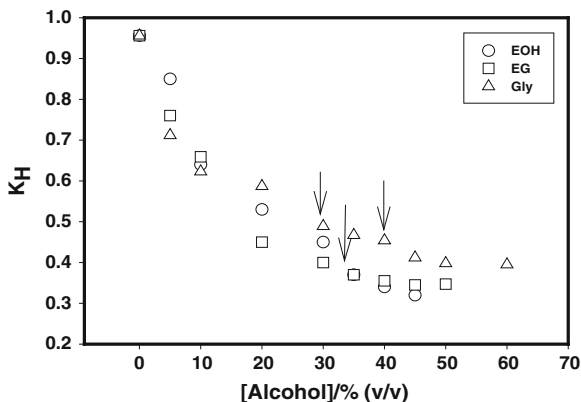


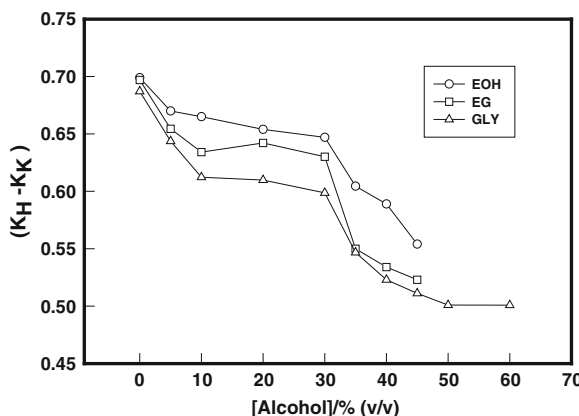
Fig. 34 Variation of Huggins interaction parameter (K_H) with alcohol concentration at room temperature. Sharp reduction in the value of K_H was observed at characteristic alcohol concentrations (arrows)

$$\text{Kraemer: } \frac{\ln \eta_r}{c} = [\eta] + K_K [\eta]^2 c \quad (7)$$

where c is the concentration of polymer solution, K_H is the Huggins coefficient and K_K is the Kraemer coefficient and theoretically it has been shown that $(K_H - K_K) = 0.5$.

The variation of intrinsic viscosity and the interaction parameters as function of organic phase concentration is shown in Figs. 33 and 34. These figures are quite revealing. Alike the radius data, the intrinsic viscosity value exhibited sharp

Fig. 35 Relative variation of Huggins and Kraemer parameter (K_H and K_K) and with alcohol concentration at room temperature



decrease at well defined concentrations of alcohol (Fig. 9). The K_H and K_K parameters are compared in Fig. 35.

The values of the K_H and K_K were observed to be decreasing with alcohol concentration and sharp change in their value was noticed at ≈ 60 , 35 and 40 % (v/v) of glycerol, ethylene glycol and ethanol solutions. Interestingly, the size and hydration data of chains exhibited qualitatively similar behavior at identical organic phase concentrations. This is also in agreement with the R_g/R_h ratio data. The reducing values of the coefficients K_H and K_K indicated lesser repulsive force between chain segments that facilitates chain collapse at threshold alcohol concentrations.

The three alcohols used in this work as solutions in water were observed to have remarkable effect on gelatin chain conformation. A clear identifiable coil-sphere conformational phase transition was detected at the characteristic alcohol concentration. And exactly at this concentration the binary solvent exhibited freezing point depression and maximum inter solvent hydrogen bonding. The contraction in chain volume was maximum for glycerol, intermediate for ethyl glycol and minimum for ethanol. The propensity of hydrogen bonds is maximum in glycerol solution followed by ethylene glycol and ethanol. Raman data helps to explore the water structure involved in solution phase.

4 Intermolecular Complexation and Coacervation

Biopolymer- biopolymer interactions have caught the attention of many scientists in recent past due to its inherent potential to generate new biomaterials. The formation of biopolymer-biopolymer supra-molecular structures as coacervates induced by electrostatic interactions is a fundamental physicochemical phenomenon, relevant to a number of known biological processes such as protein transcription, antigen-antibody reactions or enzymatic channeling. Recent Ref. [112]

reveals that complex formation between weakly charged polyelectrolytes is driven by the negative enthalpy ΔH due to electrostatic attraction, with counter ion release entropy playing only a minor role. On the other hand, the complex formation between highly charged polyelectrolyte is driven by large counter ion release entropy and opposed by a positive enthalpy change. A large variation of counter ion release entropy as function of salt concentration was only detected for highly charged polyelectrolytes [112]. The molar heat capacity ΔC_p of the system plays a vital role in variation of binding enthalpy with the temperature. This originates from the changes in degree of surface hydration in the free and complex molecules. If ΔC_p has large positive values, the system leads to charge neutralization via ionization process (protein-polysaccharide systems), if ΔC_p is negative, the system provokes hydrophobic interactions and if ΔC_p is positive with negative ΔH at all temperatures, there is significant contribution of H-bonding [112].

Coacervation is usually defined as a process during which a homogenous solution of charged macromolecules, undergoes liquid–liquid phase separation, giving rise to a polyelectrolyte rich dense phase. It is the spontaneous formation of a dense liquid phase of poor solvent affinity. The loss of salvation arises from interaction of complementary macromolecular species. The formation of such fluids is well known in mixtures of complementary polyelectrolytes and can also occur when mixing polyelectrolytes with colloidal particles.

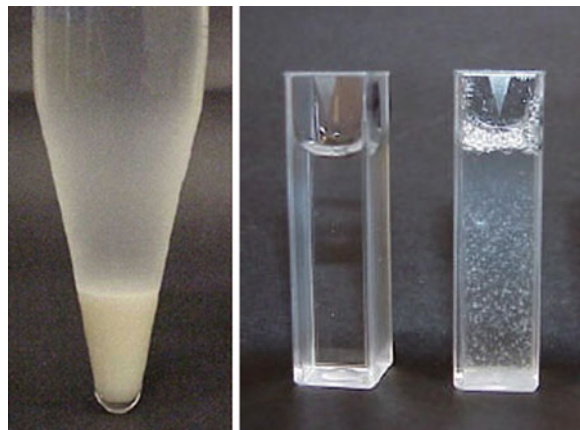
Following the pioneering work of Bungenberg De Jung [17], coacervates are either categorized as *Simple* or *Complex* based on the process that leads to coacervation. In simple coacervation, the addition of salt promotes coacervation [58]. In complex coacervation, oppositely charged polyelectrolytes can undergo coacervation through associative interactions. The other liquid phase, the supernatant, remains in equilibrium with the coacervate phase. These two liquid phases are immiscible and therefore, incompatible. Complex coacervation of polyelectrolytes can be achieved through electrostatic interaction with oppositely charged proteins and polymers. The charges on the polyelectrolytes must be large enough to cause significant electrostatic interactions, but not precipitation.

In a polyelectrolyte solution, the phase transition is driven by electrostatic solute-solvent interaction which results in a gain in the configurational entropy and the formation of amorphous randomly mixed polymer-rich phase remaining in equilibrium with dilute supernatant. Physical conditions for phase separation are deduced explicitly when the complexation between oppositely charged polyelectrolytes leads to self-charge neutralization.

As far as thermodynamics of liquid-liquid phase transition leading to coacervation is concerned, not everything is known. Phase separation models proposed in the literature do not possess all the possible interactions adequately. However, there is unanimity in the following description:

- That a homogenous solution containing N_1 molecules of solvent and N_2 molecules of solute at temperature T and pressure P , will remain stable as long as the free energy of the solute F_2 in solution obeys the thermodynamic condition $\left(\frac{\partial^2 F_2}{\partial N_2^2}\right)_{N_1,T,P} > 0$

Fig. 36 Coacervating solution (*left*) and precipitation (*right*). Depicts two pictures, one representing a coacervating solution and another showing a solution undergoing precipitation



- (b) That the phase separation of the coacervate phase from the dilute supernatant is a dehydration (of the individual polyion) process
- (c) That charge neutralization of polyion segments precedes phase separation
- (d) That the polyions do not precipitate out of the solvent because of entropy gain achieved by random mixing of polyions in the coacervate phase.

In the summary, coacervation proceeds in two steps, first, the selective charge neutralization of polyions dictated by electrostatic interactions, and second, the gain in entropy achieved by random mixing of polyions in the dense phase plus the gain in entropy due to release of counter-ions to the solvent. A coacervating solution is compared with a phase separating solution in Fig. 36.

4.1 Protein–Protein Coacervation

Gelatin is a polypeptide, and is a degraded product of native collagen. The degradation is performed either through acid or base treatment protocol. This generates two types of gelatin, A and B. Gelatin B is a random coil polymer carrying positive and negative charge sites in almost 1:1 ratio. At the same time, it is associated with small persistence length ≈ 2 nm. The zeta potential curves shown in Fig. 37 imply an isoelectric pH ≈ 5 , though small concentration dependence in its value could be clearly seen.

Specifically, a gelatin solution prepared close to pH = 5 is required to be turned into a poor solvent for gelatin molecules which will ensure chain collapse facilitating intermolecular electrostatic interaction leading to charge neutralization, and finally, coacervation. This is achieved by adding ethanol (a non-solvent) to gelatin solution (Fig. 38). Figure 38 implies that as coacervation point is reached, the zeta potential of the aggregates that are formed due to associative interactions tends to a very low value indicating effective charge neutralization achieved due to strong

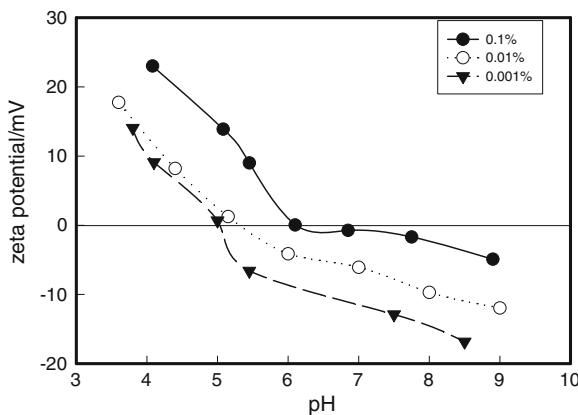


Fig. 37 Zeta potential of gelatin B molecule shown as function of concentration. Note that for the lowest protein concentration, zeta potential is zero at $\text{pI} = 5$ (Reproduced with permission from American Institute of Physics [46])

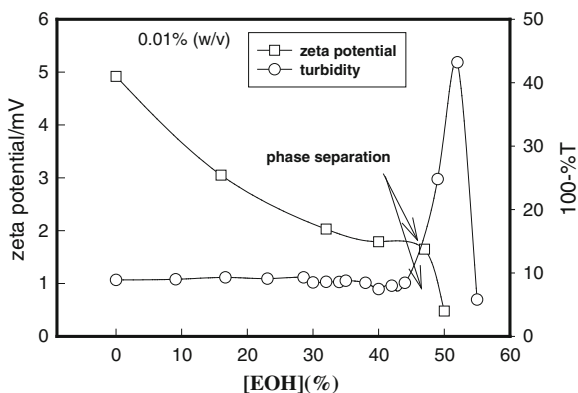


Fig. 38 Plot of zeta potential and turbidity as function of ethanol (EOH) concentration. $\%T$ represents transmittance in percentage. Note that close to 50 % (v/v) ethanol concentration, the zeta potential assumes zero value (Reproduced with permission from American Institute of Physics [46])

electrostatic binding between oppositely charged segments of the polymer. In fact, occurrence of turbidity maxima coincides with minimum zeta potential which is in complete agreement with the requirement dictated by models of phase transition [46].

The experimental data indicate the interplay of at least three different types of interactions that precede coacervation:

- Hydrophobic interactions between hydrophobic patch of gelatin molecule with aliphatic hydrocarbon tail of alcohols and,

- (b) Solute-solvent interactions.
- (c) Electrostatic interaction between oppositely charged segments.

It should also be realised that when two opposite charged segments join together, some amount of counter-ion is always released into the solvent, thereby increasing the entropy of the solution. This can also assist the process to move towards coacervation [72].

4.2 Protein–Carbohydrate

Protein-polysaccharide interactions have caught the attention of many scientists in recent past due to its inherent potential to generate new biomaterials. The formation of biopolymer-biopolymer supra-molecular structures as coacervates induced by electrostatic interactions is a fundamental physiochemical phenomenon, relevant to a number of known biological processes such as protein transcription, antigen-antibody reactions or enzymatic channeling.

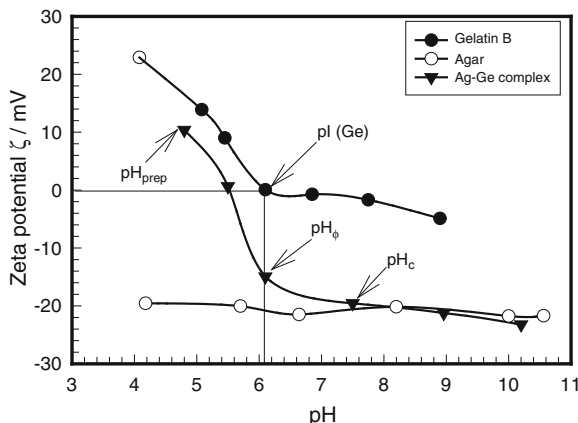
The formation of coacervates versus aggregates could be related to the stiffness and to the charge density of polysaccharides, more rigid ones leading to aggregates and flexible ones to coacervates. Agar is well known for its rigid rod shaped fiber bundles which is stiff enough due to its high charge density [14] whereas gelatin is known to bear a persistence length of 2 nm showing its flexible nature [45]. The phase separation could be visualized as a spinodal decomposition [82] or nucleation and growth [57] mechanism. However, it appears that all the systems have their signature interaction mechanisms. For instance, the coacervation behavior of some polymers such as elastin [57] appears to be an example of mixed coacervation intermediate between the classes of uni-complex and simple coacervation as defined by Bungenberg de Jong [17]. Again in some literature, we find that complex coacervates are highly unstable and sometimes a toxic chemical agent such as glutaraldehyde is added to stabilize the material [94].

The phenomenology of formation of intermolecular complexes leading to phase separation depends on the physical environment of the system. Thus the pH, polymer charge density, ionic strength, temperature and mixing ratio, all play a vital role in the formation of the complexes. The intermolecular complex formation is an associative interaction involving the attractive forces and entropy of the system. Thus, it is imperative to begin such studies with the electrophoretic characterization of the samples.

4.2.1 Agar-Gelatin Binding

This section has been adopted from our previous work [13]. The electrophoretic behaviour of agar and gelatin molecules as well as their intermolecular complexes was studied at room temperature. In order to understand the mechanism of

Fig. 39 Zeta-potential versus pH plot of 0.1 % (w/v) gelatin-B, 0.1 % (w/v) agar and Ag-Ge complexes (diluted 10 times). Note the pI of gelatin-B is at pH = 6 (Reproduced with permission from American Chemical Society [13])



formation of the Ag-Ge complex, the zeta-potential of 0.01 % (w/v) agar and 0.01 % (w/v) gelatin-B solutions were measured separately at different pH. Measurement on agar-gelatin intermolecular complexes at different pH was also carried out after dilution of the samples by 10 times. Since the net surface charge of the system is not much affected by its dilution, the data can be assumed to be comparable to the original system. No reliable measurements could be performed on samples prepared with salt. The representative data is shown in Fig. 39. The results reveal that the pI of gelatin was close to 6 and agar was a polyanionic molecule with zeta potential ≈ -20 mV. Beyond pH = 6, gelatin molecules were weakly charged with a small negative zeta potential ≈ -5 mV. The titration profile shown in Fig. 39 implies that first appearance of turbidity was noticed at pH_C = 7.4.

This refers to the formation of intermolecular soluble aggregates. Thus, the two polyions could form aggregates when the net charge on both was negative. The turbidity continued to rise and a peak was observed at pH_φ \approx 6 and even at this pH, both the biopolymers continued to carry similar charge. The soluble aggregates precipitated out of the interacting solution at pH_{prep} \approx 4.5. This is the point of maximum interaction and a stage for rapid formation of coacervates.

4.2.2 Coacervation Phenomena

Turbidity measurements were performed on gelatin B-agar solutions prepared with mixing ratio = 1:1 and NaCl concentrations of 0, 0.01, 0.05 and 0.1 M at various pHs ranging from 10 to 4 (Fig. 40). This figure shows clearly how various transition pHs vary with NaCl concentration. At pH_C (=7.4, Fig. 39) there is slight turbidity showing the initiation of intermolecular binding between gelatin and agar chains forming soluble aggregates. Here both agar and gelatin molecules are negatively charged, since pH_C > pI of gelatin-B (pI \approx 6). But gelatin, being a

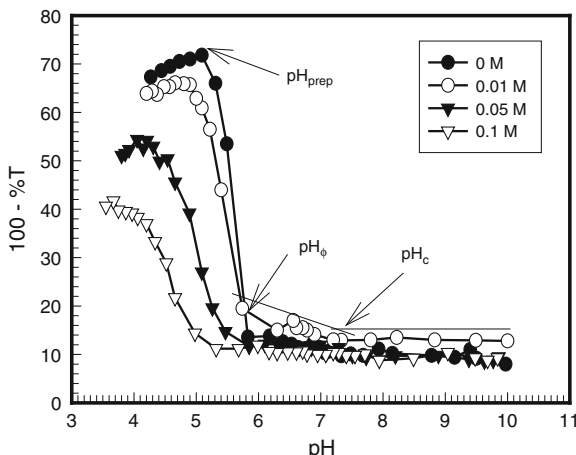


Fig. 40 Titration profile of interacting solutions of the two biopolymers recorded at 20 °C. The titration was performed from pH = 10 towards lower pH values. The change in turbidity was observed at pH_c, pH_φ and pH_{prep}. The first appearance of turbidity seen at pH_c is indicated as a change in the slope of turbidity versus pH curve (Reproduced with permission from American chemical society [13])

polyampholyte, still has some positively charged patches on its surface to promote surface selective binding at these locations. One could observe no change in pH_c with change in NaCl concentration suggesting no significant role played by the mobile ions in screening the interactions and affecting the binding. At pH_φ (near pI of gelatin) the gelatin molecules have a minor net positive charge on its surface, and hence the coacervation process is enhanced showing rapid charge neutralization and significant increase in turbidity. With further lowering of pH, similar trend was observed until the soluble aggregates precipitated out at pH_{prep} ($=5 \pm 0.2$, see Fig. 39). Salt screening effect is clearly not seen from the data presented in the Fig. 5, where pH_c and pH_φ values remained invariant of the ionic strength which is a characteristic signature of surface patch binding phenomenon. This indicated that the intermolecular interactions were poorly screened by mobile ions. The ability of the system to undergo coacervation transition in absence of salt implies that the two biomolecules followed a symmetric binding character as far as the stoichiometry was concerned. There was a notable change in pH_{prep} from pH 5 to 4.2 which was observed on increasing salt concentration. This depicts that the mobile ions stabilize the system on pH change.

Normally, for $\text{pH} > \text{pH}_\phi$, one observes the formation of large insoluble complexes that undergo precipitation immediately, which is observed in turbidity-pH profile data as a sharp drop in measured turbidity values [98, 58]. In the present case, it was observed that for $\text{pH} > \text{pH}_\phi$ the turbid solution did not undergo precipitation instantaneously, and we found a flat or saturated type of curve extending beyond the maximum turbidity pH, but the precipitation occurred within 15 min. This can be explained in the following way. Initially the size of the

insoluble aggregates was small which was not conducive for instantaneous precipitation. These aggregates grew to a larger size with time following Ostwald ripening and eventually precipitation ensued. These insoluble aggregates were not amenable to electrophoresis measurements because these dispersions sedimented gradually. At pH_Φ , a binding saturation was reached that was dictated by the stoichiometry of the polymers involved.

The microscopic structure can be imagined as the flexible gelatin chain binds to the stiff chain of agar at specific locations and the surface charge is influenced by the surrounding gelatin molecules. But the change in the thermo-mechanical properties must be attributed to the presence of both the gelatin and the agar molecules present inside the coacervate material. However, it will be appropriate to argue that the microscopic structure of the coacervate material comprised of weakly cross-linked polymer-rich zones separated by polymer-poor regions having characteristic viscoelastic length. Such systems are associated with two characteristic relaxation processes: one due to concentration fluctuation and another arising from viscoelastic relaxation. In summary, it has been unambiguously shown that surface selective binding promotes coacervation transition in the present system of biopolymers, though the electrostatic interactions are not screened by the presence of mobile ions. However, these ions create salt-bridges between the two biopolymers that enhance the thermo-mechanical characteristics of the complex coacervates formed. Surface selective binding is a poorly understood physical phenomenon and the present work intends to improve this understanding.

4.3 Protein–DNA

Binding of DNA to proteins [61, 73] and oppositely charged spherical macroions [75] has revealed interesting results. Mrevlishvili and Svintradze [73] have reported interaction between worm-like chains of DNA duplex of persistence length 50 nm, contour length 3,000 nm and width 2 nm with collagen rod-like structures of length 300 nm and width 1.5 nm. The DNA-collagen complex was found to have overlapped hydration shells of the two structures that yielded destruction of collagen triple helix and stabilization of DNA duplex.

Proteins can interact with DNA either specifically or non-specifically. In the case of non-specific interactions, the sequences of nucleotides do not matter, as far as the binding interactions are concerned. Histone (protein)–DNA interactions are an example of such interactions, and they occur between functional groups on the protein and the sugar-phosphate backbone of DNA. Specific DNA–protein interactions, however, depend upon the sequence of bases in the DNA and on the orientation of the bases that can vary with twisting and super-coiling. These DNA–protein interactions are strong, and are mediated by: (i) Hydrogen bonding mediated by water molecules, (ii) Ionic interactions like formation of salt bridges, protein side chains—DNA backbone interaction and (iii) van der Waals and hydrophobic interactions.

Herein, we discuss interaction between a low charge density polypeptide (gelatin A) and 200 base pair DNA in salt-free aqueous solutions at room temperature (25 °C). The binding profile indicated following dependence on protein concentration: DNA condensation ($GA < 0.05\% \text{ (w/v)}$), formation and growth of DNA-GA complex ($0.05 < GA < 0.1\% \text{ (w/v)}$), and finally formation of overcharged intermolecular soluble complexes followed by complex coacervation [$GA > 0.1\% \text{ (w/v)}$]. The material used here is adapted from our earlier work [3, 4].

4.3.1 DNA-Gelatin a Binding

This section has been adopted from our previous work [3, 4]. Figure 41 depicts the binding data clearly where zeta potential and size of the complex along with the solution turbidity shown. The binding profile has three distinguishable regions of interaction of DNA with GA: (i) in the first region which ends at $C_{GA} = 0.05\% \text{ (w/v)}$, the turbidity increase was marginal (less than 10 %), zeta potential decreased from -70 to -60 mV (25 %) and hydrodynamic radii decreased by close to 50 %; (ii) significant change in solution properties was observed for $0.05 < C_{GA} < 0.1\% \text{ (w/v)}$, the turbidity increased fivefold, zeta potential decreased from -50 mV to zero (complete charge neutralization) and hydrodynamic radii increased twofold and (iii) for $C_{GA} > 0.1\% \text{ (w/v)}$, the complexes were found to be positively charged (overcharging), turbidity decreased sharply and so was the complex size, leading to liquids-liquid phase separation (see Fig. 5).

4.3.2 Condensation of DNA [$C_{GA} < 0.05\% \text{ (w/v)}$]

The pH of the DNA, GA and the mixed solutions were close to 6.0 ± 0.5 . At this pH, the zeta potential of DNA and GA were measured to be -70 and $+5 \text{ mV}$ respectively, which attributes high linear charge density to DNA and considerably low charge density to the protein. In salt-free environment, DNA and GA molecules are expected to interact strongly through Coulomb interactions and form intermolecular complexes. Figure 41 data reveals considerable decrease in the size of DNA-GA complex as the protein concentration was varied in the range $0\text{--}0.05\% \text{ (w/v)}$. This clearly indicated DNA-GA binding through electrostatic interactions which was evident from the fact the charge on the DNA reduced by close to 25 % during this interaction (Fig. 41). In our experiment however large amount of GA was required for the occurrence of condensation and neutralization of DNA. This phenomenon can be understood as follows. Firstly, because of the high charge ratio (DNA: GA = 16:1), more of GA is required to bind and neutralize DNA backbone. Secondly, because of large and random coil structure of GA, DNA will feel steric hindrance while attaching to incoming GA molecule, regardless, the surface patch binding [12, 46] of GA to DNA backbone was realized. Gelatin A is a polyampholyte molecule containing both positive and

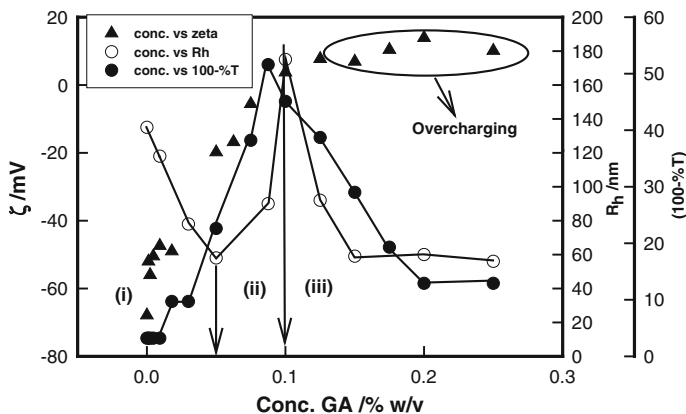
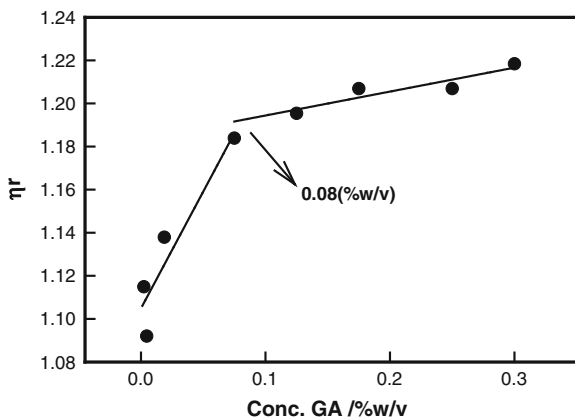


Fig. 41 Variation of hydrodynamic radii, zeta potential of DNA-GA complex, and solution turbidity at different GA concentrations in region (i) condensation, primary binding, (ii) secondary binding, (iii) overcharging and complex coacervation. DNA concentration was fixed at 0.005 % (w/v). Experimental data pertain to 25 °C. Solid lines are guide to eye (Reproduced with permission from American Chemical Society [3, 4])

negatively charged residues [16]. Thus, the positively charged segments of the chain will preferentially bind to DNA. Such interaction of DNA ($R_{DNA} \sim 140$ nm) with GA ($R_{GA} \sim 55$ nm), was responsible for reducing the size of DNA-GA complex, $R_{complex}$. It is to be noted that the stiffness of DNA molecule was reduced as more and more number of GA molecules bind to it because of the concomitant reduction in the electrostatic persistence length of DNA. This interaction, which was electrostatic in nature, was supported by zeta potential data which depicts partial charge neutralization of DNA-GA complex upon addition of GA in this concentration region. This has been referred to as primary binding.

As GA molecule approaches DNA, primary intermolecular electrostatic binding between GA and DNA occurs that tries to neutralize the DNA charge. As a consequence, electrostatic persistence length of DNA decreases, as more GA molecules bind this decrease progresses in a cooperative way giving rise to condensation of the DNA-GA complex. Therefore, effective hydrodynamic radius of DNA, $R_{DNA} \sim 140$ nm, in the presence of GA, reduces to ~ 60 nm at $C_{GA} = 0.05$ % (w/v). In this region, the solution turbidity remained largely invariant and the zeta potential of dispersed moieties decreased from -70 to -50 mV indicating partial charge neutralization of DNA due to its surface selective binding with GA molecules. This generated small, but stable soluble complexes through a process which we refer to as primary binding.

Fig. 42 Variation of relative viscosity as a function of C_{GA} . Notice the change in slope at $C_{GA} \approx 0.1\% \text{ (w/v)}$ (Reproduced with permission from American Chemical Society [3, 4])



4.3.3 Growth of Complex [$0.05 < C_{GA} < 0.1\% \text{ (w/v)}$]

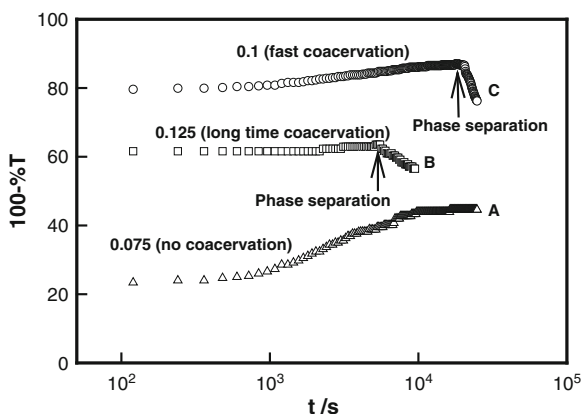
Compact complexes that are partially charge neutralized as stated in the previous section continued to attract more GA for further binding and as a consequence size of complex increased till complete charge neutralization of complex was achieved (secondary binding). Size of the complex, R_{complex} started to rise from 60 nm to a maximum size of $R_{\text{complex}} \sim 180$ nm with the increase in C_{GA} as is clear from the data (Fig. 41). This increase in size of complex get saturated at $C_{GA} \approx 0.1\% \text{ (w/v)}$, which was also the charge neutralization point (zeta potential = 0) and maximum turbidity loci. Interestingly, the viscosity data revealed the same information; notice the change in slope of the relative viscosity profile at $C_{GA} \approx 0.08\% \text{ (w/v)}$ in Fig. 42. Thus, the DLS and viscosity data collectively defined the region for secondary binding.

After condensation of the DNA-GA complex in region $C_{GA} < 0.05\% \text{ w/v}$, further electrostatic attraction was unfavorable due to substantial screening of DNA charge by GA counter-ions. In the absence of Coulombic interactions, van der Waal attractive forces will be dominant between the partially charge neutralized DNA-GA complex and free GA molecules. This attractive force will further drive the binding process causing the size of these soluble complexes to increase until maximum sustainable size is realized. In this region, the turbidity increased sharply, zeta potential of moieties reduced significantly (-50 to 0 mV) and their size grew threefold from 60 to 180 nm. These characteristic signatures indicated secondary binding between DNA-GA complex and existence of free GA molecules.

4.3.4 Complex Coacervation ($C_{GA} \geq 0.1\% \text{ (w/v)}$)

In the GA concentration range $0.05\text{--}0.1\% \text{ (w/v)}$, the size of DNA-GA complex was found to rise considerably while the zeta potential value reduced and approached zero, clearly indicating charge neutralization of the complex. Correspondingly,

Fig. 43 Variation of turbidity as function of time for three GA concentrations: (A) below, (B) above and at (C) $C_{GA} = 0.1\text{ % w/v}$ (neutralization point). Note that for a sample coacervation is absent



the turbidity increased and revealed a maximum at $[GA] = 0.1\text{ % (w/v)}$ followed by a sharp decrease in its value for $GA > 0.1\text{ % (w/v)}$. Thus, the zeta potential and turbidity profiles carried the distinctive signature [58, 81, 111] of complex coacervation at and after $GA = 0.1\text{ % (w/v)}$.

Overcharging of the DNA-GA complex was seen beyond the charge neutralization point which will be discussed in the next section. Formation of charge neutralized intermolecular complexes is known to precede complex coacervation transition which has been observed in a wide variety of interacting polyelectrolyte systems [12, 18, 17, 46, 58, 81, 103, 107, 111]. This phenomenon is supported by data shown in Fig. 8 where it is shown that below charge neutralization point no coacervation existed while dynamics of coacervation was maximum close to neutralization point. Beyond neutralization point dynamics of coacervation was again slowed down due to overcharging phenomena. The overcharged complexes in solution, because of their excess positive charge, try to repel each other and can remain in stable dispersion for sufficient amount of time, thus inhibiting coacervation. However, at longer time, these undergo phase separation as indicated in Fig. 43.

5 Biological Nanoparticles, Encapsulation and Drug Release

5.1 Chitosan-Nanoparticle

This section has been adopted from our previous work [59]. The term chitosan embraces a series of polymers that vary in molecular weight (from approximately 10,000–1 million Da) and degree of deacetylation (in the range of 50–95 %). Chitosan (CS) is the second most abundant naturally occurring polysaccharide which is a cationic polyelectrolyte ($pK_a = 6.3\text{--}7$). The chitosan nanoparticles and

their coacervates are selectively formed as per chitosan concentration [59]. It is a biodegradable polysaccharide produced by partial deacetylation of Chitin derived from naturally occurring exoskeletons of crustaceans and arthropods [95]. Structurally, this co-biopolymer consists of β -(1,4)-2-acetamido-2-deoxy-D-glucose and β -(1,4)-2-anaino-2-deoxy-D-glucose units. Thus, it comprises of copolymers of glucosamine and N-acetyl glucosamine with molecular formula C₆H₁₁O₄N. CS exhibits favorable biocompatibility characteristics as well as the ability to increase membrane permeability, both in vitro and in vivo, and gets degraded by lysozyme in serum [29].

Normally, Chitosan nanoparticles are made via ionic gelation of this polysaccharide with Tripolyphosphate, TPP [19]. In this protocol the Chitosan nanoparticles (CS NPs) are formed through the extensive inter molecular crosslinking of amino groups of CS with the negatively charged phosphate groups of TPP. The size of CS NPs could be altered by interacting PEG with CS and TPP. It has been shown that high degree of CS deacetylation and narrow CS molecular weight distribution preferentially generated NPs with size less than 100 nm [126]. The following is adapted from the Ref. [59].

5.1.1 Preparation of Chitosan and Chitosan-PEG Nanoparticles

Chitosan-TPP nanoparticles were prepared according to Calvo's method of ionic gelation [19]. Various Chitosan solutions with concentrations (0.5, 1, 1.5, 2, 2.5 mg/ml) were prepared in 1 % (v/v) acetic acid aqueous solution at room temperature and stirred for 2 h at high speed to obtain a clear dispersion. TPP was prepared in aqueous medium with a fixed concentration of 1 mg/ml. Chitosan and TPP were mixed in various ratios ([Chitosan/TPP] = 2, 3, 4, 5 and 6), by slowly adding TPP drop wise under constant stirring to a particular Chitosan solution. These solutions were kept under magnetic stirring for 30 min. The pH of the solutions remained in the range = 3.5–4 depending on the Chitosan concentration and mixing ratios. Chitosan-TPP nanoparticles were formed in these solutions due to electrostatic interaction and intermolecular crosslinking between amino groups of Chitosan to the phosphate group of TPP. These aliquots were subjected to centrifugation for purification at 11,500 rpm on 0.45 μ l glycerol bed. Supernatant and nanoparticle rich phase (pellet) were collected. Nanoparticles were washed with deionized water and kept for stabilization for 1 day after which they were used for further study. No nanoparticles could be formed under following conditions: (i) Chitosan concentration <0.5 mg/ml, mixing ratio less than 2; and (ii) Chitosan concentration 1–2.5 mg/ml and for mixing ratio in the range 2–6.

PEG is normally used to "mask" the agent from the host's immune system (leading to reduced immunogenicity and antigenicity), which also prolong its circulatory time by reducing renal clearance. Chitosan-PEG nanoparticles were made by adding 1 % PEG to Chitosan solutions, subsequently, TPP solutions were added dropwise and mixed (using stir bars) resulting in the formation of CS-PEG NPs. The remaining procedure of extraction and purification of the nanoparticles

was same as described for Chitosan nanoparticle synthesis. In order to the study of effect of PEG concentration on size of CS nanoparticles, 0.5 mg/ml Chitosan stock solution was used and [Chitosan/TPP] ratios was varied in the range 3–6. Seven PEG concentrations considered were: 0.05, 0.1, 0.3, 0.5, 1, 2, 3 % (v/v). During this study, syntheses of nanoparticles of smaller size were targeted as small nanoparticles have the ability to move across the blood vessels and membranes much easily as compared to large nano or micro-particles. Nanoparticles were prepared using same procedure as described for Chitosan-PEG nanoparticles.

When the [Chitosan/TPP] ratio >2, the pH of the solution mixture becomes quite sensitive to value of the mixing ratio. Thus, in the mixing ratio range 2–6 the solution remains weakly acidic ($\text{pH} > 5$) and both the tripolyphosphoric and hydroxyl ions abound. But, the hydroxyl ions due to their higher mobility preferentially bind to NH_3^+ binding sites of the biopolymer that produces charge neutralization of the polymer chain. Such a condition softens the considerably (intramolecular electrostatic repulsion is reduced significantly). Thus, generating folded Chitosan chains, the residual NH_3^+ sites are now linked via tripolyphosphoric ions that complete the formation of nanoparticles.

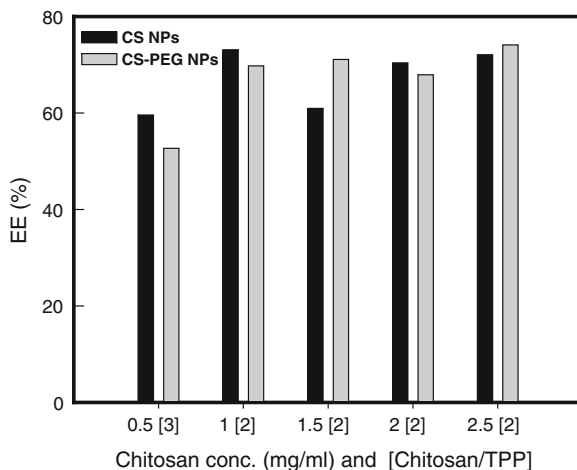
5.1.2 Drug Loading and Release

In the discussions that follow, we make a relative comparison between chitosan nanoparticles and chitosan coacervates details of which can be found elsewhere [59]. For drug loading into nanoparticles and coacervates the following protocol was used. Cycloheximide (CHX) being a hydrophobic drug is soluble in chloroform and not in water. A known amount of drug dissolved in chloroform (5 mg/100 μl) was added to a known amount of nanoparticles solution (4 ml) using sonication bath until turbid solution turned clear. Free drug gets entrapped inside the hydrophobic core of the nanoparticles. Absorbance of free drug was determined using UV-visible spectrophotometer.

A known amount (5 mg/100 μl) of drug dissolved in chloroform, was added to a known amount of coacervates (4 ml) and stirred vigorously. This enabled the drug dissolved in chloroform to get entrapped in the hydrophobic core of Chitosan-TPP coacervates. Coacervate samples were kept at room temperature for 4 days for efficient encapsulation and homogenization of drug inside the matrix. Samples were centrifuged at 10,000 rpm for 15 min and supernatant was tested to determine free drug concentration. Free drug concentration was deducted from original drug concentration which gave drug entrapped inside the coacervates. Entrapment efficiency was calculated using UV-absorbance determined for each sample.

$$\text{Entrapment Efficiency (\%)} = \text{EE(\%)} = \frac{(\text{CHX})_{\text{Total}} - (\text{CHX})_{\text{Free}}}{(\text{CHX})_{\text{Total}}} \times 100 \quad (8)$$

Fig. 44 Entrapment efficiency of Chitosan and Chitosan-PEG nanoparticles shown as function of Chitosan concentration varying in the range 0.5–2.5 mg/ml and for various mixing ratios



The entrapment efficiency of natural and induced coacervates, and Chitosan and Chitosan-PEG nanoparticles is shown in Fig. 44 respectively. The natural coacervate could encapsulate 80 % of the drugs present whereas the same for induced coacervate was close to 60 %. In case of CS NPs it was between 60 and 70 %, but the CS-PEG NPs showed slightly lower entrapment efficiency which could be due to their small size. In both the systems (NPs and coacervates) no significant polymer concentration or mixing ratio dependence was observed.

Drug release kinetics was studied in two physiologically important media in vitro at 37 °C. These were: Phosphate buffer (pH 7.4) which mimics the blood pH and simulated intestinal fluid (SIF) (pH 6.8) which mimic intestinal pH without pancreatic enzyme. Drug release was monitored for Cycloheximide loaded coacervates, and CS NPs and CS-PEG NPs. Typically, 3 ml of Chitosan-TPP coacervates were taken in dialysis bag and dialyzed against the medium considered. After regular time intervals a known amount (3 ml) was pipetted from the buffer solution for UV measurement. To decrease error to the minimal, blanks for each sample were also examined. Blanks were formed using Chitosan-TPP coacervates without drug. The absorbance was calculated as the difference between control and blank at a specific time. Concentration of sample at that instance was derived from the standard calibration curve of the drug pertaining to a particular buffer medium. Release kinetics was not explored in simulated gastric fluids (SGF) because the coacervates matrix dissolved immediately upon exposure to this medium.

5.1.3 Chitosan-TPP Nanoparticle Formation

It was possible to synthesize CS NPs through ionic gelation of Chitosan and TPP [Calvo et al. [19]]. This happened at all Chitosan concentrations considered in this study (0.5–2.5 mg/ml) provided that the mixing ratio was kept greater than 2 and

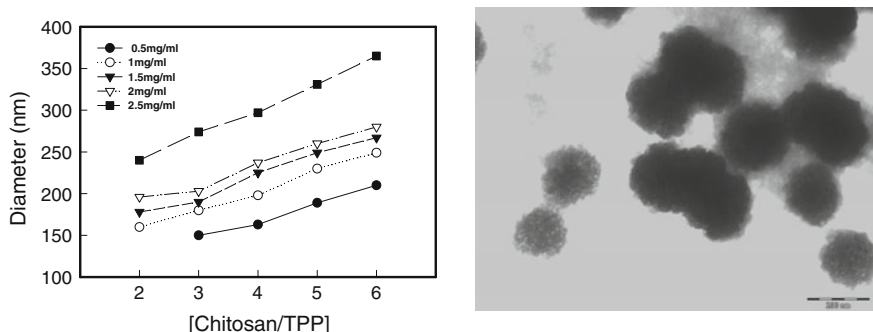


Fig. 45 Dependence of size of Chitosan nanoparticles on [Chitosan/TPP] mixing ratio and Chitosan concentration measured at 25 °C. Solid lines are guide to the eye. The TEM panel shown on the right corresponds to 1.5 mg/ml Chitosan concentration sample with [Chitosan/TPP] = 4. The average size obtained from TEM was 220 nm which is in excellent agreement with the DLS data. TEM scale bar = 300 nm (Reproduced with permission from Elsevier [59])

pH ≈ 5. Nanoparticles were observed to form even when the mixing ratio was close to 2 in solutions having Chitosan concentration in the range 1–2.5 mg/ml. Figure 45 depicts the variation in CS NP size as function of polymer concentration and [Chitosan/TPP] mixing ratio. Formation of larger nanoparticles was favored at higher Chitosan concentration and higher mixing ratios. The polymer concentration and [Chitosan/TPP] mixing ratio dependence of CS NPs is shown in Fig. 45. These preparations had typical polydispersity ≈ 20 %.

A typical TEM panel is shown in Fig. 2 which clearly depicts 220 nm the chitosan nanoparticles and its small clusters. Zeta potential of nanoparticles was found to be 44 ± 4 mV invariant of mixing ratio. This result is in excellent agreement with the findings of Zhang et al. [[126]].

As PEG was added to the Chitosan-TPP solutions the nanoparticles formed were found to have significantly reduced size (by typically 40 %) particularly at low PEG concentrations. This is shown in Fig. 3. Within the same [Chitosan/TPP] mixing ratio minimum size was obtained when PEG concentration was 1 % v/v. Based on present studies, it is noted that CS NPs formed only in a narrow range of Chitosan concentration ($0.5 \text{ mg/ml} \leq [\text{Chitosan}] \leq 5 \text{ mg/ml}$) and only when $[\text{Chitosan/TPP}] > 2$. This grossly agrees with past observations [19, 126]. However, our CS NPs were observed to be polydisperse as opposed to the monodisperse preparations obtained by Zhang et al. [126]. They used combination of post-deacetylation and fractionation of Chitosan to synthesize particles in the size range $\approx 90\text{--}200$ nm having polydispersity ≈ 8.3 % (Fig. 46).

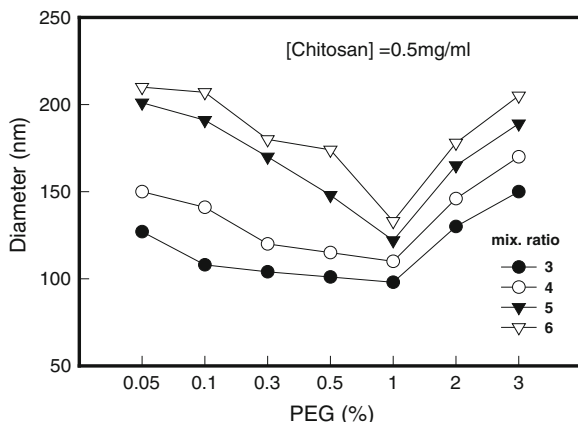


Fig. 46 Variation of size of Chitosan-PEG nanoparticles with [Chitosan/TPP] mixing ratio given in the inset and PEG concentration. The minimum size was obtained when PEG concentration was 1 % v/v (Reproduced with permission from Elsevier [59])

5.1.4 Study of Release Kinetics

Typical cumulative release profiles of the drug from the Chitosan and Chitosan-PEG nanoparticles, and coacervates, to the phosphate buffer and simulated gastric fluid (SIF) media are shown in Figs. 47 and 48. Several factors contribute to the release kinetics which includes viscosity of the matrix, concentration of the drug and its size, solubility of the drug, diffusion coefficient of the drug inside the matrix etc. It is nearly impossible to account for all these contributions and tailor it into a model. Thus, though many models for describing release kinetics have been proposed none of these capture all the observed experimental features.

The experimental data pertaining to the release occurring ($Q(t)$ in %) in the first 8 h could be least-squares fitted to the mathematical function (arbitrarily chosen)

$$Q(t) = Q_{\infty}[1 - \exp(-kt)] \quad (9)$$

$$Q(t) = Q_0 + Q_1 \exp(kt) \quad (10)$$

The exponential growth to saturation is described by Eq. (9) and the same without saturation is given by Eq. (10). These are associated with release time constant k and at saturation the released quantity is Q_{∞} . The initial release quantity in Eq. (10) is $Q_0 + Q_1$. This equation is devoid of saturation, thus, is applicable only in a well defined time window. Regardless, it was possible to fit the experimental data pertaining to the release of the drug from coacervate samples to Eq. (10) with chi-squared values >97 %. The k values obtained were $3 \times 10^{-6} \text{ s}^{-1}$ and $0.3 \times 10^{-6} \text{ s}^{-1}$ for induced coacervates in phosphate and SIF release media respectively. The same for natural coacervates were $2 \times 10^{-6} \text{ s}^{-1}$

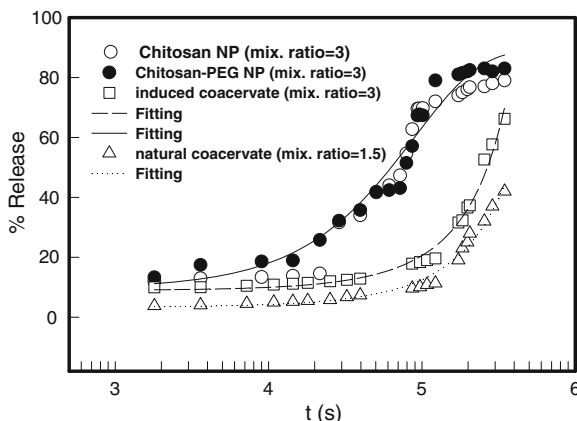
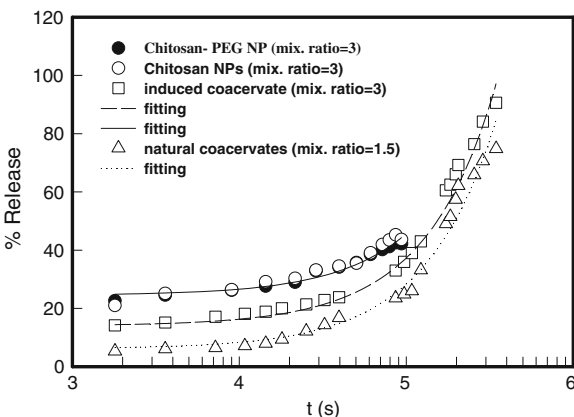


Fig. 47 Cumulative release profile of Cycloheximide in phosphate buffer measured at 37 °C. Solid lines are least-squares fitting of the data to Eqs. (2) and (3) for the nanoparticles and coacervate samples respectively (Reproduced with permission from Elsevier [59])

and $1.7 \times 10^{-7} \text{ s}^{-1}$ respectively. The release profile from Chitosan and Chitosan-PEG nanoparticles were identical for both the release media. The k value obtained was $1 \times 10^{-5} \text{ s}^{-1}$ for release in the phosphate buffer medium. The release profile in SIF medium could be fitted to Eq. (10) which yielded $k = 2 \times 10^{-7} \text{ s}^{-1}$. Thus, in summary it can be stated that coacervate samples provide sustained release over a long period of time.

Let us look at the release profile qualitatively. The kinetic of drug release from dispersion of nanoparticles and coacervates containing CHX was evaluated using equilibrium dialysis technique. This suggested that during the first hour of dialysis $\approx 25\%$ (for NPs) of drug was found in the external solution. In case of coacervates, this was $\approx 15\%$. After 18 h approximately 50 % of the drug is found in the external solution (25 h in case of coacervates). Approximately 80 % was released by the end of 24 h (30 h in case of coacervates). There was slow release of the drug initially for a period of 3 h. The above mentioned release features not too different in the two release media. This demonstrates that biological agents can be immobilized within the nanoparticle and coacervate matrices and can be used in delivery of the drug, thereby enhancing the circulation time of the drug. Release from these matrices is due to the time dependent swelling in aqueous solutions. The diffusion coefficient of a drug in a matrix is related to its diffusion coefficient in water, its molecular weight, and the percentage of polymer in the matrix. The results suggest that these formulations can be effectively exploited in drug delivery protocols. Thus, CS NPs, per se can be customized to encapsulate both hydrophilic and hydrophobic drugs offering additional advantage over other biopolymeric nanoparticles.

Fig. 48 Cumulative release of Cycloheximide in simulated intestinal fluid medium measured at 37 °C. The *lines* represent fitting of the data to Eq. (2) (Reproduced with permission from Elsevier [59])



5.2 Gelatin Nano and Microparticles

5.2.1 Preparation of Nano-particles

The solvent pH (using 0.1 M HCl) and ionic strength of the solvent was first set as per the experimental requirement (ionic strength = 0.1 M NaCl) and the gelatin solutions (1 % w/v) were prepared by dispersing gelatin in this medium at 60 °C. The macromolecules were allowed to hydrate completely; this took 30 min to 1 h. Initially at room temperature the solution pH was 5.15 ± 0.01 . Three drops of HCl were added to set the pH = 5 ± 0.01 , which is the iso-electric point of type-B gelatin (see Fig. 48). This formed the stock solution. The stock solution was titrated with ethanol and the titration profiles clearly established the transition points in terms of the percentage of volume of ethanol added relative to that of solvent until the turbidity attained its maximum value. Addition of more ethanol drove the system towards precipitation point. This characterized the initiation of intermolecular folding and intra molecular aggregate formation of the charge neutralized gelatin molecules, and the subsequent micro coacervate droplet formation. The turbid material was subjected to high speed centrifugation (relative centrifugal force $\sim 6,637$ g). The supernatant which contained gelatin nanoparticles was collected by Pasteur pipette from the top of the centrifuge cells and were used for different experiments.

5.2.2 Preparation of Micro-particles

Gelatin nanoparticles were prepared by a two-step desolvation method described by Coester method [52]. Briefly, 25 ml of 5 % (w/v) gelatin solution was prepared at room temperature. Gelatin was desolvated by slowly adding an equal volume of acetone, a non-solvent for gelatin and kept for sedimentation. The supernatant was

discarded; sediment was dissolved in water and re-desolvated at pH 2.5. Gelatin particles were further crosslinked with 500 μl of 8 % glutaraldehyde, the excess of which was neutralized by adding 500 mg of L-cysteine. Purification was done by centrifugation at 8,000g, and the desolvating agent removed by slow vaporization over 24 h. In the two-step desolvation method, after the first desolvation step, the low molecular weight gelatin fractions present in the supernatant were removed by decanting. The sediment having high molecular weight fractions were re-desolvated and crosslinked. In a second set of experiments the gelatin concentration was raised to 8 % (w/v) and rest of the protocol was maintained.

5.2.3 Surface Charge Characterizations

In a bid to calibrate the electrophoresis instrument independently, we carried out iso-electric pH (pI) measurements on gelatin solutions having concentrations 0.001, 0.01 and 0.1 % (w/v). The measured electrophoretic mobility (μ) values could be converted to equivalent zeta potential (ζ) values through the Helmholtz-Smoluchowski relation $\mu = \epsilon \epsilon_0 \zeta / \eta$, where the solvent dielectric constant and viscosity are given by ϵ and η respectively. The permittivity of vacuum is $\epsilon_0 = 8.85 \times 10^{-12} \text{ C V}^{-1} \text{ m}^{-1}$ and the value used for $\eta \approx 10^{-3} \text{ Pa s}$. Figure 2 depicts the dependence of ζ on solution pH. The measured $\text{pI} = 5.5 \pm 0.5$ value did not show concentration dependence within the limits of the experimental error. The value provides excellent matching with the nominal pI value cited by the manufacturer ($\approx 5.0 \pm 0.2$). This established the reproducibility, reliability and robustness of our measured electrophoretic mobility data.

5.2.4 Particle Size Characterizations

Average particle size, size distribution and morphology were also examined by Fei-Philips Morgagni 268D transmission electron microscope (Digital TEM with image analysis system and Maximum Magnification = 2, 80,000) at a voltage of 100 kV. The aqueous dispersion of the particles was drop-cast onto a carbon coated copper grid and grid was air dried at room temperature (25 °C) before loading on the microscope. Some representative Dynmic light scattering and TEM data are shown in Figs. 49 and 50.

The time dependent stability of these particles was monitored over a period of 2 months and the result is presented in Fig. 7 which shows excellent temporal stability. The measured zeta potential and corresponding charge density (apparent) values are given in Table 10 along with the particle dimension parameters. A qualitative feeling of surface charge density can be obtained from the measured zeta potential data. Since the surface charge on a hard sphere particle of radius R is given as $Q \approx 4\pi\epsilon_0\epsilon\zeta R$, the surface charge density, $\sigma = Q/4\pi R^2 \approx \epsilon_0\epsilon\zeta/R$ [69]. In a given situation only the ratio ζ/R is relevant which is shown as apparent charge density in Table 10. It is clearly seen that gelatin chain constitutes a low charge

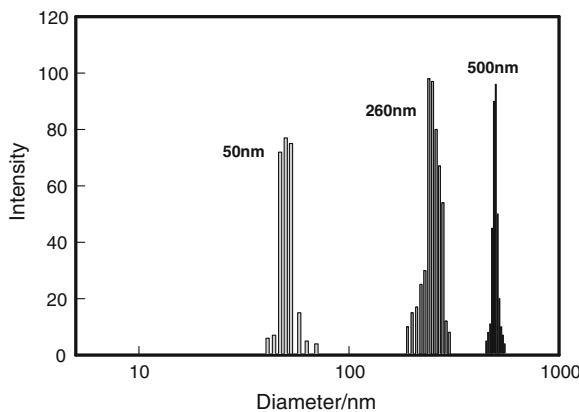


Fig. 49 Particle size distribution of nano and microparticles of mean diameter = 50, 260 and 500 nm dispersed in water

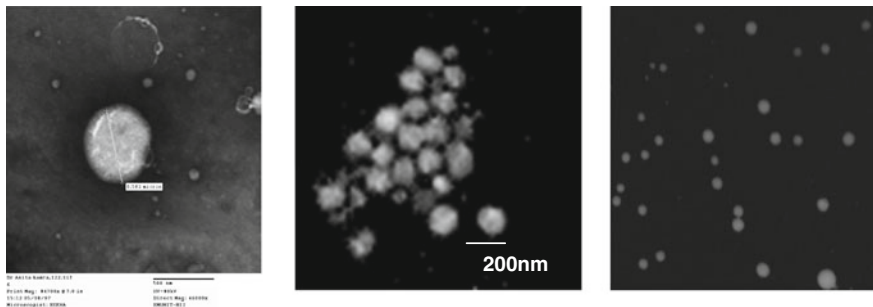


Fig. 50 Particle size from TEM data for nano and microparticles of mean diameter (*left to right*) = 500, 260 and 50 nm dispersed in water

Table 10 Physical characteristics of gelatin chain, and its nano and micro-particles measured at 20 °C

Sample	Shape	Diameter (nm)	Zeta Potential/mV	Apparent charge density/mV/nm
Gelatin chain	Random coil	–	–5	–
Micro-particle	Sphere	500	–40	$\approx 10^{-1}$
Micro-particle	Sphere	260	–30	$\approx 10^{-1}$
Nano-particle	Sphere	50	–24	$\approx 5 \times 10^{-1}$

Solution pH = 5.5 in all cases

density molecule whereas its nano and micro particles are associated with larger surface charge density.

It is seen that the surface charge density increases by a factor of 5 when the particle assumes nano-form. The large surface charge density enables the particles to remain in stable suspension without undergoing associative aggregation of any kind. In fact, this was found to be true even for micro-particles. The polydispersity remained within 20 % for all these dispersions.

The synthesis of nano (50 nm) and microparticles (260 and 500 nm) was achieved through phase transition and phase separation pathways. This can be understood through following phenomenology. Ethanol is a non-solvent for gelatin whereas it readily forms hydrogen bond with water molecules. Thus, the solvent changes from a good to marginal one when ethanol is added to water which enables the previously extended gelatin chain to assume a more compact conformation (coil to globule transition). The positively charged segment interacts with the negatively charged segment through electrostatic forces and causes the chain to undergo conformational transition to a globular shape. Such a process also generates large intermolecular clusters through systematic charge neutralization and, consequently liquid-liquid phase transition ensues. The final product is a dense polymer condensate (called coacervate) and a supernatant. The supernatant contains the nanoparticles.

5.3 Pectin Nanoparticles

This section has been adopted from our previous work [114]. Pectins are plant polysaccharides present in primary cell walls of all higher plants as an intercellular cementing material. Structurally, they are linear sequences of 1, 4-linked α -D-galactopyranosyluronic acid residues interrupted by 1, 2 linked L-rhamnosyl units providing ‘kinks’ in an otherwise stiff molecular chain. Naturally occurring pectins from apple pomace and citrus rind are 20–60 % methyl esterified. Pectin chains are known to get crosslinked with divalent or multivalent metal ions especially Calcium. It has been previously reported that CDDP complexes with polyanions such as CM-dextrans [54] as well as Alginates [90]. Pectin scores over other polysaccharides in terms of its numerous beneficial effects on gastric emptying, gastric ulcer, lowering serum cholesterol level. The most pressing need is to design new biodegradable polymeric carriers that can be used at relatively high molecular weight to promote greater EPR-mediated targeting and then be safely eliminated. Therefore, we hypothesized that Pectin, being a highly hydrophilic polyanion could be complexed to Cisplatin through association of platinum (Pt) atoms with the carboxylate anion (COO^-) of pectin. Such pectin-cisplatin conjugate system is expected to reduce toxicity of the drug thereby altering its pharmacokinetics and biodistribution pattern in tissues.

Cisplatin is highly suitable for use in carrier systems, since by replacing its ‘Cl’ ligands, usually called ‘leaving groups’, it forms complexes of varying degrees of

stability with a variety of reactive groups. Donor groups which comprise carboxylates, amides and alcohols form low affinity bonds with platinum (II) and are therefore potentially suitable to serve as active drug carriers. Such macro-molecularized drug derivatives, even if non-specific, are expected to increase the efficacy of the drug through more effective distribution, retardation of chemical or metabolic degradation and maintenance of prolonged non-toxic levels of the drug due to its slow release. Moreover, these polymers possess some advantages as a drug carrier: high water solubility, the presence of multiple functional groups that are easily modified chemically, low immunogenicity and low toxicity.

5.3.1 Preparation of the Pectin Nano-conjugate

In order to prepare the nano-conjugate complex, both Pectin and CDDP were dissolved in aqueous media at their respective concentrations in 5:1 ratio. The pectin-cisplatin nano-conjugate complex was prepared by dropwise addition of cisplatin solution to the pectin solution under vigorous magnetic stirring for ~48 h. After the incubation period the nano-conjugate complex was purified by loading onto Sephadex G-25 column using deionized water as the eluent at a flow rate (1 ml/min). The first fraction containing the high molecular weight complex was collected, lyophilized and redispersed before doing further characterization. The formation of the complex was verified by UV absorption spectra analysis, where a slight shift in the pectin peak was observed (See Figs. 51 and 52).

A coordination bond between the Platinum (II) atom and the carboxylic group in the galacturonate of pectin causes spontaneous folding to form a nano-conjugate. It should be noted that only 9 % galacturonate residues are methyl esterified while the rest is available for the drug molecules. The platinum atom can dock itself at both intra-chain as well as inter-chain positions to crosslink the pectin chains in such a way that it folds upon itself to form a nano-conjugate. The formation of the nano-conjugate complex was verified by UV absorption spectral analysis, where a slight shift in the pectin peak was observed.

The size of the conjugate was measured by DLS and was found to be in the size range 100–150 nm. A representative graph of the distribution profile has been shown in (Fig. 51). The conjugate was stable in aqueous media and can be lyophilized and stored. The formation of a nano-conjugate was evident from TEM (Fig. 52). The size and surface hydrophilicity are crucial factors in drug targeting.

Zeta potential is a useful indicator of surface charge property and can be employed as an index to the stability of the nano-conjugate. The negative Zeta Potential value of pectin chains imply negative charge on the surface and may be attributed to the presence of ionized carboxyl groups on the pectin surface. The measurement of the pectin-cisplatin conjugate depicts that the highly polyanionic pectin chains gets shielded, over ~7 times, on addition of cisplatin. The reduced negative charge might favour its interaction with cellular membranes. The negative charge on the pectin molecule is due to presence of COO^- anion and reduction

Fig. 51 DLS Spectra of Pectin-Cisplatin complex

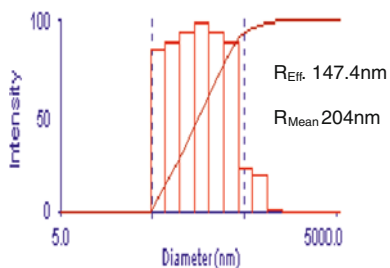
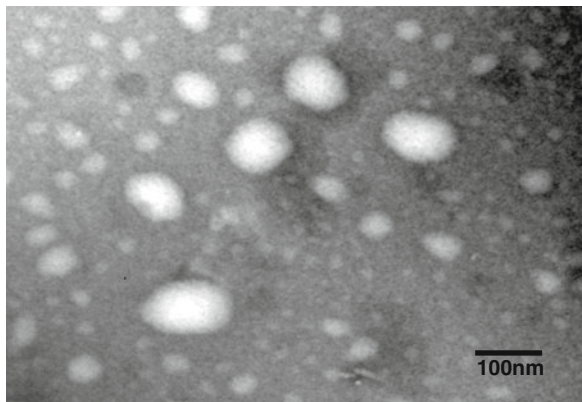


Fig. 52 TEM of pectin cisplatin complex



in negative potential sufficiently proves our hypothesis that Pt (II) atom binds to the free carboxylate group in a reversible fashion.

5.3.2 In Vitro Release Kinetics

The pectin-cisplatin nano-conjugate was lyophilized and re-dispersed in phosphate buffer saline (PBS, pH 7.4) and time dependant release kinetics study was carried out both at physiological pH (7.4) and acidic pH (5.8) by dynamic dialysis technique (Spectra/Por-7; MWCO: 10kD) under constant magnetic stirring. The complex was incubated with sera at a ratio 1:1 and the effect of plasma proteins on the release profile of the drug was also studied. Cisplatin was sampled at defined time intervals and detected in UV-Vis Spectrophotometer at 355 nm, taking into account the absorption of the platinum complex in the range 330–390 nm. After measurement the aliquot was replaced in the receiving solution to maintain the volume (See Figs. 53 and 54).

Cisplatin is a very potent anticancer drug. However, the full therapeutic exploitation of cisplatin is limited by its toxicity in healthy tissues especially nephrotoxicity ad neurotoxicity are well known. There has been an increased interest in the emerging field of polymer-drug conjugates as nanomedicines will play an

Fig. 53 Release Kinetics of CDDP in sera and PBS (pH 7.4)

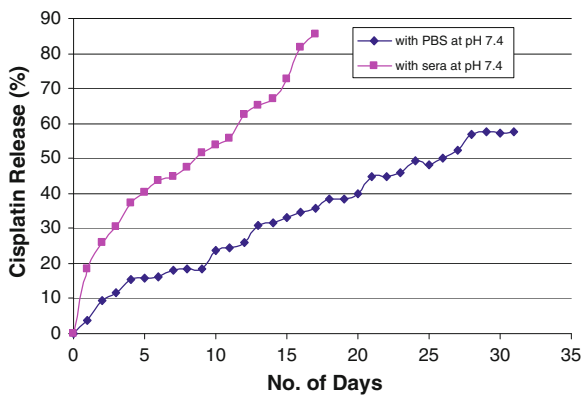
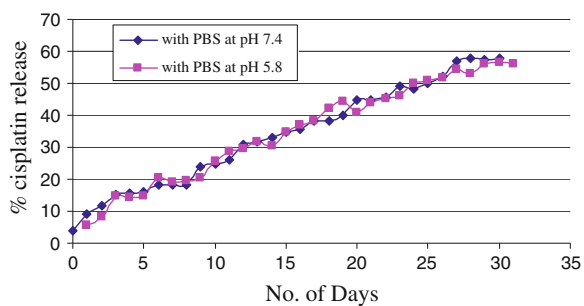


Fig. 54 Release Kinetics of CDDP at different pH



important future role in cancer diagnosis and treatment. We have developed a new drug delivery formulation for Cisplatin which is a highly active antitumor drug against a wide range of malignancies including testicular, ovarian, bladder, head and neck, small-cell and non-small cell lung cancers. Our pectin-cisplatin conjugate was designed to have the advantages of noanoscale delivery system, coupled with low toxicity and enhanced blood circulation times.

5.3.3 In-Vitro Release Profile

Pectin is ideally suited for a long circulating drug delivery vehicle. Indeed, CDDP incorporated pectin behaves as a drug delivery depot with a sustained release of the drug over a period of almost a month with no initial burst. The release profile of the pectin-cisplatin nano-conjugate complex was monitored for over a period of month at physiological pH 7.4. The release pattern of cisplatin was sustained, during which only 57 % of the conjugated drug was released in the receiving solution outside the dialysis bag Altering the pH of the buffer to slightly acidic pH 5.8 does not alter the pattern and the release was almost super-imposable over the release pattern obtained in physiological pH. However, when incubated with sera,

the plasma proteins seem to greatly facilitate release of the bound cisplatin with 85–89 % of the drug being released in 17 days, as against only 57 % drug released over a 30 day period without sera. The bond between the drug and reactive groups on the macromolecule is reversible and the drug can dissociate in favour of other ligands that have higher affinity towards platinum (II). The CDDP release is due to an inverse ligand substitution of the Pt(II) atom from a galacturonate residue of pectin chain to chloride. On intravenous administration of the pectin-cisplatin complex, the conjugated drug could be slowly dissociated in presence of physiological saline (NaCl) or by other ligands that form thermodynamically more stable links with platinum, particularly DNA which is the main target of Cisplatin.

The cisplatin passively permeates the cell membranes from the extracellular fluid. In most cells of the body, the intracellular Cl^- concentration is much lower than the extracellular fluid. The presence of high chloride concentration suppresses the aquation reaction products, which is a prerequisite for cisplatin to get activated and react with cellular machinery. Hence, when cisplatin is released from the pectin-cisplatin nano-conjugate, the drug remains in its native state before entering into the cell by way of diffusion. Inside the cell, when the Cl^- concentration dips, aquation products are formed which is the rate limiting step in all biological reaction exerted by cisplatin.

It has also been suggested that more than 90 % of platinum in the blood, following intravenous administration of cisplatin, is covalently bound to the plasma proteins. Complexation with pectin is expected to obviate plasma protein binding due to stearic hindrance thereby prolonging circulation in bloodstream and adequate drug release to elicit the pharmacological activity at the delivery site. The therapeutic potential of this nano-conjugate can be validated against solid tumors, as the tumor cells are generally located outside of microvasculatures, so that the extravasation of drug vehicles, which is a passive process governed by their molecular size and longevity in blood circulation, is a prerequisite for their specific interaction with tumor cells. Cisplatin is less soluble in water as well as in lipid. This also interferes with its treatment regime. Once cisplatin becomes attached to a macromolecular carrier, its solubility increases up to ~4 times.

The Pectin-Cisplatin nanoconjugate, a self folding nanoparticulate suspension in aqueous media shows sustained release of the drug. The complex is unaffected by change in pH. The Zeta potential measurement depicts that the polyanionic pectin chains gets shielded when Cisplatin combines to form low affinity bonds. Such conjugation with macromolecular carrier has so far been unreported in the literature for cisplatin delivery.

6 Conclusion

Novel and smart soft materials like polymer and colloidal gels, glasses, inter penetrating network structures (IPNS) and polyelectrolyte complexes (coacervates) have generated adequate interest in the recent past due to their enormous

application potential. In this chapter we have provided an extensive review on biological polyelectrolytes (biopolymers) that included proteins, nucleic acids and carbohydrates. Some generalized observations are made here in conclusion.

The nanoparticles of the biopolymers are formed largely through both inter and intra molecular electrostatic interactions. In the initial stages of nanoparticle formation there is competition between intra-molecular folding versus intermolecular aggregate formation. It is possible to approximately estimate the change in entropy for folding. The simplest polymer chain is an unrestricted random coil with degree of polymerization N , length of each segment l for which the normalized end-to-end length distribution is a Gaussian function given by [20]

$$W_N(r)dr = 4\pi r^2(3/2\pi Nl^2)^{3/2} \exp(-3r^2/2Nl^2)dr \quad (11)$$

This equation cannot actually apply to a polyelectrolyte, but can be used to estimate entropy changes. The two charged segments join together through electrostatic attraction if and only if these come within a distance (say a) less than the Debye–Hückel screening length. The volume (V_i) of closest approach will be $V_i \approx 4\pi a^3/3$. This leads to Jacobson–Stockmayer equation written for the present system as [20]

$$\Delta S_{folding} = -(3/2)R \ln N + R \ln[(3/2\pi l^2)^{3/2} V_i] \quad (12)$$

It is difficult to estimate $\Delta S_{folding}$ because of the vagueness of the term V_i . Regardless, the folding versus aggregation behavior can be explored through the usage of Eq. (13). The dynamics of DNA cyclization versus polymerization has been studied using Eqs. (11) and (12). The same framework can be at least qualitatively imposed on the present system by identifying the DNA-cyclization with folding of gelatin molecules and DNA-polymerization with gelatin aggregation. This leads to

$$\frac{[Folding]}{[Aggregation]} \propto c^{-1} M^{-1/2} \quad (13)$$

implying the preferential formation of folded molecules at lower polyion concentration c and formation of more aggregates at high c , at fixed molecular weight M . This observation infers that any polyampholyte molecules can be turned into a nanoparticle via suitable manipulation of inter and intra molecular forces. Much of this can be achieved through soft chemistry.

We have provided several examples of intermolecular complex formation that has led to coacervation. In the past coacervate samples were probed by an array of techniques in order to determine the details of their micro-structure. The experimental results taken together reveals that the coacervate phase is a heterogeneous viscous material. The polymer-rich phase comprises physically crosslinked networks of constituent biomolecules. The presence of inter-penetrating networks of

these biopolymers cannot be claimed with certainty at this stage. A pertinent question arises here: what is the physical difference between a complex coacervate and gels of its constituent biomolecules? Let us for example take agar-gelatin case. These two biopolymers form a complex coacervate [102, 100], it is appropriate to make a physical comparison between agar-gelatin complex coacervate with agar, and gelatin gels, and gelatin coacervates. The agar-gelatin coacervate has been found to retain the thermal properties of its constituents to a remarkable extent. This indicates the presence of physically entangled networks of agar and gelatin in the coacervate phase. The viscoelastic response of this phase to external stress is dependent on the specific nature and density of these crosslinks. Thus, determination of the degree of helicity present in the coacervate phase will be of significant importance much of which remains unexplored. Coacervates, like gels, are biphasic in nature comprising the solvated polymer and solvent in various structural forms. Thus, the exact determination of the amount of interstitial and free water present in this material is required to be evaluated which will provide a better understanding of the thermal and temporal stability of this material.

Let us take the following case: it is interesting to observe that gelatin coacervates (simple) and agar-gelatin coacervates (complex) share a generality as far as their microscopic structures are concerned. Though the characteristic melting temperatures differ by a few degrees, the rest of the physical signatures are identical. Thus it will be appropriate to argue that the microscopic structure of the coacervate material comprised of crosslinked polymer-rich zones separated by polymer-poor regions having characteristic viscoelastic length. Such systems are associated with two characteristic relaxation processes ([110], Hishimoto et al. 2004): one due to concentration fluctuation and another arising from viscoelastic relaxation. This has been adequately described by models and supported by experiments in the past. The model involves dynamic coupling between stress and diffusion in a complex and rigorous way [28, 79]. Thus, the coacervate phase is in a dynamically evolving state that makes this system extremely interesting [72]. The results presented provide a significant insight into the distinctive microscopic features of this coacervate vis-à-vis gelatin and agar gels, and gelatin coacervates. This paper does not answer all the questions related to the structure of coacervates, yet it makes an attempt to give some foundation to its understanding.

The investigation on biopolymer gels remained outside the purview of this chapter because it is a discipline on its own and cannot be dealt in a limited discussion. However, some general observations can be made. Polymer gels constitute a special class of soft matter as far as their supramolecular structure and viscoelastic properties are concerned. A gel can be defined as a three dimensional interconnected percolating (mechanically) network structure with the continuous phase (solvent) interacting synergistically with the network. The dispersed phase (polymer) can be present in a disordered and non-ergodic state. Regardless, these disordered systems are often found to be trapped far away from equilibrium, and typically relax slowly, exhibiting complex and interesting dynamics. Moreover, aging effects make the dynamics slow down significantly and often the response functions could still be scaled onto a master curve [23, 76].

Physical gels and complex networks made of two (bio)-polymers (often called co-gels) produce new biomaterials with customized and controlled properties. Sodium caseinate- β -glucan gels generate a bicontinuous topology governed by the mechanical strength and thermal stability of the β -glucan network structure [63]. Agar- κ -carrageenan co-gels were characterized by rheology and it was found that incorporation of κ -carrageenan reduced gel rigidity (Young's modulus) significantly. Moreover, distinctive agar and κ -carrageenan polymer-rich zones, well segregated inside the gel phase, were observed with the agar-rich phase providing the continuous phase and κ -carrageenan-rich phase constituting the discontinuous gel phase [77]. Pectin-chitosan co-gels were studied and their phase stability behaviour was investigated. It was concluded that though the gel strength was dependent on the mixing ratio of the two polymers, the relaxation behaviour and microscopic geometrical structure (fractal dimension of the network) remained invariant of the same [76]. In earlier studies involving co-gels of agar-gelatin (biopolymers had concentrations far above their gelation concentration), it was concluded that phase separated micro-domains of the two biopolymers was formed inside the co-gel phase [24, 117]. All these studies imply that it is possible to generate new soft biomaterials by adjusting the mixing ratio of two intelligently chosen biopolymers.

Acknowledgments Authors are thankful to their collaborators Dr. Anita K. Verma, Dr. Biswaranjan Mohanty, Dr. Amarnath Gupta, Dr. S. Boral, Mr. Najmul Arfin, Ms. Mandeep Kaloti, Ms. Ananya Tiwari and Ms Sonal Bindal whose work is cited in this review extensively. Authors acknowledges Department of Science and Technology, Government of India for financial support. Authors are thankful AIRF of the University for providing access to instrumentation.

References

1. Anderson, J.L., Pino, V., Hagberg, E.C., Sheares, V.V., Armstrong, D.W.: *Chem. Commun.* **19**, 2444–2445 (2003)
2. Archer, W.L.: *Ind. Eng. Chem. Res.* **30**, 2292–2298 (1991)
3. Arfin, N., Bohidar, H.B.: *Int. J. Biol. Macromol.* **50**, 759–767 (2012)
4. Arfin, N., Bohidar, H.B.: *J. Phys. Chem. B* **116**, 13192–13199 (2012)
5. Armstrong, D.W., He, L., Liu, Y.S.: *Anal. Chem.* **71**, 3873–3876 (1999)
6. Ascot, P.G., Ma, C., Wenner, J.R., Bloomfield, V.A.: *Biopolymer* **36**, 345–364 (1995)
7. Behrends, R., Fuchs, K., Kaatze, U., Hayashi, Y., Feldman, Y.: *J. Chem. Phys.* **124**, 144512-1–144512-8 (2006)
8. Benoit, H., Doty, P.: *J. Phys. Chem.* **57**, 958–963 (1953)
9. Biswas, A., Shogren, R.L., Stevenson, D.G., Willett, J.L., Bhovvamik, P.K.: *Carbohydr. Polym.* **66**, 546–550 (2006)
10. Biswas, A., Shogren, R.L., Willett, J.L.: *Ind. Crops Prod.* **30**, 172–175 (2009)
11. Bonner, G., Klipanov, A.M.: *Biotechnol. Bioeng.* **68**, 339–344 (2000)
12. Boral, S., Bohidar, H.B.: *J. Phys. Chem. B* **114**, 12027–12035 (2010)
13. Boral, S., Bohidar, H.B.: *J. Phys. Chem. B* **116**, 7113–7121 (2012)
14. Boral, S., Saxena, A., Bohidar, H.B.: *J. Phys. Chem. B* **112**, 3625–3632 (2008)
15. Brennecke, J.F., Maginn, E.J.: *AIChE J.* **47**, 2384–2389 (2001)
16. Budavari, S. (ed.): *Merck Index*, vol. 742, 12th edn., p. 4388 (1996)

17. Bungenberg de Jong, G.: Chapter 3. In: Krut, H.R. (ed.) *Colloid Science*, vol. 2. Elsevier Academic Press, New York (1949)
18. Burgess, J.J.: *Colloid Interface Sci.* **140**, 227–238 (1990)
19. Calvo, P., Rumunan-Lopez, C., Vila-Jato, J.L., Alonso, M.J.: *J. Appl. Polym. Sci.* **63**, 125–132 (1997)
20. Cantor, C.R., Schimmel, P.R.: *Biophysical Chemistry*, vol. 3. AH Freeman and Company, New York (1980)
21. Chandran, A., Ghoshdastid, D., Senapati, S.: *J. Am. Chem. Soc.* **134**, 20330–22033 (2012)
22. Cheng, N.S.: *Ind. Eng. Chem. Res.* **47**, 3285–3288 (2008)
23. Cipelletti, L., Manley, S., Ball, R.C., Weitz, D.A.: *Phys. Rev. Lett.* **84**, 2275–2278 (2000)
24. Clark, A.H., Richardson, R.K., Ross-Murphy, R.K., Stubbs, J.M.: *Macromolecules* **16**, 1367–1374 (1983)
25. Dan, A., Ghosh, S., Moulik, S.P.: *J. Phys. Chem. B* **113**, 8505–8513 (2009)
26. Dashnau, J.L., Nucci, N.V., Sharp, K.A., Vanderkooi, J.M.: *J. Phys. Chem. B* **110**, 13670–13677 (2006)
27. Davis-Searles, P.R., Saunders, A.J., Erie, D.A., Winzor, D.J., Pielak, G.: *J. Ann. Rev. Biophys. Biomol. Struct.* **30**, 271–306 (2001)
28. Doi, M., Onuki, A.: *J. Phys. II: France* **2**, 1631–1656 (1992)
29. Dumitriu, S., Chornet, E.: *Adv. Drug Deliv. Rev.* **31**, 223–246 (1998)
30. Earle, M.J., Seddon, K.R.: *Pure Appl. Chem.* **72**, 1391–1398 (2000)
31. Eastman, N.C., Rose, J.K.: *Hydroxyethyl Cellulose in Water Soluble Resins* [In: Davidson, R.L., Sittings, M. (eds.)], pp. 63–90. Reinhold, New York (1968)
32. Egorov, V.M., Smirnova, S.V., Formanovsky, A.A., Pletnev, I.V., Zolotov, Y.A.: *Anal. Bioanal. Chem.* **387**, 2263–2269 (2007)
33. Eisenberg, H.: *Acc. Chem. Res.* **20**, 276–282 (1987)
34. Erkselius, S., Karlsson, O.: *J. Carbohydrate Polym.* **62**, 344–356 (2005)
35. Fendt, S., Padmanabhan, S., Blanch, H.W., Prausnitz, J.M.: *J. Chem. Eng. Data* **56**, 31–34 (2011)
36. Ferrand, M., Djabourov, M., Coppola, M.: *Macromol. Symp.* **273**, 56–65 (2008)
37. Fletcher, K.A., Pandey, S.: *Langmuir* **20**, 33–36 (2004)
38. Forsyth, S.A., MacFarlane, D.R.: *J. Mater. Chem.* **13**, 2451–2456 (2003)
39. Fort, D.A., Swatoski, R.P., Moyna, P., Rogers, R.D., Moyna, G.: *Chem. Commun.* 714–716 (2006)
40. Fukaya, Y., Hayashi, K., Wada, M., Ohno, H.: *Green Chem.* **10**, 44–46 (2008)
41. Fukaya, Y., Sugimoto, A., Ohno, H.: *Biomacromolecules* **7**, 3295–3297 (2006)
42. Geng, F., Zheng, L., Yu, L., Li, G., Tung, C.: *Process Biochem.* **45**, 306–311 (2010)
43. Gomez, E., Gonzalez, B., Dominguez, A., Tojo, E., Tojo, J.: *J. Chem. Eng. Data* **519**, 696–701 (2006)
44. Graenacher, C.U.S.: Patent 1(943), 176 (1934)
45. Gupta, A.N., Bohidar, H.B.: *Biomacromolecules* **6**, 1623–1627 (2005)
46. Gupta, A.N., Bohidar, H.B.: *J. Phys. Chem. B* **111**, 10137–10145 (2007)
47. Hammouda, B., Worcester, D.: *Biophys. J.* **91**, 2237–2242 (2006)
48. Handy, S.T.: *Chem. Eur. J.* **9**, 2938–2944 (2003)
49. Hayashi, Y., Puzenko, A., Balin, I., Ryabov, Y.E., Feldman, Y.: *J. Phys. Chem. B* **109**, 9174–9177 (2005)
50. Heinze, T., Schwikal, K., Barthel, S.: *Macromol. Biosci.* **5**, 520–525 (2005)
51. Hirota, M., Furihata, K., Saito, T., Kawada, K., Isogai, A.: *Angew. Chem. Int. Ed.* **49**, 7670–7672 (2010)
52. Howe-Grant, M.E., Lippard, S.J.: Aqueous platinum (II) chemistry: binding to biological molecules. In: Sigel, H. (ed.) *Metal Ions in Biological Systems*, vol. 11, pp. 63–125. Marcel Dekker, New York (1980)
53. Huggins, M.L.: *J. Am. Chem. Soc.* **64**, 2716–2718 (1942)
54. Imai, T., Fujii, K., Shiraiishi, S., Otagiri, M.: Alteration of pharmacokinetics and nephrotoxicity of Cisplatin by Alginates. *J. Pharm. Sci.* **86**, 244–247 (1997)

55. Ishii, D., Saito, T., Isogai, A.: *Biomacromolecules* **12**, 548–550 (2011)
56. Isogai, A., Saito, T., Fukuzumi, H.: *Nanoscale* **3**, 71–85 (2011)
57. Jamieson, A.M., Simic-Glavesci, B., Tansey, K., Walton, A.G.: *Faraday Discuss., Chem. Soc.* **61**, 194–204 (1976)
58. Kaibara, K., Okazaki, T., Bohidar, H.B., Dubin, P.L.: *Biomacromolecules* **1**, 100–107 (2000)
59. Kaloti, M., Bohidar, H.B.: *Colloids Surf. B* **81**, 165–173 (2010)
60. Kaloti, M., Saxena, A., Bohidar, H.B.: *Int. J. Biol. Macromol.* **48**, 263 (2011)
61. Kaya, M., Toyama, Y., Kubota, K., Nodasaka, Y., Ochiai, M., Nomizu, M., Nishi, N.: *Int. J. Biol. Macromol.* **35**, 39–46 (2005)
62. Kimizuka, N., Nakashima, T.: *Langmuir* **17**, 6759–6761 (2001)
63. Kontogiorgos, V., Ritzoulis, C., Biliaderis, C.G., Kasapis, S.: *Food Hydrocolloids* **20**, 749–756 (2006)
64. Kraemer, O.: *Ind. Eng. Chem.* **30**, 1200–1203 (1938)
65. Lee, S.H., Dang, D.T., Ha, S.H., Chang, W.J., Koo, Y.M.: *Biotechnol. Bioeng.* **99**, 1–8 (2008)
66. Legoff, J., Tanton, C., Lecerf, M., Grésenguet, G., Nzambi, K., Bouhlal, H., Weiss, H., Belec, L.: *J. Virol. Methods* **138**, 196–200 (2006)
67. Liu, Q.B., Janssen, M.H.A., van Rantwijk, F., Sheldon, R.A.: *Green Chem.* **7**, 39–42 (2005)
68. Lukin, M., de los Santos, C.: *Chem. Rev.* **106**, 607–686 (2006)
69. Matsumura, Y., Maeda, H.: A new concept for macromolecular therapeutics in cancer chemotherapy: Mechanism of tumoritropic accumulation of proteins and the antitumor agent Smancs. *Cancer Res.* **46**, 6387–6392 (1986)
70. Micka, U., Kremer, K.: *Europhys. Lett.* **38**, 279–284 (1997)
71. Mikkola, J.P., Kirilin, A., Tuuf, J.C., Pranovich, A., Holmbom, B., Kustov, L.M., Murzin, D.Y., Salmi, T.: *Green Chem.* **9**, 1229–1237 (2007)
72. Mohanty, B., Aswal, V.K., Kohlbrecher, J., Bohidar, H.B.: *J. Polym. Sci.: Part B* **44**, 1653–1667 (2006)
73. Mrevlishvili, G.M., Svintradze, D.V.: *Int. J. Biol. Macromol.* **35**, 243–245 (2005)
74. Mudalige, A., Pemberton, J.E.: *Vib. Spectrosc.* **45**, 27–35 (2007)
75. Nguyen, T.T., Shklovskii, B.I.: *J. Chem. Phys.* **115**, 7298–7308 (2001)
76. Nordby, M.H., Kjoniksen, A.L., Nystrom, B., Roots, J.: *Biomacromolecules* **4**, 337–343 (2003)
77. Norziah, M.H., Foo, S.L., Karim, A.A.: *Food Hydrocolloids* **20**, 204–206 (2006)
78. Ohno, H., Fukaya, Y.: *Chem. Lett.* **38**, 2–7 (2009)
79. Onuki, A., Taniguchi, T.: *J. Chem. Phys.* **106**, 5761–5770 (1997)
80. Park, P., Kazlauskas, R.J.: *J. Org. Chem.* **66**, 8395–8401 (2001)
81. Park, J.M., Muhoberac, B.B., Dubin, P.L., Xia, J.: *Macromolecules* **25**, 290–295 (1992)
82. Pawar, N., Bohidar, H.B.: *J. Polym. Sci., Part B: Phys.* **48**, 555–565 (2010)
83. Pezron, I., Djabourov, M., Bosio, L., Leblond, J.: *J. Polym. Sci. Part B: Phys.* **1990**, 28 (1823)
84. Pezron, I., Djabourov, M., Leblond, J.: *Polymer* **32**, 3201–3210 (1991)
85. Polson, J.M., Zuckerman, M.J.: *J. Chem. Phys.* **116**, 7244–7254 (2002)
86. Rawat, K., Bohidar, H.B.: *J. Mol. Liq.* **169**, 136–143 (2012)
87. Rawat, K., Bohidar, H.B.: *J. Phys. Chem. B* **116**, 11065–11074 (2012)
88. Remsing, R.C., Swatoski, R.P., Rogers, R.D., Moyna, G.: *Chem. Commun.* **12**, 1271–1273 (2006)
89. Roder, B., Fruhwirth, K., Vogl, C., Wagner, M., Rossmanith, P.: *J. Clin. Microbiol.* **48**, 4260–4262 (2010)
90. Rolin, C., Nielsen, B.U., Glahn, P.E., Pectin, D.S. (eds.): *Polysaccharides: Structural Diversity and Functional Versatility*, pp. 377–431. Marcel Dekker, New York (1998)
91. Saito, T., Hirota, M., Tamura, N., Kimura, S., Fukuzumi, H., Huex, L., Isogai, A.: *Biomacromolecules* **10**, 1992–1996 (2009)
92. Saito, T., Kimura, S., Nishiyama, Y., Isogai, A.: *Biomacromolecules* **8**, 2485–2491 (2007)

93. Saito, T., Nalepa, D.E.: *J. Appl. Polym. Sci.* **22**, 865–867 (1978)
94. Sanchez, C., Renard, D.: *Int. J. Pharm.* **242**, 319–324 (2002)
95. Sanford, P.A., Hutchings, G.P.: *Genetic Engineering: Structure-Property Relations and Applications*. Elsevier, New York (1987)
96. Sanwalani, S., Bohidar, H.B.: *J. Phys. Chem Biophys.* **3**, 100114-1–6 (2013)
97. Scherage, A., Mandelkern, L.: *J. Am. Chem. Soc.* **75**, 179–184 (1953)
98. Seyrek, E., Dubin, P.L., Tribet, C., Gamble, E.A.: *Biomacromolecules* **4**, 273–282 (2003)
99. Shankar, P.N., Kumar, M.: *Proc. R. Soc. Lond. A* **444**, 573–581 (1994)
100. Singh, S.S., Aswal, V.K., Bohidar, H.B.: *Int. J. Biomacromol.* **41**, 301–307 (2007)
101. Singh, T., Boral, S., Bohidar, H.B., Kumar, A.: *J. Phys. Chem. B* **114**, 8441–8448 (2010)
102. Singh, S.S., Siddhanta, A.K., Meena, R., Prasad, K., Bandyopadhyay, S., Bohidar, H.B.: *Int. J. Biol. Macromol.* **41**, 185–192 (2007)
103. Smith, A.E.: *Nature* **214**, 1038–1040 (1967)
104. Streit, S., Sprung, M., Gutt, C., Tolan, M.: *Phys. B* **357**, 110–114 (2005)
105. Tanford, C.: *Physical Chemistry of Macromolecules*. Wiley, New York (1961)
106. Swatloski, R.P., Spear, S.K., Holbrey, J.D., Rogers, R.D.: *J. Am. Chem. Soc.* **124**, 4974–4975 (2002)
107. Tiwari, A., Bindal, S., Bohidar, H.B.: *Biomacromolecules* **10**, 184–189 (2009)
108. Tokuda, H., Hayamizu, K., Ishii, K., Susan, Md.A.B.H., Watanabe, M.: *J. Phys. Chem. B* **109**, 6103–6110 (2005)
109. Towey, J.J., Soper, A.K., Dougan, L.: *J. Phys. Chem. B* **115**, 7799–7807 (2011)
110. Toyoda, N., Takenaka, M., Saito, S., Hashimoto, T.: *Polymer* **42**, 9193–9203 (2001)
111. Tsuchida, E., Abe, K.: *Intermacromolecular Complexes*. Springer, Heidelberg (1982)
112. Turgeon, S.L., Schmitt, C., Sanchez, C.: *Curr. Opin. Colloid Interface Sci.* **12**, 166–178 (2007)
113. Veis, A.: *Macromolecular Chemistry of Gelatin*. Academic Press, New York (1964)
114. Verma, A.K., Sachin, K.: *Curr. Drug Deliv.* **5**, 120–126 (2008)
115. Vijayaraghavan, R., Izgorodin, A., Ganesh, V., Surianarayanan, M., MacFarlane, D.R.: *Angew. Chem. Int. Ed.* **49**, 1631–1633 (2010)
116. Vitz, J., Erdmenger, T., Haensch, C., Schubert, U.S.: *Green Chem.* **11**, 417–424 (2009)
117. Watase, M., Nishinari, K.: *Rheol. Acta* **19**, 220–225 (1980)
118. Watson, J.D., Crick, F.H.C.: *Nature* **171**, 737–738 (1953)
119. Welton, T.: *Chem. Rev.* **99**, 2071–2083 (1999)
120. Wu, Y., Sasaki, T., Irie, S., Sakurai, K.: *Polymer* **49**, 2321–2327 (2008)
121. Xie, H., Zhang, S., Li, S.: *Green Chem.* **8**, 630–633 (2006)
122. Xu, Q., Kennedy, J.F., Liu, L.: *Carbohydr. Polym.* **72**, 113–121 (2008)
123. Xu, Y., Mazzawi, M., Chen, K., Sun, L., Dubin, P.L.: *Biomacromolecules* **12**, 1512–1522 (2011)
124. Yamazaki, S., Takegawa, A., Kaneko, Y., Kadokawa, J., Yamagata, M., Vlshikawa, : *Electrochim. Commun.* **11**, 68–70 (2009)
125. Zech, O., Thomaier, S., Bauduin, P., Ruck, T., Touraud, D., Kunz, W.: *J. Phys. Chem. B* **113**, 465–473 (2009)
126. Zhang, H., Oh, M., Allen, C., Kumacheva, E.: *Biomacromolecules* **5**, 2461–2468 (2004)
127. Zhang, G., Wu, C.: *Phys. Rev. Lett.* **86**, 822–825 (2001)
128. Zhang, H., Wu, J., Zhang, I., He, J.: *Macromolecules* **38**, 8272–8277 (2005)

Polyelectrolyte Hydrogels: Thermodynamics

Xue-Song Jiang, Mohit Philip Mathew and Jian Du

Abstract Polyelectrolyte hydrogel is a three dimensional networks forming by charged polymer chains. The hydrophilic networks capable of imbibing large amount of water or biological fluids, mimics biological tissues. Because of this nature, great attention was devoted to these systems for biomedical applications by tuning the physicochemical properties with varying the degree of crosslinking either by physical or chemical or physical-chemical means. Numerous approaches have been investigated for formulation of polyelectrolyte hydrogels. In this chapter, an attempt was made to narrate the synthetic and natural materials and their mechanism to form cross-linked polyelectrolyte hydrogels. It was also tried to explain the importance of ionotropic gelation and polyelectrolyte complexation approaches, as these methods show great promise as a tool for the development in their application process. For further understanding in this area, a mathematical model was introduced to describe the thermodynamic behavior of polyelectrolyte hydrogels and derives conditions for thermodynamic phase equilibrium; the physical and chemical characterization of hydrogels, as well as special considerations that need to be made when characterizing polyelectrolyte hydrogels, were also discussed. In the end, a number of biomedical applications of polyelectrolyte hydrogel were given, such as in controlled release systems, different types of tissue reconstitution, for the enzyme and protein separations, etc.

X.-S. Jiang · M.P. Mathew · J. Du (✉)

The Translational Tissue Engineering Center, The Johns Hopkins University,
Baltimore, MD, USA
e-mail: jdu4@jhu.edu

X.-S. Jiang
e-mail: xjiang11@jhu.edu

X.-S. Jiang
Department of Materials Science and Engineering, The Johns Hopkins University,
Baltimore, MD, USA

M.P. Mathew · J. Du
Department of Biomedical Engineering, The Johns Hopkins University,
Baltimore, MD, USA

1 Introduction

Polyelectrolyte hydrogels have attracted tremendous research interest over the past few decades owing to their ability in respond to external chemical or physical stimuli. A polyelectrolyte hydrogel is a three dimensional networks forming by charged polymer chains that can swell in water and retain a significant amount of water while maintaining their structure [1]. Their ability to swell in water is dependent on the presence of ions on the polymer chains and counter ions localized in the network frame. The pendant acidic groups (e.g. carboxylic acid, sulfonic acid) or basic groups (e.g. amine groups) on the polymer backbone become ionized at high or low pH. Polyampholyte hydrogel networks contain both positively and negatively charged moieties and show entirely different properties from their originate polyelectrolyte polymers [2–4]. Due to the ionic interactions between charged polymer and free ions, polyelectrolyte hydrogels are able to undergo large reversible and nonlinear volume phase transitions in response to environmental stimuli, such as pH [5], polarity of solvent, ionic strength, or electric field [6, 7]. In some circumstances, these stimulus-responsive polyelectrolyte hydrogels are referred to as environment-sensitive or intelligent hydrogels [8, 9]. This peculiarity has stimulated the interest for these materials in the applications such as actuators [10] and sensors [11], separation and filtration processes [12].

Many applications require hydrogels that have high sensitivity and a short response times. Because the volume phase transition of hydrogels is a diffusion-limited process, the fast swelling property can be achieved by either reducing the particle size of the hydrogels or creating pore structures in the hydrogels. Both methods will generate larger surface areas and reduce diffusion distance, which improve the swelling kinetics.

More recent work has addressed the development of novel biomaterials for biomedical and pharmaceutical applications. Polyelectrolyte hydrogels have similar physical properties as that of biological tissues. The living tissues consist of polyelectrolyte such as charged polysaccharide and filamentous proteins and their properties originate from the polyelectrolyte nature. Therefore, polyelectrolyte hydrogels have been extensively used in the development of controlled drug delivery system and scaffolds for tissue engineering. However, one of the inherent limitations of the hydrogel networks formed by irreversible covalent crosslinking is the non-biodegradability when being used in applications such as implantable devices. Alternative types of networks, formed by cleavable bond or physical interactions between polymer chains, have been developed. These biocompatible, nontoxic and biodegradable polymers are now acquiring unique place for biomedical application for various purposes such as scaffolds for tissue engineering [13] and drug delivery system [13–15]. In addition, the weak mechanical property of swollen polyelectrolyte hydrogel is another main hurdle that limits its practical applications. Studies have been done to improve the mechanical properties by grafting hydrogels onto a stronger support surface via covalent bonds. The other

approach is to form a polyampholyte gels which have supramolecular structure, contain much less water than that of conventional hydrogels. Most importantly, they have a high toughness and fatigue resistance [16].

2 Classification of Polyelectrolyte Hydrogels

Polyelectrolyte hydrogels can be of synthetic or natural in origin. Combining natural occurring polymer with synthetic materials produces novel natural-synthetic hybrid polymers. This section describes the properties of polymers that have been used for designing and fabricating polyelectrolyte hydrogels.

2.1 Synthetic Polyelectrolyte Hydrogels

Compared with natural polymers, synthetic polymers possess defined structures and more reproducible chemical and physical properties. Desirable hydrogels with suitable block structures, morphology, mechanical strength and biodegradability can be designed and synthesized. Of the many synthetic polyelectrolyte hydrogels, poly (acrylic acid) (PAA), poly (methacrylic acid) (PMAA), and their derivatives are the most widely investigated polymers. The wide variety of monomers enables one to prepare the hydrogel with desired physical properties for a given application. Furthermore, the side carboxylic groups of PAA can be easily modified with various functional groups, such as imide, amine, or attached to other molecules or bioactive agents.

The change in the pH of the external environment will act as a stimulus, and the response to the stimulus is the change in swelling properties of the hydrogels. The dynamic swelling change of the ionic hydrogels is used in the design of intelligent controlled release devices for site-specific drug delivery of therapeutic proteins to the target place, where the biological activity of the proteins is prolonged. The pH sensitivity of anionic hydrogels of poly (methacrylic acid-g-ethylene glycol) has been used to deliver proteins to the colon [17, 18]. Electrically stimulated drug delivery systems has also been studied using PAA polyelectrolyte hydrogel [19].

Hydrogels composed of amino groups containing polymers, such as units of poly(2-(dimethylamino)ethyl methacrylate) (PDMA), poly(2-(diethylamino)ethyl methacrylate), poly(2-(diisopropylamino) ethyl methacrylate) (PDPA), poly(2-vinylpyridine), poly(ethyleneimine) (PEI), have been frequently studied.

Cationic hydrogels have been used in the development of self-regulated insulin delivery systems [20, 21]. In these system, glucose oxidase catalyze the oxidation of glucose to produce gluconic acid. Therefore, the local pH decreases with the increase in glucose concentration, swelling the pH sensitive cationic hydrogels, which results in the release of encapsulated insulin in response to changing glucose concentration.

The swelling and pH sensitivity of these gels can be adjusted by using neutral comonomers such as 2-hydroxyethyl methacrylate and maleic anhydride. In addition, the hydrogels can be made temperature-sensitive, by incorporating poly(N-isopropylacrylamide) units. Interpenetrating polymer network (IPNs, details in 7.3) hydrogels formed by PAA and polyacrylamide (PAAm) or poly poly(acrylamide-co-butyl methacrylate) have positive temperature dependence of swelling. While the P(NIPAAm-co-BMA-co-AA) hydrogels are negatively thermosensitive [22].

Hydrogels prepared from the copolymerization of various vinylated monomers are nonbiodegradable, thus are limited in applications where biodegradability is desired. Poly amino acids were used in synthesis of biodegradable hydrogels because of their more regular arrangement of amino acid residues than those derived from natural proteins. Examples of such type of hydrogels include polymer of aspartic acid, glutamic acid and lysine. In addition to normal electro-static effects associated with most pH-sensitive synthetic polymer hydrogels, Poly amino acids backbone may also contribute to the pH-sensitive swelling behavior [23, 24].

2.2 Natural Polyelectrolyte Hydrogels

Many natural polymers have charged polymer chains that can form polyelectrolyte hydrogels. They are frequently used to make hydrogel scaffolds for tissue-engineering applications owing to their biocompatibility, inherent biodegradability and critical biological functions. These polymers include polysaccharides, such as alginate, heparin, heparan sulfate, hyaluronic acid (HA) and chitosan, proteins/polypeptides, such as collagen, gelatin and DNA.

A variety of polysaccharides like HA, heparin, chitosan, dextran [25] and alginate have been explored as hydrogels. Crosslinking among polymer chains can be formed by covalent bond or physical interaction. If direct crosslinking is not achievable, the polymer chains need to be modified with the attachment of various functional groups such as vinyl, amine or sulfhydryl groups for hydrogel formation [26, 27]. In addition, polysaccharides have been combined with other components such as collagen, gelatin, laminin and fibrin to form an interpenetrating network or composite hydrogels.

Many methods have been employed for preparation of protein-based hydrogels hydrogels, including thermal gelation, photopolymerization and chemical cross-linking with agents such as glutaraldehyde, genipin, adipic dihydrazide and bis(sulfosuccinimidyl) suberate [28, 29].

DNA molecule is composed of two highly negatively charged polynucleotide chains. Both chains are held together by weak intermolecular forces, forming a double helix. DNA has drawn considerable attention as a building material for fabricating hydrogels due to its ability to form ordered hydrogel networks through self-assembly [30].

2.3 Natural/Synthetic Hybrid Polyelectrolyte Hydrogels

The combination of the characteristics of synthetic and natural polymers to make hybrid hydrogels has become a direct approach to create bioactive hydrogel expands the design and application of hydrogels.

Many naturally occurring polymers, such as collagen, fibrinogen, hyaluronic acid, chitosan and heparin, have been used to make hybrid hydrogels with synthetic polymers, such as PEG, PNIPAm and PVA [31–35]. The hybridization can be performed by covalent bonding or physically interactions. For example, the IPN hydrogel composed of sodium alginate (SA) and poly(diallyldimethylammonium chloride) (PDADMAC) exhibited pH and electrical sensitive behavior [36].

3 Synthesis of Polyelectrolyte Hydrogels

Hydrogels are crosslinking stabilized networks. A wide variety of approaches have been employed to prepare polyelectrolyte hydrogels. Crosslinking can be provided by covalent bonds, or by physical interaction, such as electrostatic interaction, hydrogen bonding, and van der Waals force. An IPN is a combination of two polymer networks that interlaced on a molecular scale but not covalently bonded to each other. The networks may be synthesized independently in the immediate presence of the other without any covalent bonds between them.

3.1 Copolymerization from Monomers

Free radical copolymerization is the most commonly used method to synthesize hydrogel from vinyl monomers. The ionic or neutral monomers and the cross-linking agents are copolymerized in bulk, in solution, or in suspension. The reaction is normally initiated with chemical initiator, heat, or radiation, e.g. UV light or gamma ray. After polymerization the hydrogels need to be washed with water in order to remove the residual monomers and homopolymers not incorporated into the network.

Water is the most commonly used solvent since monomers used to synthesis the polyelectrolyte hydrogels are highly water soluble. However, when copolymerize with monomers insoluble in water, suspension polymerization and emulsion polymerization [37] can be used.

3.2 Crosslinking of Linear Polymers

Linear polymers can be converted to hydrogels by irradiation. The irradiation of polymer with high energy radiation like UV light, gamma ray and electron beam,

in aqueous solution or in dry state, results in the formation of free radicals on the polymer chains. Free radicals initiate the formation of covalent bonds or grafting polymerization, and form a network structure. The major advantage over chemical initiation is the production of relatively pure, residue-free hydrogels. PAA and other polymers have been crosslinked by radiation method [38].

The presence of functional groups, such as hydroxyl, carboxyl or primary amine group, on the water soluble polymer chain, can be used to prepare hydrogels by forming covalent linkages between the polymer chains and complementary reactivity, such as amine/carboxylic acid, isocyanate/hydroxyl/amine group or by reductive amination. Polymers can be converted to hydrogels by crosslinking of polymers containing reactive groups with a bi-functional crosslinking agent like divinylsulfone [39] and 1,6-hexanedibromide [40]. Gluteraldehyde has been widely used as a crosslinker to prepare hydrogels of polymers containing primary amine groups (e.g. gelatin, chitosan) [41, 42]. The reaction is usually performed in aqueous solution, and the gel point is reached very quickly.

Recently, a method combining chemical crosslinking and physical self-assembly for fabricating *in situ* biodegradable hydrogels based on a pH-responsive thiol–disulfide exchange reaction dependent on the pKa of the involved thiols was reported by Wu et al. [43]. In this system, core-shell structures were produced using two-step Michael addition polymerization, stabilizing the hydrogel network.

3.3 Modifying Neutral Hydrogels

Ionic hydrogels can also be prepared by hydrolysis of neutral hydrogels, resulting in an acidic hydrogel. Different degrees of ionization can be introduced in the polymeric backbone by hydrolysis of already existing groups in neutral hydrogel, such as esters, amides and nitriles. The resulting distribution of ionizable groups in the backbone will be different than the distribution after copolymerization of the two corresponding monomers. A polyelectrolyte hydrogel was prepared by partial hydrolysis of N-vinyl-pyrrolidinone and methyl methacrylate copolymer resulting in formation of acidic groups to improve corneal epithelial cell adhesion and bind to fibronectin or peptides [44]. One unique method to synthesize polyelectrolyte hydrogel has been reported by modifying a functional neutral polymer, charges can be introduced by a crosslinker [45].

3.4 Physical (Non-Covalent) Crosslinking of Polymers

Hydrogels rely on physical bonds to undergo volume-phase transition. In some cases, non-covalent crosslinking reversibly transforms a solution of polymers into a gel. The crosslinks of the network have a physical origin (charge-charge interaction, hydrogen bonding, Van der Waals forces) and therefore are sensitive to variations of temperature, pH, ionic content, etc. [46, 47].

3.4.1 Polyelectrolyte Complexes Formed Through Charge–Charge Interaction

Hydrogel may also be obtained by using anionic and cationic polymers to form polyelectrolyte complexes, where ionic forces hold the polymers together forming a network through ionic bridges between the polymeric chains. The ionic cross-linking is reversible as the hydrogel will dissociate at extreme ionic strength.

The polyelectrolyte complex undergoes slow erosion, which gives a more biodegradable material than covalently crosslinked hydrogels [48, 49]. Such complex can also be formed by layer-by-layer self-assembly of oppositely charged polymers [50, 51]. When polyelectrolytes are mixed with multivalent counter-ions in aqueous solutions, the multivalent ions can cross-link the polymer to form hydrogels. Examples of such ionotropic gelation pairs are alginate/calcium [52] and chitosan/tripolyphosphate [53, 54].

3.4.2 Crosslinking Through Hydrogen Bond and Van der Waals Force

Hydrogen bond and Van der Waals force are weak interactions that are formed or broken during a phase transition are a combined effect of cooperative interactions between polymer chains and polymer-solvent interactions [46, 47, 55]. These weak interactions occur as in the case of poly(methacrylic acid) and poly(ethylene glycol) hydrogel formation. Poly(methacrylic acid-g-ethylene glycol) showed pH dependent swelling due to the reversible formation of interpolymer complex, stabilized by hydrogen bonds between the oxygen of poly(ethylene glycol) and carboxylic acid group of poly(methacrylic acid) [56, 57].

Some commonly used protein-based gels, e.g. Matrigel and collagen type I, rely on a change in temperature to induce gelation. When denatured collagen forming gelatin, the thermally induced changes are caused by segments of gelatin chains organizing intra molecularly into the collagen fold. Although hydrogen bonds, ionic bonds and Van der Waals interactions participates in bonding, gelatin gels formation depends on concentration and exist over only a small temperature range.

Polyampholyte hydrogels can be fabricated by utilizing hydrogen bond and Van der Waals forth. The self-assembly of peptides and proteins provide a method to control the gel structure and properties precisely [58–60].

Stronger interactions can be observed when polymers form ordered complexes such as microcrystals, peptides helices and specific binding of biomolecules. For example, hyaluronic-acid based hydrogel can be crosslinked through antigen-antibody [61] or biotin-avidin [62] binding.

3.5 Interpenetrating Networks

Two physically entangled crosslinked polymer networks form an interpenetrating network, even they may be incompatible with each other. Such a network

combines individual properties of two polymers and in some cases, exhibits entirely new properties that are not found in individual network [63].

The same principles that used to form a crosslinking network can be applied to IPN systems. For instance, IPN can be prepared initiating polymerization of a monomer in an existing polymer network. The first hydrogel network was composed of crosslinked poly(oxyethylene). The secondary polymerization was taken place in a mixture of acrylic acid, crosslinker and initiator with the poly(oxyethylene) soaked in it, resulting in interpenetrating pH-sensitive networks of poly(oxyethylene) and PAA [64]. IPN can also be formed simultaneously using two different polymerizations mechanisms such as condensation and free radical polymerizations [65]. If linear polymer penetrate on a molecular scale of cross-linked polymer network, a semi-IPN is formed [66].

4 Polyelectrolyte Hydrogels: Thermodynamics

An understanding of the thermodynamic properties of polyelectrolyte hydrogels provides the theoretical framework necessary to predict and understand the behavior of these gels. Of particular importance is a means to study swelling and shrinking properties of gels, to this end attention needs to be paid to the conditions necessary for phase equilibrium. Polyelectrolyte hydrogel swelling and shrinking behavior has an added layer of complexity introduced by the charges that exist within the gel and the charges that can be present as ions in the surrounding liquid. While different models have been developed over the years to describe the thermodynamics of polyelectrolyte hydrogels, this section will focus on the model developed by Maurer and Prausnitz [67]. This model was chosen as it derives a comprehensive framework for the description of a polyelectrolyte hydrogel system that can be applied to diverse conditions starting from the fundamental laws of thermodynamics. Also this model pays specific attention to the equilibrium partitioning of solute molecules which is especially useful for chemical engineering applications.

4.1 The Gel Model

This model for a hydrogel as depicted in Fig. 1 considers three phases: the bath, the gel and the surface of the gel (that is modelled as an elastic membrane).

The membrane serves a couple of functions. It behaves in an analogous way to a semi-permeable membrane in osmosis, allowing solvent particles to freely pass through but only allowing select solute particles to transit in and out. Unlike the membrane in osmosis that is assumed to be invariant, the membrane in this model is defined as elastic; as a result the energy of the membrane varies with the volume of the gel. The elasticity of the membrane is important in incorporating the

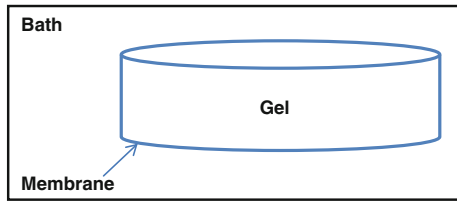


Fig. 1 Schematic of the gel model, the gel phase is surrounded by an elastic membrane and together they are immersed in a liquid bath

mechanical properties of the gel and the pressure differences that result between the gel and fluid phases as the gel swells or shrinks. Hence for the system to reach phase equilibrium it needs to not only be in chemical equilibrium but also in a mechanical equilibrium.

4.2 Derivation of Conditions for Phase Equilibrium

Starting by applying the first law of thermodynamics to an isothermal system kept under constant external pressure (these conditions are appropriate for most chemical engineering and biological situations where external pressure applied is usually not changed and temperatures are held fairly constant). The system includes the gel phase, the liquid phase and the elastic membrane. Heat (Q) and work (W) can be transferred to and from the system thus altering its internal energy (U). Both Q and W are defined as positive when energy is transferred to the system.

$$Q + W = \Delta U \quad (1)$$

Focusing on the case wherein work can only be done on the system in conjunction with a volume change and applying the 1st and 2nd laws of thermodynamics we derive the following expression:

$$TdS - pdV \geq dU \quad (2)$$

where T is the absolute temperature, S is entropy, p is pressure and V is volume (all with respect to the entire system). The system consists of 3 phases as discussed in Fig. 1, the gel phase, the bath and the membrane. Hence each of the state functions can be represented as the sum of the individual contributions of the three phases (phase is designated in superscript, bath for fluid phase, gel for gel phase and m for elastic membrane).

$$dU = dU^{bath} + dU^m + dU^{gel} \quad (3)$$

$$dV = dV^{bath} + dV^m + dV^{gel} \quad (4)$$

$$dS = dS^{bath} + dS^m + dS^{gel} \quad (5)$$

The model assumes that the volume of the membrane remains constant, and hence:

$$dV^m = 0 \quad (6)$$

At a fixed temperature, the only factor that affects the elastic behavior of the membrane is the volume of the gel phase. p in Eq. (2) refers to external pressure (p^{bath}). Thus combining Eqs. (4) and (6) gives:

$$pdV = p^{bath}(dV^{gel} + dV^{bath}) \quad (7)$$

Substituting Eqs. (3)–(7) into Eq. (2) results in:

$$-T(dS^{bath} + dS^m + dS^{gel}) + p^{gel}(dV^{gel} + dV^{bath}) + dU^{bath} + dU^m + dU^{gel} \leq 0 \quad (8)$$

Since the membrane separates the gel and fluid phases it is important to realize that there is a pressure difference between the two phases ($p^{gel} \neq p^{bath}$).

The Helmholtz energy, A , is defined as the useful work that can be obtained from a closed system at a constant temperature and is described by:

$$A = U - TS \quad (9)$$

Another commonly used measure of thermodynamic energy is the Gibbs energy, G , it is defined as the amount of useful work that can be obtained from a system at a fixed temperature and pressure and is described by:

$$G = U + pV - TS \quad (10)$$

Since the system is isothermal (temperature is constant) and held at a constant external pressure (p^{bath} is constant) Eqs. (9) and (10) give rise to:

$$dG^{bath} = dU^{bath} + p^{bath}dV^{bath} - TdS^{bath} \quad (11)$$

$$dA^m = dU^m - TdS^m \quad (12)$$

$$dG^{gel} = dU^{gel} + p^{gel}dV^{gel} + V^{gel}dp^{gel} - TdS^{gel} \quad (13)$$

Using Eqs. (11)–(13) to rewrite Eq. (8):

$$dG^{bath} + dA^m + dG^{gel} + (p^{bath} - p^{gel})dV^{gel} - V^{gel}dp^{gel} \leq 0 \quad (14)$$

At Constant p^{bath}

$$(p^{bath} - p^{gel})dV^{gel} - V^{gel}dp^{gel} = -d\{V^{gel}(p^{gel} - p^{bath})\} \quad (15)$$

Hence Eq. (14) simplifies to:

$$d\{G^{bath} + A^m + G^{gel} - V^{gel}(p^{gel} - p^{bath})\} \leq 0 \quad (16)$$

We can assume that the gel is incompressible at a fixed temperature and composition (T and n^{gel} are constant, where n^{gel} denotes the mole numbers of the various components of the gel). i.e. that volume changes are accompanied by changes in the composition of the gel. Therefore if we consider a change in pressure for the gel phase from p^{bath} to p^{gel} using Eq. (13):

$$G^{gel}(T, p^{gel}, n^{gel}) = G^{gel}(T, p^{bath}, n^{gel}) + V^{gel}(p^{gel} - p^{bath}) \quad (17)$$

Substituting Eq. (17) into Eq. (16) results in:

$$d\{G^{bath}(T, p^{bath}, n^{bath}) + A^m(T, V^{gel}) + G^{gel}(T, p^{bath}, n^{gel})\} \leq 0 \quad (18)$$

Equation (18) demonstrates when the temperature and external pressure of the system are held constant the only changes that are thermodynamically allowed are ones wherein the sum of the Gibbs free energy of the gel and the bath and the Helmholtz energy of the membrane decreases or remains constant.

In a system when you have a small isothermal change in volume, work is done on the system and hence the work that the system is now capable of performing increases (the Helmholtz Energy of the membrane increases), this change is described by:

$$Work = PdV = -(p^{bath} - p^{gel})dV^{gel} = (dA^m)_T \quad (19)$$

4.3 Solving for Conditions for Phase Equilibrium

As discussed previously Eq. (18) describes the conditions for phase equilibrium. At equilibrium the sum of these energies must reach a minimum. The equilibrium conditions can be mathematically formulated by the following equations. For notational convenience we define a variable Y :

$$Y = G^{bath}(T, p^{bath}, n^{bath}) + A^m(T, V^{gel}) + G^{gel}(T, p^{bath}, n^{gel}) \quad (20)$$

At equilibrium the sum of the energies needs to reach a constant/stable, minimum value.

$$\left(\frac{\partial Y}{\partial n_{water}^{gel}} \right)_{T,p^{bath}} = 0 \quad (21)$$

Equation (21) describes the equilibrium criterion that ensures that the sum of the energies is constant. The second derivative of Y shown in Eq. (22) sets the criteria for the sum of the energies of system being a minimum.

$$\left[\frac{\partial^2 Y}{\partial n_{water}^{gel}} \right]_{T,p^{bath}} > 0 \quad (22)$$

Using Eqs. (21) and (22) the phase equilibrium of the system can be mathematically determined.

4.4 Developing the Model to Better Describe Polyelectrolyte Gels

The Gibbs energy is related to the chemical potentials by the following relationship:

$$G(T, p^{bath}) = \sum_{i=1}^N n_i \mu_i \quad (23)$$

where N is the number of chemical species in the respective phase and:

$$\mu_i = \left(\frac{\partial G}{\partial n_i} \right)_{T,p^{bath},n^{gel}} \quad (24)$$

Differentiating Eq. (23) at constant temperature and external pressure gives rise to:

$$(dG)_{T,p} = \sum_{i=1}^N \mu_i dn_i \quad (25)$$

From the law of mass conservation the following expression is arrived at:

$$dn_i^{bath} = -dn_i^{gel} \quad (26)$$

Substituting Eq. (25) into Eq. (18) we get the reformulated equation:

$$d\{G^{bath} + A^m + G^{gel}\} = d\left(\sum_{i=1}^{N^{bath}} n_i^{bath} \mu_i^{bath}(T, p^{bath}, n^{bath}) + \sum_{i=1}^{N^{gel}} n_i^{gel} \mu_i^{gel}(T, p^{bath}, n^{gel}) + A^m\right) \quad (27)$$

Now substituting Eq. (26) into Eq. (27) results in:

$$d\{G^{bath} + A^m + G^{gel}\} = \sum_{i=1}^N (\mu_i^{bath}(T, p^{bath}, n^{bath}) - \mu_i^{gel}(T, p^{bath}, n^{gel})) dn_i^{bath} + dA^m \quad (28)$$

Since polyelectrolyte gels have the added property of containing various charge carrying species the model needs to be adapted to incorporate the effect these charges will have on the system. In particular how this affects the partitioning of the different species into and out of the gel. There are two main approaches to doing this: (1) Taking into account the electrical potential differences that may occur between the phases or (2) assuming electroneutrality, i.e. that each phase while containing a number of charges is overall neutral. Since the potential differences that are generated between the phases are often too small to be accurately measured the most common approach is to assume electroneutrality. It is important to point out that this assumption allows the exact description of the distribution of the various charged species between the two phases [68–70].

4.4.1 Using Assumption of Electroneutrality

Introducing the condition for electroneutrality:

$$\sum_{i=1}^{N^{gel}} n_i^{gel} z_i = 0 \quad (29)$$

Here N^{gel} is the number of different species i within the gel, z_i is the charge number of each species i (for cations $z_i > 0$, for anions $z_i < 0$), Eq. (29) can be reorganized to give:

$$dn_q^{gel} = - \sum_{\substack{i=1 \\ i \neq q}}^N z_i n_i^{gel} / z_q \quad (30)$$

where q is an ionic species that can partition between the gel and fluid phases.

At this stage partial molar volumes \bar{v}_i^{gel} can be defined as:

$$\bar{v}_i^{gel} = \left(\frac{\partial V^{gel}}{\partial n_i} \right)_{T, p^{bath}, n^{gel}} \quad (31)$$

Taking into account that not all the components of the hydrogel can partition in and out of the gel phase (for example the network constituents are assumed to be limited to the gel) we can replace N^{gel} with N, where N is defined as the number of species that can partition between the two phases. We can therefore express the change in volume of the gel phase as:

$$dV^{gel} = \left(\sum_{\substack{i=1 \\ i \neq q}}^N \bar{v}_i^{gel} dn_i^{gel} \right) + \bar{v}_q^{gel} dn_q^{gel} = - \sum_{\substack{i=1 \\ i \neq q}}^N \left(\bar{v}_i^{gel} - z_i \bar{v}_q^{gel} / z_q \right) dn_i^{bath} \quad (32)$$

Equation (28) can be expressed as:

$$dY = \sum_{i=1}^N (\mu_i^{bath}(T, p^{bath}, n^{bath}) - \mu_i^{gel}(T, p^{bath}, n^{gel})) dn_i^{bath} + dA^m \quad (33)$$

Since

$$dA^m = \left(\frac{\partial A^m}{\partial V^{gel}} \right)_T dV^{gel} \quad (34)$$

Substituting Eqs. (31) and (34) into the first equilibrium condition that can be defined from Eq. (33):

$$\sum_{i=1}^N (\mu_i^{bath}(T, p^{bath}, n^{bath}) - \mu_i^{gel}(T, p^{bath}, n^{gel}) + \left(\frac{\partial A^m}{\partial V^{gel}} \right)_T \bar{v}_i^{gel}) dn_i^{bath} = 0 \quad (35)$$

Substituting Eq. (32) into Eq. (35) results in:

$$\sum_{i=1}^N \left\{ \mu_i^{bath}(T, p^{bath}, n^{bath}) - \mu_i^{gel}(T, p^{bath}, n^{gel}) - \left(\frac{\partial A^m}{\partial V^{gel}} \right)_T \left(\bar{v}_i^{gel} - \frac{z_i \bar{v}_q^{gel}}{z_q} \right) \right\} dn_i^{bath} = 0 \quad (36)$$

Separating the components of the summations and introducing Eq. (30) leads to the following expression:

$$\begin{aligned}
& \sum_{i=1}^N \left\{ \mu_i^{bath}(T, p^{bath}, n^{bath}) - \mu_i^{gel}(T, p^{bath}, n^{gel}) - \left(\frac{\partial A^m}{\partial V^{gel}} \right)_T \left(\bar{v}_i^{gel} - \frac{z_i \bar{v}_q^{gel}}{z_q} \right) \right\} d n_i^{bath} \\
& i \neq q \\
& - \left\{ \mu_q^{bath}(T, p^{bath}, n^{bath}) - \mu_q^{gel}(T, p^{bath}, n^{gel}) \right\} \left(\sum_{\substack{i=1 \\ i \neq q}}^N z_i d n_i^{bath} / z_q \right) = 0
\end{aligned} \tag{37}$$

This expression can be reorganized and simplified to give the condition for phase equilibrium in a polyelectrolyte system at constant temperature and external pressure:

$$\begin{aligned}
\mu_i^{bath}(T, p^{bath}, n^{bath}) &= \mu_i^{gel}(T, p^{bath}, n^{gel}) + \left(\frac{\partial A^m}{\partial V^{gel}} \right)_T \bar{v}_i^{gel} + \\
& \left(\frac{z_i}{z_q} \right) \left\{ \mu_q^{bath}(T, p^{bath}, n^{bath}) - \mu_q^{gel}(T, p^{bath}, n^{gel}) - \bar{v}_q^{gel} \left(\frac{\partial A^m}{\partial V^{gel}} \right)_T \right\} \quad i = 1 \dots N; \quad i \neq q
\end{aligned} \tag{38}$$

This equation is versatile and can describe both the ionic and neutral species ($z_i = 0$) encountered in the system. This model thus enables the determination of equilibrium compositions of both the gel and the bath in almost any polyelectrolyte system: polyelectrolyte gels in pure water, polyelectrolyte gels in an aqueous electrolyte bath, etc. However, it does make the assumption of electro-neutrality, and hence an alternative way to describe the equilibrium of a polyelectrolyte system is also commonly used wherein an electric potential difference is defined between the two phases [70, 71].

4.4.2 Allowing for Potential Difference Between Phases

In this method the potential difference between the two phases is described by:

$$z_q F \Delta \Psi = \mu_q^{bath}(T, p^{bath}, n^{bath}) - \mu_q^{gel}(T, p^{bath}, n^{gel}) \tag{39}$$

F = Faraday's constant and $\Delta \Psi$ is the electric potential difference (as defined in Eq. (40)).

$$\Delta \Psi = \Psi^{gel} - \Psi^{bath} \tag{40}$$

Apart from this a new variable is introduced to account for the mechanical effects of an electric potential difference and the ‘electromechanical’ potential difference $\Delta\Xi$ is defined as:

$$z_q F \Delta\Xi = \bar{v}_q^{gel} (p^{gel} - p^{bath}) \quad (41)$$

where $\Delta\Xi$ is:

$$\Delta\Xi = \Xi^{gel} - \Xi^{bath} \quad (42)$$

Using Eqs. (39) and (41) the condition for phase equilibrium derived previously (Eq. (38)) can now be expressed in terms of $\Delta\Psi$ and $\Delta\Xi$. Hence at constant temperature and external pressure, the condition for phase equilibrium is given by:

$$\begin{aligned} \mu_i^{bath}(T, p^{bath}, n^{bath}) &= \mu_i^{gel}(T, p^{bath}, n^{gel}) + (p^{gel} - p^{bath})_T \bar{v}_i^{gel} \\ &\quad + z_i F \{\Delta\Psi - \Delta\Xi\} \quad i = 1 \dots N; i \neq q \end{aligned} \quad (43)$$

It is important to note that it is often difficult to accurately measure p^{gel} and that of $\Delta\Psi$ and $\Delta\Xi$ cannot be measured. As a result, p^{gel} is usually calculated based on the elastic properties of the polymer gel using Eq. (19). Both $\Delta\Psi$ and $\Delta\Xi$ have to be calculated based on Eqs. (39) and (41), this is usually possible as long as appropriate expressions exist for the Gibbs energy of the fluid mixture that forms the gel phase and A^m of the polymer network.

In summary, this gel model while not the only model developed to describe the thermodynamics of polyelectrolyte gel systems, builds on the concepts developed over time by a number of different people, weaving them together into a comprehensive versatile model. It also provides a very solid framework to study equilibrium partitioning of solute molecules which is not seen in many of the other models. This model provides a straightforward means to determine the phase equilibrium of a number of different polyelectrolyte gel systems and is very useful in understanding and possible predicting the behavior of not just different polyelectrolyte gels, but also how they behave in different surroundings.

5 Characterization of Polyelectrolyte Hydrogels

Characterization of a polyelectrolyte hydrogel begins similarly to the characterization of any hydrogel. However more stringent characterization is required thereafter to account for the behavioral complexity that is introduced by the charges they contain. As alluded to in the thermodynamic examination of these systems, the charges in the system affect the swelling of these gels, the partitioning of different charged species in the system, etc. As a result more detailed characterization is required for these gels. This section will first deal with common

characterization methods that are used to help describe hydrogels in general and then focus on the special conditions and properties that are further studied in the case of polyelectrolyte hydrogels. This section will focus primarily on physical characterization which is widely applicable rather than chemical characterization that is usually specific to the particular polyelectrolyte gel being prepared.

5.1 Characterization of Hydrogel

5.1.1 Swelling Behavior of Hydrogels

Swelling is one of the key properties of hydrogels, and the swelling ratio (Q) is the most commonly used means of quantifying this effect [72–74]. The swelling ratio of a hydrogel is defined as the ratio of weight of water in the hydrogel (W_s) to the dry weight of the gel (W_d).

$$Q = W_s/W_d$$

W_s is determined by measuring the weight of the gel after it has reached equilibrium in a bath of deionized water and subtracting the dry weight of the gel from that.

In addition to this sometimes the kinetics of swelling may be measured wherein the gel is weighed at different times during its incubation in the deionized water bath. The deswelling kinetics may also be determined by transferring the swollen hydrogel after it has reached equilibrium into a deionized water bath at a temperature greater than its Lower Critical Solution Temperature (LCST) and measuring the decrease in weight of the hydrogel over time, the deswelling kinetics are studied in terms of water retention [72, 74]. The water retention of a hydrogel is defined as follows:

$$\% \text{ Water retained} = 100 * (W_t - W_d)/(W_s - W_d)$$

where W_t is the weight of the hydrogel at a given time. The LCST of a hydrogel can be determined using spectrophotometer measurements or a differential scanning calorimeter to study the behavior of the hydrogel as the temperature is varied, the LCST is determined as the temperature corresponding to the break point of the curve. The reswelling kinetics after deswelling are also sometimes measured [72], here the gel after deswelling is transferred back into a deionised bath at a temperature below its LCST and the kinetics of reswelling are measured in terms of water uptake that is given by:

$$\% \text{ Water uptake} = 100 * (W_t - W_d)/(W_s - W_d)$$

Some studies go further and study the swelling behavior at various temperatures, pressures, etc. [74, 75].

5.1.2 Mechanical Properties of Hydrogels

The bulk mechanical properties of hydrogels are usually determined next. The tensile strength and compression modulus can be determined using a tensile strength tester, here the gel is placed on top of a compression load cell and compressed between this and a parallel plate at a constant rate. By measuring the deformation of the gel at different pressures a stress-strain curve can be produced and used to determine the compression modulus [74, 76–78]. The compression modulus is the slope of the linear region of the stress-strain curve; it is analogous to the Young's modulus of tensile strength.

The Young's modulus or tensile modulus is also sometimes determined using a tensile strength tester, this presents some unique challenges as unlike most materials that are tested, gels are difficult to grip, as a result the gels need to be cut into a specific shape that allows solid supports to be glued onto either end of the gel thus enabling the machine to grip either end of the gel. For example the gel can be cut using dies into a dumbbell shape and then wooden supports can be glued onto the wide portions of the dumbbells [74].

Dynamic viscoelastic parameters such as the storage modulus and the loss modulus offer another measure of the mechanical properties of hydrogels. The storage and loss moduli represent the stored energy (elastic portion) and the heat dissipated (viscous portion) respectively of a viscoelastic solid. These are determined using a rheometer. The most commonly used set up for these measurements is the rotational rheometer wherein the sample is placed between two discs, the top disc rotates in an oscillatory manner in order to introduce a small strain oscillatory shear, while the torque exerted by the sample on the lower disc is measured. This allows a shear stress-strain relationship to be determined and thus for the moduli in turn to be found. Usually an amplitude sweep will be done to ensure that the sample is in the linear viscoelastic range [73, 75, 79, 80].

5.1.3 Pore Size Distribution and Interior Morphology

The final level of physical characterization that is sometimes done is to determine the pore size distribution and the interior morphology of the hydrogel. While there are a number of slightly varying methods to measure the pore size distribution most of them utilize the concept of size-exclusion, i.e. particles that are larger than the size of the pores are excluded.

Initial studies used mercury intrusion porosimetry, here the pressure required to force mercury into the pores is measured and then used to estimate the size of the pores [81–83]. However this method tends to be quite harsh and so a number of different methods have since been adopted. Some groups use FITC labelled

dextran molecules of varying sizes, here the entry of solute particles into the hydrogel can be easily tracked using fluorescence [72]. Other studies use various solute particles of different size and measure amount of solute lost from the bath using differential refractometry [84]. The pore size distribution can also be studied by inverse size exclusion chromatography, wherein the gel is used as a column and solute particles of different sizes are flowed through, the pore size distribution can be obtained based on the differences in retention times of the various particles [85].

Determination of the interior morphology is generally done using scanning electron microscopy [79, 81]. Here thin slices of the hydrogel are first allowed to swell in distilled water and then ethanol is gradually added. This treatment makes the gel a little more rigid and opaque. The gel block is then placed in a vacuum to dry and then coated with gold before the sample is examined in a scanning electron microscope [79]. Freeze drying of the swollen gel is also sometimes used as a means of sample preparation [81]. However it should be noted that drying of these hydrogels is likely to have an effect of the porous structure and hence the SEM images generated may not be representative of the structure *in vivo*.

5.1.4 Chemical Characterization

While a number of different techniques may be used to chemically characterize the hydrogel, a common method used is nuclear magnetic resonance, here the gel is dried and deuterized and then the NMR spectrum is used to determine the composition of the various constituent building blocks that are used to prepare the gel. [75, 80] Sometimes the molecular weight distribution of the monomers is also determined using size exclusion chromatography [80].

5.2 Special Considerations for Polyelectrolyte Hydrogels

While the overall properties studied aren't very different in the case of a polyelectrolyte hydrogel there are some added considerations that need to be made. These considerations are mostly based on the effect the surrounding bath has on the behavior of these gels. As highlighted in the previous section on the thermodynamics of polyelectrolyte hydrogels the presence of ions both in the gel and in the bath can have an effect on the swelling and equilibrium composition of these gels. As a result a lot of attention is usually given to the how these gels behave at different pH and in various electrolyte baths.

5.2.1 Effect of PH on Swelling Behavior

Different pH has different effects on the ionization of various species. As a result in the case of a polyelectrolyte gel this could alter the charges present on some of the

species which in turn could have an effect on the swelling behavior of the gel. As a result, studying the effect of pH variations is often done for polyelectrolyte gels as a means of better characterizing them [86–88]. The procedure for this is the same as the swelling studies for a simple hydrogel except that the gel is allowed to swell in a bath buffered at various pH instead of in deionized water.

5.2.2 Effect of Ionic Strength on Swelling Behavior

Another factor in these polyelectrolyte gels is the effect of ions in the bath, i.e. an electrolyte bath. This is of particular interest since most biological applications would likely entail the gel at some point being in contact with an electrolyte. Again the thermodynamic model presented previously can give some intuitive understanding of how the presence of ions can alter the behavior of these gels. Movement of ions into and out of the gel would lead to electrostatic changes such as charge shielding that could alter the swelling of the gel. Hence, another level of characterization usually done in the case of polyelectrolyte gels is to study their behavior in a variety of electrolyte solutions [86, 88]. Here too the procedure is almost identical to the swelling studies of a simple hydrogel except that the gel is made to swell in an electrolyte solution instead of deionized water.

5.2.3 Effect of Electric Field on Swelling Behavior

While not as common, some groups go as far as to look at what effect that altering the electric field across the gel has on its swelling and deswelling behavior. Here an electric field is applied across the gel and the swelling and deswelling behavior is studied as described earlier. Here too different electrolyte baths may be used [89–92]. The exact mechanism that results in this effect is still under examination. One theory is that the electric field leads to localized pH zones on either side of the gel which in turn leads to different swelling behavior in each zone.

5.2.4 Electromechanical Properties

Finally a very unusual technique that can be used to characterize polyelectrolyte gels is to study their electromechanical properties. To do this the gel is placed on top of a concentric array of platinum electrodes and then a well-defined pressure distribution is applied to the top of the gel using a spherical indenter. The potential generated due to the applied mechanical force is measured using the electrodes. Polyelectrolyte gels due to their charged species may be able to transduce mechanical forces and deformation applied on them into electrical potentials, these can be measured using this kind of a setup [93].

While for the most part the characterization of polyelectrolyte is carried out on similar lines to that of any other hydrogel due to their unique properties some extra

characterization is required to effectively describe them. While some of this characterization is simply to understand the effect different surroundings have on the gel, further characterization may focus on characterizing the electromechanical properties and electrical responsiveness of the gels.

6 Biomedical Applications of Polyelectrolyte Hydrogels

Although the polyelectrolyte hydrogels are being used in a variety of applications, they have gained much attention in the past decades because of their potential biomedical applications, such as in controlled release systems, for different types of tissue reconstitution, as supports for catalyst, and for isolation and fractionation of proteins. Many of these applications are based on the functional properties of the polyelectrolyte.

6.1 Drug Delivery

Synthetic hydrogels, with their ability to absorb water, flexibility, and biocompatibility, are ideal carriers for the development for novel pharmaceutical formulations and for the delivery of drugs, proteins, and as targeting agents for drug delivery. The concept of polyelectrolyte complex (PEC) in the design of drug delivery systems may be useful due to the advancements made during the last two decades [94]. The polyelectrolyte hydrogels respond to external pH stimuli that enable sustained drug delivery corresponding to the network structure and the nature of components. The use of polyelectrolyte hydrogels allows not only delivery of drugs, but also controlled release, for example, drugs can be delivered only when needed, may be directed to specific site, and can be delivered at specific rates required by the body. These types of polymers not only convert the active substances into a non-deleterious form which can be administered, but also have specific effect on the biodistribution, bioavailability or absorption of the active substances and hence increasingly gaining importance in modern pharmaceutical technology.

6.1.1 Oral Drug Delivery

The pH-sensitive hydrogels have been most frequently used to develop controlled release formulations for oral administration. The pH in the stomach (<3) is quite different from the neutral pH in the intestine, and such a difference is large enough to elicit pH-dependent behavior of polyelectrolyte hydrogels [95]. These hydrogels have been investigated in a number of therapeutic oral delivery systems either as

controlled release matrices or functional biomaterials for the delivery of drugs to specific sites of the body such as oral cavity, stomach, small intestine and colon.

Win et al. [96] developed PEC gel beads based on phosphorylated chitosan (PCS) for controlled release of ibuprofen in oral administration. The PCS gel beads were prepared from soluble phosphorylated chitosan by using an ionotropic gelation with counter polyanion, tripolyphosphate at pH 4. This study suggested that the PCS gel beads may be useful for controlled drug delivery system through oral administration by avoiding the drug release in the highly acidic gastric fluid region of the stomach. Chang et al. [97] developed amoxicillin-loaded pH-sensitive hydrogels composed of chitosan and poly(γ -glutamic acid) for the treatment of *Helicobacter pylori* (*H. pylori*) infection in the peptic ulcer disease. Hydrogel of chitosan and PAA containing amoxicillin and clarithromycin were also clinically evaluated for *H. pylori* eradication [98]. Clinical trial experiments indicated that the polyionic hydrogel could serve as suitable candidates for amoxicillin and clarithromycin site-specific delivery in the stomach. A 5-amino salicylic acid colon-specific delivery system is based on chitosan-Ca²⁺-alginate by spray drying and followed by ionotropic gelation/polyelectrolyte complexation [99]. The highly cooperative ionic bonds between the positively charged chitosan and negatively charged alginate, the main driven force binding of the intermolecular and intramolecular hydrogen bonds and hydrophobic forces between the drug and the polymers, increased the mechanical strength of the gels network and decreased its porosity/permeability. “In vivo,” these microspheres have been localized in the colon of Wistar male rats that were previously induced with colitis.

6.1.2 Ocular Drug Delivery

One of the main problems encountered in ophthalmic drug delivery is the rapid and extensive elimination of conventional eye drops from the eye. Only a small amount (1–6 %) actually penetrates the cornea and reaches the intra ocular tissues [100]. The administration of ophthalmic drugs in hydrogels has been shown to increase the contact time of the drugs with cornea, thereby increasing ocular bioavailability.

Cohen et al. [101] reported on the use of alginate as in situ forming hydrogel for the controlled release of pilocarpine in the eye. The extent of alginate gelation and consequently the release of pilocarpine were found to be dependent upon the percentage of glucuronic acid residues in the polymer backbone. Alginates with a G content of more than 65 % instantaneously formed hydrogels upon addition of lacrimal fluid, whereas alginates with a low G content relatively slowly formed only weak hydrogels. A diffusion-controlled release of pilocarpine from alginate gels for 24 h was observed. Additionally, a prolonged pharmacodynamic effect was obtained as shown by an intra-ocular pressure reduction for 10 h, when compared to 3 h for pilocarpine nitrate solution. Another in situ thermosensitive hydrogel composed of chitosan and poly (*N*-isopropylacrylamide) was prepared for ocular delivery of timolol maleate. The bio-availability, efficacy, and

compliance of eye drugs were improved [102]. To increase its ocular bioavailability, Genta et al. [103] prepared bioadhesive chitosan microspheres for ophthalmic administration of acyclovir. In vivo ocular studies on rabbits indicated a high concentration of acyclovir for an extended period of time.

6.1.3 Rectal Drug Delivery

This route has been used to deliver many types of drugs for treatment of diseases associated with the rectum. There are however, some drawbacks associated with rectal delivery. For example, due to discomfort arising from given dosage forms, there is substantial variability in patient's acceptance of treatment. Also, if drugs diffusing out of the suppositories are delivered in an uncontrolled manner, they are unable to be retained at a specific position in the rectum, and tend to migrate upwards to the colon. This leads to variation of availability of drugs, especially those that undergo extensive first-pass elimination. Hydrogels offer a way in which to overcome these limitations, provided that the hydrogels show bioadhesive properties. Considering the advantageous for the rectal administration of non-steroidal anti-inflammatory drugs, the diclofenac-sodium chitosan microspheres were incorporated into hydrogels containing hydroxypropyl methylcellulose and carbopol 934 for rectal administration [104]. The viscosity of rectal hydrogels influences the drug release and distribution of hydrogels in the distal portion of the large intestine.

6.1.4 Protein Drug Delivery

Advances in recombinant protein technology have identified several protein and peptide therapeutics for disease treatment. However, the problem which plagued researchers was how to effectively deliver these biomolecules. Due to their large molecular weight, and three dimensional structures, the most commonly used route for drug administration is by intravenous or subcutaneous injection. Unfortunately proteins and peptides are prone to proteolytic degradation, thus they experience short plasma circulation times and rapid renal clearance, leading to multiple daily injections or increased dosage in order to maintain the required drug therapeutic levels. Multiple injections are difficult for the patient, while high doses might be toxic, and induce serious immune response. PEC hydrogels provide relatively mild network fabrication technique and drug encapsulation conditions, making them the ideal material for use in protein drug delivery.

Charged microspheres were prepared by copolymerization of either methacrylic acid or *N,N*-dimethylamino ethyl methacrylate with hydroxyethyl methacrylate-derivatized dextran [105]. Protein mobility in the hydrogels and protein release from the matrices were investigated [106]. The gels could be loaded with proteins by simply mixing the microsphere dispersions with a protein solution, avoiding the use of potentially damaging factors (organic solvents, extreme pH, temperature,

etc.). At pH 7, a diffusion-controlled release of the proteins, in accordance to their hydrodynamic radii, was observed with 50 % of the initial amount of lysozyme, BSA and IgG released in respectively 4, 6 and 13 days. Lysozyme was quantitatively released in about 25 days, with full preservation of its enzymatic activity, confirming the protein-friendly preparation technology.

In additional, chitosan–alginate [107] and chitosan–konjac glucomannan [108, 109] PECs also have the advantage of not destroying the drug structure loaded, and are especially suitable for the encapsulation of biological products with low stability, such as peptides, proteins, vaccines, and so on. The chitosan–alginate PECs are also an effective controlled release carrier for nerve growth factor [110]. Polyelectrolyte complex beads made from polysaccharide mixtures show protein release behavior that is highly dependent on both complex pH and stoichiometry [109, 111]. The release of protein from PEC vesicles is dependent on the ionic strength, i.e. high ionic strengths—on the order of physiological salt concentrations—trigger near instantaneous disassembly of the PEC micelles, resulting in the release of proteins due to disruption of attractive electrostatic forces [108, 112]. Conversely when salt concentrations are decreased, the release of lysozyme becomes even slower due to increased attractive interactions [113]. Alginate-based insulin nanoparticles have been shown to be capable of releasing proteins at intestinal pH [114]. Complexes of alginate and chemically modified carboxymethyl chitosan were loaded with both BSA and lysozyme, with efficient release observed at elevated/physiological temperature, and desirable swelling behavior and subsequent release of proteins occur at low pH [115]. Similarly, PEC nanoparticles assembled from water soluble chitosan and poly(aspartic acid) have been used for controlled release of BSA at physiological pH and at two acidic pHs, showing an initial burst followed by gradual protein release over 24 h [116].

6.2 Tissue Engineering

Polyelectrolyte hydrogels are attractive as tissue engineering matrices as these hydrophilic networks are capable of absorbing great amounts of water while maintaining structural integrity [117]. They also offer the possibility of fabrication in a variety of different shapes, e.g., rods, disks, films, microparticles, depending on the intended applications and sites of administration, and can easily be washed, following production, to remove any undesired molecules such as unreacted initiators, monomers, etc. Importantly, cells and growth factors can be incorporated and suspended in the gels precursors prior to gelation, enabling homogenous cell seeding and easy implantation [118].

The concept of “cell encapsulation” was first proposed by Chang [119] in the early 1950s. A primary requirement of microcapsule-surrounding membranes are that they are amenable to the diffusion of nutrients (e.g., glucose) and molecules such as oxygen and growth factors essential for cell survival [120]. Twenty years later, Lim and Sun presented the first implantable alginate-poly(L-lysine) PEC

microcapsules harboring rat islet cells, that naturally secreted insulin, for the treatment of diabetes [121]. In the three decades since then, the permselective capsule environment has been shown to be capable of supporting cellular metabolism, proliferation, differentiation and cellular morphogenesis and micro-encapsulation has become a preferred system for cell transplantation and for forming functional new tissues. The encapsulation of cells instead of small molecule or even protein or nucleic acid-based therapeutic products allows the delivery of the product for a longer period of time because of the ability of cells to release the products continuously over time periods of days, weeks, or in some cases even months. Moreover, cell encapsulation allows the use of cells from a variety of sources such as primary or stem cells, or genetically engineered cells which can be modified to express any desired protein *in vivo* without the modification of the host's genome [122].

Rat osteoblasts were cultured on PEC composed of phosphated and carboxymethylated chitin as a polyanion, and chitosan (CS) as a polycation, and adhere to them without the aid of fibronectin [123]. CS-PECs containing carboxymethyl groups as anionic sites cause the human periodontal ligament fibroblast (HPLF) to aggregate and promote differentiation because the carboxymethyl groups offer similar conditions as *in vivo* to HPLF. On the contrary, PECs containing sulfate groups cause HPLF to form a spreading morphology and proliferate well [124]. A higher adhesion number of cells on the chitosan/chondroitin sulfate surface are better than that on pure chitosan films [125]. This is explained by taking into account that complex formation removes the individual charges of the polymers and the chemical structure of chitosan, which is necessary for cell recognition changes.

The cell cycle analysis is carried out to assess the proliferation of L929 rat fibroblasts on chitosan/gelatin PEC films in comparison with that on chitosan films. It is found that blending chitosan and gelatin can induce cells to enter the cell cycle and to begin to proliferate. Chitosan/gelatin PECs can promote cell proliferation and inhibit cell apoptosis. This effect may be attributed to the decline in positive charge density of chitosan that may benefit cell migration [126]. A chitosan/gelatin PEC scaffold is fabricated by freezing and lyophilizing methods. Autologous chondrocytes from pigs' auricular cartilage are seeded onto the scaffold, and elastic cartilages have been successfully engineered at porcine abdomen subcutaneous tissue [127]. Moreover, chondrocyte proliferation is more distinct in chitosan–gelatin–DNA PEC scaffolds [128]. These studies indicate that the chitosan/gelatin PECs can be used as a suitable scaffold for tissue engineering.

Chitosan–alginate PECs show good compatibility *in vitro* with the mouse/human fibroblasts, osteoblasts, and chondrocytes [129]. The chondrocytes on chitosan tend to form a monolayer, a possible marker of chondrocyte dedifferentiation and fibroblastic phenotype [130]. In contrast, the chondrocytes on chitosan–alginate PECs materials form much larger cell clusters. And cell proliferation on chitosan–alginate scaffolds is found to be faster than that on a pure chitosan scaffold [131]. Kratz et al. [132] found that the chitosan/heparin PEC can stimulate wound healing in human skin. Moreover, the chitosan/heparin complex

networks are supposed to exist as a network to create an appropriate environment for the regeneration of hepatocytes, as well as to induce growth angiogenesis for the regeneration of livers. The collagen–chitosan–heparin [133] and alginate–galactosylated chitosan/heparin [134] scaffolds, which are similar to the liver extracellular matrix, play important roles in the regulation of the morphological appearance of hepatocytes.

6.3 Enzyme Immobilization

Enzymes or ‘biocatalysts’ are remarkable discovery in the field of bioprocess technology. Biocatalysis has been widely accepted in diverse sectors owing to their ease of production, substrate specificity and green chemistry. However, for large extent commercialization of these bio-derived catalysts, their reusability factor becomes mandatory, failing which they would no longer be economic. Maintenance of their structural stability during any biochemical reaction is highly challenging. Consequently, immobilized enzymes with functional efficiency and enhanced reproducibility are used as alternatives in spite of their expensiveness. Immobilization of enzymes on charged supports via electrostatic interactions constitutes a common and not expensive approach for preparing industrial biocatalyst [135]. This immobilization method also allows the reuse of the matrix [136].

Different approaches have been utilized to immobilize enzymes on modified electrode surface, and layer-by-layer adsorption (LBL) technique based on electrostatic force between polyelectrolytes and proteins has received great attention and interests. LBL has been introduced to fabricate multilayer films, and it represents a promising and environmental preparation method because no complicated instruments or chemical reactions are involved, and ultrathin multicomponent architecture can be constructed only by alternate adsorption in cationic and anionic polyelectrolytes. A pair of biomacromolecules, positively charged chitosan and negatively charged hyaluronic acid was successfully assembled onto the surface of a poly(ethylene terephthalate) microfluidic chip using layer-by-layer deposition for the formation of a microstructured and biocompatible scaffold to immobilize trypsin. This simple technique may offer a potential solution for low-level protein analysis [137]. Leblanc shows a way of immobilizing organophosphorus hydrolase using several bilayers of chitosan and negatively charged poly (thiophene-3-acetic acid) for detecting the presence of paraoxon. This five-bilayer macromolecular structure compared with the solid substrate rendered stability to the enzyme by giving functional integrity in addition to the ability to react with paraoxon solutions [138].

Except the LBL deposition for the enzyme immobilization, lactose has been hydrolyzed using covalently immobilized β -galactosidase on thermally stable carrageenan coated with chitosan. The immobilized enzyme showed lactose conversion of 70 % at 7 h compared to 87 % for the free enzyme. However, the

reusability of the immobilized enzyme for tens of times reduces the enzyme cost tremendously [139]. Aranaz et al. [140] used alginate–chitosan polyelectrolyte capsules for coimmobilization of enzymes to reproduce a multistep enzymatic route for the production of d-amino acids. Encapsulation of a crude cell extract from *Agrobacterium radiobacter* containing d-hydantoinase and d-carbamoylase activities into the PECs was accomplished with negligible leakage from the formed capsules. The biocatalysts were able to hydrolyze L-d-hydroxyphenylhydantoin into p-hydroxyphenylglycine with yields ranging from 30 to 80 %. Taqieddin and Amiji [141] described the development of a core–shell microcapsule technology for enzyme immobilization. The enzyme is localized and protected in the core matrix, while the shell can regulate the entry and exit of the substrate and product, respectively. A model enzyme, β -galactosidase, was immobilized in either calcium alginate or barium alginate core surrounded by a perm-selective chitosan shell. Sankalia et al. [142] explored, using response surface methodology, the main and interaction effects of some process variables on the preparation of a reversed chitosan–alginate PEC with entrapped α -amylase for stability improvement. Yapar et al. [143] reported that cholesterol oxidase was immobilized in the conducting network via complexation of chitosan with alginic acid. The polymer electrolyte matrix protects entrapped cholesterol oxidase; hence the enzyme shows higher stability over broader temperature and pH ranges.

6.4 Protein Separations

Polyelectrolytes Complexes or nanoparticles can be used to recover proteins from their mixtures by selective phase separation (precipitation or coacervation) [144]. The ability of polyelectrolytes to remove proteins from solutions represents tremendous potential in the area of protein fractionation. Protein separation may occur at two steps in the protein complexation/recovery process: at the point of complex formation, or at the point of complex redissolution. The use of polyelectrolyte-precipitation to separate proteins offers several advantages over other protein fractionation techniques. The recovery of proteins through the formation of insoluble complexes with polyelectrolytes appears to be a non-denaturing process. Furthermore, compared to other methods for protein separation, e.g. chromatography, selective precipitation offers great economy with regard to materials and process, and, furthermore, is virtually unlimited in scale. Thus, an elucidation of the principles governing protein selectivity in polyelectrolyte separation would be of considerable applied significance [145]. De Vasconcelos et al. [146] showed that assembling nanoparticles from binary mixtures of polycation chitosan and poly(methacrylic acid) (PMMA) will result in the formation of negative PMAA coated particles. Subsequent interactions with BSA first occur near pI where a positive protein domain interacts with the PMAA coating and a negative charge patch interacts with the positive chitosan core [146]. Hartig examined the effects of the MW and stoichiometry of the polymers comprising binary PEC complexes

[147]. The results suggest that the chain lengths and charge densities of the polycationic and polyanionic components must be closely matched to allow for the formation of soluble complexes that can persist and interact with proteins over a wide pH range. Polyelectrolyte complexes of poly(acrylate) and poly(ethyleneimine) also showed good separation properties from complex protein mixtures. When attaching a ligand, the triazine dye Cibacron Blue to poly (ethyleneimine), an affinity PEC was formed capable of binding lactate dehydrogenase at high yields of 85 % and a purification factor of 11-fold. The subsequent harvesting of the affinity complex was done by adding, e.g., phosphate ions which induced quantitative precipitation. Furthermore, it was observed that the precipitate consisted of compact [148].

7 Conclusions

This chapter gives a lot of information on polyelectrolyte hydrogels that obtained by mixing aqueous solutions of two polymers carrying opposite charges. There are three different types of polyelectrolyte hydrogels obtained according to the origins, synthetic, natural, natural/synthetic hybrid polyelectrolyte hydrogels. The formation of these hydrogels is influenced not only by chemical properties like stereochemical fitting, their molecular weight, charge densities, etc. but also by secondary experimental conditions like concentration of polyelectrolytes prior to mixing, their mixing ratio, ionic strength of the solution, mixing order, etc. The thermodynamic model and characterizations of polyelectrolyte hydrogels provide a better understanding to the behavioral complexity of these hydrogels, and thus open the mind for better designing their structures for specific applications. The utilization of expensive and toxic organic solvents in the gelation process has been drastically reduced due to evolution of ionotropic gelation and polyelectrolyte complexation techniques. Combining with the fast progress on molecular biology, these have inspired researchers to design of polyelectrolyte hydrogels with multifunctional properties on demand for biomedical applications. The polyelectrolyte hydrogels have great utility in developing controlled release formulations of almost all types of bioactive molecules, and ensure the constant release over the desired period by retaining their structural integrity. Artificial extracellular matrices combining polyelectrolyte hydrogel scaffolds, cells and growth factors hold great promise for cell transplantation and tissue regeneration both in vitro and in vivo, and pave the way for treatment of diseases and replacement of organs. In addition, the self-assembled or self-organized polyelectrolyte hydrogels as well as those based on more biocompatible and environment friendly natural polymers are expected more prevalently in the future.

References

1. Osada, Y., Gong, J.P.: *Adv. Mater.* **10**, 827 (1998)
2. Nisato, G., Munch, J.P., Candau, S.J.: *Langmuir* **15**, 4236 (1999)
3. Pafiti, K.S., Philippou, Z., Loizou, E., Porcar, L., Patrickios, C.S.: *Macromolecules* **44**, 5352 (2011)
4. Takeoka, Y., Berker, A.N., Du, R., Enoki, T., Grosberg, A., Kardar, M., Oya, T., Tanaka, K., Wang, G.Q., Yu, X.H., Tanaka, T.: *Phys. Rev. Lett.* **82**, 4863 (1999)
5. Firestone, B.A., Siegel, R.A.: *J. Appl. Polym. Sci.* **43**, 901 (1991)
6. Tanaka, T., Nishio, I., Sun, S.T., Uenonishio, S.: *Science* **218**, 467 (1982)
7. Mohammadi, A.: *Phys. Fluids* , **25** (2013)
8. Ito, Y., Casolaro, M., Kono, K., Imanishi, Y.: *J. Controlled Release* **10**, 195 (1989)
9. Miyata, T., Uragami, T., Nakamae, K.: *Adv. Drug Deliv. Rev.* **54**, 79 (2002)
10. Beebe, D.J., Moore, J.S., Bauer, J.M., Yu, Q., Liu, R.H., Devadoss, C., Jo, B.H.: *Nature* **404**, 588 (2000)
11. Richter, A., Paschew, G., Klatt, S., Lienig, J., Arndt, K.F., Adler, H.J.P.: *Sensors* **8**, 561 (2008)
12. Nagase, K., Kobayashi, J., Okano, T.: *J. R. Soc. Interface* **6**, S293 (2009)
13. Seliktar, D.: *Science* **336**, 1124 (2012)
14. Stuart, M.A.C., Huck, W.T.S., Genzer, J., Muller, M., Ober, C., Stamm, M., Sukhorukov, G.B., Szleifer, I., Tsukruk, V.V., Urban, M., Winnik, F., Zauscher, S., Luzinov, I., Minko, S.: *Nat. Mater.* **9**, 101 (2010)
15. Liu, L., Wang, W., Ju, X.J., Xie, R., Chu, L.Y.: *Soft Matter* **6**, 3759 (2010)
16. Sun, T.L., Kurokawa, T., Kuroda, S., Bin Ihsan, A., Akasaki, T., Sato, K., Haque, M.A., Nakajima, T., Gong, J.P.: *Nat. Mater.* **12**, 932 (2013)
17. Torres-Lugo, M., Peppas, N.A.: *Macromolecules* **32**, 6646 (1999)
18. Kim, B., Peppas, N.A.: *Biomed. Microdevices* **5**, 333 (2003)
19. Sawahata, K., Hara, M., Yasunaga, H., Osada, Y.: *J. Controlled Release* **14**, 253 (1990)
20. Kost, J., Horbett, T.A., Ratner, B.D., Singh, M.: *J. Biomed. Mater. Res.* **19**, 1117 (1985)
21. Ishihara, K., Kobayashi, M., Ishimaru, N., Shinohara, I.: *Polym. J.* **16**, 625 (1984)
22. Ramkisson-Ganorkar, C., Baudys, M., Kim, S.W.: *J. Biomater. Sci. Polym. Ed.* **11**, 45 (2000)
23. Markland, P., Zhang, Y.H., Amidon, G.L., Yang, V.C.: *J. Biomed. Mater. Res.* **47**, 595 (1999)
24. Hynes, S.R., McGregor, L.M., Rauch, M.F., Lavik, E.B.: *J. Biomater. Sci. Polym. Ed.* **2007**, 18 (1017)
25. Chiu, H.C., Hsiue, G.H., Lee, Y.P., Huang, L.W.: *J. Biomater. Sci. Polym. Ed.* **10**, 591 (1999)
26. Leach, J.B., Bivens, K.A., Patrick, C.W., Schmidt, C.E.: *Biotechnol. Bioeng.* **82**, 578 (2003)
27. Ramamurthi, A., Vesely, I.: *J. Biomed. Mater. Res., Part A* **66A**, 317 (2003)
28. Drury, J.L., Mooney, D.J.: *Biomaterials* **24**, 4337 (2003)
29. Brandl, F., Sommer, F., Goepferich, A.: *Biomaterials* **28**, 134 (2007)
30. Qi, H., Ghodousi, M., Du, Y., Grun, C., Bae, H., Yin, P., Khademhosseini, A.: *Nat. Commun.* **4**(2013)
31. Jin, R., Teixeira, L.S.M., Krouwels, A., Dijkstra, P.J., van Blitterswijk, C.A., Karperien, M., Feijen, J.: *Acta Biomater.* **2010**, 6 (1968)
32. Li, F., Griffith, M., Li, Z., Tanodekaew, S., Sheardown, H., Hakim, M., Carlsson, D.J.: *Biomaterials* **26**, 3093 (2005)
33. Wang, C., Stewart, R.J., Kopecek, J.: *Nature* **397**, 417 (1999)
34. Chen, J.P., Cheng, T.H.: *Macromol. Biosci.* **2006**, 6 (1026)
35. Tan, H.P., Ramirez, C.M., Miljkovic, N., Li, H., Rubin, J.P., Marra, K.G.: *Biomaterials* **30**, 6844 (2009)

36. Kim, S.J., Yoon, S.G., Kim, I.Y., Lee, Y.H., An, K.H., Kim, N.G., Hong, C.U.: Smart Sensors, Actuators, and Mems, Pts 1 and 2, **5116**, 756 (2003)
37. Oliveira, M.A.M., Boyer, C., Nele, M., Pinto, J.C., Zetterlund, P.B., Davis, T.P.: Macromolecules **44**, 7167 (2011)
38. Jabbari, E., Nozari, S.: Iran. Polym. J. **8**, 263 (1999)
39. Gehrke, S.H., Uhden, L.H., McBride, J.F.: J. Controlled Release **55**, 21 (1998)
40. Coviello, T., Grassi, M., Rambone, G., Santucci, E., Carafa, M., Murtas, E., Riccieri, F.M., Alhaise, F.: J Control Release **60**, 367 (1999)
41. Stevens, K.R., Einerson, N.J., Burmania, J.A., Kao, W.Y.J.: J. Biomater. Sci. Polym. Ed. **13**, 1353 (2002)
42. Mirzaei, B.E., Ramazani, S.A.A., Shafiee, M., Danaei, M.: Int. J. Polym. Mater. Polym. Biomaterials **62**, 605 (2013)
43. Wu, D.C., Loh, X.J., Wu, Y.L., Lay, C.L., Liu, Y.: J. Am. Chem. Soc. **132**, 15140 (2010)
44. Cunanan, C.M., Graham, R.S., Manesis, N.J., Pettit, D.K., Deacon, J., Knight, P.M.: Surf. Modif. Polym. Biomaterials **129** (1997)
45. Ruiz, J., Mantecon, A., Cadiz, V.: Polymer **42**, 6347 (2001)
46. Liu, Y., Vrana, N.E., Cahill, P.A., McGuinness, G.B.: J. Biomed. Mater. Res. B Appl. Biomater. **90B**, 492 (2009)
47. Hennink, W.E., van Nostrum, C.F.: Adv. Drug Deliv. Rev. **54**, 13 (2002)
48. Nge, T.T., Yamaguchi, M., Hori, N., Takemura, A., Ono, H.: J. Appl. Polym. Sci. **2002**, 83 (1025)
49. de la Torre, P.M., Torrado, S., Torrado, S.: Biomaterials **24**, 1459 (2003)
50. Decher, G., Hong, J.D., Schmitt, J.: Thin Solid Films **210**, 831 (1992)
51. Decher, G.: Science **277**, 1232 (1997)
52. Li, Z.Q., Guan, J.J.: Polymers **3**, 740 (2011)
53. Shu, X.Z., Zhu, K.J.: Int. J. Pharm. **233**, 217 (2002)
54. Ko, J.A., Park, H.J., Hwang, S.J., Park, J.B., Lee, J.S.: Int. J. Pharm. **249**, 165 (2002)
55. Zhang, H.B., Zhang, F., Wu, J.: React. Funct. Polym. **73**, 923 (2013)
56. Eagland, D., Crowther, N.J., Butler, C.J.: Eur. Polymer J. **30**, 767 (1994)
57. Lowman, A.M., Peppas, N.A.: Macromolecules **30**, 4959 (1997)
58. Kopecek, J., Yang, J.: Acta Biomater. **5**, 805 (2009)
59. Kumar, P., Pillay, V., Modi, G., Choonara, Y.E., du Toit, L.C., Naidoo, D.: Recent Pat. Drug Deliv. Formul. **5**, 24 (2011)
60. Rajagopal, K., Schneider, J.P.: Curr. Opin. Struct. Biol. **14**, 480 (2004)
61. Wei, Y., Cui, F., Tian, W.: Front. Mater. Sci. China **3**, 353 (2009)
62. Cui, Y., Li, Y.H., Duan, Q., Kakuchi, T.: Appl. Biochem. Biotechnol. **169**, 239 (2013)
63. Ekici, S., Saraydin, D.: Polym. Int. **56**, 1371 (2007)
64. Nishi, S., Kotaka, T.: Macromolecules **18**, 1519 (1985)
65. Touhsaent, R.E., Thomas, D.A., Sperling, L.H.: J. Polym. Sci., Part C: Polym. Symp. **175** (1974)
66. Kim, I.Y., Yoo, M.K., Kim, B.C., Kim, S.K., Lee, H.C., Cho, C.S.: Int. J. Biol. Macromol. **38**, 51 (2006)
67. Maurer, G., Prausnitz, J.M.: Fluid Phase Equilib. **115**, 113 (1996)
68. Haynes, C.A., Benitez, F.J., Blanch, H.W., Prausnitz, J.M.: AIChE J. **39**, 1539 (1993)
69. Haynes, C.A., Blanch, H.W., Prausnitz, J.M.: Fluid Phase Equilib. **53**, 463 (1989)
70. Großmann, C., Maurer, G.: Fluid Phase Equilib. **106**, 17 (1995)
71. King, R.S., Blanch, H.W., Prausnitz, J.M.: AIChE J. **34**, 1585 (1988)
72. Wu, X.S., Hoffman, A.S., Yager, P.: J. Polym. Sci., Part A: Polym. Chem. **30**, 2121 (1992)
73. Lutolf, M.P., Hubbell, J.A.: Biomacromolecules **4**, 713 (2003)
74. Zhang, X.-Z., Wu, D.-Q., Chu, C.-C.: Biomaterials **25**, 3793 (2004)
75. Stile, R.A., Burghardt, W.R., Healy, K.E.: Macromolecules **32**, 7370 (1999)
76. Zhang, Y., Chu, C.-C.: J. Mater. Sci. Mater. Med. **13**, 773 (2002)
77. Sayil, C., Okay, O.: Polymer **42**, 7639 (2001)
78. Okay, O., Durmaz, S.: Polymer **43**, 1215 (2002)

79. Fumio, U., Hiroshi, Y., Kumiko, N., Sachihiko, N., Kenji, S., Yasunori, M.: *Int. J. Pharm.* **58**, 135 (1990)
80. Stavrouli, N., Aubry, T., Tsitsilianis, C.: *Polymer* **49**, 1249 (2008)
81. Kim, S.H., Chu, C.C.: *J. Biomed. Mater. Res.* **53**, 258 (2000)
82. Gemeinhart, R.A., Chen, J., Park, H., Park, K.: *J. Biomater. Sci. Polym. Ed.* **11**, 1371 (2000)
83. Maia, J., Ferreira, L., Carvalho, R., Ramos, M.A., Gil, M.H.: *Polymer* **46**, 9604 (2005)
84. Kuga, S.: *J. Chromatogr. A* **206**, 449 (1981)
85. DePhillips, P., Lenhoff, A.M.: *J. Chromatogr. A* **883**, 39 (2000)
86. Gonzales, D., Fan, K., Sevoian, M.: *J. Polym. Sci., Part A: Polym. Chem.* **1996**, 34 (2019)
87. Shimokuri, T., Kaneko, T., Akashi, M.: *J. Polym. Sci., Part A: Polym. Chem.* **42**, 4492 (2004)
88. Yao, B., Yang, C., Zhang, K., Ni, C., Song, H., Ni, Z., Chen, M.: *Mater Sci Poland* **27**, 319 (2009)
89. Grimshaw, P.E., Nussbaum, J.H., Grodzinsky, A.J., Yarmush, M.L.: *J. Chem. Phys.* **93**, 4462 (1990)
90. Kim, S.Y., Shin, H.S., Lee, Y.M., Jeong, C.N.: *J. Appl. Polym. Sci.* **73**, 1675 (1999)
91. Segalman, D.J., Witkowski, W.R., Adolf, D.B., Shahinpoor, M.: *Smart Mater. Struct.* **1**, 95 (1992)
92. Tanaka, T., Nishio, I., Sun, S.-T., Ueno-Nishio, S.: *Science* **218**, 467 (1982)
93. Prudnikova, K., Utz, M.: Characterization of electromechanical transduction in polyelectrolyte gels for mechanical sensor applications. In *MRS Proceedings*, 1 edn., Cambridge University Press, p. 1006/
94. Shojaei, A.H.: *J. Pharm. Pharm. Sci.: Publ Can Soc Pharm. Sci. (Societe canadienne des sciences pharmaceutiques)* **1**, 15 (1998)
95. Qiu, Y., Park, K.: *Adv. Drug Deliv. Rev.* **64**, 49 (2012)
96. Win, P.P., Shin-ya, Y., Hong, K.J., Kajuchi, T.: *Carbohydr. Polym.* **53**, 305 (2003)
97. Chang, C.-H., Lin, Y.-H., Yeh, C.-L., Chen, Y.-C., Chiou, S.-F., Hsu, Y.-M., Chen, Y.-S., Wang, C.-C.: *Biomacromolecules* **11**, 133 (2010)
98. Gisbert, J.P., Torrado, G., Torrado, S., Olivares, D., Pajares, J.M.: *J. Clin. Gastroenterol.* **40**, 618 (2006)
99. Mladenovska, K., Raicki, R.S., Janevik, E.I., Ristoski, T., Pavlova, M.J., Kavrakovski, Z., Dodov, M.G., Goracinova, K.: *Int. J. Pharm.* **342**, 124 (2007)
100. Wood, R.: *Int. J. Pharm.* **23**, 175 (1985)
101. Cohen, S., Lobel, E., Trevgoda, A., Peled, Y.: *J. Controlled Release* **44**, 201 (1997)
102. Cao, Y., Zhang, C., Shen, W., Cheng, Z., Yu, L., Ping, Q.: *J. Controlled Release* **120**, 186 (2007)
103. Genta, I., Conti, B., Perugini, P., Pavanetto, F., Spadaro, A., Puglisi, G.: *J. Pharm. Pharmacol.* **49**, 737 (1997)
104. El-Leithy, E.S., Shaker, D.S., Ghorab, M.K., Abdel-Rashid, R.S.: *Aaps Pharmscitech* **11**, 1695 (2010)
105. Van Tomme, S.R., van Steenbergen, M.J., De Smedt, S.C., van Nostrum, C.F., Hennink, W.E.: *Biomaterials* **26**, 2129 (2005)
106. Van Tomme, S.R., De Geest, B.G., Braeckmans, K., De Smedt, S.C., Siepmann, F., Siepmann, J., van Nostrum, C.F., Hennink, W.E.: *J. Controlled Release* **110**, 67 (2005)
107. Li, S., Wang, X.-T., Zhang, X.-B., Yang, R.-J., Zhang, H.-Z., Zhu, L.-Z., Hou, X.-P.: *J. Controlled Release* **84**, 87 (2002)
108. Du, J., Sun, R., Zhang, S., Zhang, L.-F., Xiong, C.-D., Peng, Y.-X.: *Biopolymers* **78**, 1 (2005)
109. Du, J., Zhang, S., Sun, R., Zhang, L.F., Xiong, C.D., Peng, Y.X.: *J. Biomed. Mater. Res. B Appl. Biomater.* **72**, 299 (2005)
110. Kim, S.J., Lee, K.J., Kim, S.I.: *J. Appl. Polym. Sci.* **2004**, 93 (1097)
111. Shi, X., Du, Y., Sun, L., Zhang, B., Dou, A.: *J. Appl. Polym. Sci.* **100**, 4614 (2006)
112. Lindhoud, S., de Vries, R., Schweins, R., Stuart Cohen, M.A., Norde, W.: *Soft Matter* **5**, 242 (2009)

113. Johansson, C., Hansson, P., Malmsten, M.: *J. Colloid Interface Sci.* **316**, 350 (2007)
114. Sarmento, B., Ribeiro, A.J., Veiga, F., Ferreira, D.C., Neufeld, R.J.: *J. Nanosci. Nanotechnol.* **7**, 2833 (2007)
115. El-Sherbiny, I.M.: *Carbohydr. Polym.* **80**, 1125 (2010)
116. Shu, S., Zhang, X., Teng, D., Wang, Z., Li, C.: *Carbohydr. Res.* **344**, 1197 (2009)
117. Peppas, N.: *Eur. J. Pharm. Biopharm.* **50**, 27 (2000)
118. Kim, J., Kim, I.S., Cho, T.H., Lee, K.B., Hwang, S.J., Tae, G., Noh, I., Lee, S.H., Park, Y., Sun, K.: *Biomaterials* **2007**, 28 (1830)
119. Chang, T.M.S.: *Science* **146**, 524 (1964)
120. Uludag, H., De Vos, P., Tresco, P.A.: *Adv. Drug Deliv. Rev.* **42**, 29 (2000)
121. Lim, F., Sun, A.M.: *Science* **210**, 908 (1980)
122. Hernandez, R.M., Orive, G., Murua, A., Pedraz, J.L.: *Adv. Drug Deliv. Rev.* **62**, 711 (2010)
123. Hamano, T., Chiba, D., Nakatsuka, K., Nagahata, M., Teramoto, A., Kondo, Y., Hachimori, A., Abe, K.: *Polym. Adv. Technol.* **13**, 46 (2002)
124. Denuziere, A., Ferrier, D., Damour, O., Domard, A.: *Biomaterials* **19**, 1275 (1998)
125. Peniche, C., Fernández, M., Rodríguez, G., Parra, J., Jimenez, J., Bravo, A.L., Gómez, D., San Román, J.: *J. Mater. Sci. Mater. Med.* **18**, 1719 (2007)
126. Mao, J.S., Cui, Y.L., Wang, X.H., Sun, Y., Yin, Y.J., Zhao, H.M., De Yao, K.: *Biomaterials* **25**, 3973 (2004)
127. Xia, W., Liu, W., Cui, L., Liu, Y., Zhong, W., Liu, D., Wu, J., Chua, K., Cao, Y.: *J. Biomed. Mater. Res.* **71B**, 373 (2004)
128. Guo, T., Zhao, J., Chang, J., Ding, Z., Hong, H., Chen, J., Zhang, J.: *Biomaterials* **2006**, 27 (1095)
129. Yan, X.-L., Khor, E., Lim, L.-Y.: *J. Biomed. Mater. Res.* **58**, 358 (2001)
130. Nettles, D.L., Elder, S.H., Gilbert, J.A.: *Tissue Eng.* **2002**, 8 (1009)
131. Li, Z., Zhang, M.: *J. Biomed. Mater. Res. Part A* **75A**, 485 (2005)
132. Kratz, G., Arnander, C., Swedenborg, J., Back, M., Falk, C., Gouda, I., Larm, O.: *Scand. J. Plast. Reconstr. Surg. Hand Surg.* **31**, 119 (1997)
133. Wang, X.H., Yan, Y.N., Lin, F., Xiong, Z., Wu, R.D., Zhang, R.J., Lu, Q.P.: *J. Biomater. Sci. Polym. Ed.* **2005**, 16 (1063)
134. Seo, S.J., Choi, Y.J., Akaike, T., Higuchi, A., Cho, C.S.: *Tissue Eng.* **12**, 33 (2006)
135. Villalonga, R., Fernández, M., Fragoso, A., Cao, R., Mariniello, L., Porta, R.: *Biotechnol. Appl. Biochem.* **38**, 53 (2003)
136. Gómez, L., Ramírez, H.L., Neira-Carrillo, A., Villalonga, R.: *Bioprocess Biosyst. Eng.* **28**, 387 (2006)
137. Liu, Y., Lu, H., Zhong, W., Song, P., Kong, J., Yang, P., Girault, H.H., Liu, B.: *Anal. Chem.* **78**, 801 (2006)
138. Constantine, C.A., Mello, S.V., Dupont, A., Cao, X., Santos, D., Oliveira, O.N., Strixino, F.T., Pereira, E.C., Cheng, T.-C., Defrank, J.J., Leblanc, R.M.: *J. Am. Chem. Soc.* **2003**, 125 (1805)
139. Elnashar, M.M.M., Yassin, M.A.: *Appl. Biochem. Biotechnol.* **159**, 426 (2008)
140. Aranaz, I., Acosta, N., Heras, A.: *J. Mol. Catal. B Enzym.* **58**, 54 (2009)
141. Taqieddin, E., Amiji, M.: *Biomaterials* **2004**, 25 (1937)
142. Sankalia, M.G., Mashru, R.C., Sankalia, J.M., Sutariya, V.B.: *Eur. J. Pharm. Biopharm.* **65**, 215 (2007)
143. Yapar, E., Kayahan, S.K., Bozkurt, A., Toppare, L.: *Carbohydr. Polym.* **76**, 430 (2009)
144. Izumrudov, V.A., Galaev, I., Mattiasson, B.: *Bioseparation* **7**, 207 (1998)
145. Kayitmazerb, Basak: D.S.A., Minsky, B.B., Dubina, P.L., Xu, Y. *Soft Matter* **9**, 2553 (2013)
146. de Vasconcelos, C.L., Bezerril, P.M., Dantas, T.N.C., Pereira, M.R., Fonseca, J.L.C.: *Langmuir* **23**, 7687 (2007)
147. Hartig, S.M., Carlesso, G., Davidson, J.M., Prokop, A.: *Biomacromolecules* **8**, 265 (2007)
148. Dissing, U., Mattiasson, B.: *J. Biotechnol.* **52**, 1 (1996)

Thermodynamic and Rheological Properties of Polyelectrolyte Systems

Ruben H. Manzo, Alvaro F. Jimenez-Kairuz, María E. Olivera,
Fabiana Alovero and María V. Ramirez-Rigo

Abstract The chapter provides a treatment of the interaction between acidic or basic polyelectrolytes (PE) and ionizable organic molecules (selected model drugs) in aqueous environments, in terms of acid-base reactions. The electrostatic attraction between the ionized pending groups of the PE and the organic ions yields a high proportion of counterionic condensation with affinity constants in the range of 10³ to 10⁵. The high proportion of counterionic condensation in PE-drug aqueous dispersions determines many of the particular properties of these systems such as the effects of addition of electrolytes and non-electrolytes, the kinetic of drug release under different conditions, the raise of compatibility of low solubility drugs, the increase of chemical stability and the rheological behavior. The aqueous systems of acidic PE are characterized by their building viscosity capacity. Flow curves of PE-drug systems reflex the behavior of model PE-Na systems. However, complexes of a set of model drugs under similar conditions exhibit a wide range of viscosities. The determination of the kinetic of water sorption of PE-drug complexes in solid state provides valuable complementary information related to their swelling capacity. Rheology of PE-drug aqueous dispersions as well as their swelling capacity are relevant properties in the fields of mucoadhesivity and drug release.

Abbreviations

AA	Alginic acid
AA-Na	Sodium alginate
AH	Acidic organic molecule
AH _{st}	Stoichiometric concentration of an acidic organic molecule

R.H. Manzo (✉) · A.F. Jimenez-Kairuz · M.E. Olivera · F. Alovero
Departamento de Farmacia, Facultad de Ciencias Químicas, Universidad Nacional de
Córdoba (UNC), Unidad de Tecnología Farmacéutica (UNITEFA, CONICET-UNC),
Ciudad Universitaria (5000), Córdoba, Argentina
e-mail: rubmanzo@fcq.unc.edu.ar

M.V. Ramirez-Rigo
Planta Piloto de Ingeniería Química (PLAPIQUI, CONICET-Universidad Nacional
del Sur), Camino La Carrindanga Km 7 (8000), Bahía Blanca, Argentina

A^-	Dissociated species of an acidic organic molecule (*)
AH	Neutral species of an acidic organic molecule (*)
B_{st}	Stoichiometric concentration of a basic organic molecule
B	Neutral species of a basic organic molecule
BH^+	Protonated species of a basic organic molecule (*)
C	Carbomer
C934	Carbomer 934 P
C-Na	Sodium carbomer
CMC-Na	Sodium carboxymethylcellulose
CMC-Na (LV)	Low viscosity sodium carboxymethylcellulose
CMC-Na (MV)	Medium viscosity sodium carboxymethylcellulose
CMC-Na (HV)	High viscosity sodium carboxymethylcellulose
c^*	Critical concentration
DC	Diffusion coefficient
DC_f	Fast mode of the diffusion coefficient
DC_s	Slow mode of the diffusion coefficient
EE	Eudragit E 100
EL	Eudragit L-100
ES	Eudragit S-100
HA	Hyaluronic acid/hyaluronan
HA-Na	Sodium hyaluronate
$[HCl]_{st}$	Stoichiometric concentration of hydrochloric acid
K_{cc}	Affinity constant for counterionic condensation
PE	Polyelectrolyte
RAH	Acidic pending groups of a polyelectrolyte
RAH	Undissociated fraction of the acidic pending groups of a polyelectrolyte (*)
RA^-	Dissociated fraction of the acidic pending groups of a polyelectrolyte (*)
$[RA^-BH^+]$	Counterionic condensed fraction between the dissociated acidic pending groups of a polyelectrolyte and a protonated basic organic molecule (*)
RNR_1R_2	Basic pending groups of a polyelectrolyte
RNR_1R_2	Non-protonated fraction of the amino pending groups of a basic polyelectrolyte (*)
$RNR_1R_2H^+$	Protonated fraction of the amino pending groups of a basic polyelectrolyte (*)
$[RNR_1R_2H^+A^-]$	Counterionic condensed fraction between the protonated basic pending groups of a polyelectrolyte and a dissociated acidic organic molecule (*)
(*)	italics denote the dissociated or protonated species of a polyelectrolyte or a drug

Symbols

ζ	Electrokinetic potential
$\dot{\gamma}$	Shear rate
γ	Strain
τ	Shear stress
τ_0	Yield stress fluid
η	Dynamic viscosity
Tg δ	Loss tangent

1 Introduction

This chapter deals mainly with the thermodynamic and rheological properties of aqueous colloidal dispersions of complexes of polyelectrolytes (PE) with ionizable organic molecules, in particular model drugs. In addition, it follows with a description of a survey of several applications based on the unique properties of these systems.

PE can be defined as polymers carrying either positively or negatively charged ionizable groups [1].

The interaction of water soluble PE with inorganic or organic counterions generally generates stable colloidal dispersions also regarded as solutions when they are optically isotropic systems. These PE dispersions also exhibit electrokinetic potentials (ζ) which are negative or positive for acidic or basic PE respectively [2].

In most of acidic PE the ionizable moiety is the carboxylic group. Such is the case of carbomers (C, also known as carbopol or carboxyvinyl polymers), alginic acid (AA), hyaluronic acid (HA, also known as hyaluronan). Other acidic PE such as dextran sulfate, cellulose sulfate and nucleic acids are based on sulfate, or phosphoric ionizable groups.

Among basic PE, the nitrogen atom is the protonable center. There are also PE having a quaternary ammonium as a permanent cationic group. Chitosan, Eudragit E100 (EE) and trimethyl chitosan are representative members of this group. Figure 1 shows the chemical structure of some currently used acidic and basic PE.

There are several properties of the PE that are clearly different from that of uncharged polymers. The electrostatic interactions between the charges of PE lead to a rich behavior of their solutions, qualitatively different from those of uncharged polymers [3–5]. Thus, electrically charged PE chains follows unentangled dynamics in a much wider concentration range than solutions of uncharged polymers do.

Reports dealing with light scattering of flexible linear PE with acidic pending groups neutralized with monovalent inorganic cations (mainly Na^+) showed that such systems exhibit two clearly differentiated diffusion modes, one with diffusion coefficient (DC) ranging from 10^{-7} to $10^{-5} \text{ cm}^2/\text{s}$, and the other ranging from

10^{-9} to 10^{-8} cm²/s, which are regarded as “fast” (DC_f) and “slow” (DC_s) modes, respectively [6–8].

The DC_s has been associated with the presence of multichain domains (clusters) with dimensions appreciably exceeding the size of single chains. Both, the origin of these domains as well as the mechanism by which macromolecules of the same charge interact themselves are not satisfactorily understood. The DC_s has been found in a wide variety of synthetic and biological polymers. Therefore, it appears that it is a universal property of charged macromolecules dispersed in polar solvents [7].

Another interesting property of PE is the osmotic pressure. The osmotic pressure of PE in salt-free solutions exceeds by several orders of magnitude that of neutral polymers at similar polymer concentrations. Besides, it increases almost linearly with polymer concentration and is independent of the chain molecular weight in a wide range of polymer concentrations. This almost linear concentration dependence of the osmotic pressure, together with its strong dependence on added salt, demonstrates that osmotic pressure is mainly due to the counterions contribution [1].

It is well known that the properties of the colloidal microenvironments that arise from the interaction of PE with small counterions largely determine their rheological behavior. For example, the viscosity of PE solutions is proportional to the square root of polymer concentration (Fuoss' law) [9], while for solutions of uncharged polymers, at the same concentration, the viscosity is proportional to polymer concentration.

Among acidic PE, C, different degrees of sodium carboxymethylcellulose (CMC-Na), HA and AA (Fig. 1) are currently used to build aqueous viscosity [10]. With such purpose they are generally presented salified with alkaline metals as Na⁺ or K⁺, so that their carboxylic groups are essentially dissociated. As shown in Fig. 1, C is a family of linear polyacrylic acid cross-linked with allyl sugars whose viscosifying properties are clearly associated to the crosslink density. Although, CMC, AA and HA are linear PE, their monomer unities are composed of highly hydrophilic carbohydrate structures.

Although basic PE have been used for a variety of purposes, they do not exhibit valuable viscosifying properties as the acidic ones [10].

2 Interaction of Polyelectrolytes with Organic Molecules

The interaction of acidic or basic PE with model organic molecules, as those shown in the Fig. 2 currently yields stable dispersions; however in some cases the complementary addition of an inorganic counterion contributes to the required compatibility [11–14].

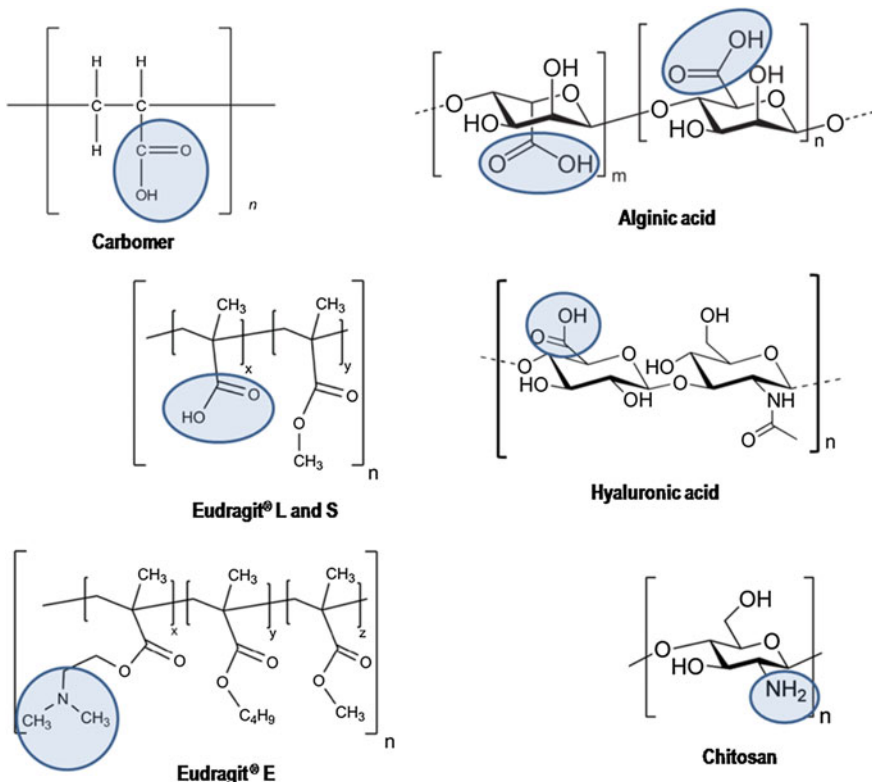


Fig. 1 Structural formula of some polyelectrolytes

2.1 Counterionic Condensation

The interaction of acidic or basic PE with model organic molecules having basic or acid groups respectively yields a high proportion of counterionic condensation [11–14].

Equation 1 depicts the reaction between acidic pending groups of a PE (RAH) with the basic groups of an organic molecule (B).



where B and BH^+ are the neutral and protonated species, RAH and RA^- represent the undissociated and dissociated fractions of the pending groups of the PE and $[RA^-BH^+]$ the counterionic condensed fraction.

In the same way, PE having protonable amino groups (RNR_1R_2) can react with the acidic groups of an organic molecule (AH) generating an analogue process of counterion condensation [12], in which AH and A^- are the neutral and anionic species, and RNR_1R_2 , $RNR_1R_2H^+$ and $[RNR_1R_2H^+A^-]$ have the same meaning of Eq. 1.

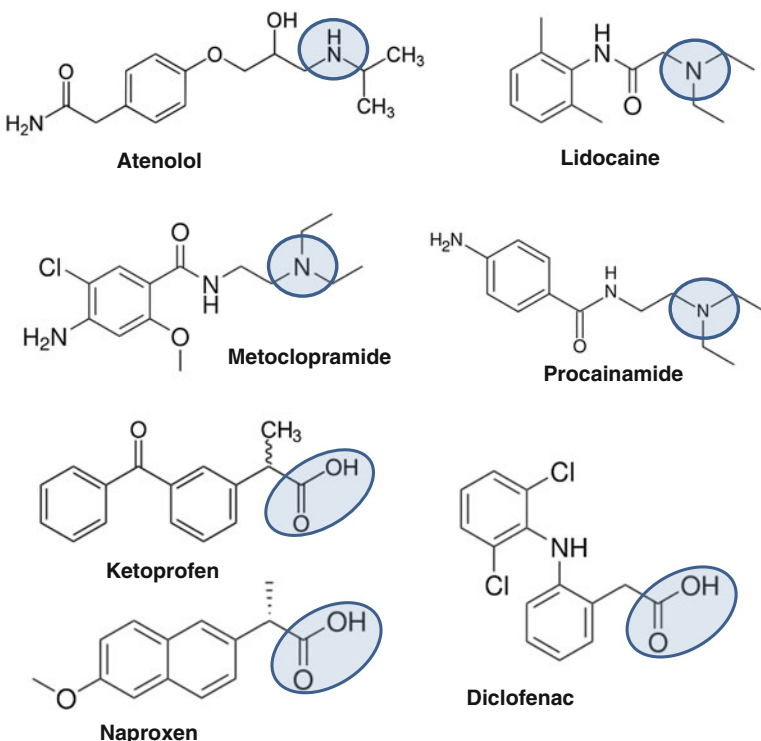
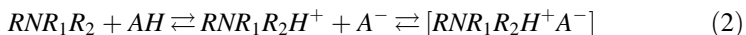


Fig. 2 Molecular structure of some of the model drugs used in several studies



Equations 1 and 2 describe the main interaction between the ionized groups of the macromolecule and its opposite charged partners. However, owing to the structural complexity of such systems other kind of contributions such as hydrogen bonding and hydrophobic interactions, among others, would also play a role in the association process.

As happen with inorganic counterions, the acid-base interaction described by Eqs. 1 and 2 originates high ζ that contribute to the physical stability of the dispersions. Figure 3 shows the ζ of aqueous dispersions of acidic and basic PE loaded with ionizable model drugs. As expected, the dispersions obtained with acidic PE yield a negative ζ while those obtained with basic PE display a positive ζ .

The knowledge about the factors that determine the interaction between ionic or ionizable drugs and PE is relevant in several fields. At present, a detailed description about the factors governing such interaction is not fully available. The classical description of ion–ion interaction recognizes two relative stable regions: one referred to as a solvent separated ion pair, or as a loose ion pair and the other referred to as a contact ion pair, which is also known as a tight ion pair [20]. In the

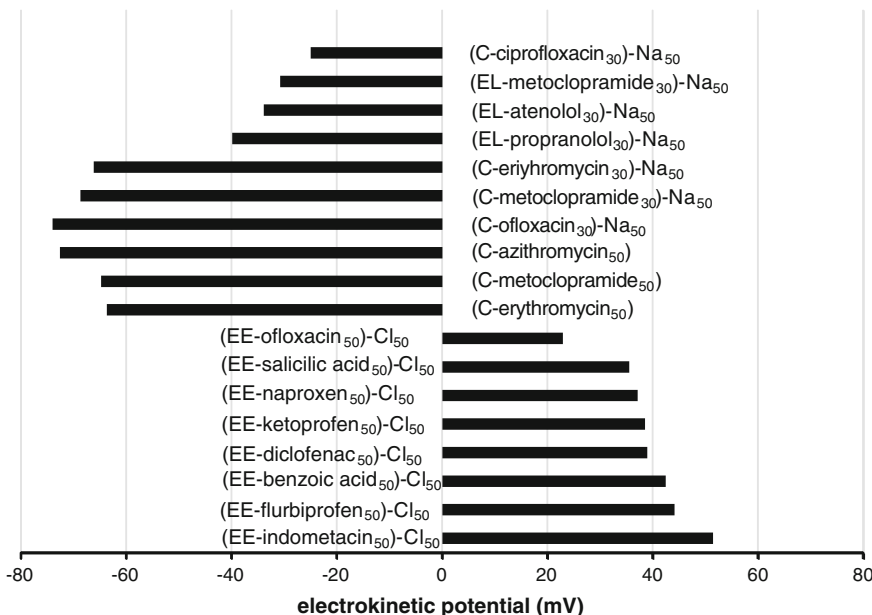


Fig. 3 Electrokinetic potentials (ζ) exhibited by aqueous dispersions of acidic and basic PE loaded with ionizable drugs. Carbomer data corresponds to C₉₃₄. The subscript numbers indicate the proportion of drug and inorganic counterion expressed in mol % which neutralizes the ionizable groups of each PE. (Data adapted from references [15–19])

same line, within the framework of the counterion condensation theory of PE, a common point in the theoretical treatments proposed is the recognition of two extreme modes of counterion association with the PE, currently referred to as loose and covalent bonding. The former is the delocalized confinement of the counterions within a condensation volume in the immediate vicinity of the PE, due only to long-range interactions, while the latter is a short range, site-specific interaction [21–23].

Theoretical treatments mainly address the interaction of acidic linear PE with inorganic cations. However, with organic counterions, although the main contribution to the overall interaction arises from the electrostatic attraction, non-electrostatic contributions would also play a role in the association process.

3 Species Distribution

Since drug speciation produces the free forms B and BH^+ or AH and A^- together with ion pairs with the ionizable groups of the PE, $[RA^-BH^+]$ or $[RNR_2H^+AD^-]$, the stoichiometric concentration B_{st} or AH_{st} are distributed as:

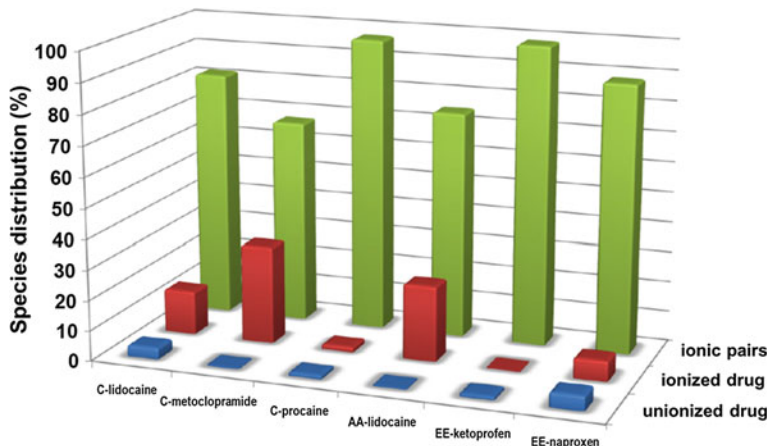


Fig. 4 Species distribution of model drugs from various hydrogels after partitioning in an organic solvent. C is Carbomer 934. (Data adapted from references [16] and [25])

$$B_{st} = (B) + (BH^+) + ([RA^-BH^+]) \quad (3)$$

$$AH_{st} = (AH) + (A^-) + ([RNR_1R_2H^+A^-]) \quad (4)$$

Species distribution in PE-drug dispersions has been determined through dialysis, selective solvent extraction of the neutral species of the drug, ultrafiltration and NMR spectroscopy. Typical results of species distribution of model organic molecules are shown in Fig. 4.

4 Affinity Constants for Counterionic Condensation

4.1 Acidic Polyelectrolytes

According with Eq. 1, the affinity constant for the counterionic condensation (K_{cc}) is expressed as:

$$K_{cc} = ([RA^-BH^+])/((RAH).(B)) = ([RA^-BH^+])/((RA^-).(BH^+)) \quad (5)$$

The following approach can be used to solve Eq. 5 in an aqueous dispersion:

$$(RA^-) + (HO^-) = (BH^+) + (H^+) \quad (6)$$

Then, under conditions in which $(RA^-) \gg (HO^-)$ and $(BH^+) \gg (H^+)$, Eq. 6 reduces to $(RA^-) = (BH^+)$.

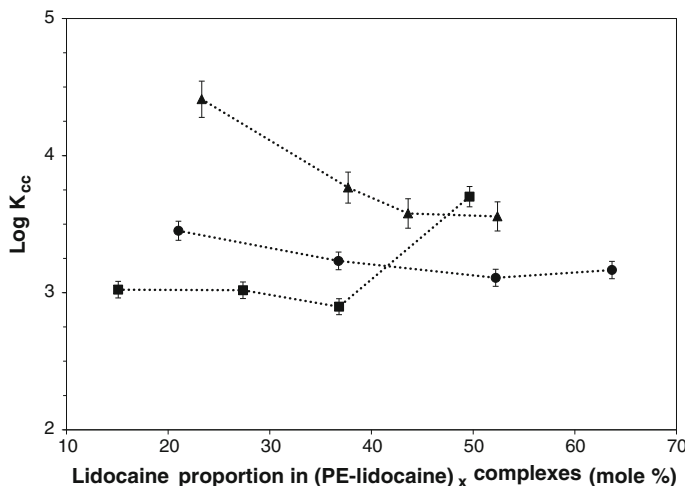


Fig. 5 Effect of the proportion of lidocaine loaded in some PE-drug complexes on the affinity constant K_{cc} . Black triangle Carbomer 934; black circle Eudragit L; black rectangle Eudragit S. (Data adapted from references [16] and [25])

The equilibrium properties of aqueous dispersions of complexes between model basic drugs lidocaine, atenolol and metoclopramide with three structurally related acidic PE was reported. Thus, K_{cc} of dispersions of polymetacrylates, EL, ES and C934 neutralized with increasing proportions of lidocaine and metoclopramide, were determined.

Figure 5 shows the K_{cc} of the three PE-drug systems loaded with increasing proportions of lidocaine.

It is worth emphasizing that, in these systems, the increase in the degree of neutralization of the acidic groups of the PE with model drugs produces an increase in their conductivity, viscosity and transparency [16, 24]. Also, the resulting dispersions exhibit high negative ζ . Such observations are consistent with the idea that a significant population of the condensed counterions keeps some degree of hydration and that charges are not fully neutralized. Therefore, the counterionic condensation generates the expansion of the PE chains, turning PE-drug complexes more hydrophilic than the PE alone.

With regard to PE-drug affinity, the branched PE C934 exhibited the highest K_{cc} at low lidocaine loading. This observation is consistent with its lower chain mobility, which correlates with its ability to build viscosity. However, the affinity decreases as the proportion of lidocaine was increased. This behavior would be primarily related to the close proximity between carboxylic groups, which would affect the ionic interaction through steric hindrance.

In spite, the linear PE EL exhibited a lower K_{cc} than C, which remains almost constant along a wide range of lidocaine loading. In addition, ES having the most

hydrophobic backbone exhibits the lowest K_{cc} at low lidocaine loading. However, at higher degrees of neutralization, K_{cc} is significantly raised. The long distance between ionizable groups, together with the expanding effect of the progressive ionization, seems to produce a positive effect to raise the ES-lidocaine affinity. Then, the distance between the acidic pending groups of the PE seems to play a significant role in K_{cc} . Thus, as lidocaine loading increases, C lowers K_{cc} , while ES raises it, and that of EL remains unchanged.

On the other hand, metoclopramide having an amino group of higher basic strength than lidocaine yields $(EL\text{-metoclopramide})_{50}$ and $(ES\text{-metoclopramide})_{50}$ with higher $\log K_{cc}$, as it was also observed with $(C\text{-metoclopramide})_{50}$ [25].

4.2 Basic PE

Several basic PE has been used for a variety of purposes. In all of them, basic nitrogen is the interacting atom susceptible of protonation in aqueous medium. Among them, chitosan and EE a polymethacrylate with diethylamino pending groups has been extensively studied.

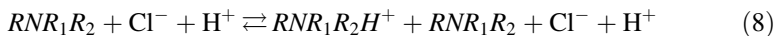
The interaction of the linear polymethacrylate EE with organic acids yields stable aqueous dispersions when an inorganic anion (example Cl^-) is incorporated in the system.

The affinity constant K_{cc} for the complex $(EE\text{-diclofenac}_{50}\text{Cl}_{50})$ at 0.5 % of EE was determined for a model non-steroidal anti-inflammatory drug.

The constant was determined according with Eq. 2.

$$\begin{aligned} K_{cc} &= ([RNR_1R_2H^+A^-])/(RNR_1R_2)(AH) \\ &= ([RNR_1R_2H^+A^-])/([RNR_1R_2H^+](A^-)) \end{aligned} \quad (7)$$

To solve Eq. 7 the approach that equilibrium 8 was essentially shifted to the right was considered.



Therefore $[\text{HCl}]_{\text{st}} = (\text{Cl}^-)$ and the charge balance is

$$(RNR_1R_2H^+) + (\text{H}^+) = (\text{HO}^-) + (A^-) + (\text{Cl}^-) \quad (9)$$

Equation 9 under the experimental conditions used is reduced to $(RNR_1R_2H^+) = (A^-) + (\text{Cl}^-)$ or $(RNR_1R_2H^+) = (\text{Cl}^-)$ that let to solve Eq. 7.

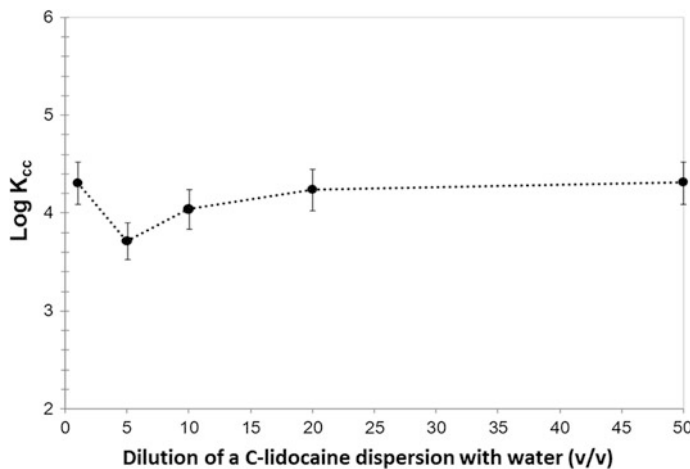


Fig. 6 Effect of the dilution of a dispersion C-lidocaine on the affinity constant K_{cc} . (Data adapted from reference [16])

4.3 Effects of Dilution

With regard to the effect of the PE-drug concentration on K_{cc} , available results indicate that the mass law exerts the control. In fact, Fig. 6 shows that in accordance with Eq. 1 $\log K_{cc}$ of the dispersion of $(C\text{-lidocaine})_{75}$ [16] remained essentially constant over 50 times dilution (from 0.5 to 0.01 % C). A similar behavior was observed on a $\log K_{cc}$ of $(EL\text{-lidocaine})_{50}$ which also remained constant over 10 times dilution [25].

5 Release of Drugs from Polyelectrolyte-Drug Dispersions

The reversibility of the PE-drug interactions described in the previous sections determines the rate and extent of the release of the loaded drugs from the complexes in aqueous dispersions [11–14, 26, 27]. In fact, experiments performed in bicompartimental cells limited by a semipermeable membrane that prevents the diffusion of the complex demonstrate that:

1. The release of drug towards water as receptor medium is mainly produced by the diffusion of the neutral species B or AH able to freely diffuse since the fraction of free charged species (A^- or BH^+) are compromised with the electrical gradient of the PE. Thus, the diffusion of the neutral species promotes the dissociation of ionic pairs according with the equilibria described in Eqs. 1 and 2 producing a feedback mechanism. In other words, the fraction of ionic pairs is a reservoir of drug and has been shown that the release rate is proportional to such fraction.

Fig. 7 Release profile of atenolol from the hydrogel C₉₃₄-atenolol in a Franz cell against water (black square) or NaCl solution (black circle) as receptor media. (Data adapted from reference [16])

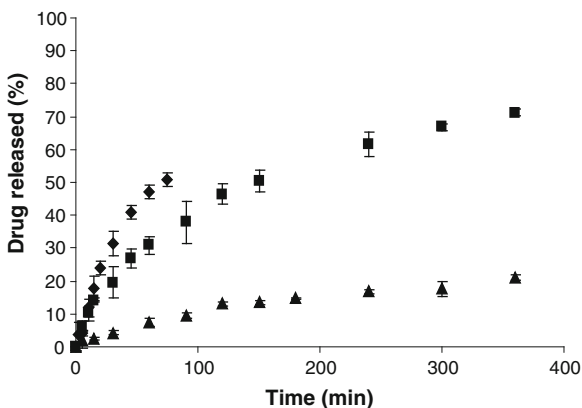
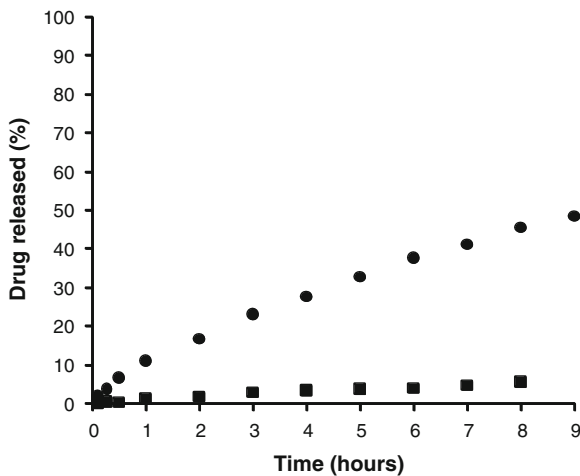


Fig. 8 Release profile of benzoic acid from drug solution (black diamond) and drug-containing EE aqueous dispersions against water (black triangle) or NaCl solution (black square) as receptor media. (Data adapted from reference [18])

2. As a saline solution (0.9 % NaCl) is placed as receptor medium in order to simulate a biological fluid, the diffusion of Na^+ and Cl^- into the donor compartment promotes an ionic exchange with the complex that raises the concentration of free species able to diffuse. As a consequence the release rate is increased as is shown in Figs. 7 and 8.

6 Rheological Properties of Polyelectrolyte Dispersions

6.1 Basic Concepts on Reology of PE

Rheology has been properly defined as the study of the flow and deformation of materials, with special emphasis being usually placed on the former [28]. There exist many fluids whose flow cannot be described by the linear response of the Newtonian flow equations. These materials are called as complex fluids, or non-Newtonian materials, since they display behaviors that range from that of viscous liquids to that of an elastic solid to some combination of the two. PE in aqueous dispersions exhibit behaviors of complex fluids [29].

Basically and considering the case of a slab of material sheared between two parallel plates (Fig. 9), there are two kinds of flows with relative movement of adjacent particles of liquid; they are called *shear* and *extensional* flows. The simple shear flow is the continual movement of particles of liquid *over* or *past* each other, by applying an external force to the top plate, while extensional (or *elongational*, or *stretching*) flows are where particles of liquid flow *towards* or *away from* each other. Then, from this deformation of material is possible calculate the resulting strain (γ). The *gradient* of the velocity in the direction at the right angles to the flow is called the *strain rate or shear rate* ($\dot{\gamma}$), and the force per unit area produced by the flow is called the *shear stress* (τ).

For a simple fluid, the dynamic viscosity (η) is simply the proportionality constant between stress and strain rates [28]:

$$\tau = \eta \dot{\gamma} \quad (10)$$

To thoroughly study the rheological behaviors observed in complex liquids it is necessary to perform a viscoelastic test by modifying the applied force both, by changing its magnitude and by adding a driving frequency. Dynamic oscillatory shear tests are performed by subjecting a material to a sinusoidal deformation and measuring the resulting mechanical response as a function of time.

Two principal models are used to describe much of the observed behavior seen in PE and other complex fluids; the Herschel-Bulkley and Maxwell models. The first is an empirical model that describes the flow of a yield stress fluid (τ_0) in response to varying shear rates, according to following equation [30]:

$$\tau = \tau_0 + k \dot{\gamma}^n \quad (11)$$

This model accounts for a yield stress combined with power law behavior in stress as a function of shear rate. Besides, this model predicts a viscosity that diverges continuously at low shear rates and is infinite below the yield stress. When $n = 1$, the Herschel-Bulkley model reduces to the Bingham fluid model where the flow above the yield stress would be purely Newtonian and the constant k would represent the viscosity [28].

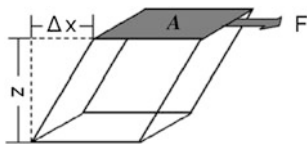


Fig. 9 Illustration of shear (a force “ F ” applied to a slab of height “ z ”, over an area “ A ”, results in a stress “ $\sigma = F/A$ ”, and get a deformation along the x-axis of “ Δx ”, which results in a strain “ $\gamma = \Delta x/z$ ”)

On the other hand, the Maxwell fluid model explains the response of complex fluids to an oscillatory shear rate. The frequency-dependent behavior of this model, displayed into linear responses to applied shear rates has been found to be applicable to a variety of complex fluid systems. Although the linear viscoelasticity is useful for understanding the relationship between the microstructure and the rheological properties of complex fluids, it is important to bear in mind that the linear viscoelasticity theory is only valid when the total deformation is quite small. Therefore, its ability to distinguish complex fluids with similar micro- and nano-structure or molecular structures (e.g. linear or branched polymer topology) is limited. However, complex fluids with similar linear viscoelastic properties may show different non-linear viscoelastic properties [31].

7 Flow Properties of Representative Sodium Salts of Acid Polyelectrolytes

7.1 Carbomer

As early mentioned, C is a family of PE of very high molecular weight composed of linear poly(acrylic acid) cross-linked with allyl sugars. Both, the degree of crosslinking and the agent used for this purpose generate the different types and applications of C shown in Table 1.

In solid state, the molecules of C are basically folded. In contact with water C chains become rapidly hydrated and spread out generating an increase in viscosity. Due to the crosslinks they do not produce true hydrogels. However, neutralization with inorganic bases generates the dissociation of C carboxylic pending groups along the chains leading to their full deployment as a result of electrostatic repulsion between the generated charges [32].

The rheology of hydrogels of C was extensively studied since, after its synthesis in the 60th, its use became popular in pharmaceutical and cosmetic technology and also in other industries because of their excellent properties as a viscosifying agent and stabilizer in suspension and emulsions, even at concentrations below 0.5 % [32, 33]. At 0.25 % w/w aqueous concentration of C yield the viscosity described in Table 2.

Table 1 Pharmaceutical and cosmetic applications of different carbomers

Applications	Type of carbomer NF
Topical use (external use only)	907, 910, 934, 940, 941, 980, 1342, 5984EP, ETD2020, Ultrez 10
Oral and mucosal use (internal use)	934P, 971P, 974P, 71G

Table 2 Dynamic viscosity of different polyelectrolyte sodium salts in aqueous dispersions

PE-Na	PE dispersion (%)	Shear rate (r.p.m)	η (cps.)
C934-Na ^a	0.25	40	1,261
CMC-Na (LV) ^d	1.0	60	10–15
CMC-Na (MV) ^d	1.0	30	1,500–2,500
CMC-Na (HV) ^d	1.0	30	8,000–12,000
AA-Na ^b	1.0	55	46
HA-Na ^c	1.0	100	407

^{a–d} Data extracted from references [10, 16, 41, 42] respectively

In cross-linked polymers as C, the crosslink keeps the strands of the polymer chains from displacing very far from the initial position during a disturbance and prevent the flow of the polymer strands relative to each other. Then, the macromolecule is able to recover its original structure. This behavior is described by the parameter known as elastic modulus and is proportional to the crosslink density [34].

Hydrogels of C are low concentrated dispersions neutralized by alkaline hydroxides and display a near Newtonian behavior. The appearance of the yield stress is observed at the critical concentration (c^*), which marks the limit between the dilute and semi-dilute regime. The onset of this behavior occurs at around 0.5 % w/v depending on the type of C. These hydrogels show little to non-thixotropic behavior [1, 34].

7.2 Sodium Carboxymethylcellulose

This PE is described in the USP as the sodium salt of polycarboxymethyl ether of cellulose. Its typical molecular weight is 90,000–700,000. The rheological properties of CMC depend on the polymer concentration and on the degree of substitution (conversion of $-\text{OH}$ into $-\text{O}-\text{CH}_2-\text{COO}^-$) which varies from 0.5 to 1.2 [35, 36]. Thus, various grades of CMC with different aqueous viscosities are available, currently regarded as low-, medium-, and high-viscosity (CMC-Na (LV), CMC-Na (MV) and CMC-Na (HV), respectively). At 1 % w/v aqueous concentration they yield the viscosities described in Table 2 [10].

The c^* of CMC has been established at around 1 % w/v. Below the c^* value CMC dispersions exhibit pseudoplastic flow without yield stress. However, at high concentrations, CMC dispersions exhibit thixotropic and viscoelastic behavior.

7.3 Alginic and Hyaluronic Acids

These PE are biopolymers. The first can be obtained from vegetal and the second from animal and microorganism sources [10].

AA swells but does not dissolve in water. However it is soluble in alkali hydroxides producing viscous dispersions. Various grades of sodium alginate (AA-Na) are available, yielding aqueous dispersions of varying viscosity within a range of 20–400 mPas in 1 % solution at 20 °C [10].

The precise composition of alginates varies markedly with the season and seaweed species, with the result that the rheological properties vary enormously from different suppliers, and even from different batches from the same supplier [37, 38].

The basic rheological properties of low concentration AA-Na dispersions have been extensively studied. They exhibit non-Newtonian pseudoplastic behavior (shear thinning) at concentrations between 0.125 and 1.5 % w/v, while at lower concentrations they behave as low viscosity Newtonian fluids [37].

In the presence of an electrolyte, e.g., increasing the concentration of NaCl up to 100 mM, a reduction in the viscosity of AA-Na dispersion was observed [10].

HA is currently presented as sodium hyaluronate (HA-Na). A number of rheological studies of HA-Na dispersions have been presented in the literature. These studies are difficult to compare when different sources of HA-Na are used. The rheology of HA-Na is extremely sensitive to protein contamination [39, 40]. Comparable results are obtained using protein free samples obtained from bacterial sources. Some of these studies were conducted in saline aqueous medium to reproduce physiological conditions in which dilute and semidilute HA-Na dispersions exhibit Newtonian behavior in a wide shear rate range. However, aqueous dispersions of 1 % w/v HA-Na exhibit shear thinning behavior without yield stress (Fig. 10). The viscosity of AA and HA dispersions is presented in Table 2.

8 Flow Properties of Acid PE-Drug Dispersions

Equilibrium and release properties of aqueous systems PE-drug dispersions can be reasonably predicted from the physicochemical properties of both partners. However such systems exhibit a wide variability in their rheological properties. Thus, Table 3 shows that C934 at 0.25 % w/v neutralized at 50 % with a set of representative basic D exhibits a wide range of apparent viscosities that in all cases are lower than that of C-Na. Table 3 also shows that the linear AA requires higher

Fig. 10 Flow curve of HA-Na 1.0 % w/v aqueous dispersion. (Data adapted from reference [41])

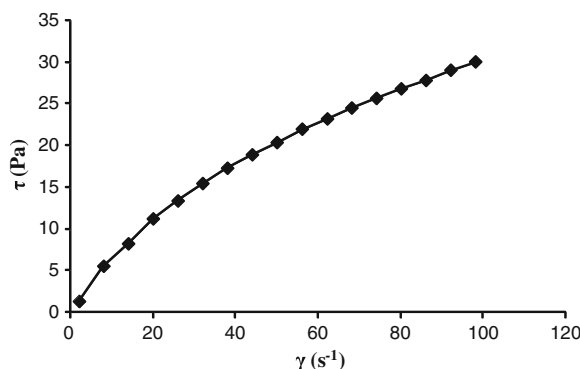


Table 3 Apparent viscosity at 25 °C of a set of PE-drug aqueous dispersions in which the PE was 50 % neutralized by drugs. (Data obtained from references [16] and [42])

PE-drug	Viscosity (mPa.s)	% PE	Shear rate (s^{-1})
C-atenolol	666.9	0.25	100
C-procainamide	435.0	0.25	100
C-pilocarpine	438.7	0.25	100
C-lidocaine	199.6	0.20	100
C-metoclopramide	31.58	0.25	100
C-naphazoline	17.03	0.25	100
C-erythromycin	14.29	0.25	100
C-azithromycin	11.99	0.25	100
AA-lidocaine	229.0	5.00	50
AA-atenolol	80.00	5.00	50

concentrations to build viscosities of the same range. On the other hand, the acidic form of CMC, obtained from CMC yields CMC-drug complexes that are not dispersible in aqueous medium.

8.1 Carbomer as a Model of Cross-Linked Polyelectrolyte to Produce Polyelectrolyte-Drug Hydrogels

C934 is a hydrophilic mucoadhesive polymer suitable for internal use that was introduced in 1960. This acidic PE swells in contact with water. Upon neutralization with strong bases as NaOH or KOH, it forms hydrogels of high viscosity at very low concentrations (from 0.1 %) and in a wide pH range between 4.5 and 8. Rheological studies were conducted on C hydrogels partially or fully neutralized with inorganic bases or with simple organic molecules containing amino groups, for example triethanolamine [32].

8.2 Properties of Carbomer-Drug Hydrogels

In general C-drug dispersions are prepared starting from an aqueous dispersion of C, at concentrations of 0.1, 0.2, 0.25 or 0.5 % w/v that is neutralized with an appropriate proportion of the organic molecule. Compositions are identified as C-drug_x, where the subscript x is the proportion of drug expressed in mol % which neutralizes the carboxylic groups of C [11–13].

Dispersions of C in water have a pH between 3.0 and 3.4. Neutralization with basic molecules increases pH which generally ranges between 5.00 and 8.40 for the range between 25 and 100 % of neutralization of their carboxylic groups.

Neutralization of C934 with different basic drugs originates different kinds of dispersions. Some of them are presented as translucent hydrogels, for example those neutralized with lidocaine, atenolol, procaine, procainamide or pilocarpine. Others are presented as relatively opaque hydrogels as that obtained with metoclopramide. In other instances the neutralization products are low viscosity opaque dispersions that after a time generate a sediment easily redispersible by agitation. C-erythromycin and C-naphazoline are examples of that behavior. The physical stability of these products, as well as their viscosity and the transparency can be increased by adding Na⁺ to the C-drug dispersion, obtaining systems C-drug_xNa_y. This strategy is useful in cases where the dispersion does not have the viscosity and/or physical stability required [13, 16].

Figure 11 shows the flow curves of dispersions of C neutralized at 50 % with a set of representative drugs, which are transparent - translucent hydrogels. They exhibit a behavior similar to that produced by (C–Na) since yield stress and shear thinning without thixotropy are also observed in all these systems.

Besides, the series of C-lidocaine_x hydrogels prepared at 0.2 % C, with increasing proportions of lidocaine (25, 50, 75 and 100 mol %) exhibits a similar pattern along the full range of compositions (Fig. 12).

Figure 13 shows that the dynamic viscosity of the C-drug_x hydrogels increases with the proportion of drug incorporated in the dispersion, between 0 and 75 %. However, at higher loading proportions it remains constant or even decreases, which is consistent with the behavior reported in literature for C–Na [32].

As early mentioned, the viscosity of PE dispersions is highly dependent on the concentration as it is shown in Fig. 14 for the system C-lidocaine. It was also observed that the elastic modulus of C varies from almost purely newtonian properties in diluted dispersion to the pseudoplastic behavior. At concentrations above 0.25 % C dispersion show a yield stress value with a plastic behavior which can be described by the Bingham fluid model [43, 44].

Fig. 11 Flow curves of 0.25 % Carbomer 934 P hydrogels loaded with different drugs. (Black diamond) atenolol; (black square) pilocarpine; (asterisk) procainamide; (white triangle) lidocaine. (Data adapted from reference [16])

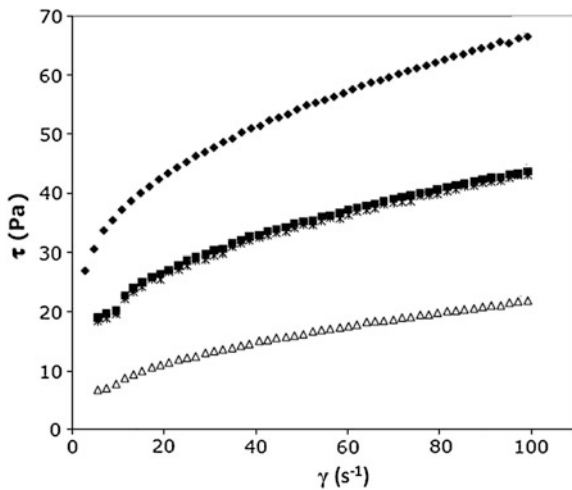
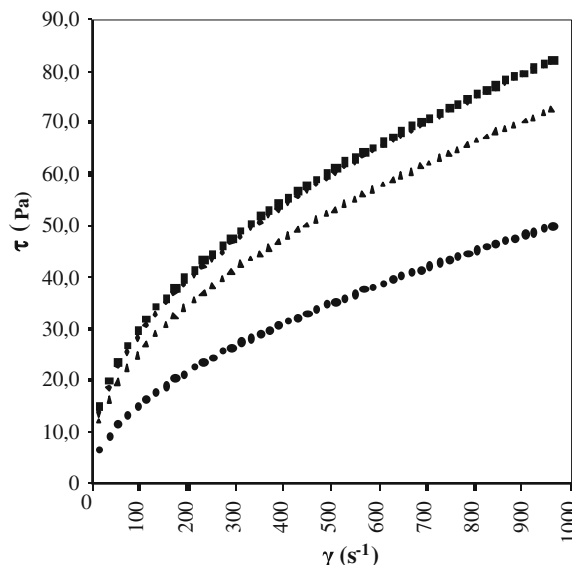


Fig. 12 Flow curves of 0.2 % carbomer hydrogels loaded with increasing proportions of lidocaine prepared in situ. (Black diamond) C-lidocaine₁₀₀; (black square) C-lidocaine₇₅; (black triangle); C-lidocaine₅₀; (black circle) C-lidocaine₂₅. (Data adapted from reference [16])



8.3 Effect of the Addition of Other Species on Carbomer-Drug Dispersions

The introduction of inorganic ions in aqueous dispersions of macromolecules generates a set of complex interactions such as changes in conformation, in the ζ and the hydration of their hydrophilic groups among others that affect their rheological behavior. In particular, the addition of salts to PE dispersions produces a

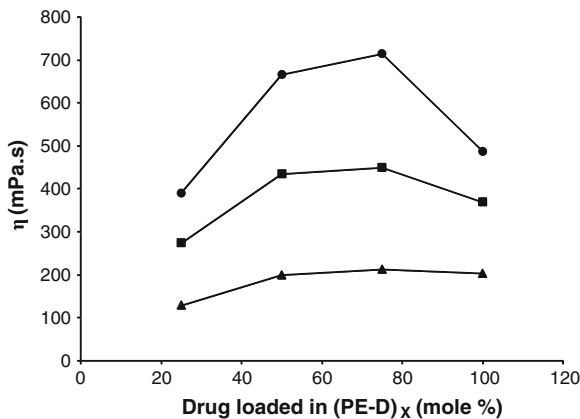
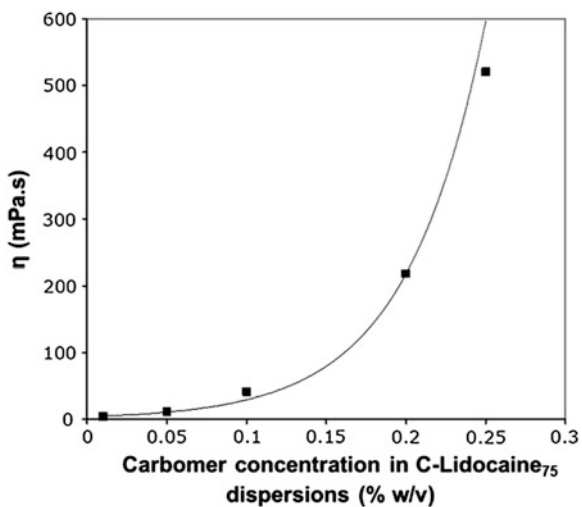


Fig. 13 Effect of drug proportion loaded in 0.25 % C dispersions on dynamic viscosity. (Black circle) atenolol; (black square) lidocaine; (black triangle) procainamide. Measurements were recorded at 25 °C and 100 s⁻¹. (Data adapted from reference [16])

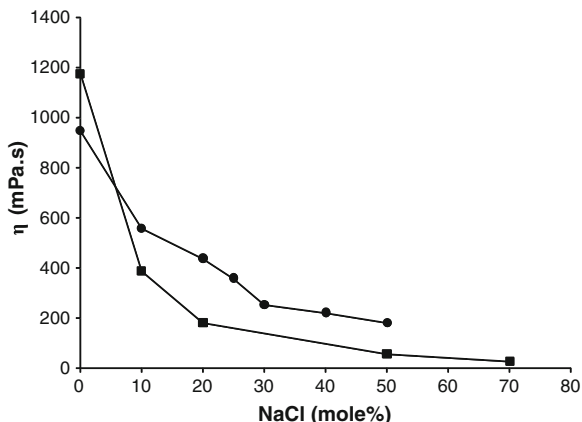
Fig. 14 Effect of concentration on viscosity of C-lidocaine₇₅ hydrogels prepared in situ. (Data adapted from reference [16])



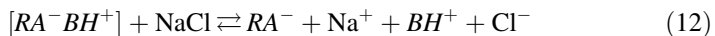
significant lowering of viscosity that has been related to the reduction of the degree of swelling of the macromolecules [34].

In aqueous dispersions of cross-linked PE-drug the osmotic pressure generated by the accumulations of ions inside the microenvironment of the complex is one of the main factors that determine the high level of swelling. Therefore, the addition of inorganic ions decreases the osmotic difference between the macromolecular environment and the bulk medium with the consequent lowering of swelling that affect the rheology of the system [34].

Fig. 15 Effect of addition of NaCl on the dynamic viscosity of 0.25 % C hydrogels loaded with lidocaine (black square) or atenolol (black circle). Measurements recorded at 25 °C and 100 s⁻¹. (Data adapted from reference [16])



Besides, the addition of inorganic salts (i.e. NaCl) to the PE-drug system also produces a displacement of organic ionic species from the PE environment as a consequence of the ionic exchange depicted in Eqs. 12 and 13:



The increase of the concentration of NaCl produces a decrease in the proportion of $[RA^-BH^+]$ with the consequent increase of BH^+ and Cl^- in the bulk phase. The incorporation of small ions (having higher mobility than the organic ones) in the PE environment would contribute to keep the level of hydration. However, a dramatic drop of viscosity is produced as depicted in Fig. 15. It should be noted that polymethacrylates, having a hydrophobic backbone without other hydrophylic moieties than carboxylic groups are particularly susceptible to the saline effect.

8.4 Properties of Alginic-Drug Dispersions

The rheological behavior of AA-drug dispersions is similar to that observed with AA-Na. In fact this linear PE requires higher concentrations than C to build comparable viscosities. Figure 16 shows the flow curve of a dispersion of AA-lidocaine₂₅ at a concentration of 5 % w/v which exhibits a modest shear thinning [42]. Since the concentration is clearly above c^* the effect of the temperature on lowering the viscosity is important with an activation energy (E_a 1,770 kJ/mole) typical of entangled systems. A similar behavior was observed with other model drugs such as atenolol [42].

The viscosity of AA-lidocaine remains constant by increasing the proportion of lidocaine until 50 % but higher loading produces a dramatic drop of this property.

Fig. 16 Flow curve of AA-lidocaine₂₅ dispersion at 5.0 % w/v at 25 °C. (Data adapted from reference [42])

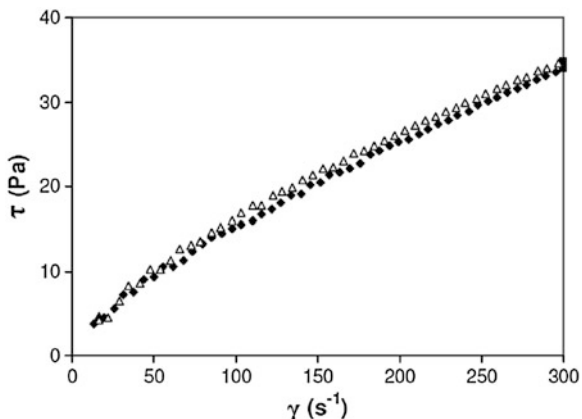
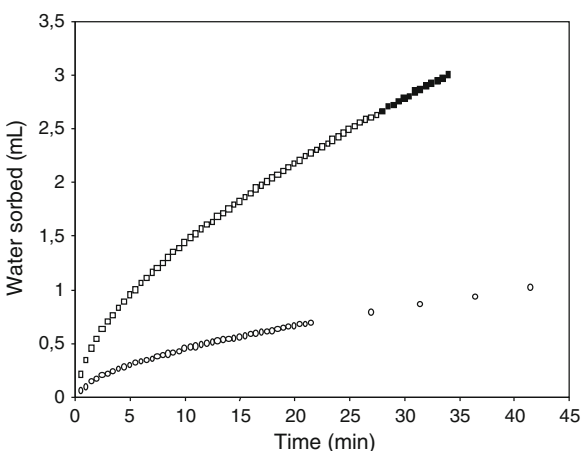


Fig. 17 Rate of water sorption (mL) by 0.100 g of C-lidocaine₇₅ (white square) and C 934P (white circle) as particulate solids. (Data adapted from reference [16])



8.5 Polyelectrolyte-Drug Complexes in Solid State

The PE-drug complexes are also obtained in solid state. They are presented as stable amorphous solids that in contact with water easily revert to the original dispersion [24, 45, 46]. Figure 17 shows that a C-lidocaine complex as particulate solid in contact with water swells quickly reversing the hydrogel state.

The same phenomenon is observed in complexes that have been compacted under the shape of circular matrices. In fact, it can be seen in Fig. 18 that water sorption rate is proportional to the viscosities reported in Table 3. Thus, the high swelling capacity exhibited by the complexes of atenolol and lidocaine in salt free medium makes them highly susceptible to the saline effect. Thus, the sorption rate decreases when a NaCl solution is used instead of water. On the other hand, the complex with metoclopramide has a very low rate of water sorption reveal a limited swelling capacity whose rate is barely affected in NaCl solution.

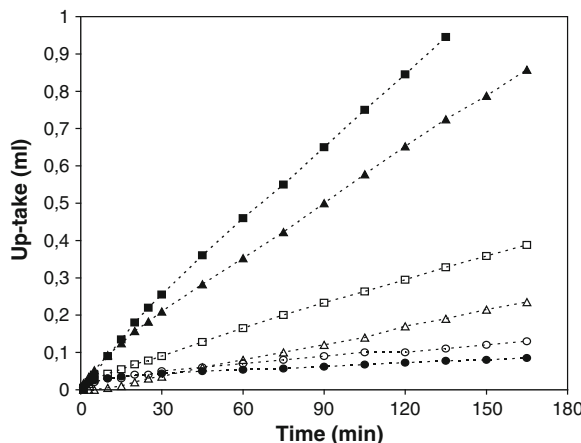


Fig. 18 Water sorption exhibited by discs 12 mm in diameter obtained by compaction of 200 mg PE-drug complexes in a hydraulic press. (Black square) C-atenolol₅₀; (black square) C-lidocaine₅₀; (black circle) C-metoclopramide₅₀. Filled and empty symbols are water and 0.9 % NaCl, respectively. (Data adapted from reference [16])

9 Remarks on Thermodynamic and Rheological Properties of Polyelectrolytes

The treatment of the interaction in aqueous environments between acidic or basic PE and ionizable organic molecules (selected model drugs) in terms of acid-base reactions provides solid basis to understand many of the properties of such systems.

The acid-base reaction renders organic ions that have lower ionic mobility than the small inorganic ions currently used as PE partners. Thus, the electrostatic attraction between the ionized pending groups of the PE and the organic ions yields a high proportion of counterionic condensation with K_{cc} in the range of 10^3 – 10^5 . Available results have shown that the K_{cc} are not affected by the dilution of the dispersions.

The high proportion of counterionic condensation in PE-drug aqueous dispersions determines many of the particular properties of these systems such as the effects of addition of electrolytes and non-electrolytes, the kinetic of drug release under different conditions, the raise of compatibility of low solubility drugs, the improvement of chemical stability and the rheological behavior.

The available rheological studies performed with acidic PE characterized by their building viscosity capacity provide information on the basic rheological behavior of PE-drug systems. In a general way, the flow curves of acidic PE-drug systems reflex the behavior of model PE-Na systems. However, complexes of a set of model drugs under similar conditions exhibit a wide range of viscosities. At present, systematic studies that relate relevant structural properties of ionizable

organic molecules with the rheological behavior of their model PE complexes are not available.

The determination of the kinetic of water sorption of PE-drug complexes in solid state provides valuable complementary information related to their swelling capacity. At present, there are few reports addressing viscoelastic properties of these systems that would complement the present results. Then, it is an interesting field yet to be explored.

10 Field of Projections Based on the Properties of PE-Drug Complexes

The dynamic of sorption and swelling is an important property in the field of modified-release of drugs, in particular in the development of so-called hydrophilic matrices.

In fact, in experiments in which the matrices of the complexes are placed between 2 glass plates the dynamic of radial wetting may be registered (Fig. 19).

Penetration of water generates a dry core surrounded by a layer of gelled complex that modulates the rate of water penetration. The Figs. 20 and 21 show the development of the wetting and erosion fronts. Besides, inside the gel layer a diffusion front is also recognized in which the displacement of equilibria described in Eqs. 1 and 2 became evident by pH changes, detected by a pH-indicator.

The hydrogel layer generated by swelling modulates release of D as has been described in previous sections.

Complexes of C because of its branched structure generate a hydrogel layer resistant to erosion and the release mechanism of the drug is predominantly by diffusion of free species toward the bulk medium. However, complexes of the linear PE AA produce a gel layer of lower resistance to erosion and the main mechanism of the drug release is the diffusion to the bulk medium of AA-drug complex macromolecules.

Last, as expected, matrices of CMC-drug complexes in contact with water do not produce a gel layer [47].

Another application related to PE rheology is in the field of mucoadhesion. There is profuse scientific literature about the topic. An interesting and complete review was published by Caramella et al. [48] in the early nineties.

The task of dealing with the rheological aspects of mucoadhesión is rather intriguing, as is always the case when rheology is involved in explaining the behavior of a system. In this regard, mucoadhesive hydrogels represent no exception.

Most of mucoadhesive polymers are either a water-soluble cross-linked polymer with limited swelling capacity or a hydrophilic polymer that swells indefinitely and eventually undergoes complete dissolution.

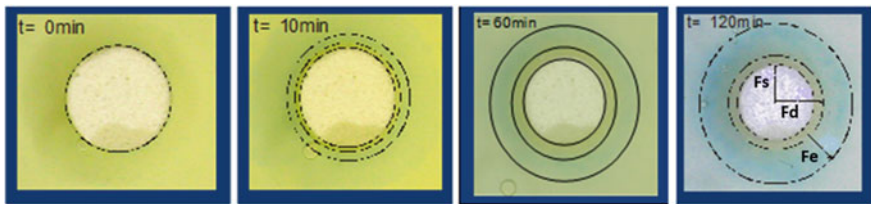


Fig. 19 Evolution in time of swelling fronts exhibited by matrices carbomer-atenolol₁₀₀ in aqueous media. F_s swelling front; F_d diffusion front; F_e erosion front

Fig. 20 Front movements of the C-atenolol₇₅ matrix in water: (black diamond) erosion front, (black square) diffusion front, (black triangle) swelling front. (Data adapted from reference [16])

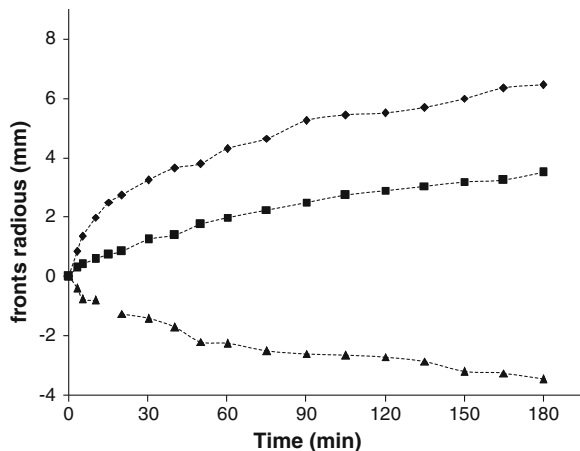
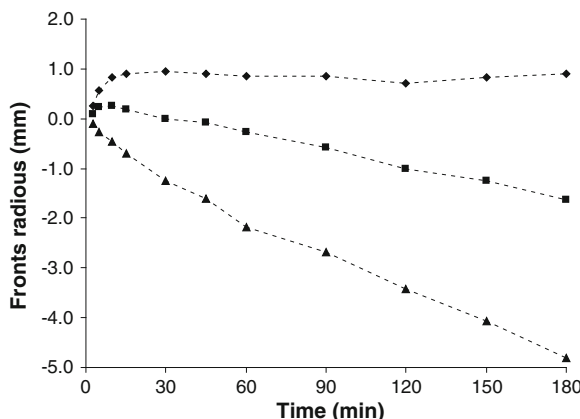


Fig. 21 Front movements of the AA-atenolol₅₀ matrix in water: (black diamond) erosion front, (black square) diffusion front, (black triangle) swelling front. (Data adapted from reference [42])



Mucoadhesion invariably involves the presence of a hydrated gel phase. The hydrogel may be applied as such to the mucosal surface or the hydrated gel phase can be formed in situ upon hydration of a solid mucoadhesive system in contact

with the mucus layer. As in the case of molecular weight, it can occur that mucoadhesivness increases with increasing viscosity up to a maximum value corresponding to optimal adhesion.

It has been reported that the viscoelastic nature of C gels is a good predictor of their adhesive properties. They also observed a substantial decrease in the rheological storage moduli for all samples, while no changes were observed in mucoadhesion and proposed that a redistribution of cations between the polymer cluster and the bulk of medium is a possible additional mechanism of ageing of C hydrogels [49].

From a methodology point of view, the rheological approach involves the investigation of the changes in rheological properties that mucoadhesive PE and hydrogels undergo when they are mixed with mucins.

There is plenty of experimental evidence to support that rheologic changes are observed when bioadhesive polymers and mucin are mixed. In this context it was shown that when a mucoadhesive polymer and mucin are mixed together there is a synergistic increase in viscosity. It is known that the viscosity of a mucin dispersion is the net result of the resistance to flow exerted by individual chain segments, physical chains entanglements and non-covalent molecular interactions, which are the same as the interactions involved in the process of mucoadhesion. Then, it has been proposed that the interaction forces involved in a mucin bioadhesive system could be evaluated by viscosity measurements since both, physical and chemical bonds in mucin-polymer mixtures cause changes in the shape or arrangements of macromolecules that are the bases for viscosity changes. It has been observed that there are variations in the elastic and viscous behavior. The balance between them is represented by $\text{tg } \delta$ (loss tangent). Thus, $\text{tg } \delta$ has been proposed as a suitable parameter to compare the viscoelastic behavior of polymers with different elastic and viscous profile. The more pronounced the elastic behavior with respect to the viscous one, the lower the loss tangent.

The measurement of the dynamic properties is useful for the differentiation of bioadhesive PE based on their interaction with mucin. The loss tangent parameter provides a complete characterization of these rheological changes. For homologous series or for similar PE the same order of mucoadhesion observed in the rheology will be found in the tensil strength.

Whenever the PE-mucin interaction produces a rheological synergism in the mixture a hardening of the gel in the corresponding interface will be observed.

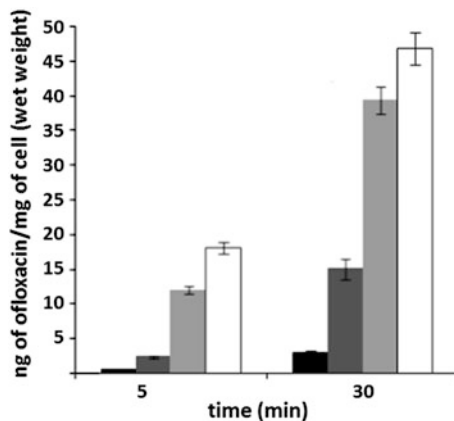
Romero et al. [50] investigated the rheological properties of C971, C934 and C940 hydrogels loaded with ofloxacin (Table 4) and related them with their antimicrobial properties against both fluoroquinolone-sensitive and -resistant *Pseudomonas aeruginosa*.

The analysis of bactericidal index values after a short time of drug exposure confirms the higher potency of hydrogels compared with that of ofloxacin (Fig. 22).

The improved uptake in fluoroquinolone-resistant isolates was correlated with the viscosity of hydrogels. The performance of hydrogels seems to be related to

Table 4 Physicochemical and rheological properties of carbomer-ofloxacin hydrogels

Hydrogel	Ofloxacin concentration (mg/ml)	pH	Electrokinetic potential (ζ) (mV)	Viscosity (mPa.s), 37 °C
C971-ofloxacin	2.64	6.93	-52.67	910
C934-ofloxacin	2.68	7.03	-65.13	1,340
C940-ofloxacin	2.68	6.94	-53.22	28,970

**Fig. 22** Bacterial uptake of ofloxacin from (black square) ofloxacin solution, (grey square) C971-ofloxacin hydrogel, (ash square) C934-ofloxacin hydrogel and (white square) C940-ofloxacin hydrogel. (Data adapted from reference [19])

their bioadhesive properties that allow prolonged contact time and the release of an effective amount of drug close to bacterial cells.

References

1. Dobrynin, A., Rubinstein, M.: Theory of polyelectrolytes in solution and at surfaces. *Prog. Polym. Sci.* **30**, 1049–1118 (2005)
2. Jimenez-kairuz, A.F., Ramirez Rigo, M.V., Quinteros, D., Vilches, A., Olivera, M.E., Alovero, F.L., Manzo, R.H.: Recent contributions on drug carrier systems based on polyelectrolytes. Part I: aqueous dispersions. *Rev. Farm. Rev.* **150**, 11–25 (2008)
3. Doi, M., Edwards, S.F.: *The Theory of Polymer Dynamics*. Clarendon Press, Oxford (1989)
4. de Gennes, P.G.: *Scaling Concepts in Polymer Physics*. Cornell University Press, Ithaca, NY (1979)
5. Rubinstein, M., Colby, R.H.: *Polymer Physics*. Oxford University Press, New York (2003)

6. Sedlák, M.: Structure and dynamics of polyelectrolyte solution by light scattering. In: Radeva, T. (ed.) *Physical Chemistry of Polyelectrolytes*, 99. Surfactant Science Series. Marcel Dekker, New York (2001)
7. Sedlák, M.: Mechanical properties and stability of multimaproton domains in polyelectrolyte solutions. *J. Chem. Phys.* **116**(12), 5236–5245 (2002)
8. Oosawa, F.: *Polyelectrolytes*. Marcel Dekker Inc., New York (1997)
9. Rabin, Y., Cohen, J., Priel, Z.: Viscosity of polyelectrolyte solutions—the generalized Fuoss law. *J. Polym. Sci. Part C: Polym. Lett.* **26**, 397–399 (1988). doi:[10.1002/pol.1988.140260904](https://doi.org/10.1002/pol.1988.140260904)
10. Rowe, R.C., Sheskey, P.J., Quinn, M.E. (eds.): *Handbook of Pharmaceutical Excipients*, 6th edn. Pharmaceutical Press and American Pharmacists Association, USA (2003)
11. Jimenez-Kairuz, A., Allemandi, D., Manzo, R.H.: Mechanism of lidocaine release from carbomer-lidocaine hydrogels. *J. Pharm. Sci.* **91**(1), 267–272 (2002)
12. Jimenez-Kairuz, A.F., Allemandi, D.A., Manzo, R.H.: Equilibrium properties and mechanism of kinetic release of metoclopramide from carbomer hydrogels. *Int. J. Pharm.* **250**(1), 129–136 (2003)
13. Vilches, A.P., Jimenez-Kairuz, A., Alovero, F., Olivera, M.E., Allemandi, D.A., Manzo, R.H.: Release kinetics and up-take studies of model fluoroquinolones from carbomer hydrogels. *Int. J. Pharm.* **246**(1–2), 17–24 (2002)
14. Quinteros, D.A., Ramirez Rigo, M.V., Jimenez Kairuz, A.F., Olivera, M.E., Manzo, R.H., Allemandi, D.A.: Interaction between a cationic polymethacrylate (Eudragit E100) and anionic drugs. *Eur. J. Pharm. Sci.* **33**(1), 72–79 (2008)
15. Vilches, A.P.: Polielectrolitos solubles como portadores de fármacos ionizables, preparación y estudio de sus propiedades farmacotécnicas. M. Sc. thesis, Universidad Nacional de Córdoba, Córdoba, Argentina (2003)
16. Jimenez-kairuz, A.F.: Investigación y desarrollo de nuevos materiales con potencial uso en tecnología farmacéutica para diseño de sistemas terapéuticos. Ph. D. thesis, Universidad Nacional de Córdoba, Córdoba, Argentina (2004)
17. Esteban, S.L.: Sistemas Poliméricos Portadores de Macrólidos. Diseño y Evaluación. M. Sc. thesis, Universidad Nacional de Córdoba, Córdoba, Argentina (2007)
18. Quinteros, D.A.: Desarrollo de nuevas estrategias de formulación de fármacos mediante el acomplejamiento con polielectrolitos. Ph. D. thesis, Universidad Nacional de Córdoba, Córdoba, Argentina (2010)
19. Romero, V.L.: Evaluación de los efectos de polímeros aniónicos y catiónicos en el desempeño y la eficacia de agentes antimicrobianos Fluoroquinolónicos. Ph. D. thesis, Universidad Nacional de Córdoba, Córdoba, Argentina (2012)
20. Grant, D.W., Higuchi, T.: Ion Pairs and Solubility Behavior. *Solubility Behavior of Organic Compounds*, XXI. In: *Techniques of Chemistry*. Wiley Interscience, New York (1990)
21. Drifford, M., Delsanti, M.: Polyelectrolyte solutions with multivalent added salts: stability, structure, and dynamics. In: Radeva, T. (ed.) *Physical Chemistry of Polyelectrolytes*, 99. Surfactant Science Series. Marcel Dekker, New York (2001)
22. Porasso, R.D., Benegas, J.C., Van den Hoop, M.A.G.T., Paoletti, S.: Chemical bonding of divalent counterions to linear polyelectrolytes: theoretical treatment within the counterion condensation theory. *Phys. Chem. Chem. Phys.* **3**(6), 1057–1062 (2001)
23. Benegas, J.C., Paoletti, S., Van Den Hoop, M.A.G.T.: Affinity interactions in counterion-polyelectrolyte systems: competition between different counterions. *Macromol. Theory Simul.* **8**(1), 61–64 (1999)
24. Ardusso, M., Manzo, R.H., Jimenez Kairuz, A.F.: Comparative study of three structurally related acid polyelectrolytes as carriers of basic drugs: Carbomer, Eudragit L-100 and S-200. *Supramol. Chem.* **22**, 289–296 (2010)
25. Ardusso, M.: Utilización de materiales portadores polielectrolito-fármaco (PE-F) en el desarrollo de sistemas de liberación de fármacos. Ph. D. thesis, Universidad Nacional de Córdoba, Córdoba, Argentina (2012)

26. Esteban, S., Manzo, R.H., Alovero, F.L.: Azithromycin loaded on hydrogels of carbomer: chemical stability and delivery properties. *Int. J. Pharm.* **366**, 53–57 (2009)
27. Quinteros, D.A., Allemandi, D.A., Manzo, R.H.: Equilibrium and release properties of aqueous dispersions of non-steroidal anti-inflammatory drugs complexed with polyelectrolyte Eudragit E 100. *Sci. Pharm.* **80**(2), 487–496 (2012)
28. Barnes, H.A.: A Handbook of Elementary Rheology. Cambrian Printers, Wales (2000)
29. Graessley, W.W.: Polymeric Liquids and Networks: Dynamics and Rheology. Taylor & Francis Group, New York (2008)
30. Nguyen, Q.D., Boger, D.V.: Measuring the flow properties of yield stress fluids. *Annu. Rev. Fluid Mech.* **24**, 47–88 (1992)
31. Hyuna, K., Wilhelm, M., Kleibn, C.O., Choc, K.S., Namd, J.G., Ahnd, K.H., Leed, S.J., Ewoldse, R.H., McKinley, G.H.: A review of nonlinear oscillatory shear tests: analysis and application of large amplitude oscillatory shear (LAOS). *Prog. Polym. Sci.* **36**, 1697–1753 (2011)
32. Goodrich Company, B.F.: Technical Literature: Carbopol, Noveon, Pemulen Resins Handbook (1995)
33. Al-Malah, K.: Rheological properties of carbomer dispersions. *Ann. Trans. Nord. Rheol. Soc.* **14**, 1–9 (2006)
34. Gutowski, I.: The effect of pH and concentration on the rheology of carbopol gels. M. Sc. thesis, McGill University, Israel (2008)
35. Togrul, H., Arslan, N.: Production of carboxymethyl cellulose form sugar beet pulp cellulose and rheological behavior of carboxymethyl cellulose. *Carbohydr. Polym.* **54**, 73–82 (2003)
36. Khaled, B., Abdelbaki, B.: Rheological and electrokinetic properties of carboxymethylcellulose-water dispersions in the presence of salts. *Int. J. Phys. Sci.* **7**(11), 1790–1798 (2012)
37. Junyi, M., Yanbin, L., Xiangling, Ch., Baotang, Z., Ji, Z.: Flow behavior, thixotropy and dynamical viscoelasticity of sodium alginate aqueous solutions. *Food Hydrocolloids* **38**, 119–128 (2014)
38. Funami, T., Fang, Y., Noda, S., Ishihara, S., Nakauma, M., Draget, K., Nishinari, K., Phillips, G.: Rheological properties of sodium alginate in an aqueous system during gelation in relation to supermolecular structures and Ca^{2+} binding. *Food Hydrocolloids* **23**, 1746–1755 (2009)
39. Krause, W., Bellomo, E., Colby, R.: Rheology of sodium hyaluronate under physiological conditions. *Biomacromolecules* **2**, 65–69 (2001)
40. Rinaudo, M.: Rheological investigation on hyaluronan-fibrinogen interaction. *Int. J. Biol. Macromol.* **43**, 444–450 (2008)
41. Battistini, F.D., Olivera, M.E., Manzo, R.H.: Pharmacotherapeutic potential of ionic complexes Hyaluronan-Drug. Personal communication. 3rd Argentine Symposium of Nanomedicine. Buenos Aires, Argentina (2013)
42. Ramírez Rigo, M.V.: Preparación y estudio de sistemas portadores de fármacos. Ph. D. thesis, Universidad Nacional de Córdoba, Córdoba, Argentina (2006)
43. Kumar, S., Himmelstein, K.J.: Modification of in situ gelling behavior of carbopol solution by hydroxypropyl methylcellulose. *J. Pharm. Sci.* **84**(3), 344–348 (1995)
44. Barry, B.W., Meyer, M.C.: The rheological properties of carbopol gels I. Continuos shear and creep properties of carbopol gels. *Int. J. Pharm.* **2**, 1–25 (1979)
45. Jimenez-Kairuz, A.F., Llabot, J.M., Allemandi, D.A., Manzo, R.H.: Swellable drug-polyelectrolyte matrices (SDPM): characterization and delivery properties. *Int. J. Pharm.* **288**(1), 87–99 (2005)
46. Ramírez Rigo, M.V., Allemandi, D.A., Manzo, R.H.: Swellable drug-polyelectrolyte matrices (SDPM) of alginic acid: characterization and delivery properties. *Int. J. Pharm.* **322**, 36–43 (2006)
47. Ramírez Rigo, M.V., Allemandi, D.A., Manzo, R.H.: Swellable drug-polyelectrolyte matrices of drug-carboxymethylcellulose complexes. Characterization and delivery properties. *Drug Delivery* **16**(2), 108–115 (2009)

48. Caramella, C.M., Rossi, S., Bonferoni, M.C.: A rheological approach to explain the mucoadhesive behavior of polymer hydrogels. In: Mathiowitz, E., Chickering III, D., Lehr, C.-M. (eds.) *Bioadhesive Drug Delivery Systems*, pp. 25–65. Marcel Dekker Inc., New York (1999)
49. Tamburic, S., Craig, D.Q.: The effects of ageing on the rheological, dielectric and mucoadhesive properties of poly(acrylic acid) gel systems. *Pharm. Res.* **13**(2), 279–283 (1996)
50. Romero, V., Manzo, R., Alovero, F.: Enhanced bacterial uptake and bactericidal properties of ofloxacin loaded on bioadhesive hydrogels against *Pseudomonas aeruginosa*. *J. Chemother.* **22**, 328–334 (2010)

Complexes Formation Between Proteins and Polyelectrolytes and Their Application in the Downstream Processes of Enzyme Purification

Ph Guillermo Alfredo Picó and Bc Nadia Woitovich Valetti

Abstract Natural and synthetic polyelectrolytes have acquired notable importance in recent years due to their increasing application in different areas. One of these is downstream process methods which include the recovery, separation, concentration and purification of target enzymes from their natural sources. Polyelectrolytes interact with proteins to form soluble or non-soluble complexes. The interaction is driven by experimental variables of media such as pH, protein isoelectrical value, polyelectrolyte pK_a, ionic strength and the presence of salts. The concentration of polyelectrolytes necessary to precipitate a protein completely is of the order of 10⁻⁴ – 10⁻² % p/v. Precipitation of protein by PE is a novel technique integrating clarification, concentration and initial purification in a single step. This chapter presents some properties of aqueous solutions of natural and synthetic PE as a tool to use them in the protein downstream process.

Abbreviations

PE	Polyelectrolytes
PEC	Polyelectrolytes complex
PE-P	Polyelectrolytes-protein complexes
CAT	Catalase
Eu	Eudragit
PAA	Poly (acrylic acid)
PVS	Poly (vinylsulfonic acid)
Chy	Chymotrypsin
PEI	Polyethylenimine

Ph G.A. Picó (✉)

National Scientific and Technical Research Council, Buenos Aires, Argentina
e-mail: gpico@fbioyf.unr.edu.ar; pico@inv.rosario-conicet.gov.ar

Ph G.A. Picó · Bc N. Woitovich Valetti

Biotechnological Process Laboratory, Faculty of Biochemical and Pharmaceutical Sciences,
National University of Rosario, S2002RLK Rosario, Argentina
e-mail: nwoitovich@fbioyf.unr.edu.ar

1 Introduction: Polyelectrolytes Applications in Biotechnological Processes

The increasing number of articles on polyelectrolytes (PE) reflects the growing scientific and industrial interest in this family of substances [1–5]. Many industries such as food, medicine and pharmaceutical use PE to manufacture products used in everyday life. Initially, a small number of PE were used, and most of them were obtained from industrial processes. However, the most popular was a natural chemical modified derivative, carboxymethyl cellulose, used for the first time in a solid form as support or drug stabilizer.

In the last 20 years, the number of natural and synthetic PE used in different areas has dramatically increased. Nowadays, the interest is centered in PE obtained from natural polymers which have been chemically modified favoring an increase in their solubility in aqueous media [6]. At present, there are many natural PE, whose use is allowed by the food codex as food additives, for skin products, as drugs carriers and for controlled drug delivery, etc. These products are environmentally friendly, so they can be disposed without producing a negative impact. The list below details different applications of PE:

Uses and Applications of Polyelectrolytes:

1. Enzyme immobilization for bioreactor catalysis [7].
2. Enzyme- PE non-soluble complexes: enzymes isolation by precipitation [8].
3. Enzyme-PE soluble complexes: enzymes stabilization [9].
4. Inclusion of drugs and enzymes in non-soluble PE matrices for controlled drug delivery systems [10].
5. Non-soluble matrices with a controlled size of particles for expanded bed chromatography [11].
6. Bioremediation of waste water containing heavy metals such as: Pb^{++} , Cr^{+++} by non-soluble complex formation with a PE of opposite electrical charge [12].
7. To build selective electrodes [13].
8. Health and personal care products: viscosity enhancers for shampoos, deodorants and body lotions [6].
9. Foods and food industry: as clarification agent of wine, juice and beer [6]; besides as gelling, thickening and stabilizing agents [14].
10. Paper industry: as retention aids as well as flocculating agent [15].

This chapter presents some properties of aqueous solutions of natural and synthetic PE as a tool to use them in the protein downstream process.

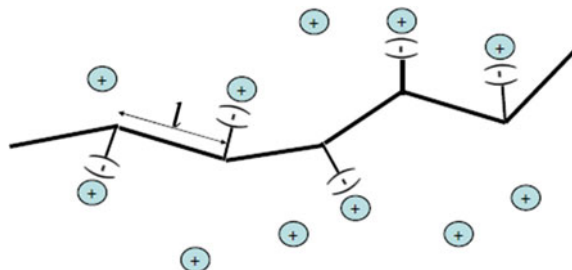


Fig. 1 Diagram of a flexible chain PE which shows the charged groups and interacting ions of opposite charge

2 Aqueous Solutions of Polyelectrolytes: Behavior and Properties

2.1 Electrostatic Properties

The study of electrostatic properties is important as it will help us to characterize the conformation of polymers at various experimental conditions (pH, ionic force, temperature) [16].

According to the theories of PE [17–19], a charged macromolecule is characterized by the charge density parameter (ξ), defined by:

$$\xi = \frac{e^2}{l \cdot D \cdot k \cdot T} \quad (1)$$

In this expression, e is the charge of the electron, D the dielectric constant, l the average distance between charges along the polymer chain (Fig. 1) and kT the Boltzmann term.

Another important parameter is the charge parameter (λ) [16], which is proportional to the linear charge density and depends on the chemical composition of the polymer and the length of the chain. This parameter is proportional to ξ , according to the equation:

$$\lambda = \frac{v \cdot e^2}{h \cdot D \cdot k \cdot T} = \frac{v \cdot l}{h} \xi \quad (2)$$

where v is the number of ionic sites and h the PE chain length.

For weak PE, λ varies with the degree of ionization of the ionizable groups which depends on pH, PE concentration and ionic strength of the medium. The ionic sites may be: $-\text{COO}^-$ (in pectins, alginates or hyaluronan), NH_3^+ (for chitosan in acidic medium), SO_3^- (carrageenan). In the cases of polyelectrolytes with $-\text{COO}^-$ and NH_3^+ groups, the net charge will strongly depend on the medium pH, which is related to the dissociation equilibrium.

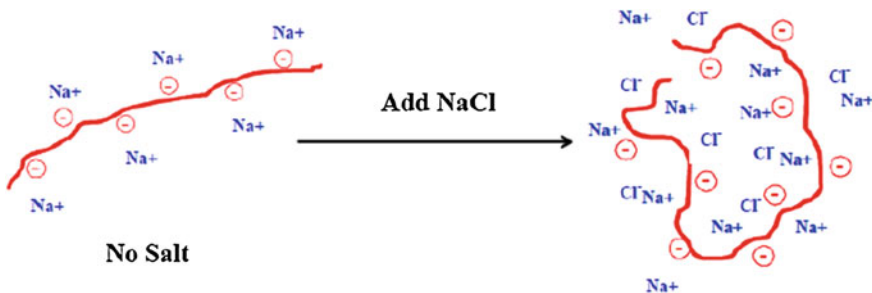


Fig. 2 The effect of salt presence on the flexible chain conformation of a PE in aqueous medium

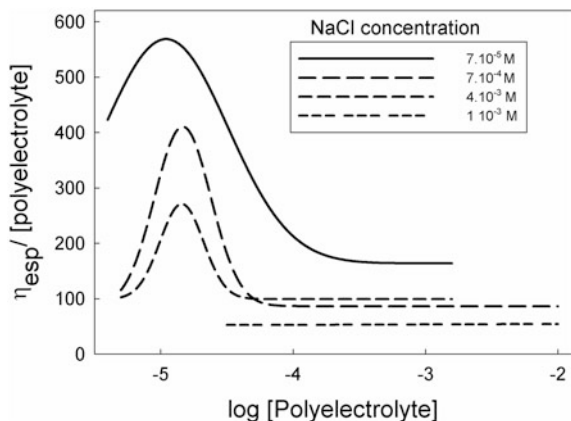
Among the factors influencing the charge parameter, we can highlight the effect of the presence of salts. Figure 2 shows salt effect on the shape of the PE molecule. It has been experimentally observed that small ions are capable of promoting compaction of flexible PE chains [20]. It is observed that longer chains tend to achieve relatively more compact conformations than shorter ones, and the dimensions of the collapsed structures do not significantly vary with contour length. The influence of contour length and intrinsic stiffness in the process of ion condensation is studied by analysis of the ion-ion nearest-neighbor distribution. The general trend is an increase in the degree of ion condensation as the chain length increases, in accordance with experimental evidence. A decreased importance of end-effects and, especially, larger volume charge densities are responsible for such behavior. The influence of chain stiffness depends on salt concentration, pH, PE concentration, etc. [16].

In the case of PE, another important parameter is the hydrodynamic volume, which depends on the molecular weight and the number and distribution of ionic groups in the polymer chain. The ionic groups can cause repulsion between the chains, which leads to an expansion of the molecule and, consequently, to an increase in solution viscosity. This behavior has been traditionally explained in terms of chain extension of the PE [21]. By decreasing the concentration of the PE, the degree of ionization increases. In dilute solutions, the ionic atmosphere is larger than the molecular diameter of the charged groups and they repel each other, increasing the rigidity of the chain and expanding the polymer with a consequent increase in viscosity. Such situation can be seen in Fig. 3.

2.2 The pH Effect on the Polyelectrolyte Solubility

PE have a high number of polar and electrically charged groups with capacity to interact with water molecules by water dipole–dipole and water dipole-charge interactions. So, they are soluble in water at high concentrations. However, in the case of PE which possesses groups capable of losing protons, solubility depends on

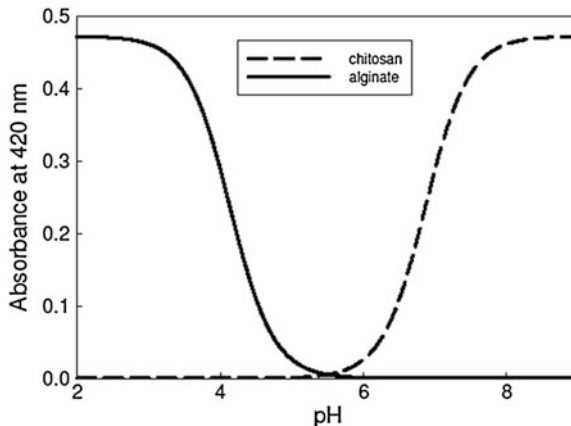
Fig. 3 Reduced viscosity versus the log of PE concentration in presence of increasing NaCl concentration



the pH of the medium and the type of charged groups. Thus, if sulphonate groups are present, as they have lost their proton around pH 0.5–1.0 at pH values above 1.5 the PE has a net electrical charge and will be soluble. On the other hand, in the presence of chemical groups such as carboxylic or amine, which tend to lose a proton at a given pH, the PE will be soluble only when the groups have a net electrical charge because the charges will repel each other favoring the interaction with the solvent molecules [22]. PE with carboxylic groups, at a pH where all they are protonated, as in the case of at pH below 4, there is no repulsion between the PE chains, which favours the interaction between them, so an aggregation process results decreasing the PE solubility.

Figure 4 shows a simulated acid-base titration curve for two natural PE: chitosan and alginate. It can be seen that in the case of alginate (an acid PE), turbidity starts to increase at pH below 4.0 [23]. In this area of acidic pH, the carboxylic groups of the PE molecule are protonated, which decreases PE

Fig. 4 Acid-base turbidimetric titration curves for chitosan and alginate in aqueous medium. The curves are expressed as turbidity at 420 nm versus pH



solubility. In the case of chitosan (a basic PE), it is non-soluble above pH 7.0, because the amino groups are non-protonated, increasing the attraction between the chain (Fig. 4) [22].

2.3 The Difference Between pK , pK_o and pH_{50}

Weak acid and basic groups present in PE can be titrated with strong basic or acid solutions so; the pK value can be calculated from the titration curve [16]. This experimental pK value is an apparent value because it depends on experimental variables such as ionic strength, dielectric constant of the solvent and the presence of cosolutes which modifies the structure of the water solvent. The pK_o value (the true dissociation equilibrium constant of the acid and basic groups) depends on the PE concentration and especially on the interaction between the PE chains. These interactions are time-varying, so the pK_o value is not constant over a period of time [24]. The pK_o value is determined by extrapolation of the experimental pK value at ionic strength zero and at PE concentration in infinite dilution [16]. This value is not the true microscopic value of the i-ésim acid or basic group and should be considered as a mean pK_o value of all the acid or base groups present per PE molecule.

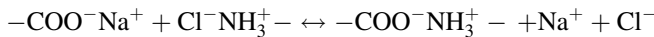
The pH solubility effect is easily followed by turbidimetry measurements, as shows in Fig. 4. From the experimental data, the pH_{50} can be calculated as the pH value where half of the PE is in solution with net electrical charge and the other half is non-soluble under neutral form. The question is if the pK of a PE determined from the acid-base titration has the same significance as pH_{50} . At first glance, it seems that both values match, because they come from an acid–base titration and they represent the same chemical process of gain or loss of a proton.

When a PE loses protons during acid–base titration, the environment of its acid or basic groups changes because they partially lose contact with the solvent molecules, so the pH_{50} will be a mean of all pK of the acid or basic groups. Then pH_{50} is a macroscopic variable and only represents the overall process of loss of solubility by the effect of pH. However, pH_{50} is an important value that allows us analyze the variation of experimental variables (ionic strength, presence of salts modifying the structure of the solvent, etc.), on PE solubility.

2.4 Polyelectrolytes–Polyelectrolytes Interaction in Dilute Aqueous Solution

Polyelectrolyte complexes (PEC) are formed by interactions between macromolecules that carry oppositely charged ionizable groups [30]. The gain in entropy of the system due to the release of counterions and water molecules is the main driving force for the PEC formation [1].

When an anionic polymer, such as alginate, is mixed with a cationic polymer (like chitosan in acidic condition), an electrostatic complex is formed whose stability depends on the pH and salt concentration. The mechanism of complex formation can be expressed by the following equilibrium [25]:



Generally, PEC are formed by electrostatic interactions between the PE chains, but Van der Waals forces, hydrogen bonds and hydrophobic interactions may also be present [23].

There are 3 models of PEC formation:

- The interaction may be stoichiometric and ordered (1:1 ratio of charges). The complex thus formed is, in most cases, neutral.
- It may be stoichiometric and disordered, leading to structures of various shapes.
- It may be non-stoichiometric, where PE interacts in different ratios to 1:1.

It is known that the stoichiometry of both components in the PEC obtained depends on the type of PE used, charge density and any environmental conditions which affect the charge state of PE such as pH values of the media, ionic strength, concentration and sometimes the order of mixing [26, 27]. Therefore, depending of such conditions, the same PE set can form PEC of different shapes and stoichiometries [28].

Over the last years, there has been a growing interest in PECs based on natural and synthetic polymers. Chitosan is a natural polyaminosaccharide and a weak base. Its PECs with different natural and synthetic polyacids such as, carboxymethylcellulose [29, 30], alginic acid [23], poly (acrylic acid) [31] are known. Besides alginate, carboxymethylcellulose, carrageenan, and dextran sulfate are the most extensively studied polysaccharides used in the formation of polyelectrolyte complexes [32, 33]. Some synthetic polyelectrolytes, like poly(l-lysine) and polyacrylates, have been used to make complexes with these polysaccharides [34]. In the above mentioned literature one can find different examples of PEC as well as various methods of forming them.

PEC have many applications in different fields [35]. They have been proposed for the design of drug delivery systems [35, 36], protein separation [37], anticoagulant coatings, and membranes for separating materials or even as skin substitutes, among other applications. Recently, the use of natural polymers for encapsulation of drugs, proteins, and viable cells has received much attention because of their biocompatibility. In some applications, the polymer matrix has been coated with another polymer to control the release of encapsulated material. The success of the coatings is largely attributed to the coulombic interactions between the PE. This property has been used as an entrapment matrix for cells and enzymes as well as for pharmaceuticals and food adjuvant.

3 The Formation of Complexes Between Polyelectrolytes and Proteins

PE are known to strongly interact with proteins of opposite charge to form soluble and non-soluble complexes according to the experimental conditions of the medium [5, 38]. By changing these conditions, such as pH or ionic strength, the protein can be released, keeping its secondary and tertiary structure as well as its biological activity. When the complexation yields insoluble products, this interaction can be employed for protein separation [8, 39, 40].

Precipitation with PE requires inexpensive chemicals in small amounts, only the amount of PE required to neutralize the protein charge. Thus, the method is suitable for large-scale processing and for dealing with dilute solutions. A variety of PE have been tried out, but the same cannot be said of polyampholytes, which are PE capable of acquiring both positive and negative charges.

The interaction between proteins and synthetic polymers has been extensively studied, in particular for the modulation of living processes, immobilization or stabilization of enzymes, modification of substrate affinity, changing properties of food products, and for the development of many pharmaceutical applications [5, 41–43]. Precipitation finds a place in most protein purification protocols and has traditionally been applied as a simple and rapid technique to protein concentration at the beginning of downstream processing [39, 40, 44–46].

A wide variety of synthetic and natural PE can interact with globular proteins to form stable protein–polyelectrolyte complexes (PE-P) that result in the formation of soluble or non-soluble complexes [5, 47]. The non-soluble complex can be easily separated by centrifugation or simple decantation. Precipitation as a concentration step offers several advantages in that it is easy to scale up, uses simple equipment and can be based on a large variety of alternative precipitants. When PE-P is specifically formed with one of the proteins in the crude extract followed by a phase separation, the process could be used as a convenient strategy for the isolation and purification of the target protein [8].

3.1 Theory of the Polyelectrolyte—Protein Complex Formation

3.1.1 Participation of Intermolecular Forces in PE-P Formation

The forces which contribute to complex formation between PE and proteins are mainly coulombic: ion–ion, ion–dipole and dipole–dipole interaction. It has been reported that the interaction between proteins and non electrical charged polymers like the polyethylene glycol family involves very weak interaction forces of the type Van der Waals, judging by the low interaction heat involucrated in the interaction [5]. Picó et al. [48] found enthalpic changes associated to the

interaction of polyethyleneglycol and polyethylene polypropylene oxide with lysozime and ovoalbumin in the order of 1 kcal, which suggests a poor interaction. However, scene changes in a dramatic manner for the interaction between a protein and a PE due to the presence of hundreds electrical charge groups per PE molecule, being the interaction between them clearly coulombic.

All PE have a hydrophobic chain in their structure, which makes the total absence of hydrophobic interactions in PE-P complexes difficult to deny. The strongest evidence for hydrophobic interactions arises from the effects of systematic structural variations, or from thermodynamic data that exhibit the temperature dependence of the entropy and enthalpy associated to the PE-P formation [5]. The predominance of electrostatic interactions is widely accepted but there are several points of discussion about the presence of other type of intermolecular forces that participate in the PE interaction with a protein, as following:

- (a) *The effect of ionic strength of the medium:* The PE-P complex formation is driven by three variables: the protein surface electrical charge density (σ), PE linear electrical charge density (ξ), and ionic strength (I) of the medium, typically included in the Debye–Hückel parameter (κ). An important consequence of this theory is the finding of a transition from a bound to an unbound state with a change in any of those three variables, so that the critical conditions for binding at constant temperature could be expressed as [49]:

$$\sigma = \frac{cte \cdot \kappa}{\xi} \quad ; \quad \kappa \propto I^{1/2} \quad (3)$$

Figure 5 shows a typical turbidimetric titration curves of the enzyme catalase (CAT) with two cationic PEs: chitosan and Eudragit E 100 (EuE), (a cationic polyelectrolyte derived from the poly (acrylic acid)) (Fig. 5 inset) [50]. It can be seen in both cases that the increasing concentration of NaCl induces a significant decrease in the complex formation. However, at high salt concentration, about 25 % of the complex with EuE remained and chitosan showed a similar behavior. These results suggest the presence of a columbic component in the formation of these complexes which is destroyed by the increasing of the ionic strength; however, a fraction of PE-P is not affected by high salt concentration, which suggests the presence of a non-columbic component. Similar finding have been reported for other PE-P [8, 38, 51].

- (b) *Heat involved in the PE-P formation:* Isothermal titration calorimetry (ITC) is a perfect method to measure the true heat involved in a PE-P formation and it is obtained by titrating the protein with a PE. This methodology requires small amounts of solution volume and allows determining the stoichiometry of the reaction in the form of protein molecules bound per PE molecule, the affinity constant of interaction (K) and the values of the thermodynamic variables associated with complex formation: enthalpy and the entropic

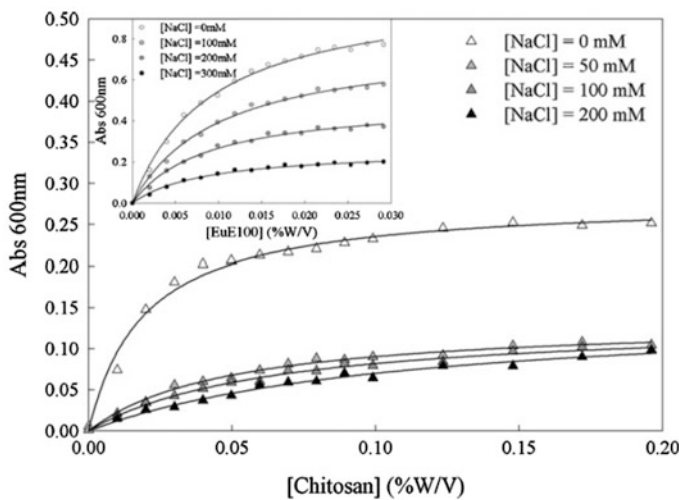


Fig. 5 Turbidimetric titration curve of CAT with chitosan and EuE (inset) at increasing ionic strength given by NaCl

change can be easily determined. This method gives information about the molecular mechanics of interaction.

McClements et al. [52] studied the influence of pH on the enthalpy changes associated with the β -lactoalbumin—sodium alginate interaction at different pHs. The heat involved in the interaction between PE and this protein was found to be highly dependent on the pH of the medium. At pH 3, a relatively high exothermic enthalpy change was observed for the interaction while at pH 4 a high exothermic enthalpy change was observed, both results suggests the presence of coulombic interaction in the PE-P formation. However, at pH 5, a relatively high endothermic enthalpic change was observed while at pH 6 and 7 the observed enthalpic change was relatively small throughout the entire range of sodium alginate concentrations studied. The isoelectric point of the β -lactoalbumin is around pH 4.8, so that the electrical charge of β -lactoalbumin changed from positive to negative as the pH increased from 3 to 7. The sodium alginate was negative at all pH values, but was appreciably lower in magnitude at pH below 4.0 due to partial protonation of carboxyl groups (pK_a 3.5). Taking this into account, we can see that at a pH above 5.0 the protein and the polymer are negatively charged, however, an interaction between them can be observed. This is accomplished at pH 6.0 and 7.0 where the heat involved is nearly zero, suggesting the absence of a electrostatic interaction. However, at pH 5.0 the heat involved was positive, and this is an interesting fact because, under this condition, no interaction between both particles is expected. The positive enthalpic change is suggesting the presence of other non-electrostatic forces present in the complex formation.

Table 1 Thermodynamic function values associated to the Eu-Chy complex formation

	Chy-EuL	Chy-EuS
ΔH (kcal/mol of Chy)	0.34 ± 0.04	≈ 0
ΔS (cal/grade mol of Chy)	21.1 ± 0.1	27.6 ± 0.2
K (M^{-1})	$(2.1 \pm 0.1) 10^4$	$9.9 \pm 0.9 10^5$
N (mol Chy/mol Eu)	60 ± 2	33 ± 1
Number of charged monomers per Eu molecule	800	500

Medium buffer phosphate 50 mM pH 7.00

Romanini et al. [53] using ITC studied the interaction of lysozyme with two anionic PE: poly (acrylic acid) (PAA) and poly (vinylsulfonic acid) (PVS). The results were obtained at pH 5.5, region in which the PVS will be fully ionized while in PAA only the 90 % of the carboxylic groups are dissociated. They found negative and high heat associated with the protein-polymer interaction expected for interactions of electrostatic nature. Besides, the larger negative enthalpic change value observed for the lisozyme -PVS complex is consistent with a greater interaction between them due to the higher number of negatively charged present in this PE.

Picó et al. [54] using ITC, measured the heat associated to the chymotrypsin (Chy)—Eu interaction at neutral pH as shown Table 1. Positive changes in the enthalpic and entropic values were associated to both interactions, which suggest the participation in a major grade of a non—coulombic component in the complex formation. The positive enthalpic change is the total resulting change which include an enthalpic change due to the coulombic interaction, because the PE and the enzyme at pH 7.00 have appositive electrical charge and other enthalpic change due to the lost of ordered water molecules around the PE hydrophobic chains when the Chy molecules are bound to the PE. This enthalpic change is of high value, so the resulting ΔH of the interaction is endothermic. A similar explain can be do for the entropic change, which is positive in value due to the great number of water molecules those are lost during the complexation process.

- (c) *PE effect on the tertiary and secondary structure and the biological activity of the enzymes:* It is well documented that the presence of a PE should produce a modification in the biological activity of an enzyme due to a change induced by PE on the secondary and tertiary structure [55]. This may be caused by interaction due to either the electrostatic forces or the hydrophobic effect involved in the complex formation. Consequently, PE can break interactions between groups inside the protein necessary to remain its structure or the PE may interfere with the active site of the enzyme. So, it is necessary to assay the behavior of PE on the target enzyme. The recommended studies are:

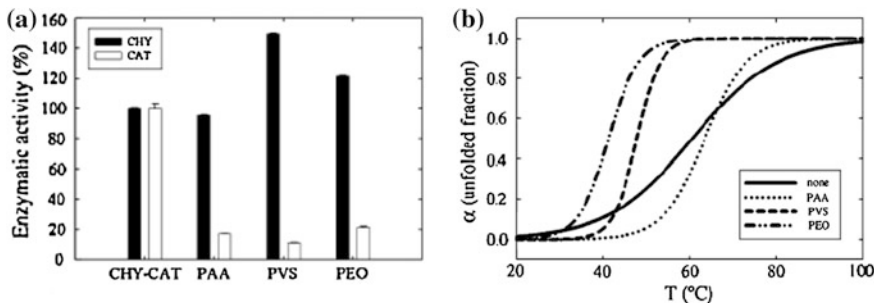


Fig. 6 (a) Biological activity for the enzymes Chy and CAT in the presence of different polymers: PAA and PVS. The enzyme activities have been expressed according to a control in the absence of polymer as 100 % of activity. (b) Unfolding fraction of enzyme CAT and Chy versus the temperature in the absence and presence of polymer

- Biological activity of the enzyme in the absence and presence of PE increasing concentration.
- Circular dichroism spectra of the enzyme in the absence and presence of PE increasing concentration. This technique is very useful because it shows modifications in the secondary and tertiary structure of the protein PE induced.
- Enzyme thermal stability in the PE presence. This technique allows us to know the melting temperature of a macromolecule (T_m), the temperature where 50 % is in native form and 50 % is in its denatured form. Also, the enthalpy and entropic changes of the denaturalization process can be calculated in this way. The information given by this technique is useful in the sense that it allows us to determine whether the PE presence increases or decreases the thermal stability of an enzyme [38].

Picó et al. [56] studied the complex formation between Chy and CAT with different PE as shown in Fig. 6a. It can be seen that for Chy the presence of the polymers did not modify the enzyme activity with respect to the control in the absence of polymer, except for PVS, which induced a significant increase in the enzyme activity, showing a stabilizing effect on this protein. An opposite effect was observed for CAT: all the polymers decreased the enzyme activity of this protein significantly, suggesting a modification of the tertiary structure in the catalytic site. Figure 6b shows the thermal denaturalization shape of CAT in the absence and presence of PVS and PAA. It can be seen that PAA increased the T_m of the enzyme significantly, contributing to increase its resistance to the temperature attack, while PVS induced a decrease in the T_m value in the order of 13 $^{\circ}$ C.

The conclusion is that PAA form a more thermodynamical stable complex with Chy than the enzyme alone does, so if Chy is isolated from its natural source by non-soluble complex formation, PAA is the most appropriate PE to be used in the process.

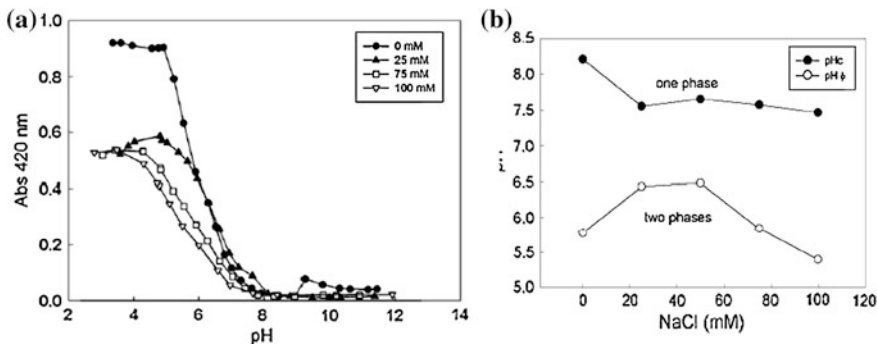


Fig. 7 **a** Acid-base turbidimetric titration curve of chy in the presence of carrageenan at different ionic strengths. **b** pH_c and pH_ϕ versus the ionic strength of the medium. The data were taken from Fig. 7a

3.1.2 Influence of pH in the PE-P Formation

It has been reported [57, 58] that the formation of soluble PE-P complexes is initiated at a specific pH called the critical pH (pH_c), which is a function of ionic strength, the protein isoelectric point, and the PE density charge [59]. For polycations, pH_c preceded the pH of visual phase separation, named pH_ϕ . This parameter is defined as the pH at which the half maximal value of turbidity is achieved. Since these non-soluble complexes can be considered a phase separation, the ionic strength dependences of both pH_c and pH_ϕ , can be viewed as phase boundaries. The phenomenon has been ascribed to the attraction between PE charges and oppositely charged “patches” on the protein surface [5]. This could be applied to complexation between oppositely charged proteins and PE.

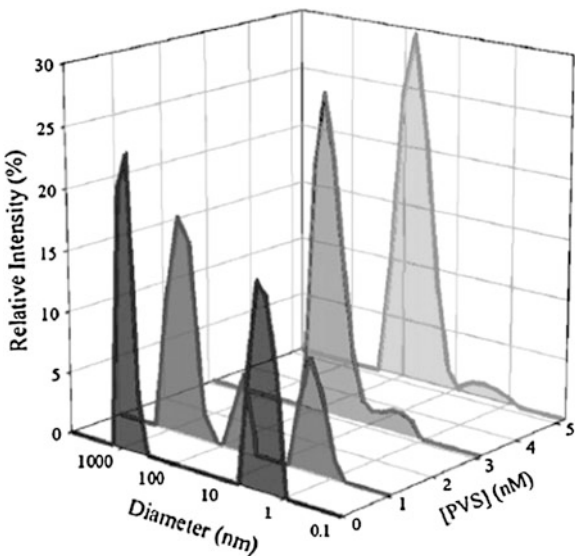
Figure 7a shows a acid-base turbidimetric titration curve for the PE carrageenan and Chy (a basic protein) in the presence of different NaCl concentrations [38]. The pH_c was calculated as the intersection of the tangent at the inflection point with the plateau of the plot while the pH_ϕ was obtained by fitting the data to a 4-parameter sigmoid function.

Figure 7b shows the experimental values obtained for pH_c and pH_ϕ . It can be seen that the increase in the salt concentration does not influence the pH_c values, which suggests that the zeta potential of the protein is not influenced by ionic strength in this zone. However, the pH_ϕ value decreases with the ionic strength, suggesting that the presence of salt affects the amount of complex formed.

3.1.3 The Size of the PE-P

It was found that under certain experimental conditions, the complex formed is not big enough to induce the formation of a new solid phase, so no turbidity can be

Fig. 8 Results from the light scattering intensities and size for chy in solution in the absence and presence of increasing concentration of PVS. Temperature 25 °C. Medium 50 mM citrate buffer



observed in the medium [60]. Such is the case of the interaction between Chy and PVS: in given conditions the interaction between them forms complex which can only be detected by light scattering measurements such as shown in Fig. 8.

Three varieties of particles with different sizes were observed in the Chy–PVS mixtures. The size of the small particles was similar to that of the free enzyme and independent of the concentration of PE and protein. Therefore, we may assign this particle to uncomplexed Chy. The increase in PVS concentration induced a decrease in the largest particle population, which corresponds to the aggregated enzyme, while an increase in the intermediate population suggests that it corresponds to the PE-P soluble complex formation.

Picó et al. [61] studied the formation of soluble complexes between Chy and Eu L100 and S100 (two anionic PE) using dynamic light scattering in the pH range from 6.80 to 8.50. The hydrodynamic radii (R_h) of the formed complex were determined as shown in Table 2.

Table 2 Hydrodynamic radii (R_h) of EuL and EuS and of the soluble complexes they form with Chy at different pH values

	R_h EuL (nm)	R_h EuS (nm)
Eu	85 ± 5	57 ± 3
Eu + Chy (pH 6.80)	48 ± 4	51 ± 4
Eu + Chy (pH 7.20)	53 ± 3	70 ± 4
Eu + Chy (pH 7.90)	66 ± 4	65 ± 5
Eu + Chy (pH 8.50)	61 ± 4	80 ± 10

Polymer concentration: 0.005 % (w/v), Chy 1 mg/mL

No changes in the R_h of each Eu were observed when varying the pH value in that range. This is expected since the electric charge of both Eu does not change within the assayed pH range because the pH is far from the pKa of the COOH groups and the behavior and conformation of these polymers in solution is highly dependent on the electrical charge density. Both polymers have the same molecular mass value; however, the R_h of EuL was higher than that of EuS, as shown in Table 2. This difference can be explained taking into account the difference in the number of electrically charged monomers in both PE. In the molecule of EuL, the electrical charge density is higher than in EuS [62]. This may induce a higher repulsion in the backbone, explaining the more extended conformation in the case of EuL.

When the size of the Chy-Eu soluble complexes was determined, the profile of the scattered light was altered by the pH and the presence of Chy (Table 2). In the case of EuL, the R_h significantly decreased in the presence of Chy. The same effect was observed in all the ranges: Chy-EuL complexes have a smaller size than free EuL. The interaction of EuS with Chy induces a decrease in the size of EuS at pH 6.80. However, the Chy-EuS complex size was always larger than the size of free EuS between pH 7.20 and 8.50. As the conformation of free EuS is compact, the binding of Chy to EuS requires the opening of the EuS chain to allow the Chy to interact with it.

A main effect takes part in the Eu-Chy complex conformation: the neutralization of a significant number of negative electrical charges of Eu molecule by Chy. However, Chy is a basic protein and carries positive electrical charge in the pH range assayed, (the charge of Chy varies from approximately +4 at pH 6.80 to +1 at pH 8.50) and the enzyme becomes less efficient in neutralizing the Eu negative electrical charges when the pH is increased.

Both Eu have identical vertebral chain, the difference lies in the ratio of the free COOH groups to the ester groups which is approximately 1:1 in EuL and 1:2 in EuS. The higher number of COOH groups present in the molecule of EuL, which gives it a greater electric charge density, implies a greater capacity of this Eu to bind Chy. This binding produces a loss of negative electrical charge of EuL, diminishing the repulsion in the EuL chain. This is reflected in a more compact structure of the Chy-EuL complex.

In EuS, COOH groups are widely separated in the chain. Their molecules acquire a more compact spatial disposition. In this case, the effect of the Chy-EuS interaction is to increase the volume of the complex when Chy molecules are bound to the EuS chain. The opening of the structure is more significant than the decrease of the volume due to the decrease in the repulsion between the hydrocarbon chains of EuS.

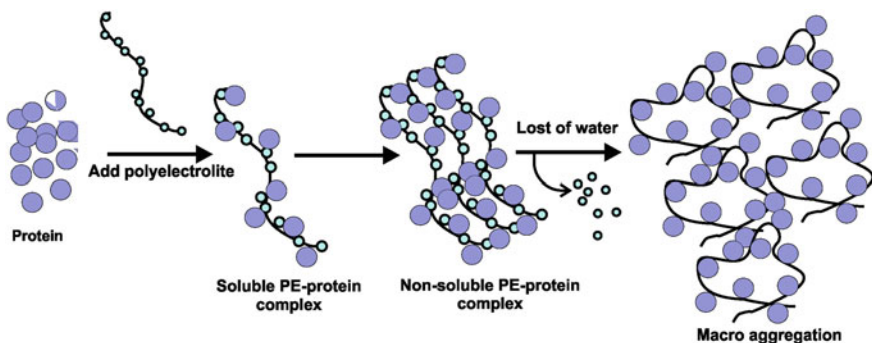


Fig. 9 Sequence of PE-P formation, showing the different steps, in agreement with Dubin et al. [63] and Picó et al. [38, 60] proposed molecular mechanism

3.2 The Molecular Mechanism of PE-P Formation

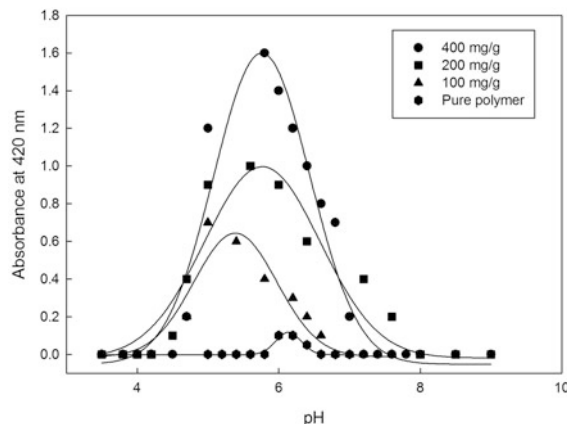
Previous studies of Dubin et al. [63] have demonstrated that the PE-protein interaction occur in two steps; however, recent reports from Picó group [38, 60] showed the presence of a third step where the particles of non-soluble complexes interact between them.

Figure 9 shows the steps in PE-P formation. In the first step, an interaction is carried out between the free electrical charge of PE and the opposite electrical charge of the protein. The complex formed involves the interaction between one PE molecule and several ones, in some cases even hundreds of protein molecules. According to the pH and ionic strength of the medium, this complex could be soluble; the formation of the soluble complex can be followed by light scattering measurements. In a second step, an interaction is produced between the soluble complex particles, so, a non-soluble complex (of high molecular mass) is produced, and this is evidenced as a precipitate. This second step is easily followed by turbidimetry (measuring the absorbance of the medium at 420 nm). Finally, the non-soluble particles interact between them to form a macro-aggregate state.

3.3 The Protein-Polyampholyte Complex Formation

One interesting option is the interaction of polyampholytes with proteins; this system has been studied by several authors [64, 65]. Polyampholytes are exclusively from the industrial synthesis, they are derivatives of the polymethacrylates such as: (a) block polyampholytes with block sequences (dimethylamino) ethyl methacrylate (cationic residue), methyl methacrylate (neutral, hydrophobic residue), and methacrylic acid (anionic residue) and (b) random polyampholytes of (dimethylamino) ethyl methacrylate, methyl methacrylate, and acrylic acid have

Fig. 10 Turbidity-pH profiles for random polyampholyte-protein mixtures at different ratios



been studied by turbidimetric titration. It may be possible to manipulate their dual electrostatic nature as well as their hydrophobic character to achieve different interactions with proteins.

As the polyampholytes have in their molecule both acidic and basic groups, their solubility is highly dependent of the medium pH. Polyampholytes form complexes with proteins, according their electrical charge. Figure 10 represents simulated turbidimetric acid-base titration curves of an polyampholyte in the absence and presence of a basic protein of pI 10. The pure polymer self-aggregates around its isoelectric point (around 6.5) for a range of pH's; its solubility increases with pH on either side of the pI because has a net charge in this zone. In the protein presence, the critical pH of the polyampholyte-protein mixture (the pH values were the complex begin to precipitate) were found to be lower than that of pure polyampholyte (4.7). In other words, the critical pHs and the pI of polyampholyte shifts to the left. One reason might be the interaction between the electrical charged group of the polymer and the protein which induces an important modification in the micro dielectric constant environment where the prototropic groups are, this result in a modification of the pK of the COOH or NH₃⁺ groups. Similar finding has been reported by Boeris et al. [50] for the interaction of chitosan with CAT, where the presence of the enzyme induces a modification of the pK₅₀ of this PE.

Other interesting option is the formation of the so called pseudo-polyampholytes, in this case a PE interacts with a ion of low molecular mass of opposite electrical charge producing a non-soluble complex, the particles formed have net electrical charge, the isoelectrical pH value of these depends on the type of the small ion [66].

Polyethyleneimine (PEI) is a positively charged polyelectrolyte with a pKa of 9.7, with the structural formula (-CH₂-NH-CH₂-)_n. In the presence of citrate or phosphate PEI has been found to form an insoluble complex in the pH interval between 3.5 and 7 or 8, where it behaves as an amphotyte. Figure 11 (a and b)

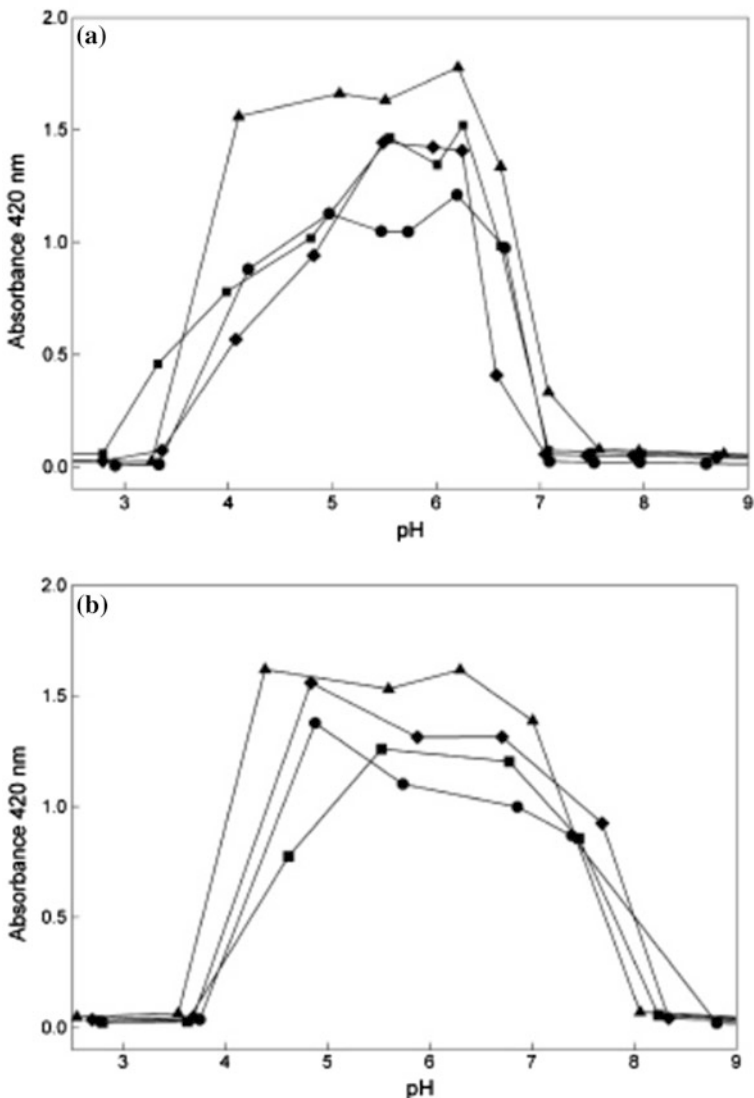


Fig. 11 (a) pH effect on the precipitation of PEI-phosphate complexes at different ratios. PEI/phosphate ratio (filled circle) 4×10^{-5} , (filled square) 7.7×10^{-5} , (filled down-pointing triangle) 1.13×10^{-4} , (filled up-pointing triangle) 1.5×10^{-4} (b) pH effect on the precipitation of poliethyleneimine-citrate complexes at different ratios. PEI/Citrate (filled circle) 0.003, (filled diamond suit) 0.006, (filled square) 0.009, (filled up-pointing triangle) 0.012

shown an acid-base turbidimetric curve of PEI, the turbidity of the medium is increased, reaching a maximal value of pH about 5.5 in a phosphate medium and pH 6.0 in citrate. Each curve has a trapezoidal shape with a plateau which is the

Table 3 Capacity of pseudo-polyampholytes to adsorb model proteins

Protein	Recovery (%)	
	Phosphate-PEI pH 5.0	Citrate-PEI pH 7.0
Pepsin	49	16
Chy	40	45
Bovine albumin	6	4

height of a trapezium. It depends on polyethyleneimine concentration. The pH values corresponding to the edges of the trapezium are the critical pHs at which the transition from complete dissolution to precipitation occurs.

The lower critical pHs of 4.0 for citrate and 3.5 for phosphate will be referred to as the acidic critical pH. The higher critical pH are 7.0 (phosphate) and 8.0 (citrate) and will be referred to as the basic critical pHs.

This behaviour has been used to precipitate acidic proteins such as pepsin [66]. Both complexes do not show exactly the same pH value of precipitation, because the PEI-anion stoichiometry is different. The mechanism of formation of the complex can be interpreted in a first stage as the interaction of the high density positive electrical charge of the polymer with the polivalent anion (phosphate), which can precipitate themselves. The adjustment of pH can cause the complex to contain an excess of positive or negative charge, which then allows the interaction with the protein to precipitate jointly like a ternary complex.

Table 3 shows the capacity of these pseudo-polyampholytes to adsorb model proteins: pepsin (pI 1), albumin (pI 4.6) and Chy (pI 9.2).

4 The Downstream Processes of Proteins and Their Scaling up Process by PE-P Formation

An ideal polyelectrolyte for protein precipitation must:

- Contain free electrically charged groups for ligand coupling
- Not interact strongly with the impurities to prevent non-specific co-precipitation
- Give complete phase separation of the polymer upon a change of some medium properties
- Preserve the secondary and tertiary structure of the protein without adversely affecting their biological activity.
- Give good yield and purification.
- Be commercially available and cheap.
- Besides, the precipitate formed should be easily solubilized: the precipitation-solubilization process should be carried out by pH changes or by ionic strength.

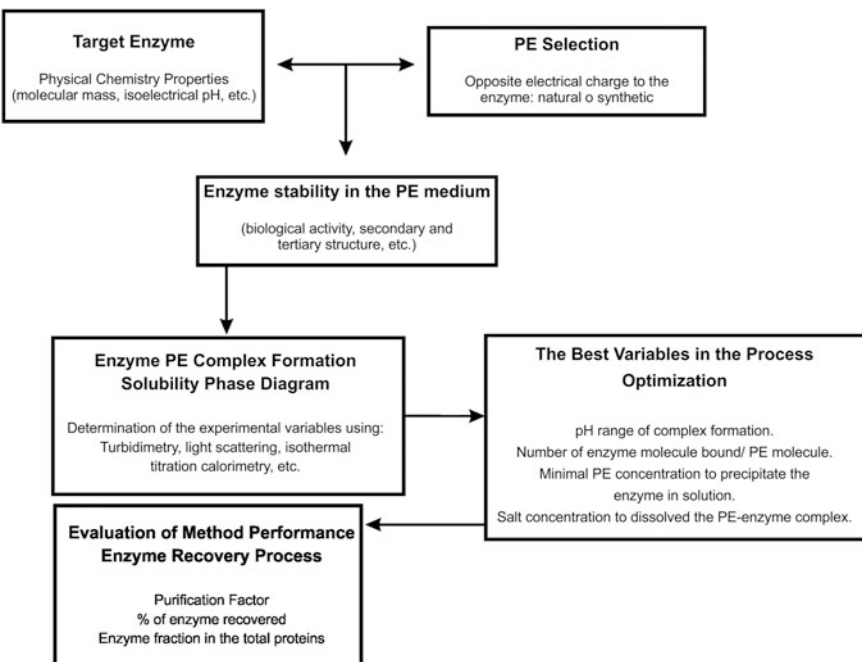


Fig. 12 Practical strategy for the enzyme isolation process by using PE-enzyme complex formation development and scale-up for the downstream processing of industrial enzymes

The complex formation between PE and a target enzyme is carried out in the natural source where the target molecule is. In general, these natural sources are microorganisms suspensions, plant or animal homogenates. The strategy applied is shown in the Fig. 12.

In general, purification of enzymes using PE involves essentially the following steps:

First step: Selection of a PE having an opposite charge to the target enzyme that is to be separated. In order to do this, is it necessary to know the isoelectric pH of the PE and the protein. Figure 13 shows the general strategy for this selection.

Following, the pH effect on the PE-P solubility is determined by turbidimetric titration.

Figure 14 (left) shows an example of an insoluble complex between a basic protein and an anionic PE. From this acid-base turbidimetric titration curve, it can be seen that the higher turbidity is produced in the pH range from 4.0 to 4.5, due to the non-soluble complex formed by the appositive electric charge of both. At pH values 6.0 or higher, the loss of the positive charge of the enzyme induces a minor complex formation, so a decrease in turbidity can be seen. From these data, two important pH values can be determined: the pH of the precipitation and the pH wherein the complex is soluble.

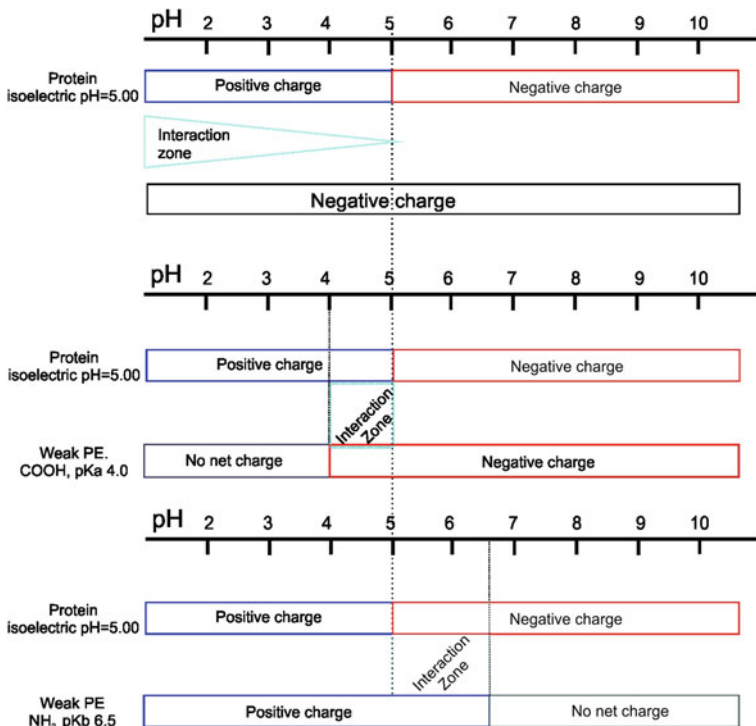


Fig. 13 Diagram showing the strategy to choose the appropriate PE to precipitate a protein with a isoelectrical pH of 5

After selecting the PE, we must verify that it does not affect the secondary and tertiary structure of the enzyme and thus its biological activity. This condition is important to validate the method to be applied. This is accomplished at the pH wherein the complex is soluble and using the pure form of the target enzyme.

Then, the pH value at which precipitation PE-P is higher should be selected, and a turbidimetric titration curve at a constant enzyme amount with increasing PE concentration is carried out (Fig. 14 (right)). The stoichiometric ratio mass of enzyme /mass of PE can be calculated from the non-lineal fitting of the experimental data. This parameter is important because it allows us to know the minimal amount of PE necessary to precipitate the protein. Table 4 shows the stoichiometry data obtained for different systems previously studied [8, 22, 38, 50].

As shown in Table 4, the stoichiometries obtained for the different complexes depended on the characteristics of the protein and the PE. The system carrageenan-Chy shows a high stoichiometric ratio, in agreement with the great number of negatively charged groups of PE, while for the lipase- chitosan system the ratio was in agreement with a steric hindrance between the positively charged groups.

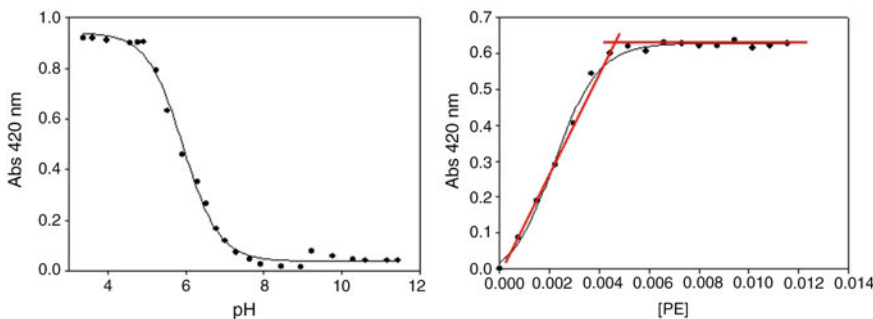


Fig. 14 *Left* Example of an acid-base turbimetric titration curve of a mixture protein-PE. *Right* Turbidimetric titration curve of protein with polymer at pH 4.5. This pH was obtained from the left data

Table 4 Stoichiometries obtained for the different complexes depended on the characteristics of the protein and the PE

PE—protein complex	Stoichiometry ratio enzyme mass (g)/polyelectrolyte mass (g)
Chy—carrageenan [67]	24 ± 2
Lipases—chitosan [8]	11 ± 0.8
Bovine serum albumin—chitosan [22]	6.9 ± 0.3
Liver catalase—chitosan [50]	1.6
Liver catalase—Eu E100 [50]	3.4

However, the value determined from the stoichiometric ratio for the formation of the complexes showed values between 100 to 1,000 enzyme molecules per PE molecule [53, 60]. This causes that the required concentrations of PE to obtain complete precipitation of the enzyme are in most cases in the order of 10^{-2} – 10^{-4} % w/v.

Second step: The next step is to assay the precipitation of the target macromolecule from its natural sources (animals and plant homogenates or microbial suspension). Obviously, a great concentration of biomass which represents around 99.9 % of the total protein concentration with respect to the concentration of target protein is present and has a negative influence on the experimental variables determined for pure enzyme precipitation in buffer solution. In a complex system such as a homogenate, there is an interaction between the protein and cellular rest, such as membrane and other proteins. One consequence is that part of the PE reacts with other macromolecules and cellular rest, thus producing a major requirement of the PE mass, so part of the impurities precipitate with the target protein, contributing to decrease the yield of the process significantly.

Ours experience shows that for target enzymes present in very low concentration in animal or microorganism homogenates, the yield of the precipitation process by PE addition is in the order of 50–70 %, with a purification factor around 1.5–4.0 [39, 40, 45, 68, 69]. Analyzing both variables, a recovery of 50–70 % in a process of precipitation of enzyme by PE could be considered of moderate performance, but it must be taken into account that a single operation unitary is being applied (precipitation) to a system which has not been previously treated. On the other hand, the second variable (the purification factor with values of 1.5–4.0) would seem to be very low. However, given the low concentration at which the target enzyme is present in its original source, this value be considered as well.

5 Application of PE-P in Downstream Processes

Production of proteins by genetically engineered microorganisms, yeasts and animal cells became a very important technique for the preparation of pharmaceuticals and other molecules used in Biotechnology. The feedstocks from which proteins are prepared are generally complex, containing solids, soluble and dissolved biomass of various sizes and molecular mass. Bioseparation steps for the recovery of the final product can account for 50–80 % of overall production costs. Most purification technologies use precipitation of proteins as one of the initial operations aimed at concentrating the product for further downstream steps. Enzymes have been traditionally purified from a variety of sources by ammonium sulfate precipitation and different chromatography techniques. These methods involve a large number of steps, which make them time-consuming and difficult to scale up.

In recent years, the field of protein isolation and purification in macro scale has grown significantly as a result of the need for large amounts of enzymes to be used in biotechnological processes. Thus, many traditional methods are no longer used because of their high cost, short life and polluting effects on the environment. The first report of isolation and purification of enzymes was in 1926 [70] where urease was isolated from a soybean paste, by precipitation of the enzyme with a mixture of 33 % acetone in water. A precipitation method based on the loss of protein solubility by adding an aqueous solution of ethanol was applied in the 40 s. It was effective for some macromolecules, non-expensive and allowed the recovery of part of the organic solvent. However, the appearance of new enzymes with different chemical characteristics required the development of new techniques such as affinity chromatography. This technique was very specific but had the disadvantage of its high cost which makes it difficult to scale up. On the other hand, it could not be used to obtain low cost enzymes.

The main problem in the scaling up purification process of an enzyme is the use of large volumes of the source where the target enzyme is present (homogenates or microbial suspensions) and the need to reduce these volumes immediately.

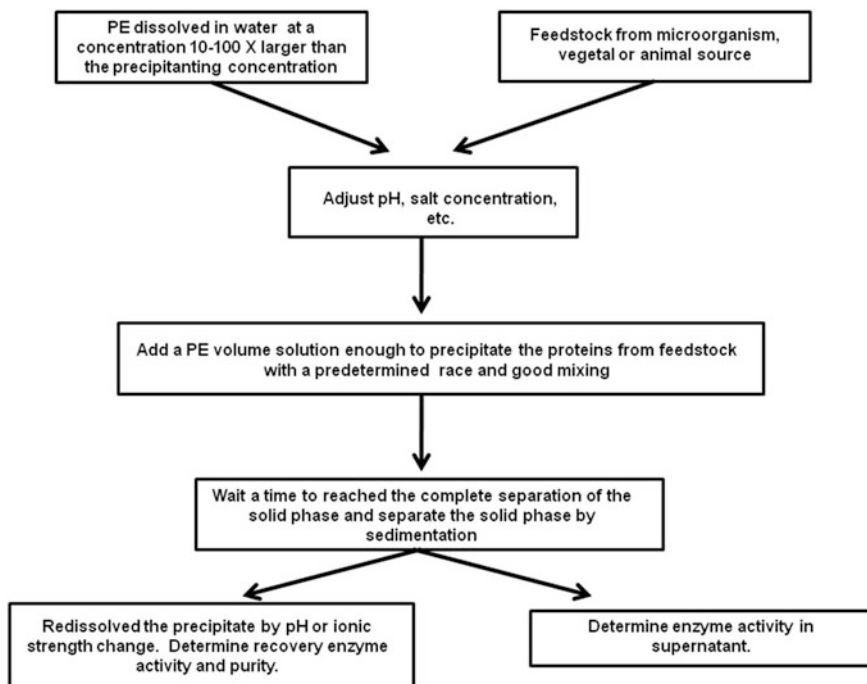


Fig. 15 General way to apply in scaling up the PE–P method for isolation of a target protein

The homogenates are formed by suspensions of cells, cell debris, membranes and proteases released from the destruction of tissues. All these give the homogenate low stability and high degradation within hours. The downstream process is to obtain a concentrate where the target enzyme is present in a great amount. The target protein precipitation from a homogenate using a PE satisfies the conditions for pre-purification steps and the total volume can be decreased significantly. In many cases the PE-P complex may be separated, dried and stored to apply another purification method. This is advantageous in the case of scaling up because the target enzyme is concentrated in a smaller volume.

In order to establish a competitive biotechnological process for protein purification in our laboratory, we have developed bioseparative methodologies based on the use of PE by forming non-soluble PE complexes with enzymes [39, 51]. These methodologies can be applied in scaling up, because they are environmentally friendly and have low cost.

Precipitation of protein by PE is a novel technique integrating clarification, concentration, and initial purification in a single step [1, 3, 5]. It allows the capture of bio-molecules from feedstock without prior removal of particulates, thus enabling clarification of a cell suspension or cell homogenate and the concentration of the desired product in one operation [39, 45].

In precipitation with PE, viscous and particulate-containing feeds can be easily treated by adding a PE solution. Once the feed is loaded and the target product is bound to the PE forming the non-soluble complex, a wash step is performed to remove particulates and unbound contaminants. Elution of the target product is then performed via pH change or by salt addition.

The non-soluble complex formation between macromolecules and PE has been known for over 50 years. However, its development was stopped during years due that PEs were obtained from industrial synthesis in small quantities, they were often toxic and cannot be removed after the solubilizing step. The development of the chemistry of natural polyelectrolytes from the 80's allows to have non-toxic, environmentally friendly PE (most were polysaccharides), which were easily degradable by microorganisms. In turn, the development of technologies to study macromolecules, and especially complexes such as circular dichroism, isothermal titration calorimetry, scanning calorimetry, dynamic and static light scattering took place in the 80's. These technologies significantly contributed to the knowledge of the molecular mechanism by which the PE-P is carried out.

In the last 10 years, there was a significant increase in the number of jobs that are intended to address the formation, the knowledge and molecular mechanism of these complexes, especially when involving natural polyelectrolytes. All the experience gained allowed the development of scaling methodologies applicable to macromolecules, especially enzymes with application in biotechnological processes.

The precipitation technique of a macromolecule by forming a poorly soluble PE-P was quickly introduced as a viable alternative to compete with the precipitation using salts such as ammonium sulfate, polyethyleneglycol, etc. But, saline precipitation cannot compete with precipitation with PE, since the PE total concentrations are in the order of 0.001–0.15 % W/V against values of 20–50 % w/w salts and non-charge polymer loaded. Besides, as PE are polysaccharides, they are capable of thermodynamically stabilizing macromolecules in solution. Their low cost and low concentration required for precipitation makes the process inexpensive. They do not interfere with the process where the enzyme is being used nor have negative effects on the final product, since most of them meet the standards of FDA (USA) regulations.

Figure 15 resumes the general way to apply in scale up the PE-P method for isolation of a target protein. The importance of the PE-P as scaling up method is useful as a previously step to concentrate an enzyme from its feedstock; this is supported in the number of patents published about the use of PE as primary concentrative way for large volume [71–73].

Acknowledgments This work was supported by a grant from CONICET PIP00196. We thank María Robson, Geraldine Raimundo, Mariana De Sanctis and Marcela Culasso for the language correction of the manuscript.

References

- Thünenmann, A., et al.: Polyelectrolyte complexes. In: Schmidt, M. (ed.) *Polyelectrolytes with Defined Molecular Architecture II*. Springer Berlin Heidelberg. pp. 113–171 (2004)
- Quinteros, D.A., et al.: Interaction between a cationic polymethacrylate (Eudragit E100) and anionic drugs. *Eur. J. Pharm. Sci.* **33**(1), 72–79 (2008)
- Renault, F., et al.: Chitosan for coagulation/flocculation processes—an eco-friendly approach. *Eur. Polym. J.* **45**(5), 1337–1348 (2009)
- Bouyer, E., et al.: Stabilization mechanism of oil-in-water emulsions by β -lactoglobulin and gum arabic. *J. Colloid Interface Sci.* **354**(2), 467–477 (2011)
- Cooper, C.L., et al.: Polyelectrolyte–protein complexes. *Curr. Opin. Colloid Interface Sci.* **10**(1–2), 52–78 (2005)
- Rinaudo, M.: Chitin and chitosan: properties and applications. *Prog. Polym. Sci.* **31**(7), 603–632 (2006)
- Schillemans, J.P., Hennink, W.E., van Nostrum, C.F.: The effect of network charge on the immobilization and release of proteins from chemically crosslinked dextran hydrogels. *Eur. J. Pharm. Biopharm.* **76**(3), 329–335 (2010)
- Bassani, G., Farruggia, B., Picó, G.: Cationic polyelectrolytes–lipases complexes formation as tool for recovery of these enzymes from their natural sources. *Int. J. Biol. Macromol.* **49**(3), 351–355 (2011)
- Liao, Y.-H., Brown, M.B., Martin, G.P.: Investigation of the stabilisation of freeze-dried lysozyme and the physical properties of the formulations. *Eur. J. Pharm. Biopharm.* **58**(1), 15–24 (2004)
- Simonoska Crcarevska, M., Glavas Dodov, M., Goracinova, K.: Chitosan coated Ca-alginate microparticles loaded with budesonide for delivery to the inflamed colonic mucosa. *Eur. J. Pharm. Biopharm.* **68**(3), 565–578 (2008)
- Roy, I., Sardar, M., Gupta, M.N.: Cross-linked alginate–guar gum beads as fluidized bed affinity media for purification of Jacalin. *Biochem. Eng. J.* **23**(3), 193–198 (2005)
- Radoiu, M.T., et al.: Preparation of polyelectrolytes for wastewater treatment. *J. Hazard. Mater.* **106**(1), 27–37 (2004)
- Eremenko, A., et al.: Monomolecular enzyme films stabilized by amphiphilic polyelectrolytes for biosensor devices. *Thin Solid Films* **260**(2), 212–216 (1995)
- Dyrby, M., et al.: Towards on-line monitoring of the composition of commercial carrageenan powders. *Carbohydr. Polym.* **57**(3), 337–348 (2004)
- Kadajji, V.G., Betageri, G.V.: Water soluble polymers for pharmaceutical applications. *Polymers* **3**(4), 1972–2009 (2011)
- Rinaudo, M.: Polyelectrolyte properties of a plant and animal polysaccharide. *Struct. Chem.* **20**(2), 277–289 (2009)
- Manning, G.S.: Limiting laws and counterion condensation in polyelectrolyte solutions II. self-diffusion of the small ions. *J. Chem. Phys.* **51**(3), 934–938 (1969)
- Lifson, S., Katchalsky, A.: The electrostatic free energy of polyelectrolyte solutions. II. Fully stretched macromolecules. *J. Polym. Sci.* **13**(68), 43–55 (1954)
- Manning, G.S.: Limiting laws and counterion condensation in polyelectrolyte solutions I. colligative properties. *J. Chem. Phys.* **51**(3), 924–933 (1969)
- Dobrynin, A.V., Rubinstein, M.: Theory of polyelectrolytes in solutions and at surfaces. *Prog. Polym. Sci.* **30**(11), 1049–1118 (2005)
- Klooster, N.T.M., Van der Touw, F., Mandel, M.: Solvent effects in polyelectrolyte solutions. 1. Potentiometric and viscosimetric titration of poly(acrylic acid) in methanol and counterion specificity. *Macromolecules* **17**(10), 2070–2078 (1984)
- Boeris, V., Farruggia, B., Pico, G.: Chitosan-bovine serum albumin complex formation: a model to design an enzyme isolation method by polyelectrolyte precipitation. *J. Chromatogr. B Analyt. Technol. Biomed. Life Sci.* **878**(19), 1543–1548 (2010)

23. Simsek-Ege, F.A., Bond, G.M., Stringer, J.: Polyelectrolyte complex formation between alginate and chitosan as a function of pH. *J. Appl. Polym. Sci.* **88**(2), 346–351 (2003)
24. Cleland, R.L.: Theory of potentiometric titration of polyelectrolytes: a discrete-site model for hyaluronic acid. *Macromolecules* **17**(4), 634–645 (1984)
25. Turgeon, S.L., Schmitt, C., Sanchez, C.: Protein–polysaccharide complexes and coacervates. *Curr. Opin. Colloid Interface Sci.* **12**(4–5), 166–178 (2007)
26. Chen, J., Heitmann, J.A., Hubbe, M.A.: Dependency of polyelectrolyte complex stoichiometry on the order of addition. 1. Effect of salt concentration during streaming current titrations with strong poly-acid and poly-base. *Colloids Surf., A* **223**(1–3), 215–230 (2003)
27. Kovačević, D., Borković, S., Požar, J.: The influence of ionic strength, electrolyte type and preparation procedure on formation of weak polyelectrolyte complexes. *Colloids Surf., A* **302**(1–3), 107–112 (2007)
28. Moustafine, R.I., Kemenova, V.A., Van den Mooter, G.: Characteristics of interpolyelectrolyte complexes of Eudragit E 100 with sodium alginate. *Int. J. Pharm.* **294**(1–2), 113–120 (2005)
29. Shang, J., Shao, Z., Chen, X.: Electrical behavior of a natural polyelectrolyte hydrogel: chitosan/carboxymethylcellulose hydrogel. *Biomacromolecules* **9**(4), 1208–1213 (2008)
30. Rosca, C., et al.: Interaction of chitosan with natural or synthetic anionic polyelectrolytes. 1. The chitosan–carboxymethylcellulose complex. *Carbohydr. Polym.* **62**(1), 35–41 (2005)
31. Chavasit, V., Torres, J.A.: Chitosan-Poly(acrylic acid): mechanism of complex formation and potential industrial applications. *Biotechnol. Prog.* **6**(1), 2–6 (1990)
32. Delair, T.: Colloidal polyelectrolyte complexes of chitosan and dextran sulfate towards versatile nanocarriers of bioactive molecules. *Eur. J. Pharm. Biopharm.* **78**(1), 10–18 (2011)
33. Sankalia, M.G., et al.: Stability improvement of alpha-amylase entrapped in kappa-carrageenan beads: physicochemical characterization and optimization using composite index. *Int. J. Pharm.* **312**(1–2), 1–14 (2006)
34. Calvo, P., Vila-Jato, J.L., Alonso, M.J.: Evaluation of cationic polymer-coated nanocapsules as ocular drug carriers. *Int. J. Pharm.* **153**(1), 41–50 (1997)
35. Lankalapalli, S., Kolapalli, V.R.: Polyelectrolyte complexes: a review of their applicability in drug delivery technology. *Indian J. Pharm. Sci.* **71**(5), 481–487 (2009)
36. Moustafine, R.I., et al.: Comparative evaluation of interpolyelectrolyte complexes of chitosan with Eudragit L100 and Eudragit L100-55 as potential carriers for oral controlled drug delivery. *Eur. J. Pharm. Biopharm.* **70**(1), 215–225 (2008)
37. Izumrudov, V., Galaev, I., Mattiasson, B.: Polycomplexes—potential for bioseparation. *Bioseparation* **7**(4–5), 207–220 (1998)
38. Valetti, N.W., Boeris, V., Picó, G.: Characterization of chymotrypsin- ι – carrageenan complex in aqueous solution: a solubility and thermodynamical stability study. *Int. J. Biol. Macromol.* **52**, 45–51 (2013)
39. Valetti, N., et al.: Precipitation of chymotrypsin from fresh bovine pancreas using ι -carrageenan. *Proc. Biochem.* **47**(12), 2570–2574 (2012)
40. Boeris, V., et al.: Purification of chymotrypsin from bovine pancreas using precipitation with a strong anionic polyelectrolyte. *Proc. Biochem.* **44**(5), 588–592 (2009)
41. Perez, A.A., et al.: Interactions between milk whey protein and polysaccharide in solution. *Food Chem.* **116**(1), 104–113 (2009)
42. Tolstoguzov, V.: Some thermodynamic considerations in food formulation. *Food Hydrocolloids* **17**(1), 1–23 (2003)
43. Xu, Z., et al.: Co-immobilization mechanism of Cellulase and Xylanase on a reversibly soluble polymer. *Appl. Biochem. Biotechnol.* **163**(1), 153–161 (2011)
44. Breccia, J.D., Mattiasson, B., Sifneriz, F.: Separation of bacterial Xylanase by precipitation using Eudragit S100. *J. Biotechnol.* **61**(3), 219–223 (1998)
45. Cappella, L.V., Boeris, V., Picó, G.: A simple method of chymotrypsin concentration and purification from pancreas homogenate using Eudragit® L100 and Eudragit® S100. *J. Chromatogr. B* **879**(13–14), 1003–1007 (2011)

46. Dubin, P.L., Gao, J., Mattison, K.: Protein purification by selective phase separation with polyelectrolytes. *Sep. Purif. Rev.* **23**(1), 1–16 (1994)
47. Schmitt, C., Turgeon, S.L.: Protein/polysaccharide complexes and coacervates in food systems. *Adv. Colloid Interface Sci.* **167**(1–2), 63–70 (2011)
48. Pico, G., et al.: Calorimetric investigation of the protein–flexible chain polymer interactions and its relationship with protein partition in aqueous two-phase systems. *Int. J. Biol. Macromol.* **40**(3), 268–275 (2007)
49. Cooper, C.L., et al.: Effects of polyelectrolyte chain stiffness, charge mobility, and charge sequences on binding to proteins and micelles. *Biomacromolecules* **7**(4), 1025–1035 (2006)
50. Boeris, V., et al.: Interaction and complex formation between catalase and cationic polyelectrolytes: Chitosan and Eudragit E100. *Int. J. Biol. Macromol.* **45**(2), 103–108 (2009)
51. Porfiri, M.C., et al.: Precipitation with poly acrylic acid as a trypsin bioseparation strategy. *Process Biochem.* **44**(9), 1046–1049 (2009)
52. Harnsilawat, T., Pongsawatmanit, R., McClements, D.J.: Characterization of β -lactoglobulin–sodium alginate interactions in aqueous solutions: a calorimetry, light scattering, electrophoretic mobility and solubility study. *Food Hydrocolloids* **20**(5), 577–585 (2006)
53. Romanini, D., et al.: Interaction of lysozyme with negatively charged flexible chain polymers. *J. Chromatogr. B Analyt. Technol. Biomed. Life Sci.* **857**(1), 25–31 (2007)
54. Boeris, V., et al.: Chymotrypsin—Eudragit® complex mechanism formation as potential non expensive tool to isolate this enzyme at scale up level. *Biotechnology and Bioprocess Engineering* (in press) (2013)
55. Mazzaferro, L., et al.: Polyethyleneimine–protein interactions and implications on protein stability. *Int. J. Biol. Macromol.* **47**(1), 15–20 (2010)
56. Boeris, V., et al.: Protein–flexible chain polymer interactions to explain protein partition in aqueous two-phase systems and the protein–polyelectrolyte complex formation. *Int. J. Biol. Macromol.* **41**(3), 286–294 (2007)
57. Weinbreck, F., et al.: Complex coacervation of whey proteins and gum arabic. *Biomacromolecules* **4**(2), 293–303 (2003)
58. Mattison, K.W., Brittain, I.J., Dubin, P.L.: Protein—polyelectrolyte phase boundaries. *Biotechnol. Prog.* **11**(6), 632–637 (1995)
59. Mattison, K.W., Dubin, P.L., Brittain, I.J.: Complex formation between Bovine Serum Albumin and Strong polyelectrolytes: effect of polymer charge density. *J. Phys. Chem. B* **102**(19), 3830–3836 (1998)
60. Boeris, V., et al.: Chymotrypsin–poly vinyl sulfonate interaction studied by dynamic light scattering and turbidimetric approaches. *Biochimica et Biophysica Acta (BBA)—General subjects.*, **1780**(9):pp. 1032–1037 (2008)
61. Boeris, V., et al.: Chymotrypsin—Eudragit® complex formation. *Biotechnol. Bioprocess Eng.* **18**(3), 538–545 (2013)
62. Azarmi, S., et al.: Thermal treating as a tool for sustained release of indomethacin from Eudragit RS and RL matrices. *Int. J. Pharm.* **246**(1–2), 171–177 (2002)
63. Tsuboi, A., et al.: Complexation of proteins with a strong polyanion in an aqueous salt-free system. *Langmuir* **12**(26), 6295–6303 (1996)
64. Patrickios, C.S., et al.: Precipitation of a water-soluble ABC Triblock methacrylic polyampholyte: effects of time, pH, polymer concentration, salt type and concentration, and presence of a protein. *Langmuir* **15**(5), 1613–1620 (1999)
65. Nath, S., Patrickios, C.S., Hatton, T.A.: Turbidimetric titration study of the interaction of proteins with acrylic polyampholytes. *Biotechnol. Prog.* **11**(1), 99–103 (1995)
66. Manzur, A., et al.: Polyethyleneimine phosphate and citrate systems act like pseudo polyampholytes as a starting method to isolate pepsin. *J. Chromatogr. B* **860**(1), 63–68 (2007)
67. Valetti, N.W., Boeris, V., Picó, G.: Characterization of chymotrypsin–*t*-carrageenan complex in aqueous solution: a solubility and thermodynamical stability study. *Int. J. Biol. Macromol.* **52**, 45–51 (2013)

68. Porfiri, M.C., Farruggia, B.M., Romanini, D.: Bioseparation of alpha-amylase by forming insoluble complexes with polyacrylate from a culture of *Aspergillus Oryzae* grown in agricultural wastes. *Sep. Purif. Technol.* **92**, 11–16 (2012)
69. Marini, A., et al.: Extraction of lipase from *Aspergillus niger* by insoluble complex formation with anionic and cationic polyelectrolytes. *Process Biochem.* **47**(12), 2234–2239 (2012)
70. Sumner, J.B.: The isolation and crystallization of the enzyme urease: preliminary paper. *J. Biol. Chem.* **69**(2), 435–441 (1926)
71. Montilla, A., et al.: Isolation of bovine β -lactoglobulin from complexes with Chitosan. *Int. Dairy J.* **17**(5), 459–464 (2007)
72. Snoke R.E., et al. Purification of microbial enzyme extracts using synthetic polyelectrolytes. US Patent 4,055,469. 1977
73. Luong, J. et al.: Affinity process for trypsin purification and stabilization. US Patent 4,973,554. 1990

Polyelectrolyte Complexes

Bridging the Ensemble Average: Single-Molecule Strategies

Rita S. Dias and Bjørn Torger Stokke

Abstract Polyelectrolyte complexation is mechanistic in formation of various biological structures as well as in technological applications. Such structure formation can be viewed as key in regulating biological functionality and designing functional soft materials. The formation of polyelectrolyte complexes depends on the interrelation between the counter ion exchange, entropic contribution, polymer properties, solution conditions, and process approach. Thus, a comprehensive description of the polyelectrolyte complex formation, their properties, and structures deem it necessary to apply various tools. The chapter provides a brief overview of representative polyelectrolyte complex examples from biology and man-made ones. In particular, we aim at combining information obtainable at the ensemble and single molecule level with numerical simulations to provide a more comprehensive description of the structure formation and resulting morphologies. A particular feature is the possible existence of kinetically trapped structures due to the flexible and long chain nature of the components. Possible impact of this particularity to this growing field is discussed.

1 Introduction

The inherent capacity of oppositely charged polyelectrolytes to form complexes is exploited both within nature and synthetic materials. One example of the importance of polyelectrolyte complexation supporting biological functionality is the wrapping of DNA around histones to form nucleosomes. The DNA in eukaryotic cells is organized in a highly compacted state. Well defined morphologies such as toroids have been identified as the fundamental organizational unit of mammalian

R.S. Dias · B.T. Stokke (✉)

Biophysics and Medical Technology, Department of Physics, The Norwegian University of Science and Technology, 7491 Trondheim, Norway
e-mail: bjorn.stokke@ntnu.no

sperm DNA [1]. Synthetic polymers are generally more flexible than DNA and they do not adopt similar highly organized packing geometries as found for the natural genetic material.

It is thus not surprising that these systems gather an enormous interest and, concomitantly, a large body of literature is available within this subject. However, many aspects pertinent to oppositely charged polyelectrolyte interaction, complexation and structure formation are often not very clear and may even be counterintuitive. For example, the driving force for the complexation of oppositely charged polyelectrolytes is dominated by a contribution of entropic nature. However, variations to the solution properties, such as the ionic strength, change the relative importance of enthalpy and entropy in these systems [2]. One additional aspect is that sample preparation routines can heavily influence the results, especially for highly coupled systems, suggesting strong kinetic effects. The possible impact of concentration on the interactions and the morphology of the formed complexes for kinetically trapped systems are particularly challenging.

These introductory comments indicate that it is necessary to use various tools to provide a more comprehensive description of the systems. In the following, we start by highlighting the interest of polyelectrolytes and polyelectrolytes complexes from biological and technological viewpoints, after which we briefly review the current knowledge on polyelectrolyte complex formation and structure, as well as some challenges of working with these, often very coupled, systems. By comparing observations of individual complexes with experimental approaches at the ensemble level and numerical simulations, we aim to provide a comprehensive approach to selected examples of polyelectrolyte structures and their fundamental properties. Polyelectrolyte—oppositely charged lipid systems will also be mentioned when deemed relevant.

1.1 *Polyelectrolytes in Biology*

Many biological molecules are charged. The presence of charge serves as structural motifs underpinning various functionalities. Firstly, it increases the solubility of the molecules in aqueous solution. Even though not much is known about the environment that molecules experience inside a cell, many biological processes are assumed to occur in aqueous environment and thus, the many components should be water soluble and interact in a controllable fashion. The solubility of the molecules is especially important for very large molecules, as most complex biopolymers need to be. Increased solubility is achieved not just by making the biopolymer segments more hydrophilic but mainly because it brings along counterions that when released give the dissolved biopolymer much entropy. In addition, the presence of charge along the backbone of a biopolymer prevents its aggregation and phase-separation. Of course, processes such as DNA condensation and packaging in bacteriophage capsids, bacterial nucleoids, and eukaryotic cell

nucleus are expected to be hindered by the presence of charge; however, this apparent drawback is overcome using different mechanisms such as interactions with oppositely charged polyelectrolytes (e.g., polyamines and proteins).

1.2 Polyelectrolytes Complexes in Biology

There are many examples of polyelectrolyte complexes in biology, since proteins are fundamentally polyampholytes. One of the most obvious is the chromatin fibre, composed of DNA and histones. The presence of charge and consequent electrostatic interactions dominates these systems. Proteins possess positive and negatively charged residues that often form charged patches at the surface of the proteins. The presence of such patches have been shown to induce an inhomogeneous distribution of polyelectrolyte monomers at the protein surface as well as the formation of a stronger complex than a corresponding protein model with a homogeneous surface charge [3]. Both results have interesting implications in biology. The charge pattern at the “surface” of the protein directs the interaction with an oppositely charged macromolecule partially compensating the lack of directionality and specificity of the electrostatic interaction. This is evident in the topography of the histone octamer’s surface where positive charges, together with other structural elements, guide the wrapping of the DNA around the histone complex [4]. In a cell DNA is wrapped by millions of octamers along its chain with a repeat distance of about 200 bp [5] resembling an overall pearl-necklace structure. This fibre is additionally wrapped on itself, to form what is called the chromatin fibre [6]. In this structure and higher order ones, nucleosome—nucleosome interactions are considered to play a crucial role. Experiments [7–9] and computer simulations [10–14] suggest that histone tail bridging may strongly contribute to nucleosomal attraction. Histone tails are flexible chains that extend from the octamer and which carry several positively charged residues. It has been shown that tail bridging is very sensitive to the charge density of the tails [13], which suggests a possible mechanism to control nucleosome—nucleosome interaction. In fact, experiments have shown that the cellular machinery is able to control the charge status of the histone tails via the acetylation and deacetylation of the lysine groups [15], that is, by neutralizing or charging up the tails, respectively, with consequences on the fibre condensation. Acetylated regions in the chromatin are more open and presumably more active, while deacetylated regions are more condensed both locally and on a larger scale [16].

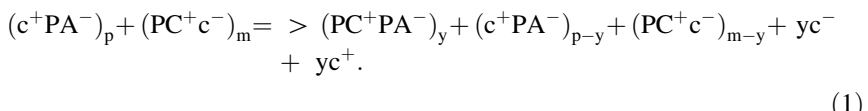
1.3 Man-Made Polyelectrolytes Complexes

An overview of various applications of polyelectrolyte complexes both as ready-made substances and the process of making such entities has recently been provided [17]. Developing polycations as non-viral delivery vehicles for gene therapy,

either for coding DNA sequences or siRNA sequences, are an active research area e.g. [18] and references therein. The requirements on the optimal polycation and process parameters need to take into account various facets. These need to fulfil requirements of sufficient stability of the resulting complexes during part of the delivery pathway while at the same time do not offset intracellular unpacking for subsequent targeted function. In addition, successful polycations need to be biocompatible. While polycations used as gene delivery vehicles is one biomedical application domain exploiting the polyelectrolyte complexation and complex properties, application of polyelectrolyte complexes (PEC) within drug delivery in general is also prominent [19]. Design of optimal PEC structures in this case is directed towards controlling the internal structure of the PEC particles through the selection of molecular and process parameters. Controlling surface properties of wood fibres by PEC either as ready-made before being introduced in the process or being formed *in situ* is an application domain directed towards tailor-making the surfaces properties of the wood fibres for, e.g. adhesion for control of strength of the resulting paper [20]. The versatility offered by selection of polyelectrolytes combined with processing conditions represents a rich experimental window into tuning the properties towards the final goal of controlled mechanical properties of paper. The need for efficient strategies for fluid–solid separation steps in various industrial processes, e.g. related to paper retention, water treatment or other, has led to exploiting of PEC at large scale [21]. These application examples illustrate the diverse application domains where either pre-formed PEC or the PEC formation process, when successful, can make a key impact. Closely related to PEC dispersed in solution is the exploitation of an electrostatic mechanisms for formation of multilayers [22].

1.4 Polyelectrolyte Complex Formation

Mixing oppositely charged polyelectrolytes leads to the spontaneous formation of polyelectrolyte complexes concomitant with the release of counterions (Fig. 1a–c). As a first approximation, such a polyelectrolyte complexation may be described as a counterion exchange reaction in a system of polyanions (PA), polycations (PC), counterions (c^+ , c^-) and solvent [23, 24], according to:



This equation is written under the assumption that the stoichiometry of the charges involved in the interaction is 1:1, but one of the components might be in excess. Additionally, either one or both polyions might exist as free polyelectrolytes in solution after mixing, depending on the mixing ratio of polyanions (p) and

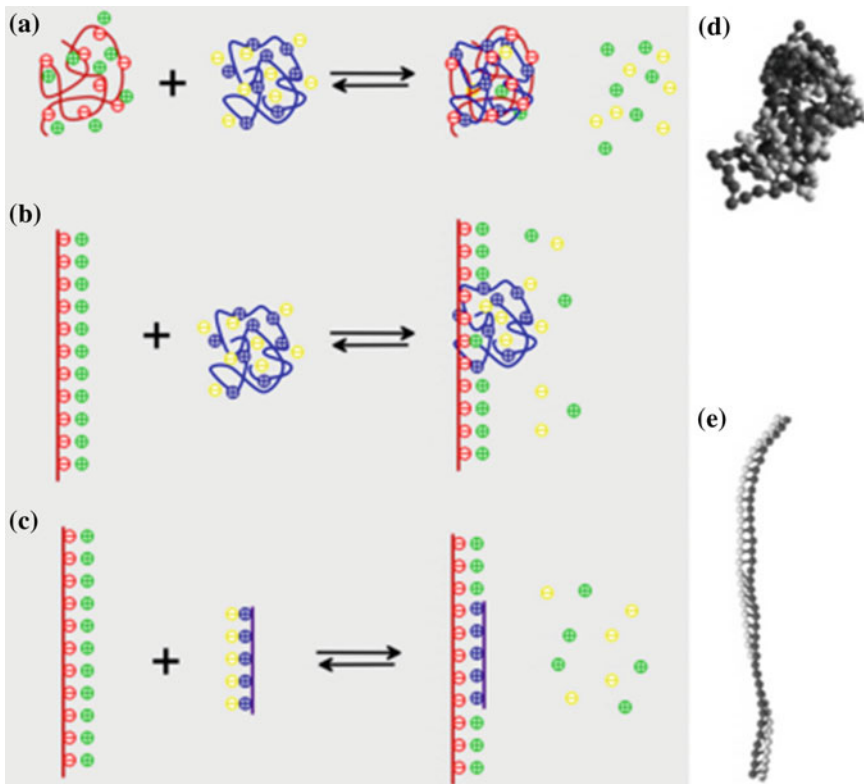


Fig. 1 Schematic illustrations of effects of chain flexibilities on structural motifs and associated entropic effects occurring on polyelectrolyte complex formation. Complexation of flexible polyanions and polycations **a** may lead to non-stoichiometric release of counterions being an important contribution to the increased entropy associated with PEC formation. Complexation of semiflexible polyanion and flexible polycation may lead to non-stoichiometric release of counterions relative to the overall valence of the polycation **(b)**. Complexation between semiflexible polyanions and polycations may yield a near stoichiometric release of counterions associated with the counterion exchange reaction in an idealized ladder-like structure **(c)**. The associated structures are often referred to as **d** “scrambled egg” and **e** “railway track” structural motifs for the flexible and inflexible, respectively, pairs of interacting polymers. Panels **d** and **e** are reproduced from ref [25] with permission from John Wiley and Sons

polycations (m). The release of counterions from both the polycations and polyanions associated with the complexation yields an entropic contribution to the thermodynamics of the complexation. Although such entropic dominated thermodynamics of polyelectrolyte complexation are abundant, there are additional contributions to the free energy. Reported experiments suggest that the counterion charge predicts condensing ability, while the counterion structure influences the morphology and dimensions of the formed complexes [26].

Upon complexation the mixing and configurational entropies of the polyanions and polycations decrease. The (at least partial) neutralization of the polyelectrolyte chains leads to a decrease in their volume, especially for long chain polyelectrolytes. Those that are relatively flexible and not very highly charged, are likely to adopt a Gaussian chain conformation in the complexes, as shown for the system poly(acrylic acid) and poly(*N,N*-dimethylaminoethyl methacrylate) using scattering techniques [27].

As the stiffness of the polyelectrolyte chains is increased, the polyplexes tend to adopt structures such as toroids or rods [28, 29] but, independently of the morphology of the resulting structures, the forces driving the complexation process are similar as has been reviewed by Bloomfield [30, 31]. As for the flexible polyelectrolytes, an important contribution to the overall driving force for condensation of stiff polyelectrolytes is the increased entropy associated with the release of counterions from the polyelectrolytes in the exchange reaction.

The theoretical account is beyond the mean-field theories, where correlated fluctuations between multivalent counterions mediate an attractive potential [32] eventually yielding compaction of a polyelectrolyte (e.g. DNA) (for review, see e.g. [33, 34]). Monte Carlo simulations have shown that the presence of multivalent species leads to effective attractions between highly charged surfaces, such as the different parts of a long polyelectrolyte molecule, yielding complexes that have smaller dimensions than the corresponding polymer [35]. In addition, the dielectric constant of the medium was found to be a key factor to determining the conformation of large DNA molecules in solution, which was attributed to an increased importance of the ion-ion correlations, due to the increase in electrostatic coupling [36].

Accordingly, two binding stages (association and condensation) during the polyelectrolyte complex formation have been successfully identified in thermodynamic characterization of the process by isothermal titration calorimetry (ITC) (Fig. 2) [37, 38]. Similar two binding stage mechanism was identified for spermidine and cobalt hexamine and were interpreted as cation binding followed by DNA condensation. The experiments verified that complexation is entropically driven and lent support to an electrostatic interaction mechanism. Nevertheless, the rather high DNA concentrations needed for the ITC characterization may also allow alternative morphologies to be formed and thus obscure a clear relation to a particular morphology of the condensed state.

It should be mentioned that ITC is a standard tool for studying the interactions between biomacromolecules and co-solutes, but has also become an invaluable tool in many other fields ranging from cell biology to food chemistry, as described in different literature reviews (see for example [39] and references therein).

The increase in entropy associated with release of counterions in a polyanion–polycation reaction has been reported for some polycation–polyanion pairs. Interestingly, data reported for binding of positively charged ligands to double stranded DNA generally confirm that the extent of counterion release is near

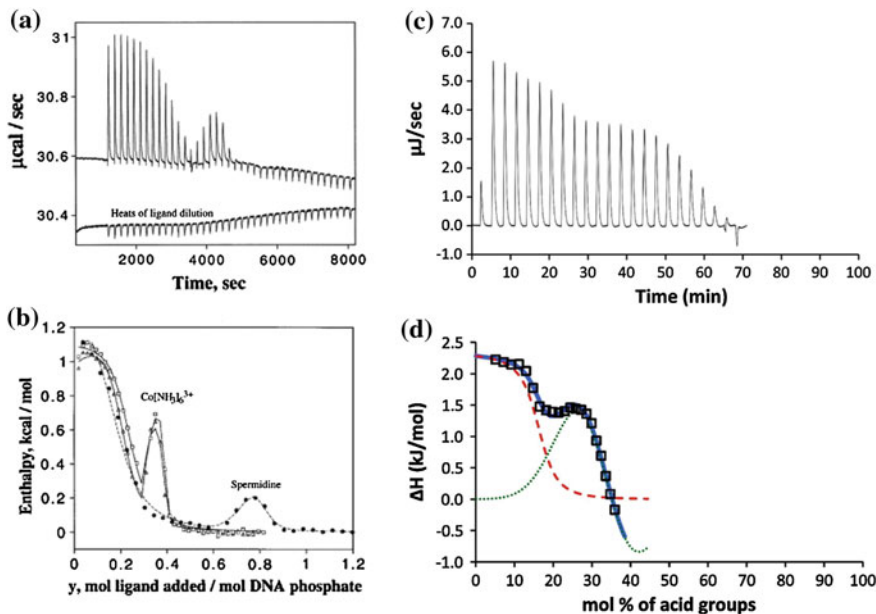


Fig. 2 Examples of isothermal titration calorimetry thermograms and binding isotherms for titration of metal ions, oligo- and polycations to polyanions. **a** Calorimetric titration curve for titrating cobalt hexamine to DNA (in 10 mM NaCl) and heat of dilution. **b** ITC titration curves for cobalt hexamine and spermidine binding to pUC118 DNA in 10 mM NaCl and 25 °C. **c** Calorimetric titration curve for titrating PGLu to a solution of PEI and **d** binding isotherm for binding of PGLu to PEI. The data (squares) were fitted to a model comprising of a sequence of two distinct binding steps each contributing to the heat change as displayed as *dashed lines*. The *red dashed line* corresponds to ion pair binding and the *green one* to the coacervate formation and dissolution. Panels **a** and **b** are reprinted from Journal of Molecular Biology, vol 296, D. Matulis, I. Rouzina, and A. Bloomfield, Thermodynamics of DNA binding and condensation: Isothermal titration calorimetry and electrostatic mechanism, Pages No. 1053–1063, Copyright (2000), with permission from Elsevier. Panels **c** and **d** are reprinted from Priftis et al. [38] Copyright (2013), with permission from Elsevier.

stoichiometric [40], whereas for single-stranded DNA it is not [41]. Studies on spermine and lipospermine binding to DNA were conducted and reported [42] to assess the importance of contribution of hydrophobic effects on DNA collapse. While ITC measurements showed a larger DNA binding affinity for the hydrophobic lipospermine than spermine, electron micrographs showed that lipospermine was incapable of condensing DNA into toroidal structures.

Models that further include packaging effects, and topological effects have been proposed in the case of ligands with low valence [43]. Thus, the relative importance of enthalpy and entropy in the complexation process is not *a priori* easy to predict and the relation to the adopted structures of the polyelectrolyte complexes need to be scrutinized.

1.5 Non-ideal Thermodynamics

When looking into polyelectrolyte complex formation, it is important to consider non-ideal thermodynamics. This is so since at least one of the components in the complex will typically have a large molecular weight which may lead to slow kinetics, especially in concentrated regimes. Systems where the two major components have a reasonable amount of charge will be strongly coupled and may additionally lead to kinetically arrested states which can be studied at the single-molecule level.

This has been directly shown in a number of different systems. For example, while studying the condensation of DNA with poly(amido amine) (PAMAM) dendrimers of different generations it was found that significant morphological rearrangements occur for DNA compacted with the lower generation dendrimers, initially forming well-structured rods and toroids [44], leading to the formation of toroid complexes with time [45]. On the other hand, higher charge density dendrimers gave rise to globular aggregates and no transient morphologies were observed, suggesting that the dendrimers become kinetically trapped when they bind to the DNA strand [45].

Although not commonly discussed, the dependence of the sample preparation protocols on the results has been known for a long time. As an example, protocols for lipoplex (DNA—cationic lipid complexes) preparation describe the order of addition of the different components according to their concentration so that the neutralization (and consequence precipitation) line in the phase diagram is not crossed [46].

Carlstedt et al. [47] have shown recently that is possibly to overcharge and redisperse DNA—cetyltrimethylammonium bromide (CTAB) complexes by quickly adding and mixing the surfactant solution to the DNA, whereas such result cannot be achieved using a step-wise addition process, that is, by preparing neutral complexes and adding excess of surfactant afterwards. A consequence of such a result is that such phenomena should be considered when performing ITC experiments where the typical procedure does consist of a stepwise titration.

Solution inhomogeneity is believed to influence conformation, aggregation and precipitation of DNA molecules. Varying the volume and concentration of the added components, in otherwise equal final samples in terms of volume and concentrations of the different components, was found to have an impact in the relative population of compacted and unfolded structures [48]. In fact, such inhomogeneous effects have been successfully used for the preparation of physical gel-like particles, by the drop-wise addition of a concentrated solution of one component over a concentrated solution of the other. These particles have been prepared using different polyelectrolytes and oppositely charged surfactants [49, 50] or surfactant mixtures [51, 52], as well as polyelectrolytes and proteins [53] or oppositely charged polyions [54]. It has been suggested that the structure of the resulting gel-like particles is governed by the solution composition and the method of preparation, while the particle stability is governed by phase behaviour

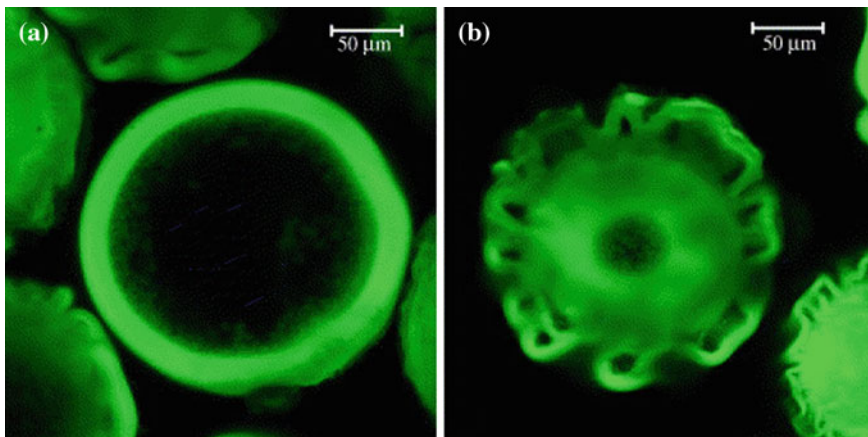


Fig. 3 Confocal microscopy images of gel particles composed of a polyelectrolyte (cationically modified hydroxyethyl cellulose (JR-400TM) and two different types of surfactants (cetyltrimethylammonium bromide, CTAB, and sodium perfluorooctanoate, FC₇). The resulting gel particles can assume two types of morphologies depending on the surfactant concentration: **a** smooth hollow particle with dense thin gel shell for lower concentrations, and **b** gel particle with sparse thick shell, and a gel corona for higher concentrations. Reprinted from Lapitsky and Kaler [51]. Copyright (2004), with permission from Elsevier

alone [51]. Interestingly, the resulting particles can have core/shell morphology or a more dense structure, depending on the solution composition [52], and undergo reversible swelling/collapse transitions according to the cross-link density, which can be tuned with the concentration of the components (Fig. 3) [52].

It has also long been acknowledged that the presence of a small amount of salt leads to a more uniform distribution of the short chain components among the polyelectrolyte with the longer chains, and thus thermodynamic equilibrium [23]. More recently it has also been demonstrated that temperature annealing can lead to more organized liquid crystalline structures of DNA—lipid systems [55] and single-molecule structures of xanthan—chitosan systems [56] (see below).

1.6 Structure of the Polyelectrolyte Complexes

Polyelectrolyte complexes adopt structures with extent of order depending on the type of molecules involved and their molecular parameters. The structures of PEC have conceptually been described to span from the formation of a lattice-like structure where the pairing of the opposite charges are viewed to induce a railway track structure of the polyanion-cation (also named a ladder-like structure), to a fuzzy type of structure coined a “scrambled egg” organization (Fig. 1) [23, 25].

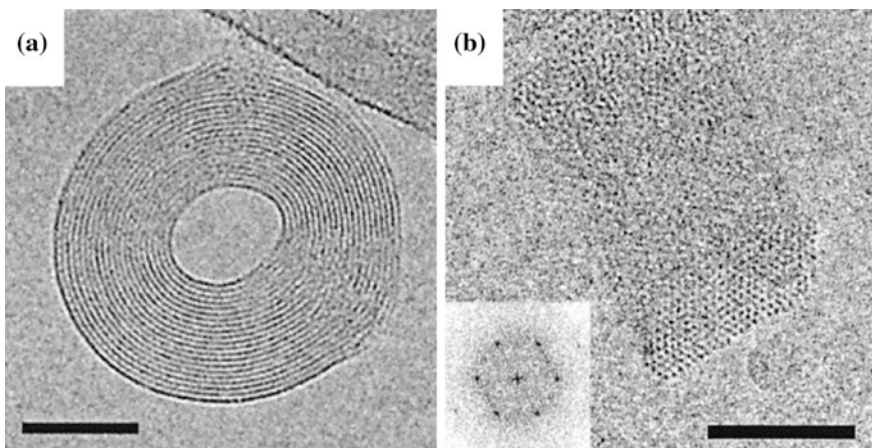


Fig. 4 Cryo-electron micrograph of lambda DNA toroids induced by cobalthexamine: **a** top-view and **b** edge-view highlighting the internal hexagonal organization. The insert in panel **b** depicts the Fourier transform of a region of the micrograph showing a highly organized structure. The scale bar is 50 nm. Reproduced with permission from Hud and Downing [57]. Copyright (2001) National Academy of Science, USA

The consecutive pairing of interaction sites, e.g. the railway track motif, within polyelectrolyte complexes exists probably within locally well-organized parts of compacted DNA. Ultramicroscopy of DNA complexes in their toroidal state by cryo-TEM [57] have revealed insight into the DNA chain intracomplex packaging (Fig. 4). The precise hexagonal polymer chain packing of compacted λ -phage DNA at the single-toroid level does contain structural information beyond the lateral intersegment interaction reported to be mechanistic in driving DNA collapse transition to the toroidal state. Recent research efforts in developing non-viral delivery vehicles for gene therapy have also increased the experimental basis for obtaining DNA toroids as a result of the compaction with cationic polymers, including e.g. polyethylenimine [58, 59], chitosans [60], poly-L-lysine [61, 62], and various synthetic co-polymers developed for tuning the transfection efficiency [63]. The finding that different polycations applied as condensing agents for DNA in most cases yield toroidal morphologies is remarkable. The limited influence of the detailed chemical structure of the polycations employed for DNA complexes indicate the importance of a general, in this case, electrostatic mechanism.

The folding of DNA to a toroid by a nucleation-and-growth mechanism is supported by the size of the toroid coinciding with the optimum cyclization probability for a wormlike chain, as investigated using direct fluorescence imaging of single DNA as well as Brownian dynamics simulation [64–66]. Thus, the initial nucleation loop is initiated by thermally activated fluctuations of the semi-flexible DNA while the polycation support formation of intersegment interactions. The

importance of the size of the initial nucleation loop has also been demonstrated by comparing the compaction of DNA with or without static curvature [67, 68]. When condensing DNA with cobalt hexamine, it has been found that inserting sequences with A-tracts can reduce the outside toroidal diameter to 45 nm as compared to 130 nm for DNA without such loops [67]. However, the reduced toroidal diameter induced by insertion of static loops did not yield a concomitant change of the toroid thickness. This suggests that the toroid diameter is determined by the nucleation loop while the thickness of the toroid depends on the solution conditions. Furthermore, the formation of larger toroids was not blocked with the incorporation of curved DNA, a small fraction of toroids with size comparable to those produced in the absence of static loops was also observed [67]. The kinetic control of toroidal size of polyelectrolyte complexes is also suggested by observation of xanthan and chitosan complexes being toroids with toroid size corresponding to optimal cyclization probability of xanthan having a persistence length of 120 nm [55].

The reports that polyelectrolyte complexes undergo rather slow processes in adoption of a state that are considered to represent the lowest free energy are challenging for the interpretation of thermodynamic data. Insight into this emerges from Brownian dynamic studies revealing that the evolution of a semi-flexible chain from an extended chain to a toroid progresses through a number of morphologies, such as racquets [69, 70]. Some of these intermediates are found to possess extended lifetimes, most likely reflecting high energy barriers to neighbouring states in the folding pathway. The resulting energetically trapped states may therefore be observed and the system will not reach the ground state, e.g., the toroidal states for complexes involving semi-flexible components. Rod-like polyelectrolyte complexes have been reported for DNA complexes [60, 62, 71, 72]. In view of the simulations, such states could represent kinetically trapped states [73, 74]. Other numerical studies suggest that the rod is a ground state, with approximately the same energy as the toroid [75–77].

AFM imaging of polycation (PEG-modified PAMAM)—DNA complexes were acquired at 5 min intervals to assess information related to the condensing pathway [78]. The data suggested co-existence of toroids and rods, but indicated also inter-conversion between toroids and rods as the condensed state. The possible toroid—rod inter-conversion in this case is probably related to the energy barrier between the morphologies. AFM imaging of heat treated xanthan—chitosan complexes indicated rearrangement of structures following duration and level of high temperature treatment [56]. Considering ultra-microscopy as snapshots of the state at the condition of sample extraction, the consecutively extracted samples revealed in the AFM topographs with an increasing fraction of toroids and reduced fraction of complex, e.g. multi-loop, morphologies (Fig. 5). These observations have been compared with recent simulations on dynamics of semi-flexible polymer chain collapse [79].

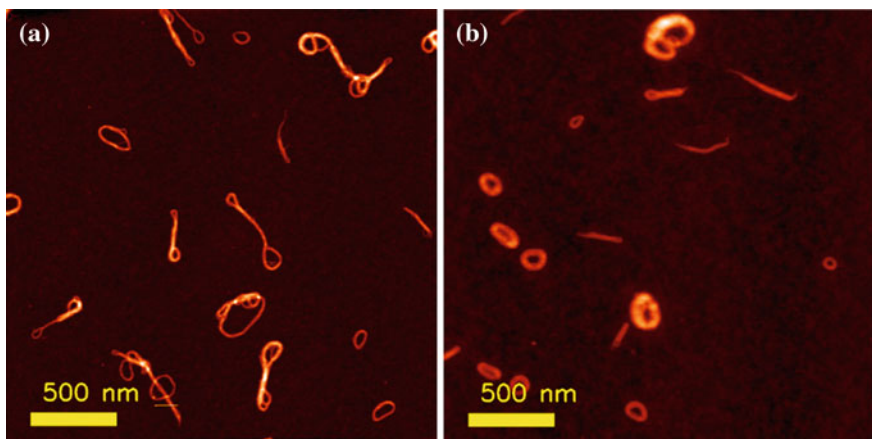


Fig. 5 AFM topography of chitosan—xanthan polyelectrolyte complexes as prepared at low concentrations at room temperature (a) and following annealing at high temperature (b). Topographs from the collections reported on in reference [56]. Reprinted with permission from Lappala and Terentjev [79]. Copyright (2013) American Chemical Society

1.7 Experimental Observations at the Individual Complex Level

Previously, single molecule studies were mostly restricted to microscopic imaging techniques and the observation of the impact of interactions on the overall structure and morphology of the complexes. Recently, the development of single-molecule techniques and their applications within molecular biology function of motor proteins and impact of external load on their processive properties has been reported. Such single-molecule strategies as supported by an experimental toolbox comprising e.g. optical tweezers, atomic force microscope or bio-membrane force probe, appears to be less exploited in the field of intra- and possibly intermolecular interactions within polyelectrolyte complexes. Nevertheless, some incipiently reported data obtained at the individual complex level illustrate the type of insight that can be generated by such an approach. The scrutiny of interaction forces within polyelectrolyte complex and the individual complex level and the possible effects of their cofactors represent a novel entry point into the understanding of their behaviour.

The direct determination of interaction forces between polyanion and polycations were recently reported by van der Gucht et al. [27]. In their study, the interaction between a cationic block copolymer (poly(*N*-methyl-2-vinylpyridinium)-block-polyethylene oxide) covalently attached to triangular SiN₃ AFM probes and a polyanionic brush were determined at ionic strengths from 0.5 to 3 M. The cationic block copolymer was covalently attached to the AFM tip by end-linking of the polymer chain through its PEO block thereby facilitating the electrostatic

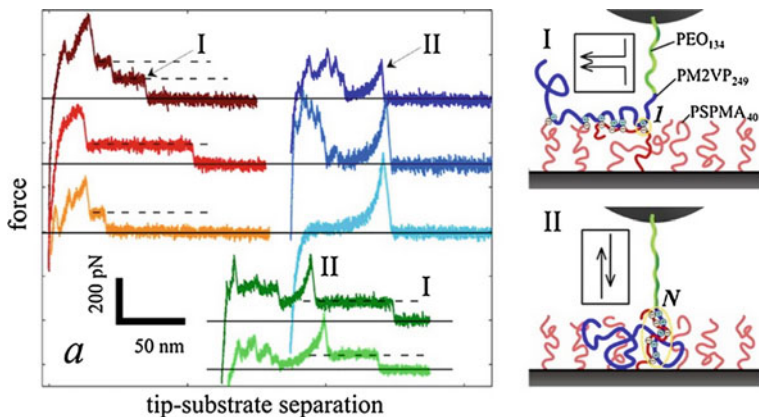


Fig. 6 Force–distance profiles observed for forced dissociation between polycation linked to an AFM tip and a polycation brush observed in aqueous 1 M NaCl solution. Successful anchoring events were observed to yield either ladder-like desorption profiles, or stretching of polymer chains just prior to the unbinding events, referred to as type *I* and *II*, respectively. The type *I* desorption profiles was interpreted to represent desorption of ionically bound train like segments of the AFM tethered polyanion from the surface of the polycation brush (*right panel*), whereas polymer stretching signatures and subsequent forced dissociation events (type *II*) was suggested to arise from polycation-polyanion pair interactions embedded within the brush, and with opposite chain polarity as for the type *I*. Reprinted with permission from Spruijt et al. [27]. Copyright (2012) American Chemical Society

interactions. The interaction forces were determined in experiments where the force-distance profiles were recorded for numerous trials and the particular unbinding profiles were observed and analysed. The authors performed experiments where they approach the polyanion surface with the polycation labelled AFM tip, to a contact force of 1–2 nN and no waiting time before starting the retraction. The speed of approach and retraction controlled by the z-piezo was kept constant at 500 nm/s. Two different unbinding profiles were observed. The first unbinding profile, denoted *I*, displayed plateaus with constant force over an extended retraction distance followed by an abrupt decrease in the observed force. Occasionally, constant force heights with twice the value of the basic level were also observed. Such type of constant force plateaus in force distance curves are also reported in forced desorption of polymers from solid surfaces [80, 81]. Such type of desorption can be referred to as a “peeling” behaviour where there is an equilibrium pullout of the polyelectrolyte within an electrostatic attractive field. The type *I* unbinding patterns was interpreted in this context by the suggestion that the polycation linked to the AFM tip associate with the polyanion layer at the exposed surface and by parallel chain orientation (Fig. 6). In general, the type *I* unbinding pattern is experienced under conditions where the individual interaction sites, ionic pairs in this case, associate and dissociate at time scales faster than that of the pulling process [81]. In addition to the type *I* unbinding profiles, Spruijt and coworkers also reported on unbinding profiles where a clear polymer stretching

signature was observed just prior to the unbinding event. This type, denoted II, was interpreted to originate from forced unbinding events of the polycationic chain that was interdispersed within the anionic brush, and with an antiparallel chain orientation. The relative occurrence of type I or type II forced dissociation events were both about 8 % of the total number of trials. Unbinding signatures similar to that identified as type II for the mentioned polycation–polyanion system, are reported for a wide variety of macromolecular pairs, and occur in general when the imposed force ramp occurs on a time scale that is faster than the characteristic lifetime of the interaction.

Types I and II unbinding of the polyanion–polycation interactions were reported to depend differently on the salt concentration in aqueous solution. For type I interactions, Spruijt and co-workers reported that the mean rupture force observed to about 110 pN at 0.5 M NaCl was decreasing upon increasing salt concentration, to 75 pN at 1.2 M NaCl. The decreasing mean unbinding force in this range of ionic strength was interpreted based on salt effect of single ionic bonds.

1.8 Correspondence to Observations at the Ensemble Level

While the forced unbinding studies do provide insight into effects of e.g. salt on fundamental, electrostatic, interactions that is driving the polyelectrolyte complex formation, application of such a strategy is not sufficient to provide a comprehensive understanding of factors affecting their thermodynamic properties.

ITC is a popular technique to study biological interactions since it directly measures enthalpy changes associated with interactions, as well as binding isotherms and concomitant quantification of equilibrium binding constants. The successful extraction of thermodynamic parameters relies on the use of nonlinear least squares curve fitting while employing an appropriate model that describes the interaction under study [82]. The simplest model is one where there is a single independent binding site (SIS), forming a 1:1 ligand/macromolecule complex. However, as the systems increase in complexity so does the evaluation of the data. Many different models have been developed to assess ITC data. For example, in order to study the complex macromolecular interactions that display cooperativity, it is necessary to use binding models that have been developed to take into account multiple binding sites and the possible cooperativity between the binding sites [82]. Other models have been developed specifically for DNA-ligand interactions and include: (1) ligand binding to macromolecules with different independent sites, each with its binding parameters (MIS); (2) non-specific electrostatic DNA binding, also based on SIS but including anti-cooperativity (Fig. 2b shows an example as such fitting, which was only applied to the initial part of the isotherm); (3) and cationic lipid binding to DNA [83].

Recently, the limitations associated with analysis of isothermal titration data of polyelectrolyte complex formation within polypeptide chains applying a lattice-

like interaction model has been suggested to be resolved by including a second process [84]. The first phase of the titration process is dominated by the ion-pairing process and represented in the model used for interpretation of ITC data as the titrant can reversibly interact with binding sites hosted by the polyelectrolyte originally in the sample cell. The second phase reported by Tirrell and co-workers, but also evident in ITC data of other polycation–polyanion titrations, is suggested to arise from thermodynamics associated with domain formation in the coacervation process. This component was in a first approximation represented as a Gaussian in the molar fraction of polyanion (titrant) relative to the total polymer content in the ITC sample chamber (Fig. 2d). This two-phase representation of the ITC data accounted well for the experimental observations of selected oppositely charged polypeptides. Trends in the derived thermodynamic quantities reveal that the initial ion-pairing phase is dominated by an entropic contribution, related to the release of counterions and restructuring of water associated with the complexation. Presence of salt during the complexation reaction leads to reduction of the strength of the electrostatic interaction, with concomitant effects of less efficient counterion release and associated changes in the entropic contribution. The enthalpic part of the term identified with the coacervation contribution was found to decrease with increasing salt concentration, ascribed also to decreased interaction strength leading eventually to less complex coacervate being formed.

The effect of ionic strength on the interaction strength in the forced unbinding studies can be compared with similar effects Tirrell and co-workers reported on complex coacervation of polyethyleneimine (PEI) and polypeptides [38]. Using turbidimetry as the observable, they report on salt effects on complex formation at an acid:base ratio 31:69 mol% and total polymer concentration of 1 mg/ml at pH 7 for a number average molecular weight of the branched PEI of 10 kg/mol, and either polyasparagine or polyglutamine. An initial increase in the turbidity was observed when salt was added to the solution. This was followed by a maximum with larger value the higher molecular weight of the polyglutamine. This maximum occurs for salt concentrations less than 200 mM. Increase of the salt concentration beyond that yielding the turbidity maximum results in decreased turbidity and the turbidity eventually disappears. The higher molecular weight of the polyglutamine extends the turbidity to larger salt concentration. The turbidity reflecting the complex coacervation thus depend on the salt concentration of the solution, mediated through the screening of the electrostatic mechanism similar to that determined directly in the forced dissociation experiments. Additionally, the finding of an increasing chain length of the polyanion substantiating the turbidity reflects differences in connectivity of the complexes at the particular total mass concentration. While similar effects of ionic strength affect the interaction in the direct unbinding assay and the turbidimetry analyses, the turbidimetric analysis additionally provide information on phenomena related chain length of the polyanion ensemble. This latter type of information is not directly accessible in the direct force unbinding strategy. In addition to offering insight of effect of the ionic strength on interaction strengths as compared with data obtained on ensembles outlined above, the data reported based on forced unbinding of polycation–

polyanion pairs are illustrative by providing direct molecular insight into coexistence of various local topologies. The indication of coexistence of various topologies within polyanion–polycation complexes reported from the forced dissociation approach is considered to be well within the concept of “scrambled egg” type of organization. However, ultrastructure observations of polyelectrolyte complexes likely to belong to such a class of organisation does not clearly indicate details of the internal structure, but is mostly limited to overall morphology. Examples of this include e.g. heparin–chitosan complexes [85, 86], and alginate–chitosan [87] complexes. Within these, the persistence length, L_p , of the stiffest polyelectrolyte is in the range of 10 nm. The transformation from dominance of scramble egg structural components, and also overall globular or apparent fuzzy morphologies can be influenced by the persistence length. Indeed, the occurrence of regular toroidal structures frequently reported for DNA, represent a polyelectrolyte complex of a polymer with persistence length 50 nm. Such toroidal structures have much more well defined morphologies than compacted alginate, L_p about 10 nm, that yield mostly non-toroidal morphologies, although a small fraction of toroids were also observed.

1.9 Cooperative Effects in DNA Condensation

Another successful combination of single molecule and ensemble techniques was achieved in the study of the condensation of long DNA molecules.

Fluorescence microscopy (FM) enables the visualization of tagged long DNA molecules, typically above 160 kbp, in solution and the study of their conformational changes upon the interaction with co-solutes, such as oppositely charged species. This technique has put in evidence a number of interesting aspects. Besides the possibility of visualizing the DNA conformational change from an extended coil to a compact structure, it was found that at intermediate concentrations of the compacting agent, the two populations coexist in solution [88].

This so-called coexistence region has been observed for most cationic condensing agents used and its width depends on the efficiency of the agents itself, with large polycations showing shorter coexistent regions, for example [89]. Such a cooperative process, in which it is more favourable to the available compacting agents to bind to DNA molecules that already possess some compacting agents than to “naked” molecules, has been proposed much earlier based on the separation of complexed DNA molecules from the mixtures by centrifugation [90]. More recently, the cooperative nature of the DNA condensation induced by PA-MAM dendrimers was shown resorting to analytical ultracentrifugation [91], cryogenic transmission electron microscopy and dynamic light scattering (DLS) [44]. The condensation of DNA by cationic surfactants has also been investigated in detail (for a recent review see [92]). The most often used cationic surfactants in DNA condensation are monovalent however their ability to self-associate into micellar aggregates provides the multivalent requirements for an efficient DNA

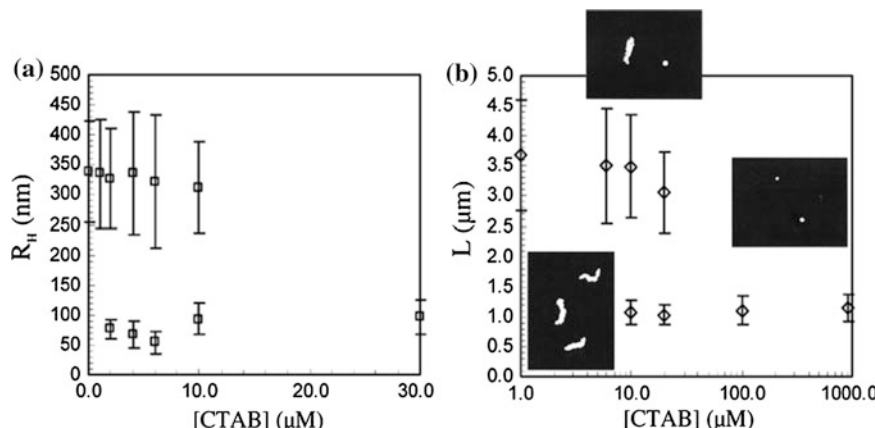


Fig. 7 **a** Hydrodynamic radius of DNA molecules, taken from the position of the peaks of the calculated intensity distribution functions versus the concentration of surfactant, CTAB. The error bars represent the width of the peak at half-height. **b** Long-axis length, L , of DNA molecules, vs. the concentration of CTAB, obtained from fluorescence microscopy experiments. Error bars indicate the statistical error in the distribution and are given by the standard deviation. Reprinted with permission from Dias et al. [96]. Copyright (2005) American Chemical Society. *Inserts* Fluorescence images of T4DNA molecules moving freely in buffer solution under different concentrations of CTAB. (*Left*) T4DNA molecules in the coil conformation, (*middle*) coexistence of coil and globule states and (*right*) all DNA molecules present a globule conformation. Reprinted with permission from Mel'nikov et al. Discrete coil-globule transition of large DNA induced by cationic surfactant J. Am. Chem. Soc. 1995; 117: 2401–2408.). Copyright (1995) American Chemical Society

condensation, the so-called double-cooperativity effect [93]. The compaction of DNA was found to occur at the critical association concentration (CAC) [94], the concentration at which the surfactant starts forming micelles in the vicinity of polymers [95]. Here we refer in particular to a DLS study that clearly shows the coexistence of extended and compacted DNA molecules in solution (Fig. 7) [96]. It is also interesting to refer that the results obtained with DLS (ensemble average technique) and FM (single-molecule technique) agree very well in terms of the size relation between the extended and compact conformations. The limits of the coexistence region did not match fully which is probably related to the fact that the sample preparation for FM includes, in addition to the fluorescence dye, an anti-oxidant to increase the observation times without significant bleaching. In this respect and taking into account that it is an ensemble average technique, the results obtained using DLS are more reliable.

As mentioned, the cooperative nature of DNA condensation has been recognised and reviewed already in 1972 by von Hippel and McGhee [90]. As they put it then, the cooperativity is somewhat counterintuitive, as one would expect that a cationic binding agent would rather bind to a “naked” and fully charged DNA molecule, than to bind to a molecule that is already partially occupied which is, in fact, that obtained using simple models [97].

If the compaction of the polyelectrolyte is abrupt above certain charge neutralization, simply the fact that different polyelectrolyte chains experience slightly different environments in solution could lead to the coexistence of extended and compact polyelectrolyte complexes. Such fluctuations in the degree of binding tend to increase with the charge of the compacting agent and are clearly significant in highly coupled systems, such as long polycations, due to the fact that the condensing agent is not likely to exchange between chains (as discussed above) [97]. However, experimental techniques such as ultracentrifugation, have shown that it is possible to separate DNA into two fractions with low- and high-density dendrimer—DNA complexes [91]. The low-density complexes, identified as being uncondensed fractions of DNA, were shown to be transcriptionally active, as opposed to the high-density complexes. Interestingly, a recent NMR study on the dynamics of DNA and PEGylated dendrimer complexes disclosed a large mobility of the dendrimers (in and out of the complexes) in this system, and suggested that the two fractions could be one in the same, with the DNA release being controlled by dendrimer mobility in the complex [98]. Although not probing dynamics, Monte Carlo simulation results suggest that in polyelectrolyte complexes with some chain length asymmetry of the polyelectrolytes, and below charge neutralization, the shorter polyelectrolyte possesses a significant translational along the longer chain which hinders to some extent the condensation of the longer chain [99]. This is more obvious for shorter and therefore less electrostatically coupled polyelectrolytes, which together with the larger probability of dissociation from the long chain, partially explains why a large excess of spermidine, for example, is required to induce the condensation of large DNA molecules in single molecules experiments [89, 100]. The reported results on DNA-dendrimer dynamics using NMR may appear contradictory to other (above mentioned) studies reporting DNA—(high generation) dendrimer complexes as being highly-coupled and kinetically-trapped. However, it should be noted that to avoid polyplex precipitation, PEGylated dendrimers were used. This has consequences on the strength of the interaction between DNA and dendrimers and, in fact, free DNA molecules were found in this system up to higher (amine/phosphate) charge ratios than that observe in systems composed of “naked” dendrimers [98]. It will be interesting to see similar dynamic determinations on non-PEGylated dendrimers of different generations, when the experimental hurdles are overcome.

Returning to the cooperative nature of DNA condensation, the suggestions put forward to explain it in 1972 [90] included (1) the favourable direct interaction between adjacent condensing agents, unlikely for the case of polypeptides but an important mechanism in the case of cationic lipids and surfactants, (2) the formation of separate phases (complex coacervation), or (3) a process in which the conformational changes induced in the DNA by the initial binding molecules favour the binding of additional condensing agents. For example, base tilting upon binding of polylysine, which would provide more easily deformed sites for additional polylysine binding than other binding sites, was given as a support for the later alternative [90]. This type of mechanism is expected to have more relevance in stiffer chains and, in fact, it has been shown that for sufficiently stiff chains the size

distribution functions show two maxima, in the presence of condensing agents, reflecting the fact that individual chains prefer to be in the elongated or compact toroid configurations [101]. The size-distribution function of semi-flexible chains on the other hand is always broader since the chains fluctuate between stretched and collapsed conformations [102]. On the other hand, and using simple models of stiff chains, no evidence was found that a mixture of fully compact and fully extended polyelectrolytes would have a lower free energy than semi-neutralised chains with homogeneously distributed condensing agents (Dias and Linse unpublished).

2 Conclusions

Characterization of the thermodynamics of driving forces in polyelectrolyte complex formation is fundamental for elucidating the impact of polyelectrolyte molecular structure on their capacity to form complexes. However, since the formation of the resulting polyelectrolyte complexes is mediated through interaction capacities along their polymer backbones of various stiffnesses, the situation is very different from “rigid body interactions”. Thus, the understanding of the thermodynamic aspects needs input from data on the structures being formed. In such a context, a combination of tools is considered essential as the way forward in providing more in depth understanding of such a field. The recent report [103] of co-assembly of PEO-PMAA block copolymer with a surfactant studied by ITC combined with nuclear magnetic resonance and time-resolved small angle X-ray scattering is an example illustrating the gathering of chemical, structural and thermodynamic parameters of the assembly process. The requirements for observing complex formation by different tools for samples prepared the same way may, however, be demanding. In the present overview, we have aimed at highlighting that polyelectrolyte complexes form with a wide diversity of structures, and that insight can be generated by the combined approach of observations at the ensemble and single-molecular level, and with the aid of computer simulations. Nevertheless, the flexible and long chain nature of the components involved represent molecular features that may lead to kinetically trapped structures. To what extent thermodynamic parameters obtained on polyelectrolyte complexation represent the parameters for the formation of the complex with the overall lowest free energy, or some kinetically trapped state, are generally difficult to assess.

References

1. Hud, N.V., Allen, M.J., Downing, K.H., Lee, J., Balhorn, R.: Identification of the elemental packing unit of DNA in mammalian sperm cells by atomic force microscopy. *Biochem Biophys Res Commun* **193**(3), 1347–1354 (1993)
2. Ou, Z., Muthukumar, M.: Entropy and enthalpy of polyelectrolyte complexation: langevin dynamics simulations. *J. Chem. Phys.* **124**, 145902–145901/145911 (2006)

3. Carlsson, F., Linse, P., Malmsten, M.: Monte Carlo simulations of polyelectrolyte–protein complexation. *J. Phys. Chem. B* **105**(38), 9040–9049 (2001)
4. Arents, G., Moudrianakis, E.N.: Topography of the histone octamer surface: repeating structural motifs utilized in the docking of nucleosomal DNA. *Proc. Natl. Acad. Sci.* **90**(22), 10489–10493 (1993)
5. Schiessel, H.: The physics of chromatin. *J. Phys. Condens. Matter* **15**, R699–R774 (2003)
6. Dorigo, B., Schalch, T., Kulangara, A., Duda, A., Schroeder, R.R., Richmond, T.J.: Nucleosome arrays reveal the two-start organization of the chromatin fiber. *Science* **306**, 1571–1573 (2004)
7. Mangenot, S., Leforestier, A., Vachette, P., Durand, D., Livolant, F.: Salt-induced conformation and interaction changes of nucleosome core particles. *Biophys. J.* **82**, 345–356 (2002)
8. Mangenot, S., Raspaud, E., Tribet, C., Belloni, L., Livolant, F.: Interactions between isolated nucleosome core particles. *Eur. Phys. J. E* **7**, 221–231 (2002)
9. Bertin, A., Leforestier, A., Durand, D., Livolant, F.: Role of histone tails in the conformation and interactions of nucleosome core particles. *Biochemistry* **43**, 4773–4780 (2004)
10. Allahyarov, E., Löwen, H., Hansen, J.P., Louis, A.A.: Nonmonotonic variation with salt concentration of the second virial coefficient in protein solutions. *Phys. Rev. E* **67**(051404), 051401–051413 (2003)
11. Boroudjerdi, H., Netz, R.R.: Interactions between polyelectrolyte-macroion complexes. *Europhys. Lett.* **64**, 413–419 (2003)
12. Boroudjerdi, H., Netz, R.R.: Strongly coupled polyelectrolyte-macroion complexes. *J. Phys. Condens. Matter* **17**, S1137–S1151 (2005)
13. Mühlbacher, F., Schiessel, H., Holm, C.: Tail-induced attraction between nucleosome core particles. *Phys. Rev. E* **74**(3), 031919 (2006)
14. Korolev, N., Lyubartsev, A.P., Nordenskiöld, L.: Computer modeling demonstrates that electrostatic attraction of nucleosomal DNA is mediated by histone tails. *Biophys. J.* **90**, 4305–4316 (2006)
15. Horn, P.J., Peterson, C.L.: Chromatin higher order folding: wrapping up transcription. *Science* **291**, 1824–1827 (2002)
16. Tse, C., Sera, T., Wolffe, A.P., Hansen, J.C.: Disruption of higher-order folding by core histone acetylation dramatically enhances transcription of nucleosomal arrays by RNA polymerase III. *Mol. Cell. Biol.* **18**, 4629–4638 (1998)
17. Müller, M.: Polyelectrolyte Complexes in the Dispersed and Solid State II: Application Aspects. Springer, Berlin (2014)
18. Bertin, A.: Polyelectrolyte complexes of DNA and polycations as gene delivery vectors. *Adv. Polym. Sci.* **256**, 103–196 (2014)
19. Müller, M.: Sizing, shaping and pharmaceutical applications of polyelectrolyte complex nanoparticles. *Adv. Polym. Sci.* **256**, 197–260 (2014)
20. Ankerfors, C., Wågberg, L.: Polyelectrolyte complexes for tailoring of wood fibre surfaces. *Adv. Polym. Sci.* **256**, 1–24 (2014)
21. Petzold, G., Schwarz, S.: Polyelectrolyte complexes in flocculation applications. *Adv. Polym. Sci.* **256**, 25–66 (2014)
22. Decher, G., Schlenoff, J.: Multilayer Thin Films, 2nd Edn. Wiley, Weinheim (2012)
23. Thünemann, A.F., Müller, M., Dautzenberg, H., Joanny, J.F., Löwen, H.: Polyelectrolyte complexes. *Adv. Polym. Sci.* **166**, 113–171 (2004)
24. Bucur, C.B., Sui, Z., Schlenoff, J.B.: Ideal mixing in polyelectrolyte complexes and multilayers: entropy driven assembly. *J. Am. Chem. Soc.* **128**(42), 13690–13691 (2006)
25. Plum, G.E., Arscott, P.G., Bloomfield, V.A.: Condensation of DNA by trivalent cations. 2. Effects of cation structure. *Biopolymers* **30**, 631–643 (1990)
26. Spruijt, E., Van Den Berg, S.A., Cohen Stuart, M.A., Van Der Gucht, J.: Direct measurement of the strength of single ionic bonds between hydrated charges. *ACS Nano* **6**(6), 5297–5303 (2012)

27. Gus'kova, O.A., Pavlov, A.S., Khalatur, P.G.: Complexes based on rigid-chain polyelectrolytes: computer simulation. *Polym. Sci. Ser. A* **48**(7), 763–770 (2006)
28. Narambuena, C.F., Leiva, E.P.M., Chávez-Páez, M., Pérez, E.: Effect of chain stiffness on the morphology of polyelectrolyte complexes. A Monte Carlo simulation study. *Polymer* **51**, 3293–3302 (2010)
29. Bloomfield, V.: DNA condensation. *Curr. Opin. Struct. Biol.* **6**, 334–341 (1996)
30. Bloomfield, V.: DNA condensation by multivalent cations. *Biopolymers* **44**, 269–282 (1997)
31. Guldbrand, L., Jönsson, B., Wennerström, H., Linse, P.: Electrical double-layer forces—a Monte-Carlo study. *J. Chem. Phys.* **80**(5), 2221–2228 (1984)
32. Grosberg, A.Y., Nguyen, T.T., Shklovski, B.I.: The physics of charge inversion in chemical and biological systems. *Rev. Mod. Phys.* **74**, 329–345 (2002)
33. Gelbart, W.M., Bruinsma, R.F., Pincus, P.A., Parsegian, V.A.: DNA-inspired electrostatics. *Phys. Today* **53**, 38–44 (2000)
34. Khan, M.O., Jonsson, B.: Electrostatic correlations fold DNA. *Biopolymers* **49**(2), 121–125 (1999)
35. Mel'nikov, S., Khan, M.O., Lindman, B., Jönsson, B.: Phase behavior of single DNA in mixed solvents. *J. Am. Chem. Soc.* **121**, 1130–1136 (1999)
36. Matulis, D., Rouzina, I., Bloomfield, V.A.: Thermodynamics of DNA binding and condensation: isothermal titration calorimetry and electrostatic mechanism. *J. Mol. Biol.* **296**(4), 1053–1063 (2000)
37. Priftis, D., Megley, K., Laugel, N., Tirrell, M.: Complex coacervation of poly(ethylene-imine)/polypeptide aqueous solutions: thermodynamic and rheological characterization. *J. Colloid Interface Sci.* **398**, 39–50 (2013)
38. Ghai, R., Falconer, R.J., Collins, B.M.: Applications of isothermal titration calorimetry in pure and applied research—survey of the literature from 2010. *J. Mol. Recogn.* **25**(1), 32–52 (2010)
39. Lohman, T.M., Dehaseth, P.L., Record, M.T.: Pentylsine-deoxyribonucleic acid interactions—a model for the general effects of ion concentrations on the interactions of proteins with nucleic-acids. *Biochemistry* **19**(15), 3522–3530 (1980)
40. Mascotti, D.P., Lohman, T.M.: Thermodynamic extent of counterion release upon binding oligosamines to single-stranded nucleic acids. *Proc. Natl. Acad. Sci. USA* **87**, 3142–3146 (1990)
41. Patel, M.M., Anchordoquy, T.J.: Contribution of hydrophobicity to thermodynamics of ligand-DNA binding and DNA collapse. *Biophys. J.* **88**, 2089–2103 (2005)
42. Park, S.Y., Harries, D., Gelbart, W.M.: Topological defects and the optimum size of DNA condensates. *Biophys. J.* **75**, 714–720 (1998)
43. Ainalem, M.-L., Carnerup, A.M., Janiak, J., Alfredsson, V., Nylander, T., Schillen, K.: Condensing DNA with poly(amido amine) dendrimers of different generations: means of controlling aggregate morphology. *Soft Matter* **5**(11), 2310–2320 (2009)
44. Carnerup, A.M., Ainalem, M.-L., Alfredsson, V., Nylander, T.: Watching DNA condensation induced by poly(amido amine) dendrimers with time-resolved cryo-TEM. *Langmuir* **25**(21), 12466–12470 (2009)
45. Lasic, D.D.: Liposomes in Gene Delivery. CRC Press, Boca Raton (1997)
46. Carlstedt, J., Lundberg, D., Dias, R.S., Lindman, B.: Condensation and decondensation of DNA by cationic surfactant, spermine, or cationic surfactant—cyclodextrin mixtures: macroscopic phase behavior, aggregate properties, and dissolution mechanisms. *Langmuir* **28**(21), 7976–7989 (2012)
47. Pinto, M.F.V., Moran, M.C., Miguel, M.G., Lindman, B., Jurado, A.S., Pais, A.A.C.C.: Controlling the morphology in DNA condensation and precipitation. *Biomacromolecules* **10**(6), 1319–1323 (2009)
48. Babak, V.G., Merkovich, E.A., Galbraikh, L.S., Shtykova, E.V., Rinaudo, M.: Kinetics of diffusionaly induced gelation and ordered nanostructure formation in surfactant-polyelectrolyte complexes formed at water/water emulsion type interfaces. *Mendeleev Commun.* **10**(3), 94–95 (2000)

49. Morán, M.C., Miguel, M.G., Lindman, B.: DNA gel particles: particle preparation and release characteristics. *Langmuir* **23**(12), 6478–6481 (2007)
50. Lapitsky, Y., Kaler, E.W.: Formation of surfactant and polyelectrolyte gel particles in aqueous solutions. *Colloids Surf. A* **250**(1), 179–187 (2004)
51. Lapitsky, Y., Eskuchen, W.J., Kaler, E.W.: Surfactant and polyelectrolyte gel particles that swell reversibly. *Langmuir* **22**(14), 6375–6379 (2006)
52. Morán, M.C., Pais, A.A.C.C., Ramalho, A., Miguel, M.G., Lindman, B.: Mixed protein carriers for modulating DNA release. *Langmuir* **25**(17), 10263–10270 (2009)
53. Morán, M.C., Laranjeira, T., Ribeiro, A., Miguel, M.G., Lindman, B.: Chitosan-DNA particles for DNA delivery: effect of chitosan molecular weight on formation and release characteristics. *J. Dispersion Sci. Technol.* **30**(10), 1494–1499 (2009)
54. McManus, J.J., Rädler, J.O., Dawson, K.A.: Observation of a rectangular columnar phase in a DNA—Calcium—Zwitterionic lipid complex. *J. Am. Chem. Soc.* **126**(49), 15966–15967 (2004)
55. Maurstad, G., Stokke, B.T.: Metastable and stable states of xanthan polyelectrolyte complexes studied by atomic force microscopy. *Biopolymers* **74**, 199–213 (2004)
56. Lazutin, A.A., Semenov, A.N., Vasilevskaya, V.V.: Polyelectrolyte complexes consisting of macromolecules with varied stiffness: computer simulation. *Macromol. Theory Simul.* **21**(5), 328–339 (2012)
57. Hud, N.V., Downing, K.H.: Cryoelectron microscopy of l-phage DNA condensates in vitreous ice: The fine structure of DNA toroids. *Proc. Natl. Acad. Sci. USA* **98**, 14925–14930 (2001)
58. Boussif, O., Lezoualc'h, F., Zanta, M.A., Mergny, M.D., Scherman, D., Demeneix, B., et al.: A versatile vector for gene and oligonucleotide transfer into cells in culture and in vivo: polyethylenimine. *Proc. Natl. Acad. Sci. USA* **92**, 7297–7301 (1995)
59. Petersen, H., Kunath, K., Martin, A.L., Stolnik, S., Roberts, C.J., Davies, M.C., et al.: Star-shaped poly(ethylene glycol)-block-polyethylenimine copolymers enhance DNA condensation of low molecular weight polyethylenimines. *Biomacromolecules* **3**, 926–936 (2002)
60. Danielsen, S., Vårum, K.M., Stokke, B.T.: Structural analysis of chitosan mediated DNA condensation by AFM: influence of chitosan molecular parameters. *Biomacromolecules* **5**, 928–936 (2004)
61. Kwoh, D.Y., Coffin, C.C., Lollo, C.P., Jovenal, J., Banaszczuk, M.G., Mullen, P., et al.: Stabilization of poly-L-lysine/DNA polyplexes for in vivo gene delivery to the liver. *Biochim. Biophys. Acta* **1444**, 171–190 (1999)
62. Liu, G., Molas, M., Grossmann, G.A., Pasumarty, M., Perales, J.C., Cooper, M.J., et al.: Biological properties of Poly-L-lysine-DNA complexes generated by cooperative binding of the polycation. *J. Biol. Chem.* **276**(37), 34379–34387 (2001)
63. Akinc, A., Lynn, D.M., Anderson, D.G., Langer, R.: Parallel synthesis and biophysical characterization of a degradable polymer library for gene delivery. *J. Am. Chem. Soc.* **125**, 5316–5323 (2003)
64. Sakaua, T., Yoshikawa, K.: Folding/unfolding kinetics of a semiflexible polymer chain. *J. Chem. Phys.* **117**, 6323–6330 (2002)
65. Matsuzawa, Y., Yonezawa, Y., Yoshikawa, K.: Formation of nucleation center in single double-stranded DNA chain. *Biochem. Biophys. Res. Commun.* **225**, 796–800 (1996)
66. Yoshikawa, K., Matsuzawa, Y.: Nucleation and growth in single DNA molecules. *J. Am. Chem. Soc.* **118**, 929–930 (1996)
67. Shen, M.R., Downing, K.H., Balhorn, R., Hud, N.V.: Nucleation of DNA condensation by static loops: formation of DNA toroids with reduced dimensions. *J. Am. Chem. Soc.* **122**, 4833–4834 (2000)
68. Conwell, C.C., Vilfan, I.D., Hud, N.V.: Controlling the size of nanoscale toroidal DNA condensates with static curvature and ionic strength. *Proc. Natl. Acad. Sci. USA* **100**, 9296–9301 (2003)

69. Schnurr, B., MacKintosh, F.C., Williams, D.R.M.: Dynamical intermediates in the collapse of semiflexible polymers in poor solvents. *Europhys. Lett.* **51**, 279–285 (2000)
70. Schnurr, B., Gittes, F., MacKintosh, F.C.: Metastable intermediates in the condensation of semiflexible polymers. *Phys. Rev. E* **65**:161904-161161–161913 (2002)
71. Rackstraw, B.J., Martin, A.L., Stolnik, S., Roberts, C.J., Garnett, M.C., Davies, M.C., et al.: Microscopic investigations into PEG-cationic polymer-induced DNA condensation. *Langmuir* **17**(11), 3185–3193 (2001)
72. Eickbush, T.H., Moudrianakis, E.N.: The compaction of DNA Helices into either continuous supercoils or folded-fiber rods and toroids. *Cell* **13**, 295–306 (1978)
73. Noguchi, H., Saito, S., Kidoaki, S., Yoshikawa, K.: Self-organized nanostructures constructed with a single polymer chain. *Chem. Phys. Lett.* **261**, 527–533 (1996)
74. Noguchi, H., Yoshikawa, K.: First-order phase transition in stiff polymer chain. *Chem. Phys. Lett.* **278**, 184–188 (1997)
75. Noguchi, H., Yoshikawa, K.: Folding path in a semiflexible homopolymer chain: a brownian dynamics simulation. *J. Chem. Phys.* **113**, 854–862 (2000)
76. Noguchi, H., Yoshikawa, K.: Morphological variation in a collapsed single homopolymer chain. *J. Chem. Phys.* **109**, 5070–5077 (1998)
77. Stevens, M.J.: Simple simulations of DNA condensation. *Biophys. J.* **80**, 130–139 (2001)
78. Martin, A.L., Davies, M.C., Rackstraw, B.J., Roberts, C.J., Stolnik, S., Tendler, S.J.B., et al.: Observations of DNA-polymer condensate formation in real time at a molecular level. *FEBS Lett.* **480**, 106–112 (2000)
79. Lappala, A., Terentjev, E.M.: Maximum compaction density of folded semiflexible polymers. *Macromolecules* **46**(17), 7125–7131 (2013)
80. Hugel, T., Grosholz, M., Claussen-Schaumann, H., Pfau, A., Gaub, H., Seitz, M.: Elasticity of single polyelectrolyte chains and their desorption from solid supports studied by AFM based single molecule force spectroscopy. *Macromolecules* **34**, 1039–1047 (2001)
81. Friedsam, C., Gaub, H.E., Netz, R.R.: Probing surfaces with single-polymer atomic force microscope experiments. *Biointerphases* **1**(1), MR1–MR21 (2006)
82. Brown, A.: Analysis of cooperativity by isothermal titration calorimetry. *Int. J. Mol. Sci.* **10**(8), 3457–3477 (2009)
83. Buruma, N.J., Haq, I.: Advances in the analysis of isothermal titration calorimetry data for ligand—DNA interactions. *Methods* **42**(2), 162–172 (2007)
84. Priftis, D., Laugel, N., Tirrell, M.: Thermodynamic characterization of polypeptide complex coacervation. *Langmuir* **28**(45), 15947–15957 (2012)
85. Boddohi, S., Moore, N., Johnson, P.A., Kipper, M.J.: Polysaccharide-based polyelectrolyte complex nanoparticles from chitosan, heparin, and hyaluronan. *Biomacromolecules* **10**(6), 1402–1409 (2009)
86. Danielsen, S., Strand, S., Davies, C.L., Stokke, B.T.: Glycosaminoglycan destabilization of DNA—chitosan polyplexes for gene delivery depends on chitosan chain length and GAG properties. *Biochim. Biophys. Acta* **1721**, 44–54 (2005)
87. Maurstad, G., Danielsen, S., Stokke, B.T.: Analysis of compacted semiflexible polyanions visualized by atomic force microscopy: influence of chain stiffness on the morphologies of polyelectrolyte complexes. *J. Phys. Chem. B* **107**(32), 8172–8180 (2003)
88. Minagawa, K., Matsuzawa, Y., Yoshikawa, K., Matsumoto, M.: Doi M Direct observation of the biphasic conformational change of DNA induced by cationic polymers. *FEBS Lett.* **295**, 67–69 (1991)
89. Takahashi, M., Yoshikawa, K., Vasilevskaya, V.V., Khokhlov, A.R.: Discrete coil-globule transition of single duplex DNAs induced by polyamines. *J. Phys. Chem. B* **101**(45), 9396–9401 (1997)
90. von Hippel, P.H., McGhee, J.D.: DNA-protein interaction. *Annu. Rev. Biochem.* **41**, 231–300 (1972)
91. Fant, K., Esbjorner, E.K., Lincoln, P., Norden, B.: DNA condensation by PAMAM dendrimers: self-assembly characteristics and effect on transcription biochemistry **47**(6), 1732–1740 (2008)

92. Dias, R.S.: DNA-surfactant interactions. *Encyclopedia of Surface and Colloid Science*, 2nd edn. Taylor & Francis, London (2010)
93. Dias, R., Mel'nikov, S., Lindman, B., Miguel, M.G.: DNA phase behavior in the presence of oppositely charged surfactants. *Langmuir* **16**(24), 9577–9583 (2000)
94. Dias, R.S., Magno, L.M., Valente, A.J.M., Das, D., Das, P.K., Maiti, S., et al.: Interaction between DNA and cationic surfactants: effect of DNA conformation and surfactant headgroup. *J. Phys. Chem. B* **112**(46), 14446–14452 (2008)
95. Holmberg, K., Jönsson, B., Kronberg, B., Lindman, B.: *Surfactants and Polymers in Aqueous Solution*, 2nd edn. Wiley, West Sussex (2003)
96. Dias, R.S., Innerlohinger, J., Glatter, O., Miguel, M.G., Lindman, B.: Coil-globule transition of DNA molecules induced by cationic surfactants: a dynamic light scattering study. *J. Phys. Chem. B* **109**(20), 10458–10463 (2005)
97. Sarraguça, J.M.G., Dias, R.S., Pais, A.A.C.C.: Coil-globule coexistence and compaction of DNA chains. *J. Biol. Phys.* **32**, 421–434 (2006)
98. Prevette, L.E., Nikolova, E.N., Al-Hashimi, H.M., Banaszak Holl, M.M.: Intrinsic dynamics of DNA—polymer complexes: a mechanism for DNA release. *Mol. Pharm.* **9**(9), 2743–2749 (2012)
99. Dias, R.S., Pais, A.A.C.C., Miguel, M.G., Lindman, B.: Modeling of DNA compaction by polycations. *J. Chem. Phys.* **119**(15), 8150–8157 (2003)
100. Khan, M.O., Mel'nikov, S.M., Jönsson, B.: Anomalous salt effects on DNA conformation: experiment and theory. *Macromolecules* **32**(26), 8836–8840 (1999)
101. Khan, M.O., Chan, D.Y.C.: Effect of chain stiffness on polyelectrolyte condensation. *Macromolecules* **38**(7), 3017–3025 (2005)
102. Dias, R.S., Linse, P., Pais, A.A.C.C.: Stepwise disproportionation in polyelectrolyte complexes. *J. Comput. Chem.* **32**, 2697–2707 (2011)
103. Uchman, M., Gradzielski, M., Angelov, B., Tosner, Z., Oh, J., Chang, T., et al.: Thermodynamic and kinetic aspects of coassembly of PEO-PMAA block copolymer and DPCl surfactants into ordered nanoparticles in aqueous solutions studied by ITC, NMR, and time-resolved SAXS techniques. *Macromolecules* **46**(6), 2172–2181 (2013)

Stratified Interpolyelectrolyte Complexes: Fabrication, Structure and Properties

Eduardo Guzmán, Marta Ruano, Francisco Ortega
and Ramón G. Rubio

Abstract The electrostatic Layer-by-Layer (LbL) technique allows the fabrication of polyelectrolyte multilayers that can be considered as a special type of interpolyelectrolyte complexes supported by a template (fluid or solid). The main characteristic that confers special interest to these interpolyelectrolyte complexes is the simplicity and versatility of the method used for their fabrication, although in some cases this may hide the complex influence of the different physico-chemical variables. The possibility to change ionic strength, pH, temperature, etc. and/or the composition makes possible to control the properties and structure of these systems. Furthermore, the compositional and structural richness of these systems opens multiple possibilities for the fabrication of nano-structured materials with tailored properties for numerous applications (from optical to nanomedical devices). This chapter deal with the physico-chemical background of the fabrication of supramolecular films by the LbL method as well as the key properties that should be managed in order to obtain functional materials following this approach.

1 Introduction: Polyelectrolyte Multilayers and Layer-by-Layer Method

The ability of the polyelectrolytes to form self-organized supramolecular structures, together to their capacity to form complexes when polyelectrolytes of opposite charge are mixed are well-known phenomena, and they have been studied from

E. Guzmán (✉)

Istituto per l'Energetica e le Interfasi (IENI), U.O.S. Genova, Consiglio Nazionale delle Ricerche (CNR), Via de Marini 6, 16149 Genoa, Italy
e-mail: e.guzman@ge.ieni.cnr.it

E. Guzmán · M. Ruano · F. Ortega · R.G. Rubio

Departamento de Química Física I, Facultad de Ciencias Químicas, Universidad Complutense de Madrid, Ciudad Universitaria s/n, 28040 Madrid, Spain

long time [1–5]. In the last 20 years, there has been an increasingly interest on the application of polyelectrolyte based systems in the design and fabrication of new materials [6, 7]. An elegant way to take advantage of these special characteristics of the polyelectrolyte systems is the fabrication of stratified interpolyelectrolyte complexes, usually known as polyelectrolyte multilayers (PEMs). They are built by the sequential assembling of opposite charged materials using the Layer-by-Layer self-assembly approach (LbL) [8–10]. This technique was first introduced by Iler [8] in the 60s, and later revisited by Decher et al. [11, 12] in the first half of the 90s of the last century [13], and it has undergone a fast development during this latter twenty years [10, 14]. This method has become a powerful technique for the fabrication of Nanomaterials with controlled structures and functions, being very frequently used technology due to its simplicity, low cost, and versatility [15, 16]. In addition, a vast number of applications in different fields of Nanotechnology (interfacial phenomena, colloids, and nanomaterials) have been described for the materials obtained following this approach [10, 15–17]. The LbL method presents many advantages over other, such as the Langmuir-Blodgett techniques (LB) [18, 19] and the fabrication of self-assembled monolayers (SAMs) [20–23]. The LbL method enables the fabrication of ultrathin polyelectrolyte films with well-defined thickness, composition, and multiple chemical functionalities [16].

The basic LbL approach as was described by Decher [24, 25] consists on the alternate deposition of opposite charged polyelectrolytes onto a solid substrate that is the template of the assembling. The alternate adsorption of the polyelectrolytes occurs mainly by direct electrostatic interaction between the successive adsorbed polyelectrolytes with opposite charge. The entropy change during the adsorption process may play an important role.

The most conventional building blocks used in the building of LbL multilayers have been opposite charged polyelectrolytes. However, the list of the components has grown to include other families of materials, both charged and non-charged, including colloidal nanoparticles [26–28], microgels [29], dyes [30], dendrimers [28, 31], clays [32–34], carbon nano-objects [35, 36], biopolymers such as enzymes, polysaccharides, proteins and nucleic acids [37–42], viruses [43] and others. The choice of these building blocks is strongly dependent on the desired application [13]. Furthermore the LbL approach is not exclusively limited to the fabrication of materials by electrostatic interactions, being possible to use other types of interactions, among these the most explored are hydrogen bonding [44, 45], charge transfer interaction [46], molecular recognition [47, 48] or coordination interactions [49]. A wide range of substrates with different nature can be used as templates for the fabrication of the complex materials: macroscopic solid flat substrates [13], colloidal particles [50–52], fluid interfaces (floating multilayers) [53–56], liposomes or vesicles [57], or even cells [58]. In summary, the LbL technique can be applied to solvent accessible surfaces of almost any shape and geometry, which allows the fabrication of PEMs with a wide variety of characteristics: from flat films to nano- and micro-capsules [56, 59].

LbL materials often present similar properties independently of the initial template. This allows important advancements in the development of new applications [60] such as optical devices [13], contact lenses [13], conductive layers [61], permselective membranes [62], sensors [63], light-emitting thin films [64], electrochromic films [65], non-linear optical devices [66], nanocapsules [67], and self-healing coatings [68–70]. In addition, an increasingly attention has been paid to the developments of the applications of LbL materials in the biomedical field, especially in tissue engineering, fabrication of medical devices, nanocapsules for drug delivery and DNA encapsulation [71, 72]. Furthermore, vesicles and liposomes coated with multilayers have received attention as delivery agents or as microrreactors [73–75]. More recently, the fabrication of biomimetic systems with multiscale organization has focused the research efforts of different groups. These systems are obtained by the integration of different PEMs capsules in a superstructure also obtained by the LbL technique [76–79].

It is worth mentioning that currently most of the works in the literature are devoted to the study of multilayers of synthetic polyelectrolytes. Some iconic examples of these systems are multilayers of type $(\text{PDADMAC} + \text{PSS})_n$ (PDADMAC: poly(diallyl-dimethyl-ammonium chloride), and (PSS: poly(4-styrene sulfonate of sodium)) where the subindex n indicates the number of bilayers in the multilayer [80–82] or $(\text{PAH} + \text{PSS})_n$ (PAH: poly(allylamine hydrochloride)) [83]. However, there is a growing interest in the last years on the fabrication of biocompatible systems, e.g. biomacromolecules [84, 85]. Some examples are multilayers of type $(\text{CHI} + \text{HEP})_n$ (being CHI Chitosan and HEP Heparin) [86] $(\text{PLL} + \text{HA})_n$ (PLL is poly(L-lysine) and HA is hyaluronic acid) or $(\text{PLL} + \text{PGA})_n$ (PGA is poly(glutamic acid)) [87, 88].

The fabrication of PEMs following the LbL approach must be considered as a multidisciplinary challenge that involves different research areas, e.g. chemistry, physics, biology, engineering, etc. However, the development of materials based in LbL systems with real world applications requires the scaling up of the laboratory work to an industrial level, which implies to be able to engineer the LbL materials following similar principles than those used for bulk materials [89]. For this purpose, new methodological approaches have been developed to replace the classical fabrication of multilayers by dipping [16]: spraying and spin-coating. These techniques allow a faster fabrication of LbL multilayer without compromising the film properties, enabling the development of LbL nanomaterials at the industrial level. This chapter reviews the current state and trends on the study of the physico-chemical features of polyelectrolyte assemblies and their applications.

The research efforts, both theoretical and experimental, have tried to understand mainly the growth mechanism, and the dependence of the adsorbed amount of material on the number of adsorbed layers, N, as well as on the developments of the potential applications of this type of materials [13]. Despite this extensive research certain physico-chemical properties related to these systems remain not well-understood yet [16]. This lack of knowledge affects especially to the understanding of the growth mechanism, internal structure and molecular properties of polyelectrolyte multilayers, and to their cross relationships [80, 90–95].

Among these variables probably those most important are: the charge density of the molecules and of the substrates [96–98], concentration [99], ionic strength [80, 81, 95], solvent quality for the precursors [81], pH [100, 101], and temperature [102]. A quantitative understanding of their effect on the final structure of the multilayers is crucial, in part because multilayers are non-equilibrium systems, and therefore their structures strongly depend on the experimental conditions and procedures used for their growth, that is critical in the fabrication of new materials.

2 Fabrication of Stratified Interpolyelectrolyte Complexes

2.1 Charge Compensation and Assembling Driving Forces: Electrostatic Versus Entropic Effects

The formation and growth of polyelectrolyte multilayers is the result of an intricate balance of interactions [103], among their components: polyelectrolyte—polyelectrolyte, polyelectrolyte—solvent, polyelectrolyte—surface, etc. The different interactions involved are governed by the complex interplay between electrostatic and entropic contributions, as well as solvent quality.

Taking into consideration that the formation of PEMs involves different charged species, it is expected that the electrostatic interaction between the polyelectrolyte adsorbed in the successive layers play a main role in this process. As a consequence, for long time charge inversion after each adsorption cycle was considered as the main driving force of the PEMs assembling. This implies that the deposition of each layer induces the charge overcompensation of the last adsorbed layer. This means that the layer deposition does not occur just till the neutralization of the charge of the previous layer, but continues till a certain degree of charge inversion is reached. The existence of this charge inversion phenomena can seem a priori counterintuitive, but it plays a key role on the formation processes of multilayers by electrostatic interaction [95], and on many other processes and phenomena with interest in both the materials and the biological fields [104].

The existence of charge overcompensation has been demonstrated both on planar substrates, [80, 105] and on colloidal-templates [52]. For this purpose it is necessary to evaluate the surface potential of the system after the deposition of each single layer. It shows an alternance between positive and negative values with the deposition of polycation and polyanion layers, respectively. Different techniques are described in the literature to evaluate the change in the surface potential during the different steps of the assembling of PEMs. Examples are: the surface potential measured with a Kelvin probe [80], the streaming potential [105] and the ζ -potential measurements of colloids coated by PEMs [52]. This latter is the most extended method in the evaluation of the charge inversion of the most frequently studied multilayers such as $(\text{PDADMAC} + \text{PSS})_n$ [13, 80, 103], $(\text{PAH} + \text{PSS})_n$ [52, 83], and other [100, 106]. In the particular case of multilayers $(\text{PAH} + \text{PSS})_n$,

the ζ -potential changes from values around (30 ± 10) mV for the adsorption of the polycation layers to values of (-40 ± 10) mV after the exposition to PSS solutions [52]. It is worth mentioning that the charge inversion degree is characteristic of each pair of polyelectrolytes, and it is not significantly affected by the assembling conditions [83, 100, 107]. The maximum level of overcompensation occurs at the surface of the layers, and its importance decreases almost in an exponential like fashion with the penetration in the layer interior [95]. Figure 1 shows some examples of charge inversion on multilayers obtained by different techniques.

As previously said it is possible to make multilayers even when charge inversion does not play any significant role [108], as in the case of $(\text{PAA} + \text{CHI})_n$ (being PAA poly(acrylic acid)) [100].

The multilayers must be electrically neutral at macroscopic level (beyond the Debye length) [80, 95]. This condition of zero net charge in the PEMs is on the bases of the possible existence of different neutralization mechanisms in polyelectrolyte multilayers. In particular, the neutrality on the PEMs can be achieved by two different mechanisms that are correlated to the different strength of the entropic factors as driving force of the assembling. The first mechanism implies the complete complexation of the polyelectrolytes of the adjacent layers that provokes the neutralization of the PEMs through the formation of complexes with stoichiometry 1:1. This type of compensation is referred to as intrinsic. The complexes formed by an intrinsic mechanism present the highest degree of ionic cross-linking that can be expected for a polyelectrolyte multilayer. This type of complexes are formed due to the release of a large amount of counterions from the polymeric matrix to the solution that provokes a significant reduction of the free energy of the system as a consequence of a strong increase on the entropy due to the counterions release. In this type of complexes the entropic contributions become the main driving force of the multilayers assembling. The second mechanism for the charge compensation of the PEMs implies the presence of counterions in the polymeric matrix in order to neutralize the charge; in this case it can be found complexes with a wide variety of stoichiometries. This is the so-called extrinsic compensation. The importance of the entropic contribution to this kind of compensation is quite limited. Figure 2 shows a scheme with the two types of charge compensation.

The most usual compensation mechanism in PEMs is the extrinsic one [26, 80, 96, 100, 109], being the intrinsic one most usual in PEMs of polyelectrolytes of high charge density [80, 110]. However, it is not possible to give general rules related to the type of expected compensation because it depends on the pair of polyelectrolytes used, and on the assembling conditions [26, 53, 80, 81, 95, 96, 100, 109]. A careful control of the type of compensation plays a critical role in the PEMs properties.

One of the most critical parameters in the control of the compensation mechanism is the ionic strength of the solutions. This is because the changes on the ionic equilibrium in the multilayers are associated to the modification of the charge density by ion condensation mechanism [111]. This fact has been pointed out for one of the classical model of PEMs, $(\text{PDADMAC} + \text{PSS})_n$, by Schlenoff and

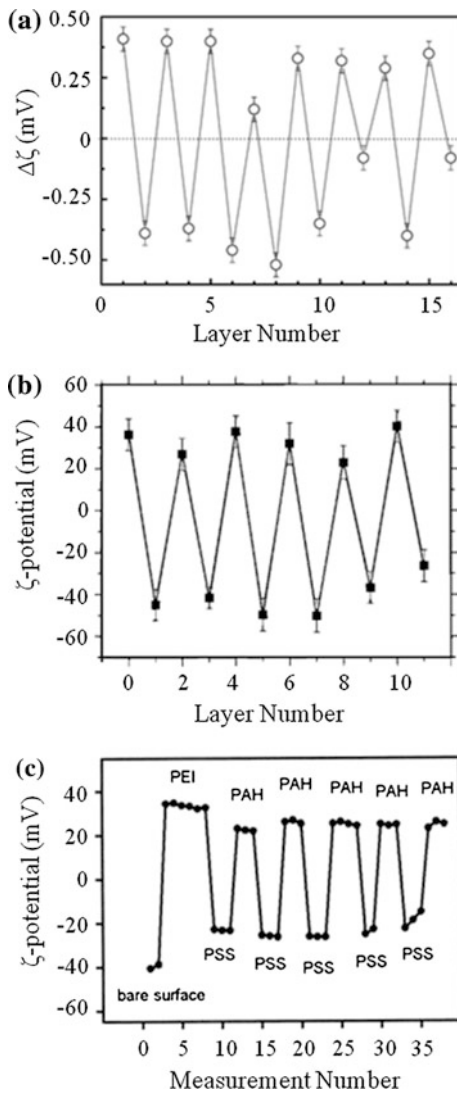


Fig. 1 Charge inversion for polyelectrolyte multilayers represented as the surface potential dependence on the number of adsorbed layer, N. **a** Charge inversion as it was obtained by the Kelvin probe for $(\text{PDADMAC} + \text{PSS})_n$ multilayers adsorbed from a NaCl solution of concentration 50 mM onto a flat surface. Adapted from Ref. [80] with permission from The Royal Society of Chemistry. **b** Zeta potential of $(\text{PSS} + \text{PAH})_n$ multilayers deposited onto colloidal microparticles of methylformamide with a positive bare charge. Adapted with permission from Ref. [52]. Copyright (1998) American Chemical Society. **c** Zeta potential changes evaluated using Streaming potential for multilayers built with PSS and PAH, the results are represented as zeta potential against number of measurement. The number of measurements is related to the number of times that each single layer was measured and it shows as accumulative number with the increase of the layer number. Adapted with permission from Ref. [83]. Copyright (2000) American Chemical Society

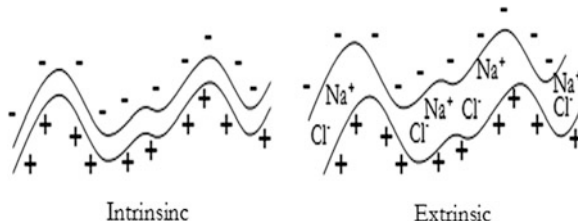


Fig. 2 Two types of charge compensation: intrinsic compensation versus extrinsic compensation. Reproduced from Ref. [80] with permission from The Royal Society of Chemistry

Dubas [95] who managed to switch the process from a mainly intrinsic like compensation to extrinsic compensation (Fig. 3). Guzmán et al. [80] have explained this transition in terms of the entropic contributions to the assembling. When the ionic strength is low, the release of the counterions to the bulk, during the multilayer assembling, strongly increases the entropy of the system, which leads to a mainly intrinsic mechanism. When the ionic strength is increased the release of counterions leads to a less important entropic contribution. In these conditions, the overall bulk concentration of ions provokes that part of the counterions remains trapped in the multilayer, thus reducing the ionic pairing between the charged groups of polyelectrolyte chains of two adjacent layers.

Recent results by Lehaf et al. [112] have pointed out that the type of compensation can be different in the two polyelectrolytes of a given PEM. In the particular case of $(\text{PDADMAC} + \text{PSS})_n$ multilayers, the PDADMAC-terminated PEMs show a compensation that can be considered strongly extrinsic, whereas the compensation of PSS layers is extrinsic. This agrees well with the fact that the compensation ratio between charged unit in PDADMAC, ρ_{PDADMAC} , and PSS layers, ρ_{PSS} , $R_c = \rho_{\text{PDADMAC}} / \rho_{\text{PSS}}$, is higher than 1 (see Fig. 4a) [80].

In accordance with the proposed by Lehaf et al. [112], the different type of compensation that present the different adsorbed polymers determines strong differences in the layer structure. In the particular case of $(\text{PDADMAC} + \text{PSS})_n$ multilayers, the PDADMAC layers present a more swollen character than those of PSS. This is ascribable to the osmotic effect induced by the higher counterions concentration associated to the PDADMAC layers. Figure 4b schematizes the different structure of the layers formed for the different polyelectrolytes. It is worth mentioning that the dependence on the nature of the last adsorbed layers of the charge compensation and swelling degree of the multilayers is reflected in the roughness of the multilayers as was recently reported by Ghostine et al. [113].

Besides the ionic strength, all the parameters that modify the ionic equilibrium in the systems alter the charge compensation mechanism in an analogous way that the described for the case of the ionic strength. Among these parameters it is possible to highlight the type of polyelectrolyte and the charge density of the chains [26, 96], the solvent quality [81] or the pH [100].

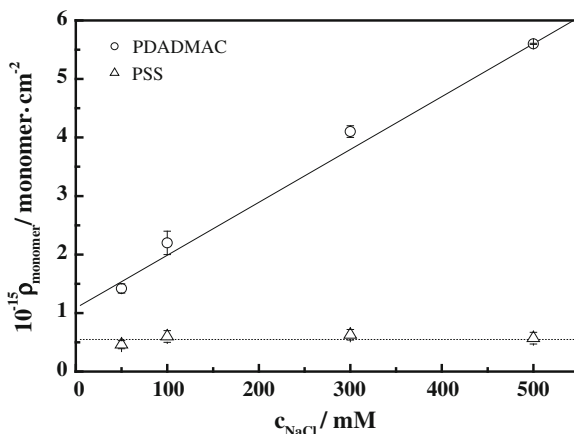


Fig. 3 Surface density of monomer, ρ_{monomer} , for polyanion and polycation layers in $(\text{PDADMAC} + \text{PSS})_n$ multilayers with different ionic strength. Notice that the different amount of adsorbed PDADMAC and PSS is a strong evidence of the existence of extrinsic compensation. Reproduced from Ref. [80] with permission from The Royal Society of Chemistry

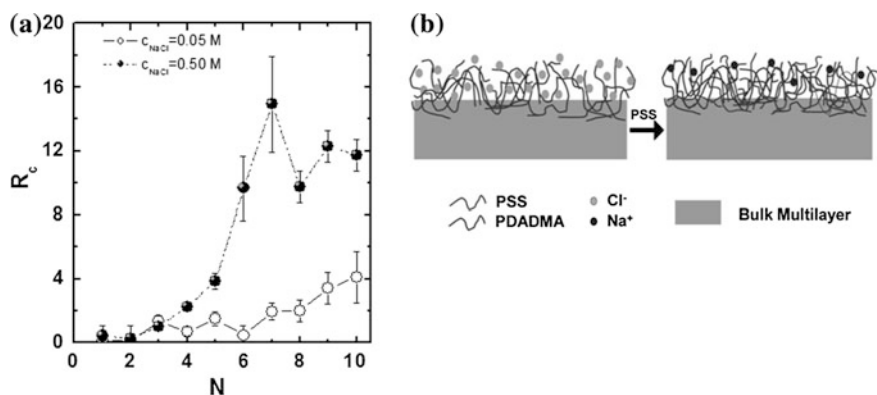


Fig. 4 **a** R_c dependence on N for $(\text{PDADMAC} + \text{PSS})_N$ films built at different ionic strengths. **b** Scheme of the distribution of extrinsic sites in $(\text{PDADMAC} + \text{PSS})_N$ films terminated in PDADMAC and PSS. Reprinted with permission from Ref. [112]. Copyright (2012) American Chemical Society

In addition to the entropic contribution already discussed, there are other entropic contributions that may play a certain role in the assembling process [114]: entropy due to the release and reorientation of water molecules associated to polyelectrolyte chains [115], and entropy penalty due to the attachment of the molecules to the surface [97, 116]. This latter always leads to the increase of the free energy of the system, but this contribution is smaller than the other ones in the majority of the systems.

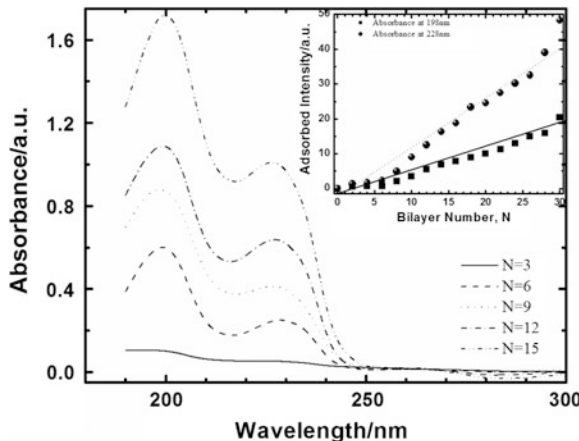


Fig. 5 Changes on the UV-visible spectrum of $(\text{PDADMAC} + \text{PSS})_n$ multilayers adsorbed from pure water solutions with the number of bilayers. Note that only PSS layers show absorbance in this region. The inserted figure represents the dependence of the absorbance on the number of adsorbed bilayers. This latter is a representation of the adsorbed amount

From all the above it is clear that the assembling of PEMs is driven by an intricate balance between the effect of electrostatic factors and the entropic contributions [13]. Considering only an electrostatic control, it would be possible to find situations where the assembling can not follow beyond the charge compensation threshold. This will be especially critical in the case of polyelectrolytes with low charge density, or under conditions of high electrostatic screening where a purely electrostatic control would not allow the formation of PEMs. The fact that it is possible to form of multilayers under the above conditions points out clearly the important role of the non-electrostatic specific interactions in the PEMs assembling [80, 117]. The existence of this non-electrostatic contribution is essential for the formation of multilayers instead of inter-polyelectrolytes complexes in the bulk, which in fact are favoured from a thermodynamic point of view.

2.2 Assembling Methods: Template-Assisted Approaches

The study of the polyelectrolyte multilayers can be done using a broad range of techniques that allow monitoring the growth of the PEMs, either during the assembling process or in a post-fabrication stage. The choice of a specific technique depends on the geometry of the substrate. In the case of flat multilayers, the use of different spectroscopic techniques (UV-Visible, Infrared, ...) [118], dissipative quart crystal microbalance (D-QCM) [80], ellipsometry [100] and reflectivity techniques (neutrons or X-Rays) [80, 119] is widely developed for studying the growth process onto flat substrates. Other techniques such as dynamic light

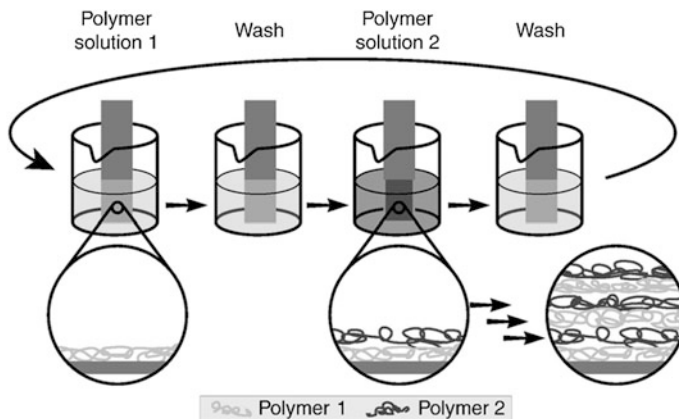


Fig. 6 Sketch of the building of LbL polyelectrolyte multilayers following a dipping methodology. Reprinted from Ref. [123], Copyright (2012), with permission from Elsevier

scattering [57], nuclear magnetic resonance (NMR) [120] give important information of the growth and properties of PEMs adsorbed onto colloidal templates. An example of a growth process followed by UV-visible spectroscopy is shown in Fig. 5, where the absorbance of $(\text{PDADMAC} + \text{PSS})_n$ multilayers with different number of bilayers, N, is shown. Since only the PSS absorb in the studied spectral region, the results point out clearly that the quantity of adsorbed PSS grows linearly with N. For other systems or under different assembling conditions (temperature, pH, ionic strength, etc.), it is possible to find a stronger dependence of the thickness on N. This type of supralinear growth are generally called as exponential growth, although the dependence may not be exactly exponential [121].

The most extended among the LbL methods is the dipping one (Fig. 6) [24]. It consists in the alternate deposition of polyelectrolytes by simple immersion of the substrate in each of the polyelectrolyte solutions. A rinsing step is included between each adsorption step to remove the polyelectrolyte chains that are not strongly adsorbed. In this way the formation of bulk complexes during the adsorption of consecutive layers is prevented. In some cases, a drying step is included after each deposition-rinsing cycle [23]. Different automatic dipping devices have been developed in the last years [23, 122, 123].

The dipping method is time-consuming and difficult for scaling up, and therefore different alternatives have been developed to overcome these problems. The most frequently used alternatives are: spin-coating (Fig. 7a) [124–126] and spraying (Fig. 7b) [127, 128]. They reduce both the time and the amount of material required for the layer deposition, which is important for the scaling-up at industrial level [13].

In spin-coating a drop of polymer solution is deposited on the substrate and afterwards it is spun at constant velocity. Once the layer is deposited, the rinsing

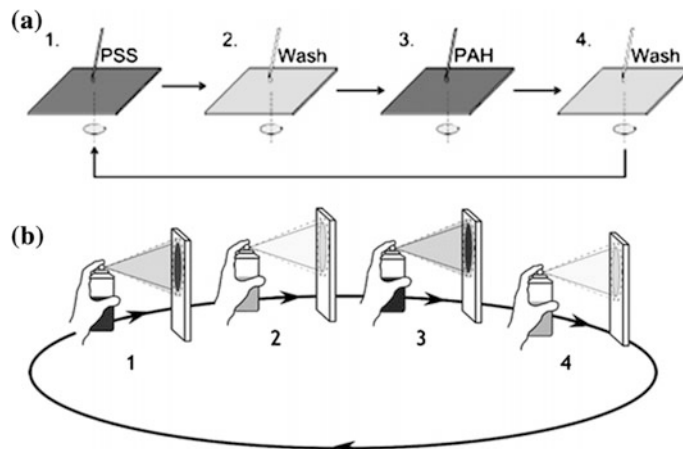


Fig. 7 Schematic representation of the alternative methodologies to the dipping for the fabrication of PEMs onto macroscopic substrates. **a** Spin-Assisted Assembling. Reprinted with permission from Ref. [129]. Copyright (2010) American Chemical Society. **b** Spray-Assisted Assembling. Reprinted with permission from Ref. [126]. Copyright (2009) American Chemical Society

step is performed following the same procedure than that used for the layer deposition, and the substrate is maintained under spinning until total drying. These cycles are repeated the number of times necessary to obtain the desired film [129, 130]. An advantage of this method is the low roughness [130] of the films obtained. Two main parameters play a key role: spinning velocity and solution concentration [131]. However, spin-coating posses many problems when one has to use aqueous solutions due to the low volatility of the water.

The spray-assisted deposition of LbL multilayers was introduced by Schlenoff et al. [132], and consists in the alternate spraying of polyelectrolyte solutions of opposite charge onto the substrate surfaces with the intermediate rinsing cycles. The films prepared by spraying present similar morphology, uniformity and chemical composition than those obtained by dipping [132]. The spraying-assisted deposition of polyelectrolyte layers implies the simultaneous occurrence of two processes: the polyelectrolyte adsorption and the drainage of the solutions. The most usual configuration for the spray-assisted deposition implies to perform the spraying perpendicular to the surface that allows the draining of the solution by gravity and the subsequent quick removal of the excess of polyelectrolyte solution. An adequate film deposition using spraying requires the optimization of the distance between the polyelectrolyte spray and the surface, as well as the control of parameters such as the times of spraying and draining, the concentration of the solutions and the volume and flow of the sprayed solution. In recent years the spray technique has strongly developed by Schaaf et al. [124, 125, 133, 134].

So far we have referred to the LbL fabrication of PEMs onto macroscopic flat substrates. Even though, the physico-chemical bases that govern the fabrication of PEMs onto colloidal particles, liposomes/vesicles or emulsions are similar to those

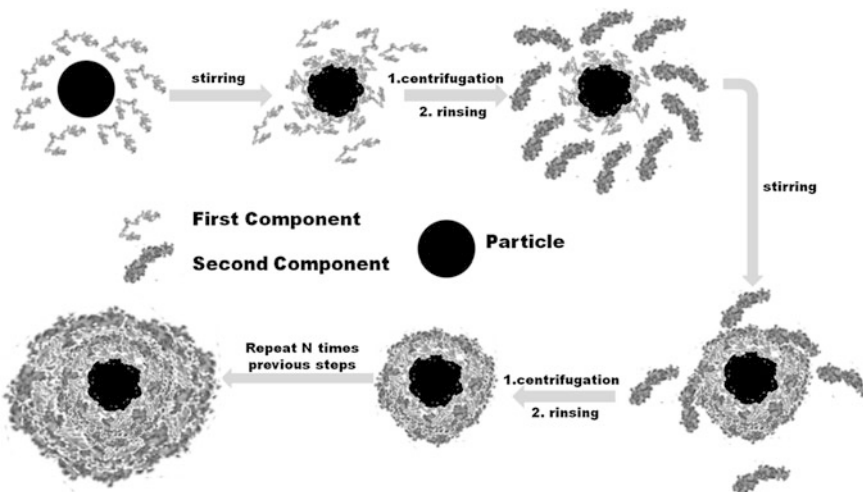


Fig. 8 Schematic representation of the fabrication process of LbL multilayers onto charged particles. The polyelectrolyte multilayer film is formed by the alternate adsorption of oppositely charged polyelectrolytes. After each adsorption step the polyelectrolyte is removed by repeated centrifugation/washing cycles. By repeating this procedure, the desired number of polyelectrolyte layers can be deposited

described for flat multilayers, modifications of the experimental methods are necessary [50, 51, 135]. Even though the coating processes of micro- and nanoparticles is slightly different than that for coating soft liposomes/vesicles, the method follows the steps shown in Fig. 8.

When particles (charged or with some specific chemical groups at the surface) are used as templates, the first step consists in mixing the particles suspension with a solution of the first component of the multilayer [50, 51]. Afterwards, the excess of weakly adsorbed polyelectrolyte is removed by centrifugation [52] or ultrafiltration [136], and the coated particles are re-dispersed in the solvent and several rinsing cycles are made to ensure that the first coating component is fully removed. Then the solution of the other polyelectrolyte is added to form the next layer. These steps are repeated several times until obtaining a capsule with the desired number of layers. In general, the maximum number of layers that can be obtained is lower than for flat substrates [13], because the particle concentration decreases at each centrifugation/ultrafiltration step.

If hollow capsules have to be obtained, a final step has to be added: the dissolution of the particle used as template. This is strongly dependent on the chemical nature of the particles, e.g. polystyrene latex particles are dissolved in tetrahydrofuran, whereas SiO₂ particles using HF [137, 138]. Of course the solvent used must not modify or destroy the assembled multilayer. One has take into account that dilute charged particle suspensions have to be used because during the adsorption of each layer the system passes through the isoelectric point when they can aggregate.

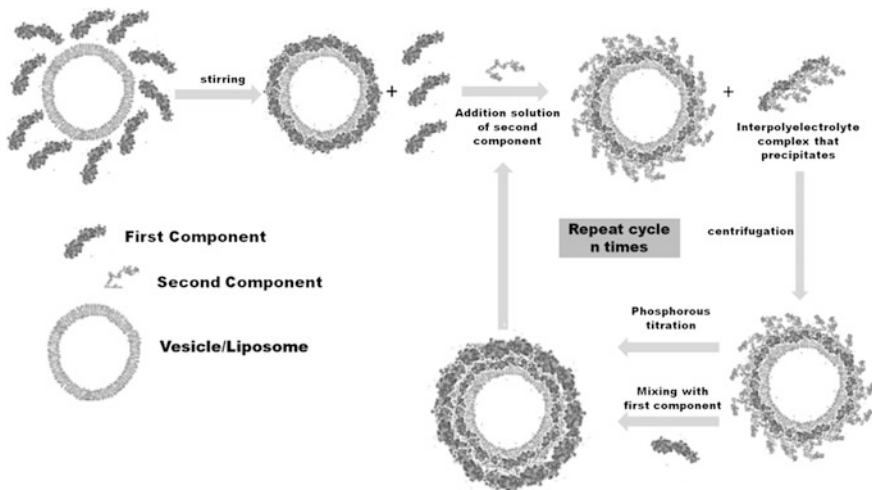


Fig. 9 Schematic representation of the fabrication process of LbL multilayers onto vesicles/liposomes following the experimental procedure by Ruano et al. [139]

The coating process is more difficult when vesicles are used as templates since the centrifugation can lead to their fusion. Nevertheless, centrifugation can be used when enough coating layers have been deposited to render the capsule rigid enough to avoid the fusion. The method shown in Fig. 9 has been demonstrated to be effective in the coating of charged liposomes [139]. A dilute charged liposomes/vesicles suspension is mixed with a solution of the first component. Afterwards, the second component is added in excess, which leads to the formation of an interpolyelectrolyte complex that precipitates, and to the formation of the second layer of the coating film. An aliquote is taken to titrate the phosphorous content in order to estimate the vesicles lost with the precipitate. The rest of the suspension is mixed with an excess of the first component (or a third one) to form the third layer, and the process is repeated until enough layers are obtained. It has been found that the lipids lost in each coating step range from 5 to 10 % depending on the charge density of the liposomes/vesicles used as templates. In general, this slightly increases with the charge density. This limits the number of layers to 8–10, which is not a problem for the capsules to be used for delivering small molecules. A similar method have recently used in Ref. [57] and [140].

It is important to recall that the multilayers are highly hydrated, and contain counterions. Furthermore, the adsorption of a polyelectrolyte layer onto a charged surface is almost irreversible. This is important for multiple potential applications of these systems because it ensures the stability of the multilayers in different environment.

2.3 Growth Mechanisms: Linear, Non-linear and Exotic Growth

A complete understanding of the different aspects that affects the multilayer growth has not been reached yet. In general, two type of dependences of the adsorbed amount on the number of deposited layers, N , (growth mechanisms) have been described in literature [103]: linear and non-linear (usually called exponential). Furthermore, new types have been recently reported [141].

In the linear growth mechanism the thickness of the multilayers depends linearly on the number of layers, N . Typical examples are $(\text{PAH} + \text{PSS})_n$ [83, 99], and $(\text{PDADMAC} + \text{PSS})_n$ when low ionic strength solutions of PDADMAC are used [80]. Other multilayers that show linear growth are $(\text{PAH} + \text{PAA})_n$ (PAA being poly(acrylic acid)) and $(\text{PM2VP} + \text{PSS})_n$ (PM2VP being poly(N -methyl-2-vinyl pyridinium chloride) [142]. Table 1 reports some examples of multilayers growing linearly and non-linearly.

The second growth mechanism is often called exponential and shows a superlinear dependence of the adsorbed amount on the number of deposition cycle. Since the dependence is not in all the case strictly exponential, it is probably more correct to call this mechanism as non-linear growth mechanism. The classical example of this type of growth are multilayer $(\text{PDADMAC} + \text{PSS})_n$ under conditions where the PDADMAC presents a low charge density (i.e. high ionic strength solutions) [80, 81, 95]. This growth is also observed for most multilayers containing biopolymers, such as $(\text{PLL} + \text{HA})_n$ or $(\text{PLL} + \text{PGA})_n$ (PGA being poly(glutamic acid)) [87, 151, 157]. Figure 10 presents a qualitative scheme of the two different growth trends.

Different physical explanations have been given for the two mechanisms. A first explanation is based on the roughness increase during the deposition of the successive layers [80]. An alternative explanation considers the non-linear growth as the result of the possible reorganization of the polyelectrolyte chains, due to the diffusion of at least one of them, through the film during the assembling of the successive layers [121, 152, 158]. In the case of linear growth the roughness of the films remains almost constant along the entire building process of the multilayers [159]. However, a significant increase in the surface roughness is observed after the deposition of a new layer for non-linear multilayers [80, 100, 109]. This leads to a significant increase of the surface area available to the adsorption, and therefore of the adsorbed amount in the successive cycles [159, 160]. These differences in the polyelectrolyte growth trends may be mainly related to differences in the polyelectrolyte conformations as was recently pointed out by Guzmán et al. [99] for multilayers of $(\text{PDADMAC} + \text{PSS})_n$ and $(\text{PAH} + \text{PSS})_n$.

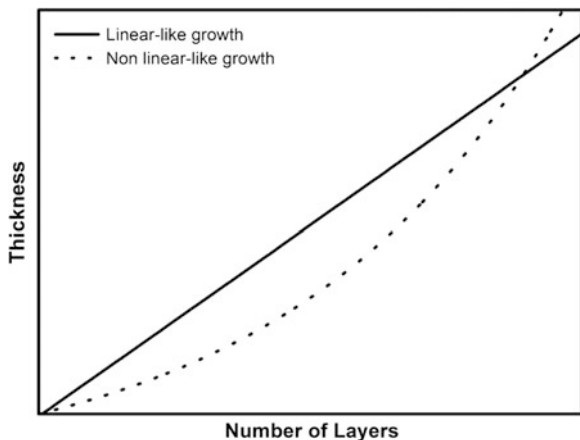
The explanation of the non-linear growth in multilayers as the result of the interdiffusion of the polyelectrolyte chains is based on the existence of a Donnan potential in the polymeric matrix due to the excess of charge due to the adsorption of the layers. This leads to an *in* and *out* interdiffusion of at least one type of

Table 1 Examples of linear growth and non-linear growth PEMs

PEMs	References	Notes
<i>Linear growth PEMs</i>		
(PDADMAC + PSS) _n	[53, 80, 81, 95, 99, 119]	Small charge screening of PDADMAC chains
(PAH + PSS) _n	[83, 99, 119]	Almost independent on the assembling conditions
(PDMAEMA + PSS) _n	[96]	PDMAEMA being a triblock copolymer PDMAEMA-PCL-PDMAEMA, where PDMAEMA is referred to poly[2-(N,N-dimethylamino)ethyl methacrylate], and PCL, to poly(epsilon-caprolactone)
(PAH + PAA) _n	[101, 142]	Dependent on the pH and charge density of the polymers
(PM2VP + PSS) _n	[142]	
(CHI + HA) _n	[143]	
(PDMA + PMAA) _n	[144]	PDMA being poly(2-(Dimethylamino)ethyl methacrylate) and PMAA poly(methacrylic acid)
(PEI + DNA) _n	[145]	PEI being poly(ethylenimine)
(PEI + BSA) _n	[146]	BSA being bovine serum albumine
(PEI + PAA) _n	[147]	
(CHI + ALG) _n	[148, 149]	ALG being alginate
(PEI + ALG) _n	[148]	
<i>Non-linear growth PEMs</i>		
(PDADMAC + PSS) _n	[53, 80, 81, 95, 99, 119]	High charge screening of PDADMAC chains
(PAH + PSS) _n	[102]	Assembling at high temperature ($T > 55$ °C)
(PAH + PAA) _n	[101]	Dependent on the pH and charge density of the polymers
(PLL + HA) _n	[87, 150–152]	
(PAH + HA) _n	[143]	
(CHI + HA) _n	[143]	
(CHI + PAA) _n	[100, 109, 143]	
(PLL + PGA) _n	[153]	
(CHI + PGA) _n	[154]	
(PLL + HEP) _n	[155]	
(Q100 M + PMAA) _n	[144]	Q100 M being a completely quaternized poly(2-(Dimethylamino)ethyl methacrylate)
(CHI + HEP) _n	[156]	

polymer through the whole multilayer structure till the potential is equilibrated [121, 161]. The result of this potential is to increase the adsorbed amount in the successive adsorption cycles, which results in a supra-linear dependence of the

Fig. 10 Linear-like versus Non linear-like growth



adsorbed amount on the number of layers. Figure 11 represents a cartoon illustrating the interdiffusion process.

Currently there is a strong controversy related to the existence of a direct correlation between the interdiffusion in polyelectrolyte multilayers and non-linear growth. Two recent works by Haynie et al. [162] and by Guzmán et al. [99] have raised new questions to this topic. Haynie et al. [162] have proposed that the non-linear growth does not require the existence of interdiffusion, being possible a explanation for this type of growth based in the growth and coalescence of polymer islands during the successive adsorption steps or by dendritic growth as it is schematized in Fig. 12. They demonstrated that this is compatible with the existence of interdiffusion in both linear and non-linear growth multilayers, as latter on pointed out Guzmán et al. [99]. Taking that into consideration, the growth mechanism is determined by the chemical characteristic of the polyelectrolytes and their conformations. In addition to the two classical growth trends above discussed, some particular polyelectrolytes can form multilayers with exotic growth patterns under certain assembling conditions as was evidenced by Cini et al. [141, 163] for the assembling of a short polyanion, poly(sodium phosphate), and PAH. In general, these exotic supramolecular architectures do not verify the main rules of the LbL polyelectrolyte multilayers.

Recent studies by Xu et al. [164] in multilayers of poly(2-(dimethylamino)ethyl methacrylate) and poly(methacrylic acid) have pointed out the correlation of the transition between linear and non-linear growth trend induced by changes of the pH of the solution and the dynamic of interpolyelectrolyte complexes in the bulk. These authors explain this as a consequence of the merging of a steric hindrance to the ionic pairing. This is in agreement with the results by Guzmán et al. [80] that pointed out the transition from a mainly intrinsic compensation for linear growth to a clearly extrinsic compensation for non-linear systems in (PDAD-MAC + PSS)_n multilayers.

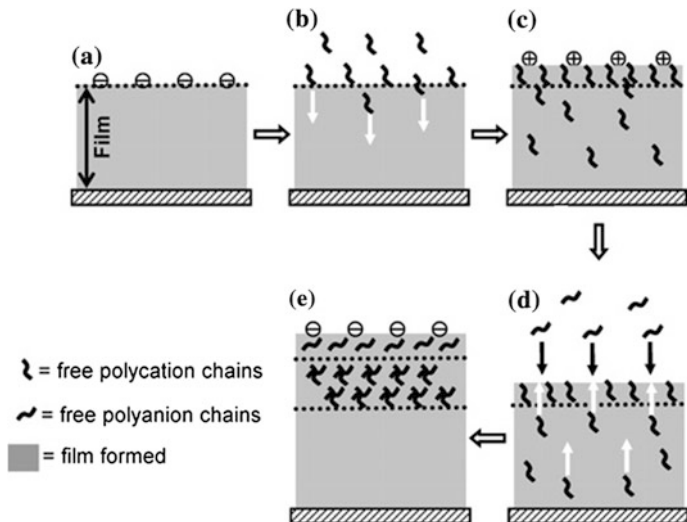


Fig. 11 Schematic representation of the interdiffusion during the layer formation in exponential multilayer growth. Reprinted with permission from Ref. [161]. Copyright (2004) American Chemical Society

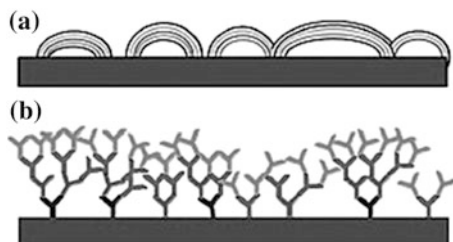


Fig. 12 Alternative models to explain the non-linear growth mechanism of polyelectrolyte multilayer. The substrate is the horizontal slab. The film resulting from successive polymer adsorption steps is shown in different level of gray. **a** Island model. **b** Dendritic model. Reprinted with permission from Ref. [162]. Copyright (2011) American Chemical Society

2.4 Adsorption Kinetics

The adsorption and growth of polyelectrolyte multilayers is determined by an intricate balance of interactions with competitive nature between the polyelectrolyte chains, substrate and solvent [103]. These interactions also affect strongly the adsorption kinetics. The adsorption of polyelectrolytes onto surfaces can be considered quasi-irreversible and it is possible to assume that once the polyelectrolyte chains are attached to the surface they remain adsorbed [165, 166]. This can be understood considering that the adsorption of a polymer chain takes places

through many monomers, and for desorption it is necessary that all the monomers detach simultaneously from the surface. Since the desorption is a dynamic process, some polymer segments can detach from the surface whereas other are reattached, that makes almost impossible the complete desorption of a polymer chain once they are adsorbed at surfaces, at least within the typical temporal scale of the experiments. This kinetic limitation to desorption allows one to explain that the polyelectrolyte layers are not washed out the substrate after their exposition to a solution of a counter-polyelectrolyte.

Despite the recognized importance that presents the study of the adsorption kinetics, a small number of studies have been devoted of this topic [53, 96, 99, 100, 109, 119, 167]. Following a simple mathematical approach, it is possible to describe the adsorption kinetics of polyelectrolytes layers by the Raposo-Avrami model [168, 169],

$$\Gamma(t) = A_1(1 - e^{-t/\tau_1}) + A_2(1 - e^{-t/\tau_2})^n \quad (1)$$

where $\Gamma(t)$ is the total amount adsorbed at time t , A_1 and A_2 are the amplitudes and τ_1 and τ_2 the characteristic times of the fast and slow adsorption steps, respectively. The second term accounted for any reorganization process of the polymer chain after its adsorption at the interface, and it was modeled according to Avrami's model, classically used for the kinetic of polymer crystallization [170, 171]. In general, most of the polyelectrolyte multilayers present adsorption kinetics compatible with $n = 1$ that allows one to rewrite the Eq. (1) in terms of the maximum adsorbed amount, Γ_∞ , as

$$\Gamma_\infty = A_1 + A_2 \quad (2)$$

$$\Gamma = \Gamma_\infty - A_1 e^{-t/\tau_1} - A_2 e^{-t/\tau_2} \quad (3)$$

In general, two well separated kinetic processes are observed and were identified by Bertrand et al. [172] as a first fast nucleation of domains followed by a second slower reorganization of the polymer chains in the multilayer. A more detailed picture allows one to describe the first step as a diffusive process coupled to the adsorption through an electrostatic or steric barrier [166, 173], whereas the second step implies all the reorganization steps that lead to the multilayer till the stationary state [167]. This latter step includes both in plane reorganization of the polymeric chains and the interdiffusion of the polyelectrolyte chains along the whole multilayer structure [99]. Figure 13 shows the adsorption kinetics of a PDADMAC layer onto a (PDADMAC + PSS)_n film.

The Fig. 13 points out clearly the validity of the model above discussed to explain the adsorption. It is worth mentioning that in most cases of the polyelectrolyte multilayers, after the first adsorption step, the adsorbed amount reaches a value around the 60–80 % of the total Γ at equilibrium.

In general, τ_1 does not depend on the number of layers [53, 100], although its value can be changed by different variables such as pH, ionic strength, T, etc., in

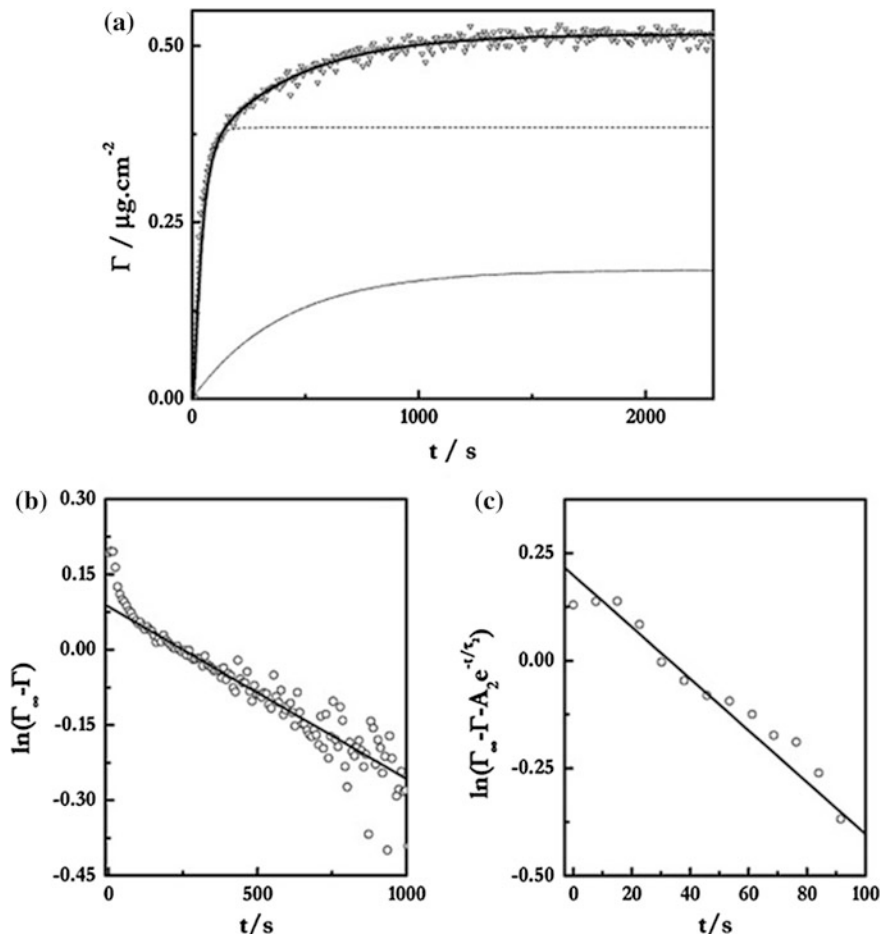


Fig. 13 Example of the analysis of the adsorption kinetics for a layer of PDADMAC adsorbed from a dipping solution with an ionic strength of 100 mM. **a** Adsorption dynamics for the layer of polymer. The *solid line* shows the best fit to Eq. (3). The two exponential components are shown: *dashed line* fast step and *dotted line* slow step. **b** Plot of logarithm of $(\Gamma_\infty - \Gamma)$ versus time, where Γ_∞ represents the surface concentration at the steady-state of the adsorption process, after long adsorption times where the fastest exponential becomes negligible, it can be fitted to a straight line (*solid line*). **c** Short time behavior of the adsorption kinetics, a plot of $\ln(\Gamma_\infty - \Gamma - A_2 e^{-t/\tau_2})$ versus time gives a straight line (*solid line*). Reprinted from Ref. [97], Copyright (2011), with permission from Elsevier

agreement with the computer simulations of Cohen-Stuart [166]. However, τ_2 can present complex dependences on N , and it has been impossible to identify general trends, as it depends on the specific characteristic of each single multilayer [99, 119]. For some systems such as $(\text{PAH} + \text{PSS})_n$ or $(\text{PDMAEMA} + \text{PSS})_n$ (PDMAEMA being a triblock copolymer PDMAEMA-PCL-PDMAEMA, where

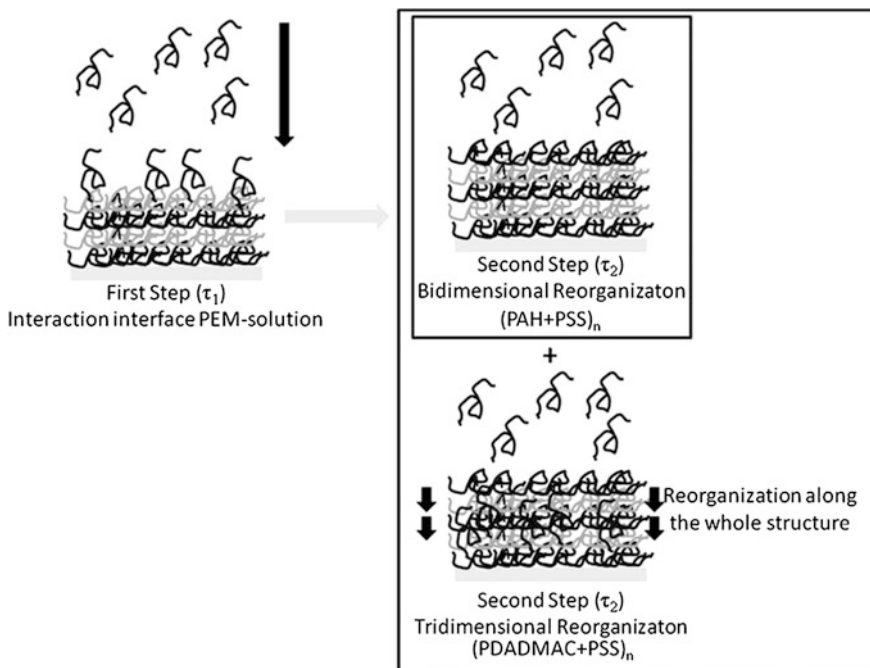


Fig. 14 Schematic representation of the different processes involved in the adsorption of polyelectrolyte multilayers. Reprinted with permission from Ref. [99]. Copyright (2012) American Chemical Society

PDMAEMA is referred to poly[2-(N,N-dimethylamino)ethyl methacrylate], and PCL, to poly(epsilon-caprolactone)) [96, 99, 119], τ_2 is linked to the reorganization process occurring at the multilayer surface, with no relationship with any diffusion through the tri-dimensional multilayer structure. However for other systems, like (PDADMAC +PSS)_n or (CHI + PAA)_n, is a little more complex [99, 100, 119]. These systems show an increase of the adsorption time with the PEMs thickness, which allows ascribing the reorganization process both the interdiffusion of the polyelectrolyte chains and the in-plane reorganization processes. This agrees with the three stage model proposed for Lane et al. [167] for the adsorption process of multilayers formed by PSS and poly[1-[4[(3-carboxy-4-hydroxyphenylazo)benzenesulfonamido]-1,2-ethanediyl sodium salt]. Figure 14 shows an schematic representation of the different processes occurring in the PEMs during the polyelectrolyte adsorption in relation to the different N-dependences of the adsorption time [99].

It is worth mentioning that a detailed study of the N-dependences of the adsorption time allows one to discriminate the possible existence of interdiffusion during the adsorption of polyelectrolyte multilayers [99, 119]. Furthermore, the adsorption times are strongly dependent on the adsorption conditions used for the assembling, and especially to the nature of the components of the PEMs

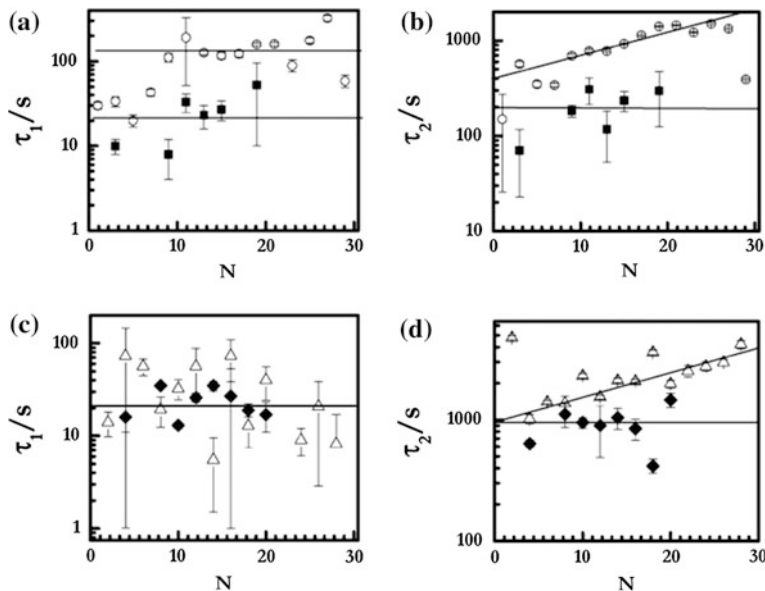


Fig. 15 Kinetic times for $(\text{PDADMAC} + \text{PSS})_n$ and $(\text{PAH} + \text{PSS})_n$ multilayers obtained using Eq. (3). **a, b** Times for the adsorption of PDADMAC (open circle, filled square) and PAH layers. **c, d** Times for the adsorption of PSS in $(\text{PDADMAC} + \text{PSS})_n$ (open triangle) and $(\text{PAH} + \text{PSS})_n$ (filled diamond) multilayers. Reprinted from Ref. [97], Copyright (2011), with permission from Elsevier

[96, 99, 100, 109]. Figure 15 shows as example of the time dependences on N the dependence of the adsorption times on N for the assembling of $(\text{PDADMAC} + \text{PSS})_n$ and $(\text{PAH} + \text{PSS})_n$ adsorbed from NaCl solution of concentration 100 mM. The results point out the different phenomena involve in the adsorption for each specific pair of polymers.

3 Controlling the Fabrication of Polyelectrolyte Multilayers: Effect of Different Physico-chemical Variables

The discussion in the previous section has focused on the description of the physico-chemical bases behind the processes leading to the formation of polyelectrolyte multilayers, and on the main characteristic of the LbL method. In what follows we will discuss how different physico-chemical variables allow controlling the assembling process of LbL architectures, and therefore the structure and properties of the obtained multilayers.

3.1 Polyelectrolytes Nature

The chemical nature of the polyelectrolytes, and the assembling conditions play a key role in the assembling of polyelectrolyte multilayers, and on their thickness, structure and properties [103, 121]. More specifically, the hydrophobic/hydrophobic balance of the chains is probably the most important factor that affects to the PEMs formation because it determines both the interaction between the polyelectrolytes and the swelling degree of the chains [174]. Comparing multilayers built with different polyelectrolytes, von Klitzing et al. [175] pointed out that increasing of the hydrophobicity of the polymer chains increases the PEMs thicknesses: $(PDADMAC + PAMS)_n$ ($PAMS$ being poly(acrylamidesulfonic acid)) < $(PAH + PSS)_n$ < $(PDADMAC + PSS)_n$. It is worth to mention that PSS is more hydrophobic than PAMS. The effect of the increase of the polymer hydrophobicity on the adsorption of polyelectrolytes is mediated by the existence of an unfavourable contribution to the solvation energy of the chains [81]. Another key variable is the flexibility of the polymer chains. This parameter plays a key role in the interaction between the chains and the adsorbed layers [99, 103, 119, 121].

3.2 Solution Concentration

The preparation of LbL multilayers requires the use of solutions with a concentration high enough to obtain an adsorbed mass able to lead to charge inversion [176], the minimum concentration is depending on the material's solubility and charge density [177]. In general, the increase in the polyelectrolyte concentration provokes the increase in the multilayer thickness [96, 119]. Shen et al. [178] pointed out that the increase in the concentration of hyaluronic acid (HA) induces a strong effect on the growth and intermolecular association in multilayers formed by poly(L-lysine) and HA. These authors pointed out that above a threshold HA concentration, around 2 mg/mL, a transition between linear and non-linear growth of the multilayers occurs. Similar dependences have been reported by Guzmán et al. for $(PDMAEMA + PSS)_n$ multilayers [96] and by Garg et al. [179] for multilayers of PAH and Poly[1-(*p*-(3'-carboxy-4'-hydroxyphenylazo)benzenesulfonamide)-1,2-ethandiyl] (see Fig. 16).

3.3 Properties of the Solutions

Some aspects that are affected by the quality of the solvent used for the assembling are the polymer charge density, conformation and solubility [103]. The fine tuning of the solution properties allows controlling the fabrication processes of PEMs and consequently their structures and properties.

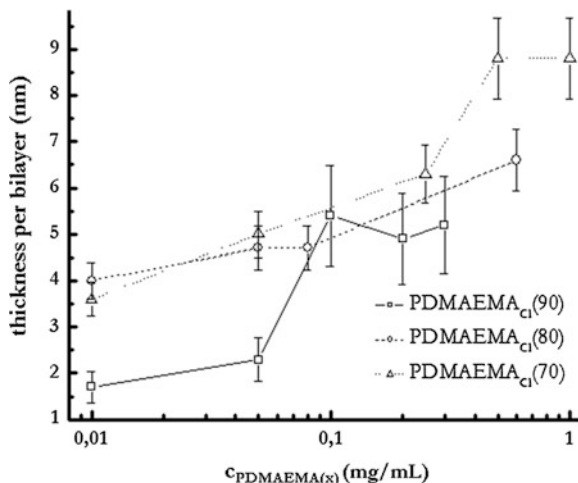
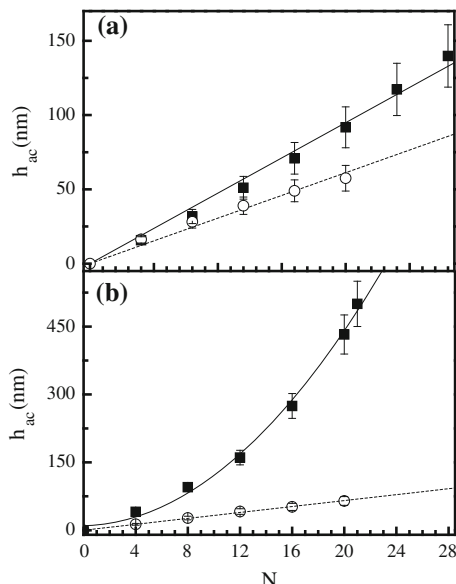


Fig. 16 Concentration dependence of the average thickness per bilayer of $(\text{PDMAEMA}(x) + \text{PSS})_n$, where x indicates the weight content of 2-(N,N-dimethylamino)ethyl-methacrylate in the copolymer. Adapted with permission from Ref. [96]. Copyright (2010) American Chemical Society

In general, polyelectrolytes can be well solubilised in water whereas are poorly soluble in organic solvents [180]. Dubas and Schlenoff [81] pointed out that the thickness of $(\text{PDADMAC} + \text{PSS})_n$ multilayers increases significantly by the use of polymer solutions in mixtures water—ethanol with increasingly content of ethanol. They explained the results as a reduction of the dielectric constant of the medium that favours coil conformation of the chains, thus, leading to an enhancement of their adsorption at the surface. Above a threshold concentration of ethanol, around 40 % in volume, the polyelectrolyte starts to precipitate. Analogous studies have been done for the building of $(\text{PAH} + \text{PSS})_n$ films in solutions containing chloroform or formamide [181, 182]. Long et al. [183] have pointed out that the use of mixtures water—methanol in the building of multilayers between PDADMAC and PAMS allows one to observe the effect of the nature of the counterions according to the Hofmeister series. The trends observed in the growth of the multilayers was the same that those described by Dubas and Schlenoff [81].

Another method for changing the solvent quality is by modifying the ionic strength, I [81]. It modifies the charge density of the polymer chains, and consequently the conformation in solution of the polyelectrolytes, thus leading to changes in the multilayer structure [80, 81, 95]. Increasing I screens the inter- and intra-chains repulsion between the polyelectrolytes, and has the same effect described above for decreasing the solvent quality that leads to the adsorption of the polymers in a more coiled conformation. This phenomena provokes an increase of the film thickness with the ionic strength as observed in Fig. 17 for

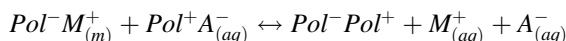
Fig. 17 Effect of I on the growth of PEMs, as h_{ac} (thickness obtained using D-QCM) versus N, for multilayers of $(\text{PDADMAC} + \text{PSS})_n$ (filled square) and $(\text{PAH} + \text{PSS})_n$ (open circle). **a** I = 100 mM. **b** I = 500 mM. The lines are guides for the eyes. Reprinted with permission from Ref. [99]. Copyright (2012) American Chemical Society



both $(\text{PDADMAC} + \text{PSS})_n$ and $(\text{PAH} + \text{PSS})_n$ multilayers [99]. However, above a threshold value of I the thickness of the multilayer does not change, and even the PEMs assembling can be completely hindered. This occurs because the level of screening of the polyelectrolyte charge reaches a high value, which prevents the efficient adsorption of the chains via electrostatic interactions [184]. The deconstruction limit of the multilayers due to the increase of I is strongly dependent on the degree of ionic association occurring in the multilayers [185].

The changes in the pH of the solutions provoke analogous effect on the chains that those above discussed when one of the polymers is a weak polyelectrolyte. This is due to the fact that the pH allows one to modify the ionization degree of the polymer chains, and consequently their charge degree [100, 101]. Good examples are PAH, poly(acrylic acid) (PAA) and most of the biopolymers. An example of the effect of the pH on the multilayer thickness is shown in Fig. 18 for PEI $(\text{PAA} + \text{CHI})_n$ [100]. In this case the effect on the ionization of the chains induces a strong change on their solubility in water. Bieker and Schönhoff [101] pointed out that for $(\text{PAH} + \text{PAA})_n$ the modification of the pH allows the modification of the growth trend of the PEMs.

pH and I change the ionic equilibrium involved in the self assembling, which can be schematized as,



where m and aq mean multilayer and aqueous phase, respectively, Pol refers to the Polyelectrolytes of different charges, and M and A to the respectively counterions.

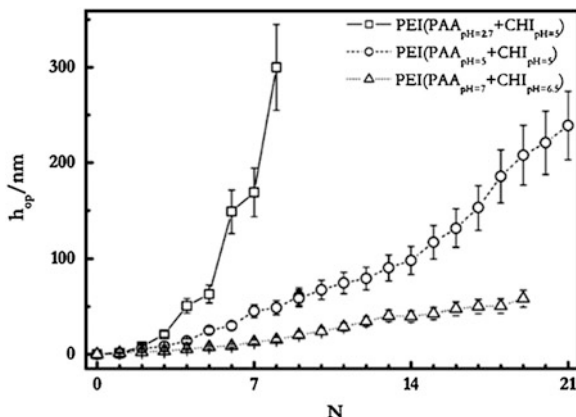


Fig. 18 Thickness obtained using ellipsometry for multilayers $\text{PEI}(\text{PAA} + \text{CHI})_n$ build using different pH combinations for the assembling of layers of PAA and CHI. Reprinted with permission from Ref. [100]. Copyright (2011) American Chemical Society

It is noteworthy that similar values of I at different pH can induce different equilibrium balances and therefore lead to different adsorption [101].

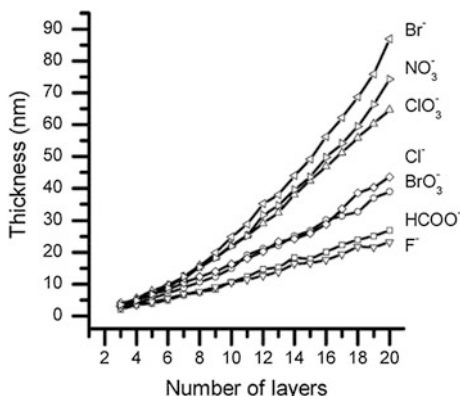
A last parameter involved in the control of the solvent quality is the temperature of the solutions, and its influence can be even stronger than that of I and pH. Despite its importance, low attention has been paid to this parameter in the literature. Salomäki et al. [102] pointed out that the modification of the temperature allows the modification of the growth trend of both $(\text{PDADMAC} + \text{PSS})_n$ and $(\text{PAH} + \text{PSS})_n$ multilayers. Special interest present the transition between linear and non-linear growth for $(\text{PAH} + \text{PSS})_n$ multilayers mediated by the temperature since this system presents a linear growth trend in almost all the I and pH assembling conditions studied in the literature [83, 151].

In summary, the control of the different parameters that affect the solvent quality is essential to tune the structure and properties of PEMs. This plays a key role in the fabrication of materials with potential applications.

3.4 Supporting Electrolyte

The effect of the supporting electrolyte is mainly governed by the well-known Hofmeister serie [186]. In general, the effect of the cations in the growth of polyelectrolyte multilayers is quite limited [187], at least in aqueous systems [183]. The increase of the ions hydrophobicity increases the thickness of the multilayer. Salomäki et al. [188, 189] used different sodium salts, and pointed out that for $(\text{PDADMAC} + \text{PSS})_n$, the multilayer thickness decrease according to: $\text{Br}^- > \text{NO}_3^- > \text{ClO}_3^- > \text{Cl}^- > \text{BrO}_3^- > \text{HCOO}^- > \text{F}^-$ (see Fig. 19). More

Fig. 19 Effect of the counter-anion in the thickness of $(\text{PDADMAC} + \text{PSS})_n$ multilayers. Reprinted with permission from Ref. [189]. Copyright (2004) American Chemical Society



hydrophobic anions bind strongly to the polymer chains and decrease their hydration degree; as a consequence the polyelectrolytes adopt a more coiled conformation, which increases the total thickness and roughness of the PEMs. Even though the effect of the cations is less important, under certain conditions they can play a significant role as it has been recently pointed out by Long et al. [183] for $(\text{PDADMAC} + \text{PAMS})_n$. The thickness of these multilayers increases following the series: $\text{Li}^+ < \text{Na}^+ < \text{K}^+$. The effect of the cations allows one to explain the salt dependence of the film properties for $(\text{PDADMAC} + \text{PSS})_n$ and $(\text{PAH} + \text{PSS})_n$ multilayers as consequence of the subtle differences of the polarizability of the cations [175].

Nevertheless, Hofmeister series is only useful to explain the effect of univalent salts on the thickness, degree of swelling, and extent of layer interpenetration of conventional polyelectrolyte multilayers [190]. However, the situation is more complex in presence of multivalent salts that can promote the formation of intra- or interchain bridge of the polyelectrolyte [191, 192]. Dressick et al. [190] pointed out that the effect of divalent salt in $(\text{PAH} + \text{PSS})_n$ films is correlated to their ability to form bridge between amino groups of the PAH chains. These bridges difficult the packing of the chains, thus leading to the formation of highly porous supramolecular films.

3.5 Drying, Rinsing and Adsorption Time

There are methodological aspects that play an important role in the building of polyelectrolytes multilayers. The adsorption time used for the layers deposition or the rinsing and drying steps between the adsorption of adjacent layers, are among the most important ones.

The time used for the adsorption of polyelectrolyte layers is critical in the fabrication of polyelectrolyte multilayers, especially for those systems where the

interdiffusion along the three-dimensional structure of the multilayers occurs. Guzmán et al. [119] pointed out that $(\text{PDADMAC} + \text{PSS})_n$ multilayers do not have a lamellar structure when the adsorption time is long enough to obtain the complete reorganization of the chains. This effect was not observed by Schmitt et al. [90], and by Lösche et al. [91] in $(\text{PAH} + \text{PSS})_n$ multilayers built using short adsorption times (15–20 min). These results allow one to conclude that the structure of the multilayers is strongly dependent on the adsorption time, and therefore short adsorption times are convenient when it wants stratified multilayer. These results are supported by the molecular dynamic simulations by Panchagnula et al. [193], who found that the multilayer can be frozen by the arrest of the adsorption process at different times. Kharlampieva et al. [131] showed that the fabrication of $(\text{PAH} + \text{PSS})_n$ multilayers using techniques with low time of contact between the layers (e.g. spraying or spin-coating: 30–180 s) lead to well stratified films contrary to what was obtained by techniques where the contact time is long enough to allow for the interdiffusion of the polymer chains (dipping method). Félix et al. [194] reported similar results for other systems.

The rinsing of the polyelectrolyte multilayers after the deposition of the successive layers allows removing the chains that are not strongly adsorbed to the PEMs. The rinsing step prevents the formation of interpolyelectrolyte complexes in solution when the next layer is formed; such complexes would precipitate onto the multilayer, thus modifying its structure and properties [13]. The effect of the rinsing process depends on the nature of the polyelectrolyte. Strong polyelectrolytes are almost unaffected by the washing due to their almost irreversible attachment through strong electrostatic interactions. However, weak polyelectrolytes can be removed easily due to the lower strength of their binding interactions [13].

The LbL approach to fabricate polyelectrolyte multilayers is a wet method [13, 172], and it is expected that the modification of the hydration of the layers by the application of drying steps between the successive deposition cycles may lead to strong structural modifications in the films. The changes that can occur by the drying include modifications in the growth mechanism of the multilayers and the hindering of the adsorption of additional layers [124]. In $(\text{POMA} + \text{PVS})_n$ multilayers (POMA and PVS being poly(o-methoxyaniline) and poly(vinylsulfonic acid), respectively), the drying steps are needed after the adsorption of each POMA layer to obtain an optimal growth of the multilayers [169]. The effect of the drying process in the multilayer structure and properties is strongly dependent on the assembling protocol used. For instance, the structure of $(\text{PAH} + \text{PSS})_n$ is different when it is dried under ambient air than under a nitrogen stream, the latter leading to a more disordered structure [195, 196].

4 Structure: Stratified and Non-stratified Systems

Understanding and controlling the internal structure of the multilayers is essential for tuning the physico-chemical properties of the obtained systems. However, as described in the previous sections, it is necessary to control many variables to obtain the desired structure of a given multilayer. As a consequence, there still is a considerable lack of knowledge in this field.

A main question is whether the film has a lamellar structure, i.e. whether consecutive layers form a stratified multilayer [119, 131, 194]. In general, depends on the specific polyelectrolytes forming the PEMs, on the assembling conditions, and on the protocol used to fabricate the film (deposition time and deposition method) [13, 119, 131, 194]. The most common techniques used to obtain information related to the internal structure and stratification of the PEMs have been reflectivity ones, mainly neutron and X-ray, together to X-ray Photoelectron Spectroscopy (XPS).

The first studies on the structural characterization of the multilayers were made in the model system $(PAH + PSS)_n$ by Schmitt et al. [90], and Lösche et al. [91] using different sequences of layers where each certain number of layers the PSS was replaced by deuterated PSS (d-PSS). These authors found certain degree of stratification, even though a total stratification between single layers was not found, and interdigitation of the layers propagating through three bilayers was observed [90, 91, 197]. Furthermore, these authors found that the degree of stratification was correlated to the multilayer thickness in accordance with the three-zone model for polyelectrolyte multilayers [13, 90, 91, 198]. The roughness of $(PAH + PSS)_n$ increase with the number of layers till it reaches a stationary value due to the effect of densification of the layers during the growing process [90, 91]. These results obtained contrast with the decrease in the roughness with the number of layers observed by Soltwedel et al. [198] for $(PDADMAC + PSS)_n$ multilayers. These differences in the roughness behaviour are ascribable to the existence of interdiffusion in the $(PDADMAC + PSS)_n$ system. From all the system studied, it is possible to distinguish between two types of roughness, topological one as in $(PAH + PSS)_n$ [90, 91] and that provoked by the interdiffusion as in the $(PDADMAC + PSS)_n$ system [198].

However, the results obtained for the $(PDADMAC + PSS)_n$ system are more intriguing than those for $(PAH + PSS)_n$ films [80, 119, 199]. Guzmán et al. [80] studied the internal structure of $(PDADMAC + PSS)_n$ by neutron reflectivity and XPS and they found a complete lack of stratification in the multilayer formed by this polyelectrolyte pair under all the assembling conditions. This was attributed to the long time used for the assembling of the layers, that was longer than that used in previous studies for the $(PAH + PSS)_n$ system [90, 91]. These results allowed hypothesizing the existence of a dynamic constrain in the fabrication of real stratified systems since the different time scale used for the layer adsorption by Guzmán et al. [80] (adsorption of the layer to reach the steady state conditions, around 1 h) and by Schmitt et al. [90] and Lösche et al. [91] (adsorption during

15–20 min). Further studies [119] for $(\text{PDADMAC} + \text{PSS})_n$ and $(\text{PAH} + \text{PSS})_n$ multilayers, using different adsorption times pointed out that there is a strong relationship between the formation of stratified structure and the adsorption kinetics for $(\text{PDADMAC} + \text{PSS})_n$ due to the interdiffusion process, whereas $(\text{PAH} + \text{PSS})_n$ multilayers present structural patterns more or less independent on the time used for the adsorbed [119]. The above scenarios allow one to distinguish between two different kind of solid supported interpolyelectrolyte complexes: stratified and non-stratified. The type of structure formed is strongly correlated to the type of polyelectrolytes used, the time used for the adsorption and the interaction involved.

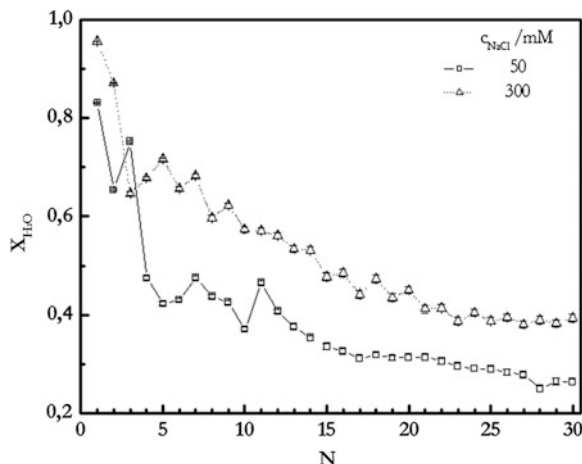
Recently, Gilbert et al. [200] have developed an elegant way to obtain stratified polyelectrolyte multilayers by the addition of single layers that allows blocking the interdiffusion of the other polymers. In absence of such layers a homogeneous blend-like film was observed.

Singh et al. [201] have revisited recently the existence of different regions in the polyelectrolyte multilayers, using (poly(ethylenimine) + PSS) multilayers. They concluded that the multilayers were formed by an inhomogeneous region near to the substrate due to the influence of the interactions between the surface and the polyelectrolyte, and a second more homogeneous region after a certain number of layers have been deposited.

5 Water Content and Hydration

The water content of the multilayers presents a great importance in the dynamic and stability of the formed structures [53, 80, 92, 96, 100, 109, 120, 202–209]. The role of the water in the polyelectrolyte multilayers is the control of the local molecular interactions, especially those related to the complexation between the polyelectrolytes [204]. Different studies have pointed out that the water content of the multilayers is in general quite high, being in the 20–80 % range of the total weight of the PEMs [208, 209]. The water content of the multilayers can be easily tuned changing the assembling conditions and/or the charge density of the polymers (see Fig. 20) [203]. This high water content in the interior of the multilayers confers a gel-like character to the films that makes possible the diffusion of small molecules along the film. This latter plays a key role in applications such as the drug delivery [208, 209]. In general, a decrease of the water content with the increase of N is observed by all the systems studied in literature [210]. This is in good agreement with the measurements of water mobility performed using NMR by Schönhoff et al. [103]. Furthermore, different studies have pointed out that the water content of the polyelectrolyte multilayers is governed by the nature of the outermost layer as deduced from even-odd effect in the water content [211]. Furthermore, Oleh et al. [103] pointed out that the water is asymmetrically distributed along the three-dimensional structure of the multilayers. This has been recently confirmed for Ghostine et al. [113] and Lehaf et al. [212] in

Fig. 20 Water content of $(\text{PDADMAC} + \text{PSS})_n$ multilayers built using solutions of different ionic strength. Reproduced from Ref. [213] with permission from The Royal Society of Chemistry



$(\text{PDADMAC} + \text{PSS})_n$ multilayers. They found that the last layer play a key role in the hydration of the multilayers. PDADMAC-capped films present a higher amount of associated water than those terminated in PSS due to the different ability to associate water of the different polymers.

Recently Dodoo et al. [214, 215] pointed out that two types of water can be identified in polyelectrolyte multilayers: hydration and swelling. The contents of these types of water in the multilayers present the opposite dependence on N .

The degree of swelling of the PEMs is quite important in numerous applications such as release or separation of materials [53, 97, 216]. The swelling degree of the multilayers can be changed by the humidity of the environment and the salt content of the solutions [215]. It controls the ionic pairing between the polyelectrolytes in the adjacent layers, and the degree of cross-linking in the multilayers which controls the mechanical properties [217]. Swelling strongly depends on the nature of polyelectrolytes used because the strength of the ionic pairing depends on their chemical structure [100, 109].

6 Rheological Properties

The control of the mechanical properties of PEMs plays an essential role in the development of materials with potential applications because they control the stability of the PEMs against different external stimuli [218]. In general, the mechanical behavior is reminiscent of both rubber-like and glass-like materials with a wide range of values of the elasticity modulus [219]. The mechanical behavior of the multilayers depends mainly on the specific interaction between the polyelectrolytes [220, 221]. However, there is a strong dependence of the

mechanical properties on the water content. Water is known to be a plastifier [113, 147, 218].

Most of the multilayers show gel-like behavior [222]. However, Nolte et al. [222] pointed out that in the dry state the multilayers have a quite rigid behavior. The changes of geometry, from flat multilayers to capsules, do not modify the mechanical response of the polyelectrolyte layers.

The increase in the ionic strength provokes the decrease in the bulk modulus of the films that allows consider this process as a counterion-plastifying phenomena [83]. More recently Blacklock et al. [80] have pointed out that these modifications of the mechanical properties of polyelectrolyte multilayers by the salt content and nature can be used to enhance the cell adhesion onto substrates modified by PEMs. Changes in pH or ionic strength can induce important transition from mainly fluid to mainly elastic films [83]. Furthermore, it is possible to introduce an additional reinforcement of the multilayers by the cross-linking of the outermost layers which provoke the rigidification of the films [80].

7 Permeability and Porosity

The porosity and permeability of the multilayers play a main role for the development of applications where the exchange of material between the interior of the multilayer and the surrounding environment is needed. In general, it would be expected that rigid films with low water content lead to the formation of non-porous structure, thus hindering the permeability of the molecules along the multilayers. Antipov et al. [222] pointed out that the porosity of polyelectrolyte multilayers can be reversibly triggered by changes in the pH due to changes in the ionization degree of the chains within the PEMs. Other external stimuli such as temperature, light, ultrasound, magnetic field or mechanical deformation can also used to modify the permeability of the multilayers [89].

Yang et al. [14] pointed out that the cross-linking of adjacent layers of PEI and PAA using glutaraldehyde reduce the porosity and consequently the permeability of the films. In this way the $(PEI + PAA)_n$ films perform as good barriers for gas permeability. Lehfaf et al. [17] have studied the effect of the mechanical properties on the salt diffusion along multilayers, and pointed out that the increase in the rigidity of the multilayers makes them less permeable to ions.

8 Response to Osmotic Stress

The response of the multilayers to the osmotic stress is governed by the ionic content in the interior of the multilayers that implies a certain correlation with the type of charge compensation in the film [17, 223]. In general, an osmotic stress can be induced in PEMs by stimuli that change the ionic equilibrium of the multilayers

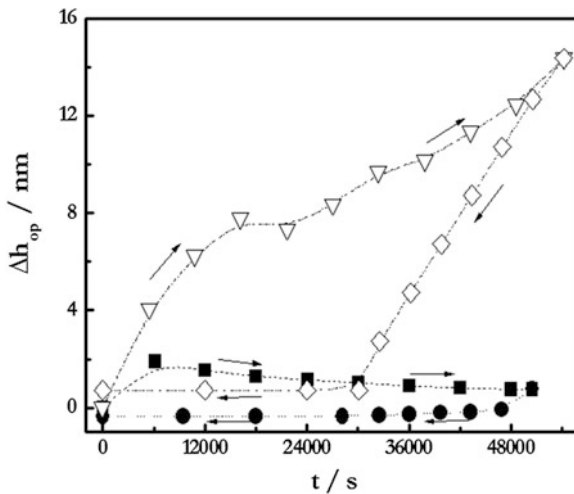


Fig. 21 Osmotic Hysteresis Loop provoked in $(\text{PDADMAC} + \text{PSS})_n$ multilayers for ionic strength changes. *Filled square* and *filled circle* represent the changes in the thickness when the salt solution is replaced for pure water and the inverse process respectively for multilayer built with a $[\text{NaCl}] = 100 \text{ mM}$. *Open inverted triangle* and *open diamond* represent the changes in the thickness when the salt solution is replaced for pure water and the inverse process respectively for multilayer built with a $[\text{NaCl}] = 300 \text{ mM}$. Reproduced from Ref. [84] with permission from The Royal Society of Chemistry

(ionic strength, pH, etc.). The response of the PEMs against osmotic stresses can be considered as anti-polyelectrolyte behavior since the effect of the modifications of the ionic strength of the environment present the opposite effects that those typically expected for polyelectrolytes in solution and adsorbed onto surfaces [224].

Ladam et al. [100, 109, 225] studied the osmotic response of $(\text{PAH} + \text{PSS})_n$ multilayers to change in the ionic strength of the surrounding medium. These authors found that the decrease in the ionic strength provoked the swelling of the multilayer due to release of the counterions from the multilayers to achieve the osmotic equilibrium. This swelling was observed to be completely reversible and the exposition of the multilayers to high ionic strength leads to the shrinking of the film by the uptaking of counterions. Similar results were found by Guzmán et al. [17, 223] for $(\text{PDADMAC} + \text{PSS})_n$. These authors evidenced that the ionic strength used for the multilayer building play a key role in the reversible release-uptaking of counterions. Multilayers built from low ionic strength show a small osmotic response whereas those built from high ionic strength solutions present a strong osmotic response (see Fig. 21). These different behaviors can be ascribed to the different types of charge compensation in the multilayer [17, 223].

Mjahed et al. [14] pointed out that under certain conditions the stress osmotic can induce the partial re-dissolution of the polyelectrolytes in the film. These authors found a critical salt concentration of 0.3 M for the dissolution of

multilayers formed by poly(L-lysine) and hyaluronic acid. The swelling induced above this critical concentration provoked the appearance of holes in the multilayer.

It is worth mentioning that these osmotic effects in polyelectrolyte multilayers play a key role in the design of functional and smart materials, since they affect both the permeability and porosity of the multilayers as well as their swelling degree.

9 Applications: A Multidisciplinary Challenge

In the previous sections, a detailed analysis of the physical-chemistry of the PEMs as well as of their properties has been presented. This section will be devoted of some of the most relevant applications. The fact that the LbL method allows a tunable design of Nanomaterials, together to the possible incorporation of multiple components of different nature into them have stimulated an increasingly interest in the application of PEMs in different areas of the Nanotechnology. Among these applications, the following are among those of special interest: separation membranes, drug delivery devices, and electrochemical and sensing devices [16]. A key role for these applications is played by the possibility to control the film composition along the thickness of the designed supramolecular architectures.

The future advancements of the LbL technology in the design and fabrication of materials with real-life applications requires the possibility to scale-up the LbL approach at industrial level. In spite of the promising origins of the LbL methodology in the fabrication of nanomaterials, the number of real applications is quite limited yet [84]. In the following, a small revision of the most promising applications of the PEMs will be presented.

9.1 Drug Delivery Systems

The most promising field of application of the PEMs is the preparation of effective drug delivery platforms for the controlled release of multiple drugs with a good patient convenience and high effectiveness [84].

Many drugs have been successfully encapsulated in PEMs: ibuprofen, furosemide, nifedipine, naproxen, biotin, vitamin K3, insulin, demathasone, tamoxifen, paclitaxel, and curcumin, as well as DNA fragments, peptides and other therapeutic agents [84]. More recently, a raising interest in the fabrication of coating for application in vaccination has been developed with promising results [85]. An additional challenge associate with the use of PEMs in drug delivery applications is the incorporation of specific functionalities in the delivery platform in order to induce molecular recognition interactions between the drug loaded devices and the cells or tissues. This will allow an increase in the effectiveness of the delivery process.

The fabrication of these systems has been developed for both flat multilayers and capsules [16]. In general, the drug release is triggered by an external stimulus such as changes of pH, temperature or ionic strength, illumination by light, or by biodegradation of the film [62, 226]. The drug contents strongly dependent on the drug nature, and its release can be extended during a time span of 1–100 h, being possible to control the switching on and off upon demand [62, 227]. Guzmán et al. [100, 109] have showed the efficiency of $(PAA + CHI)_n$ multilayers in the encapsulation and release of the β -blocker drug propranolol. They pointed out that the efficient load of drug in the multilayers only occurs when a certain number of layers have deposited due to the densification of the polymeric matrix that hinder the free release of the drug encapsulated in the multilayers. The release was efficiently triggered by changes in the environmental pH.

It is worth mentioning that the encapsulation of the drugs in PEMs is dependent on the nature of the drugs, that makes necessary to consider the hydrophilic-hydrophobic character of the drugs as well as their water solubility in order to design an adequate encapsulation methodology [228]. The encapsulation of water soluble drugs in PEMs is usually performed by the entrapping of the drugs in the polyelectrolyte shell of the capsules, whereas those drugs poorly soluble in water are encapsulated in the interior of the capsules surrounded of the protective polymer shell. This latter can be also applied for the encapsulation of drugs with good solubility in water [17]. In the case of poorly soluble drug, the most extended encapsulation approach is to perform an encapsulation in emulsion where the oil drops containing the drugs are coated by the PEMs [72, 229]. The application of emulsions stabilized by PEMs as encapsulation system open interesting perspective in the successful fabrication of nanocontainers of active species, that allows their retention in the inner volume during long times, and their immediate release on demand [135]. This opens important challenge in several fields such as the drug delivery, and the alimentary industry.

Other interesting application of PEMs in drug delivery is the fabrication of multicapsules [76, 230, 231]. Multicapsules are multicompartimental cargo systems based in the LbL assembling of multiple subunits such as polyelectrolyte layers, liposomes, and nanoparticles. The typical example of these systems consists in the coating of a colloidal template using multiple layers formed by polymers and intact vesicles. Once the supramolecular architecture is obtained, the initial template is removed by dissolution.

These multicapsules, also called capsosomes, can be used in the design and fabrication of artificial cells or organelles with therapeutic purposes [231]. The combination of liposomes and polymers layers allows one to obtain hybrid cargo systems with the advantages of both type of materials, but that overcome some of the limitation associated to the individual materials (e.g. mechanical stability of the liposomes). Furthermore, an important advantage of these multicapsules is the possibility to introduce several functionalities in the systems, that opens important challenge in the future development of drug delivery platforms.

9.2 Biomaterials

The possibility of an ease tuning of the composition of the multilayers allows the building of materials with good bio-compatibility with cells and tissues. This allows the preparation of different coating for biomedical devices, such as stents, tracheal prostheses, artificial vessels and many other applications [232].

The polyelectrolyte multilayers have been also tested as culture environment for cells. The adhesion, proliferation and differentiation of cells have been found very dependent on the nature of the multilayers [233], the stiffness of the multilayers playing a key role in this applications [234]. Furthermore, the possibility to introduce nutrients, genetic materials or different ligands allows the fabrication of culture environment with enhanced properties.

The fabrication of antifouling surfaces to avoid adhesion of organic materials is another research field where the interactions of PEMs with biomaterials have been investigated. One of the systems studied for this application have been the classical $(PAH + PSS)_n$ multilayers with grafted phosphorylcholine and ethylenoxide [235]. These components mimic the antifouling components of the erythrocyte membranes, avoiding the protein adhesion. Other PEMs that can be used as antifouling surfaces are those composed by polysaccharides. Multilayers formed by chitosan and hyaluronic acid have evidenced good properties to avoid the adhesion of serum proteins [85].

9.3 Membranes

Different polyelectrolyte multilayers have been used in the fabrication of membranes for different applications such as fuel cells or separation [16]. The multilayers have evidenced good performance in the separation of several species when they are used as separation membranes [62, 226]. The modification of separation membranes by PEMs for pervaporation or ultrafiltration applications has been widely developed to obtain a better performance of the existing media [62, 227]. Rmaile and Schlenoff [232] have designed chiral multilayers for separation of optical active compounds. Also the fabrication of membranes for selective ion separation have been developed using the LbL approach [233]. Daiko et al. [234] built PEMs optimized for proton transport in fuel cells.

9.4 Self-healing Materials

The application of LbL multilayers in the fabrication of self-healing materials is a very active research field in recent years [68–70]. This has been supported in the possibility to introduce different nano-reservoirs or nano-reactors in the interior of

the multilayers that allows conferring a self-healing character to the manufactured materials. The fabrication of this self-healing materials requires the trapping and homogeneous distribution of the reservoirs along the passive matrix. These nano-reservoirs active their healing characteristics triggered by external stimuli that can present physical, chemical or mechanical nature. The good performance of this type of self-healing materials in the protection of Aluminium surfaces against corrosion was showed by Shchukin et al. [236].

More intriguing that the introduction of nano-reservoirs in PEMs to confer them self-healing properties is the intrinsic self-healing abilities of multilayers formed exclusively by polyelectrolytes [69]. This is related to the dynamics of the chains in the PEMs. In detail, the mobility of the chains in the multilayers favors the healing of the films after a surface damage. Wang et al. [237] pointed out the self-healing character of $(\text{PEI} + \text{PAA})_n$ multilayers. These multilayers present self-healing properties triggered by the water penetration in the internal regions of the multilayers that favors the interdiffusion of the polyelectrolytes in the internal layers to the exterior region of the multilayers. In contrast with the above multilayers, $(\text{PDADMAC} + \text{PSS})_n$ did not evidence any self-healing characteristic that is ascribable to the strong interactions between the polyelectrolyte once the multilayers is formed [238]. This picture allows one to consider that the self-healing character of polyelectrolyte multilayers is confers by the weak polyelectrolytes [69].

10 Conclusions

In this chapter, a revision of the most important physico-chemical aspects involved in the fabrication and properties of PEMs has been presented. The simplicity and versatility of the LbL method in the fabrication of supramolecular materials have allowed a strong development of this approach in different applications. However, this can not hide the complex physico-chemical bases under this process. The main advantage of the LbL method in the fabrication of nano-architectures is the infinite number of control possibilities over the properties and structure of the formed systems due to subtle changes in the assembling conditions.

The formation of polyelectrolyte multilayers by the LbL approach is the result of an intricate balance between different contributions that determines both the growth and structure of the PEMs as well as the properties of the obtained films. Among the factors that govern the assembling of these polyelectrolyte layers special attention must be paid to the competence between mainly electrostatic interactions and entropic contributions to the assembling. The interplay between these contributions determines different physico-chemical properties of the obtained films such as the ionic pairing, the roughness, and the hydration of the films that play a main role in the mechanical properties and permeability of the multilayers.

Other aspects of big importance in the understanding of these systems are the adsorption kinetic and the internal structure of the films which present a strong correlation. The adsorption kinetic includes different steps that determine the distribution of the polyelectrolyte during the adsorption along the multilayers during the deposition. This phenomena allows one different degree of control over the multilayer structure, and more specifically over the stratification of the formed supramolecular architectures.

The multiple possibilities offered by the LbL polyelectrolyte multilayers open several challenges in different industrial and technological fields for the development of several applications. It is worth to mention that the extensive research efforts made in the understanding of the physico-chemical bases of the building of polyelectrolyte can not hide the lack of knowledge remaining in some aspects. This latter has provoked that a vast number of potential applications remain in the laboratory scale yet, being small the number of application that have been scale-up from this latter scale to the real industrial production.

The different aspects analyzed in this chapter have tried to present the state of the art of these intriguing systems from a physico-chemical perspective in order to contribute to a better understanding of the LbL polyelectrolyte multilayers.

Acknowledgments This work was supported in part by MINECO under Grant FIS2012-38231-C02-01, by ESA under Grants MAP AO-00-052 (FASES) and PASTA, and by EU under Grant Marie Curie ITN-COWET, and carried out in the framework of the ERF COST actions CM1101 “Colloidal Aspects of Nanoscience for Innovative Processes and Materials”. We are grateful to the UIRC of the CAI of Spectroscopy (Universidad Complutense de Madrid) for the use of their facilities.

References

1. Kabanov, V.A., Zezin, A.B.: Soluble interpolymeric complexes as a new class of synthetic polyelectrolytes. *Pure Appl. Chem.* **56**, 343–354 (1984)
2. Koetz, J., Kosmella, S.: *Polyelectrolytes and Nanoparticles*. Springer, Berlin (2007)
3. Thunemann, A.F., Muller, M., Dautzenberg, H., Joanny, J.F.O., Lowen, H.: Polyelectrolyte complexes. In: Schmidt, M. (ed.) *Polyelectrolyte with Defined Molecular Architecture II*, pp. 113–171. Springer, Berlin (2004)
4. Philipp, B., Dautzenberg, H., Linow, K.J., Kötz, J., Dawydoff, W.: Polyelectrolyte complexes—recent developments and open problems. *Prog. Polym. Sci.* **14**, 91–172 (1989)
5. van der Gucht, J., Spruijt, E., Lemmers, M., Cohen Stuart, M.A.: Polyelectrolyte complexes: bulk phases and colloidal systems. *J. Colloid Interface Sci.* **361**, 407–422 (2011)
6. Ariga, K., Moria, T., Hilla, J.P.: Evolution of molecular machines: from solution to soft matter interface. *Soft Matter* **8**, 15–20 (2012)
7. Ariga, K., Hill, J.P., Ji, Q.: Layer-by-layer assembly as a versatile bottom-up nanofabrication technique for exploratory research and realistic application. *Phys. Chem. Chem. Phys.* **9**, 2319–2340 (2007)
8. Iler, R.K.: Multilayers of colloidal Particles. *J. Colloid Interface Sci.* **21**, 569–594 (1966)
9. Decher, G., Eckle, M., Schmitt, J., Struth, B.: Layer-by-layer assembled multicomposite films. *Curr. Opin. Colloid Interface Sci.* **3**, 32–39 (1998)

10. Decher, G.: Fuzzy nanoassemblies: toward layered polymeric multicomposites. *Science* **277**, 1232–1237 (1997)
11. Decher, G., Schmitt, J.: Fine-tuning of the film thickness of ultrathin multilayer film composed of consecutively alternating layers of anionic and cationic polyelectrolytes. *Prog. Colloid Polym. Sci.* **89**, 160–164 (1992)
12. Lvov, Y., Decher, G., Möhwald, H.: Assembly, structural characterization, and thermal behavior of layer-by-layer deposited ultrathin films of poly(vinyl sulfate) and poly(allylamine). *Langmuir* **9**, 481–486 (1993)
13. Decher, G., Schlenoff, J.B.: *Multilayer Thin Films-Sequential Assembly of Nanocomposite Materials*. Wiley-VCH Verlag, Berlin (2003)
14. Schlenoff, J.B.: Retrospective on the Future of Polyelectrolyte Multilayers. *Langmuir* **25**, 14007–14010 (2009)
15. de Villiers, M.M., Otto, D.P., Strydom, S.J., Lvov, Y.M.: Introduction to nanocoatings produced by layer-by-layer (LbL) self-assembly. *Adv. Drug Deliv. Rev.* **63**, 701–715 (2011)
16. Lavalle, P., Voegele, J.-C., Vautier, D., Senger, B., Schaaf, P., Ball, V.: Dynamic aspects of films prepared by a sequential deposition of species: perspectives for smart and responsive materials. *Adv Mat* **23**, 1191–1221 (2011)
17. de Villiers, M.M., Lvov, Y.M.: Layer-by-layer self-assembled nanoshells for drug delivery. *Adv. Drug Deliv. Rev.* **63**, 699–700 (2011)
18. Langmuir, I., Schaefer, V.J.: Monolayers and multilayers of chlorophyll. *J. Am. Chem. Soc.* **59**, 2075–2076 (1937)
19. Blodgett, K.B.: Films built by depositing successive monomolecular layers on a solid surface. *J. Am. Chem. Soc.* **57**, 1007–1022 (1935)
20. Love, J.C., Estroff, L.A., Kriebel, J.K., Nuzzo, R.G., Whitesides, G.M.: Self-assembled monolayers of thiolates on metals as a form of nanotechnology. *Chem. Rev.* **105**, 1103–1170 (2005)
21. Nuzzo, R.G., Allara, D.L.: Adsorption of bifunctional organic disulfides on gold surfaces. *J. Am. Chem. Soc.* **105**, 4481–4483 (1983)
22. Bain, C.D., Whitesides, G.M.: Formation of monolayers by the coadsorption of thiols on gold: variation in the length of the alkyl chain. *J. Am. Chem. Soc.* **111**, 7164–7175 (1989)
23. Li, Y., Wang, X., Sun, J.: Layer-by-layer assembly for rapid fabrication of thick polymeric films. *Chem. Soc. Rev.* **41**, 5998–6009 (2012)
24. Decher, G., Hong, J.D.: Buildup of ultrathin multilayer films by a self-assembly process: I. Consecutive adsorption of anionic and cationic bipolar amphiphiles. *Makromol. Chem. Macromol. Symp.* **46**, 321–327 (1991)
25. Decher, G., Hong, J.D.: Buildup of ultrathin multilayer films by a self-assembly process: II. Consecutive adsorption of anionic and cationic bipolar amphiphiles and polyelectrolytes on charged surfaces. *Ber. Bunsenges. Phys. Chem.* **95**, 1430–1434 (1991)
26. Guzmán, E., Ortega, F., Prolongo, M.G., Rubio, M.A., Rubio, R.G.: On the way to functional coatings: polyelectrolyte multilayers. *J. Mat. Sci. Eng. USA* **4**(10), 1–13 (2010)
27. Gao, M.Y., Gao, M.L., Zhang, X., Yang, Y., Yang, B., Shen, J.C.: Constructing PbI₂ nanoparticles into a multilayer structure using the molecular deposition (MD) method. *J. Chem. Soc. Chem. Commun.* **1994**, 2777–2778 (1994)
28. He, J.-A., Valluzzi, R., Yang, K., Dolukhanyan, T., Sung, C., Kumar, J., Tripathy, S.K., Samuelson, L., Balogh, L., Tomalia, D.A.: Electrostatic multilayer deposition of a gold-dendrimer nanocomposite. *Chem. Mat.* **11**, 3268–3274 (1999)
29. Serpe, Michael J., Jones, Clinton D., Andrew Lyon, L.: Layer-by-layer deposition of thermoresponsive microgel thin films. *Langmuir* **19**, 8759–8764 (2003)
30. Ariga, K., Lvov, Y., Kunitake, T.: Assembling alternate dye-polyion molecular films by electrostatic layer-by-layer adsorption. *J. Am. Chem. Soc.* **119**, 2224–2231 (1997)
31. Casson, J.L., Wang, H.-L., Roberts, J.B., Parikh, A.N., Robinson, J.M., Johal, M.S.: Kinetics and interpenetration of ionically self-assembled dendrimer and PAZO multilayers. *J. Phys. Chem. B* **106**, 1697–1702 (2002)

32. Li, Y.-C., Schulz, J., Mannen, S., Delhom, C., Condon, B., Chang, S., Zammarano, M., Grunlan, J.C.: Flame retardant behavior of polyelectrolyte-clay thin film assemblies on cotton fabric. *ACS Nano* **4**, 3325–3337 (2012)
33. Zhuk, A., Mirza, R., Sukhishvili, S.: Multiresponsive clay-containing layer-by-layer films. *ACS Nano* **5**, 8790–8799 (2011)
34. Priolo, M.A., Gamboa, D., Holder, K.M., Grunlan, J.C.: Super gas barrier of transparent polymer-clay multilayer ultrathin films. *Nano Lett.* **10**, 4970–4974 (2010)
35. Correa-Duarte, M.A., Kosiorek, A., Kandulski, W., Giersig, M., Liz-Marzán, L.M.: Layer-by-layer assembly of multiwall carbon nanotubes on spherical colloids. *Chem. Mat.* **17**, 3268–3272 (2005)
36. Qin, S., Qin, D., Ford, W.T., Herrera, J.E., Resasco, D.E.: Grafting of poly(4-vinylpyridine) to single-walled carbon nanotubes and assembly of multilayer films. *Macromolecules* **37**, 9963–9967 (2004)
37. Salloum, D.S., Schlenoff, J.B.: Protein adsorption modalities on polyelectrolyte multilayers. *Biomacromolecules* **5**, 1089–1096 (2004)
38. Jackler, G., Czeslik, C., Steitz, R., Royer, C.A.: Spatial distribution of protein molecules adsorbed at a polyelectrolyte multilayer. *Phys. Rev. E* **71**, 041912 (2005)
39. Svensson, O., Lindh, L., Cárdenas, M., Arnebrant, T.: Layer-by-layer assembly of mucin and chitosan: influence of surface properties, concentration and type of mucin. *J. Colloid Interface Sci.* **299**, 608–616 (2006)
40. Watanabe, J., Shen, H., Akashi, M.: Polyelectrolyte droplets facilitate versatile layer-by-layer coating for protein loading interface. *Acta Biomat.* **4**, 1255–1262 (2008)
41. Pedano, M.L., Martel, L., Desbrieres, J., Defrancq, E., Dumy, P., Coche-Guerente, L., Labbé, P., Legrand, J.-F., Calemzuk, R., Rivas, G.A.: Layer-by-layer deposition of chitosan derivatives and DNA on gold surfaces for the development of biorecognition layers. *Anal. Lett.* **37**, 2235–2250 (2004)
42. He, P., Bayachou, M.: Layer-by-layer fabrication and characterization of dna-wrapped single-walled carbon nanotube particles. *Langmuir* **21**, 6086–6092 (2005)
43. Lvov, Y., Haas, H., Decher, G., Möhwald, H.: Successive deposition of alternate layers of polyelectrolytes and a charged virus. *Langmuir* **10**, 4232–4236 (1994)
44. Stockton, W.B., Rubner, M.F.: Molecular-level processing of conjugated polymers. 4. layer-by-layer manipulation of polyaniline via hydrogen-bonding interactions. *Macromolecules* **30**, 2717–2725 (1997)
45. Wang, L.Y., Wang, Z.Q., Zhang, X., Shen, J.C.: A new approach for the fabrication of an alternating multilayer film of poly(4-vinylpyridine) and poly(acrylic acid) based on hydrogen bonding. *Macromol. Rapid Commun.* **18**, 509–514 (1997)
46. Shimazaki, Y., Mitsuishi, M., Ito, S., Yamamoto, M.: Preparation of the layer-by-layer deposited ultrathin film based on the charge-transfer interaction. *Langmuir* **13**, 1385–1387 (1997)
47. Anzai, J., Kobayashi, Y., Nakamura, N., Nishimura, M., Hoshi, T.: Layer-by-layer construction of multilayer thin films composed of avidin and biotin-labeled poly(amine)s. *Langmuir* **15**, 221–226 (1999)
48. Bourdillon, C., Demaille, C., Moiroux, J., Savéant, J.M.: Step-by-Step immunological construction of a fully active multilayer enzyme electrode. *J. Am. Chem. Soc.* **116**, 10328–10329 (1994)
49. Xiong, H.M., Cheng, M.H., Zhou, Z., Zhang, X., Shen, J.C.: A new approach to the fabrication of a self-organizing film of heterostructured polymer/Cu₂S nanoparticles. *Adv. Mater.* **10**, 529–532 (1998)
50. Sukhorukov, G.B., Donath, E., Lichtenfeld, H., Knippel, E., Knippel, M., Budde, A., Möhwald, H.: Layer-by-layer self assembly of polyelectrolytes on colloidal particles. *Colloids Surf. A* **137**, 253–266 (1998)
51. Donath, E., Sukhorukov, G.B., Caruso, F., Davis, S.A., Möhwald, H.: Novel hollow polymer shells by colloid-templated assembly of polyelectrolytes. *Angew. Chem. Int. Ed.* **37**, 2201–2205 (1998)

52. Caruso, F., Donath, E., Möhwald, H.: Influence of polyelectrolyte multilayer coatings on Förster resonance energy transfer between 6-carboxyfluorescein and rhodamine b-labeled particles in aqueous solution. *J. Phys. Chem. B* **102**, 2011–2016 (1998)
53. Guzmán, E., Ritacco, H., Ortega, F., Svitova, T., Radke, C.J., Rubio, R.G.: Adsorption kinetics and mechanical properties of ultrathin polyelectrolyte multilayers: liquid-supported versus solid-supported films. *J. Phys. Chem. B* **113**, 7128–7137 (2009)
54. Ferri, J.K., Dong, W.-F., Miller, R., Mohwald, H.: Elastic moduli of asymmetric ultrathin free-standing polyelectrolyte nanocomposites. *Macromolecules* **39**, 1532–1537 (2006)
55. Ferri, J.K., Dong, W.-F., Miller, R.: Ultrathin free-standing polyelectrolyte nanocomposites: a novel method for preparation and characterization of assembly dynamics. *J. Phys. Chem. B* **109**, 14764–14768 (2005)
56. Shchukina, E.M., Shchukin, D.G.: Layer-by-layer coated emulsion microparticles as storage and delivery tool. *Curr. Opin. Colloid Interface Sci.* **17**, 281–289 (2012)
57. Cuomo, F., Lopez, F., Miguel, M.G., Lindman, B.: Vesicle-templated layer-by-layer assembly for the production of nanocapsules. *Langmuir* **26**, 10555–10560 (2010)
58. Kozlovskaya, V., Zaygorodnya, O., Chen, Y., Ellis, K., Tse, H.M., Cui, W., Thompson, J.A., Kharlampieva, E.: Ultrathin polymeric coatings based on hydrogen-bonded polyphenol for protection of pancreatic islet cells. *Adv Funct Mat* **22**, 3389–3398 (2012)
59. Denkbas, E.B., Ottenbrite, R.M.: Perspectives on: chitosan drug delivery systems based on their geometries. *J. Bioactive Compatible Polym.* **21**, 351–368 (2006)
60. Hammond, P.T.: Building biomedical materials layer-by-layer. *Mater. Today* **15**, 196–205 (2012)
61. Zheng, S., Tao, C., He, Q., Zhu, H., Li, J.: Self-assembly and characterization of polypyrrole and polyallylamine multilayer films and hollow shells. *Chem. Mater.* **16**, 3677–3681 (2004)
62. Dauginet, L., Duwez, A.-S., Demoustier-Champagne, R.L.S.: Surface modification of polycarbonate and poly(ethylene terephthalate) films and membranes by polyelectrolyte deposition. *Langmuir* **17**, 3952–3957 (2001)
63. Kumar, B., Park, Y.T., Castro, M., Grunlan, J.C., Feller, J.F.: Fine control of carbon nanotubes-polyelectrolyte sensors sensitivity by electrostatic layer by layer assembly (eLbL) for the detection of volatile organic compounds (VOC). *Talanta* **88**, 396–402 (2012)
64. Fou, A.C., Onitsuka, O., Ferreira, M., Rubner, M.F., Hsieh, B.R.: Fabrication and properties of light-emitting diodes based on self-assembled multilayers of poly(phenylene vinylene). *J. Appl. Phys.* **79**, 7501–7509 (1996)
65. Laurent, D., Schlenoff, J.B.: Multilayer assemblies of redox polyelectrolytes. *Langmuir* **13**, 1552–1557 (1997)
66. Laschewsky, A., Mayer, B., Wischerhoff, E., Arys, X., Bertrand, P., Delcorte, A., Jonas, A.: A new route to thin polymeric, non-centrosymmetric coatings. *Thin Solid Films* **284–285**, 334–337 (1996)
67. De Geest, B.G., Sukhorukov, G.B., Möhwald, H.: The pros and cons of polyelectrolyte capsules in drug delivery. *Expert Opin. Drug Deliv.* **6**, 614–624 (2009)
68. Shchukin, D.G., Möhwald, H.: Self-repairing coatings containing active nanoreservoirs. *Small* **3**, 926–943 (2007)
69. Skorbab, E.V., Andreeva, D.V.: Layer-by-layer approaches for formation of smart self-healing materials. *Polym. Chem.* **4**, 4834–4845 (2013)
70. Shchukin, D.G.: Container-based multifunctional self-healing polymer coatings. *Polym. Chem.* **4**, 4871–4877 (2013)
71. De Geest, B.G., De Koker, S., Sukhorukov, G.B., Kreft, O., Parak, W.J., Skirtach, A.G., Demeester, J., De Smedt, S.C., Hennink, W.E.: Polyelectrolyte microcapsules for biomedical applications. *Soft Matter* **5**, 282–291 (2009)
72. Koker, S.D., Cock, L.J.D., Rivera-Gil, P., Parak, W.J., Velty, R.A., Vervaet, C., Remon, J.P., Grooten, J., Geest, B.G.D.: Polymeric multilayer capsules delivering biotherapeutics. *Adv. Drug Deliv. Rev.* **63**, 748–761 (2011)

73. Michel, M., Vautier, D., Voegel, J.-C., Schaaf, P., Ball, V.: Layer by layer self-assembled polyelectrolyte multilayers with embedded phospholipid vesicles. *Langmuir* **20**, 4835–4839 (2004)
74. Michel, R., Plostica, T., Abezgauz, L., Danino, D., Gradzielski, M.: Control of the stability and structure of liposomes by means of nanoparticles. *Soft Matter* **9**, 4167–4177 (2013)
75. Michel, M., Arntz, Y., Fleith, G., Toquant, J., Haikel, Y., Voegel, J.-C., Schaaf, P., Ball, V.: Layer-by-layer self-assembled polyelectrolyte multilayers with embedded liposomes: immobilized submicronic reactors for mineralization. *Langmuir* **22**, 2358–2364 (2006)
76. Hosta-Rigau, L., Städler, B., Yan, Y., Nice, E.C., Heath, J.K., Albericio, F., Caruso, F.: Capsosomes with multilayered subcompartments: assembly and loading with hydrophobic cargo. *Adv. Funct. Mat.* **20**, 59–66 (2010)
77. Hosta-Rigau, L., Chung, S.F., Postma, A., Chandrawati, R., Städler, B., Caruso, F.: Capsosomes with “free-floating” liposomal subcompartments. *Adv. Mat.* **23**, 4082–4087 (2011)
78. Chandrawati, R., Caruso, F.: Biomimetic liposome- and polymersome-based multicompartmentalized assemblies. *Langmuir* **28**, 13798–13807 (2012)
79. Ejima, H., Richardson, J.J., Liang, K., Best, J.P., van Koeverden, M.P., Such, G.K., Cui, J., Caruso, F.: One-step assembly of coordination complexes for versatile film and particle engineerinh. *Science* **341**, 154–158 (2013)
80. Guzmán, E., Ritacco, H., Rubio, J.E.F., Rubio, R.G., Ortega, F.: Salt-induced changes in the growth of polyelectrolyte layers of poly(diallyl-dimethylammoniumchloride) and poly(4-styrene sulfonate of sodium). *Soft Matter* **5**, 2130–2142 (2009)
81. Dubas, S.T., Schlenoff, J.B.: Factors controlling the growth of polyelectrolyte multilayers. *Macromolecules* **32**, 8153–8160 (1999)
82. Iturri Ramos, J.J., Stahl, S., Richter, R.P., Moya, S.E.: Water content and buildup of poly(diallyl-dimethylammonium chloride)/poly(sodium 4-styrenesulfonate) and poly(allylamine hydrochloride)/poly(sodium 4-styrenesulfonate) polyelectrolyte multilayers studied by an in situ combination of a quartz crystal microbalance with dissipation monitoring and spectroscopic ellipsometry. *Macromolecules* **43**, 9063–9070 (2010)
83. Ladam, G., Schaad, P., Voegel, J.C., Schaaf, P., Decher, G., Cuisinier, F.: In situ determination of the structural properties of initially deposited polyelectrolyte multilayers. *Langmuir* **16**, 1249–1255 (1999)
84. Boudou, T., Crouzier, T., Ren, K., Blin, G., Picart, C.: Multiple functionalities of polyelectrolyte multilayer films: new biomedical applications. *Adv. Mater.* **22**, 441–467 (2010)
85. Crouzier, T., Boudou, T., Picart, C.: Polysaccharide-based polyelectrolyte multilayers. *Curr. Opin. Colloid Interface Sci.* **15**, 417–426 (2010)
86. Almodóvar, J., Mower, J., Banerjee, A., Sarkar, A.K., Ehrhart, N.P., Kipper, M.J.: Chitosan-heparin polyelectrolyte multilayers on cortical bone: Periosteum-mimetic, cytophilic, antibacterial coatings. *Biotech. Bioeng.* **110**, 609–618 (2013)
87. Picart, C., Lavalle, P., Hubert, P., Cuisinier, F.J.G., Decher, G., Schaaf, P., Voegel, J.C.: Buildup mechanism for poly(L-lysine)/hyaluronic acid films onto a solid surface. *Langmuir* **17**, 7414–7424 (2001)
88. Richert, L., Lavalle, P., Payan, E., Shu, X.Z., Prestwich, G.D., Stoltz, J.-F., Schaaf, P., Voegel, J.-C., Picart, C.: Layer by layer buildup of polysaccharide films: physical chemistry and cellular adhesion aspects. *Langmuir* **20**, 448–458 (2004)
89. Hammond, P.T.: Engineering materials layer-by-layer: challenges and opportunities in multilayer assemby. *AIChE J.* **57**, 2928–2940 (2011)
90. Schmitt, J., Griinewald, T., Decher, G., Pershan, P.S., Pershan, K., Losche, M.: Internal structure of layer-by-layer adsorbed polyelectrolyte films: a neutron and x-ray reflectivity study. *Macromolecules* **26**, 7058–7063 (1993)
91. Lösch, M., Schmitt, J., Decher, G., Bouwman, W.G., Kjaer, K.: Detailed structure of molecularly thin polyelectrolyte multilayer films on solid substrates as revealed by neutron reflectometry. *Macromolecules* **31**, 8893–8906 (1998)

92. Schönhoff, M., Ball, V., Bausch, A.R., Dejugnat, C., Delorme, N., Glinel, K., von Klitzing, R., Steitz, R.: Hydration and internal properties of polyelectrolyte multilayers. *Colloids Surf. A* **303**, 14–29 (2007)
93. Schlenoff, J.B., Ly, H., Li, M.: Charge and mass balance in polyelectrolyte multilayers. *J. Am. Chem. Soc.* **120**, 7626–7634 (1998)
94. Farhat, T., Yassin, G., Dubas, S.T., Schlenoff, J.B.: Water and ion pairing in polyelectrolyte multilayers. *Langmuir* **15**, 6621–6623 (1999)
95. Schlenoff, J.B., Dubas, S.T.: Mechanism of polyelectrolyte multilayer growth: charge overcompensation and distribution. *Macromolecules* **34**, 592–598 (2001)
96. Guzmán, E., Miguel, V.S., Peinado, C., Ortega, F., Rubio, R.G.: Polyelectrolyte multilayers containing triblock copolymers of different charge ratio. *Langmuir* **26**, 11494–11502 (2010)
97. Guzmán, E., Ortega, F., Baghdadli, N., Cazeneuve, C., Lueno, G.S., Rubio, R.G.: Adsorption of conditioning polymers on solid substrates with different charge density. *ACS Appl. Mat. Interfaces* **3**, 3181–3188 (2011)
98. Glinel, K., Moussa, A., Jonas, A.M., Laschewsky, A.: Influence of polyelectrolyte charge density on the formation of multilayers of strong polyelectrolytes at low ionic strength. *Langmuir* **18**, 1408–1412 (2002)
99. Guzmán, E., Ritacco, H.A., Ortega, F., Rubio, R.G.: Growth of polyelectrolyte layers formed by poly(4-styrenesulfonate sodium salt) and two different polycations: new insights from study of adsorption kinetics. *J. Phys. Chem. C* **116**, 15474–15483 (2012)
100. Guzmán, E., Cavallo, J.A., Chuliá-Jordán, R., Gómez, C., Strumia, M.C., Ortega, F., Rubio, R.G.: pH-induced changes in the fabrication of multilayers of poly(acrylic acid) and chitosan: fabrication, properties, and tests as a drug storage and delivery system. *Langmuir* **27**, 6836–6845 (2011)
101. Bieker, P., Schönhoff, M.: Linear and exponential growth regimes of multilayers of weak polyelectrolytes in dependence on pH. *Macromolecules* **43**, 5052–5059 (2010)
102. Salomaki, M., Vinokurov, I.A., Kankare, J.: Effect of temperature on the buildup of polyelectrolyte multilayers. *Langmuir* **21**, 11232–11240 (2005)
103. von Klitzing, R.: Internal structure of polyelectrolyte multilayer assemblies. *Phys. Chem. Chem. Phys.* **8**, 5012–5033 (2006)
104. Grosberg, A.Y., Nguyen, T.T., Shklovskii, B.I.: Colloquium: the physics of charge inversion in chemical and biological systems. *Rev. Mod. Phys.* **74**, 329–345 (2002)
105. Schwarz, S., Eichhorn, K.J., Wischerhoff, E., Laschewsky, A.: Polyelectrolyte adsorption onto planar surfaces: a study by streaming potential and ellipsometry measurements. *Colloids Surf. A* **159**, 491–501 (1999)
106. Picart, C., Sengupta, K., Schilling, J., Maurstad, G., Ladam, G., Bausch, A.R., Sackmann, E.: Microinterferometric study of the structure, interfacial potential, and viscoelastic properties of polyelectrolyte multilayer films on a planar substrate. *J. Phys. Chem. B* **108**, 7196–7205 (2004)
107. Wang, Q.: Internal structure and charge compensation of polyelectrolyte multilayers: a numerical study. *Soft Matter* **5**, 413–424 (2009)
108. Kharlampieva, E., Kozlovskaya, V., Ankner, J.F., Sukhishvili, S.A.: Hydrogen-bonded polymer multilayers probed by neutron reflectivity. *Langmuir* **24**, 11346–11349 (2008)
109. Guzmán, E., Chuliá-Jordán, R., Ortega, F., Rubio, R.G.: Influence of the percentage of acetylation on the assembly of LBL multilayers of poly(acrylic acid) and chitosan. *Phys. Chem. Chem. Phys.* **13**, 18200–18207 (2011)
110. Cerdà, J.J., Qiao, B., Holm, C.: Understanding polyelectrolyte multilayers: an open challenge for simulations. *Soft Matter* **5**, 4412–4425 (2009)
111. Ghostine, R.A., Markarian, M.Z., Schlenoff, J.B.: Asymmetric growth in polyelectrolyte multilayers. *J. Am. Chem. Soc.* **135**, 7636–7646 (2013)
112. Lehaf, A.M., Hariri, H.H., Schlenoff, J.B.: Homogeneity, modulus, and viscoelasticity of polyelectrolyte multilayers by nanoindentation: refining the buildup mechanism. *Langmuir* **28**, 6348–6355 (2012)

113. Ghostine, R.A., Jisr, R.M., Lehaf, A., Schlenoff, J.B.: Roughness and salt annealing in a polyelectrolyte multilayer. *Langmuir* **29**, 11742–11750 (2013)
114. Kotov, N.A.: Layer-by-layer self-assembly: the contribution of hydrophobic interactions. *Nanostruct. Mater.* **12**, 789–796 (1999)
115. Guzmán, E., Ortega, F., Prolongo, M.G., Starov, V.M., Rubio, R.G.: Influence of the molecular architecture on the adsorption onto solid surfaces: comb-like polymers. *Phys. Chem. Chem. Phys.* **13**, 16416–16423 (2011)
116. Guzmán, E., Ortega, F., Baghdadli, N., Luengo, G.S., Rubio, R.G.: Effect of the molecular structure on the adsorption of conditioning polyelectrolytes on solid substrates. *Colloids Surf. A* **375**, 209–218 (2011)
117. Messina, R., Holm, C., Kremer, K.: Polyelectrolyte multilayering on a charged sphere. *Langmuir* **19**, 4473–4482 (2003)
118. Lvov, Y., Yamada, S., Kunitake, T.: Non-linear optical effects in layer-by-layer alternate films of polycations and an azobenzene-containing polyanion. *Thin Solid Films* **300**, 107–112 (1997)
119. Guzmán, E., Ritacco, H., Ortega, F., Rubio, R.G.: Evidence of the influence of adsorption kinetics on the internal reorganization of polyelectrolyte multilayers. *Colloids Surf. A* **384**, 274–281 (2011)
120. Schönhoff, M., Schwarz, B., Larsson, A., Kuckling, D.: Dynamics in polymer layers investigated by NMR techniques. *Progr. Colloid Polym. Sci.* **121**, 80–87 (2002)
121. Picart, C., Mutterer, J., Richert, L., Luo, Y., Prestwich, G.D., Schaaf, P., Voegel, J.-C., Lavalle, P.: Molecular basis for the explanation of the exponential growth of polyelectrolyte multilayers. *Proc. Nat. Acad. Sci. USA* **99**, 12531–12535 (2002)
122. Gamboa, D., Priolo, M.A., Ham, A., Grunlan, J.: Note: influence of rinsing and drying routines on growth of multilayer thin films using automated deposition system. *Rev. Sci. Inst.* **81**, 036103 (2010)
123. Wohl, B.M., Engbersen, J.F.J.: Responsive layer-by-layer materials for drug delivery. *J. Controlled Release* **158**, 2–14 (2012)
124. Izquierdo, A., Ono, S.S., Voegel, J.C., Schaaf, P., Decher, G.: Dipping versus spraying: exploring the deposition conditions for speeding up layer-by-layer assembly. *Langmuir* **21**, 7558–7567 (2005)
125. Michel, M., Izquierdo, A., Decher, G., Voegel, J.C., Schaaf, P., Ball, V.: Layer by layer self-assembled polyelectrolyte multilayers with embedded phospholipid vesicles obtained by spraying: integrity of the vesicles. *Langmuir* **21**, 7854–7859 (2005)
126. Kolansinska, M., Krastev, R., Gutberlet, T., Warszynski, P.: Layer-by-layer deposition of polyelectrolytes. Dipping versus spraying. *Langmuir* **25**, 1224–1232 (2009)
127. Lee, S.-S., Hong, J.-D., Kim, C.H., Kim, K., Koo, J.P., Lee, K.-B.: Layer-by-layer deposited multilayer assemblies of ionene-type polyelectrolytes based on the spin-coating method. *Macromolecules* **34**, 5358–5360 (2001)
128. Chiarelli, P.A., Johal, M.S., Holmes, D.J., Casson, J.L., Robinson, J.M., Wang, H.-L.: Polyelectrolyte spin-assembly. *Langmuir* **18**, 168–173 (2002)
129. Kiel, M., Mitzscherling, S., Leitenberger, W., Santer, S., Tiersch, B., Sievers, T.K., Möhwald, H., Bargheer, M.: Structural characterization of a spin-assisted colloid-polyelectrolyte assembly: stratified multilayer thin films. *Langmuir* **26**, 18499–18502 (2010)
130. Cho, J., Char, K., Hong, J.-D., Lee, K.-B.: Fabrication of highly ordered multilayer films using a spin self-assembly method. *Adv. Mat.* **13**, 1076–1078 (2001)
131. Kharlamieva, E., Kozlovskaya, V., Chan, J., Ankner, J.F., Tsukruk, V.V.: Spin-assisted layer-by-layer assembly: variation of stratification as studied with neutron reflectivity. *Langmuir* **25**, 14017–14024 (2009)
132. Schlenoff, J.B., Dubas, S.T., Farhat, T.: Sprayed polyelectrolyte multilayers. *Langmuir* **16**, 9968–9969 (2000)

133. Lefort, M., Boulmedais, F., Jierry, L., Gonthier, E., Voegel, J.C., Hemmerl, J., Lavalle, P., Ponche, A., Schaaf, P.: Simultaneous spray coating of interacting species: general rules governing the poly(styrene sulfonate)/poly(allylamine) system. *Langmuir* **27**, 4653–4660 (2011)
134. Schaaf, P., Voegel, J.-C., Jierry, L., Boulmedais, F.: Spray-assisted polyelectrolyte multilayer buildup: from step-by-step to single-step polyelectrolyte film constructions. *Adv. Mat.* **24**, 1001–1016 (2012)
135. Shchukina, E.M., Shchukin, D.G.: LbL coated microcapsules for delivering lipid-based drugs. *Adv. Drug Deliv. Rev.* **63**, 837–846 (2011)
136. Arys, X., Jonas, A.M., Laguitton, B., Legras, R., Laschewsky, A., Wischerhoff, E.: Structural studies on thin organic coatings built by repeated adsorption of polyelectrolytes. *Prog. Organic Coatings* **34**, 108–118 (1998)
137. Caruso, F., Caruso, R.A., Möhwald, H.: Nanoengineering of inorganic and hybrid hollow spheres by colloidal templating. *Science* **282**, 5391–5394 (1998)
138. Peyratout, C.S., Dähne, L.: Tailor-made polyelectrolyte microcapsules: from multilayers to smart containers. *Angew. Chem. Int. Ed.* **43**, 3762–3783 (2004)
139. Ruano M, Ritacco H, Rubio RG, Ortega F (2011) Layer-by-layer assembly of polyelectrolytes onto fluid micro-interfaces: polyelectrolyte-coated liposomes. *Abs Pap the Am Chem Soc* 239:28-COLL
140. Cuomo, F., Lopez, F., Ceglie, A., Maiuro, L., Miguel, M.G., Lindman, B.: pH-responsive liposome-templated polyelectrolyte nanocapsules. *Soft Matter* **8**, 4415–4420 (2012)
141. Cimi, N., Tulun, T., Decher, G., Ball, V.: Step-by-step assembly of self-patterning polyelectrolyte films violating (almost) all rules of layer-by-layer deposition. *J. Am. Chem. Soc.* **132**, 8264–8265 (2010)
142. Johansson, E., Blomberg, E., Lingstrom, R., Wägberg, L.: Adhesive interaction between polyelectrolyte multilayers of polyallylamine hydrochloride and polyacrylic acid studied using atomic force microscopy and surface force apparatus. *Langmuir* **25**, 2887–2894 (2009)
143. Salomakki, M., Kankare, J.: Influence of synthetic polyelectrolytes on the growth and properties of hyaluronan-chitosan multilayers. *Biomacromolecules* **10**, 294–301 (2009)
144. Xu, L., Kozlovskaya, V., Kharlampieva, E., Ankner, J.F., Sukhishvili, S.A.: Anisotropic diffusion of polyelectrolyte chains within multilayer films. *ACS Macro Lett.* **1**, 127–130 (2012)
145. Ferreyra, N.F., Rivas, G.A.: Self-assembled multilayers of polyethylenimine and DNA: spectrophotometric and electrochemical characterization and application for the determination of acridine orange interaction. *Electroanalysis* **21**, 1665–1671 (2009)
146. Ji, J., Tan, Q., Shen, J.: Construction of albumin multilayer coating onto plasma treated poly(vinyl chloride) via electrostatic self-assembly. *Polym. Adv. Technol.* **15**, 490–494 (2004)
147. Yang, Y.-H., Haile, M., Park, Y.T., Malek, F.A., Grunlan, J.C.: Super gas barrier of all-polymer multilayer thin films. *Macromolecules* **44**, 1450–1459 (2011)
148. Gu, C.-H., Wang, J.-J., Yu, Y., Sun, H., Shuai, N., Wei, B.: Biodegradable multilayer barrier films based on alginate/polyethylenimine and biaxially oriented poly(lactic acid). *Carbohydr. Polym.* **92**, 1579–1585 (2013)
149. Yuan, W., Dong, H., Li, C.M., Cui, X., Yu, L., Lud, Z., Zhou, Q.: pH-controlled construction of chitosan/alginate multilayer film: characterization and application for antibody immobilization. *Langmuir* **23**, 13046–13052 (2007)
150. Jourdainne, L., Sn, Lecuyer, Arntz, Y., Picart, C., Schaaf, P., Senger, B., Voegel, J.-C., Lavalle, P., Charitat, T.: Dynamics of poly(l-lysine) in hyaluronic acid/poly(l-lysine) multilayer films studied by fluorescence recovery after pattern photobleaching. *Langmuir* **24**, 7842–7847 (2008)
151. Lavalle, P., Gergely, C., Cuisinier, F.J.G., Decher, G., Schaaf, P., Voegel, J.C., Picart, C.: Comparison of the structure of polyelectrolyte multilayer films exhibiting a linear and an exponential growth regime: an in situ atomic force microscopy study. *Macromolecules* **35**, 4458–4465 (2002)

152. Lavalle, P., Picart, C., Mutterer, Jr, Gergely, C., Reiss, H., Voegel, J.-C., Senger, B., Schaaf, P.: Modeling the buildup of polyelectrolyte multilayer films having exponential growth. *J. Phys. Chem. B* **108**, 635–648 (2003)
153. Itoh, K., Tokumi, S., Kimura, T., Nagase, A.: Reinvestigation on the buildup mechanism of alternate multilayers consisting of poly(l-glutamic acid) and poly(l-, d-, and dl-lysines). *Langmuir* **24**, 13426–13433 (2008)
154. Song, Z., Yin, J., Luo, K., Zheng, Y., Yang, Y., Li, Q., Yan, S., Chen, X.: Layer-by-layer buildup of poly(l-glutamic acid)/chitosan film for biologically active coating. *Macromol. Biosci.* **9**, 268–278 (2009)
155. Barrantes, A., Santos, O., Sotres, J., Arnebrant, T.: Influence of pH on the build-up of poly-L-lysine/heparin multilayers. *J. Colloid Interface Sci.* **388**, 191–200 (2012)
156. Yuan, W., Fu, J., Su, K., Ji, J.: Self-assembled chitosan/heparin multilayer film as a novel template for in situ synthesis of silver nanoparticles. *Colloids Surf. B* **76**, 549–555 (2010)
157. Schneider, A., Richert, L., Francius, G., Voegel, J.-C., Picart, C.: Elasticity, biodegradability and cell adhesive properties of chitosan/hyaluronan multilayer films. *Biomed. Mater.* **2**, S45–S51 (2007)
158. Hoda, N., Larson, R.G.: Modeling the buildup of exponentially growing polyelectrolyte multilayer films. *J. Phys. Chem. B* **113**, 4232–4241 (2009)
159. Porcel, C., Lavalle, P., Ball, V., Decher, G., Senger, B., Voegel, J.-C., Schaaf, P.: From exponential to linear growth in polyelectrolyte multilayers. *Langmuir* **22**, 4376–4383 (2006)
160. Kujawa, P., Moraille, P., Sanchez, J., Badia, A., Winnik, F.: Effect of molecular weight on the exponential growth and morphology of hyaluronan/chitosan multilayers: a surface plasmon resonance spectroscopy and atomic force microscopy investigation. *J. Am. Chem. Soc.* **127**, 9224–9234 (2005)
161. Lavalle, P., Vr, Vivet, Jessel, N., Decher, G., Voegel, J.-C., Mesini, P.J., Schaaf, P.: Direct evidence for vertical diffusion and exchange processes of polyanions and polycations in polyelectrolyte multilayer films. *Macromolecules* **37**, 1159–1162 (2004)
162. Haynie, D.T., Cho, E., Waduge, P.: “In and out diffusion” hypothesis of exponential multilayer film buildup revisited. *Langmuir* **27**, 5700–5704 (2011)
163. Cini, N., Tulun, T., Blanck, C., Toniazzo, V., Ruch, D., Decher, G., Ball, V.: Slow complexation dynamics between linear short polyphosphates and polyallylamines: analogies with “layer-by-layer” deposits. *Phys. Chem. Chem. Phys.* **14**, 3048–3056 (2012)
164. Xu, L., Pristinski, D., Zhuk, A., Stoddart, C., Ankner, J.F., Sukhishvili, S.A.: Linear versus exponential growth of weak polyelectrolyte multilayers: correlation with polyelectrolyte complexes. *Macromolecules* **45**, 3892–3901 (2012)
165. Holmberg, K., Jönsson, B., Kronberg, B., Lindman, B.: Surfactants and Polymers in Aqueous Solution. Wiley, Chichester (2002)
166. Cohen-Stuart, M.A.: Kinetics of polyelectrolyte adsorption. *J. Phys. Cond. Matt.* **9**, 7767–7783 (1997)
167. Lane, T.J., Fletcher, W.R., Gormally, M.V., Johal, M.S.: Dual-beam polarization interferometry resolves mechanistic aspects of polyelectrolyte adsorption. *Langmuir* **24**, 10633–10636 (2008)
168. Raposo, M., Oliveira, O.N.: Adsorption mechanisms in layer-by-layer films. *Braz. J. Phys.* **28**, 392–404 (1998)
169. Raposo, M., Pontes, R.S., Mattoso, L.H.C., Oliveira, O.N.: Kinetics of adsorption of poly(o-methoxyaniline) self-assembled films. *Macromolecules* **30**, 6095–6101 (1997)
170. Chiang, C.Y., Starov, V.M., Hall, M.S., Lloyd, D.R.: Crystallization kinetics of polymer-solvent systems: 2. experimental verification of the model. *Colloid J.* **59**, 236–247 (1997)
171. Chiang, C.-Y., Starov, V.M., Lloyd, D.R.: Crystallization kinetics of a polymersolvent system. 1. Derivation of model-equations. *Colloid J.* **57**, 715–724 (1995)
172. Bertrand, P., Jonas, A., Laschewsky, A., Legras, R.: Ultrathin polymer coatings by complexation of polyelectrolytes at interfaces: suitable materials, structure and properties. *Macromol. Rapid Commun.* **21**, 319–348 (2000)

173. Linse, P., Källrot, N.: Polymer adsorption from bulk solution onto planar surfaces: effect of polymer flexibility and surface attraction in good solvent. *Macromolecules* **43**(4), 2054–2068 (2010)
174. Burke, S.E., Barrett, C.J.: Swelling behavior of hyaluronic acid/polyallylamine hydrochloride multilayer films. *Biomacromolecules* **6**, 1419–1428 (2005)
175. von Klitzing, R., Wong, J.E., Jaeger, W., Steitz, R.: Short range interactions in polyelectrolyte multilayers. *Curr. Opin. Colloid Interface Sci.* **9**, 158–162 (2004)
176. Lvov, Y., Ariga, K., Onda, M., Ichinose, I., Kunitake, T.: A careful examination of the adsorption step in the alternate layer-by-layer assembly of linear polyanion and polycation. *Colloids Surf. A* **146**, 337–346 (1999)
177. Okubo, T., Suda, M.: Absorption of polyelectrolytes on colloidal surfaces as studied by electrophoretic and dynamic light-scattering techniques. *J. Colloid Interf. Sci.* **213**, 565–571 (1999)
178. Shen, L., Chaudouet, P., Ji, J., Picart, C.: pH-amplified multilayer films based on hyaluronan: influence of HA molecular weight and concentration on film growth and stability. *Biomacromolecules* **12**, 1322–1331 (2011)
179. Garg, A., Hefflin, J.R., Gibson, H.W., Davis, R.M.: Study of film structure and adsorption kinetics of polyelectrolyte multilayer films: effect of pH and polymer concentration. *Langmuir* **24**, 10887–10894 (2008)
180. Dobrynin, A.V., Rubinstein, M.: Theory of polyelectrolytes in solutions and at interfaces. *Progr. Polym. Sci.* **30**, 1049–1118 (2005)
181. Kamineni, V.K., Lvov, Y.M., Dobbins, T.A.: Layer-by-layer nanoassembly of polyelectrolytes using formamide as the working medium. *Langmuir* **23**, 7423–7427 (2007)
182. Tuo, X., Chen, D., Cheng, H., Wang, X.: Fabricating water-insoluble polyelectrolyte into multilayers with layer-by-layer self-assembly. *Polym. Bull.* **54**, 427–433 (2005)
183. Long, Y., Wang, T., Liu, L., Liu, G., Zhang, G.: Ion specificity at a low salt concentration in water–methanol mixtures exemplified by a growth of polyelectrolyte multilayer. *Langmuir* **29**, 3645–3653 (2013)
184. Buron, C.C., Filiâtre, C., Membrey, F., Bainier, C., Buisson, L., Charraut, D., Foissy, A.: Surface morphology and thickness of a multilayer film composed of strong and weak polyelectrolytes: effect of the number of adsorbed layers, concentration and type of salts. *Thin Solid Films* **517**, 2611–2617 (2009)
185. Dubas, S.T., Schlenoff, J.B.: Polyelectrolyte multilayers containing a weak polyacid: construction and deconstruction. *Macromolecules* **34**, 3736–3740 (2001)
186. Record, M.T., Guinn, E., Pegram, L., Capp, M.: Introductory lecture: interpreting and predicting hofmeister salt ion and solute effects on biopolymer and model processes using the solute partitioning model. *Faraday Disc* **160**, 9–44 (2013)
187. Leontidis, E.: Hofmeister anion effects on surfactant self-assembly and the formation of porous solids. *Curr. Opin. Colloid Interface Sci.* **7**, 81–91 (2002)
188. Salomäki, M., Laiho, T., Kankare, J.: Counteranion-controlled properties of polyelectrolyte multilayers. *Macromolecules* **37**, 9585–9590 (2004)
189. Salomäki, M., Tervasmäki, P., Areva, S., Kankare, J.: The hofmeister anion effect and the growth of polyelectrolyte multilayers. *Langmuir* **20**, 3679–3683 (2004)
190. Dressick, W.J., Wahl, K.J., Bassim, N.D., Stroud, R.M., Petrovykh, D.Y.: Divalent–anion salt effects in polyelectrolyte multilayer depositions. *Langmuir* **28**, 15831–15843 (2012)
191. Brunner, E., Lutz, K., Sumper, M.: Biomimetic synthesis of silica nanospheres depends on the aggregation and phase separation of polyamines in aqueous solution. *Phys. Chem. Chem. Phys.* **6**, 854–857 (2004)
192. Llamas, S., Mendoza, A.J., Guzman, E., Ortega, F., Rubio, R.G.: Salt effects on the air/solution interfacial properties of PEO-containing copolymers: equilibrium, adsorption kinetics and surface rheological behavior. *J. Colloid Interface Sci.* **400**, 49–58 (2013)
193. Panchagnula, V., Jeon, J., Dobrynin, A.V.: Molecular dynamics simulations of electrostatic layer-by-layer self assembly. *Phys. Rev. Lett.* **93**, 037801 (2004)

194. Félix, O., Zheng, Z., Cousin, F., Decher, G.: Are sprayed LbL-films stratified? a first assessment of the nanostructure of spray-assembled multilayers by neutron reflectometry. *C. R. Chim.* **12**, 225–234 (2009)
195. Silva, H.S., Uehara, T.M., Bergamaski, K., Miranda, P.B.: Molecular ordering in layer-by-layer polyelectrolyte films studied by sum-frequency vibrational spectroscopy: the effects of drying process. *J. Nanosci. Nanotechnol.* **8**, 3399–3405 (2008)
196. Silva, H.S., Miranda, P.B.: Molecular ordering of layer-by-layer polyelectrolyte films studied by sum-frequency vibrational spectroscopy. *J. Phys. Chem. B* **113**, 10068–10071 (2009)
197. Korneev, D., Lvov, Y., Decher, G., Schmitt, J., Yaradaikin, S.: Neutron reflectivity analysis of self assembled film superlattices with alternate layers of deuterated and hydrogenated polystyrenesulfonate and polyallylamine. *Phys. B* **213**, 954–956 (1995)
198. Soltwedel, O., Ivanova, O., Nestler, P., Müler, M., Köhler, R., Helm, C.A.: Interdiffusion in polyelectrolyte multilayers. *Macromolecules* **43**, 7288–7293 (2010)
199. Jomaa, H.W., Schlenoff, J.B.: Salt-induced polyelectrolyte interdiffusion in multilayered films: a neutron reflectivity study. *Macromolecules* **38**, 8473–8480 (2005)
200. Gilbert, J.B., Rubner, M.F., Cohen, R.E.: Depth-profiling X-ray photoelectron spectroscopy (XPS) analysis of interlayer diffusion in polyelectrolyte multilayers. *Proc. Nat. Acad. Sci. USA* **110**, 6651–6656 (2013)
201. Singh, S., Junghans, A., Waltman, M.J., Nagy, A., Iyer, R., Majewski, J.: Neutron reflectometry characterization of PEI–PSS polyelectrolyte multilayers for cell culture. *Soft Matter* **8**, 11484–11491 (2012)
202. Wong, J.E., Zastrow, H., Jaeger, W., von Klitzing, R.: Specific ion versus electrostatic effects on the construction of polyelectrolyte multilayers. *Langmuir* **25**, 14061–14070 (2009)
203. Schönhoff, M.: Layered polyelectrolyte complexes: physics of formation and molecular properties. *J. Phys. Cond. Matt.* **15**, R1781–R1808 (2003)
204. Schönhoff, M.: Self-assembled polyelectrolyte multilayers. *Curr. Opin. Colloid Interface Sci.* **8**, 86–95 (2003)
205. Schwarz, B., Schönhoff, M.: A ^1H NMR relaxation study of hydration water in polyelectrolyte mono and multilayers adsorbed to colloidal particles. *Colloids Surf. A* **198**, 293–304 (2002)
206. Carriere, D., Krastev, R., Schonhoff, M.: Oscillations in solvent fraction of polyelectrolyte multilayers driven by the charge of the terminating layer. *Langmuir* **20**, 11465–11472 (2004)
207. Tanchak, O.M., Yager, K.G., Fritzsche, H., Harroun, T., Katsaras, J., Barret, C.J.: Water distribution in multilayers of weak polyelectrolytes. *Langmuir* **22**, 5137–5143 (2006)
208. Dodoo, S., Steitz, R., Laschewsky, A., von Klitzing, R.: Effect of ionic strength and type of ions on the structure of water swollen polyelectrolyte multilayers. *Phys. Chem. Chem. Phys.* **13**, 10318–10325 (2011)
209. Dodoo, S., Balzer, B.N., Hugel, T., Laschewsky, A., von Klitzing, R.: Effect of ionic strength and layer number on swelling of polyelectrolyte multilayers in water vapour. *Soft Materials* **11**, 157–164 (2013)
210. Dubas, S.T., Schlenoff, J.B.: Swelling and smoothing of polyelectrolyte multilayers by salt. *Langmuir* **17**, 7725–7727 (2001)
211. Schneider, A., Francius, G., Obeid, R., Schwinté, P., Hemmerlé, J., Frisch, B., Schaaf, P., Voegel, J.-C., Senger, B., Picart, C.: Polyelectrolyte multilayers with a tunable young's modulus: influence of film stiffness on cell adhesion. *Langmuir* **22**, 1193–1200 (2006)
212. Lehaf, A.M., Hariri, H.H., Schlenoff, J.B.: Homogeneity, modulus, and viscoelasticity of polyelectrolyte multilayers by nanoindentation: refining the buildup mechanism. *Langmuir* **28**, 6348–6355 (2012)
213. Larson, R.G.: *The Structure and Rheology of Complex Fluids*. Oxford University Press, Oxford (1999)

214. Nolte, A.J., Rubner, M.F., Cohen, R.E.: Determining the young's modulus of polyelectrolyte multilayer films via stress-induced mechanical buckling instabilities. *Macromolecules* **38**, 5367–5370 (2005)
215. Jaber, J.A., Schlenoff, J.B.: Mechanical properties of reversibly cross-linked ultrathin polyelectrolyte complexes. *J. Am. Chem. Soc.* **128**, 2940–2947 (2006)
216. Nolte, A.J., Treat, N.D., Cohen, R.E., Rubner, M.F.: Effect of relative humidity on the young's modulus of polyelectrolyte multilayer films and related nonionic polymers. *Langmuir* **21**, 5793–5798 (2008)
217. Blacklock, J., Vetter, A., Lankenau, A., Oupický, D., Möhwald, H.: Tuning the mechanical properties of bioreducible multilayer films for improved cell adhesion and transfection activity. *Biomaterials* **31**, 7167–7174 (2010)
218. Lehaf, A.M., Moussallem, M.D., Schlenoff, J.B.: Correlating the compliance and permeability of photo-cross-linked polyelectrolyte multilayers. *Langmuir* **27**, 4756–4763 (2011)
219. Antipov, A.A., Sukhorukov, G.B., Leporatti, S., Radtchenko, I.L., Donath, E., Mohwald, H.: Polyelectrolyte multilayer capsule permeability control. *Colloids Surf. A* **198–200**, 535–541 (2002)
220. Delcea, M., Möhwald, H., Skirtach, A.G.: Stimuli-responsive LBL capsules and nanoshells for drug delivery. *Adv. Drug. Delivery Rev.* **63**, 730–747 (2011)
221. Köhler, K., Sukhorukov, G.B.: Heat treatment of polyelectrolyte multilayer capsules: versatile method for encapsulation. *Adv. Funct. Mater.* **17**, 2053–2061 (2007)
222. Mjahed, H., Voegel, J.-C., Senger, B., Chassepot, A., Rameau, A., Ball, V., Schaaf, P., Boulmedais, F.: Hole formation induced by ionic strength increase in exponentially growing multilayer films. *Soft Matter* **5**, 2269–2276 (2009)
223. Skirtach, A.G., Kreft, O., Villiers, M.M., Aramwit, P., Kwon, G.S.: Stimuli-sensitive nanotechnology for drug delivery. *Nanotechnology in Drug Delivery*. In: Villiers, M.M., Aramwit, P., Kwon, G.S. (eds.), pp. 545–578. Springer, New York (2009)
224. Chong, S.-F., Sexton, A., De Rose, R., Kent, S.J., Zelikin, A.N., Caruso, F.: A paradigm for peptide vaccine delivery using viral epitopes encapsulated in degradable polymer hydrogel capsules. *Biomaterials* **30**, 5178–5186 (2009)
225. Glinel, K., Déjugnat, C., Prevot, M., Schoeler, B., Schönhoff, M., von Klitzing, R.: Responsive polyelectrolyte multilayers. *Colloids Surf. A* **303**, 3–13 (2007)
226. Dubas, S.T., Farhat, T.R., Schlenoff, J.B.: Multiple membranes from “true” polyelectrolyte multilayers. *J. Am. Chem. Soc.* **123**, 5368–5369 (2001)
227. Bruening, M.L., Dotzauer, D.M., Jain, P., Ouyang, L., Baker, G.L.: Creation of functional membranes using polyelectrolyte multilayers and polymer brushes. *Langmuir* **24**, 7663–7673 (2008)
228. Guzman, E., Ruano, M., Rubio, R.G., Ortega, F.: Polyelectrolyte assemblies for drug storage and delivery: Multilayers, nanocapsules, and multicapsules. In: Prokopovich, P. (ed.) *Inhaler Devices: Fundamentals, Design and Drug Delivery*, pp. 94–145. Woodhead Publishing Limited, Sawston (2013)
229. Koker, S.D., Hoogenboom, R., Geest, B.G.D.: Polymeric multilayer capsules for drug delivery. *Chem. Soc. Rev.* **41**, 2867–2884 (2012)
230. Städler, B., Chandrawati, R., Price, A.D., Chong, S.-F., Breheny, K., Postma, A., Connal, L.A., Zelikin, A.N., Caruso, F.: A microreactor with thousands of subcompartments: enzyme-loaded liposomes within polymer capsules. *Angew. Chem. Int. Ed.* **48**, 4359–4362 (2009)
231. Städler, B., Chandrawati, R., Goldie, K., Caruso, F.: Capsosomes: subcompartmentalizing polyelectrolyte capsules using liposomes. *Langmuir* **25**, 6725–6732 (2009)
232. Rmaile, H.H., Schlenoff, J.B.: Optically active polyelectrolyte multilayers as membranes for chiral separations. *J. Am. Chem. Soc.* **125**, 6602–6603 (2003)
233. Lutkenhaus, J.L., McEnnis, K., Hammond, P.T.: Tuning the glass transition of and ion transport within hydrogen-bonded layer-by-layer assemblies. *Macromolecules* **40**, 8367–8373 (2007)

234. Daiko, Y., Katagiri, K., Matsuda, A.: Proton conduction in thickness-controlled ultrathin polycation/nafion multilayers prepared via layer-by-layer assembly. *Chem. Mater.* **20**, 6405–6409 (2008)
235. Reisch, A., Hemmerlé, J., Chassepot, A., Lefort, M., Benkirane-Jessel, N., Candolfi, E., Mésini, P., Letscher-Bru, V., Voegel, J.-C., Schaaf, P.: Anti-fouling phosphorylcholine bearing polyelectrolyte multilayers: cell adhesion resistance at rest and under stretching. *Soft Matter* **6**, 1503–1512 (2010)
236. Shchukin, D.G., Zheludkevich, M., Yasakau, K., Lamaka, S., Ferreira, M.G.S., Möhwald, H.: Layer-by-layer assembled nanocontainers for self-healing corrosion protection. *Adv. Mater.* **18**, 1672–1678 (2006)
237. Wang, X., Liu, F., Zheng, X., Sun, J.: Water-enabled self-healing of polyelectrolyte multilayer coatings. *Angew. Chem. Int. Ed.* **50**, 11378–11381 (2011)
238. Andreeva, D.V., Skorb, E.V., Shchukin, D.G.: Layer-by-layer polyelectrolyte/inhibitor nanostructures for metal corrosion protection. *ACS Appl. Mater. Interfaces* **2**, 1954–1962 (2010)

Monte Carlo Studies in Polyelectrolyte Solutions: Structure and Thermodynamics

Claudio F. Narambuena and Ezequiel P.M. Leiva

Abstract In this chapter, we summarize the basic knowledge required to implement Monte Carlo simulations applied to the study of polyelectrolytes in solution. We describe the coarse-grain model used, which emphasizes on electrostatic and excluded volume interactions. The basic foundations of statistical mechanics required to understand the implementation of this method are developed in detail. We also describe the special Monte Carlo moves required to achieve the efficient relaxation of polyelectrolyte chains. Finally, we present some results obtained for the structure of polyelectrolyte chains, counterion condensation (along with comparison with experimental results), and the morphology of polyelectrolyte complexes.

1 Introduction

A polyelectrolyte (PE) is a polymer molecule that has the capacity to ionize in a polar solvent (usually water). Functional groups in the polyelectrolyte enable charged segments of the chain to interact with each other or small ions present in solution. PE solutions show remarkable physicochemical properties as compared with those of the neutral polymer [1]. Polyelectrolytes can be classified into two major categories (strong and weak) according to the degree of ionization of their

C.F. Narambuena (✉) · E.P.M. Leiva

Departamento de Matemática y Física, Facultad de Ciencias Químicas,
Universidad Nacional de Córdoba, Haya de la Torre esq. Medina Allende. Ciudad
Universitaria, Córdoba 5000, Córdoba, Argentina
e-mail: claudionarambuena@fcq.unc.edu.ar

E.P.M. Leiva

e-mail: eze_leiva@yahoo.com.ar; eleiva@fcq.unc.edu.ar

C.F. Narambuena

Department of Biomedical Engineering, Northwestern University, 2145 Sheridan Road,
Evanston 60208, Illinois, USA

titratable groups. A strong polyelectrolyte is one, where its titratable groups are fully ionized or dissociated in a range moderate of pH. When the ionization proceeds in a partial form and is a function of solution pH, the PE is denominated weak. When a polyelectrolyte has acid groups (usually are $-COOH$, $-SO_3H$, or $-PO_3H_2$) this is called polyacid. Amines are the basic groups more common in a polybase. In general the deprotonation of an acid group AH has a equilibrium dissociation:



where A^- is the ionized group and H^+ is the proton. This dissociation reaction has an acid equilibrium constant:

$$Ka = \frac{[A^-][H^+]}{[AH]}$$

The usual values ranges of the equilibrium constant for strong and weak polyelectrolytes are $Ka \gg 1$ and $1 > Ka > 10^{-10}$ respectively.

In this book, we interpret several phenomena involving polyelectrolytes measured with different experimental techniques. In this chapter we present a computational method that attempts to achieve several purposes. The most direct goal is to reproduce qualitatively or quantitatively the experimental result of interest using a simple model to represent the structures of the polyelectrolyte and the others species present in the system. The second objective is the interpretation and explanation of the phenomenon at a molecular level to gain insight into intermolecular forces relevant to the process or behavior under study. A third objective is to denote the capacity of the model and the simulation method for the predictions of experimental result. The last purpose of the simulations is to evaluate the power of theories.

This chapter begins with the description of the simplest model used for the polyelectrolyte chain. Then, the theoretical concepts needed to understand the Monte Carlo method are developed. These concepts are related principally with statistical mechanics and their connection with thermodynamics.

The method is then applied to the study of global and local structure of polyelectrolyte chains, as well as the distribution of counterions and condensation. We also explain the morphologies (globular, rod, toroid, etc.) of polyelectrolyte complexes as a consequence of the chain stiffness itself.

The conclusions are presented in the last section of the chapter.

2 Monte Carlo Studies of Polyelectrolytes

With the advent of computers with a reasonable calculation capacity could address the application of Monte Carlo method to study of polyelectrolyte systems. The first articles appeared in the 80s [2–8], and the amount of papers has been growing

continuously to become a voluminous literature. A comprehensive review of this literature is beyond the reach of this chapter. However, we have been greatly influenced by the work of an enormous number of authors, in particular a series of articles by Wallin and Per Linse [9–11] where they studied the complexation between a charged micelle and an oppositely charged polyelectrolyte using Monte Carlo simulations and thermodynamic integration. They calculated the structural data of the micelle-PE complex and thermodynamic quantities of the complexation as a function of the PE characteristic such chain flexibility, linear charge density, etc. To represent the polyelectrolyte chain they used a very simple and useful coarse grain model, which is widely used today and is the model that we will describe below.

3 Theoretical Approach of Monte Carlo Studies

Our interest is the molecular study of a system composed of polyelectrolyte chains dissolved in a polar solvent (typically water) in presence of small ions like the countanions of polyelectrolyte, H^+ , OH^- , and/or ions from the dissociation of added salt. This small number of species can lead to a complex behavior of the system, as compared with a solution of neutral polymer. This is possible because the species interact via several types of molecular interactions with different length and time scales. Among those involved are hydrogen bonds, electrostatic, hydrophobic, van der Waals, hydrogen bonds interactions [12].

3.1 Coarse-Grain Model for Polyelectrolyte and Small Ions

A simulation study on the polyelectrolyte system must begin with the choice of the model to represent the fundamental characteristics that describe the physico-chemical phenomena, in which we are interested. Our model should be as simple as possible to optimize the computational calculation, but it has to ensure the important molecular interactions. We focus on the electrostatic interaction in the polyelectrolyte solution; that is say, the explicit electrostatic interaction between the charged segments in the chain, segments-counterions, segments-coions, and counterions-coions.

Explicit or implicit models can be used to represent the solvent. In the explicit case the solvent molecules have structure at atomic level. The implicit solvent model assumes a continuum medium (instead of the individual molecular detail of the explicit solvent model) where the dielectric aspect is emphasized and characterized by a dielectric constant.

It is possible to describe the polyelectrolyte chain at different levels of structural detail. When the model has the full atomic resolution of the chemical structure, it is called an all-atom model. While this type of model can treat microscopic scale

phenomena ($\sim 0.1\text{--}10$ nm), it is computationally expensive to study the mesoscopic scale level ($\sim 10\text{--}1,000$ nm) at which the structure and self-assembly of macromolecules emerges. To access large length scales, it is recommended to use coarse-grained models (CG), where a set of atoms is grouped into a single CG bead [13].

In a coarse grain (CG) model, called the “primitive model” a polyelectrolyte chain is represented by a set of linked charged beads (Fig. 1), and the solvent is depicted as a dielectric medium. The small ions (cations and anions) are depicted as rigid spheres (Fig. 1). Each bead is spherical and has an electrical charge in its center. The number total of particles is:

$$N = N_m N_p + N_{cat} + N_{ani} \quad (1)$$

where N_p is the number of chains in the system, and N_{cat} and N_{ani} are the number of cations and anions respectively. In addition, if the system is at pH close to 7, the electrostatic contribution of hydroxide and hydronium ions can be neglected. The principle of electroneutrality in the absence of the others charged species can be written as:

$$0 = q_m N_m N_p + q_{cat} N_{cat} + q_{ani} N_{ani} \quad (2)$$

where q_m , q_{cat} and q_{ani} are the charges of monomer, cation and anion respectively.

The coarse-grain potential energy U_{CG} can be written as the following contribution:

$$U_{CG} = U_{elect} + U_{ev} + U_{bond} + U_{ang} \quad (3)$$

where U_{elect} is the electrostatic energy, U_{ev} is the excluded volume term, U_{bond} is the connectivity energy, and U_{ang} is the angular energy term.

$$U_{elect} = \frac{1}{4\pi\epsilon_r\epsilon_0} \sum_{i=1}^{N-1} \sum_{j=i+1}^N \frac{q_i q_j}{|r_i - r_j|} \quad (4)$$

where $\epsilon_0 = 8.854 \times 10^{-12} \text{ C}^2/\text{Nm}^2$ is the permittivity of vaccum, and $\epsilon_r = 78$ is the relative dielectric constant of water. It is useful to compare the electrostatic energy with the thermal energy $k_B T$, where k_B is the Boltzmann constant and T is the absolute temperature. The charge q_i of the particle can be expressed as $q_i = e z_i$, where e is the elementary charge and z_i is the valence and Eq. 4 can be rewritten as:

$$\frac{U_{elect}}{k_B T} = l_B \sum_{i=1}^{N-1} \sum_{j=i+1}^N \frac{z_i z_j}{r_{ij}} \quad (5)$$

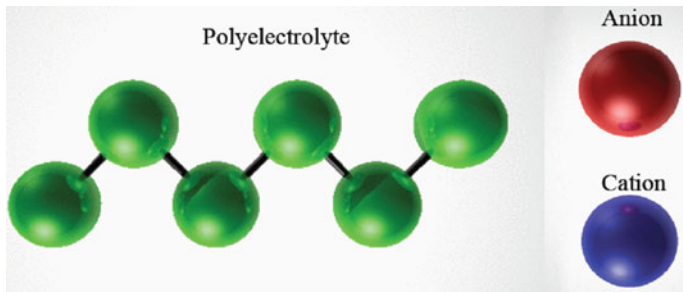


Fig. 1 Coarse grain model for the polyelectrolyte and small ions (anion and cation)

where is $r_{ij} = |r_i - r_j|$ and l_B is the Bjerrum length and has the form:

$$l_B = \frac{e^2}{4\pi\epsilon_r\epsilon_0 k_B T} \quad (6)$$

At room temperature in water the Bjerrum length has a value $l_B = 0.71$ nm. It is a key parameter and represents the distance of separation between two elemental charges, which has similar magnitude of electrostatic and thermal energies. The electrostatic potential (Eq. 5) diverges when r_{ij} approaches to zero. Therefore, it is necessary to define U_{ev} , the excluded volume potential, to avoid allowing the centers of two charges particles to be too close together. The simplest way to achieve this is to write a potential of rigid spheres as:

$$\begin{aligned} u_{RS}(r_{ij}) &= \infty && \text{if } r_{ij} \leq d, \\ u_{RS}(r_{ij}) &= 0 && \text{if } r_{ij} > d, \end{aligned} \quad (7)$$

where $d = (d_1 + d_2)/2$ is the diameter average of particles i and j .

To describe the excluded volume of the bead, we can also use a Lennard-Jones (LJ) potential of the type:

$$u_{LJ} = 4\epsilon_{LJ} \left(\left(\frac{\sigma_{LJ}}{r_{ij}} \right)^{12} - \left(\frac{\sigma_{LJ}}{r_{ij}} \right)^6 \right) \quad (8)$$

This potential has a minimum at $r_{\min} = 2^{1/6}\sigma_{LJ}$ with a depth ϵ_{LJ} . This aspect is utilized in the simulation of polyelectrolyte chains dissolved in a poor solvent, which results in an effective attraction between monomers at distances $r_{ij} > r_{\min}$, and repulsive interaction if $r_{ij} < r_{\min}$. Moreover, this potential varies smoothly and its derivate diverges only when $r_{ij} \rightarrow 0$. In contrast the derivate of the hard sphere potential diverges at $r_{ij} = d$. In molecular or Brownian dynamic simulations it is necessary to calculate the interaction force between particles. This force is obtained from the derivate of the potential. Thus, the LJ potential is usually employed since it prevents problems of divergences.

For the good solvent condition, there is a modification of the LJ potential, which does not present attractive interactions at any distance between the particles. This is possible by a little modification of the potential of Eq. 8. First the interaction range of the potential is cut at its minimum. Second this potential is translated along the ordinates such that the minimum value reaches to zero, this is achieved by the addition of ε_{LJ} to the potential. The resulting LJ modification is called truncated or purely repulsive Lennard-Jones potential, and has the following form:

$$u_{LJ} = 4\varepsilon_{LJ} \left(\left(\frac{\sigma_{LJ}}{r_{ij}} \right)^{12} - \left(\frac{\sigma_{LJ}}{r_{ij}} \right)^6 \right) + \varepsilon_{LJ} \quad \text{for } r_{ij} \leq r_c \quad (9)$$

$$u_{LJ} = 0 \quad \text{for } r_{ij} > r_c$$

where $r_c = r_{\min}$ is the cutoff radius and is equal to the minimum of the original LJ potential.

The connectivity of the linear chain is represented by an interaction potential U_{bond} between two monomers i and $i + 1$, which are two neighboring monomers in the chain localized at r_i and r_{i+1} respectively. For branched, dendritic, or non-linear polymer in general the interaction potential is similar but the order of connection of monomers defines the molecule.

The potential can be handled of different forms, usually modeled by a harmonic bond potential:

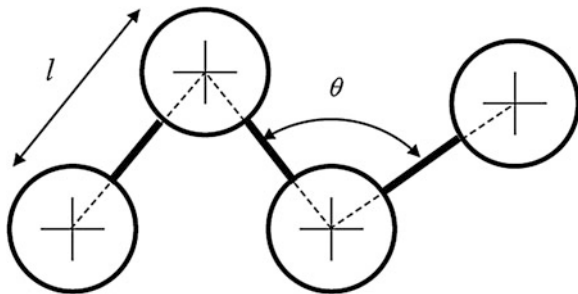
$$U_{bond} = k_{bond}(l - l_0)^2 \quad (10)$$

where $l = |r_{i+1} - r_i|$ is the distance between the monomers (see Fig. 2), l_0 is the equilibrium bond length, and k_{bond} is the spring constant for the potential. The high value of this constant $k_{bond} = 1,000 \text{ k}_B \text{T}/\text{nm}^2$ is necessary to avoid fluctuations in bond length. For simulation of polyelectrolytes in solution or polyelectrolyte adsorption on charged surfaces this potential is suitable. However, when the chain is surrounded by a high concentration of other chains, the entanglements between two segments can cause a strong strain enough to extend the bond between two monomers crossing these segments. This phenomenon is not physically realistic, and is avoided with a potential that limits the extension of the bond distance. The potential mostly used for this purpose is the finite extensible nonlinear elastic (FENE) [14]:

$$U_{FENE} = -\frac{1}{2}k_{bond}l_0^2 \ln \left(1 - \frac{l}{l_0^2} \right) \quad (11)$$

where $l = |r_{i+1} - r_i|$ is the distance between neighboring monomers, and l_0 is the maximum extension of the bond. This potential ensures that $l < l_0$ since higher distances are not defined. The potential is completed by including the repulsive part of the LJ potential, Eq. 9.

Fig. 2 Relevant distances and angles for the connectivity and stiffness of the CG chain model



In addition to the control of bond length, the chains are described by their intrinsic stiffness. In biological systems there are examples of very stiff polyelectrolytes such as chitosan and DNA, where the relative orientation between bonds is maintained at distances higher than the bond length. The intrinsic stiffness of the chain can be described by an angular harmonic potential u_{ang} between three consecutive monomers that is written as:

$$u_{ang} = k_{ang}(\theta - \theta_0)^2 \quad (12)$$

where θ is the angle between two consecutive bonds (see Fig. 2), θ_0 is the equilibrium angle with a typical value of $\theta_0 = \pi$, and k_{ang} is the angular spring constant. A fourth term can be added into the angular potential of Eq. 12 to increase the chain stiffness, this was used to simulate the condensation of DNA by polyvalent cations [15].

3.2 Ideal Gas and Excess Contribution to the Partition Function of the System: Configurational Integral

In order to theoretically understand the Monte Carlo method, we need to use the concepts of statistical mechanics. These concepts are developed in detail in books of fundamental statistical mechanics [16]. This formalism guides us in the task of calculating various quantities and/or properties that describe the behavior of the system. This is accomplished from the partition function that specifies the statistical properties of the system in thermodynamic equilibrium. There are different classes of partition functions, each corresponding to a determined statistical ensemble. The canonical ensemble is applied for a system of N particles in a volume V and temperature T . These magnitudes have fixed values and heat exchange is allowed. For this ensemble the corresponding partition function is:

$$Q = \frac{1}{h^{3N} N!} \int d\Gamma \exp[-H(\Gamma(r^N, p^N))/k_B T] \quad (13)$$

where h is the Planck constant. The integral is evaluated over all possible states of the system, where $\Gamma(r^N, p^N)$ is a point in the phase space that corresponds to a state of the system. This state is represented by all positions r^N and momenta p^N of the particles of the system. For simplicity, we use Γ to represent the state of the system. $H(\Gamma)$ is the energy of state Γ , it is called the Hamiltonian of the system, and it is related with the probability of observation of the state by:

$$\rho(\Gamma) = \frac{\exp(-\beta H(\Gamma))}{Q} \quad (14)$$

where β is called the inverse temperature, and is conventionally defined as $\beta = 1/k_B T$. The partition function and its derivatives are related with thermodynamic states functions, such energy E , entropy S , and free energy F :

$$E = -\frac{\partial \ln Q}{\partial \beta} \quad (15)$$

$$S \equiv -\frac{\partial}{\partial T}(k_B T \ln Q) \quad (16)$$

$$F = -k_B T \ln Q \quad (17)$$

The detailed derivation of these relationships can be found in classic books of statistical mechanics like that by McQuarrie [16].

The value of a quantity called an observable of the system, A , is defined as the ensemble average $\langle A \rangle$ of such quantity and has the form:

$$\langle A \rangle = \int d\Gamma A(\Gamma) \rho(\Gamma) = \frac{\int d\Gamma A(\Gamma) \exp(-\beta H(\Gamma))}{Q} \quad (18)$$

Since the total energy can be expressed as a sum of a kinetic energy contribution K (which depends only on the N particles moments p^N) and potential energy U (which depends on the particles positions r^N), the Hamiltonian can be written as:

$$H(\Gamma) = K(p^N) + U(r^N) \quad (19)$$

For simplicity r^N and p^N are denoted by r and p respectively. The partition function (Eq. 13) can factor into a product of kinetic and potential parts:

$$Q = \frac{1}{h^{3N} N!} \int dp \exp(-K/k_B T) \int dr \exp(-U/k_B T) \quad (20)$$

The first integral factor of the Eq. 20 only depends on the kinetic energy of a system and is equivalent to a system of non-interacting particles, the denominated ideal gas. Therefore this factor is called the ideal part Q^{ideal} of the partition

function. The second factor in Eq. 20 depends on the interaction potential energy of system, and is called the excess part Q^{excess} . Then we divide the total partition function into an ideal part Q^{ideal} and excess part Q^{excess} :

$$Q = Q^{ideal} Q^{excess} \quad (21)$$

The analytic calculations of the ideal part of the partition function is possible and has the form [16]:

$$Q^{ideal} = \frac{V^N}{N! \Lambda^{3N}} \quad (22)$$

The excess part depends on the interaction between the particles:

$$Q^{excess} = V^{-N} \int dr \exp(-U(r)/k_B T) \quad (23)$$

or the equivalent denominated configurational integral:

$$Z = \int dr \exp(-U(r)/k_B T) \quad (24)$$

In most systems, it is not possible to analytically calculate the excess part Q^{excess} or the configurational integral Z .

As a consequence of the uncoupling between the ideal and excess parts, the thermodynamics properties derived from the free energy can be expressed as the sum of the these two contributions. For example the chemical potential μ can be expressed as:

$$\mu = \frac{\partial F}{\partial N} = \frac{\partial}{\partial N} - k_B T \ln(Q^{ideal} Q^{excess}) = \mu_{ideal} + \mu_{excess} \quad (25)$$

In the books of classical statistical mechanics, the properties of the ideal gas have been evaluated, so we can focus on the configurational contribution. With the Monte Carlo method [17–19], we explore the configuration phase subspace according to the canonical or grand canonical distributions. The corresponding trajectory is essentially the projection of the phase space onto the subspace of coordinates, becoming independent of the subspace of moments.

3.3 Metropolis Monte Carlo Method

The exact computation of the partition function allows us to obtain all thermodynamic properties of the system; this is possible for a small number of very simple systems, such as the ideal gas. For other systems, we can reach some

approximate results after some simplifications and involved mathematical work. In most systems, it is not possible to analytically calculate the configurational integral and the properties or quantities that originate from it or its derivatives. The direct numerical estimation of Z for the polyelectrolyte system needs to generate a first point $r_{\tau=1}$ in the configuration space at $\tau = 1$, then calculate the potential energy $U(r_{\tau=1})$ for this configuration and its respective Boltzmann factor $\exp(-U(r_{\tau=1})/k_B T)$. Then a second configuration is generated $r_{\tau=2}$, and the calculation is reiterated. This operation is carried out a large number of times τ_{sample} , which is the size of the sample, and the configuration integral is estimated by:

$$Z \approx \frac{1}{\tau_S} \sum_{\tau=1}^{\tau_S} \exp(-U(r_\tau)/k_B T) \quad (26)$$

Let us considerer the specific case of a diluted polyelectrolyte chain composed of 50 monomers with their respective 50 counterions, without salt added, which is simulated in a cubic box of size W centered in the origin. This system contains 100 particles, and each system configuration contain 300 coordinates in total. Then, in order to choose a “random” point of the configurational space we can generate three random numbers between $-W/2$ and $W/2$ for each particle. In this configuration, it is unlikely that two consecutive monomers are at a relative distance close to the equilibrium bond length, given that the monomers are generated uniformly in the cubic box. This pair of monomers is more likely to be at a relative distance much greater than l_0 . Therefore, the binding energy would be very high, and the Boltzmann factor would be nearly negligible. Thus, this configuration does not contribute significantly to the configurational integral. Only the monomers distributions with distances between neighbors close to l_0 will have an important Boltzmann factor. Thus, efficient sampling of this system with a homogeneous random distribution of configurations is an impossible task for the currently available computational power.

The property A that we wish to estimate is depends only on the configuration of the system r^N . The configurational average of this quantity is:

$$\langle A \rangle = \frac{\int dr \exp(-U(r)/k_B T) A(r)}{\int dr \exp(-U(r)/k_B T)} = \frac{\int dr \exp(-U(r)/k_B T) A(r)}{Z} \quad (27)$$

This is a ratio between integrals, where we can note that the term $\exp(-U(r)/k_B T)/Z$ is the probability density of the configuration r^N . This configurational probability density is designed as:

$$\rho(r) \equiv \frac{\exp(-U(r)k_B T)}{Z} \quad (28)$$

Then Eq. 27 can be expressed numerically by:

$$\langle A \rangle_\rho = \sum_{r \in S} \rho(r) A(r) \quad (29)$$

where r is a point in the configurational space S . With the Monte Carlo method, it is not possible to calculate Z , and therefore we cannot directly evaluate the density $\rho(r)$. However it is possible to generate independent configurational point samples r_1, r_2, \dots, r_τ (from the distribution $\rho(r)$), which we can use to assess $\langle A \rangle_\rho$ through the average:

$$\langle A \rangle_{MC} \equiv \frac{1}{\tau} \sum_{i=1}^{\tau} A(r_i) \quad (30)$$

This Monte Carlo average $\langle A \rangle_{MC}$ becomes a better estimate of $\langle A \rangle_\rho$ as the sample size τ increases. Essentially the issue that remains to be resolved is how to generate points in the configurational space with relative probability proportional to the Boltzmann factor $\exp(-U(r)/k_B T)$. The Monte Carlo method builds a sequence of states that has a fundamental characteristic: it is a Markov chain of states. In this type of sequence, each configurational state is related directly to the previous configurational state. The first step is to make an initial configuration of the system $r_{i=1}$. Usually, the generation of the positions of the particles is random, avoiding the configurations with very high energy $U(r_{i=1}) \rightarrow \infty$. One example of a convenient initial configuration is a spatial distribution of rigid spheres, where particle overlap is avoided. Another example is a polymer chain where the distances between consecutive monomers in the initial configuration are close to the equilibrium length. After generating the initial configuration and calculating its potential energy $U(r_{i=1})$, a new $j = i + 1$ configuration $r_{j=i+1}$ is generated by the modification of the prior configuration $r_{i=1}$. Usually i and j are called old and new configurations, respectively. The new configuration is a trial and is not directly accepted, but an energetic criterion is used. A probability transition matrix $\pi(i \rightarrow j)$ represents this passage from one state to another. It is necessary to compute the energy of the new configuration $U(r_j)$. As we will see by comparing the initial and final energy we calculate the probability of transition. We can see that the Monte Carlo procedure generates a sequence of states, which appear with a probability $\rho^{MC}(r)$ given by the method. What we seek is that this probability distribution converges to the equilibrium states as the number of states generated is very large.

$$\lim_{\tau \rightarrow \infty} \rho_\tau^{MC}(r) = \rho(r) \quad (31)$$

The initial distribution $\rho_{\tau=0}^{MC}(r)$ has only the initial configuration $r_{i=1}$, which is evidently very different from those corresponding to equilibrium distribution $\rho(r)$. After a certain number of Monte Carlo steps, the initial distribution changes until it

converges to the equilibrium distribution given by a transition matrix $\pi(i \rightarrow j)$, which is the probability that the system will be in state j at time $\tau + 1$, given that it is in state i at time τ . The evolution of $\rho^{MC}(r)$ is governed by the master equation:

$$\rho_{\tau+1}^{MC}(r_j) - \rho_\tau^{MC}(r_j) = \sum_{i \neq j} [\rho_\tau^{MC}(r_i)\pi(i \rightarrow j) - \rho_\tau^{MC}(r_j)\pi(j \rightarrow i)] \quad (32)$$

The left hand side of this equation is the probability variation of finding the system in the configuration r_j from time τ to time $\tau + 1$. This variation is a balance between two contributions specified on the right hand side of the Eq. 32. The first term increases the probability $\rho_{\tau+1}^{MC}(r_j)$ due to the states that come from configurations $i \neq j$ and go to the configuration j . The second term decreases the probability $\rho_{\tau+1}^{MC}(r_j)$ due to the states that are in the configuration j and convert to other configurations $i \neq j$.

Eq. 32 defines that at very long time the $\rho_{\tau+1}^{MC}(r_j)$ distribution reaches a stationary distribution $\rho(r_j)$, which is constant in time $\rho_{\tau+1}^{MC}(r_j) = \rho_\tau^{MC}(r_j)$ for $\tau \rightarrow \infty$. This condition implies that:

$$\sum_{i \neq j} [\rho_\tau^{MC}(r_i)\pi(i \rightarrow j) - \rho_\tau^{MC}(r_j)\pi(j \rightarrow i)] = 0 \quad (33)$$

At very long times, the balance of contributions to the probability change of configuration j is cancelled. Usually we can use a strong condition to achieve the stationary state, where the terms in Eq. 33 are canceled in pairs.

$$\rho_\tau^{MC}(r_i)\pi(i \rightarrow j) = \rho_\tau^{MC}(r_j)\pi(j \rightarrow i) \quad (34)$$

This condition is called the detailed balance, also usually written in a very compact form as a ratio of transition probabilities and replacing $\rho_\tau^{MC}(r_j)$ by the equilibrium distribution given by Eq. 28:

$$\frac{\pi(i \rightarrow j)}{\pi(j \rightarrow i)} = e^{-\Delta U/k_B T} \quad (35)$$

where $\Delta U = U(r_j) - U(r_i)$ is the energy change due to the transition from i state to the j . In summary the chosen $\pi(i \rightarrow j)$ transition matrix must satisfy two main conditions: the detailed balance and $\pi(i \rightarrow j) \geq 0$.

In the Metropolis Monte Carlo scheme [20], the move from the state i to j is given in two stages. The first stage produces a trial move from state i to state j and is represent by a probability $\alpha(i \rightarrow j)$ called the underlying matrix of the Markov chain. For example, this trial move can consist of the translation of one particle chosen from N particles. The probability is then $\alpha(i \rightarrow j) = 1/N$. The second stage is represented by $acc(i \rightarrow j)$, which determines whether the trial move is accepted or rejected. The transition matrix $\pi(i \rightarrow j)$ is written as a function of these two stages:

$$\pi(i \rightarrow j) = \alpha(i \rightarrow j) \times acc(i \rightarrow j) \quad (36)$$

where $\alpha(i \rightarrow j) = \alpha(j \rightarrow i)$ in the Metropolis Monte Carlo original scheme [20]. The chosen symmetric α simplifies Eq. 35:

$$\frac{acc(i \rightarrow j)}{acc(j \rightarrow i)} = e^{-\Delta U/k_b T} \quad (37)$$

There are several choices for $acc(i \rightarrow j)$ satisfying this condition. The choice of Metropolis et al. [20] is:

$$\begin{aligned} acc(i \rightarrow j) &= \rho(r_j^N) / \rho(r_i^N) \quad \text{if } \rho(r_j^N) < \rho(r_i^N) \\ acc(i \rightarrow j) &= 1 \quad \text{if } \rho(r_j^N) \geq \rho(r_i^N) \end{aligned} \quad (38)$$

The transition probability matrix for going from state i to state j is given by:

$$\begin{aligned} \pi(i \rightarrow j) &= \alpha(i \rightarrow j) \quad \text{if } \rho(r_j^N) \geq \rho(r_i^N) \\ \pi(i \rightarrow j) &= \alpha(i \rightarrow j) \rho(r_j^N) / \rho(r_i^N) \quad \text{if } \rho(r_j^N) < \rho(r_i^N) \\ \pi(i \rightarrow i) &= 1 - \sum_{j \neq i} \pi(i \rightarrow j). \end{aligned} \quad (39)$$

In the Metropolis scheme the only requirement for the α matrix is that it must be symmetric, allowing significant freedom in the choice of the trial move. This is important for the speed of convergence to the equilibrium distribution since this speed depends on the type of trial move utilized.

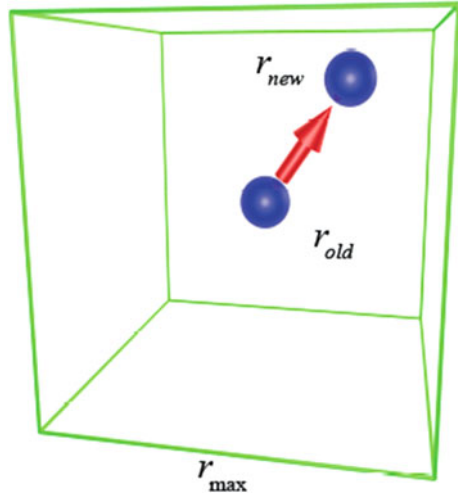
3.4 Monte Carlo Trial Moves

Translational moves of a single particle. The simplest form of creating a trial configuration is a translation move of a particle, see Fig. 3.

In this move the particle is translated from an old position r_{old} to a trial new position r_{new} in a cubic box with side $L = r_{max}$ and centered at the old position. Usually the size of the trial box where the translation is performed is lower than the size of the simulation box. This move consists of three steps:

1. Select a particle at random, and calculate its energy $U(r_{old})$.
2. Give the particle a random displacement value between $-r_{max}/2$ and $r_{max}/2$ to each coordinate measured with respect to the center of mass. We need to use $Ranf$, a random number uniformly distributed between 0 and 1.

Fig. 3 Scheme that represents the translational move of a single particle



$$\begin{aligned}x_{new}(i) &= x_{old}(i) + (Ranf - 0.5)r_{max} \\y_{new}(i) &= y_{old}(i) + (Ranf - 0.5)r_{max} \\z_{new}(i) &= z_{old}(i) + (Ranf - 0.5)r_{max}\end{aligned}\quad (40)$$

Then calculate its new energy $U(r_{new})$.

3. If the system energy decreases, $U(r_{new}) < U(r_{old})$, the trial move is accepted directly. If $U(r_{new}) > U(r_{old})$ the move to the new configuration has an acceptance probability:

$$acc(i \rightarrow j) = \exp\{-\beta \Delta U\} < 1 \quad (41)$$

where $\Delta U = U(r_{new}) - U(r_{old})$ is the energetic change from the old to the new configuration. For example, if $\Delta U = 0$ the new configuration is accepted since $acc(i \rightarrow j) = 1$. For $\Delta U > 0$ the acceptance probability is lower than 1, and the algorithm uses $Ranf$ to decide to accept the trial move or not. If $Ranf < acc(i \rightarrow j)$ the new configuration is accepted, since that the probability that the random number $Ranf$ is less than $acc(i \rightarrow j)$ is equal to $acc(i \rightarrow j)$.

If the particle is chosen at random between N particles, then the probability is $\alpha(i \rightarrow j) = 1/N$. The reverse trial move is equally probable and hence is symmetric.

The space within which the particle can be translated is the cubic box with side length equal to r_{max} and centered in the old coordinate r_i , hence defines the maximum extension of the particle translation during the simulation (see Fig. 3). If r_{max} is small, the resulting configuration has a very similar potential energy and the change $\Delta U/k_B T \rightarrow 0$. In this case, the most of the moves are accepted. However,

the sampling of the configurational space is poor because the configurations are all very similar, and there is a low number of statistically independent configurations. When the r_{\max} value is high, the change in potential energy is much larger, and it is more likely that the new configuration is rejected. This balance can be quantified by the acceptance ratio:

$$r_{acc} = \frac{N_{acc}}{N_{trial}} \quad (42)$$

where N_{acc} is the number of trial accepted of a total trials equal to N_{trial} . The maximum particle displacement is adjusted as the simulation is performed to achieve an acceptance ratio close to 0.2–0.5 depending on the particular characteristics of the system.

This simulation trial move is very efficient for finding uncorrelated configurations in condensed systems or in our case, for the small ions. However, in a system like a polymer or polyelectrolyte the degrees of freedom of particles are reduced by the connectivity between them, which generates collective movement of segments or entire chains. Hence, achieving this type of collective movement by the translation motion of one particle at a time is a laborious task. There are several collective motions: we describe two for the entire chain (translation and rotation) and two for the segment (bending and pivot). These collective motions include the counterions near the chain or segment that will move.

Translational move of chain. This move is similar to the translation of a single particle motion, but in this case we are going to move all the particles that make up a chain at a time and in the same direction.

The translation of a chain is the generalization of the translation of a single monomer (Eq. 40). In this case, we choose a random displacement vector:

$$\begin{aligned} dx &= (Ranf - 0.5)r_{\max,Trasl} \\ dy &= (Ranf - 0.5)r_{\max,Trasl} \\ dz &= (Ranf - 0.5)r_{\max,Trasl} \end{aligned} \quad (43)$$

where $r_{\max,Trasl}$ is the maximum displacement of the translation. This displacement vector is added to all particles i that make up the chain:

$$\begin{aligned} x_{new}(i) &= x_{old}(i) + dx \\ y_{new}(i) &= y_{old}(i) + dy \\ z_{new}(i) &= z_{old}(i) + dz \end{aligned} \quad (44)$$

In this way the particles move in the same direction maintaining their relative positions. The trial move is accepted with the same energetic criterion as that of Eq. 41.

Rotational move of chain. For the rotation of an entire chain, we need to choose a rotation axis determined by a unit vector $u = (a, b, c)$. For simplicity, we chose the chain center of mass as the initial point of this vector:

$$\mathbf{r}_{cm} = \frac{1}{N} \sum_{i=1}^N \mathbf{r}(i) \quad (45)$$

Then the rotation process is applied to the relative position of particles with respect to the center of mass ($\mathbf{r}_{old}(i) - \mathbf{r}_{cm}$). The expression for the rotation is:

$$\mathbf{r}_{new}(i) = A_{\theta,u}(\mathbf{r}_{old}(i) - \mathbf{r}_{cm}) + \mathbf{r}_{cm} \quad (46)$$

where $A_{\theta,u}$ is the standard matrix for a counterclockwise rotation through a random choose of the angle θ about u .

$$A_{\theta,u} = \begin{bmatrix} a^2(1 - \cos \theta) + \cos \theta & ac(1 - \cos \theta) - c \sin \theta & ac(1 - \cos \theta) + b \sin \theta \\ ab(1 - \cos \theta) + c \sin \theta & b^2(1 - \cos \theta) + \cos \theta & bc(1 - \cos \theta) + a \sin \theta \\ ac(1 - \cos \theta) + b \sin \theta & bc(1 - \cos \theta) + a \sin \theta & c^2(1 - \cos \theta) + \cos \theta \end{bmatrix} \quad (47)$$

The trial move is accepted with the same energetic criterion as that of Eq. 41.

Pivot and bending moves of chain segments. These two moves consist in the rotation of a segment of the chain. In the pivot case [21], we need to choose a rotation axis determined by a unit vector $u = (a, b, c)$. As initial point of this vector we choose the position \mathbf{r}_j of a random choose monomer j (see Fig. 4a). The segment from monomer j to one end of the chain is rotated through a random choice of the angle θ about u . For this we use:

$$\mathbf{r}_{new}(i) = A_{\theta,u}(\mathbf{r}_{old}(i) - \mathbf{r}_j) + \mathbf{r}_j \quad (48)$$

The pivot move trail is the more efficient move for the sampling of the polymer chain.

The bending move is very similar to the pivot move. In this case the rotation is carried out on a segment of the chain between the monomers j and k (see Fig. 4). The rotation axis is determined by the direction that connect the two monomers:

$$\mathbf{u} = \frac{\mathbf{r}_k - \mathbf{r}_j}{|\mathbf{r}_k - \mathbf{r}_j|} \quad (49)$$

As initial point of this vector we choose the position \mathbf{r}_j . These trial moves are accepted with the same energetic criterion as that of Eq. 41.

To achieve greater efficiency in all these moves, the small ions that are closer to the chain or segment must move as if they were part of these.

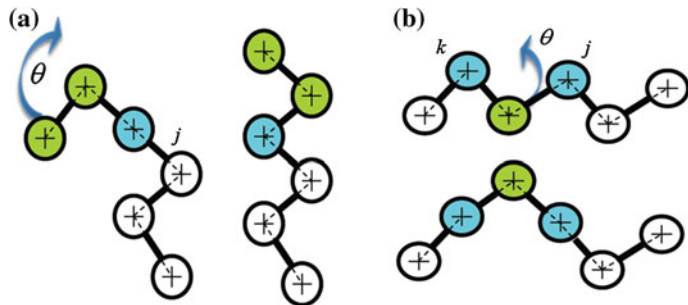


Fig. 4 Monte Carlo moves for efficient sampling of configurational space. **a** Pivot move. **b** Bending move

4 Application of Monte Carlo to Polyelectrolyte Solutions

4.1 Conformational and Persistence Length of a Single Polyelectrolyte Chain

The stiffness of the polyelectrolyte chain has an important influence on several phenomena, such as the morphology of polyelectrolyte complexes [22–24], and DNA condensation by multivalent cations [25]. The real polymer may be categorized, from the view point of its chain stiffness, into three main groups: flexible chains, in which bending is limited over the length of a few links; semiflexible chains, in which bending becomes appreciable over larger lengths; and rigid rods, where the extension of the bending radius is considerably greater than the chain dimension.

The classical parameter that quantifies the global conformation of the chain is the end-to-end distance D_{ee} :

$$D_{ee} = |\vec{R}_{ee}| = |\vec{r}_{Nm} - \vec{r}_1| \quad (50)$$

This is the distance of the vector \vec{R}_{ee} that joins the chain ends whose positions are \vec{r}_{Nm} and \vec{r}_1 . Several important properties are obtained by averaging over all conformations of the square of the end-to-end vector $\langle \vec{R}_{ee}^2 \rangle$, the first step is to write the vector in an alternative way:

$$\vec{R}_{ee} = \sum_{i=1}^{Nm-1} \vec{a}_i \quad (51)$$

where $\vec{a}_i = \vec{r}_{i+1} - \vec{r}_i$ is the vector that joins two consecutive monomers. The mean square of \vec{R}_{ee} can be written as:

$$\langle \vec{R}_{ee}^2 \rangle = \left\langle \sum_{i=1}^{Nm-1} \vec{a}_i \cdot \sum_{j=1}^{Nm-1} \vec{a}_j \right\rangle = \sum_{i=1}^{Nm-1} \langle \vec{a}_i^2 \rangle + 2 \sum_{1 < i < j < Nm-1} \langle \vec{a}_i \vec{a}_j \rangle \quad (52)$$

where $\vec{a}_i \cdot \vec{a}_j = |\vec{a}_i| \cdot |\vec{a}_j| \cos \theta_{ij}$ is a scalar product, and θ_{ij} is the angle between the vectors. The simplest model for representing a polymer is called the ideal chain or freely-jointed chain. The fundamental characteristics of this model are: (a) The bonds between neighbor monomers have a constant length of l_0 ; (b) The chain has a negligible bending potential; (c) The monomers are point particles, and the interactions of the monomers with other monomers and with the solvent are negligible. This model has important statistical properties. In particular, the segment directions are fully free, and the angle θ_{ij} has an equal probability of taking any value between 0 and π . Thus, the average relative orientation between the i and j bonds is null. Thus the averaging is:

$$\langle \vec{a}_i \cdot \vec{a}_j \rangle = l_0^2 \langle \cos \theta_{ij} \rangle = 0 \quad (53)$$

where $l_0 = \langle \vec{a}_i \rangle$. Eq. 52 yields:

$$\langle \vec{R}_{ee}^2 \rangle = (Nm - 1)l_0^2 \quad (54)$$

The root-mean-square end-to-end distance R_e for a long polymer ($Nm \gg 1$) is:

$$R_{ee} = \langle \vec{R}_{ee}^2 \rangle^{1/2} \sim l_0 Nm^{1/2} \quad (55)$$

The scaling relationship is:

$$R_{ee} \sim Nm^\nu \quad (56)$$

where ν is the scaling coefficient, which has a value of $\nu = 0.5$ for the ideal chain. The statistical properties of the ideal chain model are similar to those of the random walk case.

When the monomer has a finite volume and cannot occupy the same space as another monomer, it has an interaction denominated of excluded volume. The simplest mathematical model that represents the exclude volume chain is the self-avoiding random walk, where a segment of a chain cannot overlap of the rest of monomers. The number of possible conformations decreases with respect to the ideal chain, but the remaining conformations present the most extended form, resulting in an increase of the scaling coefficient to $\nu \approx 0.6$.

In our coarse grain model the chain stiffness is governed by two contributions: the bending constant (Eq. 12) and the long-range nature of the electrostatic interaction due to the presence the of charges on the polyelectrolyte segments.

These two contributions are compared with the chain stiffness in reference [26]. The simulations of ideal and fully flexible neutral chains are found to follow the theoretical scaling relations for R_e (Eq. 56) with $\nu = 0.5$ and $\nu = 0.6$ respectively

verifying the accuracy of the Monte Carlo algorithm. When the intrinsic stiffness of the neutral chain is increased $k_{ang} = 1 - 5$ the scaling value has a coefficient close to $v = 0.6$, however for higher values of angular constant the scaling coefficient has a significant increase until a value close to $v = 0.9$. This mean that the most extend conformations are more probable.

The scaling coefficient of polyelectrolyte chains is $v \approx 1$ for all values of angular constant, this behavior indicates that the most probable conformations are extended, something that minimizes the electrostatic repulsion between segments. For the polyelectrolyte with intrinsic full-flexible chain ($k_{ang} = 0$) the conformations are more expanded than the full-flexible neutral case, this fact is reflected in the greater value of R_e with respect to the neutral chain, however these are not fully-extended conformations [26].

The end-to-end distance probability distribution $P(R_{ee})$ is analyzed to understand the relation between the global conformation and local stiffness. For the sake of comparasion, the maximun chain stretching is also calculated, as indicated by the contour length of the chain:

$$L_{chain} = (Nm - 1)l_0 \quad (57)$$

The contour length for this 60 monomers chain is $L_{chain} = 29.5$ nm.

We compare a 60 monomers chain of a neutral polymer and polyelectrolyte chain as depicted in Fig. 5a and b respectively, at different values of the angular constant k_{ang} . The end-to-end distance probability distribution for the fully flexible neutral chain ($k_{ang} = 0$) has a symmetrical distribution around $R_{ee} = 6$ nm that is significantly lower than the contour length. The major fraction of conformations corresponds to the coiled form. The fluctuation in the R_{ee} values is of the same order of magnitude as its average value, where the stretched conformations represent an insignificant fraction.

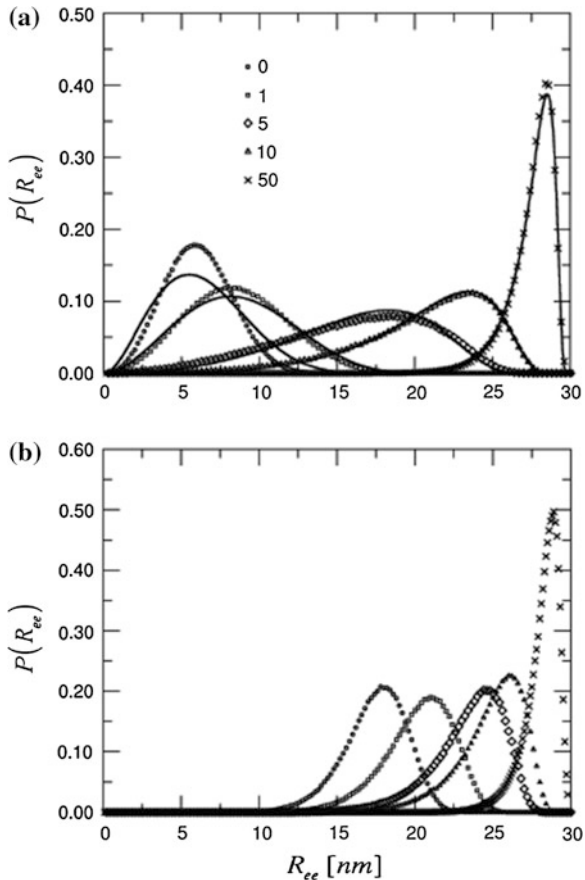
In the semiflexible chain case ($k_{ang} = 1 - 10$) the distribution $P(R_e)$ shifts to higher R_e values and increases it fluctuations around the average value.

Adopting a continuum wormlike chain model Wilhelm and Frey [27] have calculated analytically the end-to-end distance distribution function of a semi-flexible polymer. They obtained the following expression:

$$G(d_e) = \frac{2\kappa}{4\pi N} \sum_{n=1}^{\infty} \pi^2 n^2 (-1)^{n+1} e^{-\kappa\pi^2 n^2 (1-d_e)} \quad (58)$$

where $d_e = R_e/L_{chain}$ is the end-to-end distance relative to the chain contour length, $\kappa = l_p^0/L_{chain}$, where l_p^0 is the intrinsic persistence length and N is a normalization constant. The theoretical profiles $G(d_e)$ obtained by fitting Eq. 58 with the simulation result ($P(R_e)$) are shown in the Fig. 5a as full lines. The curve fitting process has a free parameter l_p^0 and reproduces the data qualitatively well and is an excellent approximation for $k_{ang} > 1$. Table 1 summarizes the values of l_p^0 as a function of k_{ang} , where a linear relation among these can be observed.[26]

Fig. 5 End-to-end distance probability distribution obtained from Monte Carlo simulations of **(a)** a Neutral polymer, **(b)** a Polyelectrolyte. The different values of angular constant k_{ang} are informed inside of the figure [26]



The combined effect of intrinsic angular potential and electrostatic interactions on polyelectrolyte conformations is shown in Fig. 5b for a chain that contains 60 monomers. The fully flexible case ($k_{ang} = 0$) is paradigmatic since the distribution $P(R_e)$ has a strong shift towards greater R_e values, but the most probable value is still far from the chain contour length. This implies that the electrostatic repulsion is capable of stretching the chain but is not strong enough to yield a rod conformation. The distribution shows a similar form at $k_{ang} = 1$, however as the angular constant increases, $k_{ang} = 5$ and $k_{ang} = 10$, the fluctuation with respect to the neutral chain are reduced considerably. The distributions are similar for neutral and charged chain when $k_{ang} = 10$. This fact indicates that the intrinsic stiffness dominates. The distribution fittings using Eq. 58 are very poor (data not shown) which mean that the polyelectrolyte conformations statistics cannot be satisfactorily interpreted in terms of a wormlike chain model. To shed light on this aspect of the polyelectrolyte structure we will use a local measure of chain flexibility.

As described above in an ideal chain (Eq. 53), two segments may have any orientation with equal probability. This can be generalized for polymers and

polyelectrolytes using the segment orientational correlation between two link \vec{a}_i and \vec{a}_j calculated according to:

$$\langle \cos \theta_{ij} \rangle = \left\langle \frac{\vec{a}_i \cdot \vec{a}_j}{|\vec{a}_i| \cdot |\vec{a}_j|} \right\rangle \quad (59)$$

We take the average over all pairs i, j while keeping the distance $s = |i - j|$ constant:

$$\langle \cos \theta(s) \rangle = \left\langle \frac{\vec{a}_i \cdot \vec{a}_j}{|\vec{a}_i| \cdot |\vec{a}_j|} \right\rangle_{s=|i-j|} \quad (60)$$

where $\langle \cos \theta(s) \rangle$ is the segment orientational correlation function (SOCF) and represents the average of the cosine of the angle between the segments separated by a length s .

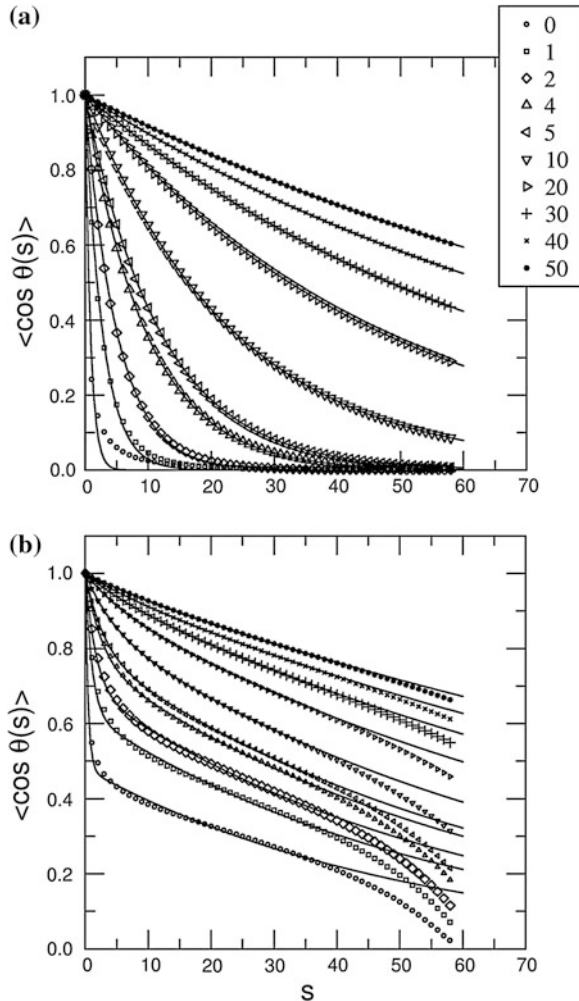
Figure 6 shows the SOCF for neutral and charged chains at different angular constant. For both cases the chain has 60 monomers. The SOCF for the neutral chain is depicted in Fig. 6a and a linear form is shown for the higher values of angular constants $k_{ang} = 40 - 50$ and a simple exponential decay form for the lower values $k_{ang} = 1 - 30$. This reproduces the behavior of a worm-like chain model, which obeys a SOCF exponential decay with distance:

$$\langle \cos \theta(s) \rangle = \exp\left(-\frac{s}{l_p^0}\right) \quad (61)$$

where l_p^0 is the intrinsic persistence length. The fitting with this expression is excellent for $k_{ang} \geq 1$, but for fully the flexible chain ($k_{ang} = 0$) the fitting is not satisfactory since the volume exclusion effects become important, this effect was not taken into account in the theoretical derivation of Eq. 61. The single exponential decay represents the main characteristic of the worm-like model that is the existence the only one relevant spatial scale, which is quantified by the intrinsic persistence length. The l_p^0 values obtained by the fitting with this equation are reported in Table 1 and are in excellent agreement with those calculated with Eq. 58.

Fig. 6b shown the SOCF of polyelectrolyte chains. We note that for the intrinsic rigid chain ($k_{ang} = 50$) the profile has a single exponential decay form similar to the neutral polymer case. However for the semi-flexible and fully-flexible chains the SOCF are qualitatively different to neutral polymer case. The electrostatic interactions between monomer-monomer and monomer-counterions originate severe difficulties to the analytical treatment of SOCF. Odijk [28] and Skolnick and Fixman [29] performed the pioneering studies on the influence of electrostatic interactions on polyelectrolyte stiffness. They applied a perturbative calculation on a slightly bent rigid charged rod using the Debye-Hückel approximation. They found a simple exponential decay for the SOCF of the type:

Fig. 6 SOCF of a neutral polymer (**a**) and a polyanion (**b**) of 60 monomers. The different values of bending constant used are reported inside the *upper graphic*. The *continuous lines* represent the fit with the theoretical expressions (61) and (64) for (**a**) and (**b**) respectively.[26]



$$\langle \cos \theta(s) \rangle = \exp\left(-\frac{s}{l_p}\right) \quad (62)$$

where l_p is the total persistence length given by [28, 29]:

$$l_p = l_p^0 + l_p^e \quad (63)$$

This is expressed as a contribution of intrinsic and electrostatic persistence lengths denoted by l_p^0 and l_p^e respectively. The concept of a unique persistence length of a polyelectrolyte works well for rigid chain. However this concept applied to a fully-flexible and semiflexible chains has been questioned using

Table 1 Intrinsic $\left(l_p^0\right)$ and electrostatic $\left(l_p^e\right)$ persistence length values for neutral polymer and polyanion chains at different bending constant and sizes.[26]

	$\left(l_p^0\right)$ [nm]	$\left(l_p^e\right)$ [nm]	$(Nm = 30)$	$(Nm = 60)$	$(Nm = 90)$	$(Nm = 120)$
k_{ang}	(Eq. 58)	(Eq. 61)				
0	0.8	0.4	10.3	25.3	43.1	59.6
1	1.3	1.4	10.5	26.2	45.1	61.5
2	2.0	2.5	10.8	26.6	46.2	64.1
4	3.8	4.8	10.8	26.9	46.4	64.0
5	4.8	6.0	10.8	27.1	44.5	65.4
10	10.0	11.5	10.6	25.6	44.7	65.0
20	20.2	23.5	9.8	24.5	41.2	58.7
30	32.4	34.8	10.5	23.2	39.7	55.4
40	43.0	46.5	10.5	21.6	39.0	56.3
50	55.6	58.0	10.4	21.2	37.9	52.0

computer simulations [30, 31]. The fitting is not satisfactory for the SOCF for the simulation results of fully and semiflexible chains presented in Fig. 6b. A better fitting of polyelectrolyte SOCF is found with a double exponential function [32]:

$$\langle \cos \theta(s) \rangle = B \exp \left(-\frac{s}{l_p^0 + l_p^e} \right) + (1 - B) \exp \left(-s \frac{l_p^e + (1 - B)l_p^0}{l_p^0 (l_p^0 + l_p^e) (1 - B)} \right) \quad (64)$$

This theoretical expression was obtained for a charged chain with a Gaussian statistics in a solution with monovalent salt [33]. The chain was assumed to be of infinite length and the electrostatic interactions were treated at a linear level with a Debye-Hückel screened interaction between charges due to the presence of monovalent salts. This treatment neglects non-linear effects connected to counterion condensation, as well as chain-end effects present in our simulations.

The fitting curves with Eq. 64 are shown in Fig. 6b, for which we use the l_p^0 values obtained with the equation corresponding to the neutral polymer case. We considered chain segment separations $s < 30$, since below this separation the two decays predicted by Eq. 64 are evident. Above this separation there is a third decay resulting from the effects of chain ends, which were not considered in the derivation of Eq. 64. The values obtained for l_p^e as a function of k_{ang} for different chain sizes are shown in Table 1.

The electrostatic persistence length does not vary significantly with the bending constant, but is highly sensitive to the chain size. The l_p^e approximate values are 10, 20, 40, and 60 nm for chains with 30, 60, 90 and 120 monomers respectively. This means that they have magnitudes comparable to the chain contour length because in the salt-free condition the electrostatic interactions have the same reach as the chain size used.

4.2 Counterions Condensation and End-Chain Effects

In order to analyze the local structure of a polyelectrolyte in solution we use the monomer-monomer radial distribution function $G_{mm}(r)$. This is defined as the ratio between the number of monomer-monomer pairs (at a distance in the interval between r and $r + dr$) and the volume enclosed between spheres of radius r and $r + dr$. In our binning dr is taken to be 0.1 nm. Analogously, we define a monomer-counterion radial distribution function $G_{mc}(r)$. These quantities are shown for a chain with 20 monomers, at a concentration of 10^{-4} monomer/nm³, in Fig. 3a and b for different equilibrium bond lengths between monomers, l_0 , ranging between 0.25 and 0.75 nm. The distance between consecutive electric charges in the chain is equal to l_0 , assuming the total dissociation of the polyelectrolyte ($f = 1$). The monomer-monomer radial distribution function was multiplied by r^2 for proper visualization. As shown there, all $G_{mm}(r)$ curves display a sharp peak at a distance close to l_0 ; this peak corresponds to the correlation among the first neighboring monomers, and reflects the connectivity of the chain [34]. The subsequent weak peaks are observed at multiples of l_0 and correspond to the correlation between neighbors of higher order.

The ratio between the distances l_0 and l_B , called the Manning parameter $\xi = l_B/l_0$ [35], plays a central role in the condensation of counterions and will be used in the present analysis. In the conditions of the present work the Bjerrum length has a value of $l_B = 0.71$ nm.

Figure 7a shows $G_{mc}(r)r^2$ for the present simulations, where the ξ values are found to be between 2.84 and 0.95. These values are close to the ones where ion condensation along the polyelectrolyte may occur, say $\xi \geq 1$. Additionally, Fig. 7b shows the $G_{mc}(r)$ distribution for the aforementioned values of l_0 . The profiles show a sharp peak that corresponds to the hardcore distance between monomers and counterions. The accumulation of counterions decreases with distance and becomes negligible at $r > 1$ nm. The effect of l_0 on the counterion atmosphere is evident: as l_0 decreases the counterion concentration increases. This phenomenon is called Manning condensation, which is quantified in our simulation with the condensation degree $\hat{\theta}$ defined as:

$$\hat{\theta} = \frac{\langle n_c \rangle}{N_m} \quad (65)$$

where $\langle n_c \rangle$ is the average number of counterions condensed on the chain made of N_m monomers. A counterion j is considered to be in a condensed state with respect to a given monomer i , if it is closer to this monomer than a given cutoff radius r_C . This is chosen here as 1 nm, consistent with the behavior of $G_{mc}(r)$. Each counterion is assumed to condense only on one charged monomer, which is supposed to be the closest to it. Using the former definition we can analyze the condensation on a given monomer, say i , by the quantity $\theta_i = \langle n_c^i \rangle$, where n_c^i is now the number of counterions condensed on the monomer i [34, 36]. This value will allow us to

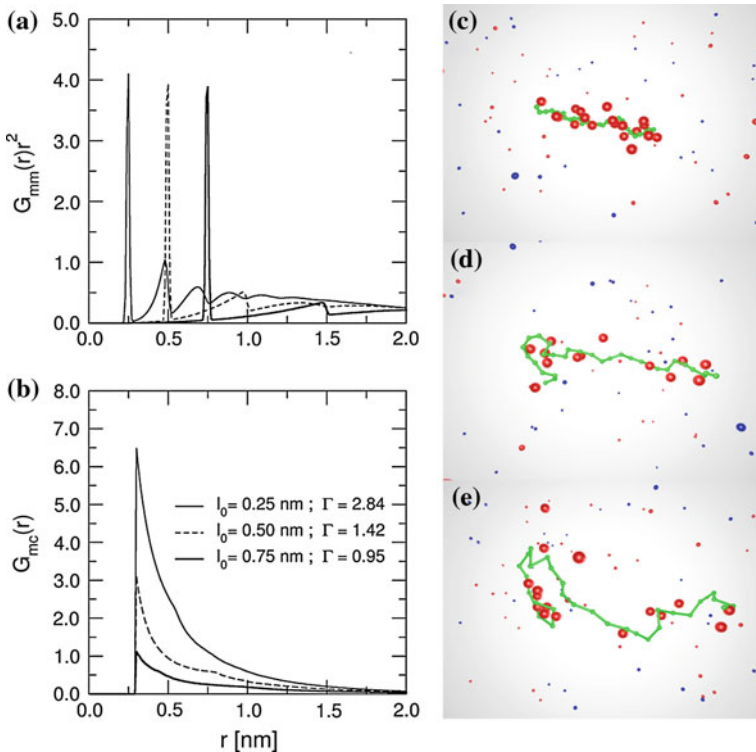
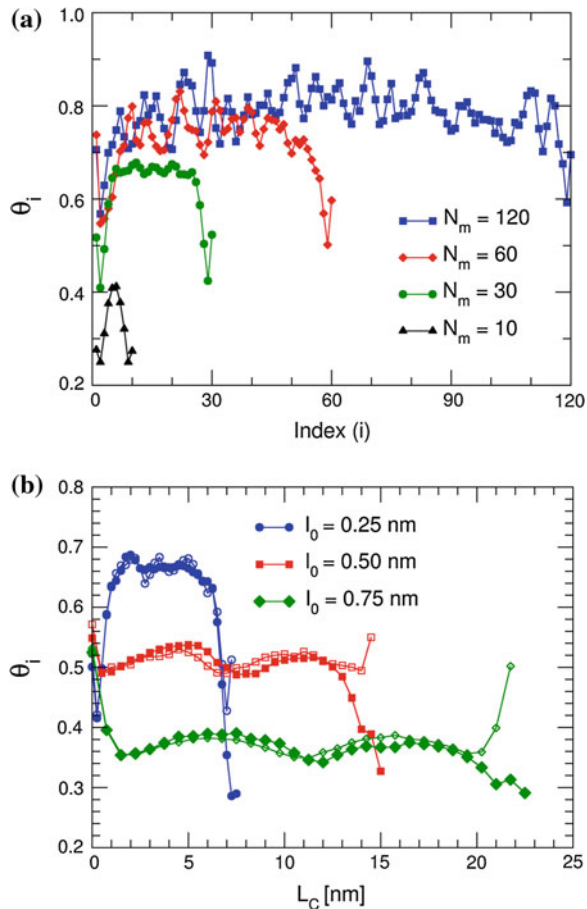


Fig. 7 Radial distribution function for (a) monomer–monomer pairs $G_{mm}(r)$ and (b) monomer–counterion pairs $G_{mc}(r)$ corresponding to different equilibrium bond lengths between monomers l_0 . Simulation frames for (c) $l_0 = 0.25 \text{ nm}$; (d) $l_0 = 0.50 \text{ nm}$ and (e) $l_0 = 0.75 \text{ nm}$

study the distribution of counterions along the chain for different values of N_m and l_0 . Besides the monomer index i , another quantity can be used to set the location of a given monomer in the chain. This is the contour length $L_C(i) = (i - 1)l_0$ which gives an interesting alternative interpretation. The condensation degree θ_i as a function of monomer index i and the contour length L_C for different values of N_m and l_0 is shown in Fig. 8.

Figure 8a depicts the distribution of θ_i values along the chain with $l_0 = 0.25 \text{ nm}$ and different polymerization degrees N_m . For the shorter chain, $N_m = 10$, the counterion condensation has small values that range between 0.25 and 0.42, with a symmetrical distribution that presents a maximum in the middle of the chain and a minimum at each end. When the chain has a size equal to $N_m = 30$, it presents a higher counterion condensation than in the former case, and there emerges a plateau between the monomers with indices 5 and 25. The condensation increases again when the size of the chain becomes $N_m = 60$, but it is slightly lower than the case of the chain with $N_m = 120$. These results suggest that the degree of condensation tends to a constant value as the size of the chain increases.

Fig. 8 Degree of counterion condensation θ_i as a function of (a) monomer index i , for chains with $l_0 = 0.25$ nm and different polymerization degrees N_m and (b) the contour length $L_C(i)$, for a chain with 30 charged monomers (empty symbol) and chain with 30 charged monomers +1 neutral monomer (filled symbol)



Ion condensation is not the same on all the monomers of a given chain because the end effects are important for finite chains. The counterions are preferentially in middle of the chain, and there are fewer counterions at the ends.

The local maximum of condensation on the first and the last monomers (end monomers) represents a special case, where $G_{mc}(r)$ for each individual monomer (data not shown) indicates that the condensation has a minimum on the end monomers, i.e. the $G_{mc}(r)$ profile for the last monomers are lower than the rest. These local maxima in Fig. 4a are an artifact and arise as a consequence of the definition of the condensation degree. The end monomers evidently have a greater volume accessible to the counterions, thus increasing the local condensation degree, but physically there is no local maximum of the counterion density at these positions, since the average charge density is smaller there. This is evident in the continuous line in Fig. 8b. This effect is not present in Monte Carlo simulations where we add a neutral monomer at the end of the chain, which does not modify the electric potential produced by the other charged monomers. This was done for

the monomer at position 30, and the results are shown as open symbols in Fig. 8b. The θ_i values are different for monomers 1 and 30 because the neutral monomer was not added for the monomer in position 1. This allows us to observe that the density of condensed counterions effectively decrease at the ends.

The average degree of condensation $\langle \theta \rangle$ can be used as a global quantity for measuring counterion condensation. The relationship between the global and the specific condensation is:

$$\langle \theta \rangle = \frac{\sum_{i=1}^{N_m} \theta_i}{N_m} \quad (66)$$

This is plotted as a function of chain size N_m at different equilibrium lengths (l_0) in Fig. 9. When the chain size is small, counterion condensation is negligible, then θ increases as the chain size increases. θ reaches a plateau $\theta^{plateau}$ at a chain size $N_m^{plateau}$ around fifty and one hundred monomers, depending on l_0 [37]. Thus $N_m^{plateau} \approx 50$ for $l_0 = 0.75$ nm, and $N_m^{plateau} \approx 100$ for the most strongly charged polyelectrolyte, with $l_0 = 0.25$ nm.

This asymptotic behavior is a consequence of the different distribution of counterions on the middle and at the extremes of the chain. Therefore, as the size of the chain increases, end-effects become less important. Polyelectrolytes with a greater linear charge density achieve a larger $\theta^{plateau}$ value at a larger chain size $N_m^{plateau}$. End effects are more important in this case, due to the larger counterion condensation in these systems. The plateau values are $\theta^{plateau} \approx 0.78; 0.63; 0.43$ for $l_0 = 0.25; 0.50;$ and 0.75 nm respectively.

The values of the counterion condensation degree predicted from the limiting Manning theory according to the equation:

$$\theta_M = 1 - \frac{1}{\xi} \quad (67)$$

are $\theta_M \approx 0.65; 0.29; 0.00$ for $l_0 = 0.25; 0.50; 0.75$ nm respectively. The flexible coarse-grained model of a polyelectrolyte chain has the ability to adopt many configurations that are more expanded than that of a neutral polymer but are more compressed than that predicted assuming a rigid rod configuration [26]. The electrostatic potential produced by the flexible model configurations is more attractive than that predicted by the rigid-rod model, being more efficient to condense counterions [38, 39]. The present results sheds light on apparent discrepancies found in the literature. On one side, the degree of ionization $\alpha = 1 - \theta$ has been found to be independent of the polymerization degree at essentially all Coulomb strengths and in solutions without added salt [34] when $N_m \geq 50$. On the other hand, Winkler et al. reported that the degree of condensed counterions increases with increasing chain length in the range $8 < N_m < 64$ [40]. Thus, the results presented above in Fig. 9 bridging the different chain sizes show that both results deliver complementary rather than opposite pictures of the problem.

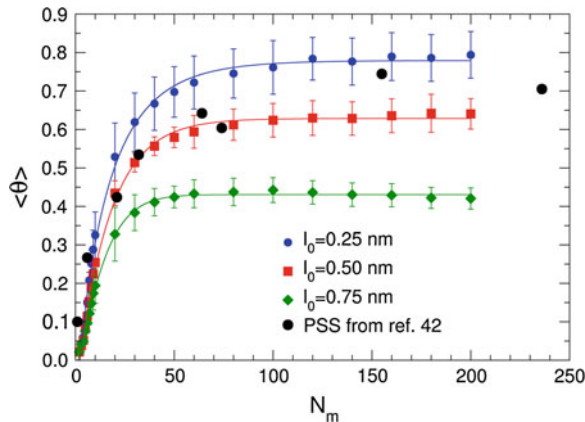


Fig. 9 Average condensation degree at a function of chain size for different values of the equilibrium bond length l_0 . The experimental values are depicted using the effective charge measurement by Böhme and Scheler [42] and Eq. 68

Comparison with recent experiment supports this assessment [41]. Böhme and Scheler [42] measured the effective charge Z_{effect} of poly-(styrene sulfonate) as a function of the degree of polymerization by means of an electrophoresis NMR experiment. The effective charge is the sum of the chain nominal charge plus the charge of condensed counterions, therefore the relationship between Z_{effect} and the counterion condensation degree is given by:

$$\theta = 1 - \frac{Z_{\text{effect}}}{N_m} \quad (68)$$

Figure 5 depicts the values of θ calculated by Eq. 68 and the experimental values of Z_{effect} obtained by Scheler. It can be noted the similarity between the experimental results and our simulation for the chain with $l_0 = 0.50 \text{ nm}$.

4.3 Morphology of Polyelectrolytes Complex. Effect of Chain Stiffness

Another remarkable physicochemical property of polyelectrolytes is the formation of complexes between oppositely charged polymer in solution [43] or on a charged surface [44]. In particular, complex formation on surfaces by alternate adsorption with oppositely charged polyelectrolyte causes self-assembling into multilayer films [45]. These structures has been experimentally investigated through their morphology [22–24], and granular, rod and toroidal structures are obtained depending of the component and conditions in which complexes are made. The chain stiffness is critical since the experiment have shown that the flexible

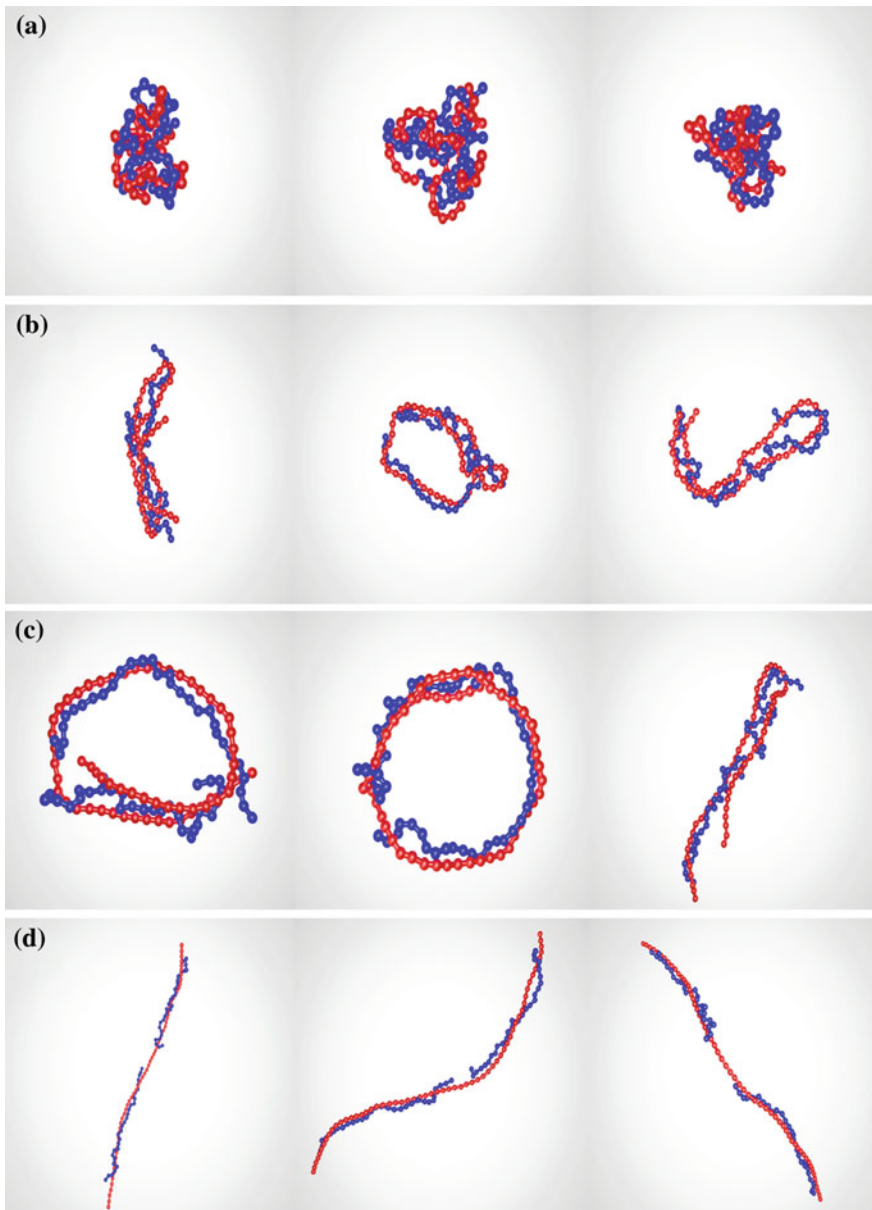


Fig. 10 Configurations obtained from Monte Carlo simulations with different values of the angular constant for the polyanion chain, (a) $k_{bend,pa} = 0$, (b) $k_{ang,pa} = 4$, (c) $k_{ang,pa} = 10$, (d) $k_{ang,pa} = 50$. The long polyanion chain contains 60 monomers and the two short fully flexible polycation chains contain 30 monomers each.[26]

polymers generally collapse to disordered globules, and stiff ones collapse to ordered structures such as toroids or folded chains [25].

In order to study the polyelectrolyte complex morphology we have chosen a system made of a “long” polyanion chain and several “short” polycation chains. The long polyanion chain was given a size $Nm_{pa} = 60$ with variable stiffness governed by the polyanion angular constant $k_{ang,pa}$ values. In the case of the polycation chains, we have considered them as totally flexible chains ($k_{bend,pc} = 0$) with $Nm_{pc} = 30$. We added as many short polycation chains as necessary to obtain a system with equal amounts of polycation and polyanion monomers.

Figure 10 shows several configurations obtain from Monte Carlo simulations with different stiffness values of the long chain (red one) combined with the short flexible chains (blue ones). Each panel corresponds to single trajectory. Panel a shows three characteristic structures formed by a fully flexible long chain complexed with shorter chains. The final complex structures present a globular shape.

When the long chain stiffness is increased $k_{bend,pa} = 4$, the structures are no longer globular and become more stretched, yielding pseudo-toroidal shapes (panel b). With a larger bending constant, $k_{bend,pa} = 10$ the presence of toroidal structures becomes evident (panel c). Some highly elongated shapes are also found. When we reach extreme rigidity setting $k_{bend,pa} = 50$, elongated structures with the shape of rigid rods are formed, but different from those obtained with $k_{bend,pa} = 10$. While the latter are obtained by roughly folding the chain in half yielding an U shaped structure, in the former case the chain is fully extended.

One of the most important factors affecting complex morphology is the chain length of the polyanion [26]. It was observed that longer chains display higher percentage of occurrence of toroids than of rods. However the structure of the toroids as characterized by SOCF and the radius do not depend significantly on chain length. This suggests that the final structure of the toroid is more dependent on the intrinsic rigidity of the chain than on the electrostatic contributions [26].

5 Conclusion

The Monte Carlo method has proven to be a powerful tool to the study of polyelectrolyte solution. This simulation technique is a convenient complement to the experimental approach, since the simulation has access to molecular details that may lead to new concepts and ideas on the physicochemical phenomena under consideration.

References

1. Radeva, T. (ed.): Physical Chemistry of Polyelectrolytes. Marcel Dekker, New York (2001)
2. Brender, C., Lax, M., Windwer, S.: J. Chem. Phys. **74**, 2576 (1981)
3. Vlachy, V., Dolar, D.: J. Chem. Phys. **1982**, 76 (2010)

4. Wennerstrom, H., Jonsson, B., Linse, P.: *J. Chem. Phys.* **76**, 4665 (1982)
5. Carnie, S.L., Christos, G.A., Creamer, T.P.: *J. Chem. Phys.* **89**, 6484 (1988)
6. Olmsted, M.C., Anderson, C.F., Record, M.T.: *Jr PNAS* **86**, 7766 (1989)
7. Valleau, J.P.: *Chem. Phys.* **129**, 163 (1989)
8. Christos, G.A., Carnie, S.L.: *J. Chem. Phys.* **91**, 439 (1989)
9. Wallin, T., Linse, Per: *Langmuir* **12**, 305 (1996)
10. Wallin, T., Linse, Per: *J. Phys. Chem.* **100**, 17873 (1996)
11. Wallin, T., Linse, Per: *J. Phys. Chem. B* **101**, 5506 (1997)
12. Israelchvili, J.N.: *Intermolecular and Surface Forces*. Cornell University Press, Ithaca, NY (1985)
13. Gregory, A. (ed.): *Coarse-Graining of Condensed Phase and Biomolecular Systems*. CRC Press, Boca Raton (2009)
14. Grest, G.S., Kremer, K.: *Phys. Rev. A* **33**, 3628 (1986)
15. Stevens, M.K.: *Biophys. J.* **80**, 130 (2001)
16. McQuarrie, D.A.: *Statistical Mechanics*. University Science Books, Sausalito, California (2000)
17. Binder, K.: *Monte Carlo and Molecular Dynamics Simulations in Polymer Science*. Oxford University Press, New York (1995)
18. Frenkel, D., Smit, B.: *Understanding Molecular Simulation: from Algorithms to Applications*, 2nd edn. Academic Press, San Diego, CA (2001)
19. Allen, M.P., Tildesley, D.J.: *Computer Simulation of Liquids*. Oxford University Press, New York (1989)
20. Metropolis, N., Rosenbluth, A.W., Rosenbluth, M.N., Teller, A.H., Teller, E.: *J. Chem. Phys.* **1087**, 21 (1953)
21. Madras, N., Sokai, A.D.: *J. Stat. Phys.* **50**, 109 (1988)
22. Maurstad, G., Danielsen, S., Stokke, B.T.: *J. Phys. Chem. B* **107**, 8172 (2003)
23. Danielsen, S., Vårum, K.M., Stokke, B.T.: *Biomacromolecules* **5**, 928 (2004)
24. Maurstad, G., Danielsen, S., Stokke, B.T.: *Biomacromolecules* **8**, 1124 (2007)
25. Bloomfield, V.A.: *Curr. Opin. Struct. Biol.* **6**, 334 (1996)
26. Narambuena, C.F., Leiva, E.P.M., Chávez-Páez, M., Pérez, E.: *Polymer* **51**, 3293 (2010)
27. Wilhelm, J., Frey, E.: *Phys. Rev. Lett.* **77**, 2581 (1996)
28. Odijk, T.: *J. Polym. Sci.* **15**, 477 (1977)
29. Skolnick, J., Fixman, M.: *Macromolecules* **10**, 944 (1977)
30. Seidel, C., Schlacken, H., Müller, I.: *Macromol. Theory Simul.* **3**, 333 (1994)
31. Micka, U., Kremer, K.: *Europhys. Lett.* **38**, 279 (1997)
32. Bacova, P.: Study of persistence length of linear polyelectrolytes in solutions. Bachelor thesis, Charles University in Prague Faculty of Science, Czech Republic (2008)
33. Mangui, M., Netz, R.R.: *Eur. Phys. J. E* **14**, 67 (2004)
34. Liu, S., Muthukumar, M.: *J. Chem. Phys.* **116**, 9975 (2002)
35. Manning, G.S.: *J. Chem. Phys.* **51**, 924 (1969)
36. Limbach, H.J., Holm, C.: *J. Chem. Phys.* **14**, 9674 (2001)
37. Frank, S., Winkler, R.G.: *Europhys. Lett.* **83**, 38004 (2008)
38. Muthukumar, M.: *J. Chem. Phys.* **120**, 9343 (2004)
39. Muthukumar, M.: *J. Chem. Phys.* **137**, 034902 (2012)
40. Winkler, R.G., Gold, M., Reineker, P.: *Phys. Rev. Lett.* **80**, 3731 (1998)
41. Scheler, U.: *Curr. Opin. Colloid. Interface Sci.* **17**, 64 (2012)
42. Böhme, U., Scheler, U.: *Macromol. Chem. Phys.* **208**, 2254 (2007)
43. Kabanov, A.V., Bronich, T.K., Kabanov, V.A., Yu, K., Eisenberg, A.: *Macromolecules* **29**, 6797 (1996)
44. Decher, G.: *Science* **277**, 1232 (1997)
45. Decher, G., Schlenoff, J.B. (eds.): *Multilayer Thin Films: Sequential Assembly of Nanocomposite Materials*. Wiley, Weinheim, Germany (2003)